ANSA-BRIDGED AND BINUCLEAR METALLOCENE COMPOUNDS OF ZIRCONIUM AND HAFNIUM

by

Gary M. Diamond

A thesis submitted in part fulfilment

of the requirements for the degree of

Doctor of Philosophy

at the University of Oxford

Balliol College,

Oxford

January 1994

ABSTRACT

ansa-Bridged and Binuclear Metallocene Compounds of Zirconium and Hafnium

Gary M. Diamond

Balliol College

D. Phil. Thesis

Hilary Term 1994

This thesis describes the synthesis and characterisation of new mononuclear and binuclear zirconium and hafnium compounds containing *ansa*-bridged ligands. Some olefin polymerization studies, employing the new compounds as catalysts, are also presented.

Chapter 1 begins with an introduction to Ziegler-Natta polymerization of olefins, concentrating on recently developed metallocene-based catalyst systems. The second part of the Chapter charts the development of group 4 *ansa*-metallocene derivatives, especially their use as stereospecific catalysts. Finally, a review of binuclear group 4 metallocene compounds containing bridging bis(cyclopentadienyl)-type ligands is presented.

Chapter 2 describes the synthesis and characterisation of some novel mononuclear metallocene compounds of zirconium and hafnium containing *ansa*-bridged ligands. The *ansa*-bridged mononuclear compounds [{$Me_2C(\eta^5\text{-}C_5H_4)(\eta^2\text{-}C_9H_6)$}$M(\eta^5\text{-}C_5H_5)Cl$] (M = Zr, Hf), [{$(CH_2)_5C(\eta^5\text{-}C_5H_4)(\eta^2\text{-}C_9H_6)$}$M(\eta^5\text{-}C_5H_5)Cl$] (M = Zr, Hf) and [{$Me_2(\eta^5\text{-}C_5H_4)(\eta^3\text{-}C_{13}H_8)$}$Zr(\eta^5\text{-}C_5H_5)Cl$] are described, along with the X-ray crystal structures of the zirconium compounds. The η^2-indenyl and η^3-fluorenyl coordination modes observed for these compounds are unprecedented. The synthesis and characterisation of the novel, mononuclear *ansa*-bridged compounds [{$Me_2C(\eta^5\text{-}C_5H_4)_2$}$M(\eta^5\text{-}C_5H_5)Cl$] (M = Zr, Hf) is also described, along with their X-ray crystal structures. The variable temperature solid state ^{13}C CP/MAS NMR spectra of [{$Me_2C(\eta^5\text{-}C_5H_4)_2$}$M(\eta^5\text{-}C_5H_5)Cl$] (M = Zr, Hf) show slow rotation of the C_5H_5 ring on the NMR timescale.

Chapter 3 describes the synthesis and characterisation of some novel homo- and hetero-binuclear metallocene compounds of zirconium and hafnium in which the metals are bridged by an unsymmetrical *ansa* ligand. The novel, chiral homobinuclear compounds $[(\eta^5\text{-}C_5H_5)MCl_2\{(\eta^5\text{-}C_5H_4)CMe_2(\eta^5\text{-}C_9H_6)\}MCl_2(\eta^5\text{-}C_5H_5)]$ (M = Zr, Hf) are described. The *ansa*-bridged mononuclear compounds $[\{Me_2C(\eta^5\text{-}C_5H_4)(\eta^2\text{-}C_9H_6)\}M(\eta^5\text{-}C_5H_5)Cl]$ (M = Zr, Hf) are used as reagents for the *selective* synthesis of the heterobinuclear analogues $[(\eta^5\text{-}C_5H_5)MCl_2\{(\eta^5\text{-}C_5H_4)CMe_2(\eta^5\text{-}C_9H_6)\}M^*Cl_2(\eta^5\text{-}C_5H_5)]$ (M = Zr, M* = Hf ; M = Hf, M* = Zr) and the unsymmetrical homobinuclear compound $[(\eta^5\text{-}C_5H_5)ZrCl_2\{(\eta^5\text{-}C_5H_4)CMe_2(\eta^5\text{-}C_9H_6)\}ZrCl_2(\eta^5\text{-}C_5Me_5)]$. The methylated derivatives $[(\eta^5\text{-}C_5H_5)M(CH_3)_2\{(\eta^5\text{-}C_5H_4)CMe_2(\eta^5\text{-}C_9H_6)\}M^*(CH_3)_2(\eta^5\text{-}C_5H_5)]$ (M = Zr, M* = Zr, Hf; M = Hf, M* = Zr, Hf) are also described. The structurally related mononuclear compounds $[(\eta^5\text{-}C_5H_5)MCl_2\{(\eta^5\text{-}C_5H_4)CMe_2(C_9H_7)\}]$ (M = Zr, Hf) and $[(\eta^5\text{-}C_5H_5)Zr(CH_3)_2\{(\eta^5\text{-}C_5H_4)CMe_2(C_9H_7)\}]$ have also been prepared.

Chapter 4 presents some olefin polymerization studies using the new compounds described in Chapter 3 as catalysts, along with either methylaluminoxane or the recently developed co-catalysts $[Ph_3C]^+[B(C_6F_5)_4]^-$ and $B(C_6F_5)_3$.

Chapter 5 provides the experimental details for the reactions described in this thesis and the characterising data for all new compounds are given in **Chapter 6**

Crystallographic data for the for the X-ray structure determinations in Chapter 2 are given in the **Appendices**.

The work described in this thesis was carried out in the Inorganic Chemistry Laboratory, South Parks Road, Oxford, from October 1990 until October 1993 under the supervision of Professor M. L. H. Green, F. R. S. All the work is my own unless stated to the contrary, and has not been submitted for a degree at this, or any other, university.

[Signature removed from online version of thesis]

To my Parents

ACKNOWLEDGEMENTS

First I wish to thank my supervisor, Professor M. L. H. Green, F. R. S., for allowing me the opportunity to carry out research in his group, and for his advice, encouragement and enthusiasm.

I would also like to thank the colleagues who contributed directly to the work in this thesis, namely Dr. Philip Mountford, Dr. Alexander Chernega and Dr. Vince Murphy for crystallographic services, Dr. Steve Heyes and Jackie Horne for solid state NMR data and Neil Popham for the mass spec.

I want to thank all those who have contributed with helpful discussions, especially Neil Popham and Philip Mountford, and Nik Kaltsoyannis for providing a copy of Richard Strittmatter's Ph.D. thesis, which was very useful. The excellent proof reading by Neil (again!), John Claridge, Jane Haggitt, Steve Barlow, John Evans, Tom James, Cliff Williams and Grant Taylor, must also be acknowledged. You never would have guessed there were so many ways to spell "diastereomer"!

I would also like to mention my old S15 lab-mates Dave Glueck, Pedro Gomes and "Tommy" Ushioda, for putting up with my mess for all these years.

On a more serious note, I would like to thank ICI plc and the SERC for a CASE award, and in particular Dr. John Kelland of ICI for inviting me up to the Wilton Plant. Thanks also to the technical staff of the ICL, especially Ken, Steve and Keith in Stores, for their unique brand of humour.

The most important acknowledgement of all, though, must go to my parents, for all their support and encouragement over the years.

When angry, count four; when very angry, swear.

Mark Twain

ABBREVIATIONS

General:

Bu	butyl
Cp	cyclopentadienyl
Cp'	substituted cyclopentadienyl
Cp*	pentamethylcyclopentadienyl
DME	1,2-bis(methoxy)ethane
Et	ethyl
$Et(Ind)_2$	ethylenebis(indenyl)
Et_2O	diethyl ether
Ind'	substituted indenyl
MAO	methylaluminoxane
Me	methyl
NMR	nuclear magnetic resonance
Ph	phenyl
Pr	propyl
r.t.	room temperature
THF	tetrahydrofuran

Nuclear magnetic resonance spectroscopic data:

br.	broad
d	doublet
Hz	Hertz
J	coupling constant
m	multiplet
ppm	parts per million
q	quartet
s	singlet
t	triplet

CONTENTS

Chapter 1

Chapter 2

CHAPTER ONE

Introduction

1.0 General Introduction

This thesis is concerned with the synthesis, structure and reactivity of new mononuclear and binuclear zirconium and hafnium compounds containing *ansa*-bridged ligands. This introductory Chapter provides an overview of previous work in the three areas of interest most pertinent to this thesis.

The first part of this Chapter provides an introduction to Ziegler-Natta polymerization of olefins, which has been one of the major driving forces for the development of group 4 organometallic chemistry, concentrating on recently developed metallocene-based catalyst systems. The second part of the Chapter charts the development of group 4 *ansa*-metallocene derivatives, especially their use as stereospecific catalysts. Finally a review of binuclear group 4 metallocene compounds is presented, with emphasis on complexes containing bridging bis(cyclopentadienyl)-type ligands.

1.1 Ziegler-Natta polymerization of olefins

1.1.1 Early history of Ziegler-Natta polymerization

The discovery, in the early 1950s, of catalysts for the low pressure polymerization of olefins won Karl Ziegler and Guilio Natta the Nobel Prize for Chemistry, and has had a dramatic effect on the shape of the worldwide petrochemical and plastics industries. Since then there has been a huge research effort towards improving the catalytic processes and understanding the reaction mechanisms involved.

The industrial production of polyethylene began in earnest during the Second World War, when it was made with a radical catalyst at very high pressures (1000-3000 atm.) and high temperatures (150-230 °C). It is hardly surprising that the discovery by Ziegler of catalysts capable of polymerizing ethylene at room temperature and one atmosphere pressure was to have such an effect on the polymer industry.

It had been known for some time that lithium alkyls were capable of catalysing the oligomerization of ethylene to low molecular weight polymers.[1] In the 1940s and early '50s Ziegler and co-workers demostrated that $LiAlH_4$ reacted with ethylene to form $LiAlEt_4$, and that ethylene undergoes oligomerization when heated with aluminium alkyl compounds by what Ziegler called the "aufbau" or growth reaction:

$$R_2AlC_2H_5 + C_2H_4 \rightarrow R_2Al\text{-}CH_2\text{-}CH_2\text{-}C_2H_5$$

$$R_2AlCH_2CH_2C_2H_5 + nC_2H_4 \rightarrow R_2Al(CH_2CH_2)_{n+1}C_2H_5$$

$$R_2Al(CH_2CH_2)_{n+1}C_2H_5 + C_2H_4 \rightarrow R_2AlC_2H_5 + CH_2CH(CH_2CH_2)_nC_2H_5$$

The propagation step requires temperatures of 100-120 °C whilst the displacement step requires still higher temperatures.

In 1953, Ziegler's group discovered, by accident, that colloidal nickel catalysed the displacement reaction and soon cobalt and platinum were found to have a similar effect. When they tried using zirconium acetylacetonate as a co-catalyst, the autoclave

was filled with polyethylene. Other transition metal compounds of groups 4 to 6 together with alkylaluminium reagents gave similar results, with the best catalysts coming from titanium compounds.[2] Characterization studies of the polyethylenes produced by the new catalysts showed them to have linear unbranched structures and high molecular weights.

Before publication, Ziegler disclosed his results to the Italian company Montecatini, and it was agreed that Natta should investigate the polymerization of propylene and other α-olefins. Using the $AlEt_3$ / $TiCl_4$ catalyst developed by Ziegler, Natta's group found that propylene could be polymerized to a mixture of crystalline and amorphous fractions. The yield of crystalline polymer could be increased by using $TiCl_3$ as the titanium component. Natta investigated the structure of the polymer and designated it **isotactic** (see below).[3] In 1962 he disclosed that high yields of another crystalline form of polypropylene, **syndiotactic** polypropylene, could be made at low temperature using a homogeneous system composed of $AlEt_2Cl$ and VCl_4.[4]

1.1.2 Stereochemical aspects of polymer structure

If the backbone of a polymer chain is drawn in a flat zig-zag form in the plane of the paper, the substituent patterns shown in Figure 1.1.1 can easily be envisaged for the case of a monosubstituted vinyl monomer such as propylene.

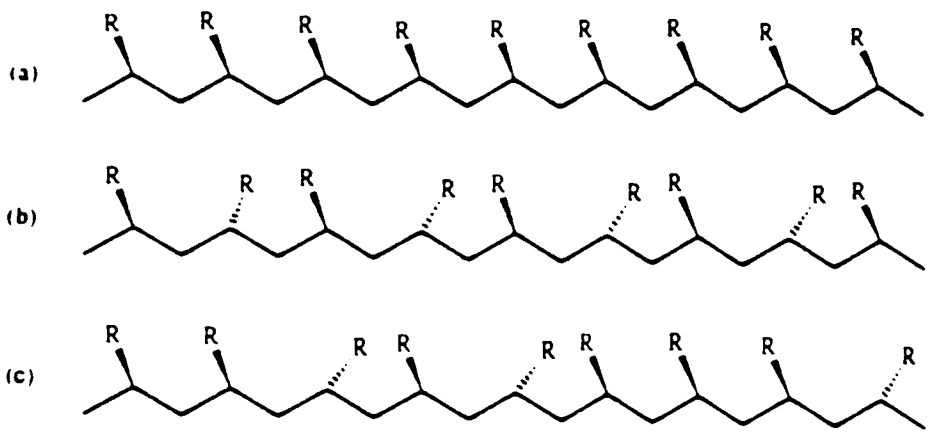

Figure 1.1.1 Planar representations of chains of poly(α-olefins); (a) isotactic (b) syndiotactic and (c) atactic

It should be noted that in (a) all the substituent R groups lie on the same side of the zig-zag plane, which Natta called **isotactic**. In (b) the substituent R groups occupy positions alternately above and below the backbone plane, this is arrangement called **syndiotactic**. In (c) there is no regular arrangement of the R groups which lie randomly above and below the plane, this is known as **atactic** polymer. Polymerization of propylene generally produces a mixture of atactic, together with either isotactic or syndiotactic, polymer.

1.1.3 Development of Ziegler-Natta catalysis

Since the early work by Ziegler and Natta, a whole industry has grown up based on their discoveries and on the work of thousands of other industrial and academic chemists. New classes of catalysts and polymers have been discovered and some insight has been gained into the detailed mechanism of polymerization. Since there have been many reviews and books published covering these developments in great detail,[5-13] I shall concentrate on the most recent advances and those most pertinent to the work in this thesis, namely homogeneous group 4 metallocene catalysts and recently developed co-catalysts.

1.1.4 Metallocene catalysts for olefin polymerization

The application of group 4 metallocenes as Ziegler-Natta catalysts has been known since 1957 when Natta reported that Cp_2TiCl_2 together with $AlEt_3$ polymerized ethylene.[14] Over the next 15 years catalysts based on bis(cyclopentadienyl)titanium(IV) compounds and various alkylaluminium reagents were to become amongst the most studied soluble catalyst systems, and, with respect to the kinetics of polymerization and side reactions, one of the best understood.[11] Such systems were not used industrially, though, due to their relatively low activity and short lifetime.

In 1980, Kaminsky reported highly active and long lived ethylene polymerization catalyst systems based on the group 4 metallocene derivatives Cp_2ZrMe_2 and Cp_2TiMe_2. The co-catalysts were oligomeric methylaluminoxanes, formed by the partial hydrolysis of trimethylaluminium.[15] During the early 1980s Kaminsky and others demostrated that bis(cyclopentadienyl) group 4 dichloride and dialkyl derivatives, together with alkyl aluminoxanes, were highly active olefin polymerization catalysts. Employment of the oligomeric aluminoxane co-catalysts apparently offered the following advantages: (i) the catalyst system was extremely long lived, (ii) the molecular weight distribution of the resulting polyethylene was surprisingly narrow, resembling those of "living polymers" and (iii) high molecular weight atactic polymers were obtained from propylene and higher α-olefins.[11, 15-18] The exact nature and role of the alkylaluminoxanes used as co-catalysts was not known, and to this day is a subject of considerable debate.

1.1.5 The role of methylaluminoxane

Methylaluminoxane (MAO) can be prepared by the partial hydrolysis of trimethylaluminium. The most commonly used procedure is the reaction between $AlMe_3$ and hydrated inorganic salts such as $CuSO_4.5H_2O$ and $Al_2(SO_4)_3.6H_2O$. The product is believed to be a mixture of linear and/or cyclic oligomers, $[-Al(CH_3)-O-]_n$, where the degree of oligomerization depend on the conditions used, but typically lies in the range n = 4 to 30.[18, 19] Unreacted $AlMe_3$ is typically also present, probably co-ordinated to the oxygen atoms of the Al-O-Al moieties. A generalised molecular structure is shown in Figure 1.1.2.

The polymerization activity of the Kaminsky-type metallocene/methyl aluminoxane catalysts has been shown to be highly dependent on the nature of the MAO used. It has been reported that high catalyst activity requires a high degree of oligomerization[15,18] and that organic Lewis bases such as ethers have a dramatic poisoning effect on polymerization.[18]

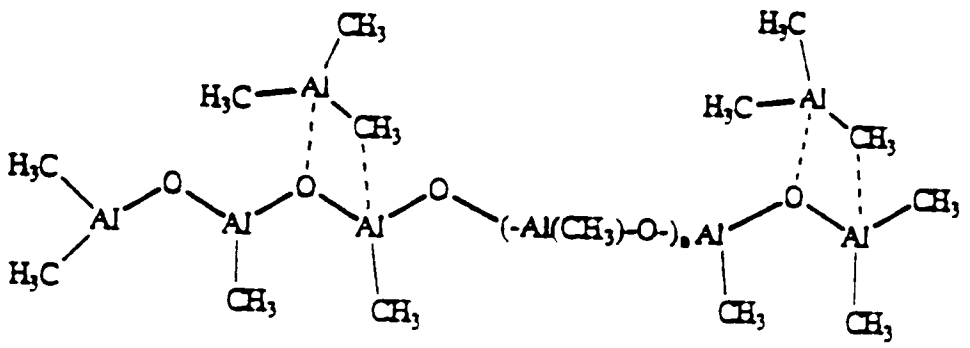

Figure 1.1.2. Generalised molecular structure of methylaluminoxane.[18]

The catalytic activity has also been shown to be strongly dependent on both the nature of substituents on the cyclopentadienyl ligand and the type of σ-alkyl ligands (R) in Cp_2MR_2 catalysts.[18] Based on such observations, both Kaminsky[19] and Giannetti[18] proposed an intimate relationship involving covalent M-O-Al bonding between the metallocene and MAO. Kaminsky suggested that the active species might be a multi-metallic cluster, whilst Giannetti proposed that an oxygen atom of an Al-O-Al moiety of the MAO may act initially as a σ-donor towards the transition metal (M), followed by insertion into an M-R bond to give an active species with M-O-Al bonds, which was proposed to have a highly polarized structure (Figure 1.1.3).

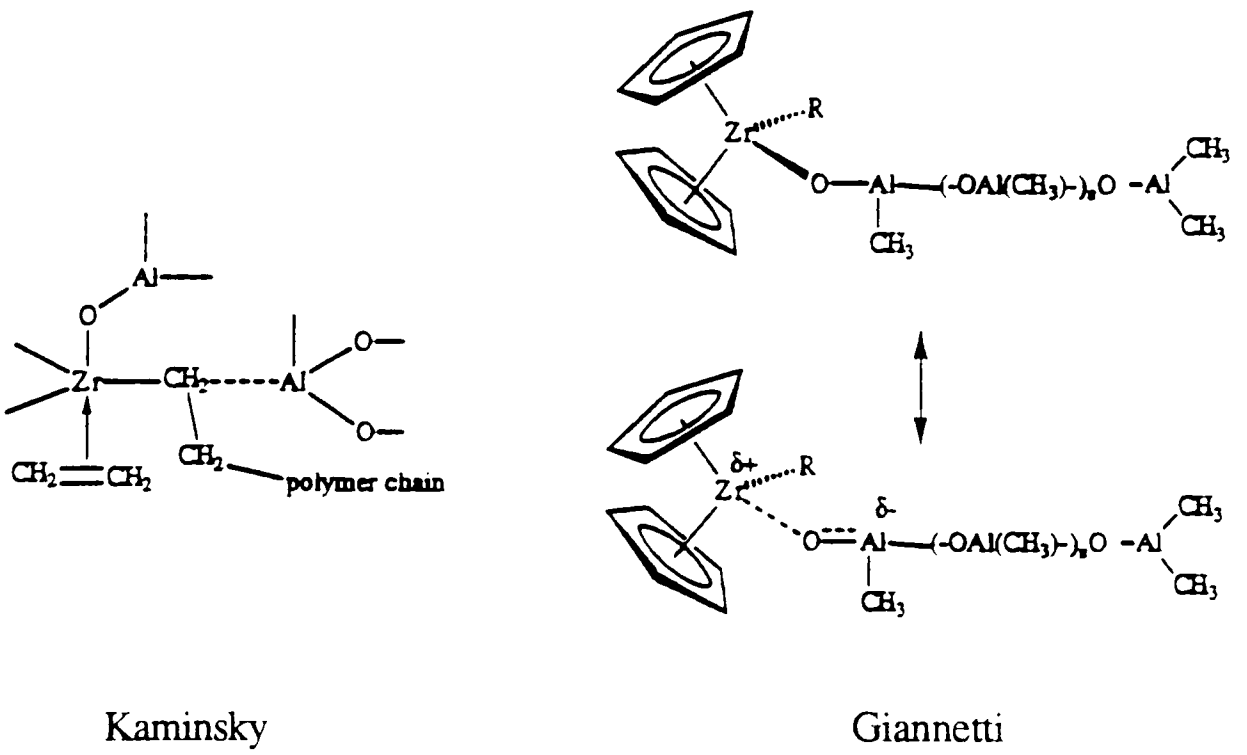

Kaminsky Giannetti

Figure 1.1.3. Active species proposed by Kaminsky[19] and Giannetti.[18]

Some researchers have suggested that the MAO might have a much less intimate role in the polymerization, behaving more like a "carrier" or "support" for the active species. Resconi has demonstrated that, for the metallocene derivatives Cp_2ZrR_2 (R = Me, Ph, CH_2Ph and CH_2SiMe_3), when $AlMe_3$ is used as a co-catalyst instead of MAO, although the polymerization activity is much lower, the activity follows the same order in both cases (R = Me < Ph < CH_2Ph < CH_2SiMe_3). Furthermore, when a chiral *ansa*-bridged isospecific catalyst ethylenebis(indenyl)zirconium dichloride was used, the polypropylene produced had the same microstructure whether the co-catalyst was $AlMe_3$ or MAO (stereospecific olefin polymerization is discussed later in this chapter, along with *ansa*-bridged metallocenes). On this evidence Resconi proposed that the actual co-catalyst in the metallocene-MAO system is $AlMe_3$, with MAO acting as a soluble carrier-activator of an ion pair formed upon the reaction of the metallocene with $AlMe_3$.[20] Soga has also recently shown that metallocene dichloride systems, when supported on Al_2O_3 or $MgCl_2$ and activated with $AlMe_3$ or $AlEt_3$, are highly active polymerization catalysts, though an order of magnitude less active than related MAO systems.[21]

The previous two paragraphs have presented opposite extreme proposals for the role of MAO, that it forms multi-metallic clusters with M-O-Al covalent bonds, or acts more like a carrier or support. The most widely supported concept for the role of MAO is as follows:

(i) in the case of metallocene dichloride precursors, the MAO (or the $AlMe_3$ co-ordinated to the MAO) alkylates the transition metal centre to form $Cp_2M(R)Cl$ or Cp_2MR_2 species,

(ii) the MAO then, at least partially, abstracts a halide or alkide group from the transition metal, forming a cationic or "cation-like" active species of the type $[Cp_2M(R)]^+$ or $[Cp_2M(R)]^{\delta+}$,

(iii) this cation-like species is closely associated with the MAO, either in the form of a tight ion pair or as a pseudo-ionic "highly polarised species",

(iv) the olefin monomer co-ordinates to the transition metal of the co-ordinatively unsaturated $[Cp_2M(R)]^{(\delta)+}$ species and then inserts into the M-R bond.

It has been shown that electron-withdrawing substituents at the 4- and 7-positions of indenyl ligands in the systems $(\eta^5\text{-}4,7\text{-}X_2C_9H_5)ZrCl_2$/MAO markedly reduce the polymerization activity, suggesting a "cation-like" active species.[22] Model studies by Jordan,[23] Turner,[24] Eisch,[25] Marks,[26] Bochmann[27] and others, implicate formation of an ion pair of the type $[Cp_2M(R)]^+[X\{Al(CH_3)\text{-}O\}_n]^-$. Strong evidence for an active species of this type has been provided by an elegant series of solid state ^{13}C NMR experiments by Marks.[28] In these experiments $Cp_2Zr(CH_3)_2$ was treated with between 5 and 20 equivalents of MAO, then the solvent was removed and the resulting solids studied by solid state ^{13}C NMR. When the Al:Zr ratio was increased, the ^{13}C NMR signals of $Cp_2Zr(CH_3)_2$ were diminished, whilst new signals assigned to $[Cp_2Zr(CH_3)]^+$ were observed to increase. By then dosing the systems with ethylene, it was shown that $[Cp_2Zr(CH_3)]^+$ underwent ethylene insertion to give the cationic species $[Cp_2Zr(CH_2CH_2)_nCH_3]^+$:

$$Cp_2Zr(CH_3)_2 + [Al(CH_3)\text{-}O]_n \rightleftharpoons [Cp_2Zr(CH_3)]^+[(CH_3)\{Al(CH_3)\text{-}O\}_n]^-$$

$$[Cp_2Zr(CH_3)]^+ + n CH_2CH_2 \longrightarrow [Cp_2Zr(CH_2CH_2)_nCH_3]^+$$

In a related experiment, Cam and Giannini[29] have shown by solution ^1H NMR studies that Cp_2ZrCl_2 is monomethylated by the trimethyl aluminium present in MAO. They also provided evidence that, in the presence of excess MAO, the $Cp_2Zr(CH_3)Cl$ formed a highly polarised species which, on dosing with ethylene, underwent ethylene insertion into the Zr-CH_3 bond:

$$Cp_2ZrCl_2 + MAO{\cdot}AlMe_3 \longrightarrow Cp_2Zr(CH_3)Cl + MAO{\cdot}AlMe_2Cl$$

$$Cp_2Zr(CH_3)Cl + [Al(CH_3)O]_n \rightleftharpoons [Cp_2Zr(CH_3)^{\delta+}\cdots ClAl^{\delta-}(CH_3)O\{OAl(CH_3)\}_{n-1}]$$

$$Cp_2Zr(CH_3)^{\delta+} + n CH_2CH_2 \longrightarrow [Cp_2Zr(CH_2CH_2)_nCH_3]^{\delta+}$$

Waymouth has shown that the activity of metallocene catalysts of the type Cp'_2MX_2 activated by MAO shows a strong dependence on the nature of X, which may suggest that a "pseudo-cationic" species, in which there is still a close association between the anionic and cationic fragments, may be closer to the true nature of the active species.[30]

1.1.6 Cationic group 4 metallocene alkyl complexes

Neutral, d^0 group 4 metal alkyl complexes of the general type Cp_2MR_2 and $Cp_2M(R)X$ (R = H, alkyl, aryl; X^- = anionic, two-electron donor) are the most extensively studied class of group 4 organometallic complexes.[31] Since the mid-1980s the chemistry of the related cationic 16-electron $[Cp_2M(R)L]^+$ complexes (L = Lewis base ligand) and base-free 14-electron $[Cp_2M(R)]^+$ complexes has been developed.[32] The cationic complexes are considerably more reactive than their neutral counterparts, as a result of the increased Lewis acidity of the cationic metal centre and also the presence of a labile ligand (L), or increased co-ordinative unsaturation for base-free cations. The low-lying unfilled molecular orbitals of these complexes are shown below (Figure 1.1.4).

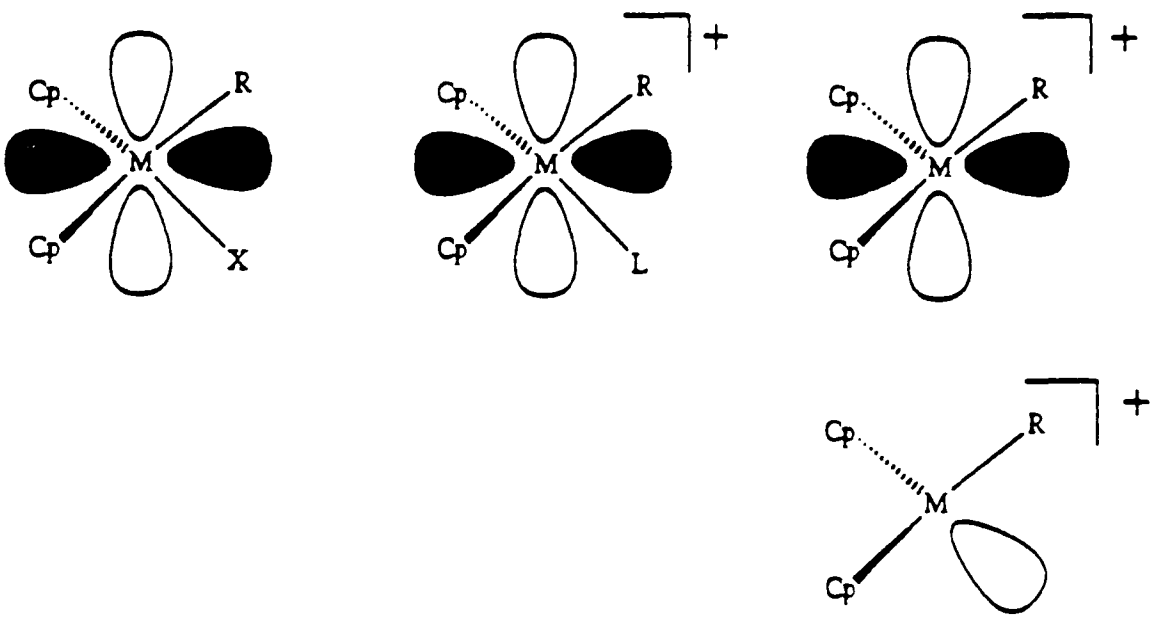

Figure 1.1.4. Low-lying unfilled orbitals of d^0 complexes $Cp_2M(R)X$, $[Cp_2M(R)L]^+$ and $[Cp_2M(R)]^+$

The $Cp_2M(R)X$ and $[Cp_2M(R)L]^+$ species both posess one low-lying metal-centred LUMO localised in the equatorial plane between the Cp ligands, in the latter case the LUMO is stabilised by the positive charge on the metal, and the metal is thus more Lewis acidic. The base-free species $[Cp_2M(R)]^+$ has two low-lying, metal-centred empty orbitals and is isolobal with AlR_2^+ and $Cp_2Ln(R)$ (Ln = Sc, Y, lanthanide).[32-35]

1.1.7 Synthesis of $[Cp_2M(R)L]^+$ and $[Cp_2M(R)]^+$ complexes

In recent years, several general synthetic routes to group 4 cationic $[Cp_2M(R)L]^+$ and $[Cp_2M(R)]^+$ complexes have been developed, namely; (i) oxidative cleavage of M-R bonds of Cp_2MR_2 complexes, (ii) protonolysis of Cp_2MR_2 complexes, (iii) abstraction of R^- group from Cp_2MR_2 complexes using $B(C_6F_5)_3$ or $[Ph_3C]^+[B(C_6F_5)_4]^-$.

1.1.7 (i) Oxidative cleavage of Zr-R bonds of Cp_2ZrR_2 complexes

In 1986, Jordan reported that cationic $[Cp_2Zr(R)L]^+$ complexes can be prepared by the reaction of Cp_2ZrR_2 complexes with one-electron oxidants such as $[(C_5H_4Me)_2Fe]^+$ or Ag^+ in the presence of ligand L.[36-38] The reaction is quite general for a variety of zirconocene dialkyl derivatives, as shown below (Figure 1.1.5), though not for the titanium analogues which are generally reduced to Ti(III) products.[32]

A key point in the development of this chemistry was the realization that weakly coordinating, inert counterions such as $[BPh_4]^-$ were required for the isolation of stable salts of $[Cp_2Zr(R)L]^+$ cations. The general trend for the ease of Zr-R bond cleavage by $[Cp'_2Fe]^+$ reagents was shown to be $Zr\text{-}CH_2Ph > Zr\text{-}CH_3 > Zr\text{-}Ph$.[39]

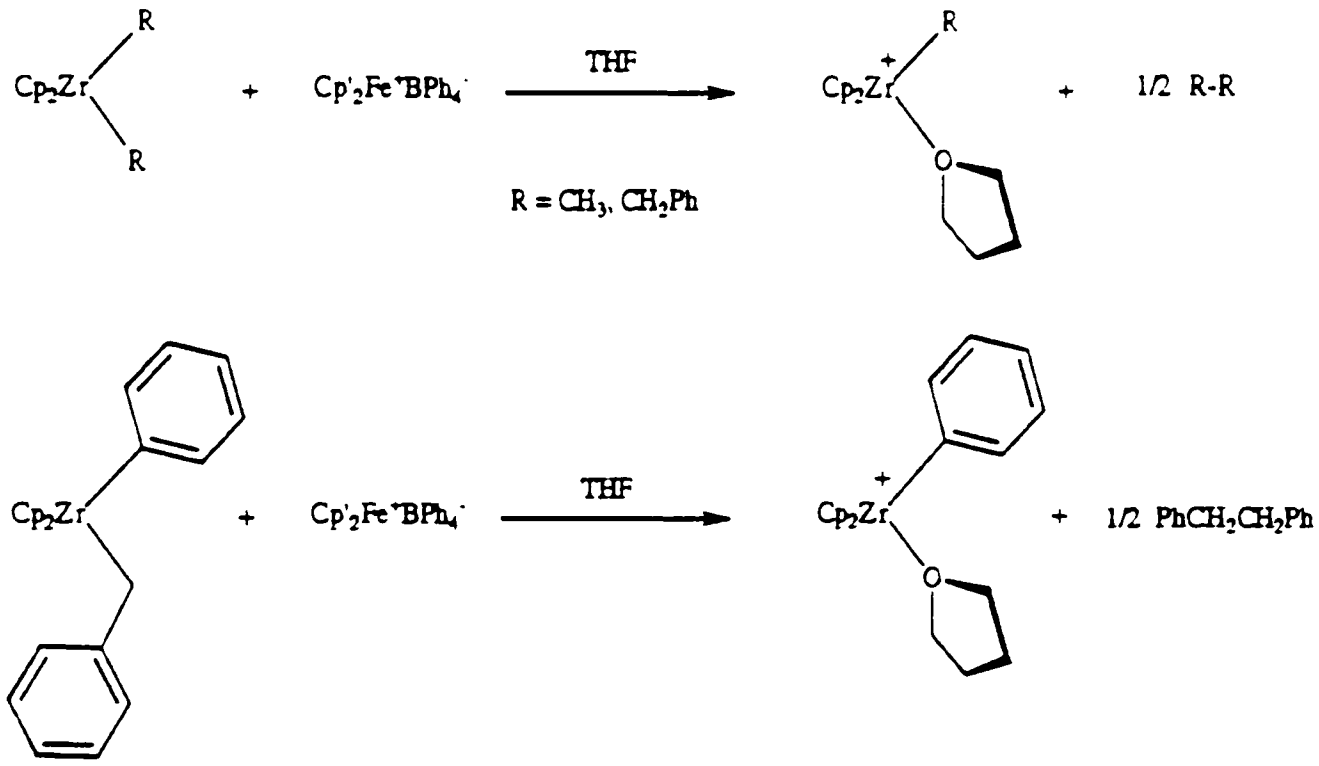

Figure 1.1.5. Synthesis of $[Cp_2Zr(R)L]^+$ complexes by oxidative cleavage.

Jordan demonstrated that CH_2Cl_2 solutions of $[Cp_2Zr(CH_3)(THF)]^+[BPh_4]^-$ catalyze ethylene polymerization in the absence of aluminium co-catalysts or supports, under mild conditions.[37] The activity of this catalyst was very low compared with Kaminsky's Cp_2MX_2/MAO systems; this was attributed to the presence of the THF ligand inhibiting the coordination and insertion of ethylene.

The crystal structure of $[Cp_2Zr(CH_3)(THF)]^+[BPh_4]^-$ showed that the cation adopts a normal four-coordinate bent-metallocene type structure with no significant cation-anion interactions. The THF ligand is orientated nearly perpendicular to the O-Zr-CH_3 plane, which, together with the short Zr-O bond length, suggests that the oxygen is acting as a 4 electron σ,π-donor to the metal, thus the metal achieves an 18-electron configuration.[37] This influences not only the reactivity but also the structures of the THF-adducts. For example, $[Cp_2Zr(CH_2Ph)(THF)]^+$ has a normal η^1-benzyl ligand (and π-donation from the THF), but reacts irreversibly with CH_3CN to form the η^2-benzyl complex $[Cp_2Zr(\eta^2\text{-}CH_2Ph)(CH_3CN)]^+$ which shows π-donation from the phenyl group (CH_3CN is a poor π-donor).[38]

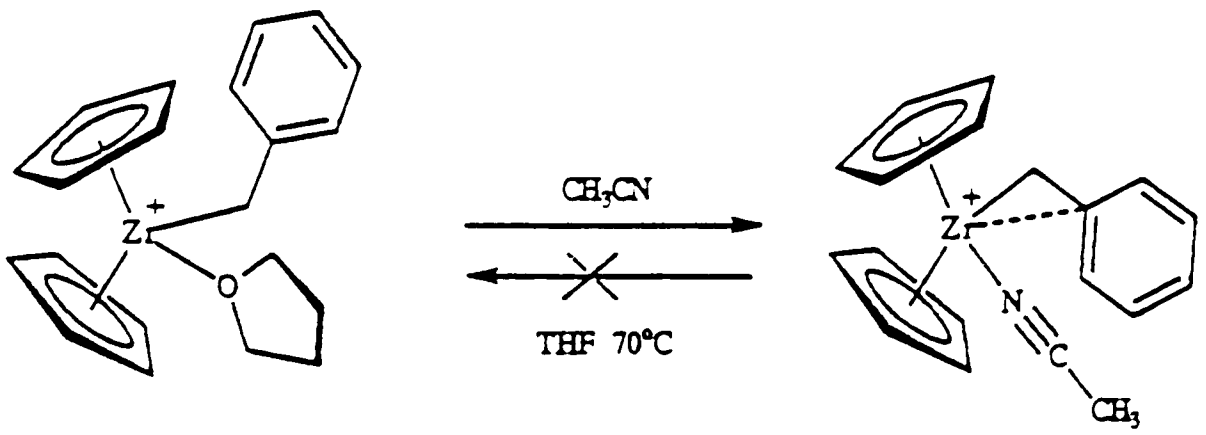

Figure 1.1.6. Reaction of $[Cp_2Zr(\eta^1\text{-}CH_2Ph)(THF)]^+$ with CH_3CN to form η^2-benzyl complex

Similarly, whilst cationic alkyl complexes $[Cp_2Zr(CH_2CH_2R)(THF)]^+[BPh_4]^-$ contain normal, undistorted alkyl groups, reaction with PMe_3 yields free THF and the PMe_3 complexes $[Cp_2Zr(CH_2CH_2R)(PMe_3)]^+[BPh_4]^-$ which exhibit strong β-agostic interactions.[40]

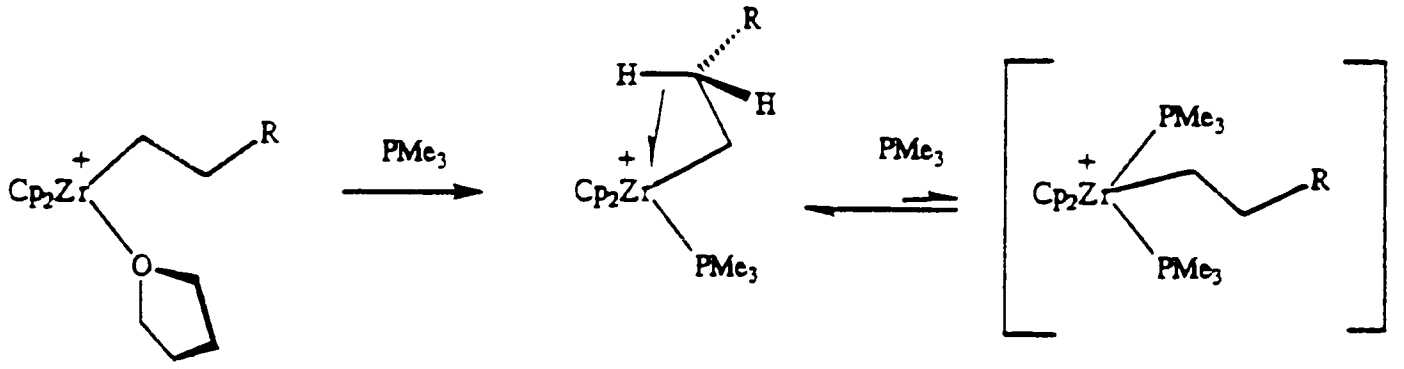

Figure 1.1.7. Reaction of $[Cp_2Zr(CH_2CH_2R)(THF)]^+$ complexes with PMe_3

1.1.7 (ii) Protonolysis of Cp_2MR_2 complexes

In 1986 Bochmann reported the synthesis of $[Cp_2Ti(CH_3)(NH_3)]^+X^-$ (X^- = PF_6^-, ClO_4^-) *via* the reaction of $Cp_2Ti(CH_3)_2$ with $[NH_4]^+X^-$ in THF.[41] The use of $[BPh_4]^-$ salts of bulkier ammonium reagents such as $[Bu_3NH]^+$ and $[PhNMe_2H]^+$ provides a general synthesis of $[Cp_2M(R)L]^+$ and $[Cp_2M(R)]^+$ complexes.[39, 42-44]

With the unhindered reagent $[Me_3NH]^+[BPh_4]^-$ the order of reactivity was shown to be Zr-Ph > Zr-CH_3 > Zr-CH_2Ph, *ie.* the reverse of the order for oxidative cleavage.[39]

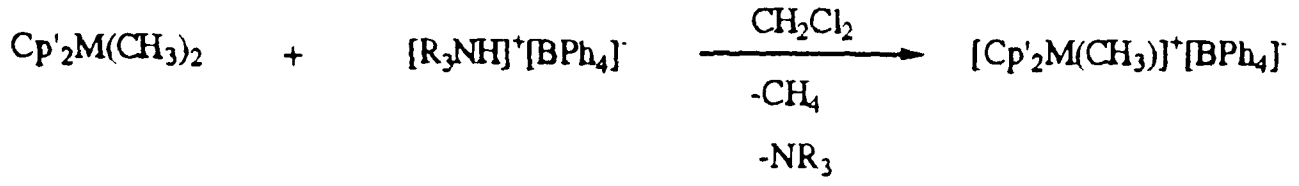

Figure 1.1.8. Preparation of $[Cp'_2M(CH_3)]^+[BPh_4]^-$

(Cp' = Cp, Ind; M = Ti, Zr; R_3N = Bu_3N, $PhNMe_2$)[43]

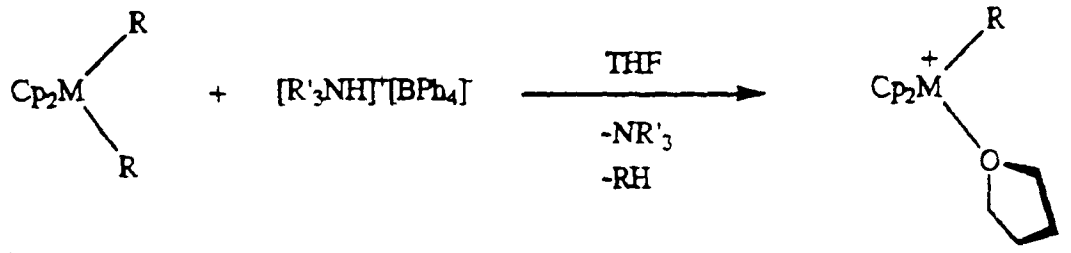

Figure 1.1.9. Preparation of $[Cp_2M(R)(THF)]^+[BPh_4]^-$

(M = Zr, Hf; R = Ph, Me; R'_3N = Bu_3N, $PhNMe_2$)[39]

Hlatky and Turner reported that the reaction between $Cp^*_2Zr(CH_3)_2$ and $[Bu_3NH]^+[BPh_4]^-$ in toluene yields the zwitterionic complex $[Cp^*_2Zr^+C_6H_4BPh_3^-]$ *via* Zr-CH_3 protonolysis followed by aryl C-H bond activation.[42]

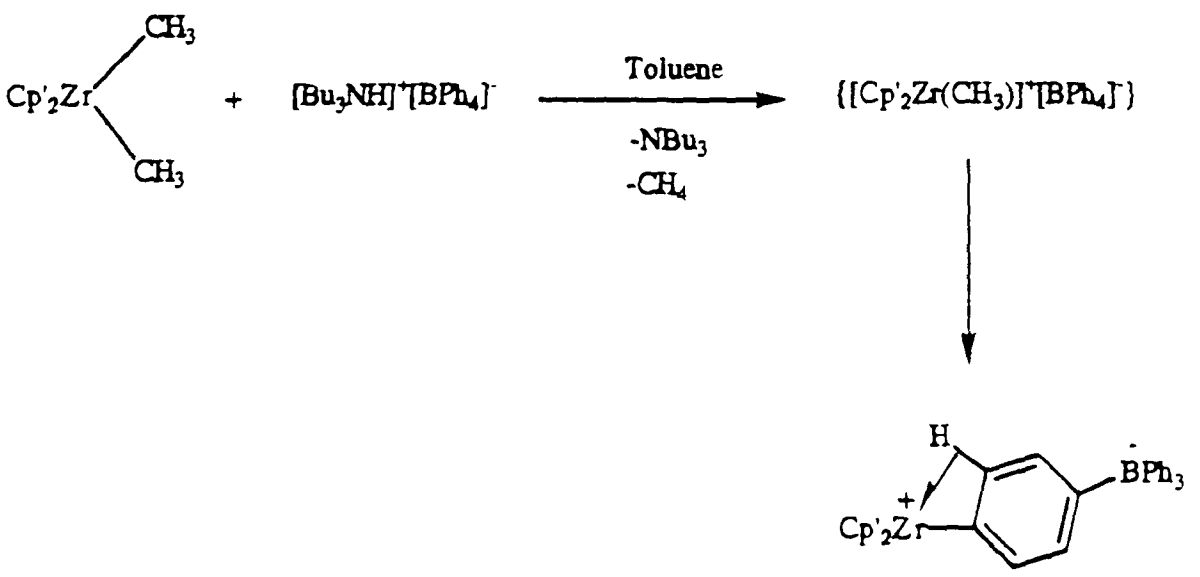

Figure 1.1.10. Synthesis of zwitterionic complex $[Cp^*_2Zr^+C_6H_4BPh_3^-]$

1.1.7 (iii) Abstraction of R^- group from Cp_2MR_2 complexes using $B(C_6F_5)_3$ or $[Ph_3C]^+[B(C_6F_5)_4]^-$

In 1991, Marks and co-workers attempted to model the supposed alkide (R^-) abstraction role of MAO to form cationic or "cation-like" active species of the type $[Cp_2M(R)]^{(\delta)+}$. They demonstrated that $B(C_6F_5)_3$, a hydrocarbon-soluble Lewis acid devoid of nucleophilic/coordinating substituents, was capable of abstracting a methide (CH_3^-) group from a variety of $Cp'_2Zr(CH_3)_2$ complexes ($Cp' = \eta^5\text{-}C_5H_5$, $\eta^5\text{-}1,2\text{-}Me_2C_5H_3$, $\eta^5\text{-}C_5Me_5$) to form the first stoichiometrically precise, isolable, crystallographically characterized, highly active "cation-like" zirconocene polymerization catalysts.[26, 45]

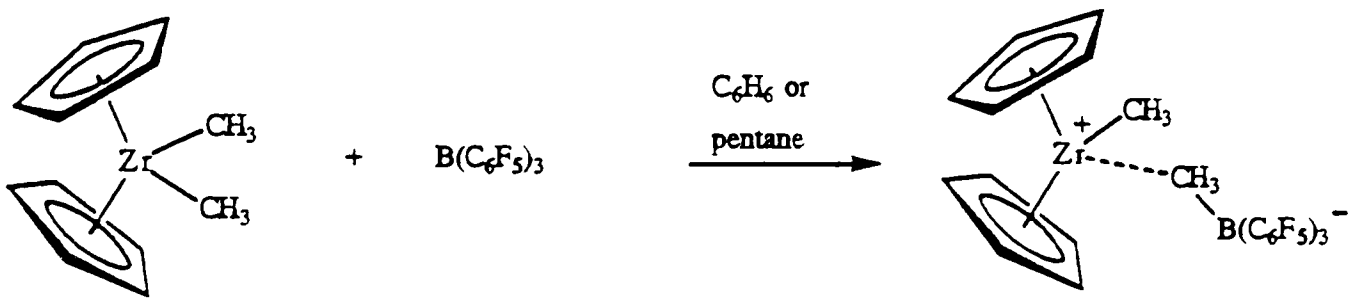

Figure 1.1.11. Preparation of "cation-like" complexes $[Cp'_2Zr(CH_3)]^+[CH_3B(C_6F_5)_3]^-$

The crystal structure of $[(\eta^5\text{-}1,2\text{-}Me_2C_5H_3)_2Zr(CH_3)]^+[CH_3B(C_6F_5)_3]^-$ shows a "bent-sandwich" $[(\eta^5\text{-}1,2\text{-}Me_2C_5H_3)_2Zr(CH_3)]^+$ cation weakly coordinated to a $[CH_3B(C_6F_5)_3]^-$ anion *via* a non-linear, highly unsymmetrical $Zr(\mu\text{-}CH_3)B$ bridge.

In 1992, Waymouth demonstrated that $[Cp^*_2Zr(CH_3)]^+[CH_3B(C_6F_5)_3]^-$ is capable of polymerizing functionalised olefins and dienes containing silyl-protected alcohols and tertiary amine groups. This is in sharp contrast to Ziegler-Natta catalysts with alkylaluminium-type co-catalysts, one of the major limitations of which is their intolerance towards Lewis base functionality.[46]

Soon after the use of $B(C_6F_5)_3$ as an alkide abstraction co-catalyst was reported, Chien and co-workers demonstrated that the triphenylcarbenium complex $[Ph_3C]^+[B(C_6F_5)_4]^-$ could play a similar role. The $[Ph_3C]^+$ was shown to abstract a CH_3^- group from the *ansa*-metallocene dimethyl derivative $[\{Et(Ind)_2\}Zr(CH_3)_2]$ to form Ph_3CCH_3 and the cationic zirconocene complex $[Et(Ind)_2Zr(CH_3)]^+[B(C_6F_5)_4]^-$, which was shown to be a highly active propylene polymerization catalyst, producing highly isotactic polypropylene[47] (stereospecific olefin polymerization is discussed later in this chapter, along with *ansa*-bridged metallocenes).

$$Et(Ind)_2Zr(CH_3)_2 + [Ph_3C]^+[B(C_6F_5)_4]^- \rightarrow [Et(Ind)_2Zr(CH_3)]^+[B(C_6F_5)_4]^- + Ph_3CCH_3$$

Figure 1.1.12. Alkide abstraction by $[Ph_3C]^+[B(C_6F_5)_4]^-$

In 1993 Bochmann showed that a variety of base-free cationic benzyl complexes $[Cp'_2Zr(CH_2Ph)]^+[B(C_6F_5)_4]^-$ could be prepared by the reaction of the metallocene dibenzyl precursors with $[Ph_3C]^+[B(C_6F_5)_4]^-$.[27] The cationic benzyl complexes $[Cp'_2Zr(CH_2Ph)]^+$ were thermally more stable than their methyl analogues, which Bochmann attributed to η^2 coordination of the benzyl group to the metal centre. These complexes were highly active ethylene and propylene polymerization catalysts, particularly at temperatures in excess of 50 °C.

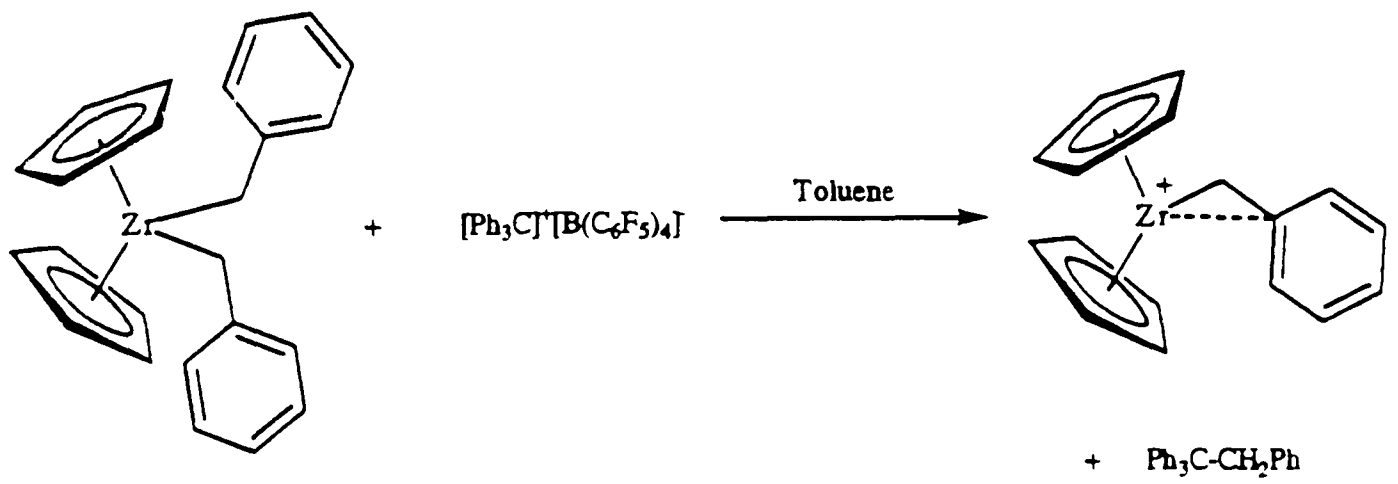

Figure 1.1.13. Reaction of metallocene dibenzyl complexes with $[Ph_3C]^+[B(C_6F_5)_4]^-$

1.2 Group 4 *ansa*-metallocene compounds

1.2.1 Early history of *ansa*-metallocenes

In 1957 Rinehart and Curby reported the synthesis of 1,1'-(α-ketotrimethylene)-ferrocene, $[\{(\eta^5\text{-}C_5H_4)COCH_2CH_2(\eta^5\text{-}C_5H_4)\}Fe]$, via the self-condensation reaction of $[(\eta^5\text{-}C_5H_5)Fe(\eta^5\text{-}C_5H_4CH_2CH_2CO_2H)]$.[48] This was the first report of a metallocene derivative with a bridge joining the two cyclopentadienyl rings (Figure 1.2.1). In the following year Luttringhaus and Kullick reported the synthesis of $[\{(CH_2)_3(\eta^5\text{-}C_5H_4)_2\}Fe]$ in low yield from the bridged sodium cyclopentadienide derivative $Na_2[(C_5H_4)CH_2CH_2CH_2(C_5H_4)]$.[49] They used the prefix "*ansa*" (latin, meaning bent handle attached at both ends) to denote the presence of an inter-annular bridge. Rinehart later showed that $[\{(\eta^5\text{-}C_5H_4)COCH_2CH_2(\eta^5\text{-}C_5H_4)\}Fe]$ could be reduced to the same trimethylene bridged *ansa*-ferrocene.[50]

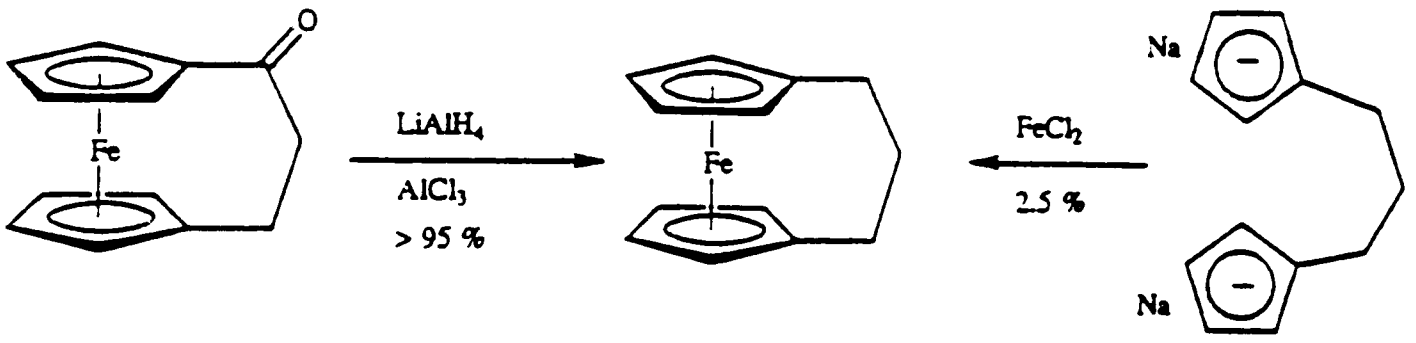

Figure 1.2.1. The first *ansa*-metallocenes

In 1970 Katz reported the synthesis (Figure 1.2.2) of the first group 4 *ansa*-metallocene, the methylene-bridged complex $[\{CH_2(\eta^5\text{-}C_5H_4)_2\}TiCl_2]$.[51] Katz also reported that this complex, together with sodium naphthalide, fixed nitrogen, and with Et_2AlCl polymerized ethylene (both known reactions of the unbridged Cp_2TiCl_2). Two years later Hillman prepared the first zirconium and hafnium *ansa*-metallocenes, the trimethylene-bridged complexes $[\{(CH_2)_3(\eta^5\text{-}C_5H_4)_2\}MCl_2]$ (M = Ti, Zr, Hf).[52]

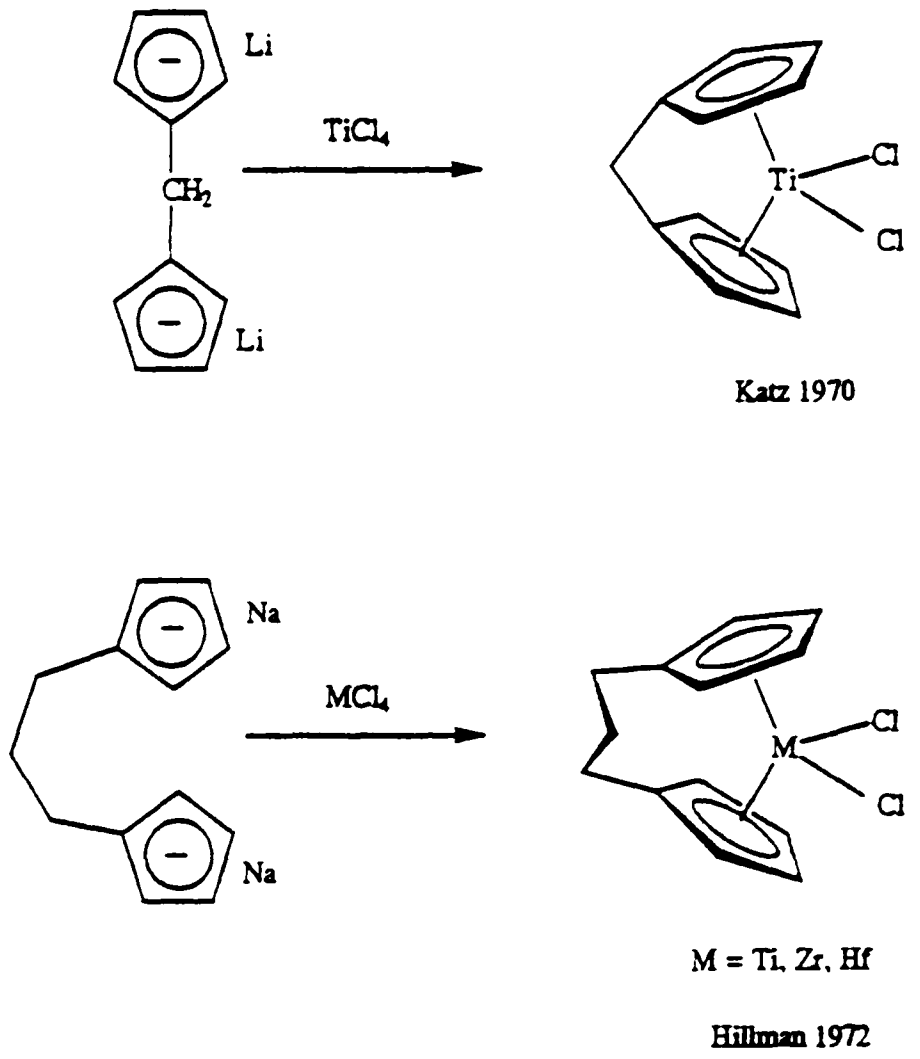

Figure 1.2.2. Synthesis of the first group 4 *ansa*-metallocenes.

1.2.2 Development of group 4 *ansa*-metallocene chemistry

After the initial reports by Katz and Hillman, group 4 ansa-metallocenes received little attention until the publication of a series of papers, from 1979 until the present day, by Brintzinger and co-workers.[53, 54] In the first of these they reported the synthesis of the ethylene-bridged titanocene $[\{(CH_2)_2(\eta^5\text{-}C_5H_4)_2\}TiCl_2]$, and compared the X-ray crystal structures of the series $[\{(CH_2)_n(\eta^5\text{-}C_5H_4)_2\}TiCl_2]$ (n = 1, 2, 3).[53] The molecular structures indicated a high degree of strain in the methylene-bridged derivative, whereas the ligand geometry of the ethylene-bridged complex did not deviate significantly from that of the unbridged Cp_2TiCl_2.

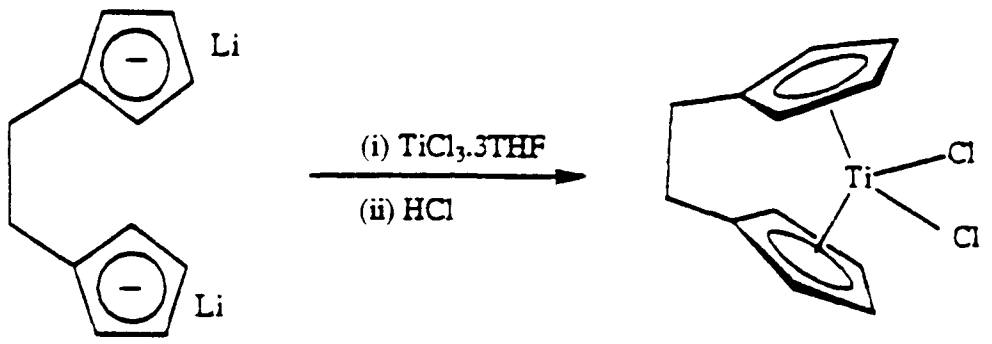

Figure 1.2.3. Synthesis of $[\{(CH_2)_2(\eta^5\text{-}C_5H_4)_2\}TiCl_2]$

1.2.3 Reactivity of *ansa*-metallocenes

Over the next few years, Brintzinger demonstrated two important aspects of *ansa*-metallocene chemistry. The first of these was the discovery that the joining of two rings of a group 4 metallocene with a suitable bridge can result in a more chemically inert metal/ring skeleton. This was seen as highly desirable as it would allow a more focussed study of the chemistry of the equatorial ligands, which might provide greater insight into several important reactions, including hydrogenation reactions and olefin polymerization. Brintzinger and co-workers showed that, in contrast to unbridged analogues, ethylene-bridged *ansa*-metallocenes did not undergo isotopic exchange at the cyclopentadienyl rings with D_2, and that the rate of hydrogenolytic alkane liberation from metallocene alkyl halide compounds was much reduced in *ansa*-derivatives. They proposed that the *ansa*-bridge prevents free ring rotation and thus blocks the ring-mediated hydrogen transfer reactions.[55, 56]

1.2.4 Chiral *ansa*-metallocenes

The second and most important aspect of group 4 *ansa*-metallocene chemistry is their high degree of stereorigidity, and, if the rings are suitably substituted, chirality. As illustrated in Figure 1.2.4, metallation of equivalently substituted bridged bis(cyclopentadienes) can produce *ansa*-metallocenes with either a C_2 symmetrical

relationship between the rings resulting in chiral (*rac*) metallocenes, or C_S symmetry which are achiral (*meso*) metallocenes.

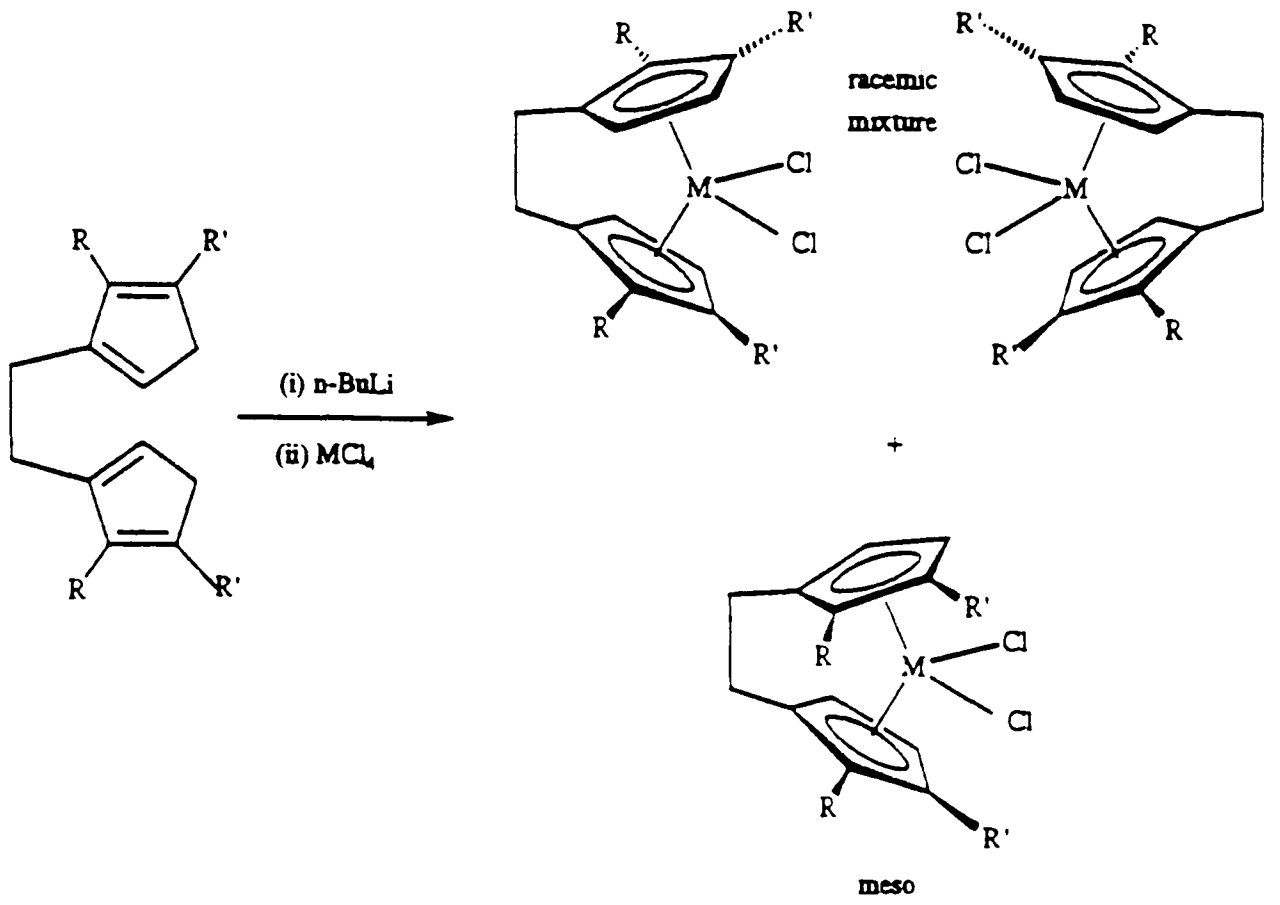

Figure 1.2.4. Chiral (*rac*) and achiral (*meso*) *ansa*-metallocenes

The first report of a chiral *ansa*-metallocene was Brintzinger's 1979 publication of $[\{(CH_2)_2(\eta^5\text{-}3\text{-}(t\text{-}Bu)C_5H_3)_2\}TiCl_2]$ as shown below (Figure 1.2.5).[57] Only the chiral titanocene dichloride diastereomer was isolated from the metallation reaction, presumably due to steric considerations preventing formation of the *meso* isomer. The racemic mixture was resolved into its enantiomers by addition of enantiomerically pure binapthol. Only one of the diastereomeric binaptholate derivatives was isolated, and treatment of this with HCl reformed the, now enantiomerically pure, *ansa*-titanocene dichloride.

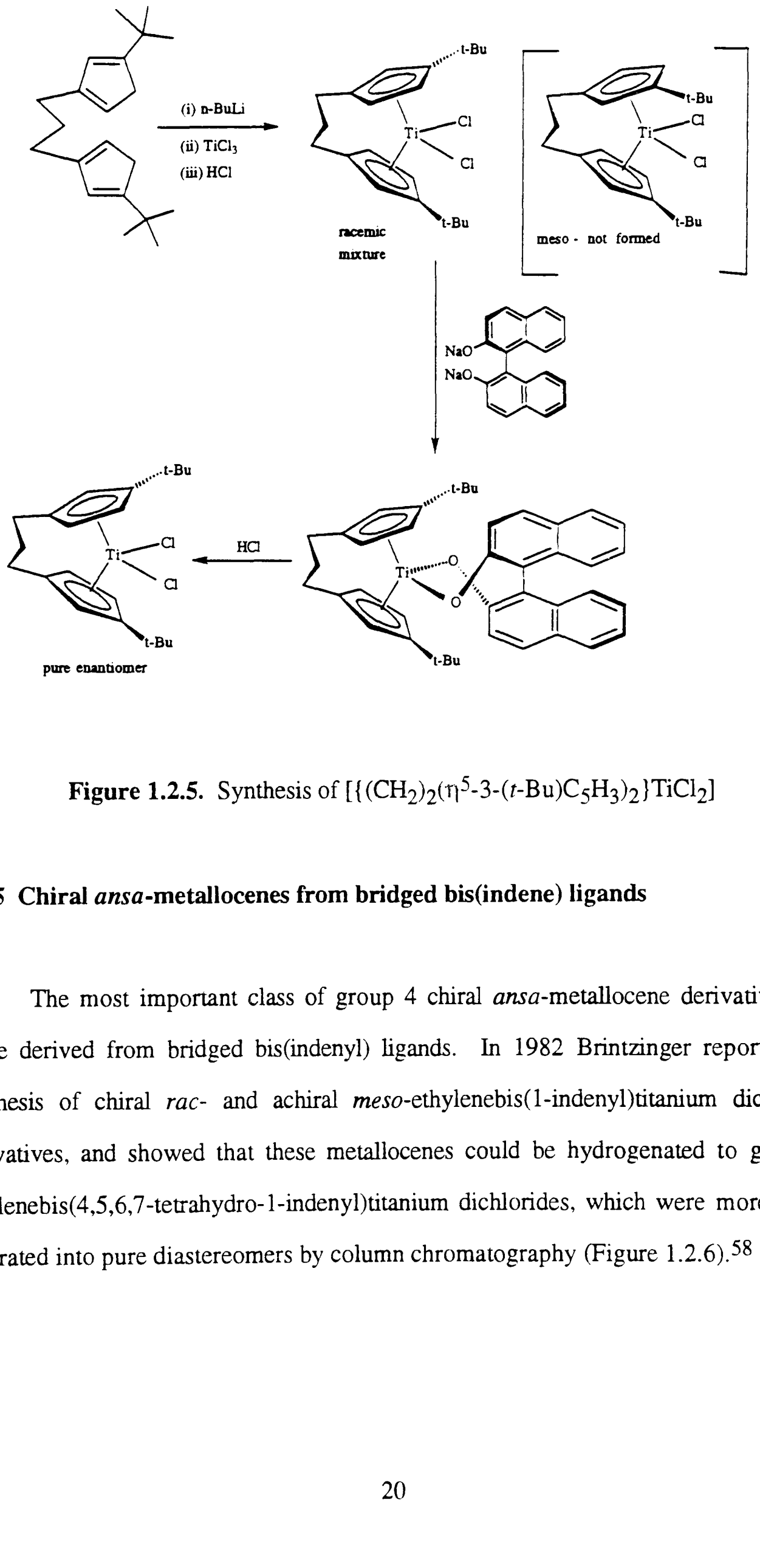

Figure 1.2.5. Synthesis of [{$(CH_2)_2(\eta^5$-3-(t-Bu)$C_5H_3)_2$}$TiCl_2$]

1.2.5 Chiral *ansa*-metallocenes from bridged bis(indene) ligands

The most important class of group 4 chiral *ansa*-metallocene derivatives are those derived from bridged bis(indenyl) ligands. In 1982 Brintzinger reported the synthesis of chiral *rac*- and achiral *meso*-ethylenebis(1-indenyl)titanium dichloride derivatives, and showed that these metallocenes could be hydrogenated to give the ethylenebis(4,5,6,7-tetrahydro-1-indenyl)titanium dichlorides, which were more easily separated into pure diastereomers by column chromatography (Figure 1.2.6).[58]

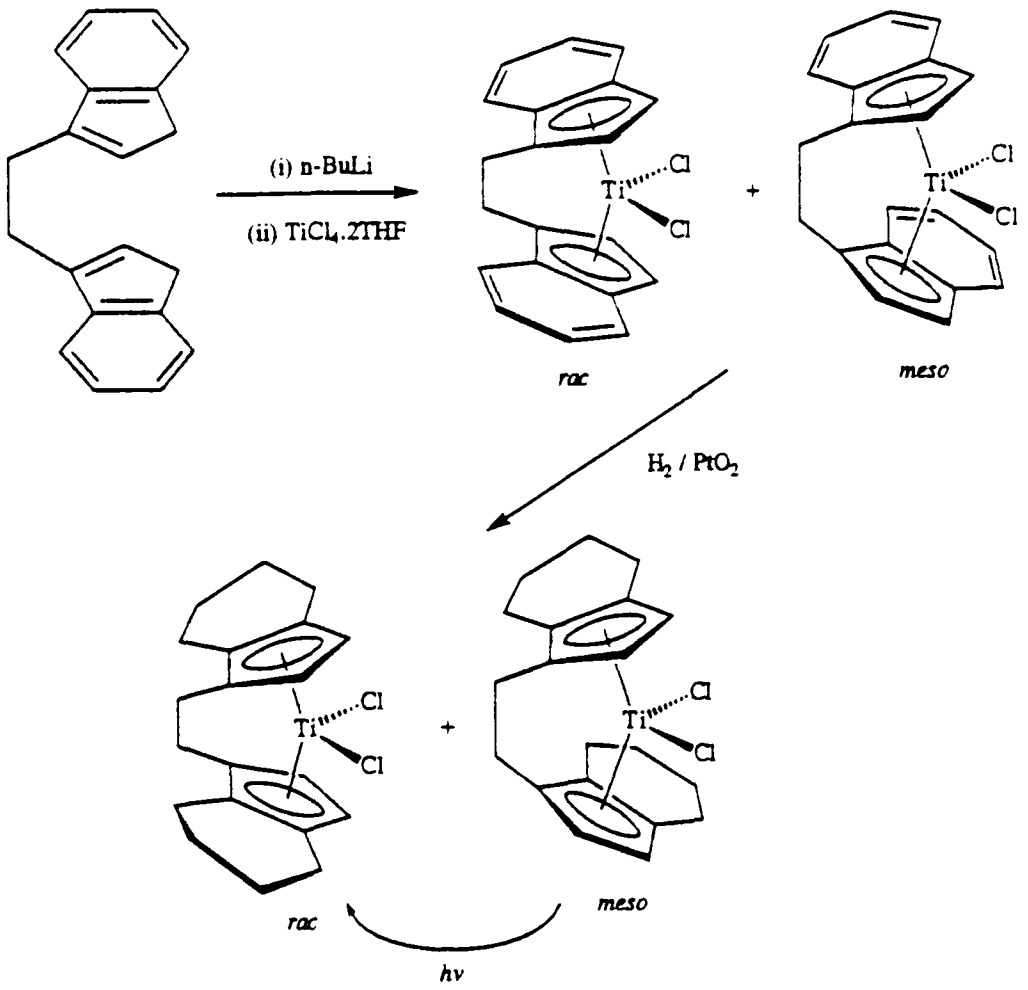

Figure 1.2.6. Synthesis of *rac*-and *meso*-[{$(CH_2)_2(\eta^5\text{-}C_9H_6)_2$}$TiCl_2$] and [{$(CH_2)_2(\eta^5\text{-}C_9H_{10})_2$}$TiCl_2$] [58, 61]

The *meso* diastereomer can be converted cleanly to the *rac* by photolysis, and solutions of the pure enantiomers (obtained using chiral binaptholate, as described above) must be shielded from light to prevent racemisation. These metallocenes, however, retain their chiral integrity during exchange of the equatorial ligands.

In the following years the syntheses and crystal structures of the analogous zirconium[59] and hafnium[60] ethylenebis(indenyl) and ethylenebis(tetrahydroindenyl) metallocene dichlorides were reported by Brintzinger and Ewen respectively (Figure 1.2.7). In both cases the chiral *rac*-ethylenebis(indenyl)metallocene dichlorides are isolated free of the *meso*-diastereomer, in contrast with titanium for which the *meso* was the major product. Brintzinger postulated that for the titanium derivatives the formation of the metal-ring linkage may be under kinetic control, whilst the larger size of the zirconium atom might allow thermodynamic control and formation of the more

stable *rac*-diastereomer. In 1988 Collins reported an improved synthesis and revised crystal structures for the titanium and zirconium ethylenebis(tetrahydroindenyl) metallocene dichlorides.[61]

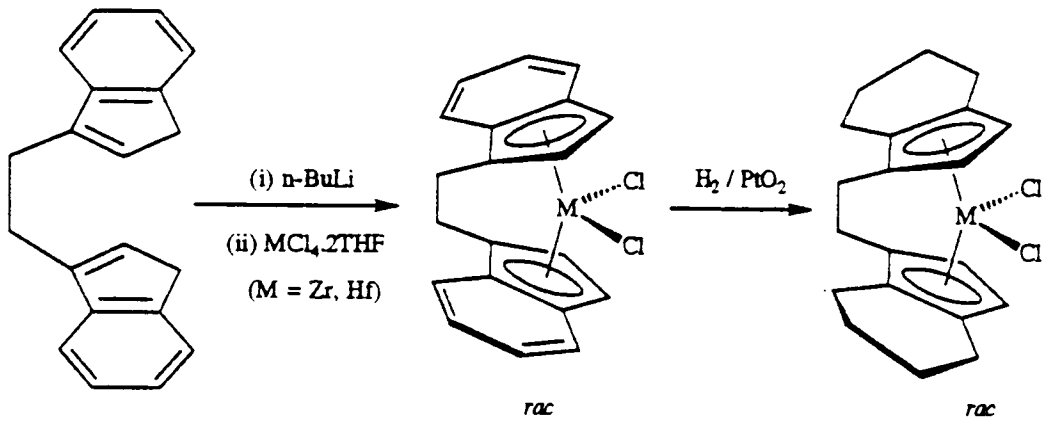

Figure 1.2.7. Synthesis of *rac*-[{$(CH_2)_2(\eta^5\text{-}C_9H_6)_2$}$MCl_2$] and [{$(CH_2)_2(\eta^5\text{-}C_9H_{10})_2$}$MCl_2$] (M = Zr, Hf)

1.2.6 Applications of group 4 *ansa*-metallocenes

Over the past few years a great variety of chiral group 4 *ansa*-metallocene derivatives have been synthesised, with a variety of bridging groups and substituted cyclopentadienyl and indenyl ligands. These have been well covered by a recent review,[62] so will not be discussed at length here. Instead, the application of group 4 *ansa*-metallocenes in stereospecific catalytic and stoichiometric reactions will be considered, with particular emphasis on the most important application as stereoselective olefin polymerziation catalysts.

1.2.7 Stereoselective olefin polymerization

In 1984 Ewen reported the first use of a chiral *ansa*-metallocene as a stereoselective catalyst for the polymerization of propene.[63] He showed that a mixture

of chiral *rac*- and achiral *meso*-ethylenebis(1-indenyl)titanium dichloride (Figure 1.2.6) together with methylaluminoxane co-catalyst produced a mixture of isotactic and atactic polypropylene. The isotactic polypropylene possessed a microstructure (determined by ^{13}C NMR) consistent with **enantiomorphic-site control**, in which the stereochemistry of olefin insertion is controlled by the chirality of the catalyst. This leads to a chain microstructure of type **I,** shown in figure 1.2.8, in which successive monomer units have the same relative configuration, with occasional placements of units with opposite handedness. In NMR notation this corresponds to ...mmmmmm**rr**mmmmmmmm**rr**mmmmmmm..., *i.e.,* stereosequences of isotactic meso (m) dyads connected by pairs of syndiotactic racemic (**r**) dyads.[63]

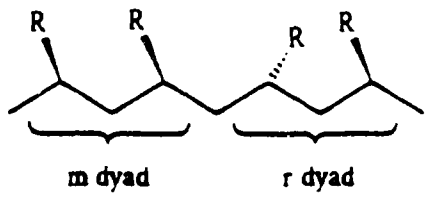

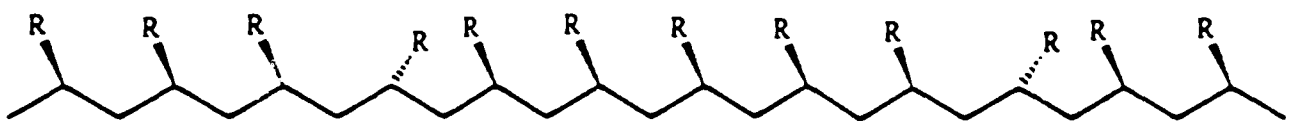

Type I enantiomorphic-site control

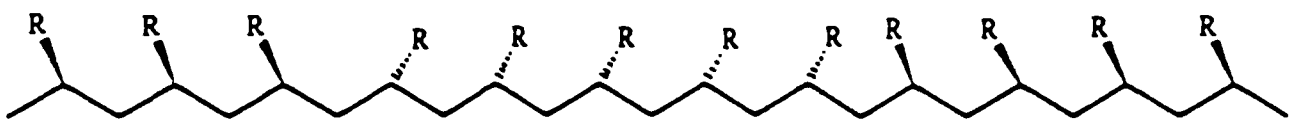

Type II chain-end control

Figure 1.2.8. Polypropylene chain microstructures consistent with enantiomorphic site control of stereoselectivity (type I) and chain end control (type II).

Ewen proposed that the isotactic polypropylene was produced by the chiral *rac*-ethylenebis(1-indenyl)titanium dichloride, whilst the atactic polypropylene was produced by the achiral *meso*-ethylenebis(1-indenyl)titanium dichloride. He also

reported that bis(cyclopentadienyl)bis(phenyl)titanium [Cp_2TiPh_2] with methylaluminoxane co-catalyst, is capable of producing polypropylene which, if the polymerization is performed at low temperature, is isotactic. However, the polymer microstructure was consistent with **chain-end control**, in which the configuration of the last inserted monomer unit determines the stereochemistry of monomer insertion.[64] This mechanism results in the propagation of the new chain-end configuration after a steric inversion defect, resulting is a stereoblock microstructure of the type ...mmmmmmrmmmmmmrmmmm...., type II in Figure 1.2.8.

In 1985 Kaminsky and Brintzinger reported that the pure *rac*-ethylenebis(4,5,6,7-tetrahydro-1-indenyl)zirconium dichloride (see Figure 1.2.7) with methylaluminoxane was a highly active catalyst for the polymerization of propylene, producing highly isotactic, high molecular weight polypropylene with a narrow molecular weight distribution.[65] Two years later Ewen showed that the *rac*-ethylenebis(indenyl) and *rac*-ethylenebis(tetrahydro-indenyl)hafnium dichlorides (with MAO) were also highly isospecific polymerization catalysts for propene.[60] The hafnium *ansa*-metallocenes, however, produced highly isotactic, high molecular weight polypropylene at conventional industrial polymerization temperatures (50-80 °C), in contrast to the titanium analogues which decomposed at these temperatures, and the zirconium analogues which produced only low molecular weight waxes. Ewen also reported that, for hafnium, the indenyl derivatives had higher activities, produced higher molecular weight polymers and were less stereospecific than the tetrahydroindenyl derivatives under equivalent polymerization conditions, and that the hafnium derivatives produced slightly more stereoregular polymers than those obtained with zirconium analogues.[60] The isotactic polymer microstructures were consistent with **enantiomorphic site control**.

In 1988 Ewen reported the **syndiospecific** polymerization of propene using zirconium and hafnium *ansa*-metallocene derivatives of the type [{$(CH_3)_2C(\eta^5\text{-}C_5H_4)(\eta^5\text{-}C_{13}H_8)$}$MCl_2$] (M = Zr or Hf, Figure 1.2.9) with MAO co-catalyst.[66] The polymer configurational microstructure was of the type

...rrrrrrrr**mm**rrrrrrrrrrrr**mm**rrrrrrr....., consistent with enantiomorphic-site control with chain migratory insertions resulting in site isomerizations, and occasional reversals in diastereoface selecivity resulting in mm triads.

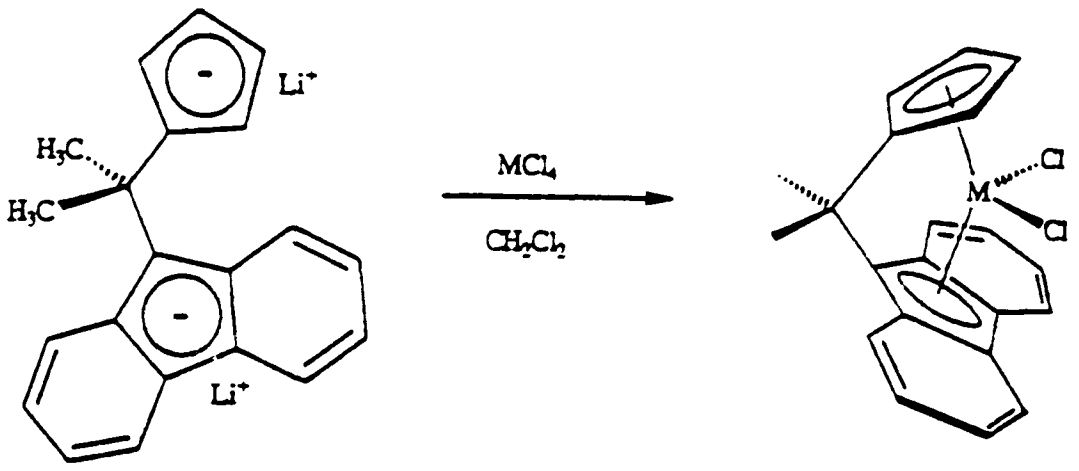

Figure 1.2.9. Syndiospecific *ansa*-metallocenes for propylene polymerization (M = Zr, Hf)

1.2.8 The effects of *ansa*-metallocene molecular structure upon reactivity

After the initial reports of isospecific and syndiospecific polymerization catalysed by *ansa*-metallocenes, attention turned to the possibility of fine-tuning the molecular structure of the catalyst precursors to produce polymers with different molecular and bulk properties. In order to achieve this goal, many researchers set out to discover structure/reactivity relationships, such as the effects of varying the metal, the *ansa*-bridge and substituents on cyclopentadienyl, indenyl and fluorenyl ligands, on activity, stereospecificity and polymer molecular weight.[67-76]

Brintzinger studied the effects on MAO co-catalysed propylene polymerization of substitution at the α (2 or 5) position and β (3 or 4) position of *ansa*-bis(cyclopentadienyl) zirconium dichloride derivatives (Figure 1.2.10).[68] He showed that increased **steric bulk at the β position** of these C_2-symmetric molecules increased the isospecificity and reduced the activity of polymerization. Collins showed that for *rac*-[{$(CH_2)_2(\eta^5$-3-(*R*)-$C_5H_3)_2$}$ZrCl_2$] where R = Me, *i*-Pr, *t*-Bu, the same

trends are observed.[71] Brintzinger also showed that α-methyl substituents suppressed regioirregular (2-1) insertion and dramatically increased the polymer molecular weight.[68] A dependence on the nature of the *ansa* bridge was demonstrated by Brintzinger; the Me_2Si bridged derivative was more isospecific and more active than the $(Me_2C)_2$ bridged analogue.[68]

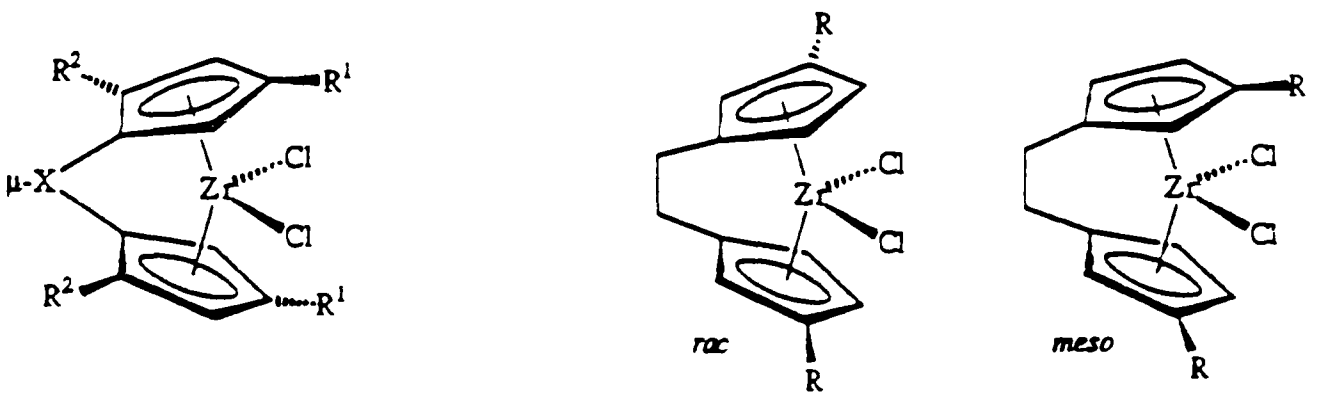

Brintzinger: μ-X = $(CMe_2)_2$, Me_2Si

R^1 = t-Bu, i-Pr R^2 =H, Me

Collins: R = Me, i-Pr, t-Bu

Figure 1.2.10. Substituted *ansa*-bis(cyclopentadienyl)zirconium dichloride catalyst precursors prepared by Brintzinger[68] and Collins.[71]

Spalek[69] and Herrmann[72] investigated the substitution of *ansa*-bis(indenyl) derivatives at the 2, 3 and 4 positions (Figures 1.2.11). Spalek showed that steric bulk at the β-position strongly influenced stereospecificity and activity. For the complexes $[\{(Me_2Si)(\eta^5\text{-}3\text{-}(R)\text{-}C_9H_5)_2\}ZrCl_2]$, when R = H the zirconocene/MAO catalyst is highly active and highly isospecific, whilst when R = CH_3 the activity is much lower and atactic polypropylene is produced. Non-C_2 symmetric chiral *ansa*-metallocenes such as $[\{(\mu\text{-}X)(\eta^5\text{-}C_5H_4)(\eta^5\text{-}C_9H_6)\}ZrCl_2]$, μ-X = Me_2Si, Me_2C, were much less isospecific than their bis(indenyl) analogues.[69, 73]

In general, highly isospecific polymerization of propene requires two, diagonally opposite, quadrants of the molecular framework (when viewed from the "open" face of the *ansa*-metallocene) to be sterically bulky, whilst the other two quadrants should be sterically uncrowded.

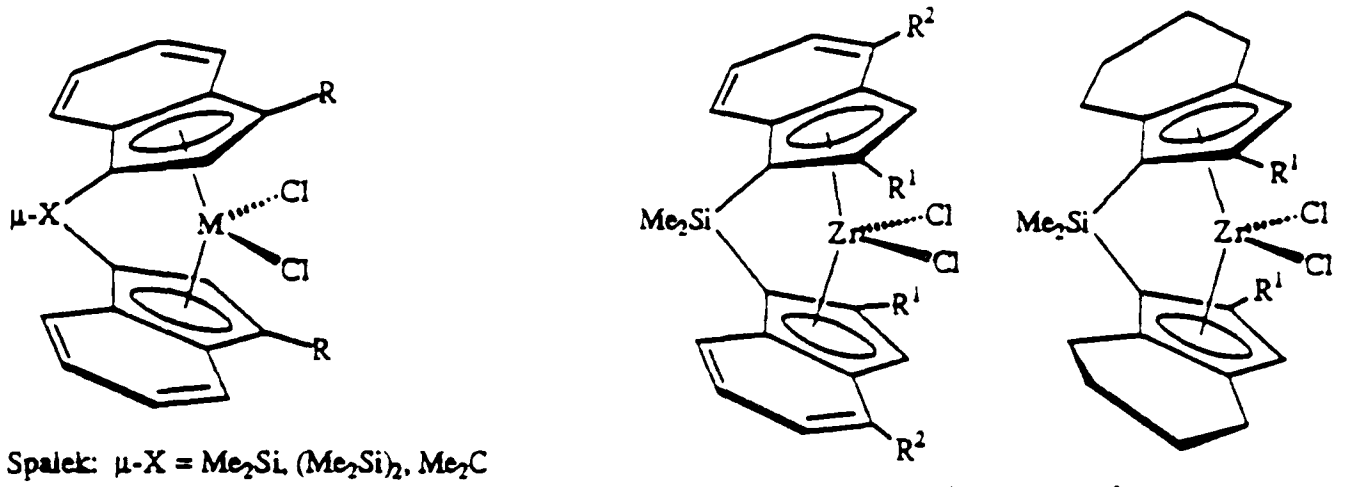

Spalek: μ-X = Me_2Si, $(Me_2Si)_2$, Me_2C

R = H, CH_3

Herrmann: R^1 = H, Me; R^2 = H, i-Pr

R = H, Me, OMe

Collins

R = H, Me

Figure 1.2.11. Substituted *ansa*-bis(indenyl) derivatives prepared by Spalek[69] Herrmann[72] and Collins[74]

A dependence of isospecificity and activity on the nature of the *ansa* bridge was demonstrated by Spalek[69] and Ewen.[70] The Me_2C bridged bis(indenyl)zirconium dichloride derivative was less isospecific and less active than the Me_2Si bridged analogue.[69] Ewen suggested that the number and size of atoms in the bridge determined the proximity of the β-substituents to the olefin coordination site and alkyl chain-end, thus contributing to the steric effects of the β-substituents on activity and stereoregularity.

Hermann showed that for the *ansa*-bis(indenyl)zirconium dichloride derivatives, replacing the α-H (at the 2-position) of both indenyl rings with a methyl or ethyl group lead to a 500 % increase in polypropylene molecular weight.[72] If an alkyl group at the 4-position of each indenyl is also included, the activity of the catalysts is

more than doubled and the polymer molecular weight is increased by a further 40 % to almost 5 x 10^6 $gmol^{-1}$. Herrmann proposed that for substituents at the 2- and 4-positions the **electronic effect** is dominant, rather than the steric effect. He proposed that electron-donating alkyl groups decreased the lewis acidity of the (cationic) zirconium atom of the active species and thus lowered its tendency to abstract a β-H atom. Thus the number of chain terminations, for which β-H elimination is the major process, is decreased and the average polymer molecular weight is increased.

The 2-Me, 4-*i*-Pr substituted *ansa*-bis(indenyl)zirconium dichloride derivative was the first *ansa*-metallocene catalyst to produce high molecular weight, highly isotactic polypropylene with high activity at conventional industrial polymerization temperatures (50 °C or higher), demonstrating the usefulness of studying structure/reactivity relationships for rational catalyst design.

The effects of molecular structural changes on the **syndiospecific** polymerization of propylene by *ansa*-metallocene/MAO catalysts was investigated by Ewen.[70] The most dramatic effect was obtained by replacing a H atom at a β-position of the C_5H_4 ring with a CH_3 group (Figure 1.2.12).

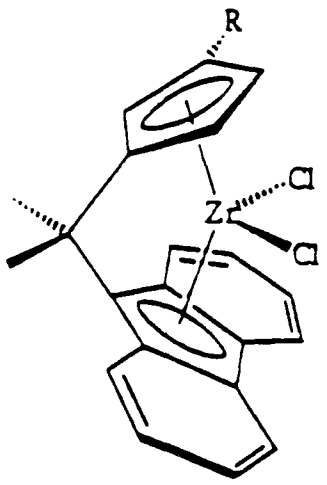

Ewen: R = H, Me

Figure 1.2.12. [{$(Me_2C)(\eta^5\text{-}3\text{-}(R)\text{-}C_5H_3)(\eta^5\text{-}C_{13}H_8)$}$ZrCl_2$], R = H, Me

Whilst [{$(Me_2C)(\eta^5\text{-}C_5H_4)(\eta^5\text{-}C_{13}H_8)$}$ZrCl_2$] produced highly syndiotactic polypropylene, [{$(Me_2C)(\eta^5\text{-}3\text{-}(CH_3)\text{-}C_5H_3)(\eta^5\text{-}C_{13}H_8)$}$ZrCl_2$] produced "hemi-isotactic" polypropylene in which every second monomer unit tends to be isotactic

whilst the others are in a random atactic arrangement. This demonstrated that steric bulk at the β-position strongly influences stereospecificity in syndioselective as well as isoselective *ansa*-metallocenes. The syndiospecific polymerization behaviour of $[\{(Me_2C)(\eta^5\text{-}C_5H_4)(\eta^5\text{-}C_{13}H_8)\}ZrCl_2]$ is strong evidence for chain migration with every insertion step, because without chain migration isospecific behaviour would be expected. The "hemi-isotactic" polymer produced by the β-methyl substituted analogue is also indicative of a chain migratory insertion mechanism.[70]

1.2.9 The mechanism of stereoselectivity

The following discussion combines ideas and evidence from many sources in the literature,[63-83] and presents the most widely accepted proposals for the mechanism of stereoselective propylene polymerization by *ansa*-metallocenes:

(i) Cationic metallocene monoalkyl active sites catalyse chain growth by a **chain migratory insertion** mechanism.

(ii) Polymerization takes place by a **regioselective [1-2] insertion** of propylene monomer into a metal-carbon bond, between the central metal atom and the first carbon atom of the polymer chain, *via* a *cis*-opening.

(iii) Before insertion, the propylene is coordinated through the **π-electrons** of its double bond at a coordination-deficient site of the metal atom. The propylene can bind to the metal via one of its two **prochiral faces**. If one of these orientations is energetically favoured, polymerization will be stereoselective.

(iv) The π-facial selectivities are governed by the chain-end orientations, the chain end orientations in turn being enforced by β-CpR substituents. This is **indirect steric control** by the enantiomorphic site. Direct contacts between the β-CpR substituents and the monomer methyl group then additionally reinforce (isotactic) or diminish (syndiotactic) stereoregulation.

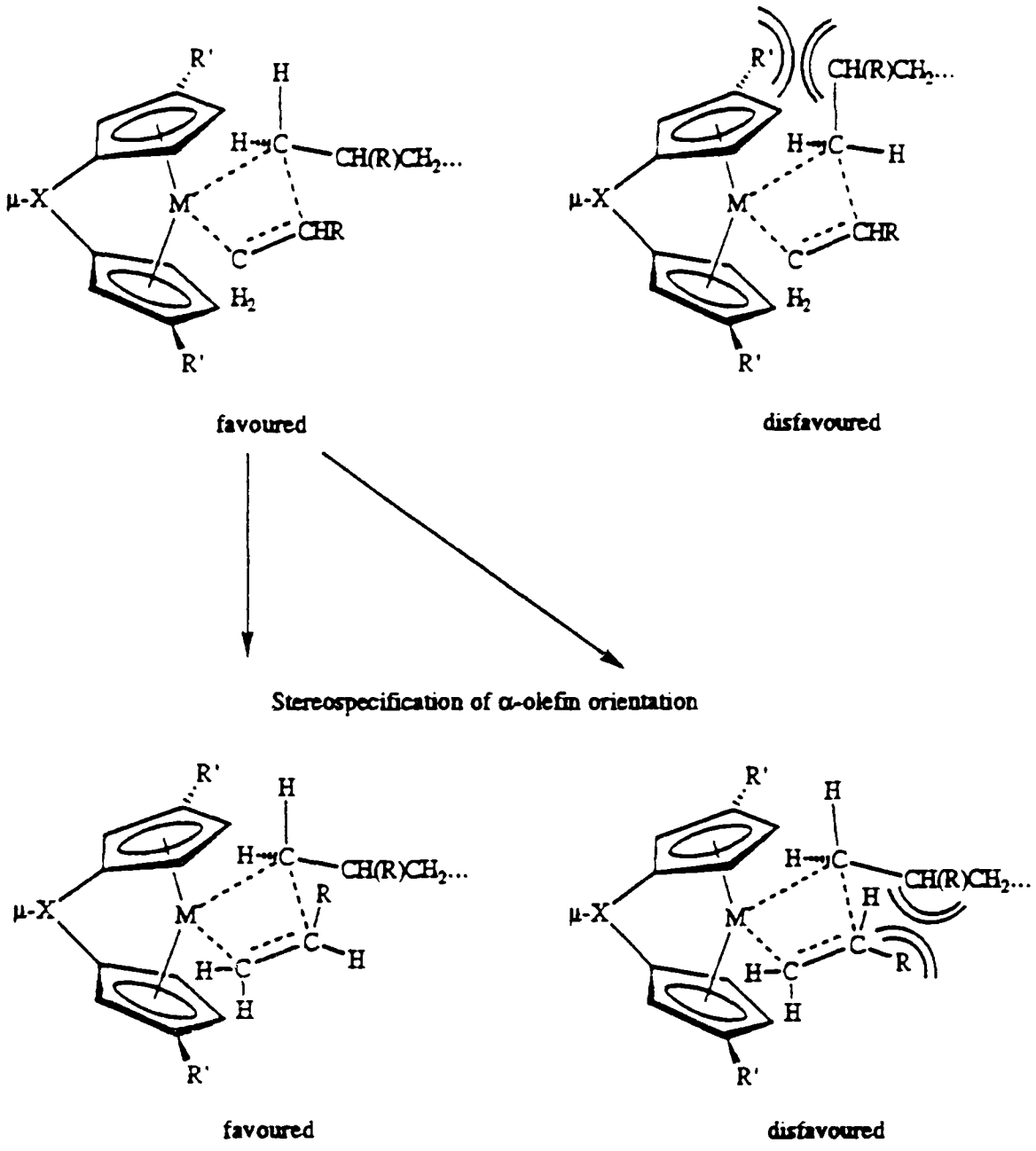

Figure 1.2.13. Proposed mechanism for isospecific polymerization[70, 77]

(v) Insertion takes place by **migration of the chain end** to the co-ordinated monomer, *i.e.* the next insertion step starts with the chain and monomer having exchanged positions with each other compared to the previous step.

The syndiospecific polymerization behaviour of [{$(Me_2C)(\eta^5\text{-}C_5H_4)(\eta^5\text{-}C_{13}H_8)$}$ZrCl_2$] is strong evidence for chain migration with every insertion step, without chain migration isospecific behaviour would be expected. The "hemi-isotactic" polymer produced by the β-methyl substituted analogue is also indicative of a chain migratory insertion mechanism.[70]

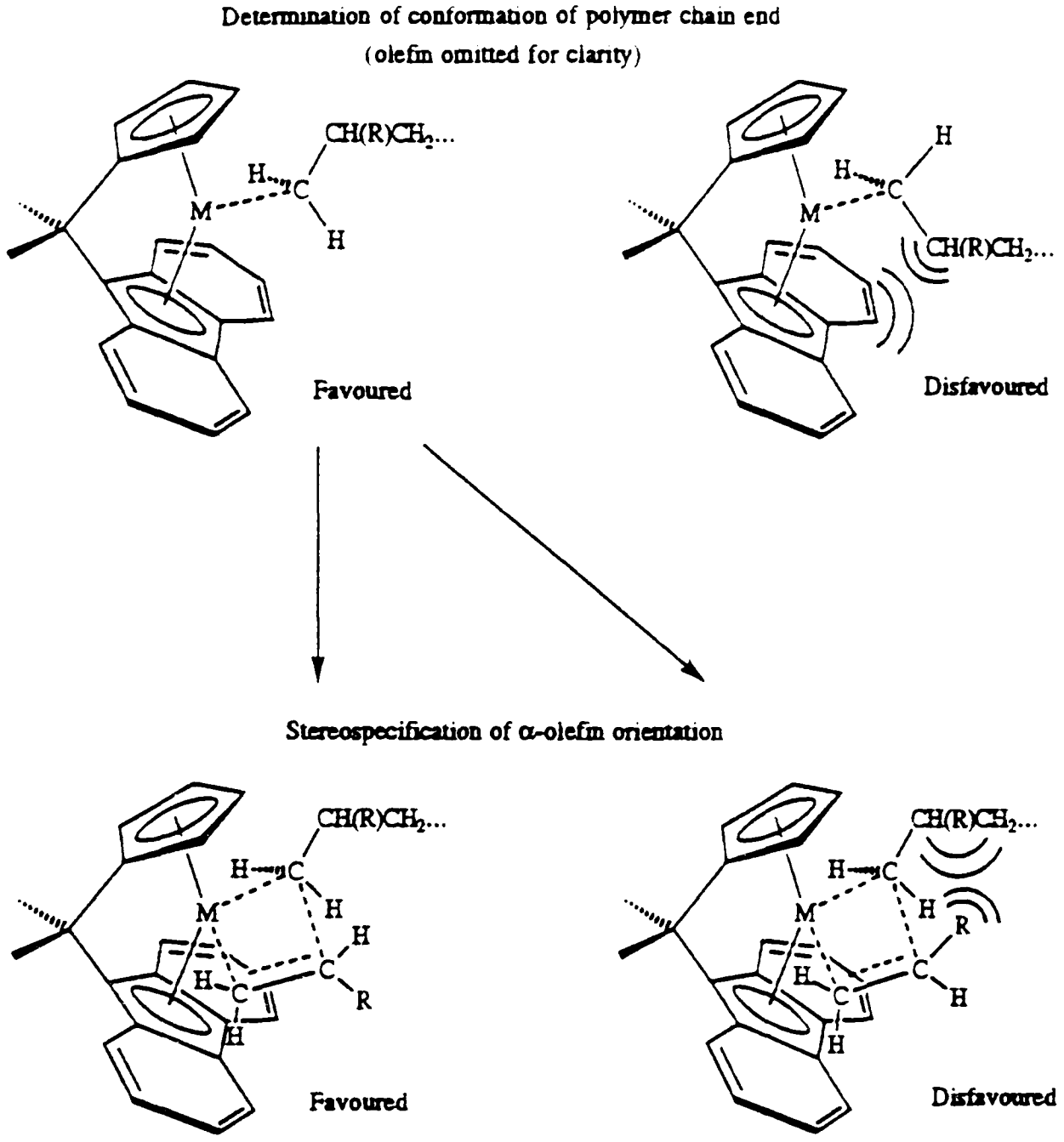

Figure 1.2.14. Proposed mechanism for syndiospecific polymerization[70, 77]

(vi) It has been proposed that an **agostic interaction**, between one of the α-H atoms of the migrating alkyl chain and the metal centre, stabilizes the the transition state of the migratory insertion step.[78-83] It has also been proposed that the α-agostic M←H-C interaction confers increased rigidity on the transition state, reinforcing the sterically preferred chain-end configuration, and thus **reinforcing the stereoselectivity** of monomer insertion.[78, 79]

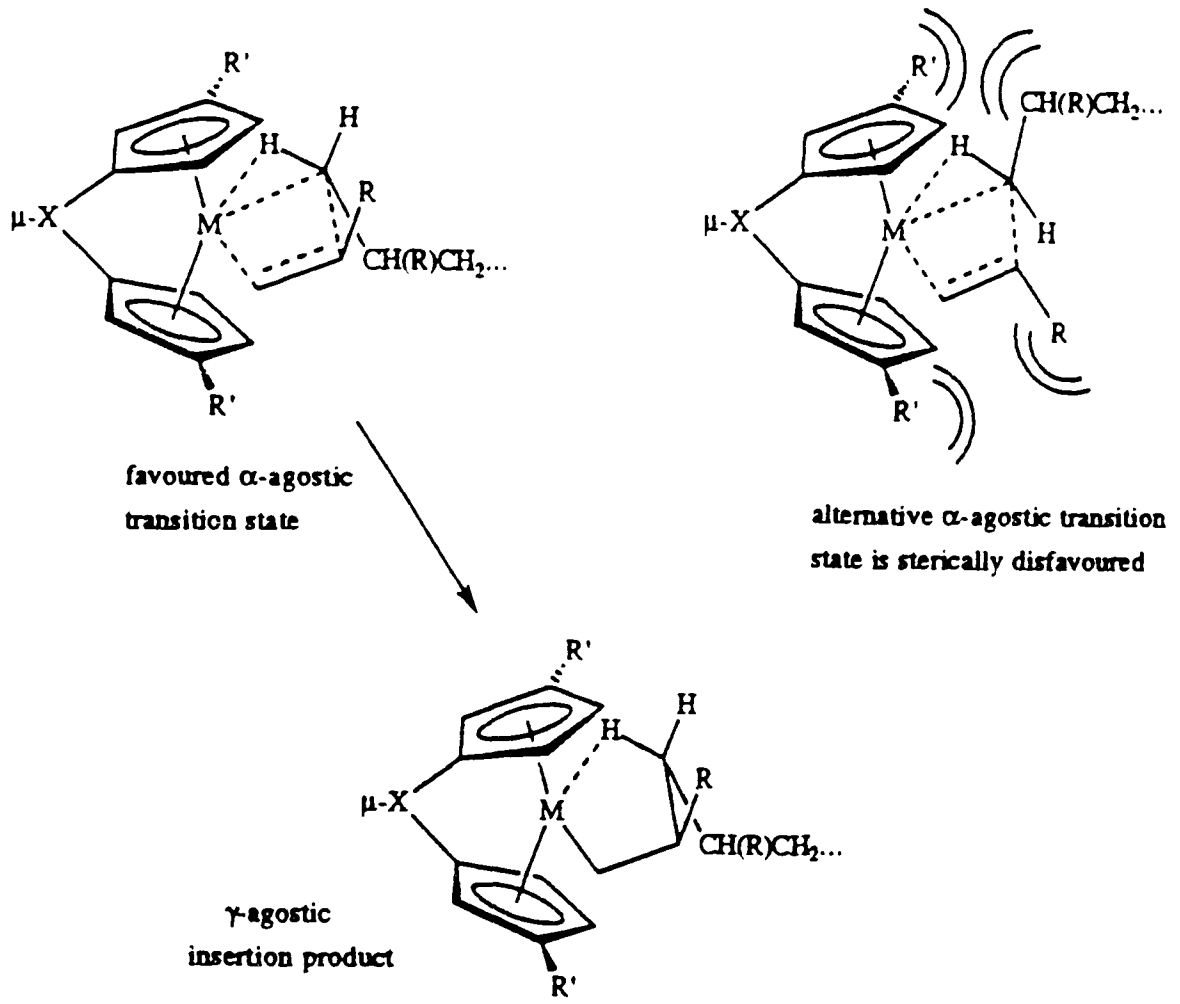

Figure 1.2.15. Proposed α-agostic assistance in stereoselectivity

Evidence for such **α-agostic assistance** was provided in 1990 by Brintzinger who showed that olefin insertion into α-deuterated alkyl derivatives of a zirconocene-based polymerization catalyst is influenced in its stereochemistry by kinetic isotope effects.[80] Bercaw observed similar isotope effects with scandocene-based catalysts.[81] These observations imply that these olefin insertions are assisted by an agostic interaction of one of the α-H atoms of the migrating alkyl chain with the metal centre, as proposed by Green and Brookhart.[82, 83] Molecular orbital calculations by Janiak support these proposals.[78, 79]

Collins has shown that the stereoselectivity of a series of substituted *ansa*-bis(indenyl)zirconium dichloride derivatives (Figure 1.2.11) is highly sensitive to the electronic effects of the substituents, an increase in electron density at the metal centre resulted in a decrease in the stereoselectivity of propylene insertion.[74] Collins proposed that increased electron density at the metal centre should render α-agostic stabilization of the transition state less important and thus decrease the stereoselectivity of insertion.

1.2.10 Optically active macromolecules using *ansa*-metallocene catalysts

In 1987 Pino demonstrated that a resolved, chiral *ansa*-metallocene derivative, (-)-(*R*)-ethylenebis(tetrahydroindenyl)dimethylzirconium with MAO, could produce optically active isotactic oligomers of propylene (in the presence of H_2) with detectable optical rotation.[84] However the symmetry of high molecular weight isotactic and syndiotactic polypropylenes is such that they usually contain mirror planes and are thus achiral.

Waymouth has recently demonstrated that the cyclopolymerization of 1,5-hexadiene can give four different stereoregular polymers, one of which, the racemo-diisotactic polymer, contains no mirror planes of symmetry and is thus chiral. When 1,5-hexadiene is polymerized using enantiomerically pure ethylenebis(tetrahydroindenyl)zirconium binaphtholate and MAO, optically active polymer is produced. The (-)-(*R,R*) enantiomer of the catalyst produces poly(methyl-1,3-cyclopentane) with a molar optical rotation of +50.1°, whilst the polymer prepared with the (+)-(*S,S*) enantiomer showed a value of -49.1°. These findings are consistent with the formation of polymers with main chain chirality. [85, 86]

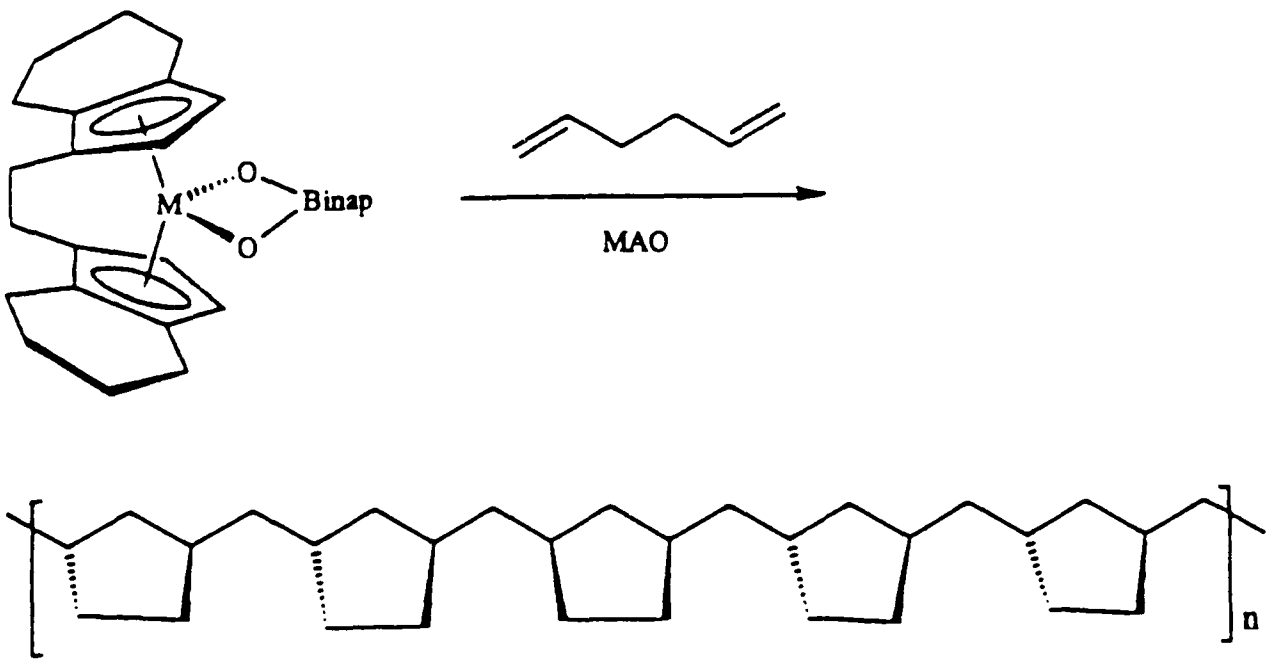

Figure 1.2.16. Synthesis of optically active polymer using chiral catalyst.

1.2.11 Other stereoselective reactions of *ansa*-metallocenes

The successful application of *ansa*-metallocene derivatives as stereoselective olefin polymerization catalysts has encouraged many researchers to investgate other catalytic stereoselective applications.[62] During the last three years, chiral group 4 ansa-metallocenes have been employed as catalysts in the following asymmetric reactions: epoxidation of alkenes,[87] hydrogenation of alkenes,[88] Diels-Alder reactions[89, 90] hydrogenation of imines,[91] carbomagnesation,[92] the oligomerization of phenylsilane,[93] and alkene isomerization.[94]

1.3 Binuclear group 4 metallocene compounds

1.3.1 Introduction

Binuclear transition metal complexes in which two reactive metal centres are held in close proximity offer the opportunity for observing cooperative chemical behaviour and may exhibit new types of reactivity not shown by otherwise analogous mononuclear species.

Much of the interest in binuclear transition metal compounds has centred on the preparation of model complexes for species thought to be present in many important heterogeneous catalytic processes. For example, Grubbs has prepared many binuclear μ-methylene species with a CH_2 bridge between titanium and a late transition metal such as rhodium or palladium, as models for proposed intermediates in Fischer-Tropsch catalysis (the conversion of CO and H_2 to hydrocarbons and oxygenates) and as models for "strong metal-support interactions", a dominant theme in heterogeneous catalysis.[95] Grubbs also prepared μ-phenyl titanium-rhodium heterobimetallic complexes (Figure 1.3.1) as models for the interaction of arene groups with heterogeneous catalysts such as Rh/TiO_2.[96]

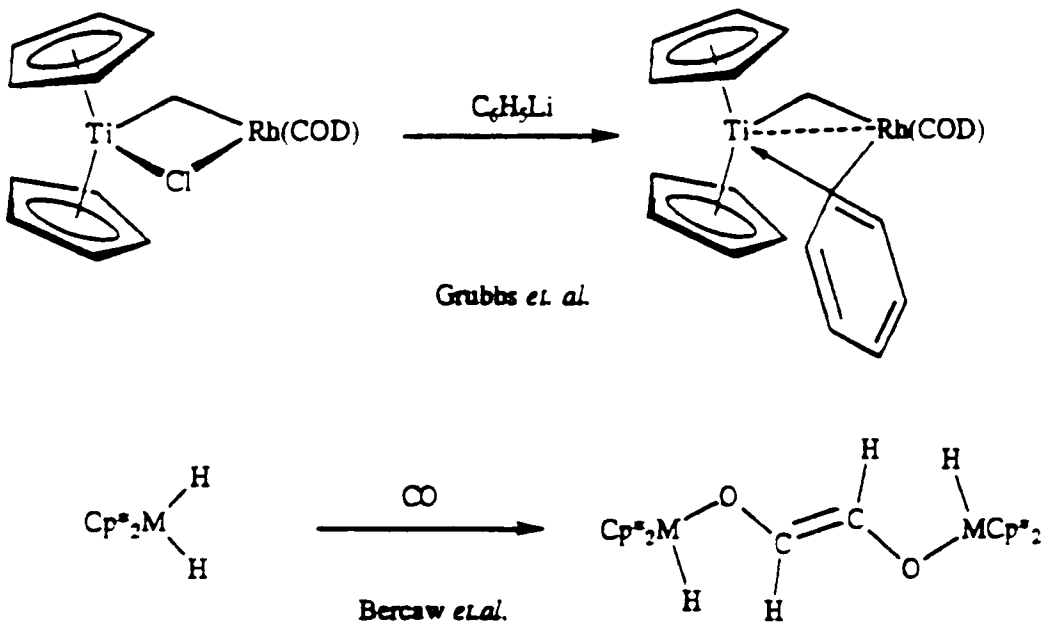

Figure 1.3.1. Bimetallic models of proposed important species in heterogeneous catalysis.[95-97]

Bercaw reported the formation of bimetallic enediolates (Figure 1.3.1) *via* the carbonylation of $Cp^*_2MH_2$ (M = Zr, Hf),[97] and several other researchers have demonstrated C-C bond forming processes *via* the reaction of metal hydride complexes with CO, as models for the Fischer-Tropsch reaction.[98]

Another area of interest has been the binuclear coordination and activation of small molecules such as N_2. Well known examples are the binuclear group 4 metallocene complexes $[\{Cp^*_2Ti\}_2(\mu\text{-}N_2)]$ and $[\{Cp^*_2M(N_2)\}_2(\mu\text{-}N_2)]$ (M = Ti, Zr, Hf) described by Bercaw.[99] An interesting recent example was provided by Fryzuk, who reported the synthesis and crystal structures of two related binuclear zirconium complexes containing Zr-N_2-Zr bridging moieties, one with unusual "side-on" coordination of N_2 to the metals, the other with an "end-on" coordination (Figure 1.3.2). Upon acidification, both of these complexes generate one equivalent of hydrazine.[100]

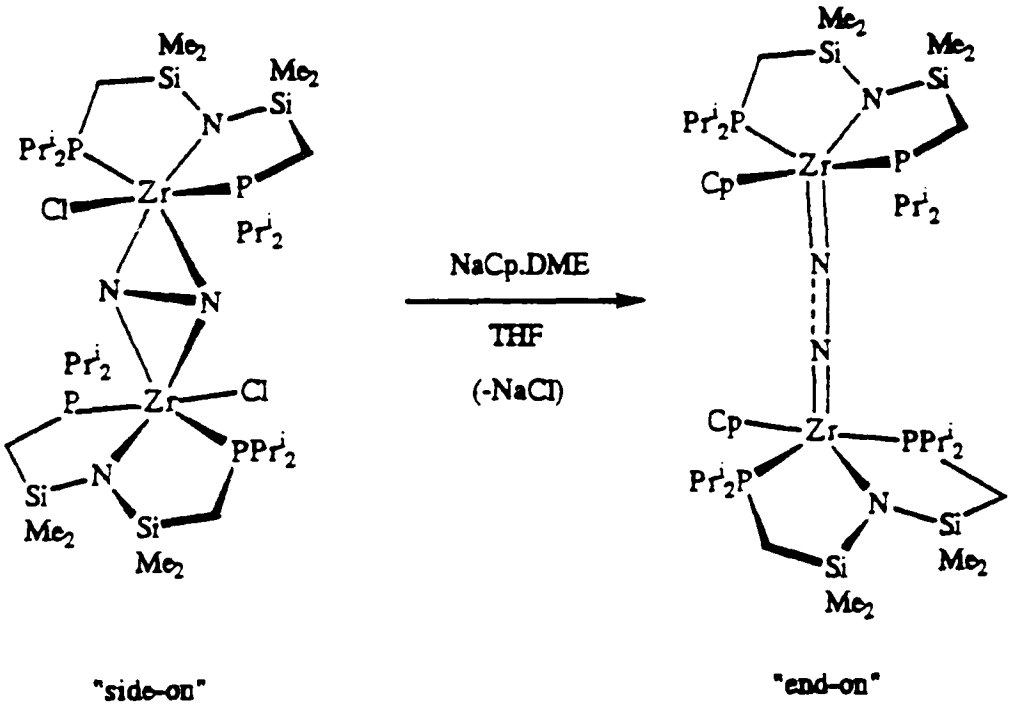

Figure 1.3.2. Bimetallic dinitrogen complexes with "side-on" and "end-on" coordination of N_2 between two metal centres

Bimetallic complexes have also been shown to exhibit new and unusual structural and bonding features. For example, Grubbs has reported a dizirconium complex with a trigonal-bipyramidal methyl bridge between the two zirconium centres

(Figure 1.3.3).[101] Erker has recently reported zirconium-aluminium and zirconium-gallium bimetallic complexes with bridging ligands containing planar tetracoordinate carbon centres.[102-104] Erker has also recently published the molecular structure of a zirconium-aluminium bimetallic complex with a highly unusual μ-(1,2-η^2-Zr):(4-η^1-Al) bridging butadiene ligand, showing η^2-σ,π coordination to the zirconium centre (Figure 1.3.3).[105]

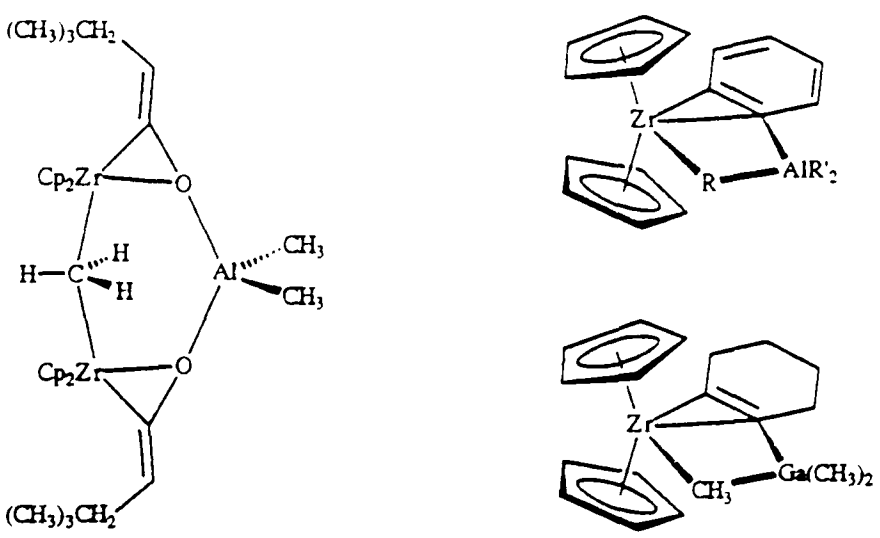

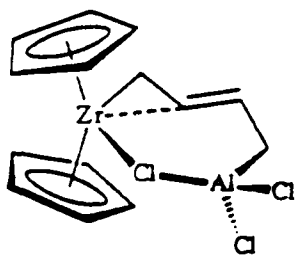

η^2-σ,π-coordination of butadiene to Zr (Erker)

Figure 1.3.3. Bimetallic complexes containing bridging moieties with new and unusual structural features.

Many multi-metallic complexes have shown reactivity enhancements when compared to the reactivity of their individual components, these enhancement effects are known collectively as synergism and may have a variety of mechanistic origins.[106] Bimetallic catalytic pathways involving the concerted action of two metals have been proposed for many processes; for example, olefin hydroformylation catalysed by

binuclear ruthenium[107] and rhodium[108] complexes, and the hydration of acrylonitrile to acrylamide catalysed by binuclear palladium complexes.[109] An interesting example involving a binuclear group 4 metallocene complex is the chemoselective hydrogenation of 1,3-cyclooctadiene to cyclooctene catalysed by an alkenyl-bridged bis(zirconocene) derivative (Figure 1.3.4).[110]

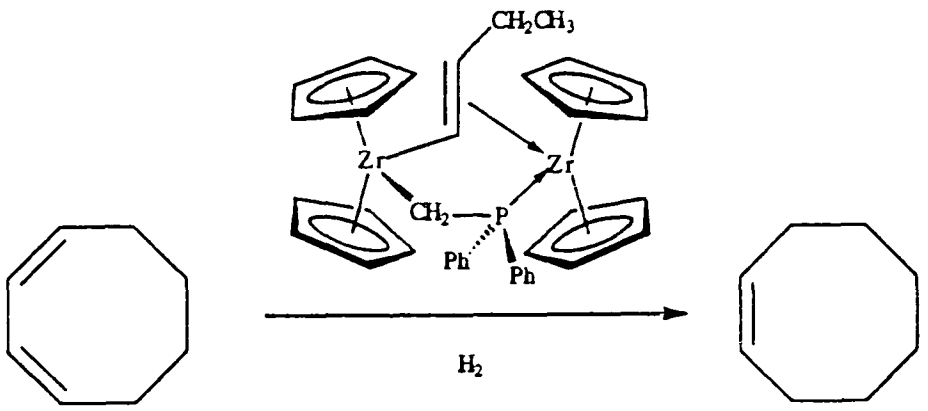

Figure 1.3.4. Hydrogenation of 1,3-cyclooctadiene to cyclooctene catalysed by a dizirconium complex

Proposed bimetallic catalytic pathways have been postulated on the basis of two ideas; (i) the flexibility of the M-L-M' bridge permits the transfer of an atom or ligand from one metal centre to the other, (ii) an electronic cooperative effect can take place between metallic centres *via* orbital interactions with the bridging ligands. Only in a few cases has there been clear evidence that bimetallic catalysts retain their integrity during the reaction.[111] For example, Bergman has reported that $[Cp_2Ta(\mu\text{-}CH_2)_2Ir(CO)_2]$ catalytically hydrogenates, isomerizes and hydrosilates olefins under mild conditions, and has obtained direct NMR evidence that the bimetallic complex remains intact during the catalysis.[112] In contrast, Maitlis has found kinetic evidence in favour of the total **cleavage** of the bridges between the metal atoms of the compounds $[Cp^*MCl_2]_2$ (M = Rh, Ir) and $[Cp^*IrClH]_2$ which catalyze the hydrogenation of olefins.[113] Similarly, Sanchez-Delgado and co-workers have

proposed on the basis of kinetic data that, for reactions catalysed by simple metal carbonyl clusters, the **fragmentation** of the clusters is a general phenomenon.[114]

One possible strategy for overcoming the problem of bridge cleavage in binuclear catalysts would be to join the mononuclear fragments with an **inter-annular bridge** between cyclopentadienyl-type ligands. Recent years have seen a growing interest in bimetallic complexes containing bridging bis(cyclopentadienyl)-type ligands.[115-121] Compared with, for example, halide or carbonyl ligands bridging the metal atoms directly, an inter-annular bridge would be expected to be considerably more resistant to cleavage during reactions at the metal centres. Since mononuclear group 4 metallocene derivatives are an important class of homogeneous catalysts, such a strategy would be especially interesting for group 4 binuclear metallocene complexes.

1.3.2. Inter-annular bridged binuclear group 4 metallocenes

Binuclear group 4 complexes in which the metals are bridged by a ligand containing two cyclopentadienyl-type rings fall into two major catagories; (i) those containing **fulvalene**-type bridging ligands, in which the two cyclopentadienyl rings are directly bonded to each other, and (ii) those containing ***ansa***-type ligands, in which the rings are bridged by a chain (X) at least one atom in length. These are illustrated below (Figure 1.3.5).

I II

Figure 1.3.5. Binuclear complexes with fulvalene (I) and *ansa* (II) bridging ligands

1.3.3 Fulvalene-bridged titanocene derivatives

One of the best known fulvalene titanium derivatives is "green titanocene", prepared by the reaction of $Cp_2Ti(CH_3)_2$ with H_2 in hexane[122] or by the reduction of Cp_2TiCl_2 with sodium naphthalide[123] or sodium sand.[124] The green, diamagnetic product of these reactions, $[(C_{10}H_{10})Ti]$, was originally thought of as a dimer of titanocene, $[(\eta^5\text{-}C_5H_5)_2Ti]_2$. In 1970 Brintzinger and Bercaw proposed, on the basis of IR data, a hydride-bridged dimeric structure.[125] They proposed that the initially formed titanocene decomposed *via* the abstraction of a hydrogen atom from a C_5H_5 ligand by titanium, followed by dimerization to form a fulvalene-bridged binuclear titanium complex with two bridging hydrides (Figure 1.3.6). During the 1970s additional evidence for such a structure was provided by a ^{13}C NMR study indicating the presence of a bridging fulvalene ligand,[126] and X-ray diffraction crystal structures of related alkylaluminium-,[127] hydroxyl-[128] and chloro-bridged[129] complexes prepared by the reaction of "green titanocene" with Et_3Al, H_2O and HCl respectively (Figure 1.3.6).

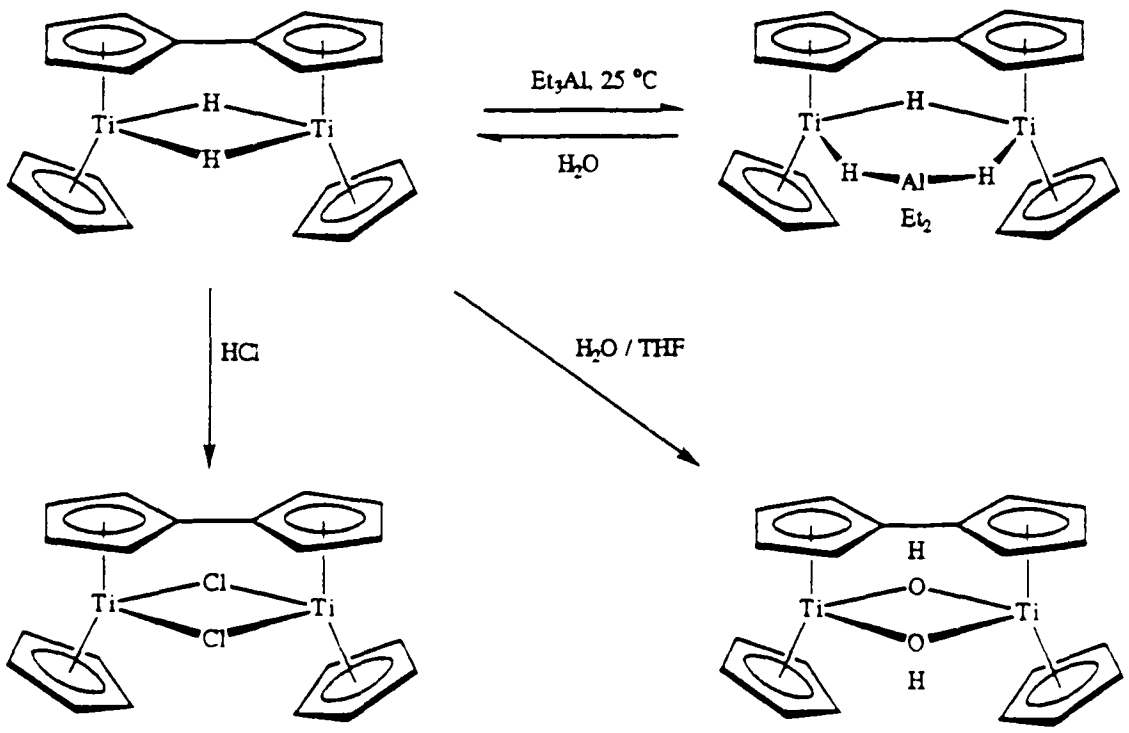

Figure 1.3.6. The fulvalene-bridged "green titanocene" and related complexes

The "green titanocene" $[\{(\eta^5\text{-}C_5H_5)Ti(\mu\text{-}H)\}_2(\mu\text{-}\eta^5\text{-}\eta^5\text{-}C_{10}H_8)]$ is diamagnetic; the diamagnetism was originally ascribed to a possible Ti-Ti bond[124] and later to strong super exchange through the hydride bridging ligands.[127] On the basis of the crystal structures of the derivatives, it was proposed that a Ti-Ti bond was unlikely, and that the diamagnetism was due largely to magnetic coupling of the two metal centres by the fulvalene ligand.[129] It was not until 1992 that an X-ray crystal structure was obtained for "green titanocene".[130] Whilst confirming the proposed $[\{(\eta^5\text{-}C_5H_5)Ti(\mu\text{-}H)\}_2(\mu\text{-}\eta^5\text{-}\eta^5\text{-}C_{10}H_8)]$ structure, the presence of a Ti-Ti bond was neither confirmed nor ruled out, and the Ti-Ti distance for a series of $[\{(\eta^5\text{-}C_5H_5)Ti(\mu\text{-}X)\}_2(\mu\text{-}\eta^5\text{-}\eta^5\text{-}C_{10}H_8)]$ derivatives was shown to reflect the size of the bridging atom or group (μ-X).

In 1993 Royo reported the reaction of "green titanocene" with chlorine to give the Ti(III) complex $[\{CpTi(\mu\text{-}Cl)\}_2(\mu\text{-}\eta^5\text{-}\eta^5\text{-}C_{10}H_8)]$ and the Ti(IV) complex $[\{CpTiCl(\mu\text{-}Cl)\}_2(\mu\text{-}\eta^5\text{-}\eta^5\text{-}C_{10}H_8)]$. The former could be oxidised to the oxo-bridged $[\{CpTiCl\}_2(\mu\text{-}O)(\mu\text{-}\eta^5\text{-}\eta^5\text{-}C_{10}H_8)]$ whilst the chloro-bridged Ti(IV) complex could be alkylated to fulvalene-bridged titanocene dialkyl complexes (Figure 1.3.8).[131] At about the same time Wohrle and Thewalt reported essentially analogous chemistry for the bromine analogues.[132, 133] In 1986 Rausch demonstrated that fulvalene dithallium, $Tl_2(C_{10}H_8)$ reacts with Cp^*TiCl_3 in refluxing benzene to give $[\{Cp^*TiCl_2\}_2(\mu\text{-}\eta^5\text{-}\eta^5\text{-}C_{10}H_8)]$ (Figure 1.3.7).[134]

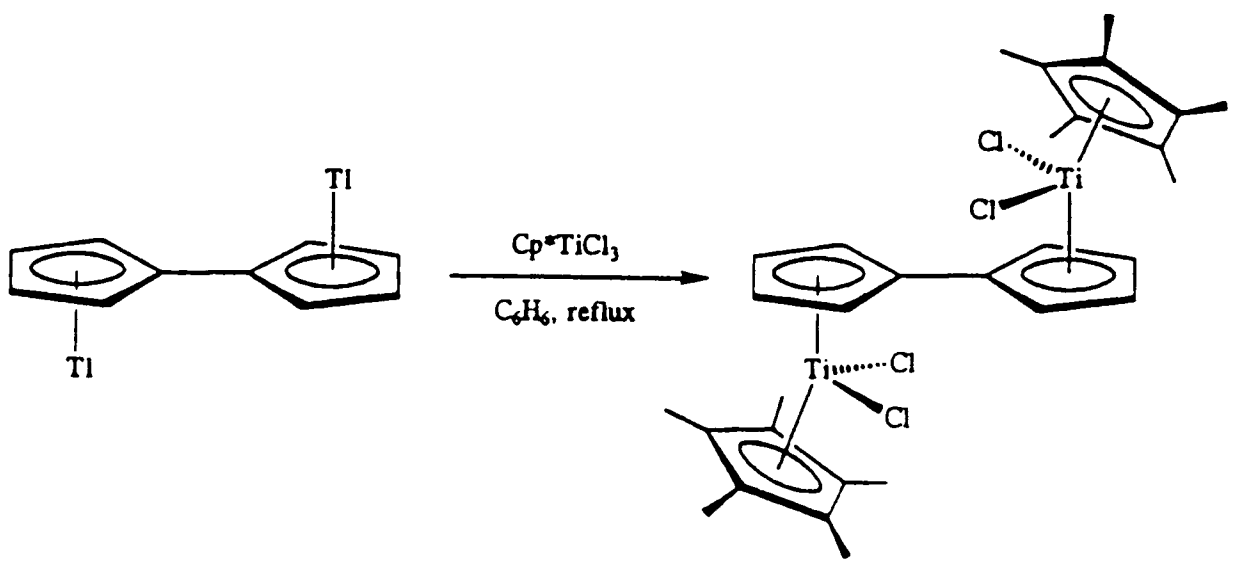

Figure 1.3.7. Synthesis of $[\{Cp^*TiCl_2\}_2(\mu\text{-}\eta^5\text{-}\eta^5\text{-}C_{10}H_8)]$ from $Tl_2(C_{10}H_8)$

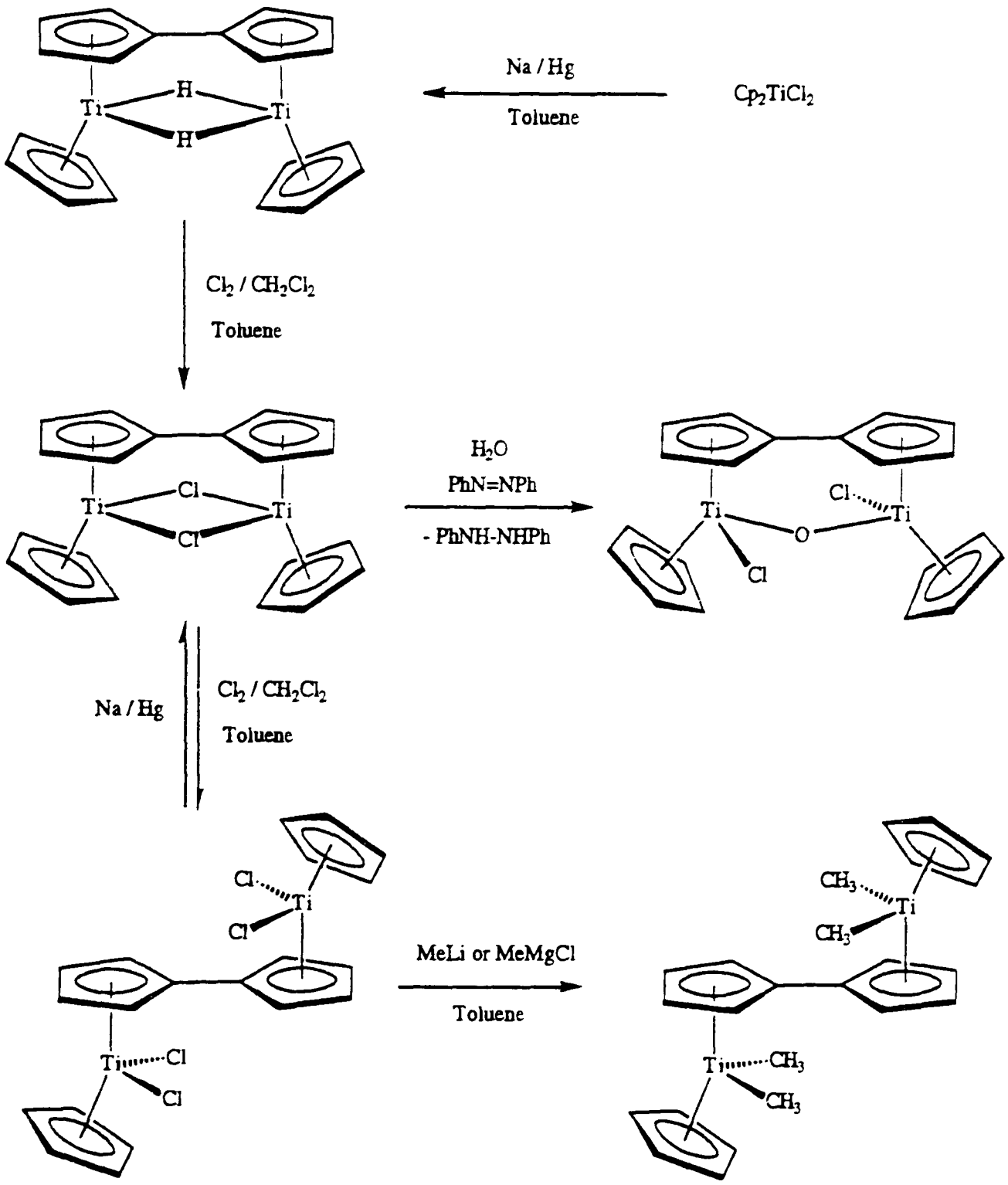

1.3.8. "Green titanocene" as a starting material for the synthesis of fulvalene-bridged dititanium compounds.[131]

In 1992 Royo reported the reaction between bis(trimethylsilyl) fulvalene or $Tl_2(C_{10}H_8)$ and $TiCl_4$ to give $[\{TiCl_3\}_2(\mu\text{-}\eta^5\text{-}\eta^5\text{-}C_{10}H_8)]$ (Figure 1.3.9).[135] Oxidation of the product gave *syn*-$[\{TiCl_2\}_2(\mu\text{-}O)(\mu\text{-}\eta^5\text{-}\eta^5\text{-}C_{10}H_8)]$ whilst reaction with benzyl Grignard reagent gave *anti*-$[\{Ti(CH_2Ph)_3\}_2(\mu\text{-}O)(\mu\text{-}\eta^5\text{-}\eta^5\text{-}C_{10}H_8)]$, both

characterised by X-ray diffraction studies (*syn* and *anti* refer to the rotomeric configuration of the fulvalene ligand, discussed in section 1.3.4).

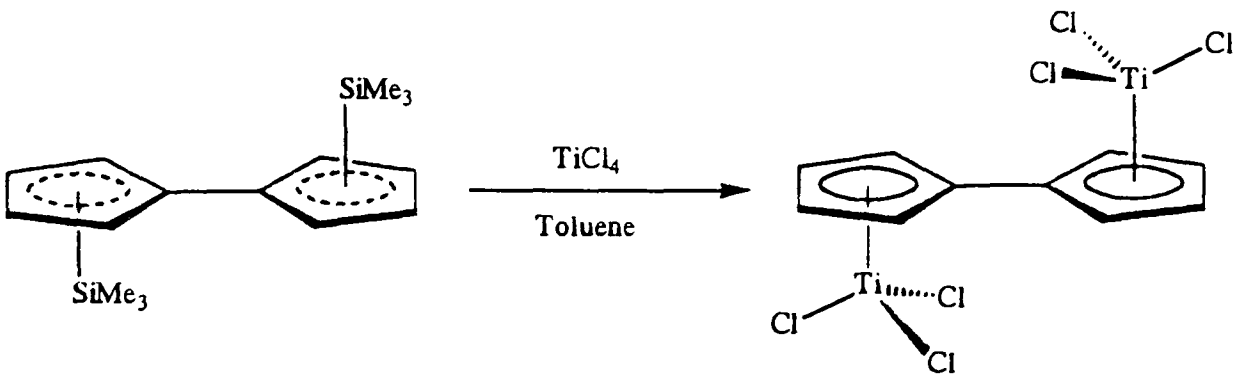

Figure 1.3.9. Synthesis of $[\{TiCl_3\}_2(\mu\text{-}\eta^5\text{-}\eta^5\text{-}C_{10}H_8)]$

1.3.4 Fulvalene-bridged zirconocene derivatives

In recent years several synthetic routes have been developed for the preparation of fulvalene-bridged zirconium derivatives, namely; (i) reduction of Zr(IV) complexes, (ii) comproportionation reactions between Zr(II) and Zr(IV) complexes, (iii) mild oxidation of Zr(II) complexes, and (iv) reaction of monocyclopentadienyl compounds with fulvalene dianion, $(C_{10}H_8)^{2-}$.

1.3.4(i) Reduction of Zr(IV) complexes

In 1986, Herrmann reported the reduction of Cp_2ZrCl_2 using sodium amalgam to give $[\{CpZr(\mu\text{-}Cl)\}_2(\mu\text{-}\eta^5\text{-}\eta^5\text{-}C_{10}H_8)]$, the first undisputed example of a dimeric Zr(III) compound containing a fulvalene ligand.[136] The bridging fulvalene ligand was thought to play a central role in stabilizing this complex, compared with the tendency of $[\{Cp_2Zr(\mu\text{-}Cl)\}_2]$ to undergo disproportionation in solution even at low temperatures.[137] The X-ray crystal structure of $[\{CpZr(\mu\text{-}Cl)\}_2(\mu\text{-}\eta^5\text{-}\eta^5\text{-}C_{10}H_8)]$ revealed a Zr-Zr distance consistent with the presence of a metal-metal bond to which the diamagnetism of the compound was ascribed.[138]

Herrmann reported the reaction of $[\{CpZr(\mu\text{-}Cl)\}_2(\mu\text{-}\eta^5\text{-}\eta^5\text{-}C_{10}H_8)]$ with oxygen to give an oxo-bridged Zr(IV) dimer,[136] and with diphenyldiazomethane and tert-butyl isocyanide to give the 1:1 addition products $[(CpZrCl)_2(\mu\text{-}\eta^1\text{-}\eta^2\text{-}N_2CPh_2)(\mu\text{-}\eta^5\text{-}\eta^5\text{-}C_{10}H_8)]$ and $[(CpZrCl)_2(\mu\text{-}\eta^1\text{-}\eta^2\text{-}CNCMe_3)(\mu\text{-}\eta^5\text{-}\eta^5\text{-}C_{10}H_8)]$ respectively (Figure 1.3.10).[139]

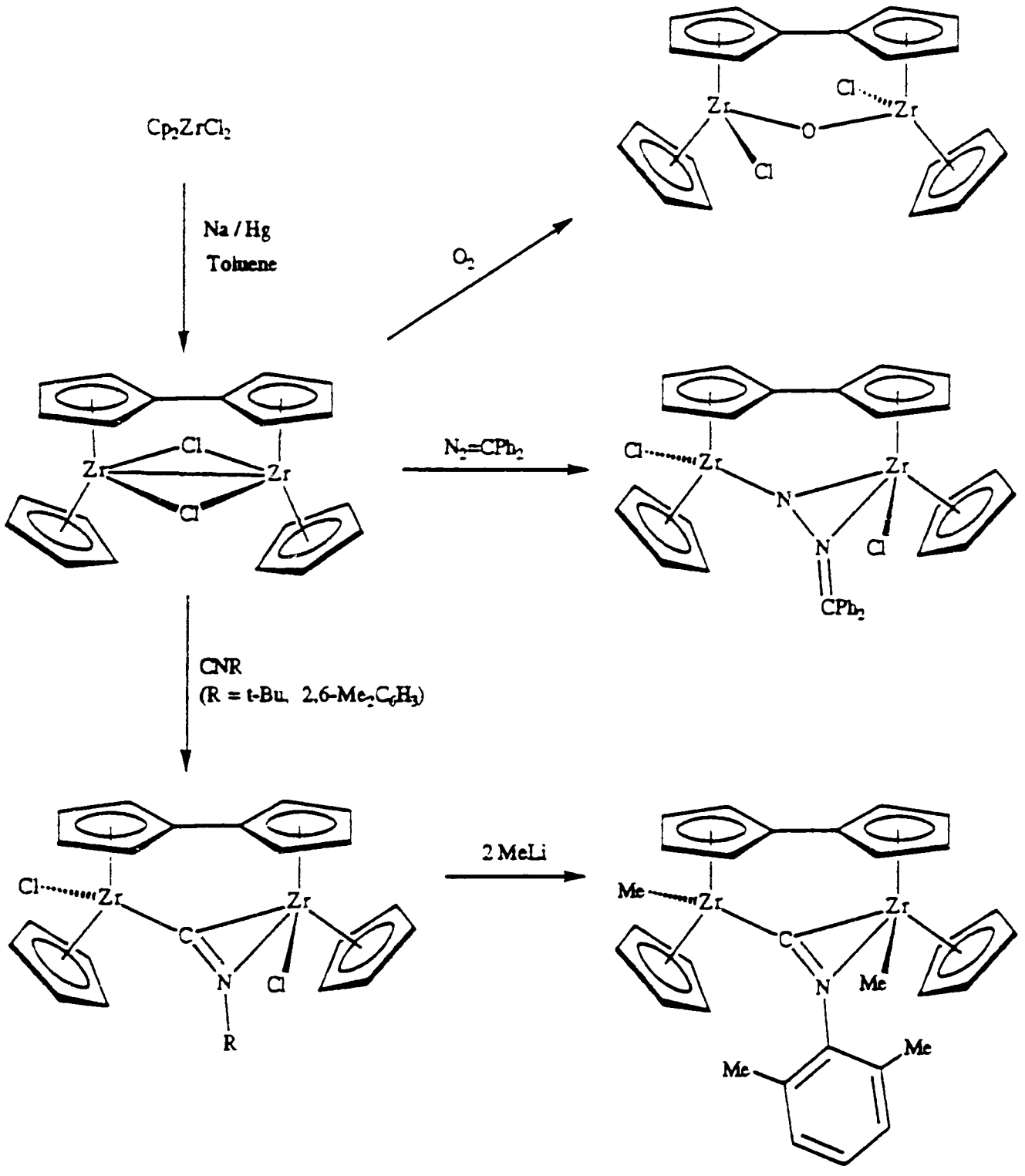

Figure 1.3.10. Synthesis of $[\{CpZr(\mu\text{-}Cl)\}_2(\mu\text{-}\eta^5\text{-}\eta^5\text{-}C_{10}H_8)]$ by reduction of Cp_2ZrCl_2, and reactions with O_2 and unsaturated organic molecules.[136-140]

The reactions were regarded as insertion of the unsaturated organic molecules into the Zr-Zr bond with concomitant splitting (opening) of the chloride bridges. The

unsaturated organic ligands then act as bridging ligands coordinated in a (σ + π) fashion. Royo later reported an analogous reaction with 2,6-dimethylphenyl isocyanide and showed that the zirconium atoms of the product could be methylated without modification of the bridging ligand.[140]

1.3.4(ii) Comproportionation reactions between Zr(II) and Zr(IV) complexes

In 1987, Gambarotta and co-workers reported that the comproportionation reaction between $Cp_2Zr^{II}(PMe_3)_2$ and $Cp_2Zr^{IV}Cl_2$ affords [{(η^5-C_5H_5)Zr(μ-Cl)}$_2$(μ-η^5-η^5-$C_{10}H_8$)] in good yields.[138] They proposed that under the reaction conditions (gentle heating, 40-50 °C) the $Cp_2Zr(PMe_3)_2$ loses H_2 and PMe_3 to form [$CpZr(PMe_3)(\eta^1$-η^5-$C_5H_4)]_2$ and verified that this complex reacts with Cp_2ZrCl_2 to give the same product (Figure 1.3.11).[141]

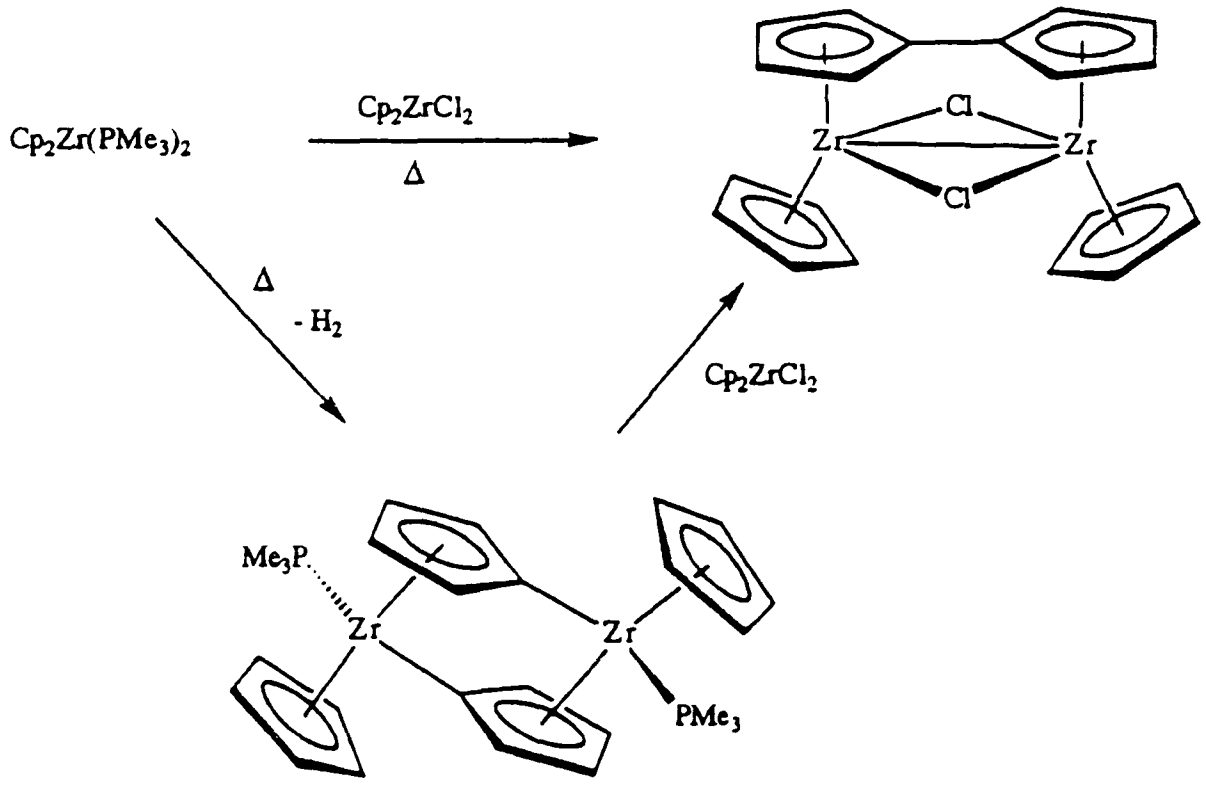

Figure 1.3.11. Comproportionation reactions between Zr(II) and Zr(IV) complexes

1.3.4(iii) Mild oxidation of Zr(II) complexes

In 1990, Gambarotta showed that the oxidation of $[CpZr(PMe_3)(\eta^1\text{-}\eta^5\text{-}C_5H_4)]_2$ with a variety of mild oxidising reagents [R_3PX_2 (R = n-Bu, Me; X = Cl, Br, I), PhSSPh, Me_2PPMe_2) resulted in the reductive coupling of the two ($\eta^1\text{-}\eta^5\text{-}C_5H_4$) rings to form a bridging fulvalene ligand. The reaction allowed the preparation of a class of fulvalene-bridged Zr(III) complexes *syn*-$[\{CpZr(\mu\text{-}X)\}_2(\mu\text{-}\eta^5\text{-}\eta^5\text{-}C_{10}H_8)]$, and Zr(IV) complexes *anti*-$[\{CpZrX_2\}_2(\mu\text{-}\eta^5\text{-}\eta^5\text{-}C_{10}H_8)]$ (Figure 1.3.12).[142, 143]

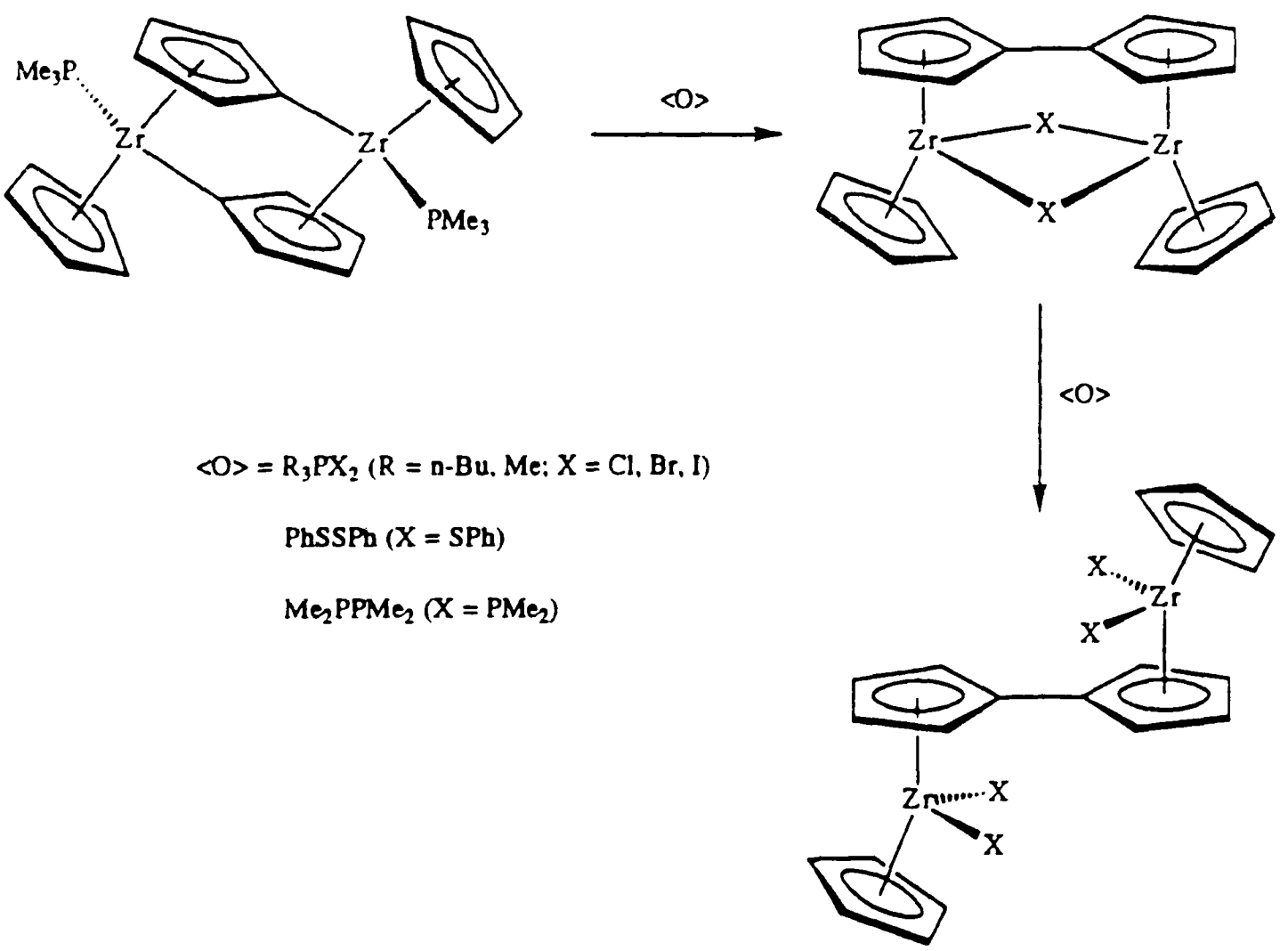

Figure 1.3.12. Synthesis of Zr(III) and Zr(IV) fulvalene-bridged complexes *via* oxidation of $[CpZr(PMe_3)(\eta^1\text{-}\eta^5\text{-}C_5H_4)]_2$

Gambarotta suggested that free-rotation of the fulvalene-bridged complexes was somewhat moderated by electronic conjugation between the two rings, the solid-state structures show only two main rotomeric configurations, *syn* and *anti*. The

former was observed in the (μ-X) bridged Zr(III) species, the latter in the Zr(IV) species in which the *anti* configuration should be sterically favoured.[143] The *anti* configuration was also observed in the crystal structures of the tetramethyl and tetraallyl fulvalene-bridged complexes [{$CpZrR_2$}$_2$(μ-η^5-η^5-$C_{10}H_8$)] [R_2 = $(CH_3)_2$, (η^1-CH_2CHCH_2)(η^3-CH_2CHCH_2)] prepared from the Zr(IV) dichloride derivative (Figure 1.3.13).[143, 144] Partial hydrolysis of *anti*-[{$CpZrMe_2$}$_2$(μ-η^5-η^5-$C_{10}H_8$)] gives *syn*-[{CpZrMe}$_2$(μ-O)(μ-η^5-η^5-$C_{10}H_8$)] in which the *syn* configuration is again imposed by a (μ-X)-type bridge.[143]

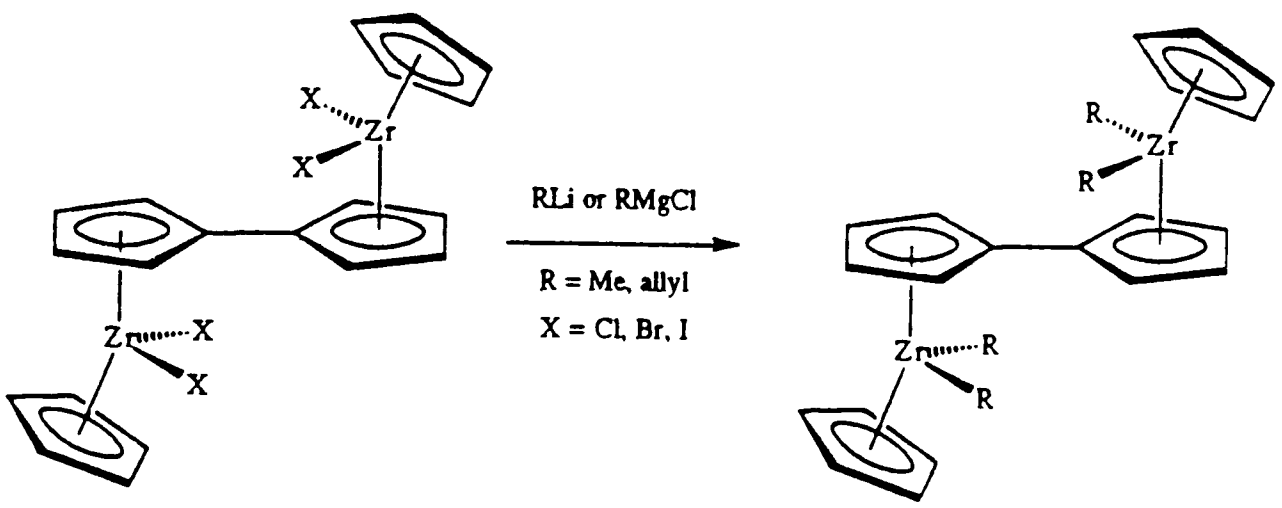

Figure 1.3.13. Synthesis of *anti*-[{$CpZrR_2$}$_2$(μ-η^5-η^5-$C_{10}H_8$)]

1.3.4(iv) Reaction of monocyclopentadienyl compounds with $(C_{10}H_8)^{2-}$

In 1991, Curtis isolated the lithium salt of the fulvalene dianion $Li_2(C_{10}H_8)$, the reaction of which with two equivalents of $(Cp^*ZrCl_3)_x$ yields [{Cp^*ZrCl_2}$_2$(μ-η^5-η^5-$C_{10}H_8$)]. Methylation of the tetrachloride complex yields [{Cp^*ZrMe_2}$_2$(μ-η^5-η^5-$C_{10}H_8$)] which reacts with H_2 to give the tetrahydride complex [{$Cp^*ZrH(\mu\text{-}H)$}$_2$(μ-η^5-η^5-$C_{10}H_8$)]. The latter reacts with CO to give the bridging formaldehyde complex [{$Cp^*Zr(\mu\text{-}\eta^2\text{-}CH_2O)$}$_2$(μ-$\eta^5$-$\eta^5$-$C_{10}H_8$)] (Figure 1.3.14).[145]

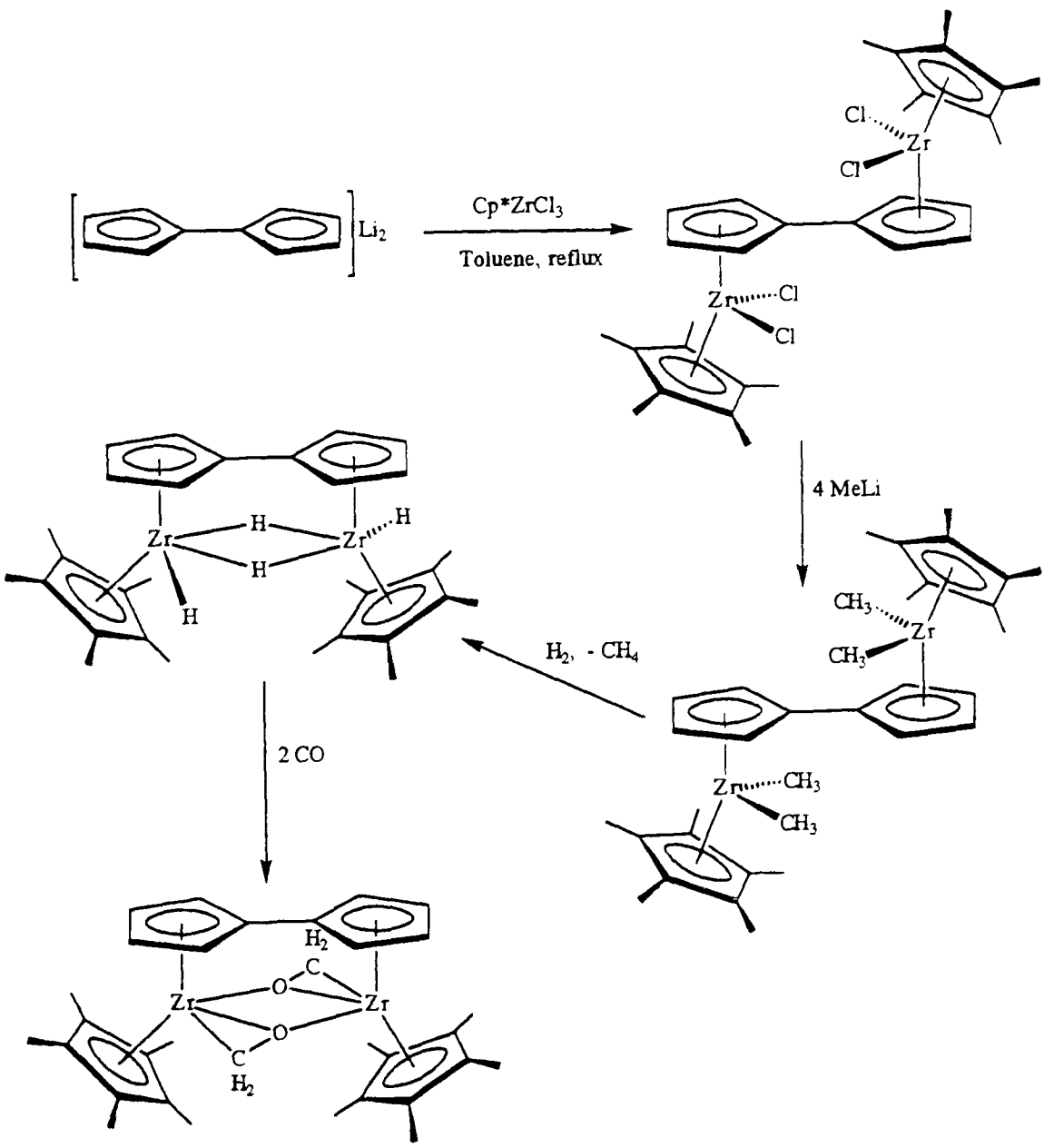

Figure 1.3.14. Synthesis and chemistry of $[\{Cp^*ZrCl_2\}_2(\mu\text{-}\eta^5\text{-}\eta^5\text{-}C_{10}H_8)]$

1.3.5. Binuclear complexes with substituted fulvalene ligands

Brintzinger has very recently reported the synthesis of iron-zirconium heterobimetallic complexes in which the metals are bridged by substituted fulvalene-type ligands (Figure 1.3.15).[146] Only the chiral *rac*-diastereomer of the bis(indenyl) derivative was isolated.

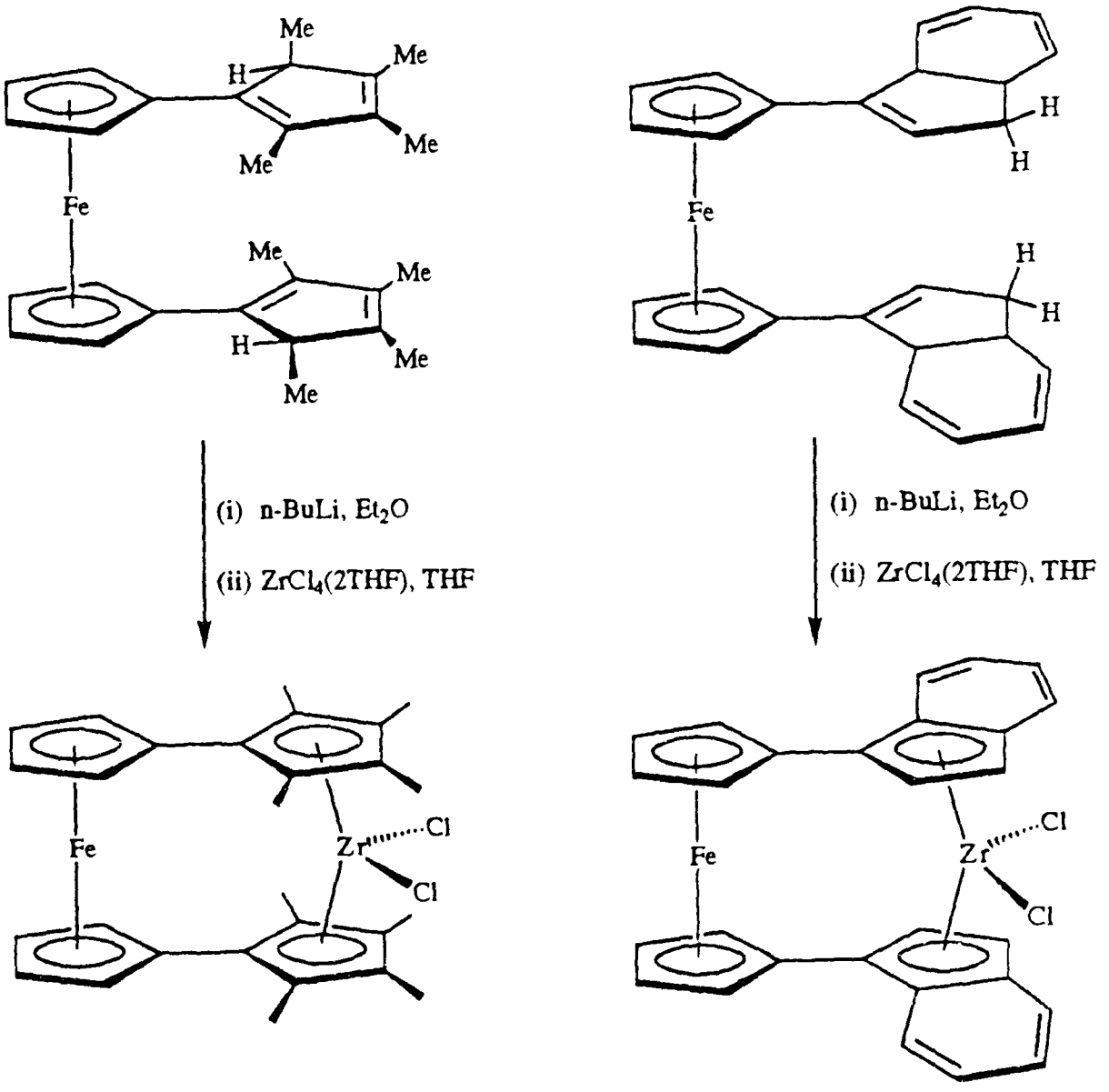

Figure 1.3.15. Heterobimetallic complexes with substituted-fulvalene bridging ligands

1.3.6 Binuclear *ansa*-bridged group 4 complexes

In contrast with the fulvalene ligand, *ansa*-bis(cyclopentadienyl) ligands can coordinate to metal centres in both **bridging** and **chelating** fashions.[147, 148] Mononuclear group 4 *ansa*-bridged metallocenes, in which the *ansa* ligand coordinates in a chelating fashion to the metal, are well known. When the *ansa* ligand is suitably substituted, they are an important class of stereospecific homogeneous catalysts, as discussed in section 1.2.

Marks[118] and Fischer[147] have shown that binuclear transition metal complexes of the general type $[R_2Si(\eta^5\text{-}C_5R'_4)_2M(\mu\text{-}X)]_2$ (M = Y, Lanthanide) may principally exist in two isomeric forms with chelating (**I**) and bridging (**II**) $R_2Si(\eta^5\text{-}C_5R'_4)_2$ ligand

coordination (Figure 1.3.16). Whether isomer **I** or **II** is preferred depends on the size of the metal, the nature of the (μ-X) bridging ligand and on the ($C_5R'_4$) ring substituents.

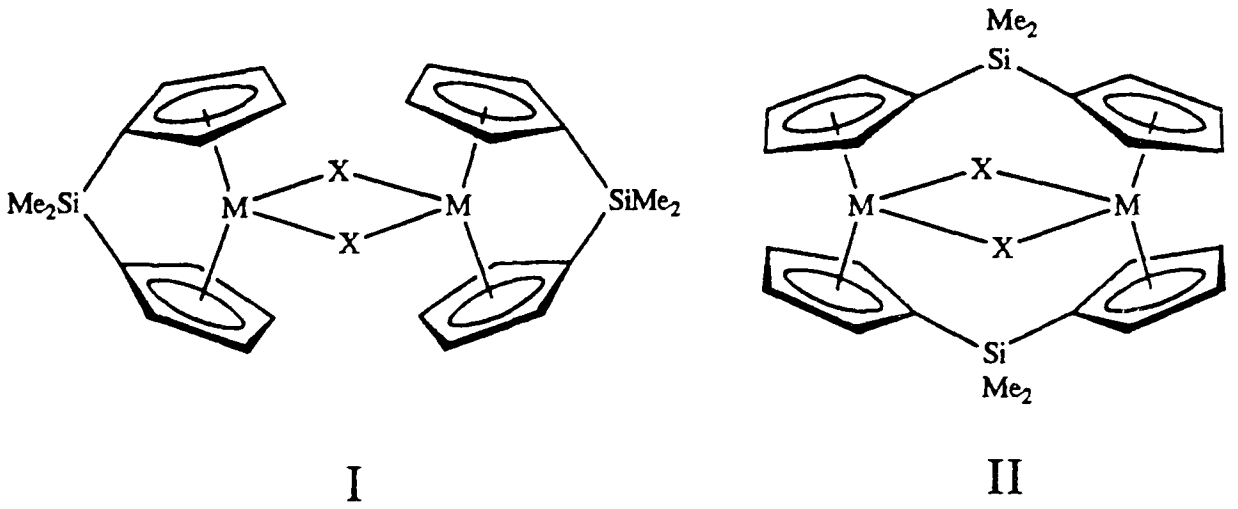

I II

Figure 1.3.16. Binuclear complexes with chelating (**I**) and bridging (**II**) *ansa* ligand coordination

A great range of *ansa* ligands have been prepared, with a variety bridging groups and substituted cyclopentadienyl, indenyl and fluorenyl rings (see section 1.2). Thus a great variety of *ansa*-bridged binuclear complexes could, in theory, be prepared, including; (i) unsymmetrical complexes with different ligand environments at each metal centre, (ii) chiral complexes, and possibly (iii) heterobimetallic complexes.

Compared with fulvalene-bridged bimetallics, a greater range of metal-metal distances should be possible with the *ansa* ligands, by varying the size/length of the inter-annular bridge. Another drawback of fulvalene-bridged bimetallics which might be avoided is their potential to undergo carbon-carbon bond cleavage leading to the formation of binuclear complexes containing (η^1-η^5-C_5H_4) bridging groups.[149]

1.3.7 Synthesis of *ansa*-bridged binuclear group 4 complexes

The syntheses of *ansa*-bridged binuclear group 4 complexes have employed three classes of ligand starting material: (i) lithium salts, (ii) thallium complexes and (iii) dimethyl tin complexes.

1.3.7(i) Homobinuclear metallocenes from $[\{X(C_5H_4)_2\}Li_2]$

In 1989, Petersen reported the metathesis of $[\{X(C_5H_4)_2\}Li_2]$ (X = CH_2, $SiMe_2$) with two equivalents of $CpZrCl_3 \cdot 2THF$ or Cp^*ZrCl_3 to give the *ansa*-bridged binuclear zirconocene derivatives $[\{X(\eta^5\text{-}C_5H_4)_2\}\{(\eta^5\text{-}C_5R_5)ZrCl_2\}_2]$ (R = H, CH_3).[150] The crystal structure of $[\{Me_2Si(\eta^5\text{-}C_5H_4)_2\}\{(\eta^5\text{-}C_5Me_5)ZrCl_2\}_2]$ showed that the configuration adopted in the solid state was intermediate between the *syn* and *anti* configurations adopted by fulvalene derivatives. In fact the "skew" angle between the C_5H_4 planes was 48°, contrasting with the strict *anti* configuration observed for fulvalene-bridged group 4 metallocenes.[134, 143, 144]

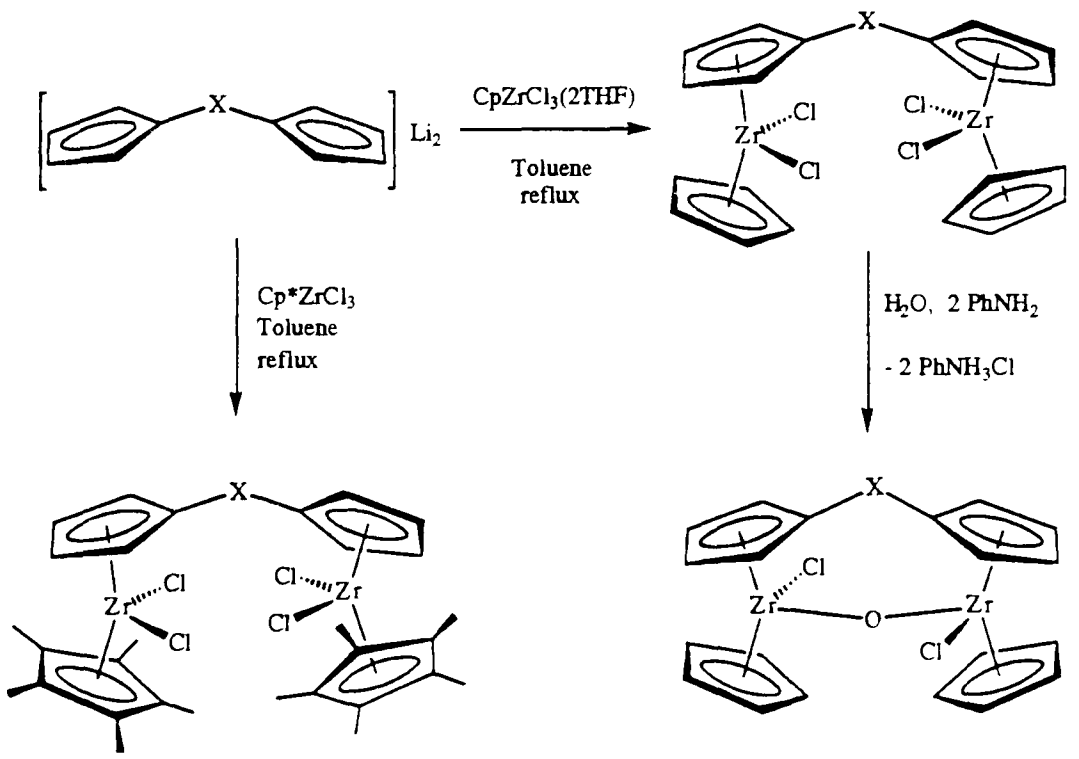

Figure 1.3.17. Synthesis of $[\{X(\eta^5\text{-}C_5H_4)_2\}\{(\eta^5\text{-}C_5R_5)ZrCl_2\}_2]$

(X = CH_2, $SiMe_2$; R = H, CH_3)

Hydrolysis of [{X(η^5-C_5H_4)$_2$}{(η^5-C_5Me_5)$ZrCl_2$}$_2$] in the presence of aniline affords the corresponding oxo-bridged derivatives [{X(η^5-C_5H_4)$_2$}{(η^5-C_5Me_5)ZrCl}$_2$(μ-O)] with an approximate syn configuration (Figure 1.3.17).

Treatment of the binuclear zirconocene derivative [{CH_2(η^5-C_5H_4)$_2$}{(η^5-C_5H_5)$ZrCl_2$}$_2$] with $LiAl(OBu^t)_3H$ yields the hydride-bridged derivatives [{Me_2Si(η^5-C_5H_4)$_2$}{CpZrCl(μ-H)}$_2$], which on treatment with ethylene at 85 °C, or on thermolysis at 130 °C, or photolysis at room temperature, affords the diamagnetic binuclear Zr(III) complex [{Me_2Si(η^5-C_5H_4)$_2$}{CpZr(μ-Cl)}$_2$].[150, 151] Treatment of the oxo-bridged derivative with $LiAlH_4$ gives [{Me_2Si(η^5-C_5H_4)$_2$}{CpZrH(μ-H)}$_2$] (Figure 1.3.18).[148]

Petersen has also recently reported that the treatment of [{Me_2Si(η^5-C_5H_4)$_2$}{CpZrH(μ-H)}$_2$] with elemental sulphur affords the (μ-S)$_2$ bridged dinuclear Zr(IV) complex [{Me_2Si(η^5-C_5H_4)$_2$}{CpZr(μ-S}$_2$]. The (μ-S) bridges are quite resistant to cleavage, no reaction is observed with PMe_3, CH_3NC or pyridine. In contrast the (μ-Cl) bridges of the diamagnetic binuclear Zr(III) complex [{Me_2Si(η^5-C_5H_4)$_2$}{CpZr(μ-Cl)}$_2$] are easily cleaved by the addition of PMe_3 or THF, to give the paramagnetic binuclear Zr(III) complexes [{Me_2Si(η^5-C_5H_4)$_2$}{CpZrCl(L)}$_2$] (L = PMe_3, THF). The presence of two Zr(III) centres in [{Me_2Si(η^5-C_5H_4)$_2$}{CpZr(μ-Cl)}$_2$] suggests that it might react as a two electron reductant. Indeed such behaviour is observed in its reaction with Ph_3PO, which produces the oxo-bridged binuclear Zr(IV) complex [{Me_2Si(η^5-C_5H_4)$_2$}{(η^5-C_5H_5)ZrCl}$_2$(μ-O)] and PPh_3 (Figure 1.3.18).[151]

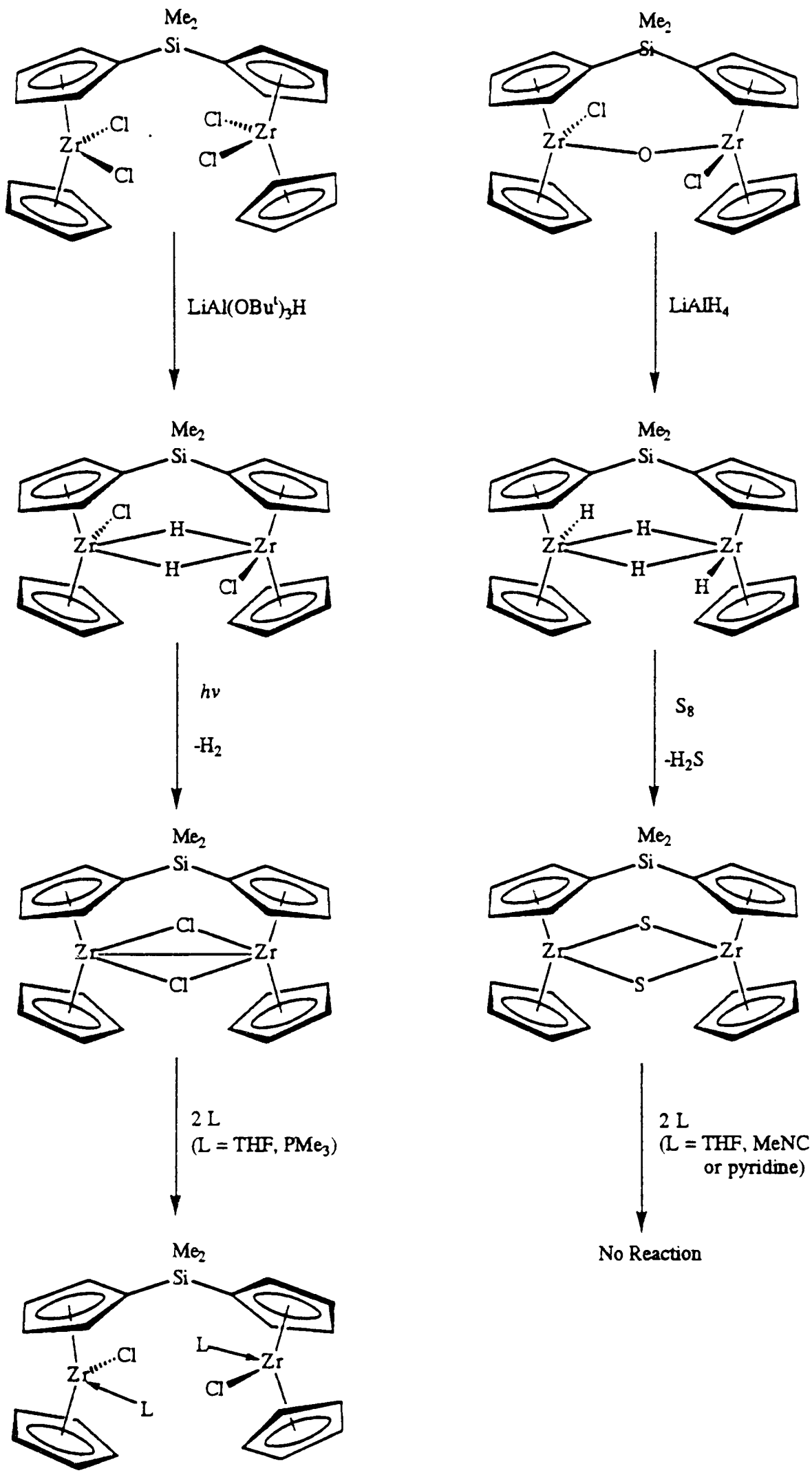

Figure 1.3.18. Synthesis and chemistry of $[\{Me_2Si(\eta^5\text{-}C_5H_4)_2\}\{CpZr(\mu\text{-}X)\}_2]$

(X = Cl, S)

1.3.7(ii) Binuclear "half-sandwich" complexes from $[\{Me_2Si(C_5H_4)_2\}Tl_2]$

Royo has recently reported the synthesis of the thallium compound $[\{Me_2Si(C_5H_4)_2\}Tl_2]$ from the reaction of $Me_2Si(C_5H_5)_2$ with thallium ethoxide. Addition of the thallium *ansa* ligand to$TiCl_4$ in dry toluene gives the binuclear complex $[\{Me_2Si(\eta^5\text{-}C_5H_4)_2\}(TiCl_3)_2]$.[152] Attempts to prepare this complex using the lithium salt of the ligand failed, instead the mononuclear complex $[\{Me_2Si(\eta^5\text{-}C_5H_4)_2\}TiCl_2]$, with chelating *ansa*-ligand coordination, was obtained.[153, 154] Nifant'ev has reported that the chelating, mononuclear complexes $[\{X(\eta^5\text{-}C_5H_4)_2\}TiCl_2]$ (X = Me_2Si, Me_2C) reacted with $TiCl_4$ in refluxing toluene to produce the binuclear complexes $[\{X(\eta^5\text{-}C_5H_4)_2\}(TiCl_3)_2]$,[155] *via* a ligand exchange reaction analogous to the original preparation of $CpTiCl_3$ from Cp_2TiCl_2 and $TiCl_4$.[156]

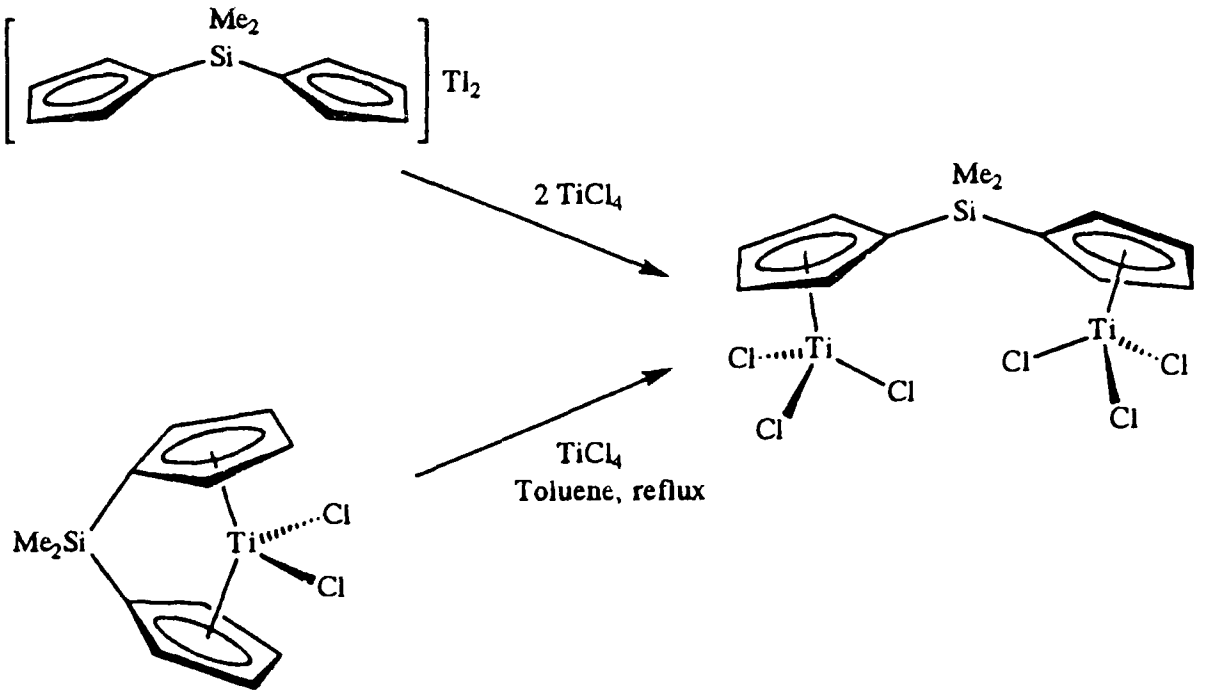

Figure 1.3.19. Synthesis of $[\{Me_2Si(\eta^5\text{-}C_5H_4)_2\}(TiCl_3)_2]$

1.3.7(iii) Homo- and heter-binuclear metallocenes from $[\{X(\eta^1\text{-}C_5H_4)_2\}SnMe_2]$

Heterobinuclear complexes containing bridging bis(cyclopentadienyl) ligands are very rare, in part because it is inherently difficult to add one metal selectively to one ring and a different metal to the second.[117]

In 1992 Nifant'ev reported the monotransmetallation reaction between the *ansa*-bis(cyclopentadienyl) dimethyltin derivatives [{$Me_2Si(\eta^1\text{-}C_5H_4)_2$}$SnMe_2$] and $CpTiCl_3$ or $CpZrCl_3 \cdot 2THF$ to give [$CpMCl_2${$(\eta^5\text{-}C_5H_4)SiMe_2(\eta^1\text{-}C_5H_4)SnClMe_2$}] (M = Ti, Zr) (Figure 1.3.20).[157] The reaction is very solvent- and temperature-dependent and produces the binuclear metallocenes [{$Me_2Si(\eta^5\text{-}C_5H_4)_2$}$(CpMCl_2)_2$] and/or the mononuclear *ansa*-metallocenes [{$Me_2Si(\eta^5\text{-}C_5H_4)_2$}$MCl_2$] as by-products, especially for the titanium derivatives.

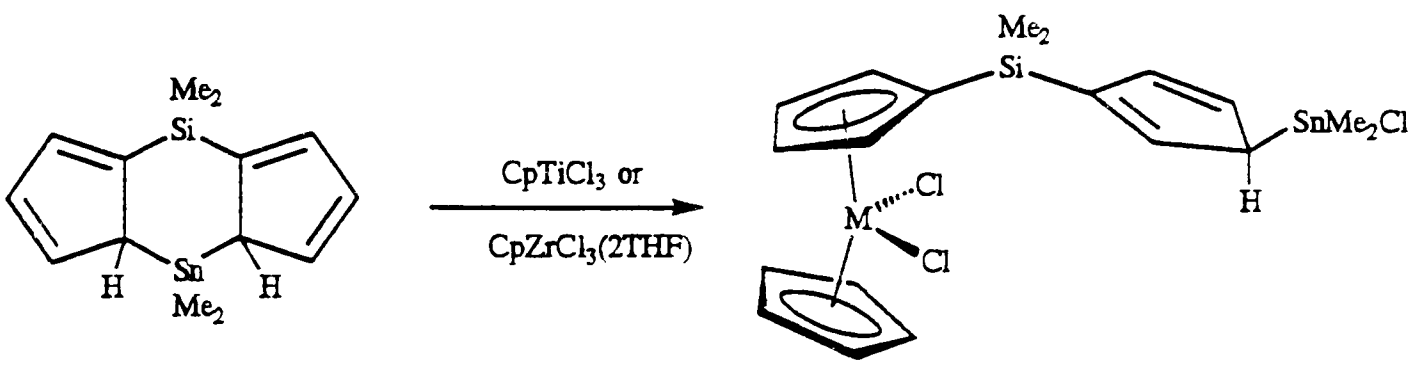

Figure 1.3.20. Synthesis of [$CpMCl_2${$(\eta^5\text{-}C_5H_4)SiMe_2(\eta^1\text{-}C_5H_5)SnClMe_2$}] (M = Ti, Zr)

Nifant'ev demonstrated that the Zr-Sn compound [$CpZrCl_2${$(\eta^5\text{-}C_5H_4)SiMe_2(\eta^1\text{-}C_5H_4)SnClMe_2$}] could be used as an intermediate in the synthesis of homo- and hetero-bimetallic *ansa*-bridged compounds in low to moderate yield (20 to 50 %).[157] These reactions are summarised in Figure 1.3.21. It was found that, due to the thermal instability of the monotransmetallated compounds, the order of metallation was important. For instance, the Zr-Ti bimetallic complex could not be prepared from the treatment of the Ti-Sn complex with $CpZrCl_3 \cdot 2THF$, instead thermal decomposition of the Ti-Sn complex gave the mononuclear titanium *ansa* compound [{$Me_2Si(\eta^5\text{-}C_5H_4)_2$}$TiCl_2$] as the major product.

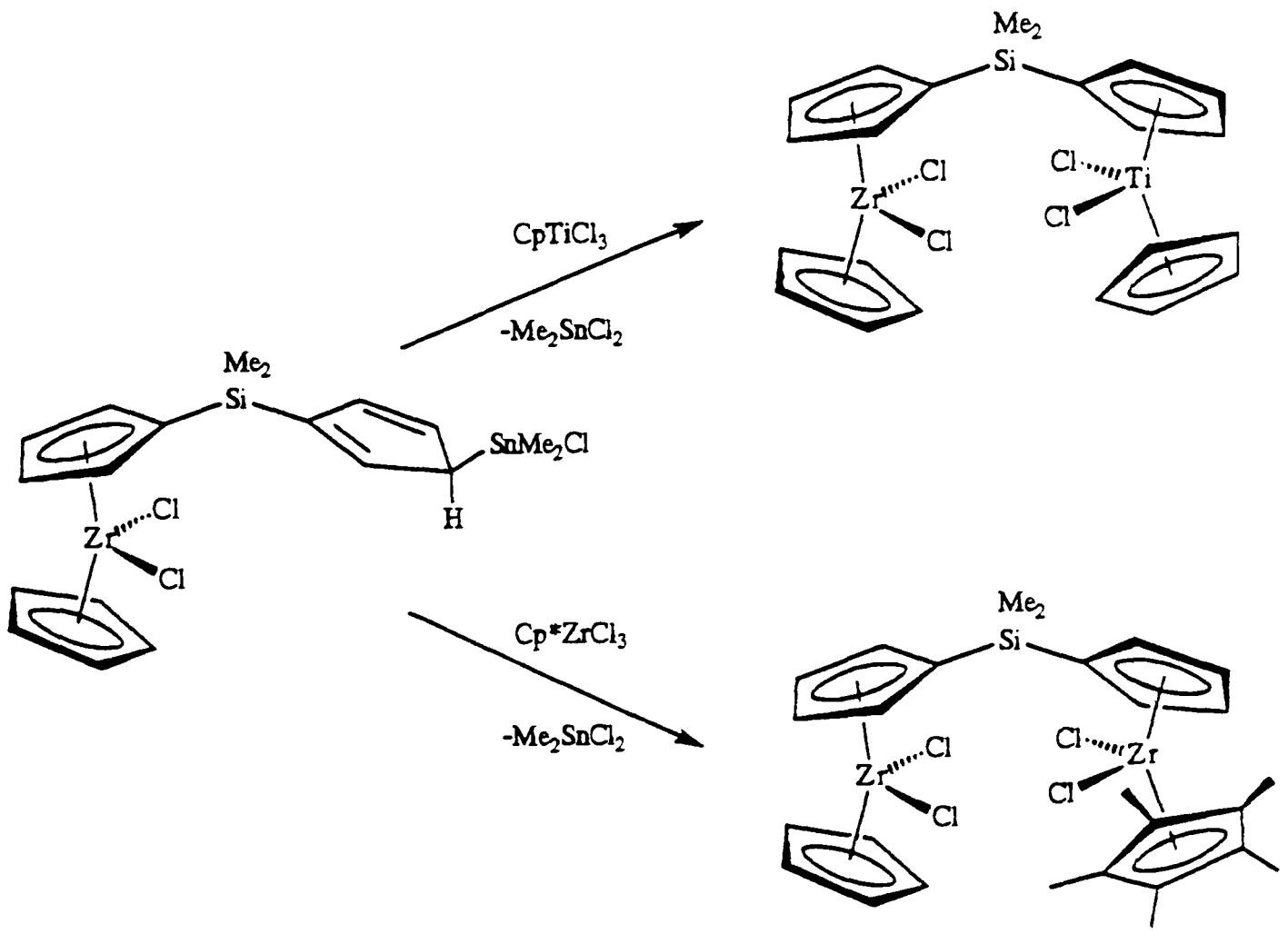

Figure 1.3.21. Synthesis of homo-and hetero-bimetallic compounds from the Zr-Sn complex

Nifant'ev also reported that the treatment of $[\{X(\eta^1\text{-}C_5H_4)_2\}SnMe_2]$ (X = Me_2Si, Me_2C) with $[\{Me_2Si(\eta^5\text{-}C_5H_4)_2\}(TiCl_3)_2]$ afforded double-bridged binuclear titanocene dicloride derivatives in low yield (15-20 %) (Figure 1.3.22). These were insoluble in all available organic solvents and characterized only by microanalysis, so may have been oligomeric. However, the reduction of these compounds (using powdered zinc) proceeded in high yield to give the binuclear chloro-bridged Ti(III) derivatives, and the crystal structure of the binuclear Ti(III) complex $[\{\mu\text{-}\eta^5\text{-}\eta^5\text{-}Me_2Si(C_5H_4)_2\}_2\{Ti(\mu\text{-}Cl)\}_2]$ was reported.[157]

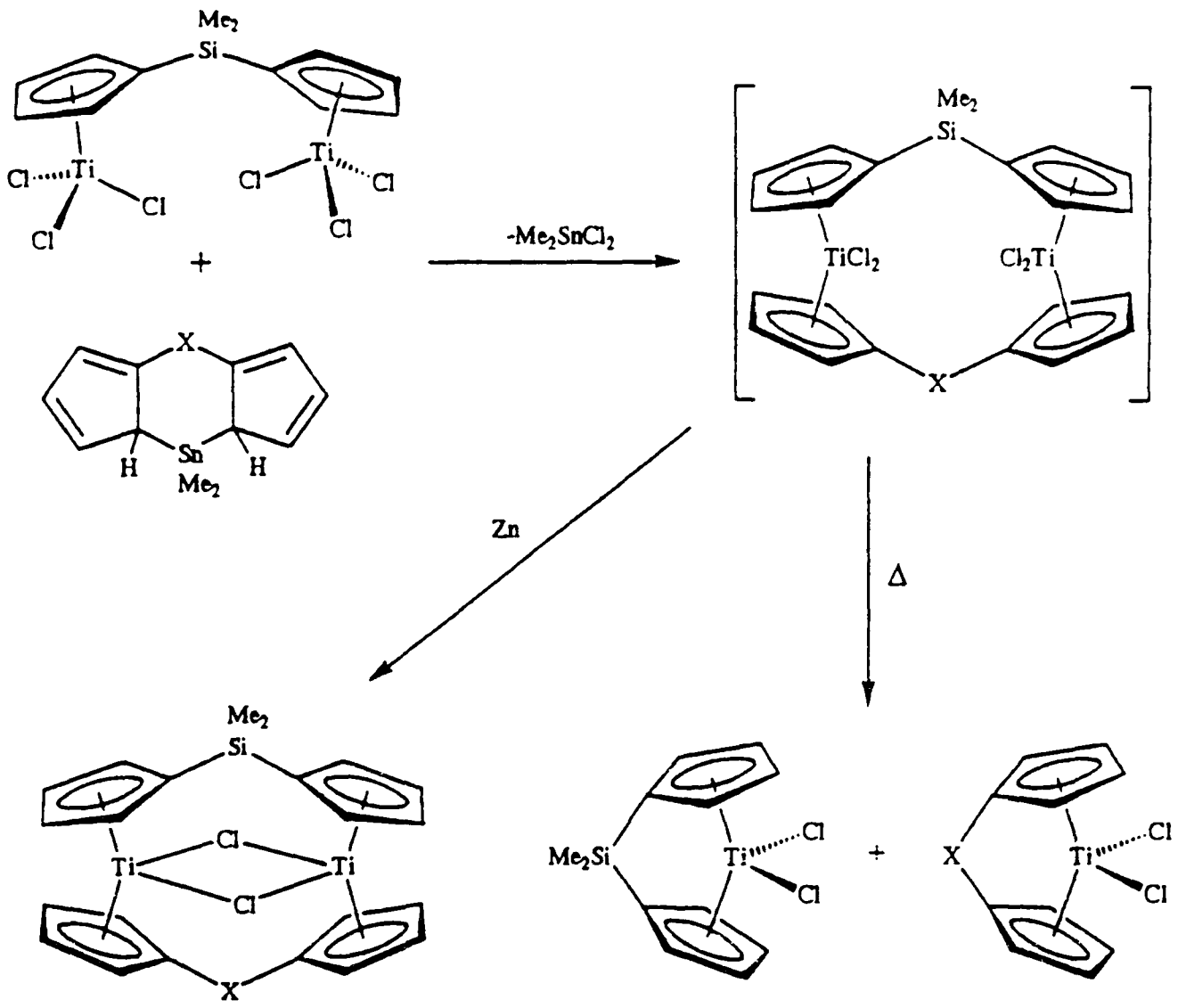

Figure 1.3.22. Synthesis of double-bridged binuclear Ti(IV) and Ti(III) complexes

1.3.8 Other *ansa*-bridged binuclear complexes

In 1992, Werner reported the synthesis of the mononuclear complexes $[M(CO)_2\{(\eta^5\text{-}C_5H_4)CH_2(C_5H_5)\}]$ (M = Rh, Ir). Treatment of these with n-BuLi afforded the lithiated derivatives $[M(CO)_2\{(\eta^5\text{-}C_5H_4)CH_2(C_5H_4)Li\}]$ from which, on reaction with $[Co(CO)_4I]$, $[Rh(CO)_2Cl]_2$ and $[(\eta^5\text{-}C_5H_5)TiCl_3]$, the heterobimetallic complexes $[M(CO)_2\{CH_2(\eta^5\text{-}C_5H_4)_2\}M^*(CO)_2]$ (M = Rh, Ir; M* = Co, Rh) and $[Ir(CO)_2\{CH_2(\eta^5\text{-}C_5H_4)_2\}TiCl_2Cp]$ were obtained.[158] Nifant'ev prepared the related group 4 / group 9 heterobimetallic complexes $[CpMCl_2\{Me_2Si(\eta^5\text{-}C_5H_4)_2\}Rh(COD)]$ (M = Ti, Zr; COD = cyclooctadiene) *via* the Ti-Sn and Zr-Sn complexes $[CpMCl_2\{(\eta^5\text{-}C_5H_4)SiMe_2(\eta^1\text{-}C_5H_4)SnClMe_2\}]$ (Figure 1.3.23).[157] Thus Werner and Nifant'ev prepared similar heterobimetallic complexes, but were able to approach them from synthetically opposite directions, illustrating the potential versatility of *ansa*-bridged bis(cyclopentadienyl)-type ligands.

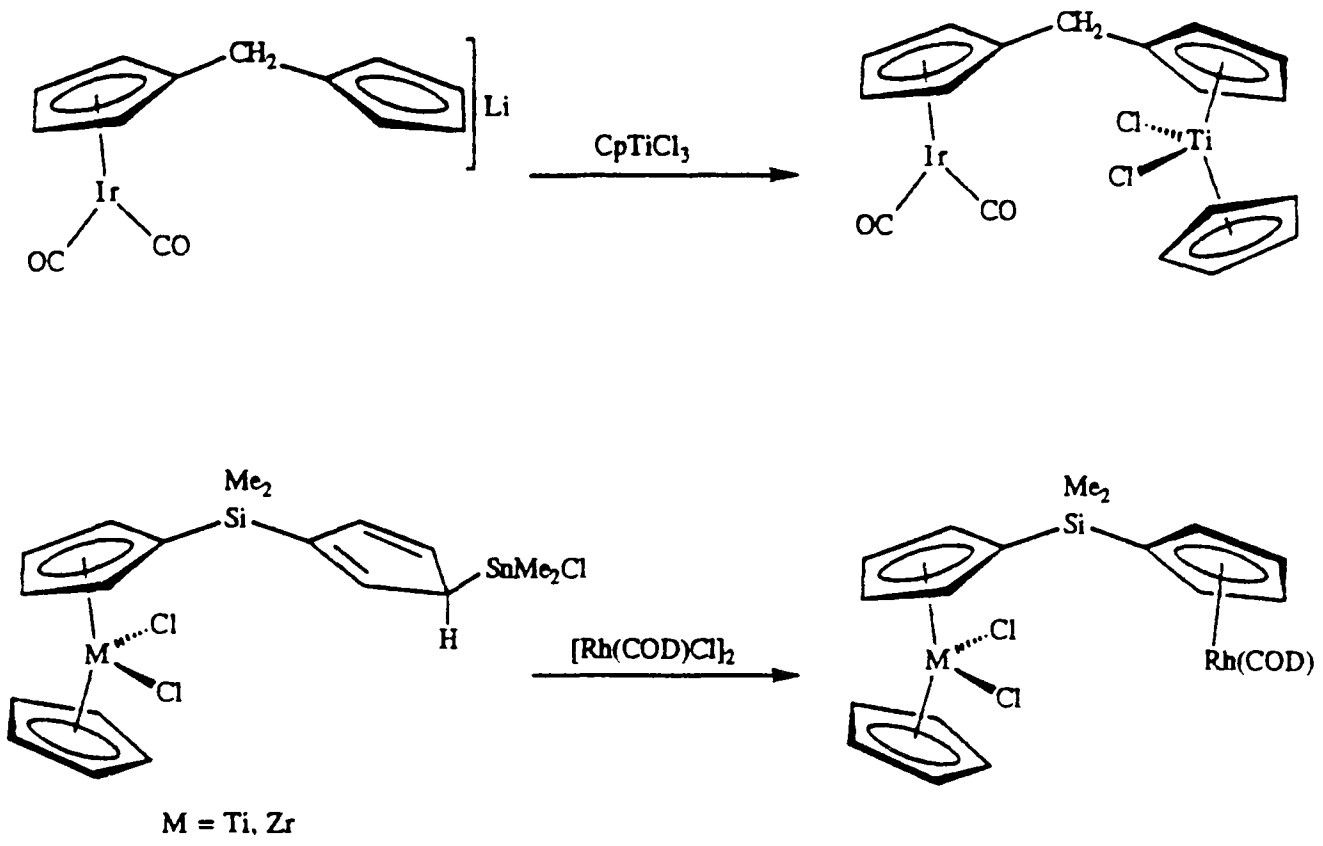

1.3.23. Synthesis of Ti-Ir, Ti-Rh and Zr-Rh heterobimetallic complexes.

1.4 Summary

In conclusion, mononuclear group 4 metallocene derivatives have become recognised as an important class of homogeneous catalysts, especially for the stereospecific polymerization of olefins. Several synthetic routes to symmetrically bridged, homobinuclear group 4 metallocenes have been developed, whilst related heterobinuclear group 4 compounds were unknown until very recently, and only one example has been reported. The chemistry of binuclear group 4 metallocene compounds remains under-developed, and the catalytic properties of such compounds have not been reported.

This Thesis is concerned with the synthesis of novel, chiral, homo- and hetero-binuclear group 4 metallocene compounds, in which non-equivalent mononuclear fragments are joined by an *ansa* bridge. The synthesis and the molecular structures of novel *ansa*-bridged mononuclear compounds will be discussed in Chapter 2, followed by the synthesis of the binuclear compounds in Chapter 3. A study of the binuclear compounds as olefin polymerization catalysts is presented in Chapter 4.

References for Chapter 1

1. M. E. P. Friedrich and C. S. Marvel, *J. Am. Chem. Soc.*, 1930, **52**, 376.
2. K. Ziegler, *Belg. Pat.*, 533 362, 1953; K. Ziegler, E. Holzkamp, H. Briel and H. Martin, *Angew. Chem.*, 1955, **67**, 541.
3. G. Natta, P. Pino and G. Mazzanti, *Ital. Pat.*, 526 101, 1954; G. Natta, *J. Polymer Sci.*, 1955, **16**, 143; G. Natta, P. Pino, P. Corradini, F. Danusso, E. Mantica, G. Mazzanti and G. Moraglio, *J. Am. Chem. Soc.*, 1955, **77**, 1708; G. Natta, *Angew. Chem.*, 1955, **67**, 430.
4. G. Natta, I. Pasquon and A. Zambelli, *J. Am. Chem. Soc.*, 1962, **84**, 1488.
5. R. P. Quirk, Ed., *Transition Metal Catalysed Polymerizations*, Cambridge University Press, Cambridge, 1988.
6. W. Kaminsky and H. Sinn, Eds., *Transition Metals and Organometallics as Catalysts for Olefin Polymerization*, Springer, New York, 1988.
7. T. Keii and K. Soga, Eds., *Catalytic Polymerization of Olefins*, Elsevier, Amsterdam, 1986.
8. P. Pino and B. Rotzinger, *Makromol. Chem. Suppl.*, 1984, **7**, 41.
9. R. P. Quirk, H. L. Hsieh, G. C. Klingensmith and P. J. Tait, Eds., *Transition Metal Catalysed Polymerization. Alkenes and Dienes.*, Harwood Publishers for MMI Press, New York, 1983.
10. P. D. Gavens, M. Bottrill, J. W. Kelland and J. McMeeking, in *Comprehensive Organometallic Chemistry*, G. Wilkinson, F. G. A. Stone and E. W. Abel, Eds., Pergamon Press, Oxford, 1982, vol. 3, ch. 22.5, pp 476-547.
11. H. Sinn and W Kaminsky, *Adv. Organomet. Chem.*, 1980, **18**, 99.
12. P. Pino and R. Mulhaupt, *Angew. Chem., Int. Ed. Engl.*, 1980, **19**, 857.
13. (a) P. J. T Tait, in *Comprehensive Polymer Science*, G. Allen and J. C. Bevington, Eds., Pergamon Press, Oxford, 1989, vol. 4, ch. 1, pp 1-25; (b) P. J. T Tait and N. D. Watkins, in *Comprehensive Polymer Science*, vol. 4, ch. 2,

pp 533-573; (c) P Corradini, V. Busico and G. Guerra, in *Comprehensive Polymer Science*, vol. 4, ch. 3, pp 29-50.

14. G. Natta, P. Pino, G. Mazzanti and U. Giannini, *J. Am. Chem. Soc.*, 1957, **79**, 2975.

15. H. Sinn, W. Kaminsky, H-J. Vollmer and R. Woldt, *Angew. Chem., Int. Ed. Engl.*, 1980, **19**, 390.

16. W. Kaminsky, M. Miri, H. Sinn and R. Woldt, *Makromol. Chem., Rapid Commun.*, 1983, **4**, 417.

17. W. Kaminsky and H. Luker, *Makromol. Chem., Rapid Commun.*, 1984, **5**, 225.

18. E. Giannetti, G. M. Nicoletti and R. Mazzocchi, *J. Polym. Sci., Polym. Chem. Ed.*, 1985, **23**, 2117.

19. W. Kaminsky and R. Steiger, *Polyhedron*, 1988, **7**, 2375.

20. L. Resconi, S. Bossi and L. Abis, *Macromolecules*, 1990, **23**, 4489.

21. M. Kaminaka and K. Soga, *Makromol. Chem., Rapid Commun.*, 1991, **12**, 367.

22. N. Piccolrovazzi, P. Pino, G. Consiglio, A. Sironi and M. Moret, *Organometallics*, 1990, **9**, 3098.

23. R. F. Jordan, *Adv. Organomet. Chem.*, 1991, **32**, 325.

24. G. G. Hlatky, H. W. Turner and R. R. Eckman, *J. Am. Chem. Soc.*, 1989, **111**, 2728.

25. J. J. Eisch, K. R. Caldwell, S. Werner and C. Kruger, *Organometallics*, 1991, **10**, 3471.

26. T. J. Marks, *Acc. Chem. Res.*, 1992, **25**, 57.

27. M. Bochmann and S. J. Lancaster, *Organometallics*, 1993, **12**, 633.

28. C. Sishta, R. M. Hathorn and T. Marks, *J. Am. Chem. Soc.*, 1992, **114**, 1112.

29. D. Cam and U. Giannini, *Makromol. Chem.*, 1992, **193**, 1049.

30. R. Waymouth and P. Pino, *J. Am. Chem. Soc.*, 1990, **112**, 4911.

31. D. J. Cardin, M. F. Lappert and C. L. Raston, *Chemistry of Organo-Zirconium and -Hafnium Compounds*, Ellis Horwood Ltd., West Sussex, England, 1986.

32. R. F. Jordan, *Adv. Organomet. Chem.*, 1991, **32**, 325.

33. J. C. Green, M. L. H. Green and C. K. Prout, *J. Chem. Soc., Chem. Commun.*, 1972, 421.

34. J. W. Lauher and R. Hoffmann, *J. Am. Chem. Soc.*, 1976, **98**, 1729.

35. L. Zhu and N. M. Kostic, *J. Organomet. Chem.*, 1987, **335**, 395.

36. R. F. Jordan, W. E. Dasher and S. F. Echols, *J. Am. Chem. Soc.*, 1986, **108**, 1718.

37. R. F. Jordan, C. S. Bajgur, R. Willet and B. Scott, *J. Am. Chem. Soc.*, 1986, **108**, 7410.

38. R. F. Jordan, R. E. LaPointe, C. S. Bajgur, S. F. Echols and R. Willet, *J. Am. Chem. Soc.*, 1987, **109**, ~~7410.~~ 4111

39. S. L. Borkowsky, R. F. Jordan, and G. D. Hinch, *Organometallics*, 1991, **10**, 1268.

40. R. F. Jordan, P. K. Bradley, N. C. Baezinger and R. E. LaPointe, *J. Am. Chem. Soc.*, 1990, **112**, 1289.

41. M. Bochmann and L. M. Wilson, *J. Chem. Soc., Chem. Commun.*, 1986, 1610.

42. G. G. Hlatky, H. W. Turner and R. R. Eckman, *J. Am. Chem. Soc.*, 1989, **111**, 2728.

43. M. Bochmann, A. J. Jaggar and J. C. Nicholls, *Angew. Chem., Int. Ed. Engl.*, 1990, **29**, 780.

44. M. Bochmann and A. J. Jaggar, *J. Organomet. Chem.*, 1992, **424**, C5.

45. X. Yang, C. L. Stern and Tobin J. Marks, *J. Am. Chem. Soc.*, 1991, **113**, 3623.

46. M. R. Kesti, G. W. Coates and R. M. Waymouth, *J. Am. Chem. Soc.*, 1992, **114**, 9679.

47. J. C. W. Chien, W. M. Tsai and M. D. Rausch, *J. Am. Chem. Soc.*, 1991, **113**, 8570.

48. K. L. Rinehart and R. J. Curby, *J. Am. Chem. Soc.*, 1957, **79**, 3290.

49. A. Luttringhaus and W. Kullick, *Angew. Chem.*, 1958, **70**, 438; A. Luttringhaus and W. Kullick, *Makromol. Chem.*, 1961, **44-46**, 669.

50. K. L. Rinehart, R. J. Curby, D. H. Gustafson, K. G. Harrison, R. E. Bozak and D. E. Bublitz, *J. Am. Chem. Soc.*, 1962, **84**, 3263.

51. T. J. Katz and N. Acton, *Tetrahedron Lett.*, 1970, **28**, 2497.

52. M. Hillman and A. J. Weiss, *J. Organomet. Chem.*, 1972, **42**, 123.

53. J. A. Smith, J. von Seyerl, G. Huttner and H. H. Brintzinger, *J. Organomet. Chem.*, 1979, **173**, 175.

54. W. Mengele, J. Diebold, C. Troll, W. Roll and H. H. Brintzinger, *Organometallics*, 1993, **12**, 1931.

55. J. A. Smith and H. H. Brintzinger, *J. Organomet. Chem.*, 1981, **218**, 159.

56. F. Wochner and H. H. Brintzinger, *J. Organomet. Chem.*, 1986, **309**, 65.

57. H. Schnutenhaus and H. H. Brintzinger, *Angew. Chem., Int. Ed. Engl.*, 1979, **18**, 777.

58. F. R. W. P. Wild, L. Zsolnai, G. Huttner and H. H. Brintzinger, *J. Organomet. Chem.*, 1982, **232**, 233.

59. F. R. W. P. Wild, M. Wasiuionek, G. Huttner and H. H. Brintzinger, *J. Organomet. Chem.*, 1985, **288**, 63.

60. J. A. Ewen, L. Haspeslagh, J. L. Atwood and H. Zhang, *J. Am. Chem. Soc.*, 1987, **109**, 6544.

61. S. Collins, B. A. Kuntz, N. J. Taylor and D. G. Ward, *J. Organomet. Chem.*, 1988, **342**, 21.

62. R. L. Halterman, *Chem. Rev.*, 1992, **92**, 965.

63. J. A. Ewen, *J. Am. Chem. Soc.*, 1984, **106**, 6355.

64. V. Venditto, G. Guerra, P. Corradini and R. Fusco, *Polymer*, 1990, **31**, 530.

65. W. Kaminsky, K. Kulper, H. H. Brintzinger and F. R. W. P. Wild, *Angew. Chem., Int. Ed. Engl.*, 1985, **24**, 507.

66. J. A. Ewen, R. A. Jones, A. Razavi and J. D. Ferrara, *J. Am. Chem. Soc.*, 1988, **110**, 6255.

67. J. A. Ewen, L. Haspeslagh, M. J. Elder, J. L. Atwood, H. Zhang and H. N. Cheng, in *Transition Metals and Organometallics as Catalysts for Olefin Polymerization*, W. Kaminsky and H. Sinn, Eds., Springer, New York, 1988.

68. W. Roll, H. H. Brintzinger, B. Rieger and R. Zolk, *Angew. Chem., Int. Ed. Engl.*, 1990, **29**, 279.

69. W. Spalek , M. Antberg, V. Dolle, R. Klein, J. Rohrmann and A. Winter, *New J. Chem.*, 1990, **14**, 499.

70. J. A. Ewen, M. J. Elder, R. L. Jones, L. Haspeslagh, J. L. Atwood, S. G. Bott and K. Robinson, *Makromol. Chem., Makromol. Symp.*, 1991, **48/49**, 253.

71. S. Collins, W. J. Gauthier, D. A. Holden, B. A. Kuntz, N. J. Taylor and D. G. Ward, *Organometallics*, 1991, **10**, 2061.

72. W. Spalek , M. Antberg, J. Rohrmann, A. Winter, B. Bachmann, P. Kiprof, J. Behm and W. A. Herrmann, *Angew. Chem., Int. Ed. Engl.*, 1992, **31**, 1347.

73. W. Kaminsky, R. Engehausen, K. Zoumis, W. Spalek and J. Rohrmann, *Makromol. Chem.*, 1992, **193**, 1643.

74. I. M. Lee, W. J. Gauthier, J. M. Ball, B. Iyengar and S. Collins, *Organometallics*, 1992, **11**, 2115.

75. K. Hortmann and H. H. Brintzinger, *New J. Chem.*, 1992, **16**, 51.

76. J. R. Hart and R. K. Rappe, *J. Am. Chem. Soc.*, 1993, **115**, 6159.

77. H. Kawamura-Kuribayashi, N. Koga and K. Morokuma, *J. Am. Chem. Soc.*, 1992, **114**, 8687.

78. M. H. Prosenc, C. Janiak and H. H. Brintzinger, *Organometallics*, 1992, **11**, 4036.

79. C. Janiak, *J. Organomet. Chem.*, 1993, **452**, 63.

80. H. Krauledat and H. H. Brintzinger, *Angew. Chem., Int. Ed. Engl.*, 1990, **29**, 1412.

81. W. E. Piers and J. E. Bercaw, *J. Am. Chem. Soc.*, 1990, **112**, 9406.

82. M. Brookhart and M. L. H. Green, *J. Organomet. Chem.*, 1983, **250**, 395.

83. M. Brookhart, M. L. H. Green and L. L. Wong, *Prog. Inorg. Chem.*, 1988, **36**, 1.

84. P. Pino, P. Cioni and J. Wei, *J. Am. Chem. Soc.*, 1987, **109**, 6189.

85. G. W. Coates and R. M. Waymouth, *J. Am. Chem. Soc.*, 1991, **113**, 6270.

86. G. W. Coates and R. M. Waymouth, *J. Mol. Catal.*, 1992, **76**, 189.

87. R. L. Halterman and T. M. Ramsey, *Organometallics*, 1993, **12**, 2879.

88. R. M. Waymouth and P. Pino, *J. Am. Chem. Soc.*, 1990, **112**, 4911.

89. Y. Hong, B. A. Kuntz and S. Collins, *Organometallics*, 1993, **12**, 964.

90. K. L. Gibis, G. Helmchen, G. Huttner and L. Zsolnai, *J. Organomet. Chem.*, 1993, **445**, 181.

91. C. A. Willoughby and S. L. Buchwald, *J. Am. Chem. Soc.*, 1992, **114**, 7562.

92. J. P. Morken, M. T. Didiuk and A. H. Hoveyda, *J. Am. Chem. Soc.*, 1993, **115**, 6997.

93. J. P. Banovetz, K. M. Stein and R. M. Waymouth, *Organometallics*, 1991, **10**, 3430.

94. Z. Chen and R. L. Halterman, *J. Am. Chem. Soc.*, 1992, **114**, 2276.

95. P. B. Mackenzie, R. J. Coots and R. H. Grubbs, *Organometallics*, 1989, **8**, 8.

96. J. W. Park, L. M. Henling, W. P. Schaefer and R. H. Grubbs, *Organometallics*, 1991, **10**, 171.

97. J. M. Manriquez, D. R. McAlister, R. D. Sanner and J. E. Bercaw, *J. Am. Chem. Soc.*, 1978, **100**, 2716.

98. C. C. Cummins, G. D. Van Duyne, C. P. Schaller and P. T. Wolczanski, *Organometallics*, 1991, **10**, 164.

99. R. D. Sanner, D. M. Duggan, T. C. McKenzie, R. E. Marsh and J. E. Bercaw, *J. Am. Chem. Soc.*, 1976, **98**, 8358; J. M. Manriquez, D. R. McAlister, E. Rosenberg, A. M. Shiller, K. L. Willimson, S. I. Chan and J. E. Bercaw, *J. Am. Chem. Soc.*, 1978, **100**, 3078; D. M. Roddick, M. D. Fryzuk, P. F. Siedler, G. L. Hillhouse and J. E. Bercaw, *Organometallics*, 1985, **4**, 97.

100. M. D. Fryzuk, T. S. Haddad, M. Mylvaganam, D. H. McConville and S. J. Rettig, *J. Am. Chem. Soc.*, 1993, **115**, 2782.

101. R. M. Waymouth, B. D. Santarsiero and R. H. Grubbs, *J. Am. Chem. Soc.*, 1984, **106**, 4050.

102. G. Erker, M. Albrecht, C. Kruger, S. Werner, P. Binger and F. Langhauser, *Organometallics*, 1992, **11**, 3517.

103. G. Erker, M. Albrecht, C. Kruger and S. Werner, *J. Am. Chem. Soc.*, 1992, **114**, 8531.

104. R. Gleiter, I. Hyla-Krispin, S. Nui and G. Erker, *Angew. Chem., Int. Ed. Engl.*, 1993, **92**, 754.

105. G. Erker, R. Noe, C. Kruger and S. Werner, *Organometallics*, 1992, **11**, 4174.

106. R. D. Adams, *Polyhedron*, 1988, **7**, 2251.

107. J. Jenck, P. Kalk, E. Pinelli, M. Siani and A. Thorez, *J. Chem. Soc., Chem. Commun.*, 1988, 1428.

108. P. Kalck, *Polyhedron*, 1988, **7**, 2441.

109. C. McKenzie and R. Robson, *J. Chem. Soc., Chem. Commun.*, 1988, 112.

110. Y. Rault, R. Choukron, D. Gervas and G. Erker, *J. Organomet. Chem.*, 1990, **399**, C1.

111. M. A. Esteruelas, M. P. Garcia, A. M. Lopez and L. A. Oro, *Organometallics*, 1991, **10**, 127.

112. M. Hostetler and R. G. Bergman, *J. Am. Chem. Soc.*, 1990, **112**, 8621.

113. P. M. Maitlis, *Acc. Chem. Res.*, 1978, **11**, 301

114. R. A. Sanchez-Delgado, A. Andriollo, J. Puga and G. Martin, *Inorg. Chem.*, 1987, **26**, 1867.

115. M. D. Rausch, W. C. Spink, B. G. Conway, R. D. Rogers and J. L. Atwood, *J. Organomet. Chem.*, 1990, **383**, 227.

116. T. Bitterwolf, *J. Organomet. Chem.*, 1986, **312**, 197.

117. J. F. Buzinkai and R. R. Schrock, *Organometallics*, 1987, **6**, 1447.

118. D. Stern, M. Sabat and T. J. Marks, *J. Am. Chem. Soc.*, 1990, **112**, 9558.

119. H. Atzkern, B. Huber, F. H. Kohler, G. Muller and R. Muller, *Organometallics*, 1991, **10**, 238.

120. U. Siemling and P. Jutzi, *Chem. Ber.*, 1992, **125**, 31.

121. H. Werner, M. Treiber, A. Nessel, F. Lippert, P. Betz and C. Kruger, *Chem. Ber.*, 1992, **125**, 337.

122. K. Claus and H. Bestian, *Justus Liebigs Ann. Chem.*, 1962, **654**, 8.

123. G. W. Watt, L. J. Baye, F. O. Drummand, *J. Am. Chem. Soc.*, 1966, **88**, 1138.

124. J. J. Salzmann and P. Mosimann, *Helv. Chem. Acta.*, 1967, **50**, 1831.

125. H. H. Brintzinger and J. E. Bercaw, *J. Am. Chem. Soc.*, 1970, **92**, 6182.

126. A. Davison and S. S. Wreford, *J. Am. Chem. Soc.*, 1974, **96**, 3017.

127. L. J. Guggenberger and F. N. Tebbe, *J. Am. Chem. Soc.*, 1973, **95**, 7870.

128. L. J. Guggenberger and F. N. Tebbe, *J. Am. Chem. Soc.*, 1976, **98**, 4137.

129. G. L. Olthof, *J. Organomet. Chem.*, 1977, **128**, 367.

130. S. I. Troyanov, H. Antropiusova and K. Mach, *J. Organomet. Chem.*, 1992, **427**, 49.

131. A. Cano, T. Cuenca, G. Rodriguez, P. Royo, C. Cardin and D. J. Wilcock, *J. Organomet. Chem.*, 1993, **447**, 51.

132. T. Wohle and U. Thewalt, *J. Organomet. Chem.*, 1993, **447**, 45.

133. T. Wohle and U. Thewalt, *J. Organomet. Chem.*, 1993, **456**, C21.

134. W. D. Spink and M. D. Rausch, *J. Organomet. Chem.*, 1986, **308**, C1.

135. L. M. Alvaro, T. Cuenca, J. C. Flores, P. Royo, M. A. Pellinghelli and A. Tiripicchio, *Organometallics*, 1992, **11**, 3301.

136. T. V. Ashworth, T. Cuenca, E. Herdtweck and W. A. Herrmann, *Angew. Chem., Int. Ed. Engl.*, 1986, **25**, 289.

137. W. Wielstra, S. Gambarotta, A. Meetsma and A. L. Spek, *Organometallics*, 1989, **8**, 2948.

138. S. Gambarotta and M. Y. Chiang, *Organometallics*, 1987, **6**, 897.

139. W. A. Herrmann, B. Menjon and E. Herdtweck, *Organometallics*, 1991, **10**, 2134.

140. T. Cuenca, R. Gomez, P. Gomez-Sal, G. M. Rodriguez and P. Royo, *Organometallics*, 1992, **11**, 1229.

141. W. Wielstra, S. Gambarotta, A. Meetsma, J. L. de Boer, *Organometallics*, 1989, **8**, 250.

142. W. Wielstra, A. Meetsma, S. Gambarotta and S. Kahn, *Organometallics*, 1990, **9**, 876.

143. W. Wielstra, S. Gambarotta, A. L. Spek and W. J. J. Smeets, *Organometallics*, 1990, **9**, 2142.

144. W. Wielstra, R. Duchateau, S. Gambarotta, C. Benismon and E. Gabe, *J. Organomet. Chem.*, 1991, **418**, 183.

145. C. J. Curtis and R. C. Haltiwanger, *Organometallics*, 1991, **10**, 3220.

146. P. Scott, U. Rief, J. Diebold and H. H. Brintzinger, *Organometallics*, 1993, **12**, 3094.

147. K. Qiau, R. D. Fischer, G. Paulicci, P. Traldi and E. Celon, *Organometallics*, 1990, **9**, 1361; T. Akhnoukh, J. Muller, K. Qiau, X. F. Li and R. D. Fischer, *J. Organomet. Chem.*, 1990, **408**, 47; K. Qiau, R. D. Fischer, G. Paulicci, *J. Organomet. Chem.*, 1993, **456**, 185.

148. K. P. Reddy and J. L. Petersen, *Organometallics*, 1989, **8**, 547.

149. M. Berry, N. J. Cooper, M. L. H. Green and S. J. Simpson, *J. Chem. Soc., Dalton Trans.*, 1980, 29.

150. K. P. Reddy and J. L. Petersen, *Organometallics*, 1989, **8**, 2107.

151. J. Cacciola, K. P. Reddy and J. L. Petersen, *Organometallics*, 1992, **11**, 665.

152. S. Ciruelos, T. Cuenca, J. C. Flores, R. Gomez, P. Gomez-Sal and P. Royo, *Organometallics*, 1993, **12**, 944.

153. R. Gomez, T. Cuenca, P. Royo, W. A. Herrmann and E. Herdtweck, *J. Organomet. Chem.*, 1990, **382**, 103.

154. R. Gomez, personal communication.

155. I. E. Nifant'ev, K. A. Butakov, Z. G. Aliev and I. F. Urazovskii, *Organomet. Chem. USSR*, 1991, **4**, 622.

156. R. D. Gorsich, *J. Am. Chem. Soc.*, 1958, **80**, 4744.

157. I. E. Nifant'ev, M. V. Borsov, A. V. Churakov, S. G. Mkoyan and L. O. Atovmyan, *Organometallics*, 1992, **11**, 3942.

158. H. Werner, D. Schneider and M. Schulz, *Chem. Ber.*, 1992, **125**, 1017.

CHAPTER TWO

ansa-Bridged Mononuclear Compounds of Zirconium and Hafnium

2.1 Introduction

The aim of this project was to synthesize novel binuclear complexes in which group 4 metallocenes are joined by an *ansa* bridge. The preceding chapter described how binuclear group 4 metallocene complexes bridged by symmetrical *ansa*-bis(cyclopentadienyl) ligands have recently been prepared. However, binuclear group 4 metallocene compounds with unsymmetrical bridging ligands, resulting in different ligand environments at each metal centre and/or chiral molecular structures, have ~~been~~ not been reported. The main objective of this project was the discovery of new synthetic routes to both homo- and hetero-binuclear, unsymmetrical and chiral compounds in which group 4 metallocenes are joined by an *ansa*-bridge.

In 1989, Petersen reported the reaction between lithium salts of *ansa*-bridged bis(cyclopentadienyl) ligands $[\{X(C_5H_4)_2\}Li_2]$ ($X = CH_2$, $SiMe_2$) with $[CpZrCl_3 \cdot 2THF]$ or $[Cp^*ZrCl_3]$ to give the symmetrical, homobinuclear zirconocene derivatives $[\{X(\eta^5\text{-}C_5H_4)_2\}\{(\eta^5\text{-}C_5R_5)ZrCl_2\}_2]$ ($R = H$, CH_3).[1] It seems highly likely that such a reaction may proceed *via* a **mononuclear intermediate** (Figure 2.1.1).

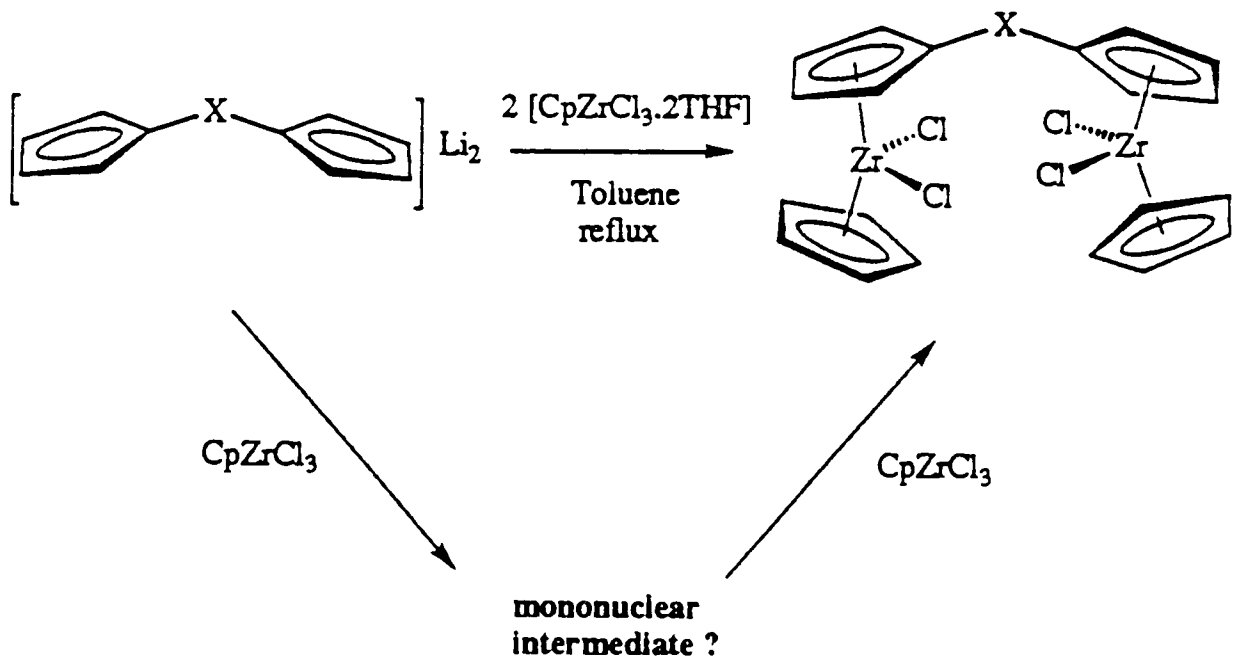

Figure 2.1.1. Reaction of $[\{X(C_5H_4)_2\}Li_2]$ with two equivalents of $[CpZrCl_3 \cdot 2THF]$

If such an intermediate could be isolated, for example by treating the dilithium salt of the ligand with one equivalent of [$CpZrCl_3 \cdot 2THF$], it may be possible to synthesize **heterobinuclear** complexes by treating the intermediate with a second, different transition metal halide complex. A synthetic route of this type to binuclear complexes would be especially useful since a great range of dilithium salts of *ansa*-bridging ligands have already been prepared for the synthesis of mononuclear *ansa*-metallocene derivatives, as described in the previous chapter.

It was decided to study the reactions of ligands of the type [{$Cp'CR_2Cp''$}Li_2], where Cp' is a cyclopentadienyl ligand and Cp'' is a cyclopentadienyl, indenyl or fluorenyl ligand. Ligands of this type are readily prepared by the reaction of a fulvene derivative with a cyclopentadienide, indenide or fluorenide salt.[2-10] This is a very versatile synthesis, since a large range of substituted fulvene derivatives may be prepared by the condensation reaction between cyclopentadiene derivatives and ketones,[11, 12] and *via* several other reactions.[12, 13] With appropriate substitution of the bridging carbon atom, or of the rings, chiral[4, 5, 10] and prochiral[3, 6-9] ligands may be prepared. The first ligand chosen for study was [{$Me_2C(C_5H_4)(C_9H_6)$}Li_2], because binuclear complexes bridged by this ligand would be chiral, and the two metals would experience different ligand environments.

2.2 Synthesis of [{$Me_2C(\eta^5\text{-}C_5H_4)(\eta^2\text{-}C_9H_6)$}$M(\eta^5\text{-}C_5H_5)Cl$]

2.2.1 Preparation of [{$Me_2C(C_5H_4)(C_9H_6)$}Li_2]

Figure 2.2.1. shows the preparation of the ligand [{$Me_2C(C_5H_4)(C_9H_6)$}Li_2] from 6,6-dimethylfulvene and lithium indenide. The 6,6-dimethylfulvene was prepared by a modification of a literature method, in which the condensation reaction between cyclopentadiene monomer and acetone is catalysed by pyrrolidine.[11] In the literature preparation, a molar ratio of acetone to cyclopentadiene to pyrrolidine of 2 : 5 : 3 was

used, and the fulvene required purification by column chromatography. Since the stoichiometry of the condensation reaction between cyclopentadiene monomer and acetone is one to one, a preparation using an acetone : cyclopentadiene : pyrrolidine molar ratio of 1 : 1 : 1.5 was attempted. This reaction provided pure 6,6-dimethylfulvene in high yield, without the need for chromatography.

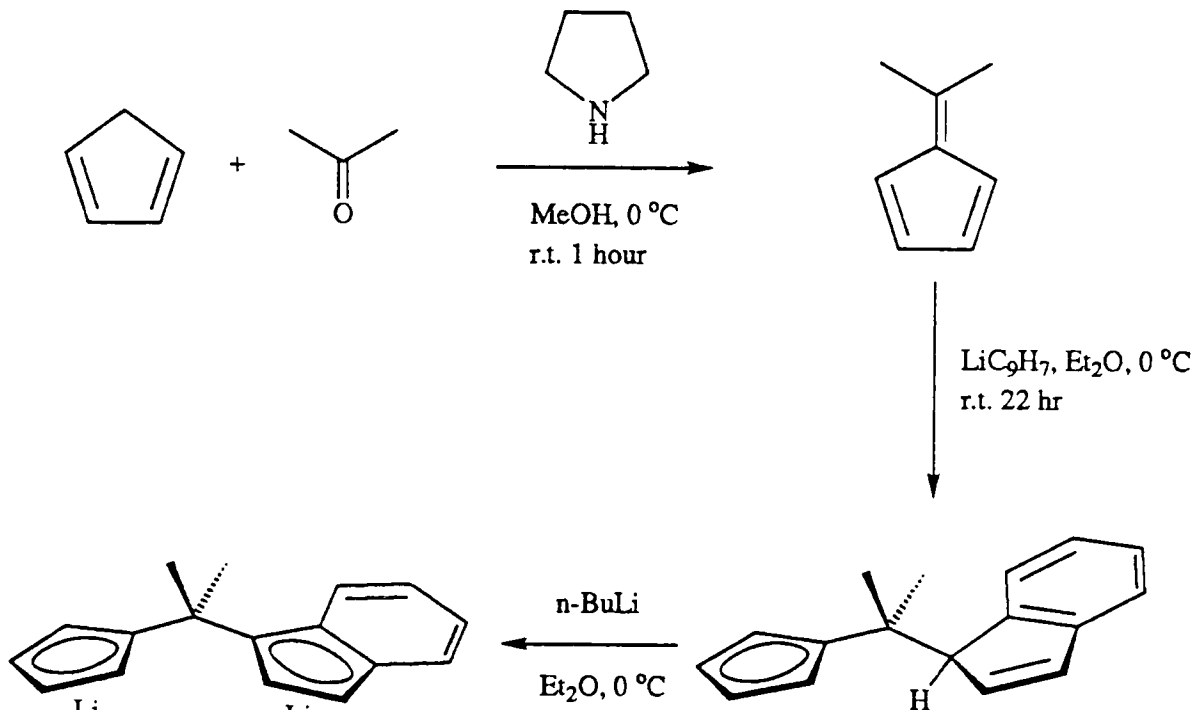

Figure 2.2.1. Preparation of $[\{Me_2C(C_5H_4)(C_9H_6)\}Li_2]$

The synthesis of $[\{Me_2C(C_5H_4)(C_9H_6)\}Li_2]$ from 6,6-dimethylfulvene and lithium indenide has been previously reported, together with the preparation of the mononuclear *ansa*-metallocenes $[\{Me_2C(\eta^5\text{-}C_5H_4)(\eta^5\text{-}C_9H_6)\}MCl_2]$ (M = Ti, Zr, Hf).[3, 14] In these syntheses, the initially formed monolithium salt of the ligand was hydrolysed, and the neutral ligand was purified by column chromatography. Subsequent deprotonation using two equivalents of n-butyllithium gave the dilithium salt of the ligand. It was decided to try to improve this ligand synthesis by eliminating the hydrolysis and chromatography steps.

A diethyl ether solution of 6,6-dimethylfulvene was added dropwise to a diethyl ether solution of lithium indenide at 0 °C, then stirred at room temperature overnight.

The monolithium salt [$Li(C_5H_4)CMe_2(C_9H_7)$] was isolated as pale orange crystals by the addition of petroleum ether (bp. 40-60 °C), followed by cooling to -80 °C. Treatment of a diethyl ether solution of [$Li(C_5H_4)CMe_2(C_9H_7)$] with n-butyllithium provided a convenient synthesis of the dilithium salt [$\{Me_2C(C_5H_4)(C_9H_6)\}Li_2\{n(Et_2O)\}$] which precipated from the solution as a pale yellow, pyrophoric solid.

It was found that the monolithium salt need not be isolated. Instead, the addition of n-butyllithium to the diethyl ether solution of [$Li(C_5H_4)CMe_2(C_9H_7)$] formed *in situ*, affords the pure dilithium salt in high yield (89 %). This improved preparation makes use of the much lower solubility of the dilithium salt in diethyl ether, compared with the monolithium salts [$Li(C_9H_7)$] and [$Li(C_5H_4)CMe_2(C_9H_7)$]. The dilithium salt, [$\{Me_2C(C_5H_4)(C_9H_6)\}Li_2\{n(Et_2O)\}$], which was isolated by filtration, washed with diethyl ether and dried *in vacuo* to constant weight, was found to contain solvating diethyl ether. The amount of diethyl ether solvate (as determined by ^1H NMR) varied between 0.6 and 0.8 equivalents in subsequent preparations.

2.2.2 Synthesis of [$\{Me_2C(\eta^5\text{-}C_5H_4)(\eta^2\text{-}C_9H_6)\}Zr(\eta^5\text{-}C_5H_5)Cl$]

It was decided to study the reaction of [$\{Me_2C(C_5H_4)(C_9H_6)\}Li_2$] with one equivalent of [$CpZrCl_3\cdot DME$]. The pale yellow powder [$\{Me_2C(C_5H_4)(C_9H_6)\}Li_2\{0.6(Et_2O)\}$] and the white powder [$(\eta^5\text{-}C_5H_5)ZrCl_3\cdot DME$] were weighed into a Schlenk tube. When toluene was added at room temperature, an immediate colour change was observed, resulting in a deep red coloured reaction mixture. After stirring for a further 16 hours at room temperature, the red solution was filtered from a pale solid residue, presumably lithium chloride.

The clear, deep red coloured filtrate was then concentrated under reduced pressure and cooled to -20 °C. After several days, red crystals separated from the solution. These were characterised as the novel, *ansa*-bridged mononuclear compound

[{$Me_2C(\eta^5\text{-}C_5H_4)(\eta^2\text{-}C_9H_6)$}$Zr(\eta^5\text{-}C_5H_5)Cl$]. Several crops of crystals were obtained, resulting in an overall yield of 64 %.

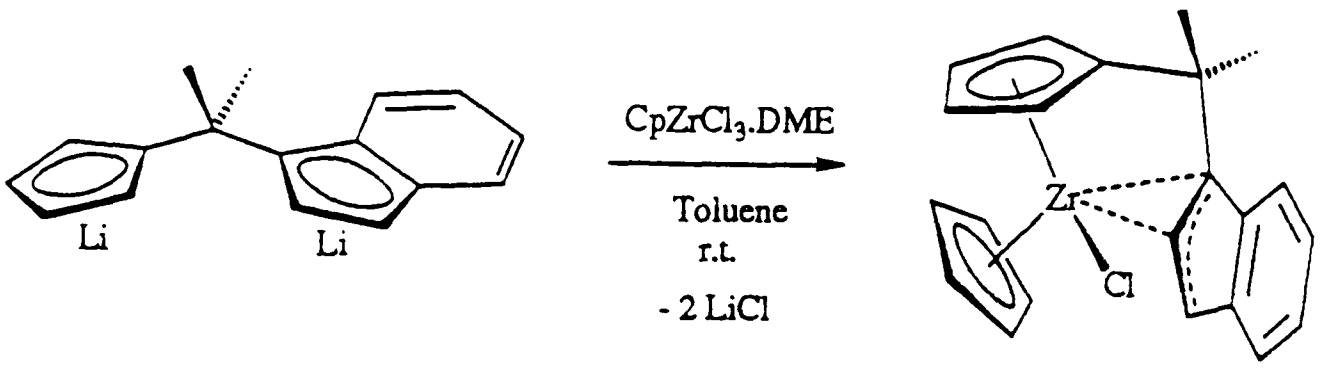

Figure 2.2.2. Synthesis of [{$Me_2C(\eta^5\text{-}C_5H_4)(\eta^2\text{-}C_9H_6)$}$Zr(\eta^5\text{-}C_5H_5)Cl$] (**1**)

It was later found that if the addition of toluene to the reactants was performed at low temperature, the yield of pure product was improved. When toluene at -78 °C was added to a stirred mixture of [{$Me_2C(C_5H_4)(C_9H_6)$}Li_2{$0.75(Et_2O)$}] and [(η^5-C_5H_5)$ZrCl_3$·DME], also at -78 °C, an orange coloured mixture was obtained. When this was allowed to warm to room temperature, it slowly darkened to a deep red colour. By following the same procedure as before, the pure product was obtained as red crystals in 75 % yield.

2.2.3 Characterisation of [{$Me_2C(\eta^5\text{-}C_5H_4)(\eta^2\text{-}C_9H_6)$}$Zr(\eta^5\text{-}C_5H_5)Cl$]

The red crystalline solid [{$Me_2C(\eta^5\text{-}C_5H_4)(\eta^2\text{-}C_9H_6)$}$Zr(\eta^5\text{-}C_5H_5)Cl$] (**1**) was initially characterised by elemental analysis, mass spectroscopy and ^1H and ^{13}C NMR studies. The elemental analysis was consistent with the molecular formula $C_{22}H_{21}ClZr$, whilst electron impact mass spectroscopy showed a molecular ion (*m/z* = 410, M^+) consistent with a mononuclear complex.

Since early attempts at growing crystals suitable for an X-ray diffraction structure determination were not successful, it was decided to try to determine the molecular structure of **1** by NMR methods. The overall molecular geometry was

determined by ^1H NMR studies, including NOESY experiments, while the unusual η^2-coordination of the indenyl group to the metal was proposed on the basis of ^{13}C NMR experiments.

Compound **1** is air and moisture sensitive, readily soluble in benzene, toluene and THF, but decomposes slowly in dichloromethane. The ^1H NMR spectra of **1** measured in both C_6D_6 and d^8-THF were very similar, though the indenyl and cyclopentadienyl signals were better separated in d^8-THF, which was thus chosen as the solvent for the NMR studies aimed at elucidating the molecular structure of **1**. The ^1H NMR spectrum of **1**, in d^8-THF at room temperature, is shown in Figure 2.2.3.

The ^1H NMR spectrum of **1** is consistent with a molecular formula [{$Me_2C(\eta^5$-$C_5H_4)(C_9H_6)$}$Zr(\eta^5$-$C_5H_5)Cl$] in which the indenyl group is coordinated, in some way, to the zirconium atom. All of the ^1H NMR signals had an intergrated intensity of 1H, except the C_5H_5 signal **m** (5H) and the CH_3 signals **g** and **h** (each 3H). Selective ^1H decoupling experiments and a COSY experiment allowed assignment of **a** and **b** as the indenyl C_5 ring protons, **c**, **d**, **e** and **f** as the indenyl C_6 ring protons, and **i**, **j**, **k** and **l** as the C_5H_4 protons. Individual assignments of each signal were made on the basis of NOESY experiments.

2.2.3 (i) Overall molecular geometry

The proposed molecular structure is chiral, the molecule in fact posesses **two chiral elements**. Inversion of the configuration at the zirconium atom would result in a diastereomer, as would coordination of the alternative face of the indenyl group to the metal. Thus two possible diastereomers (each a pair of enantiomers) are possible for a molecule of this type. The possible diastereomers of **1** are shown in Figure 2.2.4.

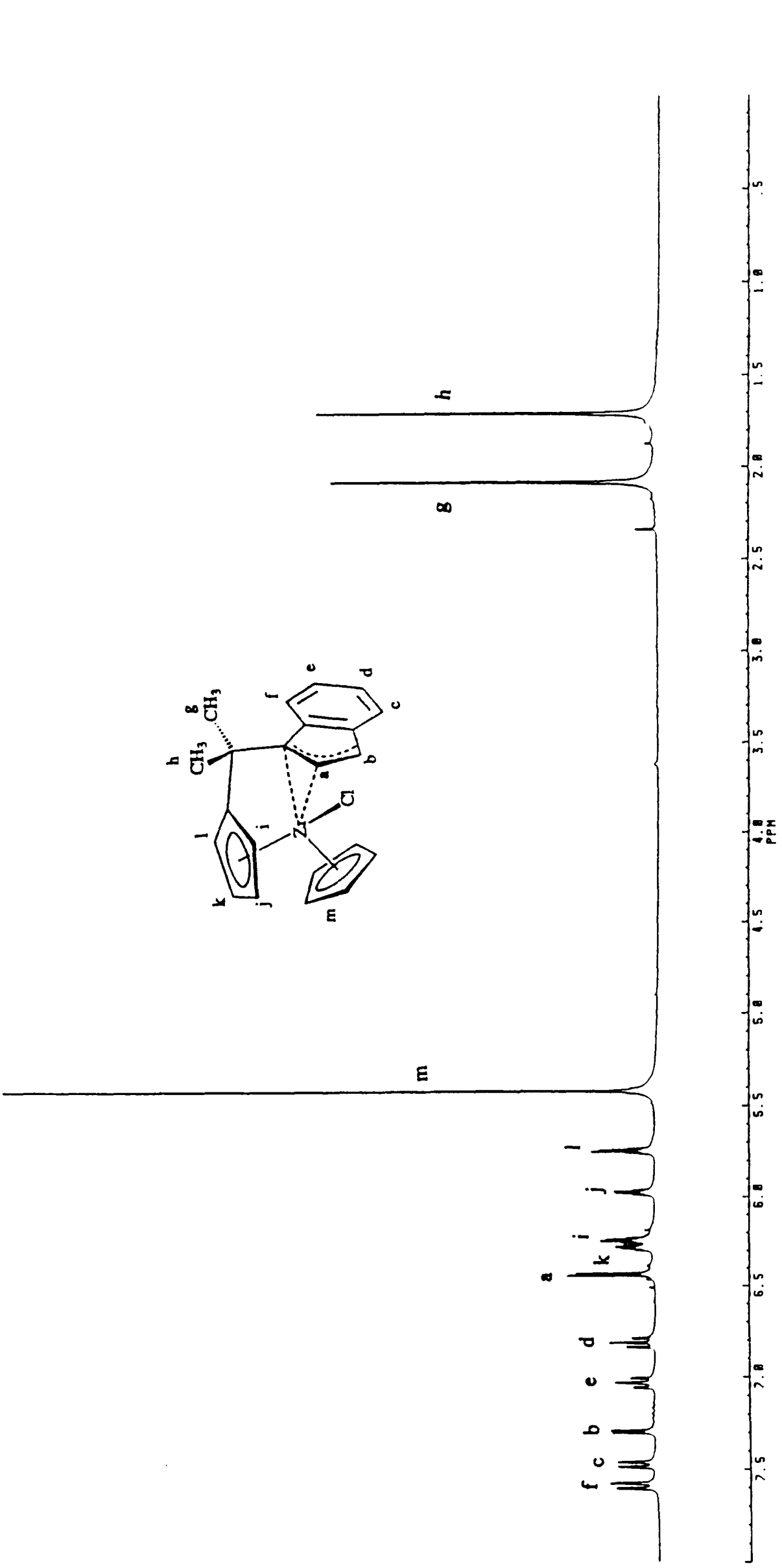

Figure 2.2.3. 300 MHz ^{1}H NMR spectrum of $[\{Me_2C(\eta^5\text{-}C_5H_4)(\eta^2\text{-}C_9H_6)\}Zr(\eta^5\text{-}C_5H_5)Cl]$ (**1**) in d^8-THF at r.t.

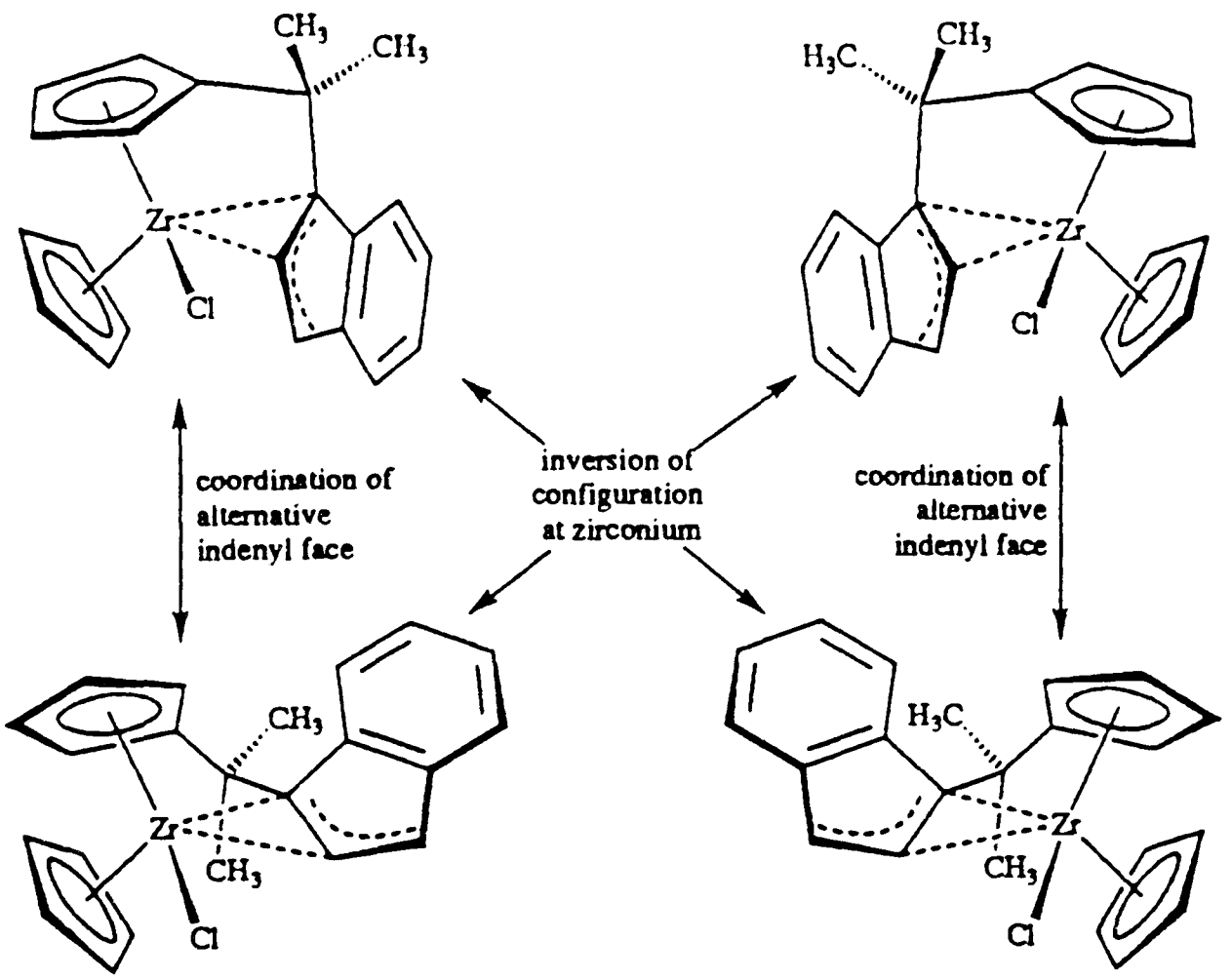

Figure 2.2.4. Possible diastereomers of [{$Me_2C(\eta^5\text{-}C_5H_4)(\eta^2\text{-}C_9H_6)$}$Zr(\eta^5\text{-}C_5H_5)Cl$]

The structures on the left are the enantiomers of those on the right, the top pair of enantiomers are diastereomers of the bottom pair of enantiomers.

The ^1H NMR spectrum of **1** shows that only one diastereomer (pair of enantiomers) is present. In an attempt to determine which diastereomeric structure is adopted, two NOESY experiments were performed. The NOESY experiment is a 2-dimensional NMR experiment in which (in the absence of chemical exchange) the off-diagonal peaks correlate spins which share a dipolar coupling due to the nuclear Overhauser effect.[15-17] The nuclear Overhauser effect (NOE) is an aspect of nuclear relaxation and depends upon dipolar (through-space) magnetic coupling between nuclei. It is revealed when one of the nuclei is irradiated at its resonance frequency and the signal of another nucleus is detected as more or less intense than usual. The interaction is dependent upon the relaxation of the observed nucleus by the irradiated nucleus and is only noticeable over short distances.[15, 16] The 2-dimensional NOESY experiment is based on transient NOE detection, which shows a strong dependence on

internuclear distance, falling off very rapidly as the distance between nuclei is increased, and may thus be used (with care) in the elucidation of molecular structure.[15]

The ^1H NOESY experiment is similar to the ^1H COSY experiment, except that an extra delay and an extra pulse are used. The extra delay is the mixing time (t_m), during which time the NOE builds up. Scalar (through-bond) coupling correlations are strongly reduced by randomly varying the exact length of the mixing time. For small molecules, the mixing time should be approximately equal to the longitudinal relaxation time T_1.

Approximate T_1 values for the protons of compound **1** were determined by the inversion recovery method[15] and ranged from about 0.5 seconds for the methyl protons (**g** and **h**); 2 seconds for **a**, **f**, **i** and **l**; 4 seconds for **d** and **e**; 6 seconds for **b**, **c**, **j** and **k**; and about 10 seconds for the C_5H_5 protons (**m**). Because of this large range of T_1 values, two NOESY experiments were performed. Experiment 1 employed a mixing time of 2 seconds and a recycle delay of 3 seconds, whilst experiment 2 employed a mixing time and recycle delay of 8 seconds each. The resulting NOESY spectra are shown in Figures 2.2.5 and Figure 2.2.6 respectively.

The proposed molecular structure of **1** is shown in Figure 2.2.7, together with the through-space (dipolar) correlations between those protons which do not show through-bond (scalar) coupling. The first NOESY spectrum (Figure 2.2.5) shows that one of the methyl signals (**h**) is correlated with one of the indenyl C_5 ring signals (**a**) and one of the C_5H_4 signals (**i**), whilst the other methyl group (**g**) is correlated with one of the indenyl C_6 ring signals (**f**) and a different C_5H_4 signal (**l**). These correlations are consistent with a **stereorigid molecular structure** without free rotation about the bridging C-C bonds of the *ansa* ligand. They also allow assignment of all of the *ansa* ligand ^1H signals except the C_5H_4 β protons **j** and **k**.

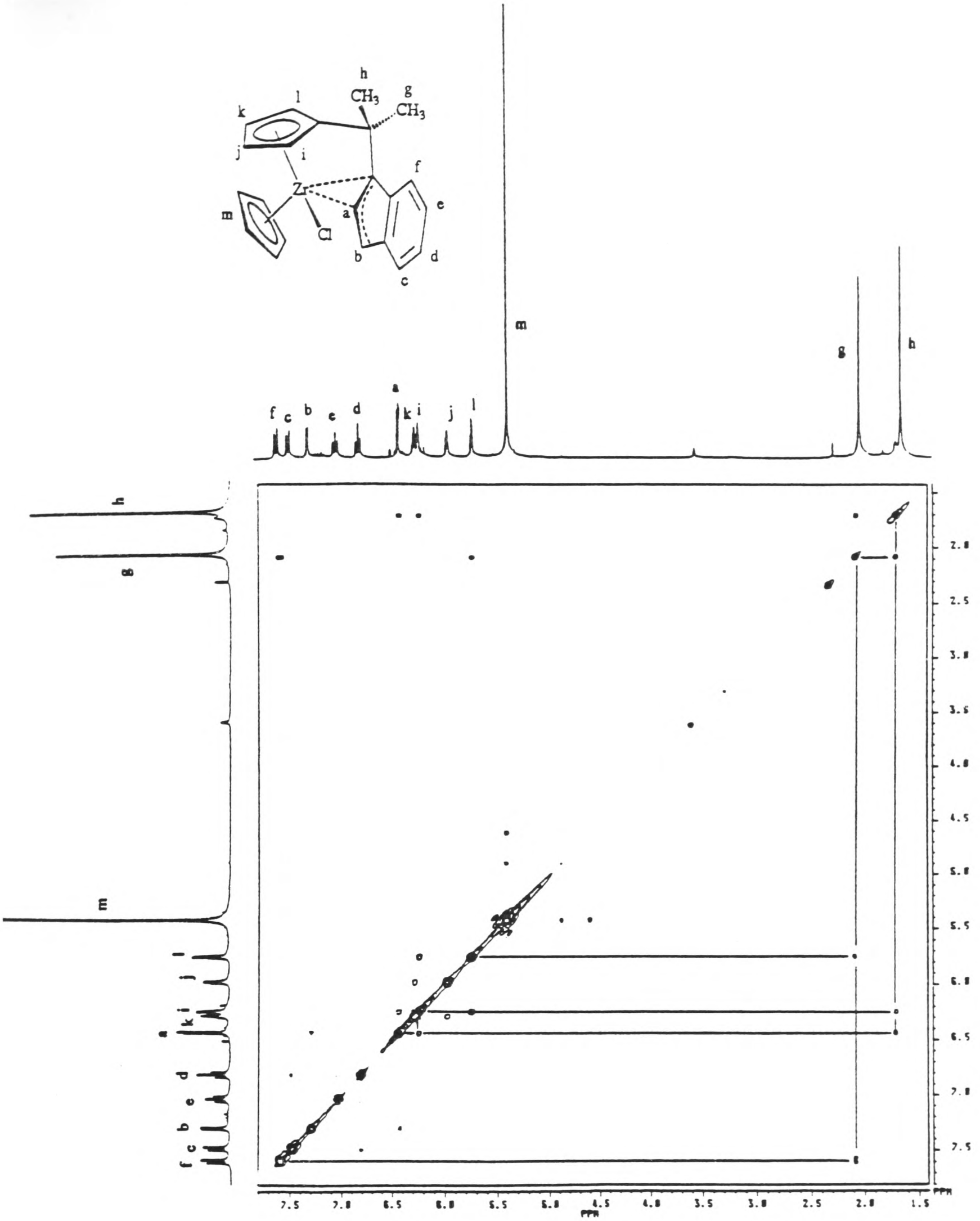

Figure 2.2.5. 300 MHz ^{1}H NOESY spectrum of

[{$Me_2C(\eta^5$-$C_5H_4)(\eta^2$-$C_9H_6)$}$Zr(\eta^5$-$C_5H_5)Cl$] (**1**) in d^8-THF at r.t.

Experiment 1 (t_m = 2 s)

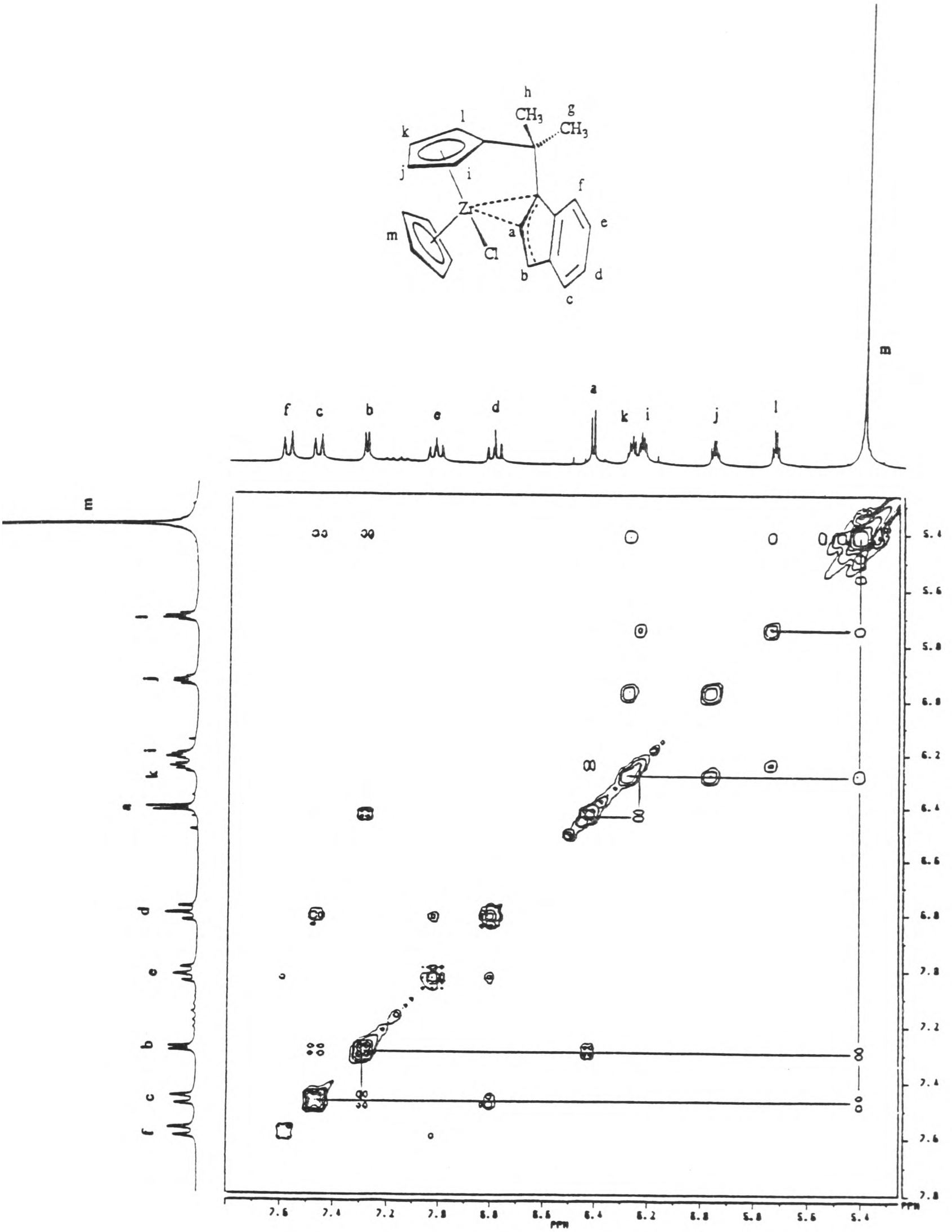

Figure 2.2.6. 300 MHz ^{1}H NOESY spectrum of

[{$Me_2C(\eta^5\text{-}C_5H_4)(\eta^2\text{-}C_9H_6)$}$Zr(\eta^5\text{-}C_5H_5)Cl$] (**1**) in d^8-THF at r.t.

Experiment 2 (t_m = 8 s)

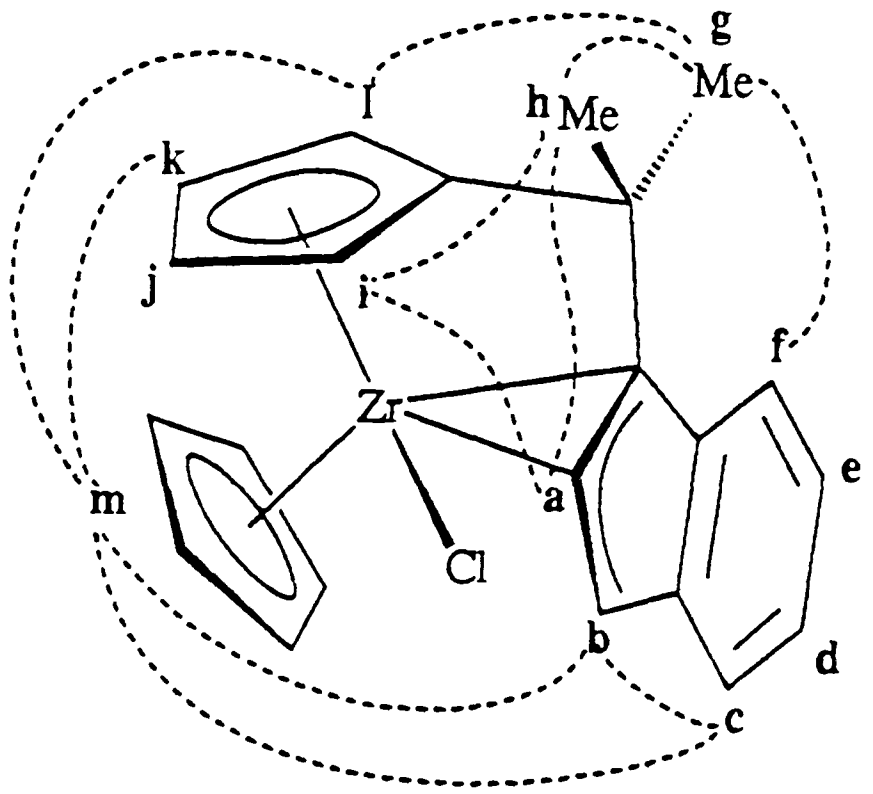

Figure 2.2.7. Proposed molecular structure of **1**, showing the through-space (dipolar) correlations between those protons which do not show through-bond (scalar) coupling.

The second NOESY spectrum (Figure 2.2.6) shows that the C_5H_5 signal (**m**) is correlated with two of the C_5H_4 signals (**k and l**). Proton **l** is correlated with methyl group **g**, which in turn is correlated with the indenyl C_6 ring signal **f**. This suggests that the diastereomer present is that which has the indenyl C_6 ring and the C_5H_5 ring on the same side of the molecule (the top pair of enantiomers in Figure 2.2.4). The correlation of the C_5H_5 signal (**m**) with the indenyl signals **b** and **c** is also consistent with this structure. The NOESY spectrum (Figure 2.2.6) also allows assignment of the C_5H_4 signals **j** and **k** as the β protons next to the α protons **i** and **l** respectively. If the other diastereomeric structure was adopted, correlations of **m** with **a**, **i** and **j** would be expected.

The proposed diastereomeric structure is consistent with the observed chemical shifts of the methyl protons. The methyl protons labelled **g** lie close to the plane of the aromatic C_6-ring of the indenyl ligand, and would thus be expected to experience a deshielding effect due to the induced ring current, and hence appear at a higher

chemical shift than the other methyl group (**h**), which is indeed observed. Also, for the proposed diastereomer the C_5H_5 protons would be expected to experience a shielding ring current effect due to the position of the indenyl ligand, which may account for the lower than usual C_5H_5 chemical shift in the ^1H NMR spectrum of **1**.

2.2.3 (ii) Coordination of indenyl group to the metal

Probably the most interesting feature of the proposed molecular structure of compound **1** is the η^2 coordination of the indenyl group to the metal. This unprecedented mode of coordination of an indenyl ligand to a transition metal was initially proposed on the basis of the ^{13}C NMR spectrum of **1**, shown in Figure 2.2.8.

The assignments of the CH and CH_3 signals were based on a ^{13}C-^1H shift correlation experiment, shown in Figure 2.2.9. The signal **n** was assigned to the ipso carbon of the C_5H_4 ring by comparison with many other *ansa*-bridged complexes. Similarly, the signals **q** and **r** were assigned as the C_6-C_5 ring junction carbons of the indenyl ligand by comparison with other spectra, as was the assignment of signal **o** as the CMe_2 bridging carbon atom.

The ^1H and ^{13}C NMR spectra of **1** are consistent with η^5 coordination of the C_5H_5 and C_5H_4 ligands to zirconium. The zirconocene derivative **1** would normally be expected to adopt a molecular structure with a valence electron count for zirconium of 16 or 18, which would correspond to η^1 or η^3 coordination of the indenyl ligand to the metal. Both of these coordination modes have been previously reported for indenyl ligands.[18]

An unprecedented η^2 coordination mode of the indenyl group to the metal was proposed on the basis of the chemical shifts of the indenyl C_5-ring carbon atoms. The bridge-head quaternary carbon signal C_p lies at 84.4 ppm, compared with 111.7 ppm for C_a and 129.8 ppm for C_b. These chemical shifts are not consistent with those expected for η^1 or η^3 coordination of the indenyl group to the metal.

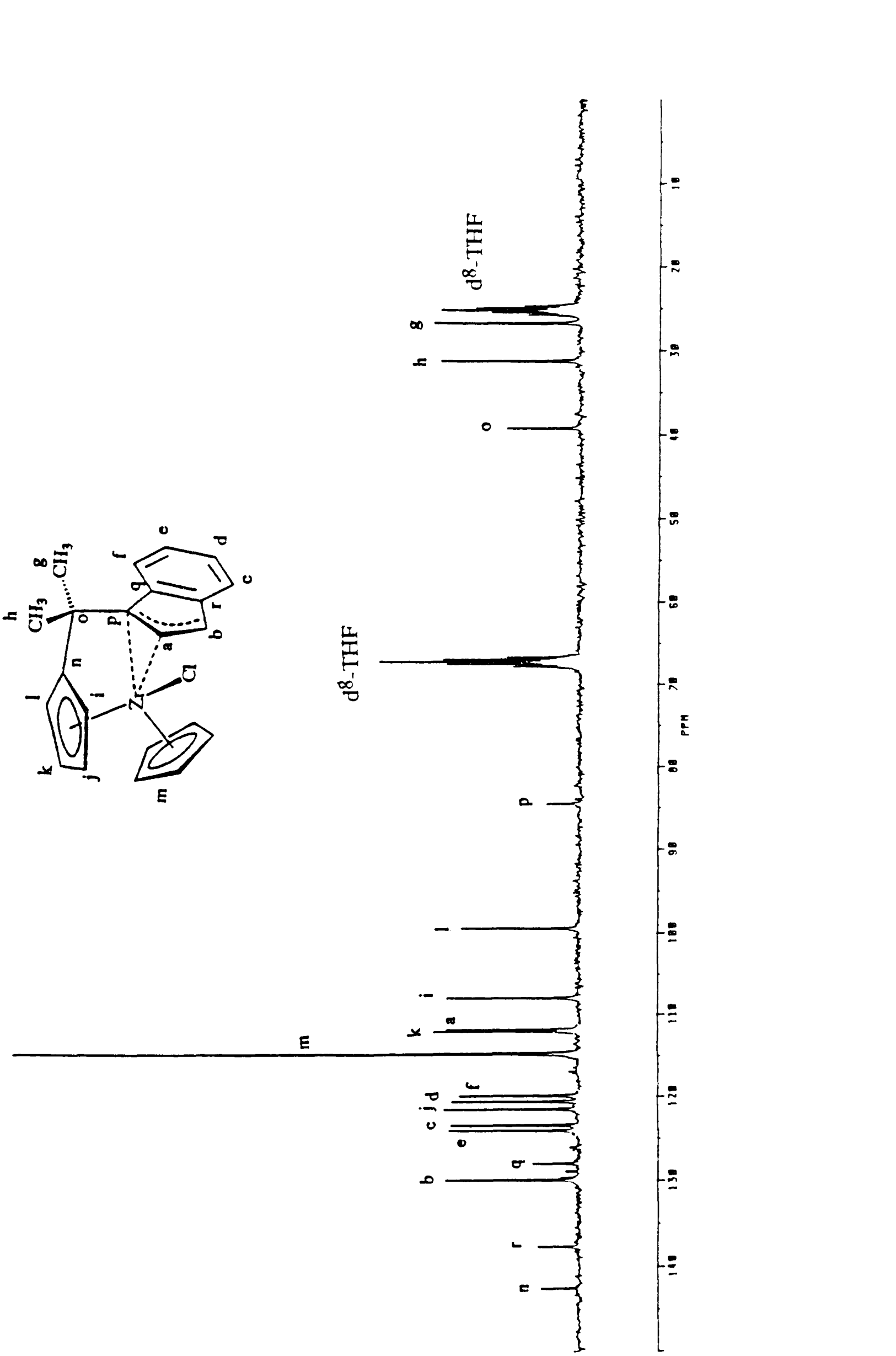

Figure 2.2.8. 75.5 MHz $^{13}C\{^{1}H\}$ NMR spectrum of $[\{Me_2C(\eta^5\text{-}C_5H_4)(\eta^2\text{-}C_9H_6)\}Zr(\eta^5\text{-}C_5H_5)Cl]$ (**1**) in d^8-THF at r.t.

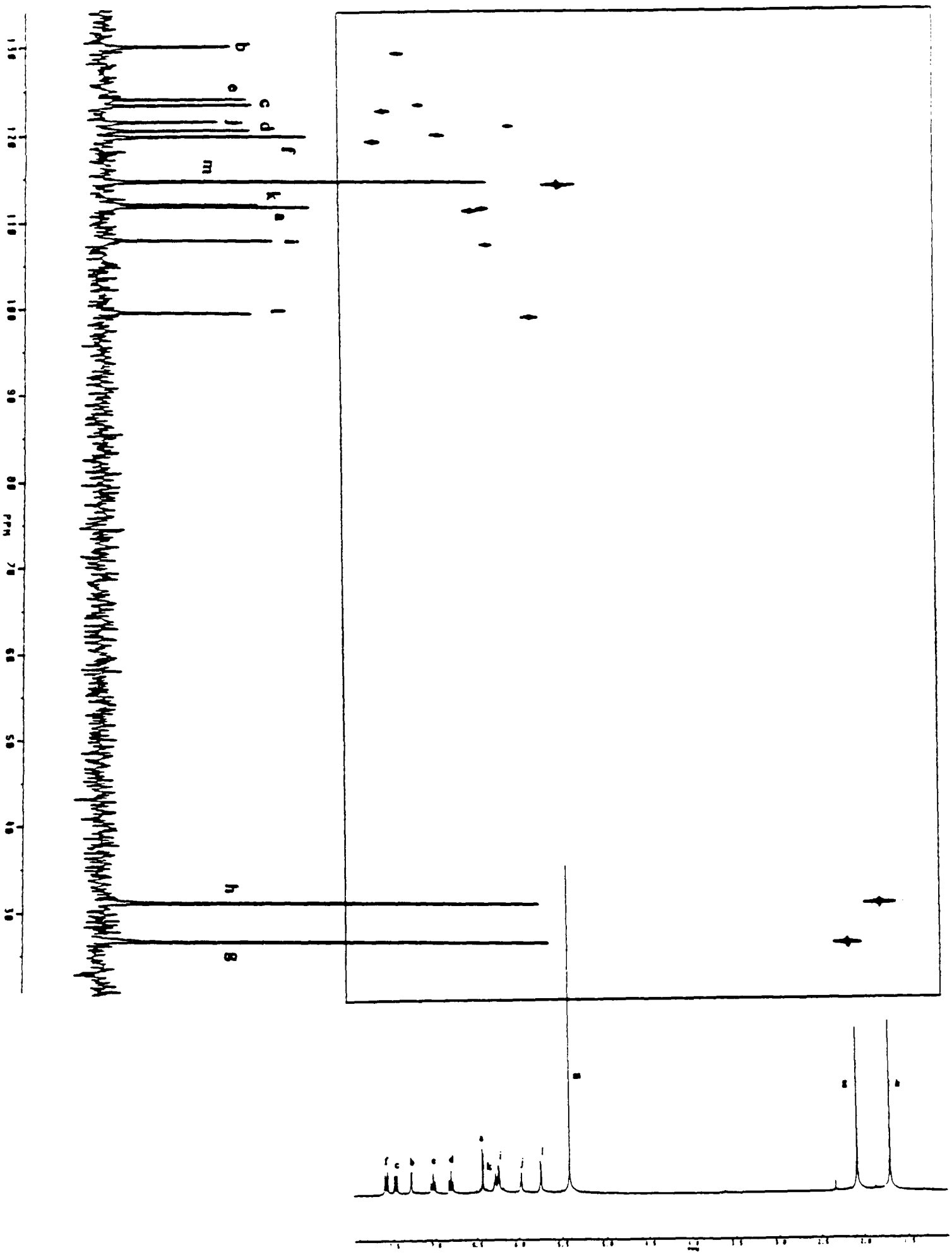

Figure 2.2.9. 75.5 MHz ^{13}C-^{1}H shift correlation NMR spectrum of [{$Me_2C(\eta^5$-$C_5H_4)(\eta^2$-$C_9H_6)$}$Zr(\eta^5$-$C_5H_5)Cl$] (**1**) in d^8-THF at r.t.

For both η^3-indenyl and η^3-allyl derivatives, the chemical shift of the "central" carbon atom of the η^3 fragment is considerably higher than those of the "terminal" carbon atoms. For example, the relevant ^{13}C chemical shifts for the η^3-indenyl complex $[(\eta^3\text{-}C_9H_7)_2Ni]$ are 106.6 ppm (central) and 67.6 ppm (terminal),[19] whilst for the η^3-allyl derivative $[\{(\eta^5\text{-}C_5Me_4)CH_2CH_2(\eta^3\text{-}CHCHCH_2)\}Zr(\eta^5\text{-}C_5Me_5)]^+$ (in which the allyl fragment is joined to the C_5Me_4 ring by a CH_2CH_2 bridge) the ^{13}C chemical shifts of the $(\eta^3\text{-}CHCHCH_2)$ fragment are 85.5, 143.1 and 83.7 ppm respectively.[20] If the indenyl group of compound **1** was coordinated in an η^3 fashion to the metal, one would expect the chemical shift of C_a to be considerably higher than both C_p and C_b.

The ^{13}C chemical shifts of compound **1** would be closer to the values expected for η^1 coordination to Zr at C_p, except that the chemical shift of C_a is considerably **lower** than C_b. The NMR data for the few η^1-indenyl complexes that have been reported show ^1H and ^{13}C chemical shifts corresponding to H_a and C_a at significantly **higher** values than for H_b and C_b,[21, 22] whilst the opposite is found for compound **1**. The chemical shift of C_a is about 20 ppm lower than the shifts of the C_5-ring, C-C double bonded carbon atoms of indene, both around 133 ppm, whilst that of C_b is quite close to these values.[19]

The ^{13}C NMR chemical shifts of compound **1** are consistent with neither η^1 σ-type coordination just at C_p, nor with η^3, π-allyl type coordination at C_p, C_a and C_b. They could, however, be consistent with an intermediate mode of coordination; η^2 coordination at C_p and C_a. This would be the first example of η^2 coordination of an indenyl moiety to a transition metal centre, although η^2 coordination of cyclopentadienyl has been observed in the crystal structure of the neutral, paramagnetic compound $[(\eta^5\text{-}C_5H_5)_2Ti(\eta^2\text{-}C_5H_5)]$ (Figure 2.2.10). The η^2 coordination of C_5H_5 ligand to titanium was described in terms of a three-centre, four-electron bonding model.[23]

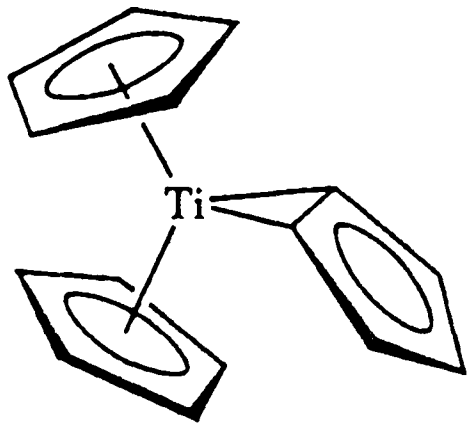

Figure 2.2.10. Structure of $[(\eta^5\text{-}C_5H_5)_2Ti(\eta^2\text{-}C_5H_5)]$

Although an η^2 coordination mode would be unprecedented for an indenyl ligand, the (butadiene)zirconocene derivative $[(\eta^5\text{-}C_5H_5)_2Zr\{\mu\text{-}(1,2\text{-}\eta^2\text{-}Zr):(4\text{-}\eta^1\text{-}Al)\text{-}C_4H_6\}(\mu\text{-}Cl)AlCl_2]$, reported in 1992 by Erker, shows possibly similar η^2 σ,π-type coordination of the butadiene ligand to zirconium.[24] This unusual compound is prepared by the reaction of (butadiene)zirconocene with $AlCl_3$, and may be considered as a member of a series of related compounds that show η^3 σ,π-type coordination of the butadiene ligand to zirconium (Figure 2.2.11).[24]

Erker has shown that for $[(\eta^5\text{-}C_5H_5)_2Zr\{\mu\text{-}(1,2\text{-}\eta^2\text{-}Zr):(4\text{-}\eta^1\text{-}Al)\text{-}C_4H_6\}(\mu\text{-}Cl)AlCl_2]$ and the related η^3 σ,π-type complexes, the ^1H and ^{13}C NMR shifts may be correlated with the zirconium-carbon distances found by X-ray diffraction, as in the table in Figure 2.2.11. The ^{13}C chemical shifts of the η^2 σ,π butadiene ligand follow the same pattern observed for C_p, C_a and C_b in compound **1**. Also, in the η^2-butadiene complex the H(2) signal lies at significantly lower chemical shift than H(3) [3.92 and 4.99 ppm respectively], which is also observed for compound **1** [$\delta(H_a)$ = 6.43, $\delta(H_b)$ = 7.29 ppm]. In contrast, for the η^3 butadiene complexes shown in Figure 2.2.11, the C(2) and H(2) signals lie at higher chemical shifts than the C(3) and H(3) signals.

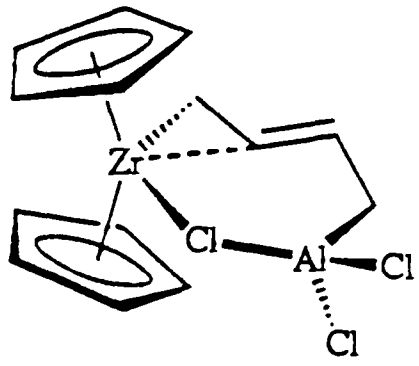

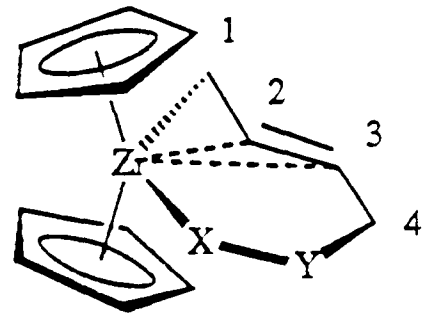

X-Y	Zr-butadiene coordination mode	^{13}C δ / ppm			Zr-C bond lengths / Å		
		C(1)	C(2)	C(3)	Zr-C(1)	Zr-C(2)	Zr-C(3)
Cl-$AlCl_2$	η^2-σ,π	42.8	102.6	140.5	2.35	2.53	3.04
CH_2-CH_2	η^3-σ,π	36.0	120.1	116.2	2.46	2.48	2.64
O-C$Cr(CO)_5$	η^3-σ,π	44.4	129.3	112.3	2.42	2.49	2.62
O-CRhCp(CO)	η^3-σ,π	40.0	126.9	111.0	2.44	2.52	2.64

Figure 2.2.11. $[(\eta^5\text{-}C_5H_5)_2Zr\{\mu\text{-}(1,2\text{-}\eta^2\text{-}Zr)\text{:}(4\text{-}\eta^1\text{-}Al)\text{-}C_4H_6\}(\mu\text{-}Cl)AlCl_2]$ and related η^3 σ,π-type complexes, with NMR and crystal structure data

Erker suggested that the unusual η^2 σ,π coordination, where a carbon-carbon double bond of the butadiene ligand is only bonded through a single sp^2-hybridised carbon atom to zirconium, might be enforced by the strained metallacyclic framework.[24] It seems likely that if a similarly unusual coordination mode is present in compound **1**, as the NMR data suggest, then the constraints on molecular geometry imposed by the short *ansa* bridge are likely to be responsible.

A well known example of η^2 σ,π coordination of a hydrocarbyl ligand to a transition metal is the η^2-benzyl ligand. For example, the zirconocene derivative $[Cp_2Zr(\eta^2\text{-}CH_2Ph)(CH_3CN)]^+[BPh_4]^-$ (Figure 2.2.12) shows η^2 coordination of the

benzyl ligand to zirconium, as evidenced by the acute Zr-CH_2-C_{ipso} angle (84.9°) and the short Zr-C_{ipso} distance (2.65 Å).[25]

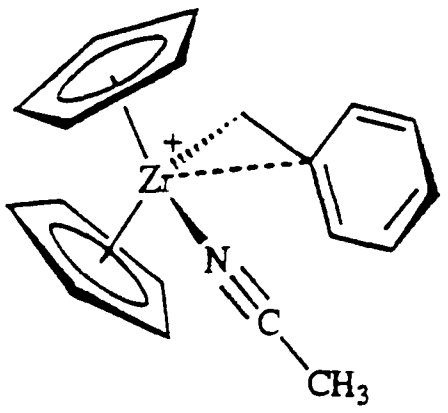

Figure 2.2.12. η^2 σ,π coordination of benzyl ligand in $[Cp_2Zr(\eta^2\text{-}CH_2Ph)(CH_3CN)]^+[BPh_4]^-$

Several other η^2-benzyl complexes, in which only one carbon atom (C_{ipso}) of the π-aromatic ring is coordinated to the metal, have been reported.[26] It has been shown that the ^{13}C chemical shift of the *ipso*-carbon atom correlates quite well with the extent of π-coordination of C_{ipso} to the metal; as the M-CH_2-C_{ipso} angle becomes more acute, $\delta(C_{ipso})$ shifts to lower values.[26] These results are consistent with Erker's observations for the η^2 butadiene coordination, and with the ^{13}C NMR-based proposal of η^2 coordination of the indenyl ligand in compound **1**.

2.2.4. X-ray crystal structure of $[\{Me_2C(\eta^5\text{-}C_5H_4)(\eta^2\text{-}C_9H_6)\}Zr(\eta^5\text{-}C_5H_5)Cl]$

It was decided at an early point in the characterisation of compound **1** that an X-ray crystal structure determination would be highly desirable, both to confirm the diastereomeric structure proposed on the basis of the NOESY experiments, and especially to test the proposed η^2 coordination of the indenyl ligand to the metal. After numerous attempts over several months, single crystals suitable for an X-ray structure analysis were obtained, by cooling a concentrated toluene solution of compound **1**. The deep red coloured crystals were isolated from the toluene solution,

washed with diethyl ether and mounted under nitrogen in Lindemann glass capillaries, which were then sealed. The X-ray structure determination was carried out by Dr. Alexander Chernega. The enantiomers of **1** crystallise separately, in the non-centrosymmetric space group $P\bar{4}2_1c$. The molecular structure of **1** is shown in Figure 2.2.13 and selected interatomic distances (Å) and angles (°) are listed in Table 2.1. Further details of the crystal structure determination are given in Appendix A.

Compound **1** adopts a bent-metallocene type structure with a centroid-Zr-centroid angle of 129.1°. The (η^5-C_5H_5) and (η^5-C_5H_4) rings are planar (deviations from best least-squares plane less than 0.008 and 0.003 Å respectively) and their zirconium-carbon and zirconium-centroid distances are similar to those reported for [(η^5-$C_5H_5)_2ZrCl_2$].[27, 28] The molecular structure shown in Figure 2.2.13 is the diastereomer predicted on the basis of NMR experiments.

The most interesting feature of the molecular structure is the coordination of indenyl ligand to the zirconium atom. The indenyl group is planar (to within 0.04 Å) and is bonded in an η^2 fashion to the metal, *via* C(14) and C(15). The Zr, Cl, C(14) and C(15) atoms are approximately co-planar (deviations from best least-squares plane less than 0.11 Å), whilst the C(16) atom lies well outside this plane. The angle between the line Zr-Cl and the plane Zr, C(14), C(15) plane is 11.2°, whilst the deviation of the Cl atom from the Zr, C(14) and C(15) plane is 0.48 Å.

Since the frontier molecular orbitals of a bent metallocene lie in the equatorial plane between the cyclopentadienyl ligands,[29-31] the ligand plane Zr, Cl, C(14) would normally be expected to coincide with the equatorial plane. For compound **1** this is not quite the case, which may arise from the constraints imposed on molecular geometry by the *ansa* bridge.

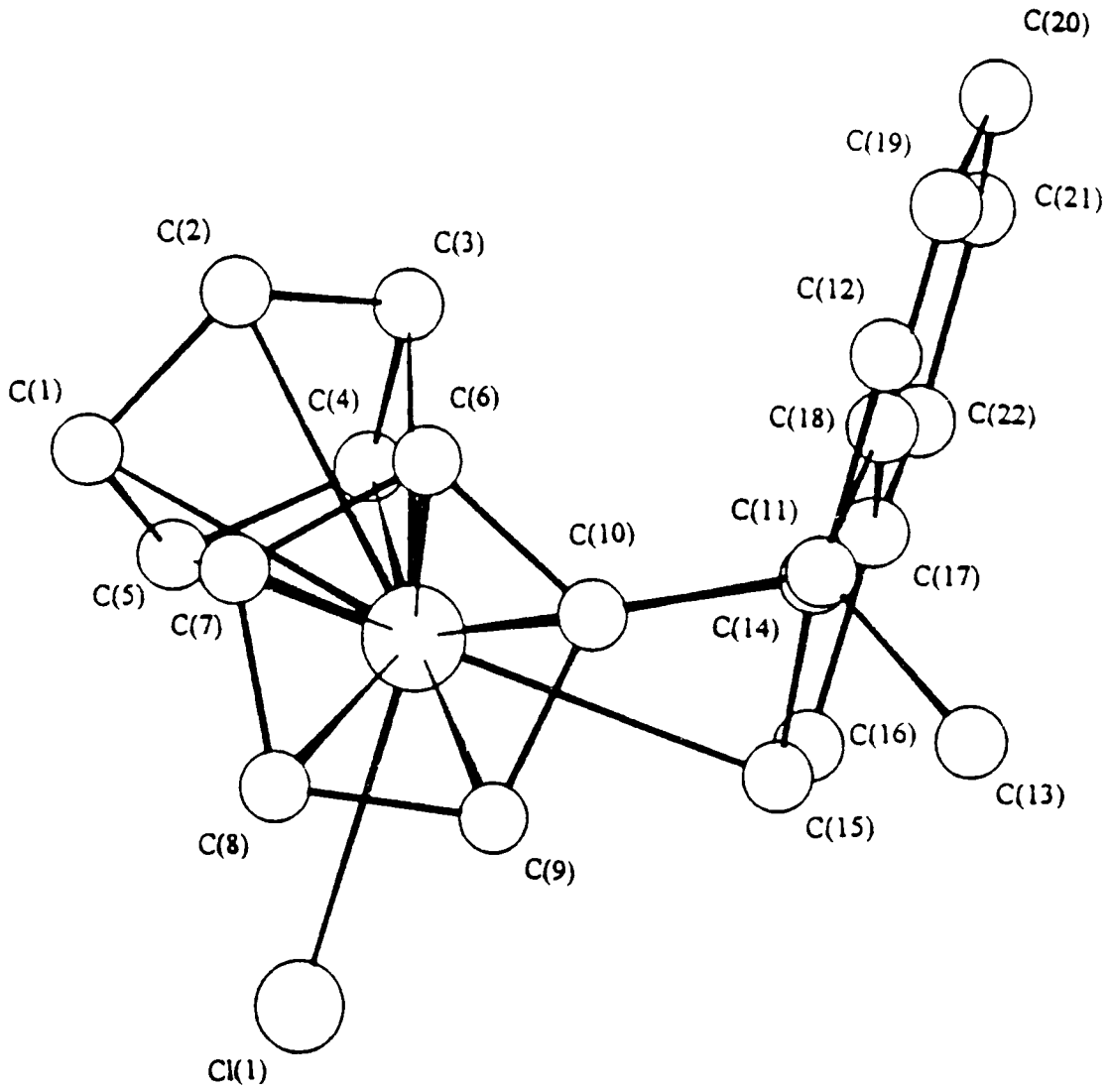

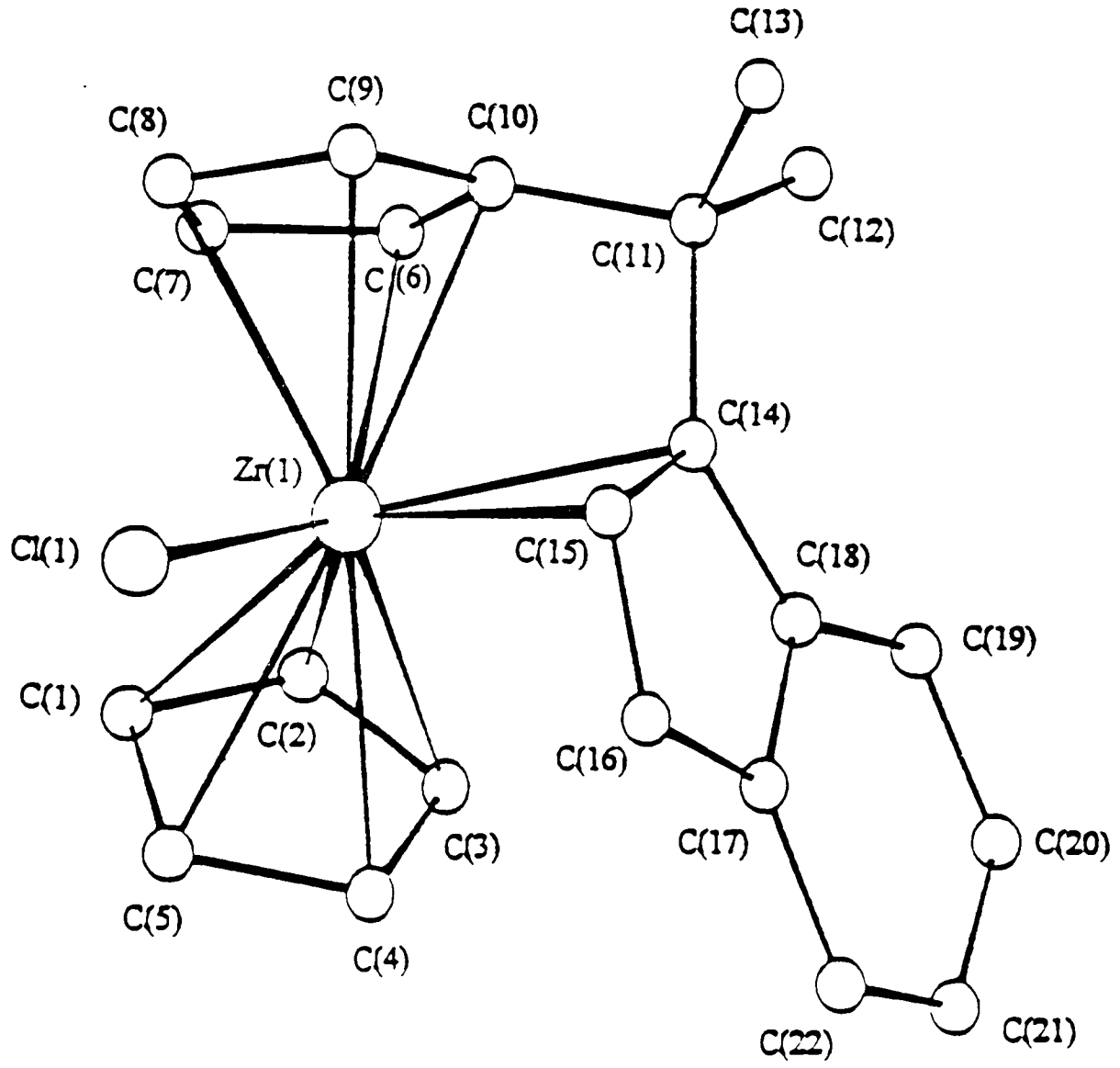

Figure 2.2.13. Two views of the molecular structure of

$[\{Me_2C(\eta^5\text{-}C_5H_4)(\eta^2\text{-}C_9H_6)\}Zr(\eta^5\text{-}C_5H_5)Cl]$ (**1**)

Table 2.1. Selected interatomic distances (Å) and angles (°) for compound **1**.

Zr(1)-C(14)	2.587(8)	Zr(1)-Cl(1)	2.489(2)
Zr(1)-C(15)	2.497(8)	Zr(1)-$C(C_5H_5)_{mean}$	2.51
Zr(1)-C(16)	3.141(9)	Zr(1)-$C(C_5H_4)_{mean}$	2.47
Zr(1)-C(17)	3.589(8)	Zr(1)-Cp	2.212
Zr(1)-C(18)	3.329(7)	Zr(1)-Cp'	2.165
C(14)-C(15)	1.43(1)		
C(15)-C(16)	1.40(1)		

C(10)-C(11)-C(14)	101.5(6)	Cp-Zr-Cp'	129.1
C(11)-C(14)-C(18)	131.8(8)	Cl(1)-Zr(1)-Cp	105.5
Zr(1)-C(14)-C(15)	70.2(4)	Cl(1)-Zr(1)-Cp'	104.7
C(14)-Zr(1)-Cl(1)	117.1(2)		

Cp and Cp' denote the centroids of the (C_5H_5) and (C_5H_4) rings respectively.

The Zr-C(14) bond length of 2.587(8) Å is about 0.09 Å longer than the Zr-C(15) bond length of 2.497(8) Å. It may be that C(14) is constrained from closer approach to the metal by the *ansa* bridge (bond strain in the *ansa* bridge is indicated by the rather small C(10)-C(11)-C(17) angle of 101.5°). The short Zr-C(15) distance and acute Zr-C(14)-C(15) angle (70.2°) suggest a pronounced bonding interaction between the electrophilic zirconium atom and C(15). The Zr-C(16) separation of 3.141(9) Å is outside the range of strong, direct covalent bonding.

The C(14)-C(15) bond length [1.43(1) Å] is only about 0.03 Å longer than the C(15)-C(16) bond length [1.40(1) Å], whilst the almost coplanar disposition of carbon atoms around C(14) is consistent with the hybridisation of C(14) being closer to sp^2 than sp^3. Thus the C(14)-C(16) bonding situation is closer to that expected for a

delocalised π-allyl system than a σ,π system with sp^3 hybridisation at C(14) and a double bond between C(15) and C(16).[32]

The Zr-Cl bond length in zirconocene chloride derivatives is highly sensitive to the extent of electronic saturation of the metal centre.[33] The Zr-Cl bond lengths found in 16-valence electron compounds [$Cp_2ZrCl(R)$] typically lie in the range 2.44-2.45 Å [34-36] whilst the Zr-Cl bond lengths of 18-electron compounds [$Cp_2ZrCl(R)(L)$] are typically around 2.55-2.58 Å.[37, 38] For compound **1** the Zr-Cl bond length of 2.489(2) Å is intermediate between the values typical of 16 and 18 electron zirconocene derivatives. This is consistent with the electron donation form the η^2-indenyl group being intermediate between η^1 (σ) and η^3 (π-allyl) indenyl coordination.

A similar Zr-Cl bond length of 2.480 Å has been reported for the zirconocene alkenyl chloride complex [$Cp_2ZrCl\{C(Ph)=CMe_2\}$].[34] The molecular structure of this compound resembles the η^2-benzyl complex shown in Figure 2.2.12, and suggests significant π-donation, from the $p(\pi)$ orbital of C_{ipso} of the phenyl group, to the vacant "ninth orbital" of the zirconium atom (which lies in the Zr-R-Cl plane, as discussed in Chapter 1).

There seems to be no simple valence-bond description for the unusual Zr-indenyl bonding situation in compound **1**. Perhaps the best bonding description, taking into account both the NMR and X-ray crystal structure data, would be η^2 coodination of a π-allyl type system, showing some tendency towards an η^2 σ,π-type coordination [evidenced by the slightly longer C(14)-C(15) bond length compared with the C(15)-C(16) distance]. This is illustrated in Figure 2.2.14.

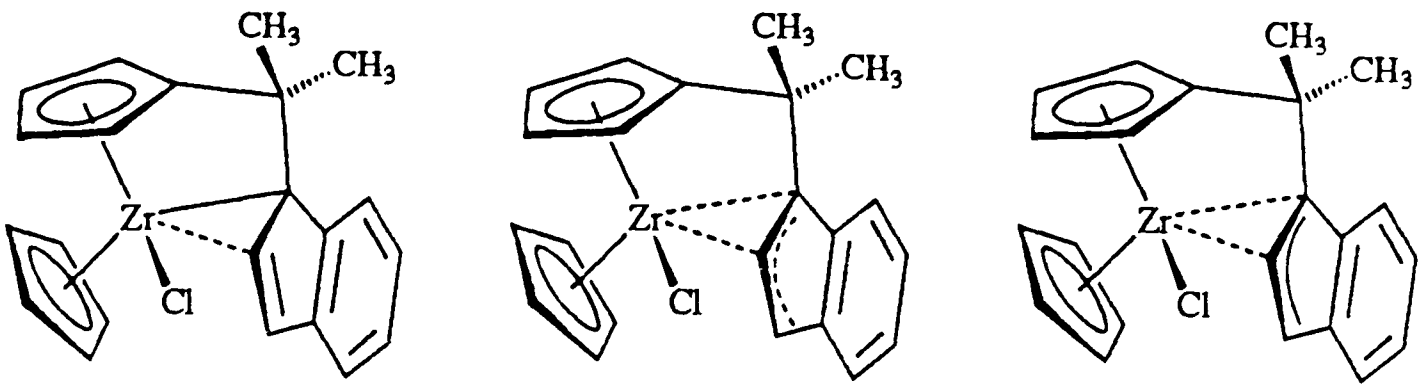

Figure 2.2.14. Alternative representations for the Zr-indenyl bonding situation in compound **1**.

It seems reasonable to propose that the indenyl ligand is constrained by the *ansa* bridge from adopting an η^3 π-allyl type coordination mode, which would lead to a favourable 18 valence electron configuration for the metal. Since the frontier molecular orbitals of a bent metallocene lie in the equatorial plane between the cyclopentadienyl ligands,[29-31] good π-orbital overlap would require the allyl fragment to lie approximately within the equatorial plane (rather than perpendicular to it), as shown in Figure 2.2.15.[30, 39]

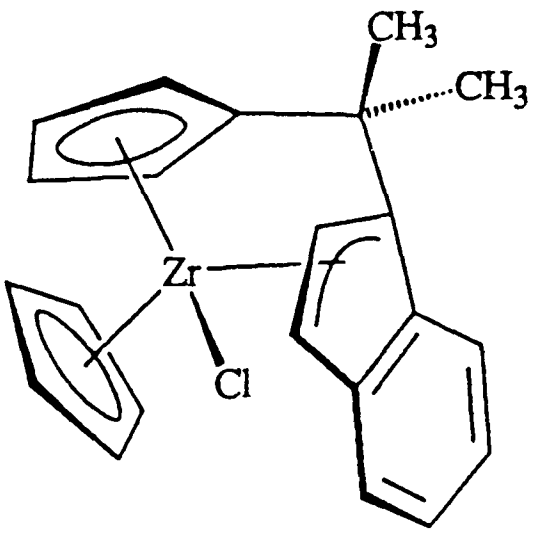

Figure 2.2.15. Molecular geometry required for η^3 π coordination of the indenyl group to zirconium in compound **1**

Even the η^2 coordination mode observed in the molecular structure of **1**, in which C(14) and C(15) are brought close to the metal, appears to result in a significantly strained *ansa* ligand, with an acute C(10)-C(11)-C(14) angle of 101.5(6)° and a large C(11)-C(14)-C(18) angle of 131.8(8)°. In order to bring the C(16) atom closer to the equatorial plane, these bond angles would have to be further distorted.

It seems reasonable to propose that the η^2 coordination mode is favoured over η^1 coordination mainly by electronic factors. Similar η^2 coordination is observed in several benzyl complexes,[25, 26] and in Erker's η^2-butadiene complex,[24] in which favourable $p(\pi)$–$d(\pi)$ interactions are thought to be responsible. Extended-Huckel molecular orbital calculations, performed by Cardin on the model compounds $[MH_3(CH_2CH{=}CH_2)]$ and $[MH_3\{C(=CH_2)\text{-}CH{=}CH_2\}]$, suggest such a $p(\pi)$–$d(\pi)$ interaction is energetically favourable, resulting in acute M-C-*C* angles for the zirconium species.[33]

It thus seems likely that the η^2-indenyl coordination is favoured over η^1 σ-coordination on electronic grounds, whilst being favoured over η^3 coordination because of the bond strain associated with the geometry required for good π overlap with three carbon atoms. The favoured η^2 bonding mode may explain the formation of the observed diastereomer. For the alternative diastereomer to adopt a similar η^2-indenyl coordination mode, one of the methyl groups of the *ansa* bridge would be brought very close to the C_5H_5 ligand, resulting in significant steric crowding (Figure 2.2.16). So it may be that the diastereoselectivity of the formation of compound **1** is based on the energetic favourability of the η^2-indenyl coordination, which in turn favours one diastereomer on steric grounds.

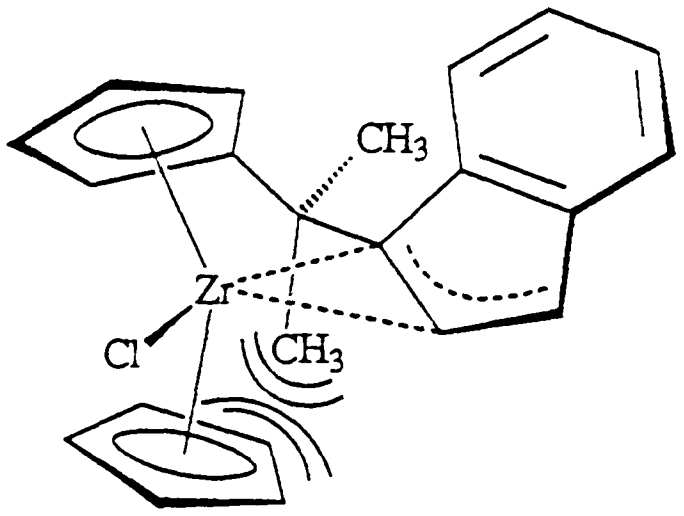

Figure 2.2.16. Alternative diastereomer of compound **1**, showing steric crowding of CH_3 and C_5H_5 groups resulting from η^2-indenyl coordination

2.2.5 Synthesis of [{$Me_2C(\eta^5\text{-}C_5H_4)(\eta^2\text{-}C_9H_6)$}$Hf(\eta^5\text{-}C_5H_5)Cl$]

Whilst the organometallic chemistry of zirconium and hafnium is broadly similar, there are some notable exceptions (as discussed later), and the catalytic properties of their complexes can show significant differences.[40-43] It was therefore decided to attempt the preparation of the hafnium analogue of compound **1**.

When toluene was added to a stirred mixture of pale yellow [{$Me_2C(C_5H_4)(C_9H_6)$}Li_2{$0.6(Et_2O)$}] and white [$(\eta^5\text{-}C_5H_5)HfCl_3\cdot 2THF$] at room temperature, an immediate colour change was observed. The resulting orange/red coloured mixture was stirred for a further 16 hours. Filtration, followed by concentration of the solution under reduced pressure and cooling to -20 °C afforded several crops of dark orange crystals, characterised as [{$Me_2C(\eta^5\text{-}C_5H_4)(\eta^2\text{-}C_9H_6)$}$Hf(\eta^5\text{-}C_5H_5)Cl$] (**2**), with a final yield of 71 % (Figure 2.2.17).

It was later found that if the addition of toluene to the reactants was performed at low temperature, the yield of pure product improved. When toluene at -78 °C was added to a stirred mixture of [{$Me_2C(C_5H_4)(C_9H_6)$}Li_2{$0.75(Et_2O)$}] and [$(\eta^5\text{-}C_5H_5)HfCl_3\cdot DME$] also at -78 °C, a yellow coloured mixture was obtained. When this was allowed to warm to room temperature, it slowly darkened to an orange colour. By

following the same procedure as before, the pure product was obtained as orange crystals in 81 % yield.

The air- and moisture-sensitive orange crystalline solid [{$Me_2C(\eta^5\text{-}C_5H_4)(\eta^2\text{-}C_9H_6)$}$Hf(\eta^5\text{-}C_5H_5)Cl$] (**2**) was characterised by elemental analysis and ^1H and ^{13}C NMR studies, including selective ^1H decoupling and a ^{13}C-^1H shift correlation experiment. The elemental analysis was consistent with the molecular formula $C_{22}H_{21}ClHf$, whilst the ^1H and ^{13}C NMR spectra were very similar to those of compound **1**, suggesting an analogous molecular structure. The ^1H chemical shift of the C_5H_5 protons was about 0.1 ppm lower than the zirconium analogue, which is typical of hafnocene derivatives compared with zirconocenes. Most interestingly, the ^{13}C chemical shifts corresponding to C_p, C_a, and C_b lie at 85.1, 108.6 and 129.4 ppm respectively, suggesting a similar η^2 coordination of the indenyl ligand to the metal.

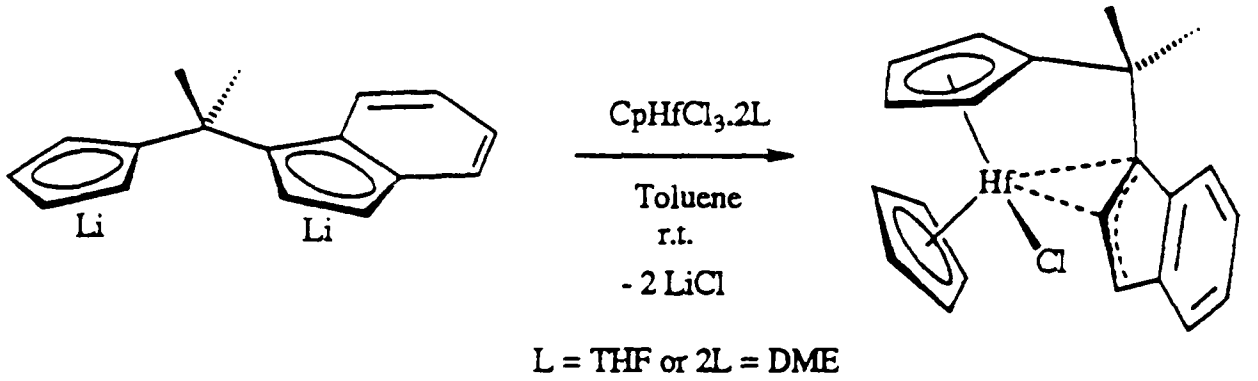

Figure 2.2.17. Synthesis of [{$Me_2C(\eta^5\text{-}C_5H_4)(\eta^2\text{-}C_9H_6)$}$Hf(\eta^5\text{-}C_5H_5)Cl$] (**2**)

2.3 Synthesis of [{$(CH_2)_5C(\eta^5\text{-}C_5H_4)(\eta^2\text{-}C_9H_6)$}$M(\eta^5\text{-}C_5H_5)Cl$]

It was decided to attempt to synthesise analogues of compounds **1** and **2** possessing cyclohexyl-bridged *ansa* ligands. This was, in part, to test the generality of the synthesis of these novel *ansa*-bridged compounds. Also, if the analogous compounds could be prepared, it was thought that the modification of the bridge substituents might prove useful in the attempt to grow crystals suitable for an X-ray

structure determination (since suitable crystals of compound **1** had not yet been obtained).

2.3.1 Preparation of $[\{(CH_2)_5C(C_5H_4)(C_9H_6)\}Li_2]$

Figure 2.3.1. shows the preparation of the dilithium salt of the cyclohexyl-bridged ligand $[\{(CH_2)_5C(C_5H_4)(C_9H_6)\}Li_2\{0.8(Et_2O)\}]$ from 6,6-pentamethylene fulvene and lithium indenide. The pure fulvene and dilithium salt of the *ansa* ligand were prepared in high yield by employing the same modifications of the literature syntheses that were developed for the CMe_2-bridged analogues. The dilithium salt was obtained as a highly air- and moisture-sensitive pale yellow powder, in high yield (92 %), with 0.8 equivalents of diethyl ether solvate (as determined by ^1H NMR).

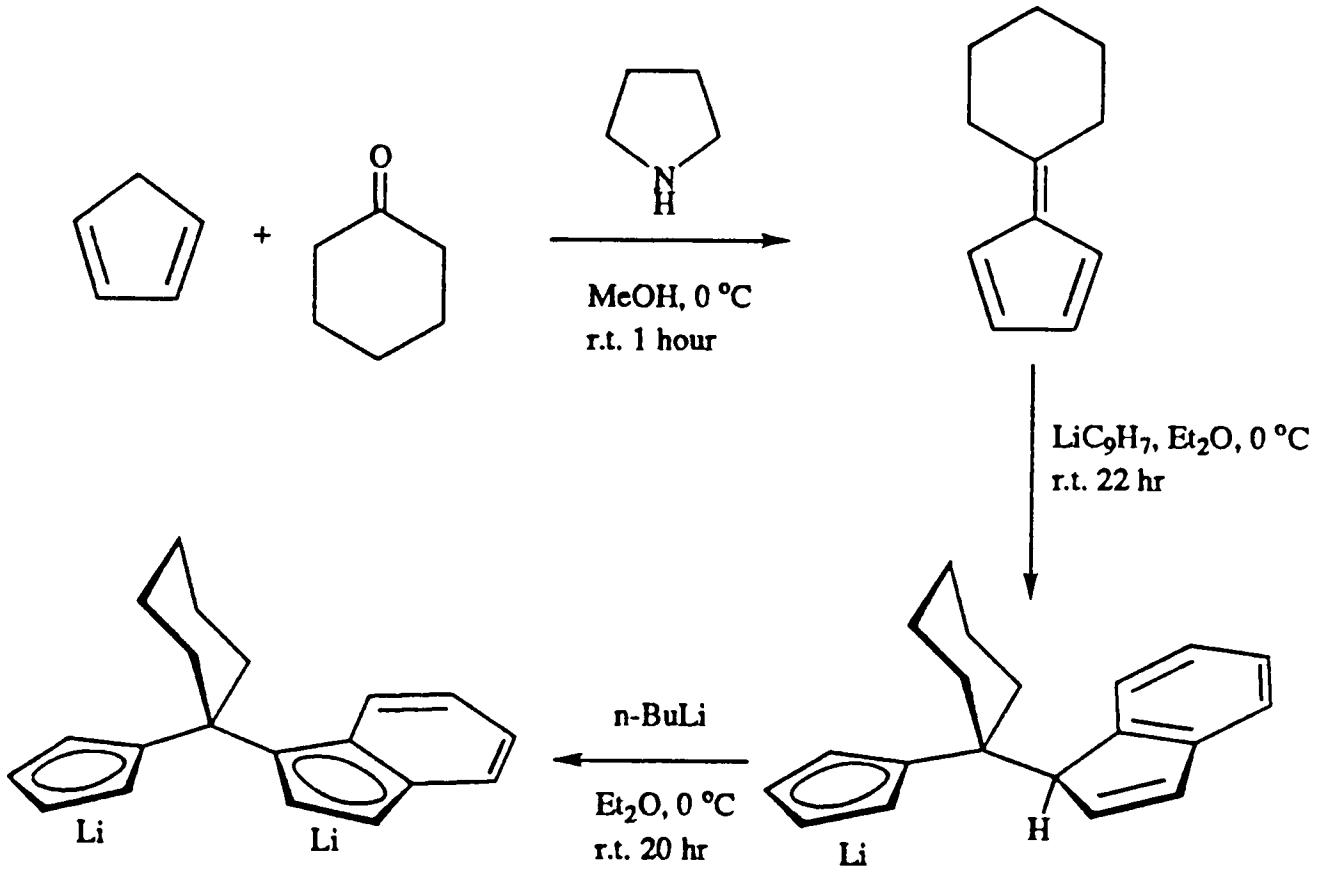

Figure 2.3.1. Preparation of $[\{(CH_2)_5C(C_5H_4)(C_9H_6)\}Li_2\{0.8(Et_2O)\}]$

2.3.2 Synthesis of $[\{(CH_2)_5C(\eta^5\text{-}C_5H_4)(\eta^2\text{-}C_9H_6)\}Zr(\eta^5\text{-}C_5H_5)Cl]$

When toluene was added to a stirred mixture of the pale yellow solid $[(CH_2)_5C(C_5H_4)(C_9H_6)]Li_2\{0.8(Et_2O)\}]$ and the white solid $[(\eta^5\text{-}C_5H_5)ZrCl_3\cdot DME]$ at room temperature, an immediate colour change was observed, giving a red coloured reaction mixture. After stirring for a further 16 hours at room temperature, the red solution was filtered from a pale solid residue, presumed to be lithium chloride.

The clear, deep red solution was then concentrated under reduced pressure and cooled to -20 °C. After several days, red needle-shaped crystals were isolated from the solution and washed with diethyl ether. These were characterised as the novel, *ansa*-bridged mononuclear compound $[\{(CH_2)_5C(\eta^5\text{-}C_5H_4)(\eta^2\text{-}C_9H_6)\}Zr(\eta^5\text{-}C_5H_5)Cl][0.5(C_6H_5CH_3)]$ (**3**). The toluene solution was again concentrated and cooled to -20 °C, giving a second crop of crystals and an overall yield of 79 %.

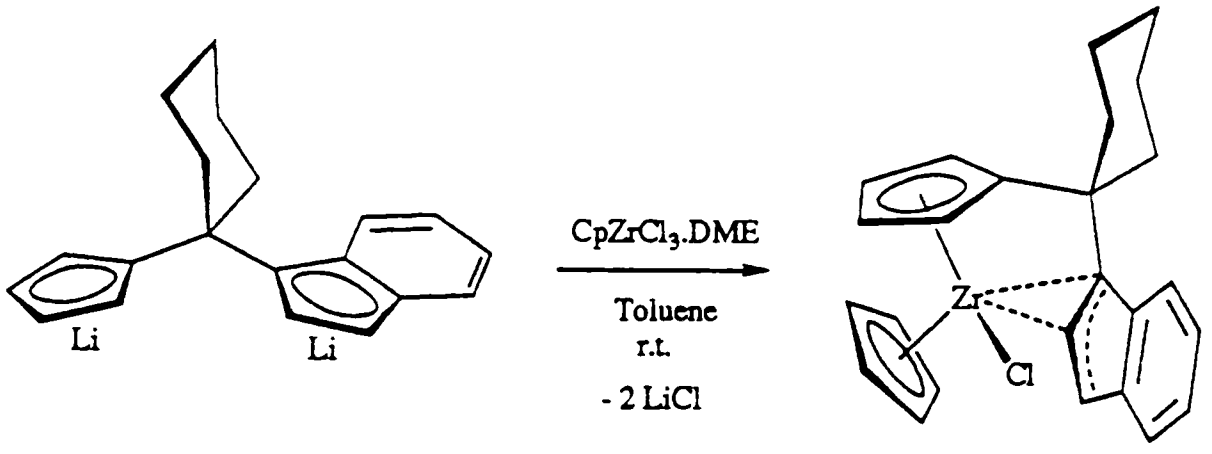

Figure 2.3.2. Synthesis of $[\{(CH_2)_5C(\eta^5\text{-}C_5H_4)(\eta^2\text{-}C_9H_6)\}Zr(\eta^5\text{-}C_5H_5)Cl]$ (**3**)

The air- and moisture-sensitive red crystalline solid $[\{(CH_2)_5C(\eta^5\text{-}C_5H_4)(\eta^2\text{-}C_9H_6)\}Zr(\eta^5\text{-}C_5H_5)Cl][0.5(C_6H_5CH_3)]$ (**3**) was characterised by elemental analysis and ^1H and ^{13}C NMR studies. The ^1H NMR spectrum of **3** in C_6D_6 is shown in Figure 2.3.3. With the exception of the signals arising from the Me_2C and $(CH_2)_5C$ bridging groups, the ^1H spectra of **1** and **3** in C_6D_6 are very similar, except that compound **3** contains a significant amount of toluene, despite being washed with diethyl ether and dried *in vacuo* overnight. Careful integration of the ^1H NMR

spectrum indicated 0.5 equivalents of toluene, and the elemental analysis was consistent with an empirical formula $C_{28.5}H_{29}ClZr$ corresponding to $[\{(CH_2)_5C(C_5H_4)(C_9H_6)\}Zr(C_5H_5)Cl][0.5(C_6H_5CH_3)]$. The ^1H NMR spectrum of **3** shows that only one diasteoromer is present, and the close resemblance to the spectrum of **1** suggests that an analogous diastereomeric structure is adopted by **3**.

The ^{13}C NMR spectrum of **3** is similar to that of **1**, and is consistent with the proposed molecular structure. In particular, the ^{13}C chemical shifts corresponding to C_p, C_a, and C_b lie at 85.7, 111.0 and 128.9 ppm respectively, suggesting a similar η^2 coordination of the indenyl ligand to the metal. Thus, the elemental analysis, ^1H and ^{13}C NMR spectra of **3** are consistent with a molecular structure analogous to that proposed for compound **1**. This proposal was confirmed by a single crystal X-ray structure determination.

2.3.3. X-ray crystal structure of $[\{(CH_2)_5C(\eta^5\text{-}C_5H_4)(\eta^2\text{-}C_9H_6)\}Zr(\eta^5\text{-}C_5H_5)Cl]$

Crystals suitable for an X-ray structure analysis of compound **3** were obtained from a concentrated toluene solution cooled to -20 °C and maintained at that temperature for several days. The deep red coloured needles were isolated from the toluene solution, washed with diethyl ether and mounted under nitrogen in Lindemann glass capillaries, which were then sealed. The X-ray structure determination was carried out by Dr. Alexander Chernega. The enantiomers of **3** crystallise together in racemic crystals with the centrosymmetric space group $P2_1/n$. The molecular structure of **3** is shown in Figure 2.3.4 and selected interatomic distances (Å) and angles (°) are listed in Table 2.2. The toluene solvate [C(26) to C(29)] lies on an inversion centre and is disordered. Further details of the crystal structure determination are given in Appendix B.

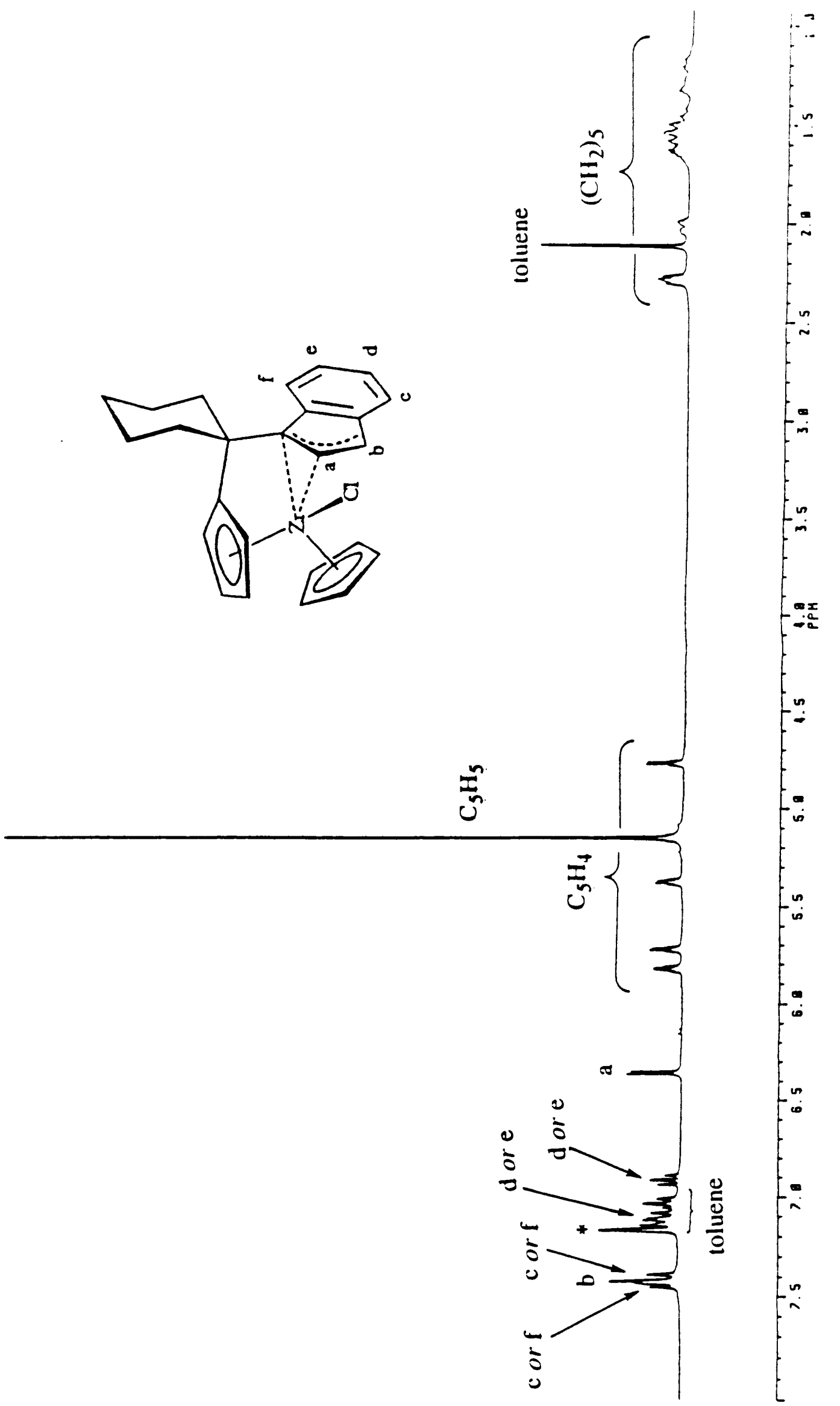

Figure 2.3.3. 300MHz ^{1}H NMR spectrum of

$[\{(CH_2)_5C(\eta^5\text{-}C_5H_4)(\eta^2\text{-}C_9H_6)\}Zr(\eta^5\text{-}C_5H_5)Cl][0.5(C_6H_5CH_3)]$ (**3**) in C_6D_6 at r.t.

(* = benzene solvent)

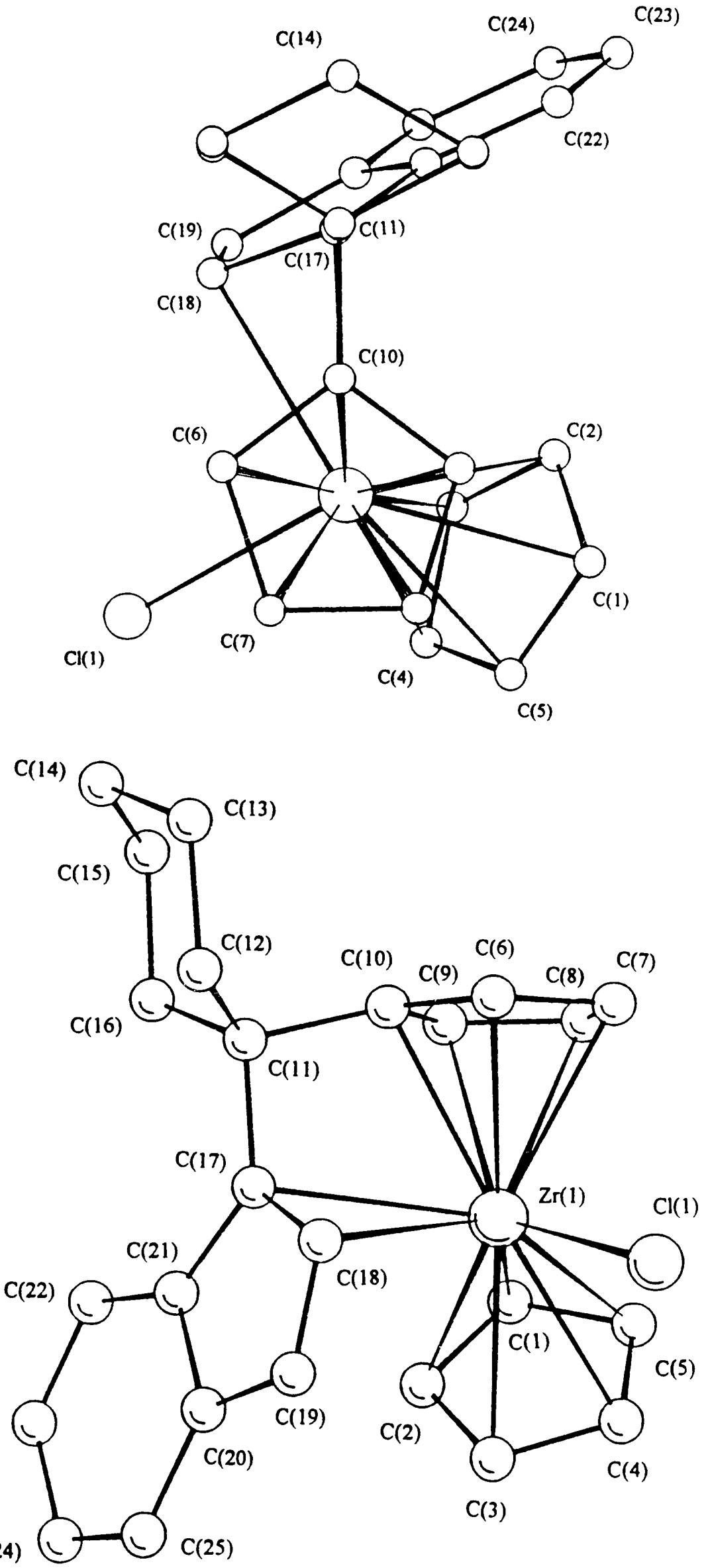

Figure 2.3.4. Two views of the molecular structure of

$[\{(CH_2)_5C(\eta^5\text{-}C_5H_4)(\eta^2\text{-}C_9H_6)\}Zr(\eta^5\text{-}C_5H_5)Cl]$ (**3**)

Table 2.2. Selected interatomic distances (Å) and angles (°) for compound **3**.

Zr(1)-C(17)	2.564(4)	Zr(1)-Cl(1)	2.500(1)
Zr(1)-C(18)	2.508(5)	Zr(1)-C(C_5H_5)$_{mean}$	2.51
Zr(1)-C(19)	3.170(5)	Zr(1)-C(C_5H_4)$_{mean}$	2.49
Zr(1)-C(21)	3.335(4)	Zr(1)-Cp	2.214
C(17)-C(18)	1.439(7)	Zr(1)-Cp'	2.174
C(18)-C(19)	1.376(7)		

Cl(1)-Zr(1)-C(17)	117.5(1)	Cp-Zr(1)-Cp'	130.4°
Zr(1)-C(17)-C(18)	71.4(2)	C(10)-C(11)-C(17)	101.5(3)
C(11)-C(17)-C(21)	130.7(5)		

Cp and Cp' denote the centroids of (C_5H_5) and (C_5H_4) rings respectively.

With the exception of the cyclohexyl bridging group, the molecular structure of compound **3** is very similar to that of compound **1**. Compound **3** adopts a bent-metallocene type structure with a centroid-Zr-centroid angle of 130.4°. The (η^5-C_5H_5) and (η^5-C_5H_4) rings are planar (deviations from best least-squares plane less than 0.003 and 0.008 Å respectively) and their zirconium-carbon and zirconium-centroid distances are similar to those of compound **1** and those reported for [(η^5-$C_5H_5)_2ZrCl_2$].[27, 28] The molecular structure shown in Figure 2.3.4 is the diastereomer proposed on the basis of the NMR data, *i.e.* the syntheses of compounds **1** and **3** show the same diastereoselectivity.

The indenyl group is planar (to within 0.02 Å) and is bonded in an η^2 fashion to the metal, *via* C(17) and C(18). The Zr, Cl, C(17) and C(18) atoms are approximately co-planar (deviations from best least-squares plane less than 0.12 Å),

whilst C(19) lies well outside this plane. The angle between the indenyl plane and the Zr, C(17) and C(18) plane is 76.6°.

The coordination of the indenyl group to the metal appears similar to compound **1**, and the best description of the bonding situation is probably the same, namely η^2 coodination of a π-allyl type system, showing some tendency towards an η^2 σ,π-type coordination. For compound **3**, the Zr-C(17) and C(18)-C(19) bond lengths are slightly shorter than the corresponding bond lengths in **1**, while the Zr-C(18) and C(17)-C(18) bond lengths are slightly longer than the corresponding distances in **1**. These differences in bond length are consistent with compound **3** having slightly more σ,π character than compound **1**. The Zr-Cl distance for compound **3** is slightly (0.01 Å) longer than in compound **1**.

Apart from these small differences, the formal substitution of the CMe_2 bridge in **1** with the cyclohexyl bridging group in **3** (which adopts a "chair" conformation) has little effect on the molecular structure. The C(10)-C(11)-C(17) and C(11)-C(17)-C(21) angles [101.5(3) and 130.7(5)° respectively] suggest a degree of strain associated with the coordination of the indenyl group to the metal similar to that found in compound **1**. The similarity of the molecular structures of **1** and **3** suggests that the same combination of electronic and steric factors are responsible for the observed η^2 coordination of the indenyl ligands, and for the diastereoselecivity of the syntheses of compounds **1** and **3**.

2.3.4 Synthesis of $[\{(CH_2)_5C(\eta^5\text{-}C_5H_4)(\eta^2\text{-}C_9H_6)\}Hf(\eta^5\text{-}C_5H_5)Cl]$

When toluene was added to a stirred mixture of the pale yellow powder $[\{(CH_2)_5C(C_5H_4)(C_9H_6)\}Li_2\{0.8(Et_2O)\}]$ and the white powder $[(\eta^5\text{-}C_5H_5)HfCl_3{\cdot}2THF]$ at room temperature, an immediate colour change was observed. The resulting orange/red mixture was stirred for 16 hours at room temperature, then a clear orange solution was filtered from the solid residues, concentrated under reduced pressure, and cooled to -20 °C. After several days, dark orange crystals were isolated

from the solution, washed with diethyl ether and dried *in vacuo*. Two further crops of crystals were obtained from the toluene solution, giving a final yield of 58 %. The air- and moisture-sensitive orange crystalline solid was characterised by elemental analysis and ^{1}H and ^{13}C NMR studies as $[\{(CH_2)_5C(\eta^5\text{-}C_5H_4)(\eta^2\text{-}C_9H_6)\}Hf(\eta^5\text{-}C_5H_5)Cl][0.5(C_6H_5CH_3)]$ (**4**), the hafnium analogue of compound **3**.

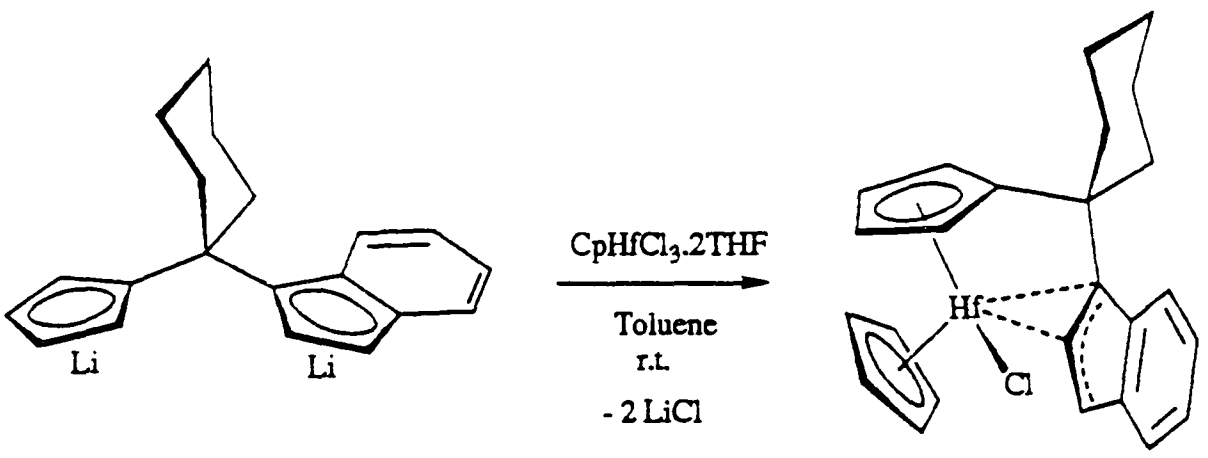

Figure 2.3.5. Synthesis of $[\{(CH_2)_5C(\eta^5\text{-}C_5H_4)(\eta^2\text{-}C_9H_6)\}Hf(\eta^5\text{-}C_5H_5)Cl]$ (**4**)

The ^{1}H NMR spectrum of **4** in C_6D_6 is shown in Figure 2.3.6. The chemical shifts of the C_5H_5, C_5H_4 and C_9H_6 protons are very similar to those of compound **2** in C_6D_6, and the spectrum as a whole closely resembles that of compound **3**. Careful integration of the ^{1}H signals indicates the presence of 0.5 equivalents of toluene, and the elemental analysis is consistent with an empirical formula $C_{28.5}H_{29}ClHf$, corresponding to the molecular formula $C_{25}H_{25}ClHf{\cdot}\frac{1}{2}(C_7H_8)$. The ^{1}H NMR spectrum of **4** shows that only one diasteoromer is present, and the close resemblance to the spectrum of **3** suggests that an analogous diastereomeric structure is adopted by compound **4**.

The ^{13}C NMR spectrum of **4** (Figure 2.3.7) is similar to that of **3**, and is consistent with the proposed molecular structure. In particular, the ^{13}C chemical shifts for the signals corresponding to C_p, C_a, and C_b, are 84.9, 108.0 and 129.5 ppm respectively, suggesting a similar η^2 coordination of the indenyl ligand to the metal. Thus, the elemental analysis, ^{1}H and ^{13}C NMR spectra of **4** are consistent with a molecular structure analogous to compound **3**.

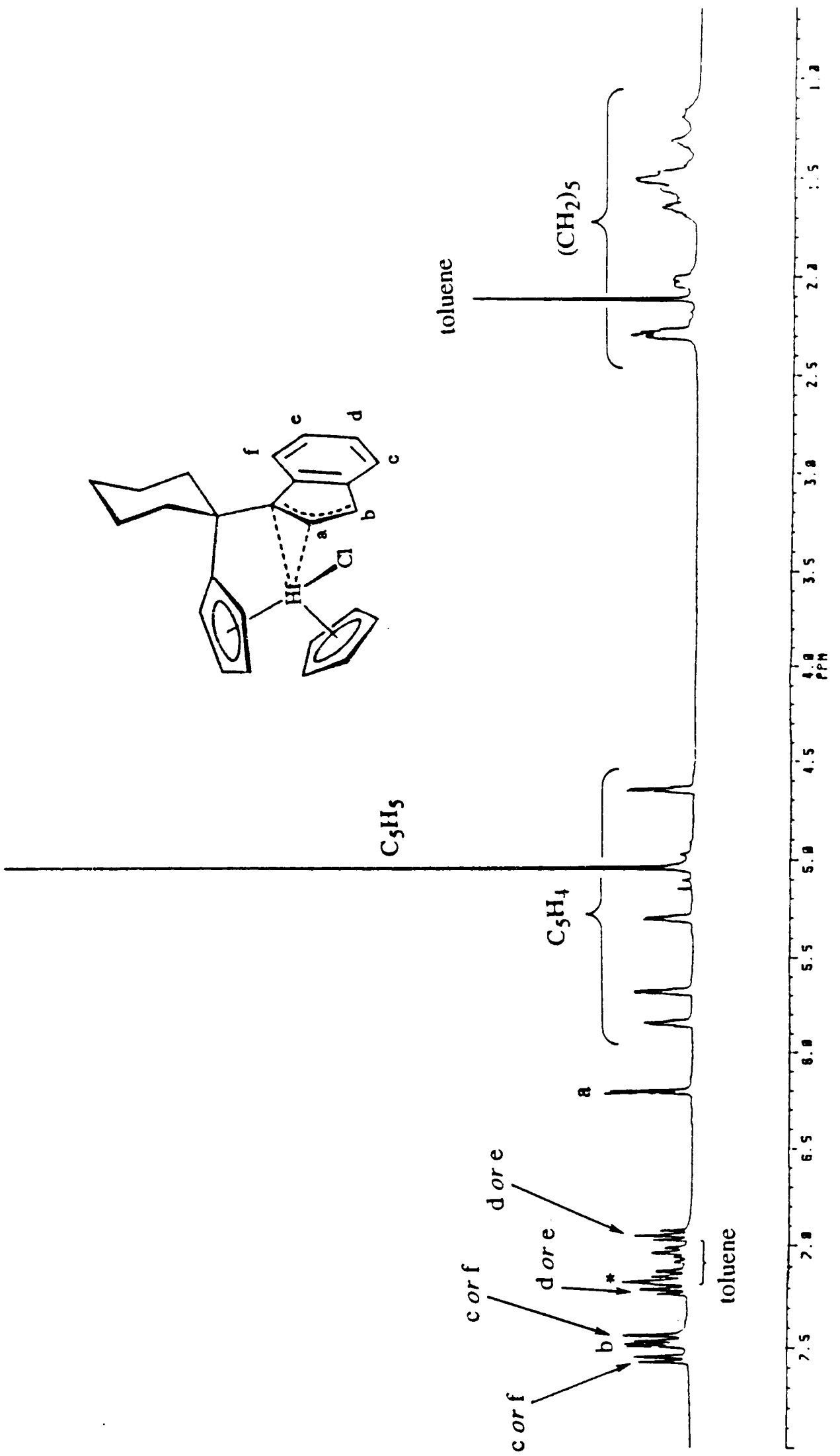

Figure 2.3.6. 300MHz ^{1}H NMR spectrum of

$[\{(CH_2)_5C(\eta^5\text{-}C_5H_4)(\eta^2\text{-}C_9H_6)\}Hf(\eta^5\text{-}C_5H_5)Cl][0.5(C_6H_5CH_3)]$ (**4**) in C_6D_6 at r.t.

(∗ = benzene solvent)

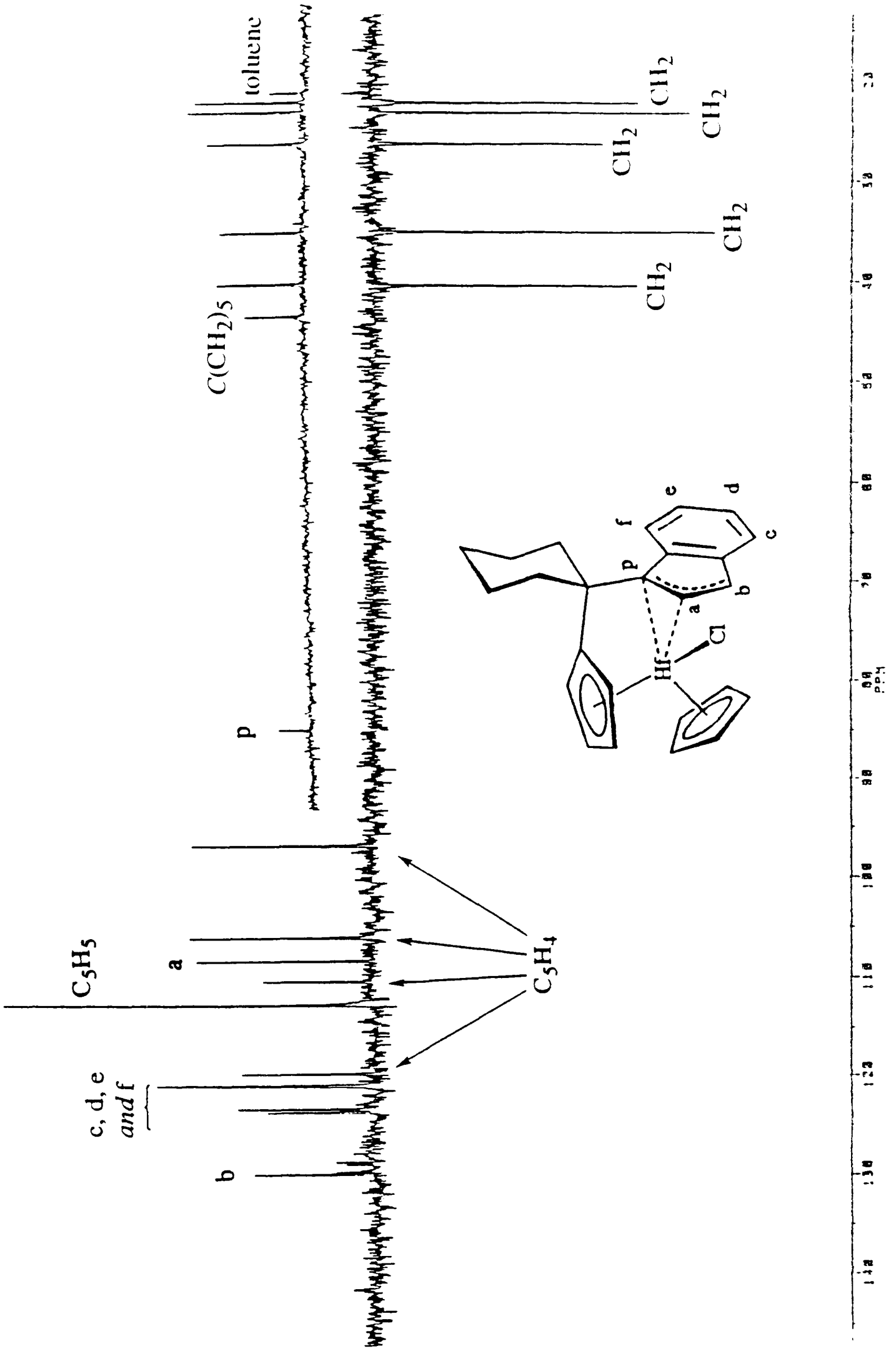

Figure 2.3.7. 75.5 MHz DEPT NMR spectrum of $[\{(CH_2)_5C(\eta^5\text{-}C_5H_4)(\eta^2\text{-}C_9H_6)\}Hf(\eta^5\text{-}C_5H_5)Cl][0.5(C_6H_5CH_3)]$ (**4**) in C_6D_6 at r.t. with part of $^{13}C\{^1H\}$ spectrum showing bridging group and C_p signals

2.4 Synthesis of [{$Me_2C(\eta^5\text{-}C_5H_4)(\eta^3\text{-}C_{13}H_8)$}$Zr(\eta^5\text{-}C_5H_5)Cl$]

So far in this chapter we have seen that the ligands [$Me_2C(C_5H_4)(C_9H_6)Li_2$] and [$(CH_2)_5C(C_5H_4)(C_9H_6)Li_2$] react with one equivalent of [$(\eta^5\text{-}C_5H_5)MCl_3\cdot 2L$] (M = Zr, Hf; 2L = DME, 2THF) to give the novel, *ansa*-bridged mononuclear complexes [{$X(\eta^5\text{-}C_5H_4)(\eta^2\text{-}C_9H_6)$}$M(\eta^5\text{-}C_5H_5)Cl$] (X = Me_2C, $(CH_2)_5C$). The unprecedented η^2-indenyl coordination mode observed in these compounds probably results not only competition between indenyl and cyclopentadienyl ligands for coordination at the metal centre, but also upon constraints imposed on the molecular structure by the short *ansa*-bridges. It was decided to further study these effects on molecular structure by investigating the reactions of other Me_2C-bridged *ansa*-ligands with [$(\eta^5\text{-}C_5H_5)MCl_3\cdot 2L$] complexes.

2.4.1 Preparation of [$Me_2C(C_5H_4)(C_{13}H_8)Li_2$]

The *ansa*-bridged ligand [{$Me_2C(C_5H_4)(C_{13}H_8)$}Li_2{$0.75(Et_2O)$}] (Figure 2.4.1) was prepared in high yield (90 %) from 6,6-dimethylfulvene and lithium fluorenide, by employing the same modifications of the literature synthesis[43] that were developed for the indenyl analogues. A solution of 6,6-dimethylfulvene in diethyl ether was added dropwise to a stirred solution of lithium fluorenide [$LiC_{13}H_9(Et_2O)$] in diethyl ether at 0 °C, and the solution was then stirred for a further 22 hours at room temperature. The reaction mixture was then cooled to 0 °C and one equivalent of n-BuLi was added. After stirring for a further 4 hours at room temperature, the very air- and moisture sensitive, bright yellow solid [{$Me_2C(C_5H_4)(C_{13}H_8)$}Li_2{$0.75(Et_2O)$}] was isolated by filtration, washed with diethyl ether and dried *in vacuo*. The ^1H NMR spectrum showed the presence of 0.75 equivalents of solvating diethyl ether. As for the indenyl analogues, the pyrophoric nature of the dilithium salt meant that elemental analysis, to confirm the amount of solvate, was not practicable.

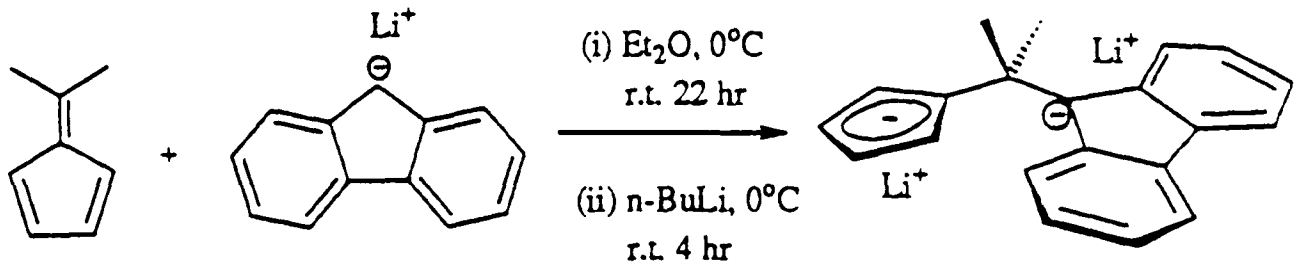

Figure 2.4.1. Preparation of [{$Me_2C(C_5H_4)(C_{13}H_8)$}Li_2]

2.4.2 Synthesis of [{$Me_2C(\eta^5\text{-}C_5H_4)(\eta^3\text{-}C_{13}H_8)$}$Zr(\eta^5\text{-}C_5H_5)Cl$]

The addition of toluene to a stirred mixture of the yellow solid [{$Me_2C(C_5H_4)(C_{13}H_8)$}Li_2{$0.75(Et_2O)$}] and the white solid [(η^5-C_5H_5)$ZrCl_3$·DME] at room temperature, resulted in an immediate colour change. The resulting red mixture was stirred for a further 16 hours at room temperature, then was filtered from pale solid residues (presumably lithium chloride) to give a clear red solution. The removal of volatiles under reduced pressure gave the crude product as a red solid, which was washed with petroleum ether (bp. 40-60 °C) then extracted into toluene. The toluene solution, when concentrated under reduced pressure and cooled to -20 °C, afforded red crystals of the pure product, the novel *ansa*-bridged mononuclear complex [{$Me_2C(\eta^5\text{-}C_5H_4)(\eta^3\text{-}C_{13}H_8)$}$Zr(\eta^5\text{-}C_5H_5)Cl$] (**5**), in 57 % yield.

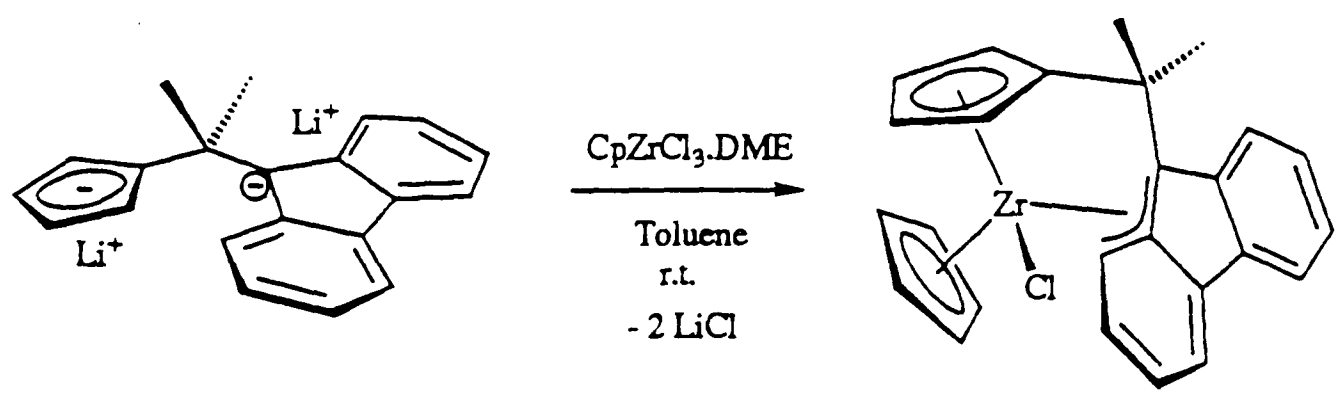

Figure 2.4.2. Synthesis of [{$Me_2C(\eta^5\text{-}C_5H_4)(\eta^3\text{-}C_{13}H_8)$}$Zr(\eta^5\text{-}C_5H_5)Cl$] (**5**)

2.4.3 Characterisation of [{$Me_2C(\eta^5\text{-}C_5H_4)(\eta^3\text{-}C_{13}H_8)$}$Zr(\eta^5\text{-}C_5H_5)Cl$]

Compound **5**, an air- and moisture-sensitive, red crystalline solid, was characterised by elemental analysis, ^1H and ^{13}C NMR studies and a single crystal X-ray structure determination. The elemental analysis was consistent with an empirical formula $C_{26}H_{23}ClZr$, corresponding to the molecular formula [{$Me_2C(C_5H_4)(C_{13}H_8)$}$Zr(C_5H_5)Cl$].

Compound **5** was less air-sensitive than **1**, and showed no sign of decomposition in dichloromethane. The ^1H NMR spectra of **5** measured in d^8-THF, C_6D_6 and CD_2Cl_2 were very similar. In each case the arene region of the spectrum was very crowded. The ^1H NMR spectrum of **5** in CD_2Cl_2 at room temperature is shown in Figure 2.4.3.

The ^1H NMR assignments are proposed on the basis of selective ^1H decoupling, COSY and NOESY experiments. As expected, the methyl groups are inequivalent, as are the C_5H_4 protons. The chemical shift of the C_5H_5 ligand (4.84 ppm) is unusually low for a zirconocene derivative, probably a result of the shielding effect of the induced aromatic ring current in the fluorenyl group.

The selective decoupling and COSY experiments revealed eight inequivalent protons for the fluorenyl ligand, in two groups of four coupled spins, corresponding to the two inequivalent C_6-rings. One of these C_6-rings (**e**, **f**, **g**, **h**) shows a chemical shift and coupling pattern similar to the C_6-ring of compound **1**, whilst the other (**a**, **b**, **c**, **d**) is quite different.

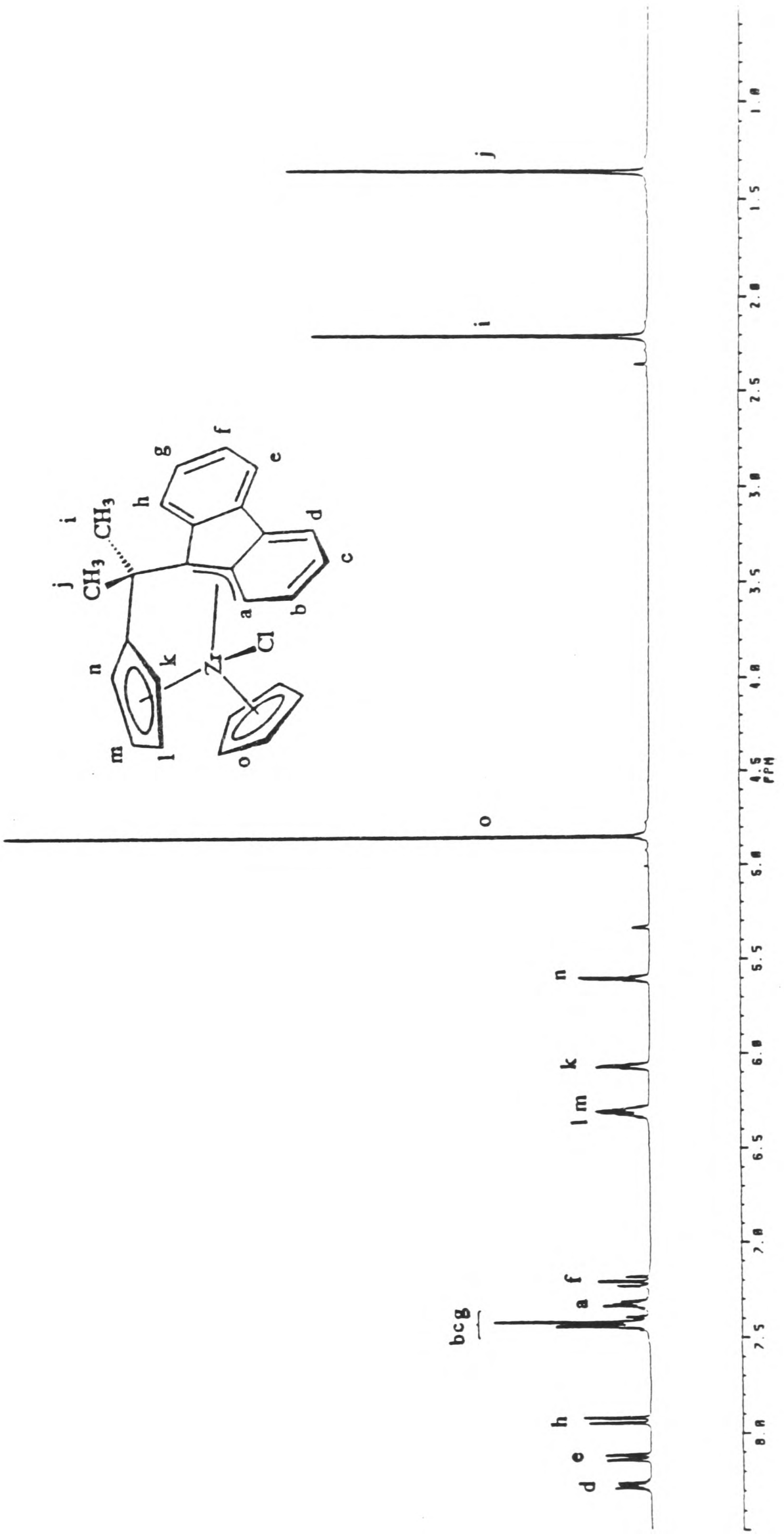

Figure 2.4.3. 300 MHz ^{1}H NMR spectrum of [{$Me_2C(\eta^5$-$C_5H_4)(\eta^3$-$C_{13}H_8)$}$Zr(\eta^5$-$C_5H_5)Cl$] (**5**) in CD_2Cl_2 at r.t.

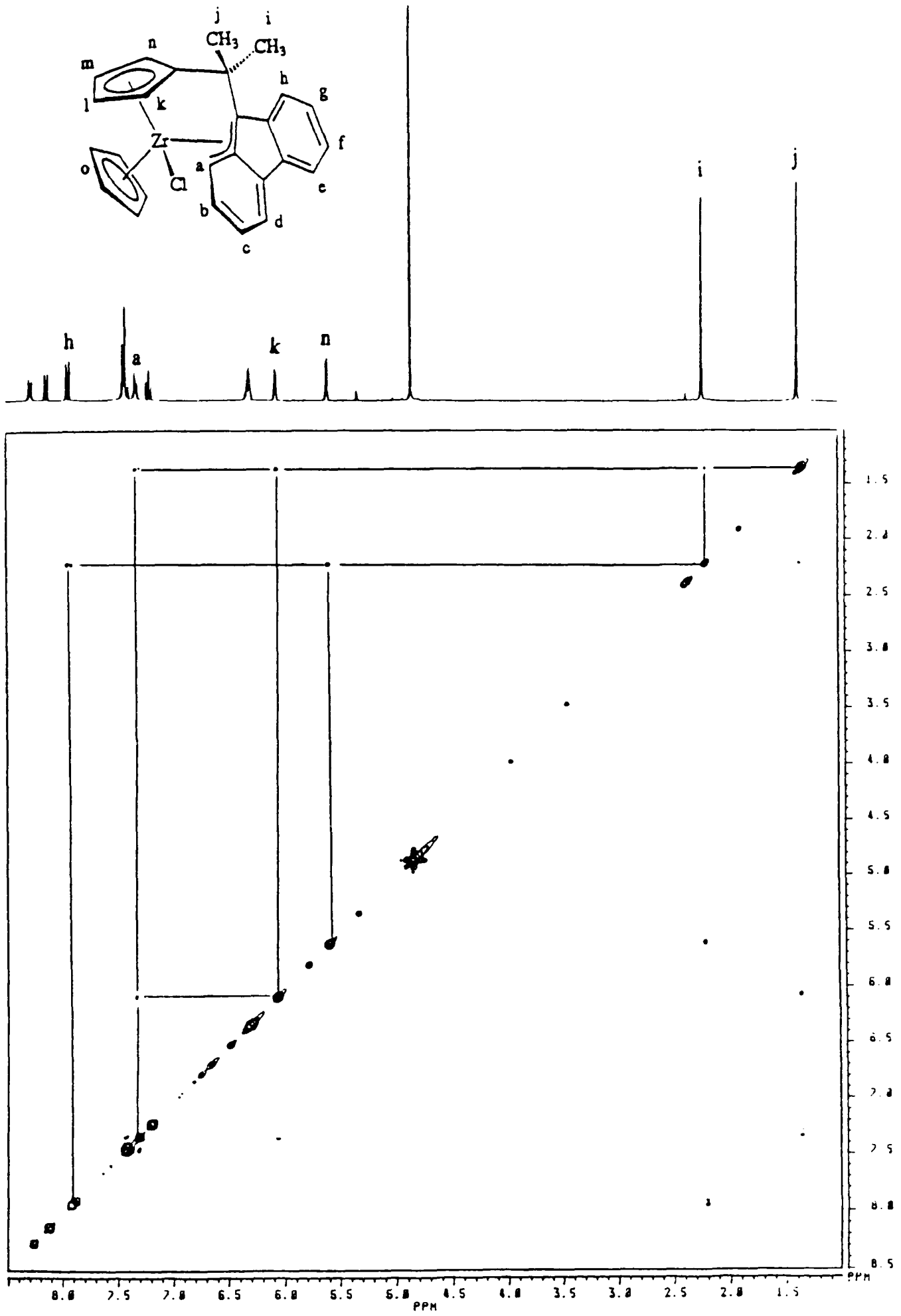

Figure 2.4.4. 300 MHz ^{1}H NOESY spectrum of [{$Me_2C(\eta^5$-$C_5H_4)(\eta^3$-$C_{13}H_8)$}$Zr(\eta^5$-$C_5H_5)Cl$] (**5**) in CD_2Cl_2 at r.t.

The 2-dimensional spectrum from a NOESY experiment employing a mixing time of 2 seconds and a recycle delay of 2.5 seconds (similar to experiment 1 for compound **1**) is shown in Figure 2.4.4. One of the methyl signals (**i**) is correlated with one of the indenyl C_6-ring signals (**h**) and one of the C_5H_4 signals (**n**), whilst the other methyl group (**j**) is correlated with a different indenyl C_6-ring signal (**a**) and a different C_5H_4 signal (**k**).

These correlations are consistent with a **stereorigid molecular structure** without free rotation about the bridging C-C bonds of the *ansa* ligand. They also allow assignment of all of the *ansa* ligand ^1H signals except the C_5H_4 β protons **l** and **m**. The same experiment showed weaker correlations of the C_5H_5 signal (**o**) with **n** and **h**, consistent with the proposed molecular structure, and weak correlations (**m**, **n**) and (**k**, **l**) consistent with the proposed C_5H_4 assignments.

The ^{13}C NMR spectrum of compound **5** in CD_2Cl_2 at room temperature is shown in Figure 2.4.5. The assignments of the CH and CH_3 signals were based on a ^{13}C-^1H shift correlation experiment, and the quaternary signal **p** was assigned to the ipso carbon of the C_5H_4 ring by comparison with many other *ansa*-bridged complexes. The quaternary signal at 70.4 ppm was assigned to the bridgehead carbon of the fluorenyl group (C_r), whilst the signals of the other quaternary carbons of the fluorenyl group (s, t, u and v) lie between 120 and 140 ppm.

The low chemical shift of C_r is not consistent with η^5 coordination of the fluorenyl group to the metal,[43] nor with η^3 coordination of the C_5-ring of the fluorenyl group with C_r as the central carbon of a π-allylic fragment.[44, 45] The chemical shift of C_a is also rather low (105 ppm), which would be consistent with η^3 coordination of the fluorenyl ligand across the C_5-C_6 ring junction, with C_r and C_a as the terminal carbon atoms of a π-allyl system coordinated to the metal. This highly unusual coordination mode was confirmed by a single crystal X-ray structure determination.

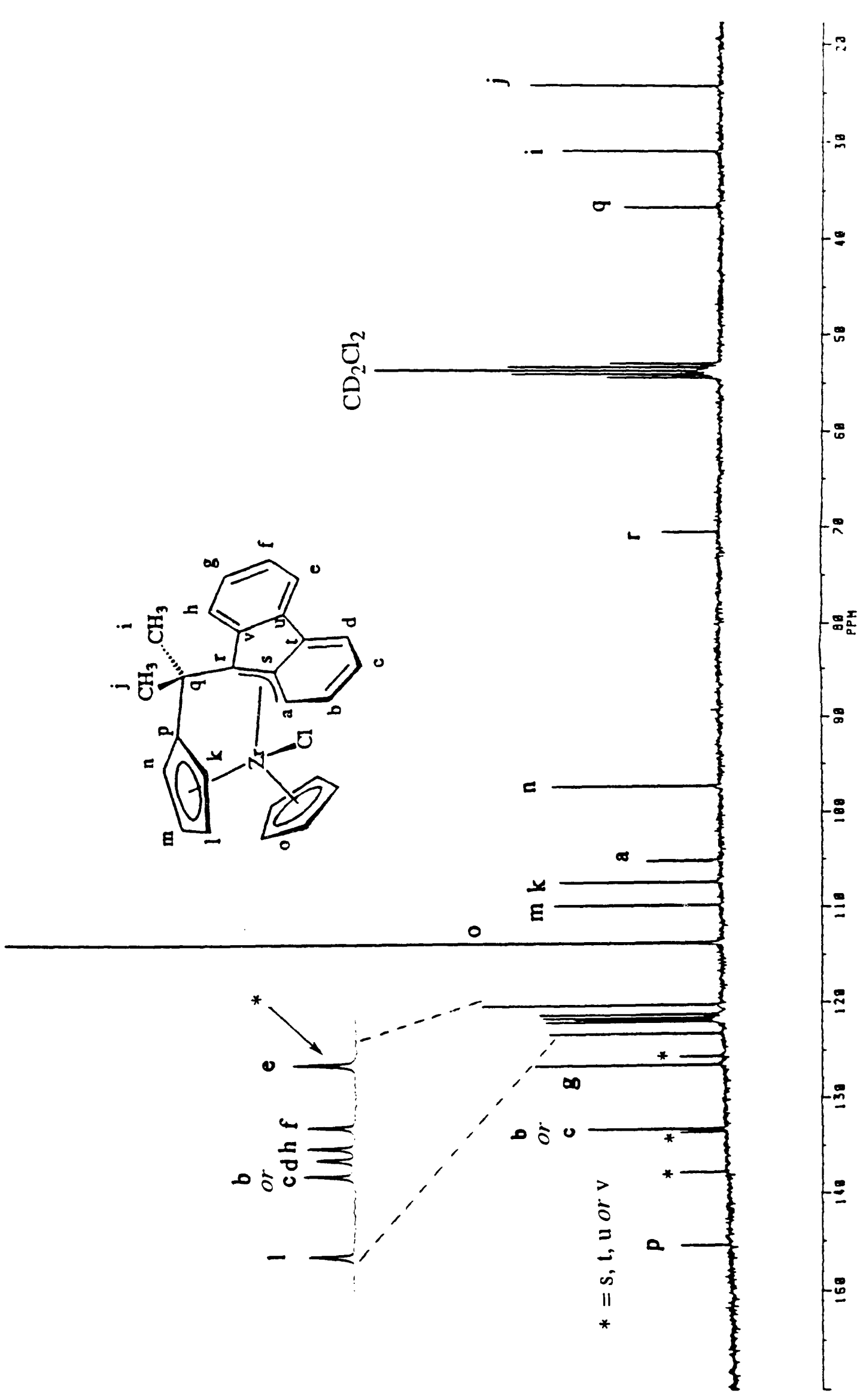

Figure 2.4.5. 75.5 MHz $^{13}C\{^{1}H\}$ NMR spectrum of $[\{Me_2C(\eta^5\text{-}C_5H_4)(\eta^3\text{-}C_{13}H_8)\}Zr(\eta^5\text{-}C_5H_5)Cl]$ (**5**) in CD_2Cl_2 at r.t.

2.4.4. X-ray crystal structure of [{$Me_2C(\eta^5\text{-}C_5H_4)(\eta^3\text{-}C_{13}H_8)$}$Zr(\eta^5\text{-}C_5H_5)Cl$]

Single crystals suitable for an X-ray structure analysis were obtained by cooling a concentrated toluene solution of compound **5**. The deep red coloured crystals were isolated from the toluene solution, washed with petroleum ether (bp. 40-60 °C) and mounted under nitrogen in Lindemann glass capillaries, which were then sealed. The X-ray data were collected by Dr. Vince Murphy and the structure was solved by Dr. Philip Mountford. The enantiomers of **5** crystallise together in racemic crystals with the centrosymmetric space group $P2_1/c$. The molecular structure of **5** is shown in Figure 2.4.6 and selected interatomic distances (Å) and angles (°) are listed in Table 2.3. Further details of the crystal structure determination are given in Appendix C.

Compound **5** adopts a bent-metallocene type structure with mean zirconium-carbon bond lengths and zirconium-centroid distances similar to compounds **1** and **3**, and $[(\eta^5\text{-}C_5H_5)_2ZrCl_2]$.[27, 28] The Zr-Cl bond length [2.560(1) Å] is typical of 18-electron zirconocene derivatives,[37,38] and is considerably longer than those of compounds **1** and **3**.

The most interesting feature of the molecular structure is the unusual η^3 coordination of the fluorenyl group to the metal, via C(7), C(6) and C(5). The fluorenyl group is not planar, but curves around the metal atom; the dihedral angle between the least-squares planes [C(1)-C(6)] and [C(7)-C(13)] is 11.8°. The coordination of the fluorenyl group to the metal resembles π-allyl type bonding, with the C(7), C(6) and C(5) atoms lying close to the equatorial plane between the cyclopentadienyl ligands, as would be required for good π-orbital overlap.[29-31]

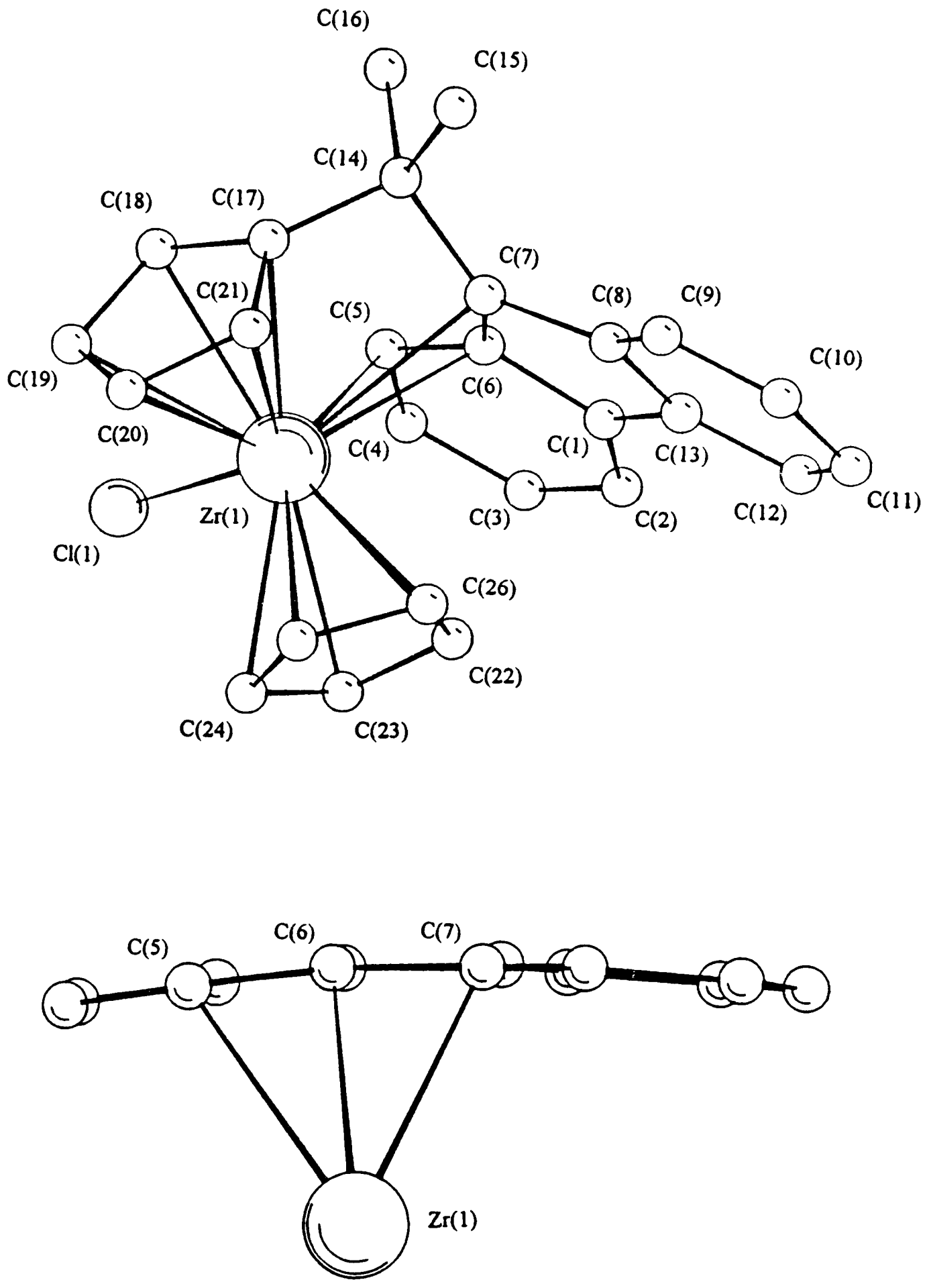

Figure 2.4.6. Molecular structure of [{$Me_2C(\eta^5\text{-}C_5H_4)(\eta^3\text{-}C_{13}H_8)$}$Zr(\eta^5\text{-}C_5H_5)Cl$] (compound **5**), showing detail of the fluorenyl-metal coordination

Table 2.3. Selected interatomic distances (Å) and angles (°) for compound **5**.

Zr(1)-C(5)	2.692(5)	Zr(1)-Cl(1)	2.560(1)
Zr(1)-C(6)	2.633(5)	Zr(1)-C(C_5H_5)$_{mean}$	2.49
Zr(1)-C(7)	2.649(5)	Zr(1)-C(C_5H_4)$_{mean}$	2.49
C(5)-C(6)	1.406(7)	Zr(1)-Cp	2.20
C(6)-C(7)	1.445(7)	Zr(1)-Cp'	2.18
C(7)-C(8)	1.489(7)	C(17)-C(14)-C(7)	103.1(4)
C(1)-C(6)	1.460(6)	C(14)-C(7)-C(6)	124.6(4)
C(1)-C(13)	1.440(7)	C(14)-C(7)-C(8)	126.3(4)

Cp and Cp' denote the centroids of the (C_5H_5) and (C_5H_4) rings respectively.

The Zr-C(7), Zr-C(6) and Zr-C(5) bond lengths [2.649(5), 2.633(5) and 2.692(5) Å respectively] are about 0.2 Å longer than typical π-allyl Zr-C bond lengths,[32] possibly due to steric crowding in compound **5** and the constraints imposed by the *ansa*-bridge. The C(5)-C(6) and C(6)-C(7) bond lengths [1.406(7) and 1.445(7) Å respectively] are consistent with some tendency towards an η^3 σ,π-type coordination mode. The other C-C bond lengths of the fluorenyl group all lie in the range 1.37 to 1.41 Å, except C(7)-C(8) [1.489(7) Å], C(1)-C(6) [1.460(6) Å] and C(1)-C(13) [1.440(7) Å]. The bond lengths of the C(8) to C(13) ring appear to be largely unperturbed by the coordination of the fluorenyl group to the metal centre.

The η^3-fluorenyl coordination observed in compound **5**, across a C_5-C_6 ring junction, is highly unusual. A different η^3-fluorenyl coordination mode has been reported for [(η^3-$C_{13}H_8$)(η^5-$C_{13}H_8$)$ZrCl_2$] (Figure 2.4.7). In this compound one of the fluorenyl ligands is bonded in the normal η^5 fashion to the metal (Zr-C distances from 2.40 to 2.65 Å), whilst the C_5-ring the other fluorenyl is coordinated in an η^3 π-allyl fashion, with only three carbon atoms bonded to the metal (Zr-C distances 2.56,

2.40, 2.59 Å) The other Zr-C distances for the C_5-ring (2.80, 2.81 Å) were considered non-bonding.[44, 45]

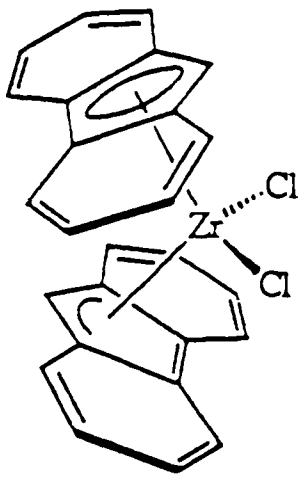

Figure 2.4.7. η^3 and η^5 fluorenyl coordination in $[(\eta^3\text{-}C_{13}H_8)(\eta^5\text{-}C_{13}H_8)ZrCl_2]$

A similar η^3 fluorenyl coordination mode was originally proposed for the *ansa*-metallocenes $[\{Me_2C(\eta^5\text{-}C_5H_4)(\eta^5\text{-}C_{13}H_8)\}MCl_2]$ (M = Zr or Hf, Figure 2.4.8) on the basis of the X-ray crystal structure of the hafnium compound, which showed a progressive increase in the Hf-C bond lengths from the bridgehead carbon (2.40 Å) and the neighbouring α carbons (2.49, 2.57 Å) to the β carbons (both 2.64 Å).[2]

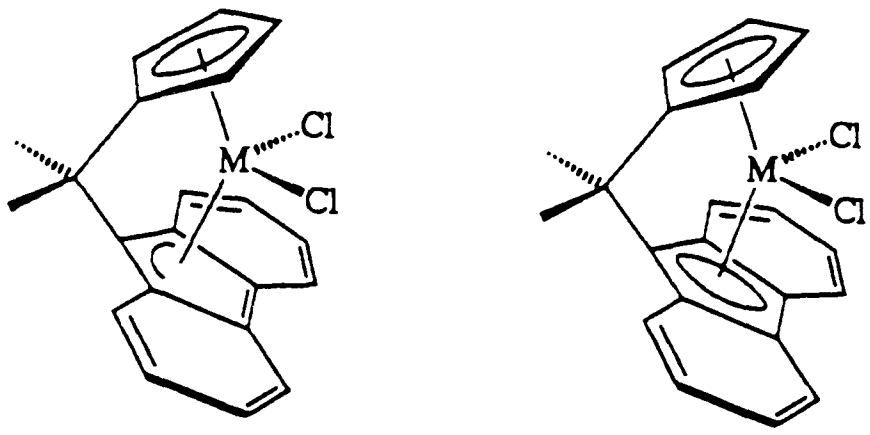

Figure 2.4.8. Original and revised structures proposed for $[\{Me_2C(\eta^5\text{-}C_5H_4)(\eta^5\text{-}C_{13}H_8)\}MCl_2]$ (M = Zr, Hf)[2, 43]

However, in the full paper following the original communication, which also reported the X-ray crystal structure of the zirconium analogue with similar Zr-C distances (2.40: 2.50, 2.53; 2.65, 2.67 Å), it was proposed that the increase in M-C distance was not large enough for η^3 coordination. Instead η^5-fluorenyl coordination was proposed for both the Zr and Hf compounds, and the increase in M-C bond length was ascribed to non-bonding interactions between the fluorenyl ligand and the chlorine atoms.[43] The thermal stability of both the Zr and Hf complexes was also thought to favour the proposed [{$Me_2C(\eta^5\text{-}C_5H_4)(\eta^5\text{-}C_{13}H_8)$}$MCl_2$] description.

The η^3 coordination of the fluorenyl group to the metal in compound **5** shows some resemblence to the η^3-benzyl coordination mode, first proposed by King and Fronzaglia in 1966 for the complex [$(\eta^5\text{-}C_5H_5)Mo(CO)_2(\eta^3\text{-}CH_2C_6H_5)$] on the basis of its fluxional NMR properties.[46] The first crystal structure of an η^3-benzyl complex was reported in 1968 by Cotton and LaPrade for the *para*-methyl analogue [$(\eta^5\text{-}C_5H_5)Mo(CO)_2(\eta^3\text{-}p\text{-}CH_2C_6H_4CH_3)$] (Figure 2.4.9).[47] Over the last 25 years many other η^3-benzyl complexes have been reported,[26] including the recently reported metallocene derivative [$(\eta^5\text{-}C_5Me_5)_2Ce(\eta^3\text{-}CH_2C_6H_5)$].[48]

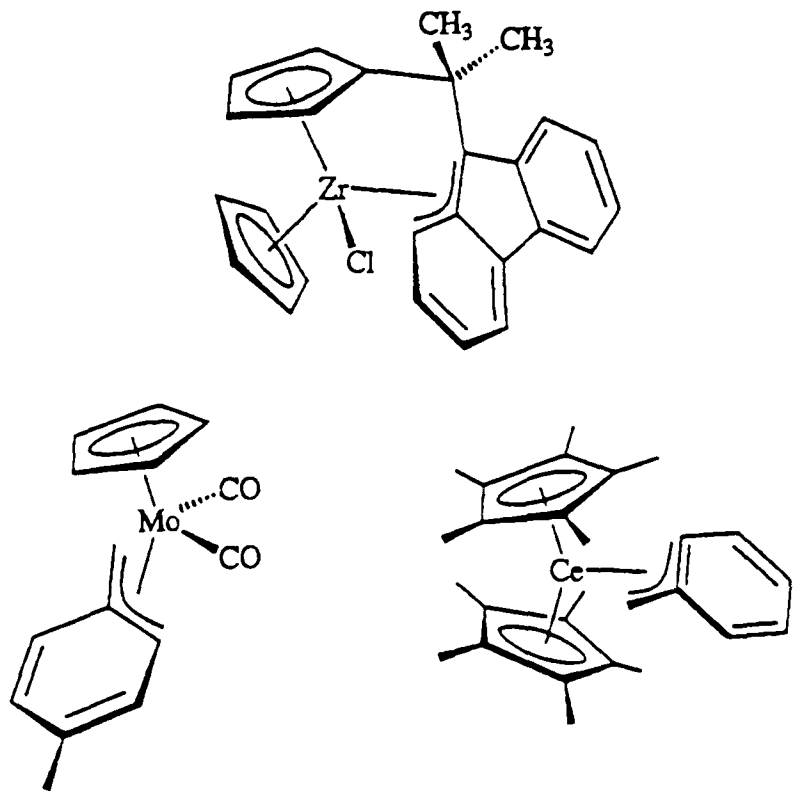

Figure 2.4.9. Compound **5** and the η^3-benzyl complexes [$(\eta^5\text{-}C_5H_5)Mo(CO)_2(\eta^3\text{-}p\text{-}CH_2C_6H_4CH_3)$] and [$Cp^*_2Ce(\eta^3\text{-}CH_2C_6H_5)$]

The C-C bond lengths in **5** more closely resemble those of [$Cp^*_2Ce(\eta^3$-$CH_2C_6H_5)$], which shows significant delocalisation over the phenyl group, compared with [$(CpMo(CO)_2(\eta^3$-*p*-$CH_2C_6H_4CH_3)$] which shows marked alternation of C-C bond lengths. The C(5)-C(6) and C(6)-C(7) bond lengths of **5** are also closer to the corresponding bond lengths of the cerium compound than of the molybdenum compound. The other C-C distances in the fluorenyl group of **5** are consistent with a relatively isolated C(8) to C(13) ring, largely unperturbed by the η^3 benzyl-like coordination of the fluorenyl group to the metal.

For compound **5** the C(17)-C(14)-C(7) angle of 103.1(4)° suggests some strain in the *ansa* ligand, though probably less than in compound **1** and [$\{Me_2C(\eta^5$-$C_5H_4)(\eta^5$-$C_{13}H_8)\}ZrCl_2$], which have corresponding angles of 101.5° and 99.4° respectively. The C(14)-C(7)-C(6) and C(14)-C(7)-C(8) angles [124.6(4)° and 126.3(4)°] in compound **5** are close to the angles expected for an unstrained system. This contrasts with the situation in compound **1**, in which the corresponding angles are significantly distorted for the η^2-indenyl coordination mode, and would have to be further distorted to allow η^3 coordination of the C_5-ring of the indenyl ligand (see Figure 2.2.15). It may be that compound **1** adopts the more strained η^2-indenyl coordination mode rather than an η^3 benzyl-like coordination mode because, although the latter would give a favourable valence electron count of 18, it probably involves more disruption of the aromaticity of the C_6-ring of the indenyl ligand.

It seems likely that the observed η^3 benzyl-like coordination observed in **5** (structure **I** in Figure 2.4.10) represents a compromise between electronic saturation at the metal centre (valence electron count), ligand aromaticity, steric crowding and bond strain. Whilst η^1 coordination at C(7) (structure **II**) would leave two intact aromatic rings in the fluorenyl ligand, the metal would only achieve a 16 valence electron count, and the *ansa* ligand would probably be more strained than in **5**. The alternative η^3 coordination of the fluorenyl C_5-ring (structure **III**), as observed for [$(\eta^3$-$C_{13}H_8)(\eta^5$-$C_{13}H_8)ZrCl_2$], would also involve more ligand strain, and would disrupt both C_6-

aromatic rings (though a 14-electron aromatic system similar to anthracene may be envisaged).

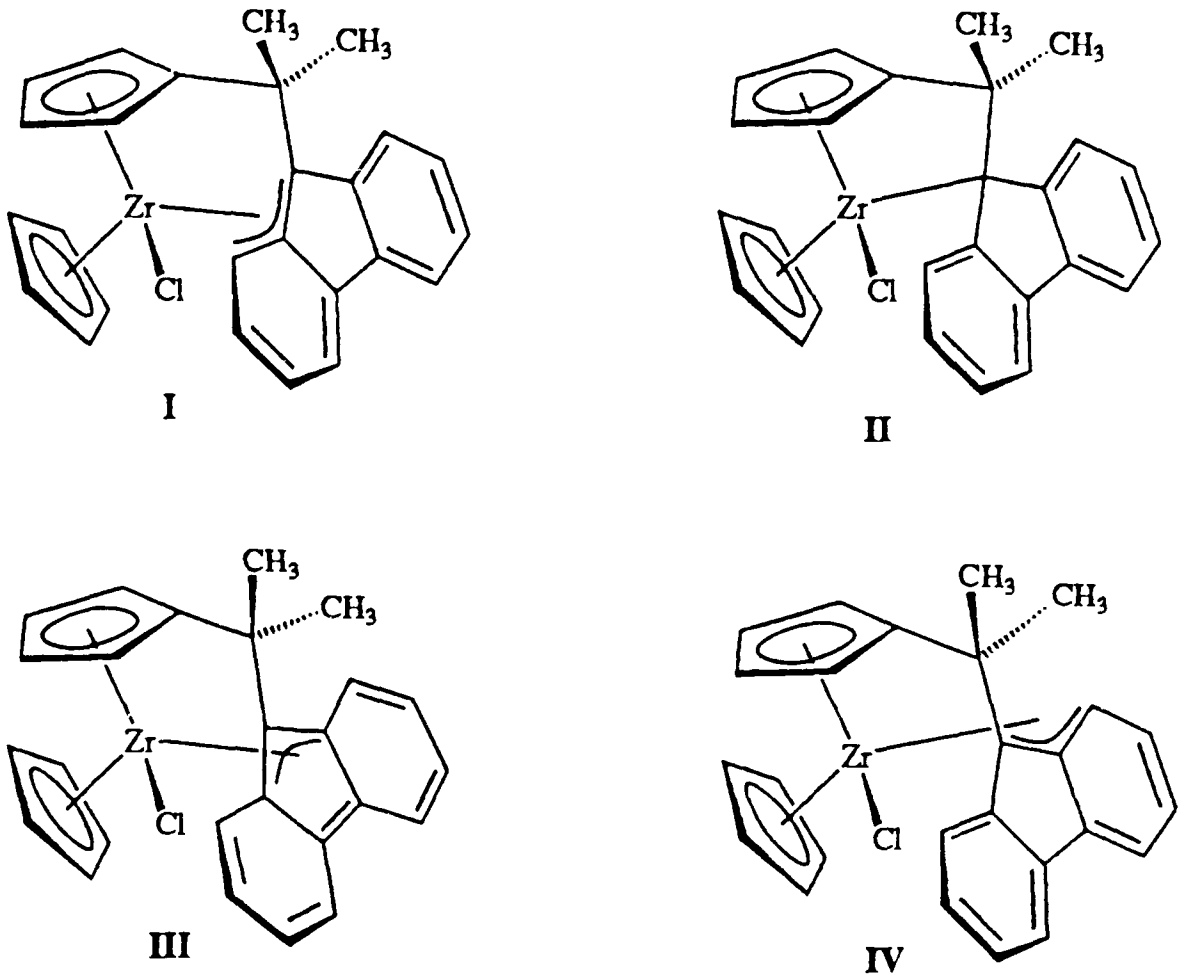

Figure 2.4.10. Alternative η^1 and η^3 fluorenyl coordination modes for compound **5**.

There is also an alternative η^3 benzyl-like coordination possible for compound **5** (structure **IV** in Figure 2.4.10). This is a diastereomer of the observed coordination mode and may be achieved by formally inverting the configuration of the zirconium atom, or by the coordination of the other face of the fluorenyl group at the same carbon atoms (or by the coordination of the same face of the other C_6-ring of the fluorenyl group).

There are two possible configurations that this alternative η^3 benzyl-like diastereomer could adopt in which the three coordinating carbon atoms lie close to the equatorial plane of the metallocene fragment, as would be required for good π-orbital overlap.[29,30] One of these [**IV(a)** in Figure 2.4.11] may be disfavoured by strain in the highly distorted *ansa* ligand geometry that would be required, while the other [**IV(b)**]

may be disfavoured by steric factors, since it would require very close approach of one of the CH_3 groups and the C_5H_5 ligand, as shown below.

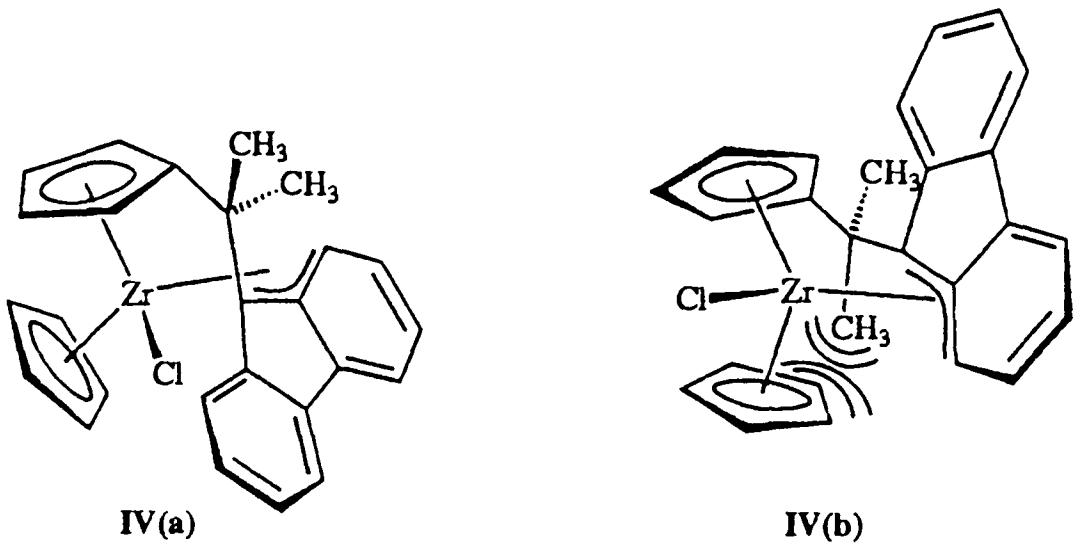

IV(a) **IV(b)**

Figure 2.4.11. Two possible conformations of the alternative η^3 benzyl-like diastereomer of **5** that would allow good π-orbital overlap.

2.5 Synthesis of $[\{Me_2C(\eta^5\text{-}C_5H_4)_2\}M(\eta^5\text{-}C_5H_5)Cl]$

The preceding sections have discussed the synthesis and molecular structures of the novel, *ansa*-bridged mononuclear complexes **1-5**, in which the bridging ligands $[Me_2C(C_5H_4)(C_9H_6)]$, $[(CH_2)_5C(C_5H_4)(C_9H_6)]$ and $[Me_2C(C_5H_4)(C_{13}H_8)]$ adopt unprecedented modes of coordination. It was decided to continue the investigation of the effects of a short *ansa* bridge on molecular structure by studying the reaction of the *ansa*-bis(cyclopentadienyl) ligand $[\{Me_2C(C_5H_4)_2\}Li_2]$ with $[(\eta^5\text{-}C_5H_5)MCl_3\cdot 2L]$ (M = Zr, Hf; 2L = DME, 2THF). The work in this section was carried out in collaboration with a colleague, Neil Popham, who prepared the zirconium compound (**6**) while the author prepared the hafnium compound (**7**).[49]

2.5.1 Preparation of $[\{Me_2C(C_5H_4)_2\}Li_2]$

The *ansa*-bis(cyclopentadienyl) ligand $[\{Me_2C(C_5H_4)_2\}Li_2]$ was prepared as shown in Figure 2.5.1. A recent literature synthesis of the neutral ligand, from the reaction of cyclopentadiene monomer and 6,6-dimethylfulvene in a NaOH / THF mixture, was employed.[9] The neutral ligand (an oil) was then dissolved in diethyl ether, cooled to 0 °C, and treated with two equivalents of n-BuLi. After stirring at room temperature overnight, the very air- and moisture-sensitive white solid $[\{Me_2C(C_5H_4)_2\}Li_2]$ was isolated by filtration, washed with diethyl ether and dried *in vacuo*. The ^1H NMR spectrum of $[\{Me_2C(C_5H_4)_2\}Li_2]$ in d^8-THF showed that no diethyl ether solvate was present.

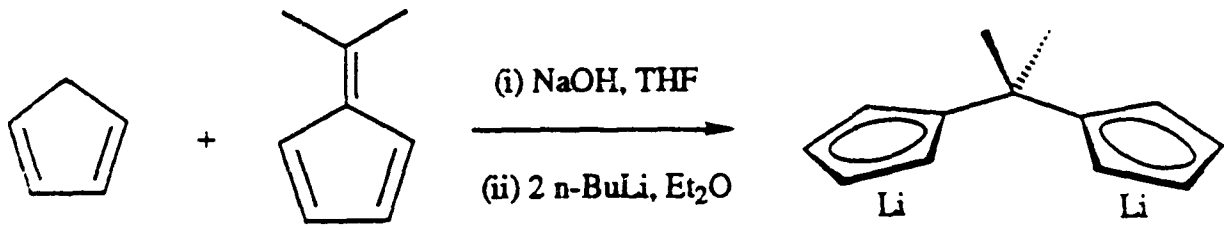

Figure 2.5.1. Preparation of $[\{Me_2C(C_5H_4)_2\}Li_2]$

2.5.2 Synthesis of $[\{Me_2C(\eta^5\text{-}C_5H_4)_2\}M(\eta^5\text{-}C_5H_5)Cl]$ (M = Zr, Hf)

$[\{Me_2C(C_5H_4)_2\}Li_2]$ and one equivalent of either $[(\eta^5\text{-}C_5H_5)ZrCl_3\cdot DME]$ or $[(\eta^5\text{-}C_5H_5)HfCl_3\cdot 2THF]$ were weighed into a Schlenk tube. Toluene was then added to the mixture of white solids at room temperature, and the resulting yellow mixture was stirred at room temperature for 60 hours. A clear yellow solution was then filtered from the solid residues, which were extracted with more toluene. The toluene solutions were then concentrated under reduced pressure and cooled to -20 °C. After several days, pale yellow crystals were isolated from solution, and characterised as the novel, mononuclear *ansa*-bridged complexes $[\{Me_2C(\eta^5\text{-}C_5H_4)_2\}M(\eta^5\text{-}C_5H_5)Cl]$ [M

= Zr (**6**) or Hf (**7**), Figure 2.5.2]. Further crops of crystals were obtained, giving final yields of 41 % (**6**) and 43 % (**7**).

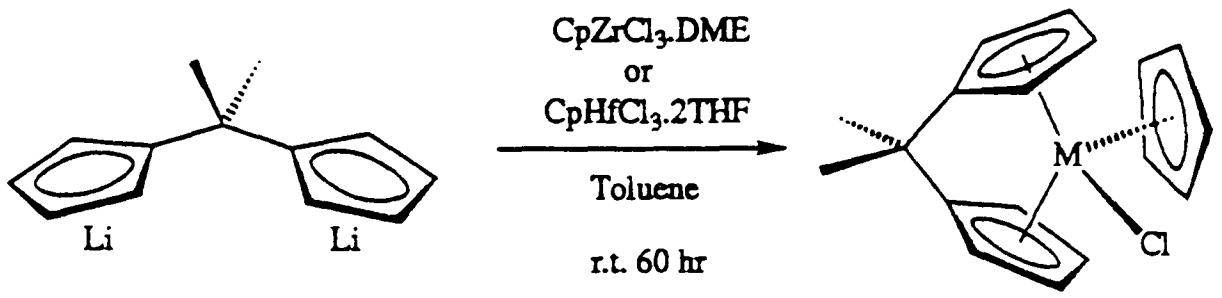

Figure 2.5.2. Synthesis of [{$Me_2C(\eta^5\text{-}C_5H_4)_2$}M($\eta^5\text{-}C_5H_5$)Cl] [M = Zr (**6**), Hf (**7**)]

2.5.3 Characterisation of [{$Me_2C(\eta^5\text{-}C_5H_4)_2$}M($\eta^5\text{-}C_5H_5$)Cl] (M = Zr, Hf)

Compounds **6** and **7**, both pale yellow, air- and moisture-sensitive crystalline solids, were characterised by elemental analysis, ^1H and ^{13}C NMR studies and single crystal X-ray structure determinations. The elemental analyses were consistent with the molecular formulae $C_{18}H_{19}ClM$, corresponding to [{$Me_2C(C_5H_4)_2$}M(C_5H_5)Cl] [M = Zr (**6**), Hf (**7**)]. The room temperature ^1H NMR spectra of **7** in C_6D_6 is shown in Figure 2.5.3, and the ^{13}C NMR spectrum of **7** in d^8-THF is shown in Figure 2.5.4. The ^1H NMR spectrum of **6** in C_6D_6 is shown in Figure 2.5.5, together with the spectra of **1** and **5** in C_6D_6.

The ^1H NMR spectra of both **6** and **7** include four C_5H_4 multiplet signals each of integrated intensity 2H, one sharp singlet of intensity 5H corresponding to C_5H_5 and two singlets (each 3H) corresponding to the methyl groups. Irradiation of any one of the C_5H_4 multiplets results in decoupling being observed in the other three. The room temperature ^1H and ^{13}C NMR spectra of **6** and **7** are consistent with a molecular structure in which the two C_5H_4 groups are equivalent and in which there is fast reorientation of the C_5H_5 ligand (compared with the NMR timescale). Low temperature NMR studies (500 MHz ^1H, d^8-THF, 304 to 173 K for **7**; 300 MHz ^1H and 75.5 MHz ^{13}C, 291 K to 173 K for **6**) show no evidence of lowering of symmetry or freezing out of any fluxionality.

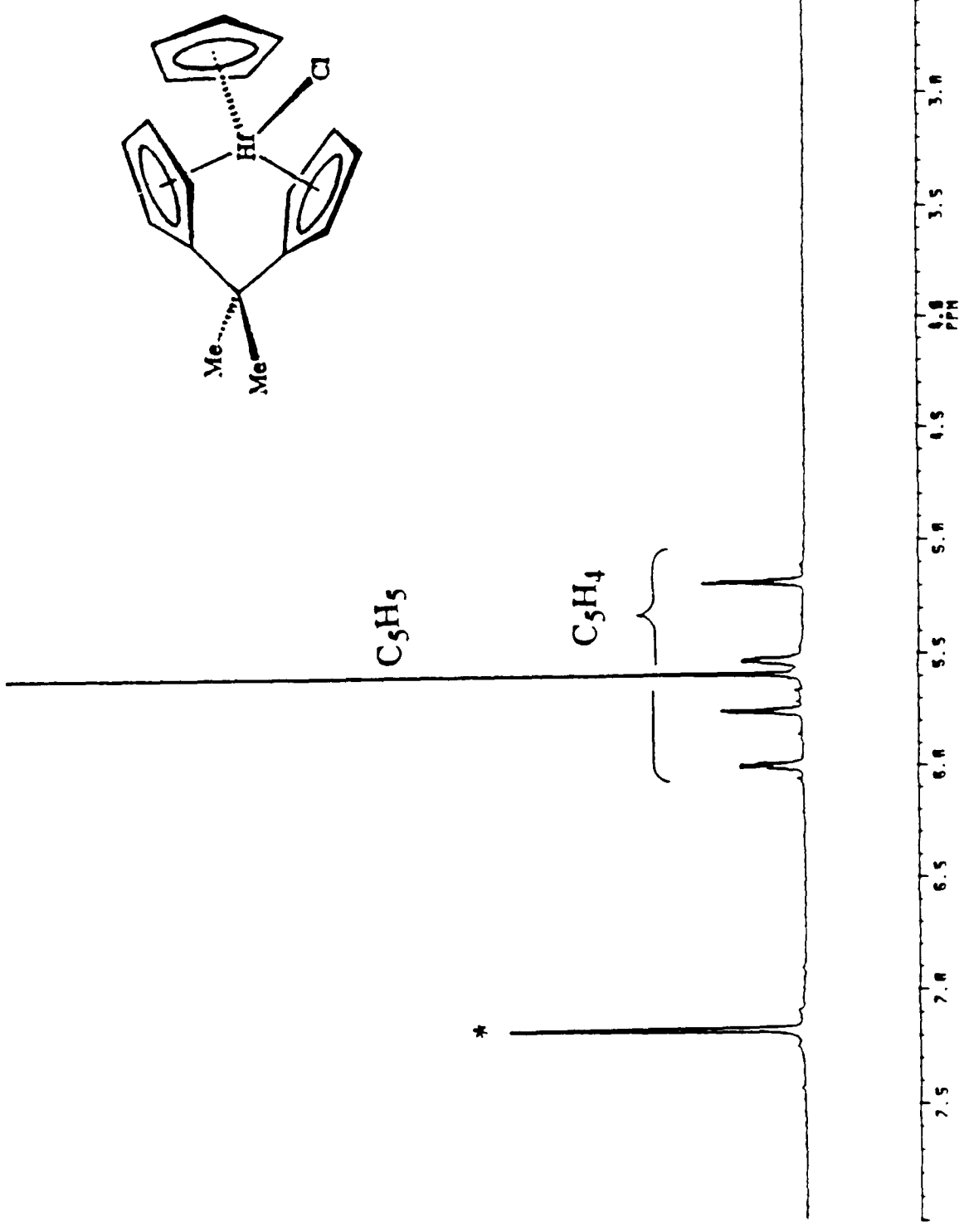

Figure 2.5.3. 300 MHz ^{1}H NMR spectrum of $[\{Me_2C(\eta^5\text{-}C_5H_4)_2\}Hf(\eta^5\text{-}C_5H_5)Cl]$ (**7**) in C_6D_6 at r.t. (* = benzene solvent)

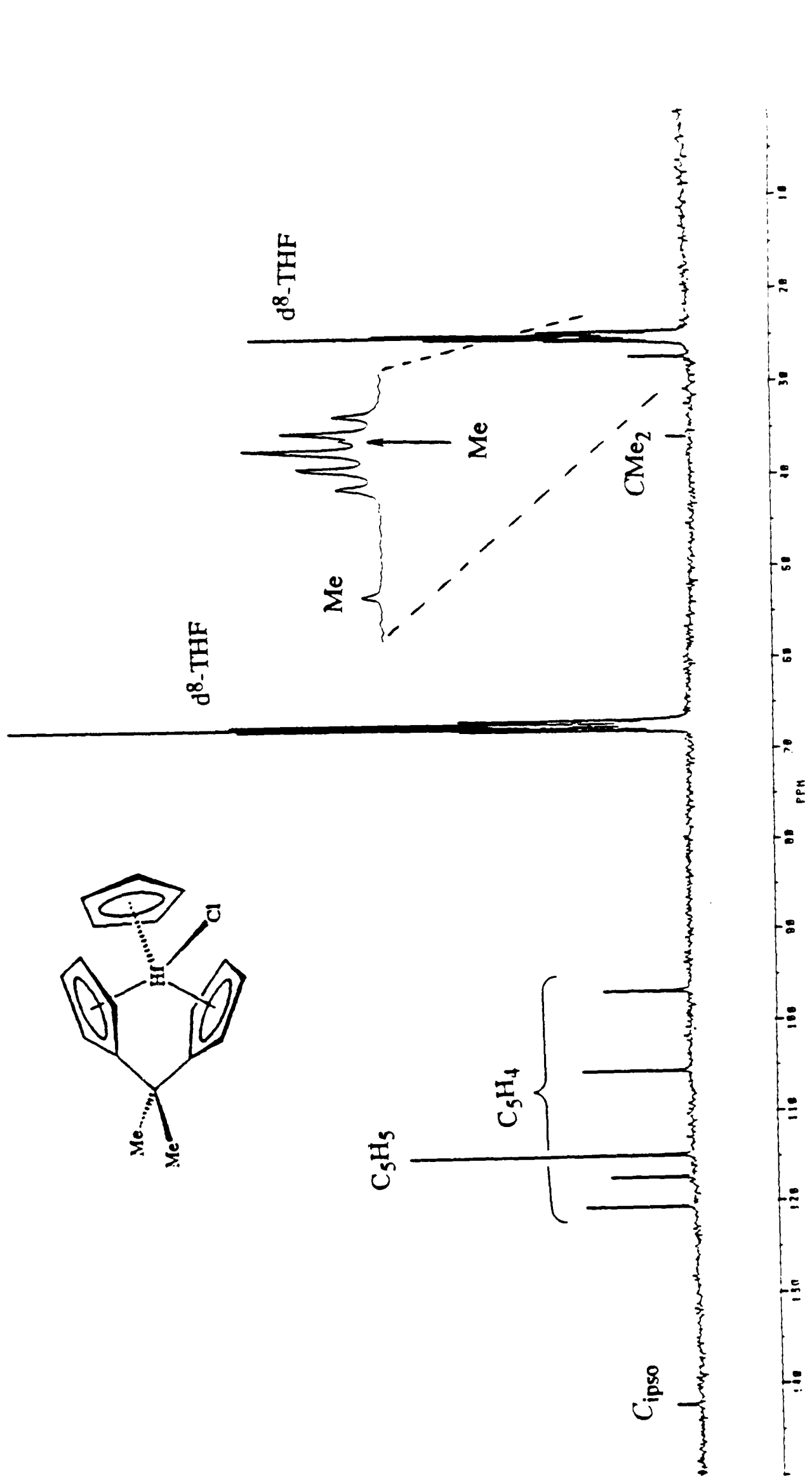

Figure 2.5.4. 75.5 MHz $^{13}C\{^1H\}$ NMR spectrum of $[\{Me_2C(\eta^5\text{-}C_5H_4)_2\}Hf(\eta^5\text{-}C_5H_5)Cl]$ (7) in d^8-THF at r.t.

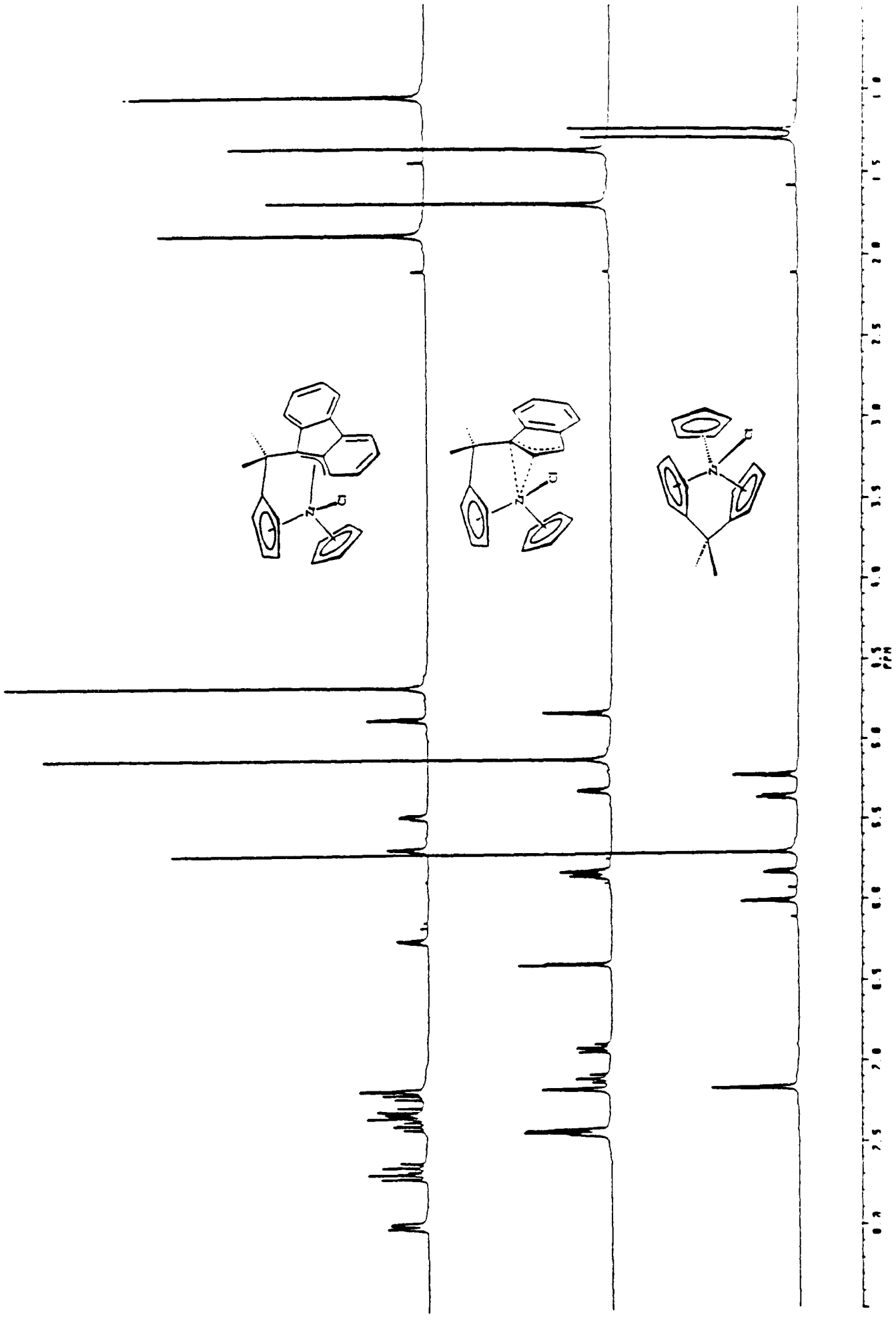

Figure 2.5.5. 300 MHz ^{1}H NMR spectra of in C_6D_6 at r.t. of

[{$Me_2C(\eta^5\text{-}C_5H_4)(\eta^3\text{-}C_{13}H_8)$}$Zr(\eta^5\text{-}C_5H_5)Cl$] (**5**)

[{$Me_2C(\eta^5\text{-}C_5H_4)(\eta^2\text{-}C_9H_6)$}$Zr(\eta^5\text{-}C_5H_5)Cl$] (**1**)

[{$Me_2C(\eta^5\text{-}C_5H_4)_2$}$Zr(\eta^5\text{-}C_5H_5)Cl$] (**6**)

2.5.4. X-ray crystal structure of [{$Me_2C(\eta^5\text{-}C_5H_4)_2$}Hf($\eta^5$-$C_5H_5$)Cl]

Single crystals suitable for an X-ray structure analysis of compound **7** were obtained from a concentrated toluene solution of **7** cooled to -20 °C and maintained at that temperature for two weeks. The pale yellow crystals were isolated from the toluene solution, washed with diethyl ether and mounted under nitrogen in Lindemann glass capillaries, which were then sealed. The X-ray structure determination was carried out by Dr. Alexander Chernega. Compound **7** crystallises in the space group $P2_1$. The molecular structure of **7** is shown in Figure 2.5.6 and selected interatomic distances (Å) and angles (°) are listed in Table 2.4. Further details of the crystal structure determination are given in Appendix D. The X-ray crystal structure of compound **6** has also been determined.[49] Compound **6** also crystallises in the space group $P2_1$ and is **isostructural** with compound **7**. The molecular structure of **6** is shown in Figure 2.5.7 and selected interatomic distances (Å) and angles (°) are listed in Table 2.5.

The molecular structures in Figures 2.5.6 and 2.5.7, and the X-ray crystal structure data, clearly show that compound **7** is essentially isostructural with compound **6**. For both **6** and **7**, all three rings show η^5 coordination to the metal centre. Only three authentic tris(η^5-cyclopentadienyl) transition metal compounds have been reported previously, and in each case the transition metal is zirconium.[50-53] When the crystal structures of the hafnium analogues of these compounds have been determined, they have ***not*** shown tris(η^5-cyclopentadienyl) coordination.[53-55]

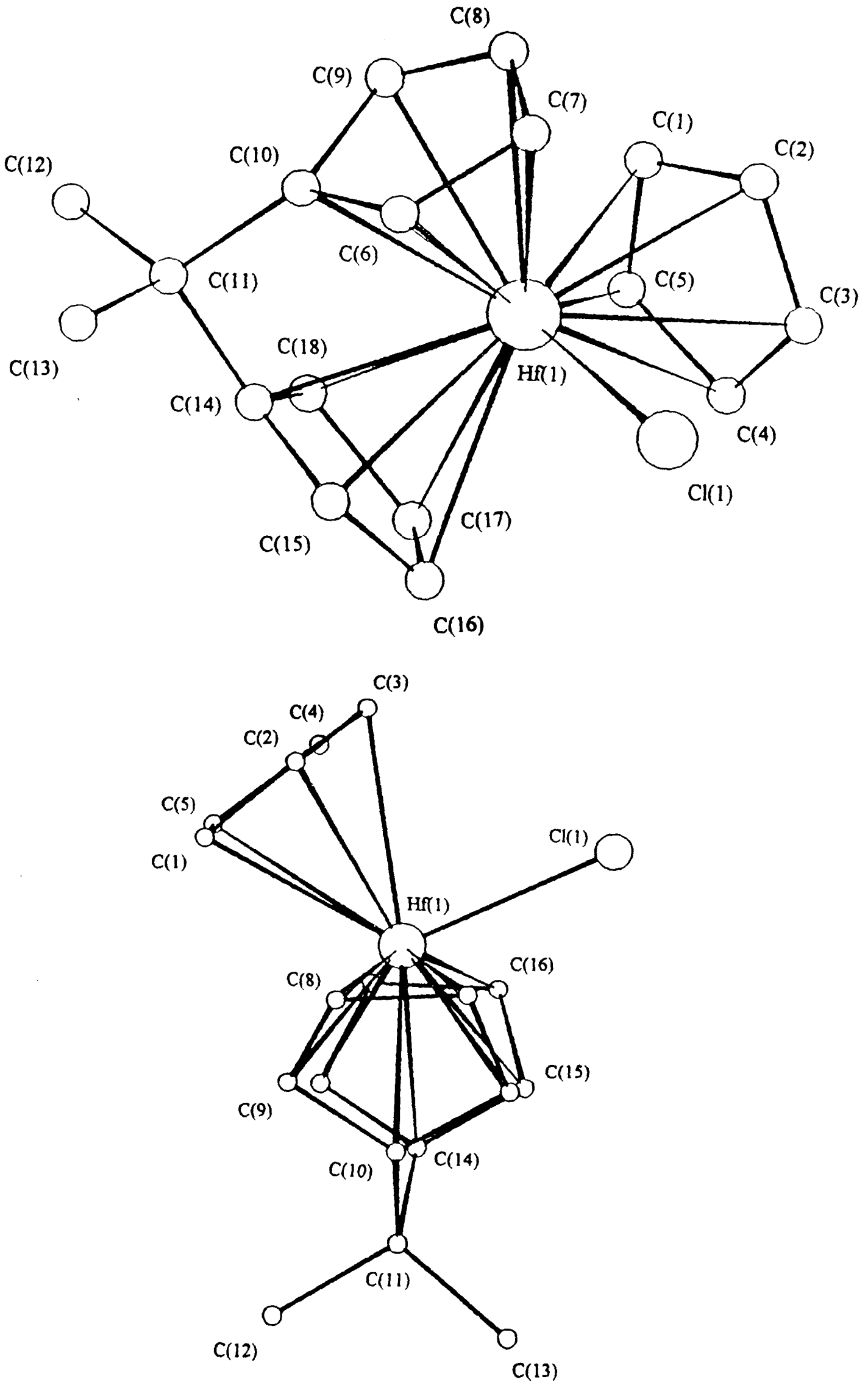

Figure 2.5.6. Two views of the molecular structure of

$[\{Me_2C(\eta^5\text{-}C_5H_4)_2\}Hf(\eta^5\text{-}C_5H_5)Cl]$ (**7**)

Table 2.4. Selected interatomic distances (Å) and angles (°) for compound **7**.

Hf(1)-Cl(1)	2.510(1)	R1'-Hf(1)-R2'	120.2
Hf(1)-$R1_{mean}$	2.59	R1'-Hf(1)-R3'	118.5
Hf(1)-$R2_{mean}$	2.57	R2'-Hf(1)-R3'	111.2
Hf(1)-$R3_{mean}$	2.58	Cl(1)-Hf(1)-R1'	100.5
Hf(1)-R1'	2.297	Cl(1)-Hf(1)-R2'	98.7
Hf(1)-R2'	2.270	Cl(1)-Hf(1)-R3'	103.0
Hf(1)-R3'	2.287	C(10)-C(11)-C(14)	97.7(5)

Hf(1)-C(1)	2.49(2)	Hf(1)-C(7)	2.64(2)
Hf(1)-C(2)	2.57(1)	Hf(1)-C(10)	2.51(2)
Hf(1)-C(3)	2.632(6)	Hf(1)-C(16)	2.63(1))
Hf(1)-C(4)	2.67(2)	Hf(1)-C(17)	2.69(2)
Hf(1)-C(5)	2.60(2)	Hf(1)-C(18)	2.48(2)

C(1)-C(2)	1.41(2)	C(6)-C(10)	1.51(2)
C(1)-C(5)	1.42(1)	C(8)-C(9)	1.31(3)
C(2)-C(3)	1.41(3)	C(14)-C(15)	1.33(2)
C(3)-C(4)	1.39(4)	C(17)-C(18)	1.52(2)
C(4)-C(5)	1.46(3)		

$Hf(1)\text{-}R1_{mean}$ is the mean Zr-C distance for the ring R1, and R1' denotes the centroid of ring R1, where R1 is C(1) to C(5), R2 is C(6) to C(10) and R3 is C(14) to C(18).

Table 2.5. Selected interatomic distances (Å) and angles (°) for compound **6**.

Zr(1)-Cl(1)	2.5363(7)	R1'-Zr(1)-R2'	119.6
Zr(1)-$R1_{mean}$	2.59	R1'-Zr(1)-R3'	119.1
Zr(1)-$R2_{mean}$	2.59	R2'-Zr(1)-R3'	110.6
Zr(1)-$R3_{mean}$	2.57	Cl(1)-Zr(1)-R1'	100.7
Zr(1)-R1'	2.301	Cl(1)-Zr(1)-R2'	100.2
Zr(1)-R2'	2.306	Cl(1)-Zr(1)-R3'	102.0
Zr(1)-R3'	2.277	C(10)-C(11)-C(14)	99.4(2)

Zr(1)-C(1)	2.55(1)	Zr(1)-C(7)	2.690(9)
Zr(1)-C(2)	2.61(1)	Zr(1)-C(9)	2.51(1)
Zr(1)-C(3)	2.634(3)	Zr(1)-C(17)	2.63(1)
Zr(1)-C(4)	2.61(1)	Zr(1)-C(18)	2.518(8)
Zr(1)-C(5)	2.56(1)		

C(1)-C(2)	1.33(2)	C(6)-C(10)	1.32(2)
C(1)-C(5)	1.418(5)	C(8)-C(9)	1.49(2)
C(2)-C(3)	1.35(2)	C(14)-C(15)	1.50(1)
C(3)-C(4)	1.45(2)	C(17)-C(18)	1.33(2)
C(4)-C(5)	1.48(2)		

$Zr(1)\text{-}R1_{mean}$ is the mean Zr-C distance for the ring R1, and R1' denotes the centroid of ring R1, where R1 is C(1) to C(5), R2 is C(6) to C(10) and R3 is C(14) to C(18).

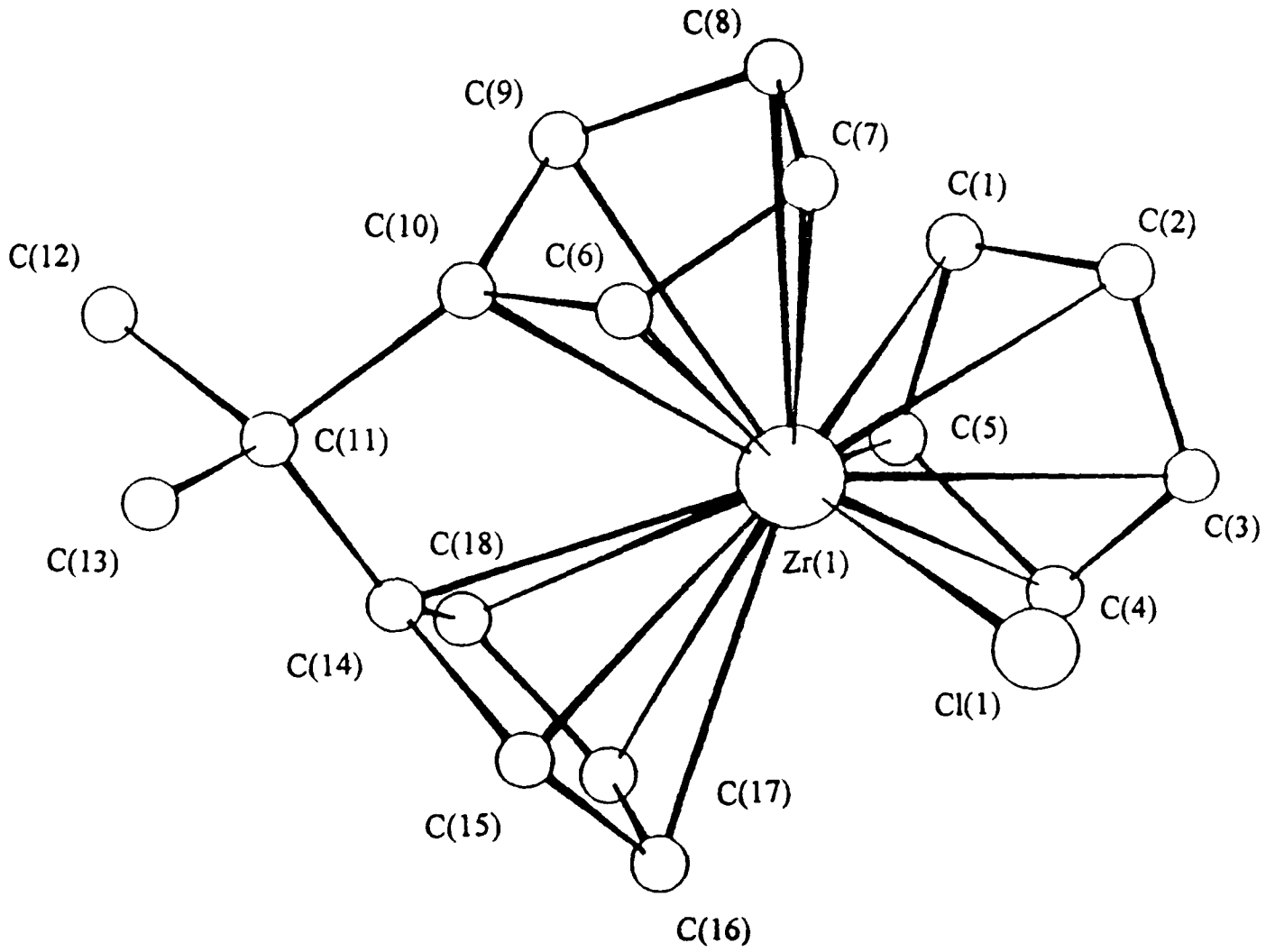

Figure 2.5.7. Molecular structure of $[\{Me_2C(\eta^5\text{-}C_5H_4)_2\}Zr(\eta^5\text{-}C_5H_5)Cl]$ (**6**)

The first crystallographically characterised tris(η^5-cyclopentadienyl) transition metal compound was $[(\eta^5\text{-}C_5H_5)_3Zr(\eta^1\text{-}C_5H_5)]$.[50, 51] This molecular structure was first proposed in 1970,[51] but the crystallographic work was of poor quality, and the tris(η^5-cyclopentadienyl) formulation was immediately questioned.[56] The molecular structures of the titanium and hafnium analogues of $[(C_5H_5)_4Zr]$ were also reported in the early 1970s, and both were shown to adopt the more normal "bent metallocene" type structure $[(\eta^5\text{-}C_5H_5)_2M(\eta^1\text{-}C_5H_5)_2]$ (M = Ti, Hf).[56, 55]

These results were considered most unusual, since zirconium and hafnium were thought to differ only slightly (but significantly) in their chemical behaviour and never in the structure of their organometallic derivatives.[54] Also, following the normal electron counting rules would result in a valence electron count of 20 for zirconium in

the proposed [(η^5-C_5H_5)$_3$Zr(η^1-C_5H_5)] molecule, which was considered unlikely.[56] In 1978 the crystal stucture of [$(C_5H_5)_4$Zr] was re-evaluated and, although the original crystallographic work was shown to be in error, the originally proposed [(η^5-C_5H_5)$_3$Zr(η^1-C_5H_5)] molecular structure was confirmed.[50] Similarly, a re-evaluation of the structure of [$(C_5H_5)_4$Hf] in 1981 confirmed the originally proposed [(η^5-C_5H_5)$_2$Hf(η^1-C_5H_5)$_2$] structure.[54] The molecular structures of [$(C_5H_5)_4$Ti], [$(C_5H_5)_4$Zr] and [$(C_5H_5)_4$Hf] are shown in Figure 2.5.8.

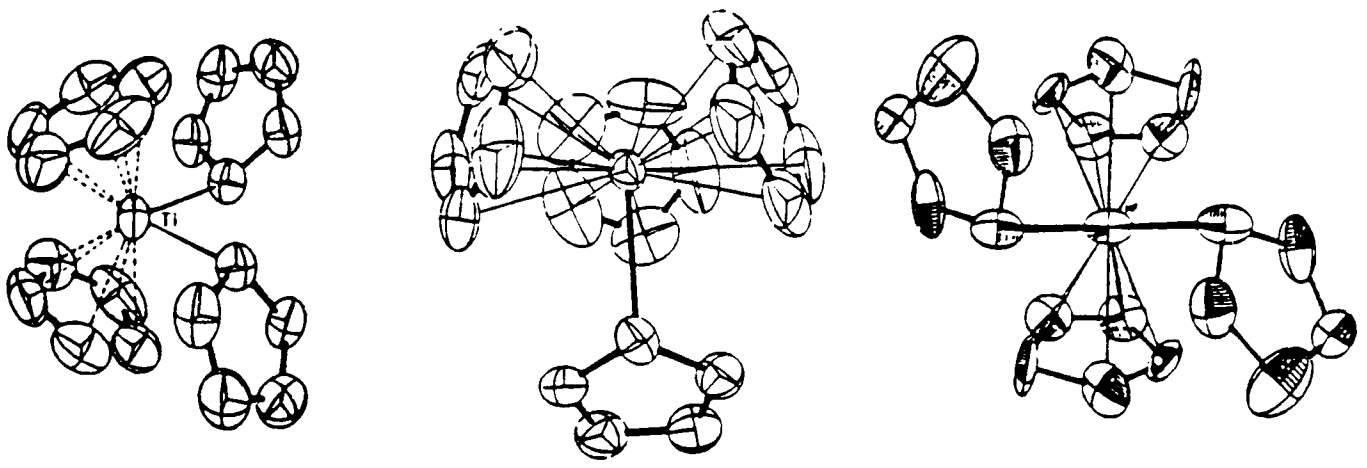

[$(C_5H_5)_4$Ti] [$(C_5H_5)_4$Zr] [$(C_5H_5)_4$Hf]

Figure 2.5.8. Molecular structures [$(C_5H_5)_4$M], M = Ti,[56] Zr,[50] Hf.[54]

These were the only structurally characterised zirconium and hafnium organometallic compounds that were not isostructural within a given ligand set. It has been suggested that the slightly smaller atomic radius of hafnium compared with zirconium, due to the "lanthanide contraction", might account for the difference in structure since the very long Zr-η^1-carbon distance (2.45 Å) in [(η^5-C_5H_5)$_3$Zr(η^1-C_5H_5)] suggests significant steric crowding, which would be expected to be worse if Zr was replaced by the slightly smaller Hf. However, the difference in the covalent radii of Zr and Hf is very small, about 0.01 Å.

Until very recently the only other structurally characterised tris(η^5-cyclopentadienyl) transition metal compound, and the only structurally characterised

tris(cyclopentadienyl) zirconium derivative, was the $AlEt_3$ aduct of $[(C_5H_5)_3ZrH]$, namely $[(\eta^5\text{-}C_5H_5)_3Zr(\mu\text{-}H)AlEt_3]$ (Figure 2.5.9).[52]

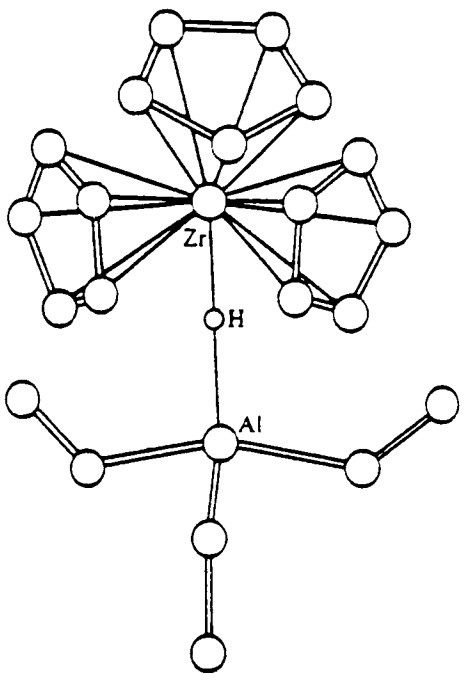

Figure 2.5.9. Molecular structure of $[(\eta^5\text{-}C_5H_5)_3Zr(\mu\text{-}H)AlEt_3]$

The molecular structures of **6** and **7** are probably best compared with the recently determined X-ray crystal structures of the non-bridged tris(cyclopentadienyl) zirconium and hafnium chloride derivatives $[(\eta^5\text{-}C_5H_5)_3ZrCl]$ and $[(\eta^5\text{-}C_5H_5)_2Hf(\eta^1\text{-}C_5H_5)Cl]$, shown in Figure 2.5.10.[53] Although the quality of the $[(\eta^5\text{-}C_5H_5)_2Hf(\eta^1\text{-}C_5H_5)Cl]$ crystal structure is poor, it is believed that the connectivity of the atoms can be trusted. Thus, as with the $[(\eta^5\text{-}C_5H_5)_4M]$ compounds, $[(C_5H_5)_3ZrCl]$ and $[(C_5H_5)_3HfCl]$ adopt different solid state structures; the zirconium derivative adopting a tris(η^5-cyclopentadienyl) structure, whilst the hafnium derivative adopts a more normal "bent metallocene" bis(η^5-cyclopentadienyl) structure, with the third C_5H_5 ligand adopting η^1 coordination. It has been predicted from molecular orbital calculations that the titanium analogue would adopt a structure similar to that found for hafnium, namely $[(\eta^5\text{-}C_5H_5)_2Ti(\eta^1\text{-}C_5H_5)Cl]$.[57]

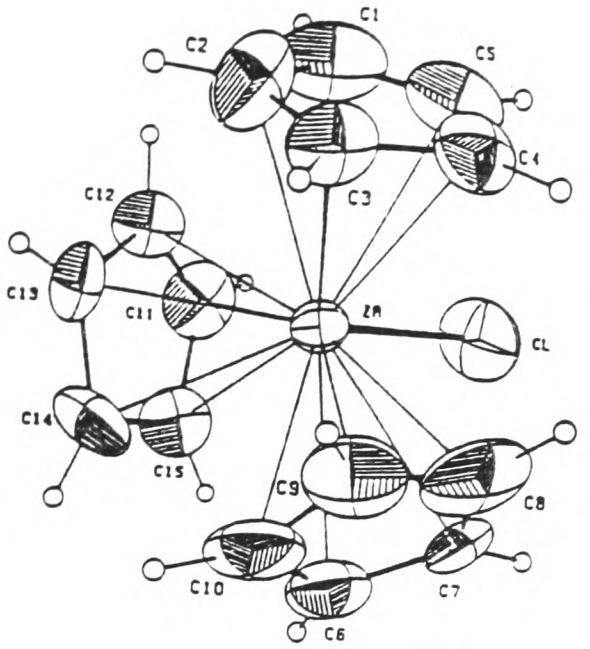

$[(\eta^5\text{-}C_5H_5)_3ZrCl]$

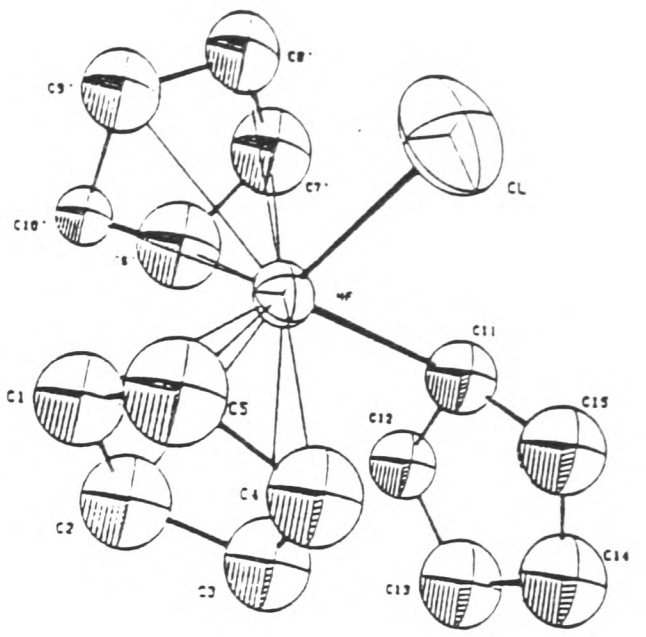

$[(\eta^5\text{-}C_5H_5)_2Hf(\eta^1\text{-}C_5H_5)Cl]$

Figure 2.5.10. Molecular structures of $[(\eta^5\text{-}C_5H_5)_3ZrCl]$ and $[(\eta^5\text{-}C_5H_5)_2Hf(\eta^1\text{-}C_5H_5)Cl]$

Bearing in mind the molecular structures of $[(\eta^5\text{-}C_5H_5)_3Zr(\eta^1\text{-}C_5H_5)]$, $[(\eta^5\text{-}C_5H_5)_2Hf(\eta^1\text{-}C_5H_5)_2]$, $[(\eta^5\text{-}C_5H_5)_3ZrCl]$ and $[(\eta^5\text{-}C_5H_5)_2Hf(\eta^1\text{-}C_5H_5)Cl]$, probably the most interesting aspect of the molecular structures of **6** and **7** is that they are essentially isostructural and that for both compounds all three rings show η^5-coordination to the metals.

In both **6** and **7** the mean M-C bond lengths of the three rings are similar. The overall mean M-C bond length is 2.58 Å for both **6** and **7**, which is identical to the values reported for the tris(η^5-cyclopentadienyl) zirconium derivatives $[(\eta^5\text{-}C_5H_5)_3Zr(\eta^1\text{-}C_5H_5)]$, $[(\eta^5\text{-}C_5H_5)_3ZrHAlEt_3]$ and $[(\eta^5\text{-}C_5H_5)_3ZrCl]$. The rings are planar to within 0.033 Å for **6** and 0.061 Å for **7**, compared with 0.04 Å for $[(\eta^5\text{-}C_5H_5)_3Zr(\eta^1\text{-}C_5H_5)]$. The M-C and C-C bond distances for compounds **7** and **6** are shown in Figure 2.5.11. It should be noted that, compared with, for example, the

molecular structures of **1**, **3** and **5**, the e.s.d. for the M-C and C-C distances in **7** and **6** are quite high. The bond distances should be viewed with this in mind.

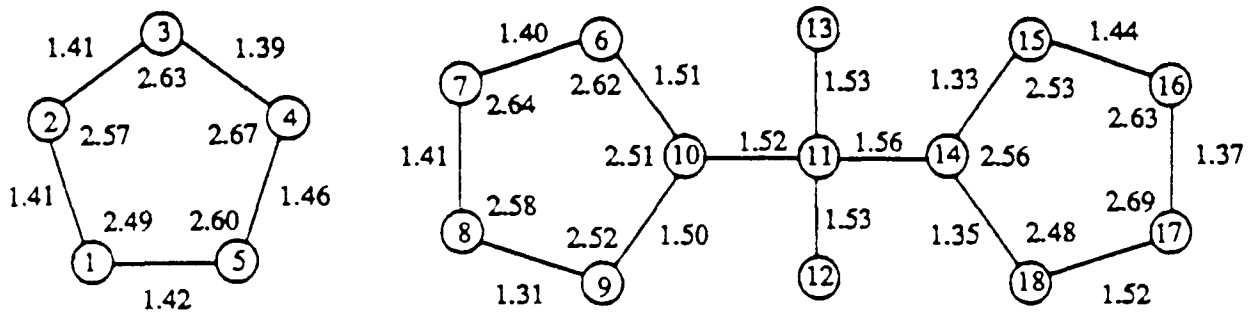

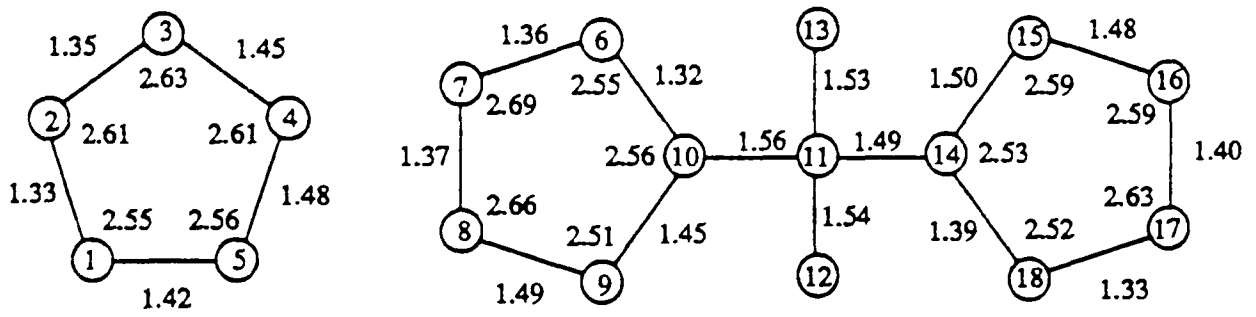

Figure 2.5.11. Some bond distances for compounds **7** (above) and **6** (below). Numerals beside carbon atoms (inside rings) give M-C distances, figures beside bond lines give C-C distances. The e.s.d. of M-C distances are up to 0.02 (Hf) and 0.01 (Zr); the e.s.d. of C-C distances are up to 0.04 (Hf) and 0.02 (Zr).

In both **6** and **7** the M-C and C-C distances for the rings show large variations. For compound **7**, $[\{Me_2C(\eta^5\text{-}C_5H_4)_2\}Hf(\eta^5\text{-}C_5H_5)Cl]$, the Hf-C distances show significant variations from the mean of 2.58 Å. For R1 the mean is 2.59 Å and the range is 2.49 to 2.67 Å; for R2, 2.57 Å and 2.51 to 2.64 Å; for R3, 2.58 Å and 2.48 to 2.69 Å. Similar bond distances and variations are observed for compound **6**. The range of M-C distances in **6** and **7** is, however, similar to those of $[(\eta^5\text{-}C_5H_5)_3Zr(\eta^1\text{-}C_5H_5)]$ in which the Zr-C distances for the $(\eta^5\text{-}C_5H_5)$ rings also have a mean of 2.58

Å, and vary from 2.52 to 2.63 Å; they are also similar to those reported for [(η^5-$C_5H_5)_3ZrCl$] (mean 2.58 Å, ranging from 2.53 to 2.66 Å). A similar range of Zr-C bond lengths (2.40 to 2.65 Å) is observed for the η^5-fluorenyl ligand in the sterically crowded [(η^3-$C_{13}H_8$)(η^5-$C_{13}H_8$)$ZrCl_2$].[44, 45]

It seems likely that the range of M-C and C-C distances in **6** and **7** reflect not only the unusual tris(η^5-cyclopentadienyl) coordination mode and the resulting steric crowding, but also significant intramolecular tension due to the short *ansa* bridge. The C(10)-C(11)-C(14) angle is 97.7(5)° for (**7**), whilst the corresponding angle for **6** of 99.4(2)° is identical to that reported for the related *ansa*-metallocene [{$Me_2C(\eta^5$-$C_5H_4)_2$}$Zr(CH_3)_2$] for which the Zr-C distances range from 2.45 Å for the bridgehead carbons to 2.57 Å for the β carbons of the C_5H_4 rings.[58]

Brintzinger has compared the molecular structures of the *ansa*-metallocenes [$(CH_2)_n(\eta^5$-$C_5H_4)_2TiCl_2$] (n = 1, 2, 3) and concluded that the C-C-C angle at the methylene carbon atom (n = 1) indicates a high degree of strain.[59] Compared with the $(CH_2)_2$ and $(CH_2)_3$ bridged analogues, the CH_2-bridged titanocene showed a large range of Ti-C bond lengths (2.30 to 2.45 Å) and the $CH_2(C_5H_4)_2$ framework showed further distortions, including C-C bond lengths ranging from 1.20 to 1.67 Å. Part of this variation was thought to be an artifact of the poor crystal shape, but Brintzinger suggested that it might also indicate some tendency towards a less delocalised, (η^3-allyl, η^2-olefinic) coordination mode for the C_5H_4 rings. It was suggested that such a distortion of the rings might serve to reduce the repulsive interaction between the two ring π-systems resulting from the close approach of the bridgehead carbon atoms.

The C_5H_4 rings of **6** and **7** are close to eclipsed, and the large range of C-C bond lengths might also reflect similar distortions of the ligand framework in order to reduce repulsive interactions. For example, the long C(6)-C(10), C(9)-C(10) and C(11)-C(14) distances in **7**, together with the short C(10)-C(11), C(14)-C(15) and C(14)-C(18) distances, might be expected to reduce the repulsive interactions between the very close bridgehead carbon atoms C(10) and C(14). Different distortions around the bridgehead carbon atoms of **6** might also have the same effect.

The unsymmetrical metal-ring bonding in **6** and **7** might also be compared with the series of compounds $[(C_5H_5)_2Mo(NO)X]$ where X = I, CH_3 or $(\eta^1\text{-}C_5H_5)$, for which the molecular formulae $[(\eta^5\text{-}C_5H_5)(\eta^3\text{-}C_5H_5)Mo(NO)X]$ were originally proposed (Figure 2.5.12).[60, 61] This was thought likely because, if the normal electron counting rules are followed (Mo has 6 electrons, univalent ligand X donates one electron and the proposed linear NO ligand donates three electrons), then two C_5H_5 rings donating 5 electrons each would give a total valence electron count of 20, which was thought highly unfavourable and unlikely.[60, 61] Following similar valence electron counting rules also gives a count of 20 for **6** and **7**, and one might expect one of the rings to adopt η^3 (or η^1) coordination, reducing the valence electron count of 18 (or 16).

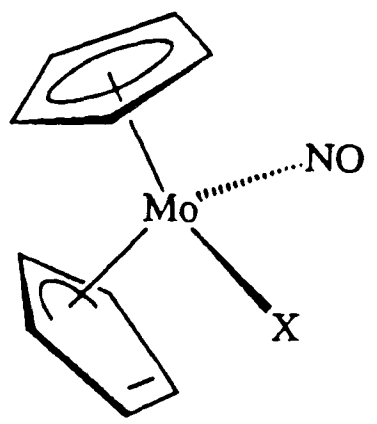

Figure 2.5.12. Originally proposed $(\eta^5\text{-}C_5H_5)(\eta^3\text{-}C_5H_5)$ structure for $[(C_5H_5)_2Mo(NO)X]$ compounds

However, the X-ray crystal structures of $[(C_5H_5)_2Mo(NO)(\eta^1\text{-}C_5H_5)]$ and $[(C_5H_5)_2Mo(NO)(CH_3)]$ showed that for both compounds the $(\eta^5\text{-}C_5H_5)(\eta^3\text{-}C_5H_5)$ formulation was incorrect and that both rings showed similar and unsymmetrical bonding to the metal atom in which there are two short (2.31 to 2.39 Å), one medium (2.42 to 2.46) and two long (2.47 to 2.71 Å) Mo-C distances.[62-64] Cotton suggested that, according to a previously proposed correlation of bond lengths with bond orders for Mo-C bonds, the short Mo-C distances indicated single bonds, the medium distances slightly weaker ones and the long Mo-C distances correspond to bond orders

of around 0.6. The important point is that these (C_5H_5) ligands showed a very unsymmetrical coordination to the metal, but all five ring atoms must be considered as bonding to the metal.[63] Thus, in so far as "hapticity" gives a topological description of the molecular structure indicating the connectivity of atoms avoiding subjective judgements about bonding details, as originally intended,[65] both (C_5H_5) rings in the compounds [$(C_5H_5)_2Mo(NO)X$] should be considered as (η^5-C_5H_5) ligands, even though normal electron counting rules suggest they should donate only four electrons each to the metal.[63]

The molecular structures of **6** and **7** and the other tris(η^5-cyclopentadienyl) zirconium complexes present similar problems of bonding description. For group 4 complexes of the type [$(\eta^5$-$C_5H_5)_3MX$], if each (η^5-C_5H_5) ring donates the normal five electrons to the metal and X donates one electron, then the metal achieves an unfavourable valence electron count of 20. Cotton disputed the originally proposed molecular structure of [$(\eta^5$-$C_5H_5)_3Zr(\eta^1$-$C_5H_5)$] on these grounds, and suggested that two of the (η^5-C_5H_5) ligands should be considered as four electron donors, by analogy with the [$(C_5H_5)_2Mo(NO)X$] complexes.[56]

However, Lauher and Hoffmann have proposed that for transition metal complexes of the type [$(\eta^5$-$C_5H_5)_3MX$] with C_{3v} symmetry, one of the molecular orbitals resulting from the combination of the three C_5H_5 rings has a_2 symmetry.[66] Since transition metals have no valence orbitals of a_2 symmetry in the C_{3v} point group, this molecular orbital cannot serve as a donor orbital. Thus group 4 complexes of the type [$(\eta^5$-$C_5H_5)_3MX$] will have, in effect, 18-electron rather than 20-electron configurations and each (η^5-C_5H_5) ring donates fewer than the normal five electrons, hence the average M-C bond order is less than one. Lauher and Hoffman's interaction diagram for Cp_3M^+ (C_{3v} symmetry) is shown in Figure 2.5.13, together with the ligand-based orbital with a_2 symmetry. The bulk of tris(η^5-cyclopentadienyl) compounds are found within the lanthanide and actinide series.[67] These metals have valence f orbitals, one of which has a_2 symmetry in the C_{3v} point group.[53, 68]

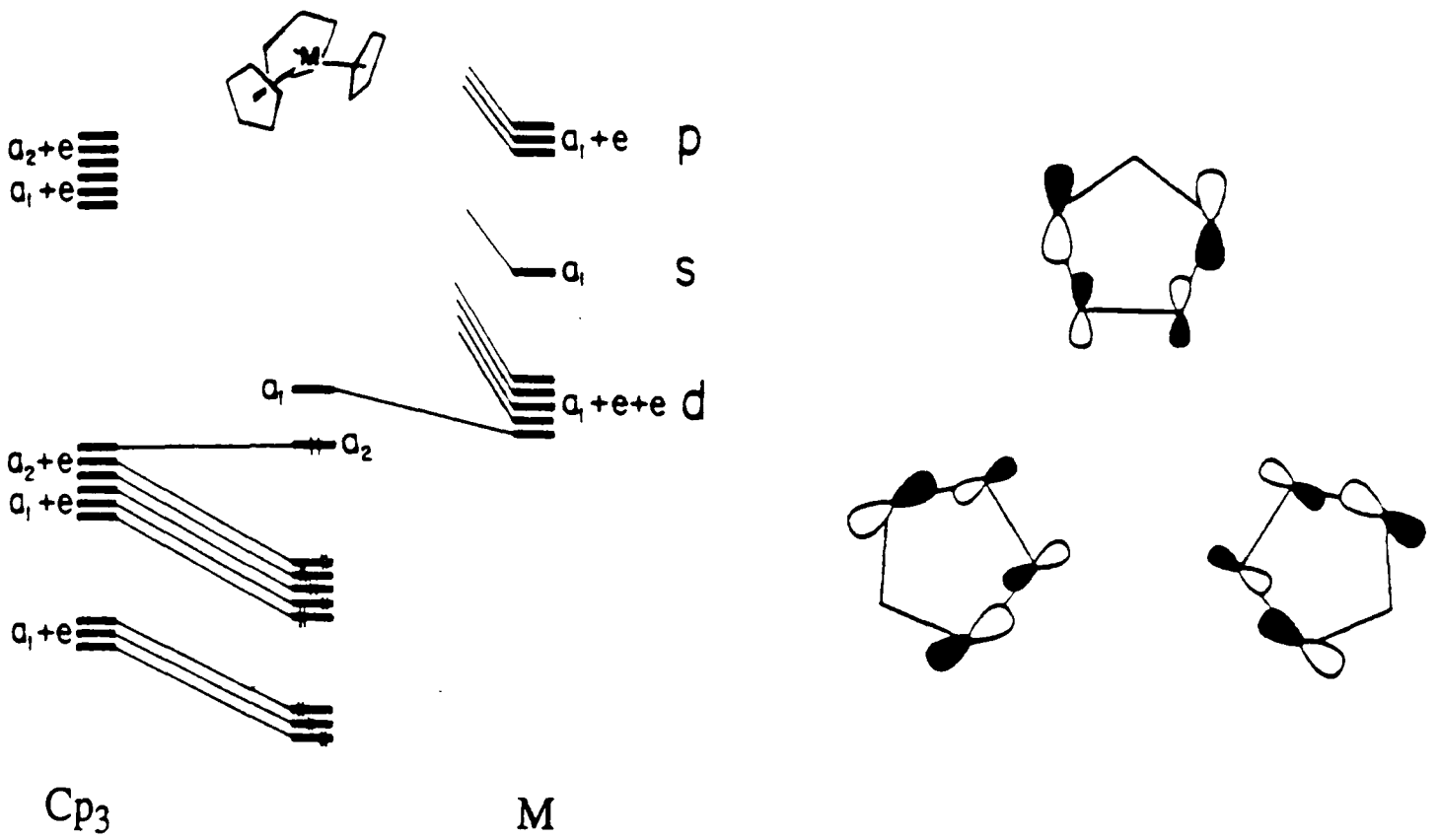

Figure 2.5.13. Interaction diagram for Cp_3M^+ (C_{3v} symmetry) showing ligand-based a_2 orbital

Although the *ansa* bridge in **6** and **7** lowers the symmetry from C_{3v}, it seems likely that a similar argument may apply. This may account for the significantly longer M-C bond lengths in **6** and **7** and the other tris(η^5-cyclopentadienyl)zirconium derivatives (all average 2.58 Å) compared with $[(\eta^5\text{-}C_5H_5)_2ZrCl_2]$ (2.49 Å)[27] and $[(\eta^5\text{-}C_5H_5)_2HfCl_2]$ (2.47 Å).[28] Even the very sterically crowded zirconocene derivative $[(\eta^5\text{-}C_5H_5)_2Zr(CH(SiMe_3)_2)(C_6H_5)]$ has a mean Zr-C(C_5H_5) bond length of only 2.54 Å.[50]

The molecular structure of **6** differs most significantly from that of the non-bridged analogue in the centroid-Zr-centroid angles. For **6**, the angle between the centroids of the bridged rings is only 110.6°, compared with over 119° for the non-bridged angles. For $[(\eta^5\text{-}C_5H_5)_3ZrCl]$ the three centroid-Zr-centroid angles are very similar and average 117.3°, compared with 127.0° for $[(\eta^5\text{-}C_5H_5)_2ZrCl_2]$. For

compound **7**, the 111.2° angle between the centroids of the rings joined by the short CMe_2 bridge is much smaller than the centroid-Hf-centroid angles in $[(\eta^5\text{-}C_5H_5)_2Hf(\eta^1\text{-}C_5H_5)Cl]$ (129°) and $[(\eta^5\text{-}C_5H_5)_2HfCl_2]$ (127.1°).

It seems likely that the structures adopted by tris(cyclopentadienyl) transition metal complexes depend on a fine balance between steric and electronic factors. Although the atomic radius of hafnium is only about 0.01 Å less than that of zirconium, average M-C and M-Cl bond lengths are about 0.02 to 0.03 Å shorter in organometallic compounds of hafnium compared with zirconium.[28, 32] The cumulative increase in steric crowding in the $[(\eta^5\text{-}C_5H_5)_2MCl]$ fragment may be sufficient to disfavour η^5 coordination of the third C_5H_5 ligand when M = Hf. The **reduced steric crowding** experienced by the C_5H_5 ligand in **7**, as a result of the **short *ansa*-bridge** between the other two rings, may allow it to adopt η^5 coordination, and complex **7** thus attains a favoured 18-electron configuration.

Compound **7**, $[\{Me_2C(\eta^5\text{-}C_5H_4)_2\}Hf(\eta^5\text{-}C_5H_5)Cl]$, is the **first example** of a tris(η^5-cyclopentadienyl) derivative of hafnium, or of any transition metal (groups 4 to 10) other than zirconium. The molecular structure of **7** compared with $[(\eta^5\text{-}C_5H_5)_2Hf(\eta^1\text{-}C_5H_5)Cl]$ demonstrates the effect that an *ansa* bridge can have on the gross structure of a complex. The molecular structures of the related *ansa*-bridged complexes $[\{Me_2C(\eta^5\text{-}C_5H_4)(\eta^2\text{-}C_9H_6)\}Zr(\eta^5\text{-}C_5H_5)Cl]$ (**1**) and $[\{Me_2C(\eta^5\text{-}C_5H_4)(\eta^3\text{-}C_{13}H_8)\}Zr(\eta^5\text{-}C_5H_5)Cl]$ (**5**) also show unexpected coordination modes which are believed to reflect the constraints imposed by the short CMe_2 *ansa* bridges.

2.6 Solid state ^{13}C NMR spectra of $[\{Me_2C(\eta^5\text{-}C_5H_4)_2\}M(\eta^5\text{-}C_5H_5)Cl]$

The X-ray crystal structures of **6** and **7** suggested that all three rings of each showed similar bonding to the metal centre. The interaction time of the X-rays with the electrons is about 10^{-18} seconds, but an X-ray crystal structure is not "snapshot" of a static "lifeless" molecule captured in its ground state form. It is in fact a time

average of all the possible atomic displacements, averaged again over the entire crystal. The "time scale" of the X-ray diffraction experiment is therefore the entire period of the data collection, usually several days.

The X-ray crystal structures of **6** and **7** indicate that all five carbon atoms of the C_5H_5 rings and the C_5H_4 rings may be considered as bonding to the metal centre, but that the actual extent of M-C bonding varies considerably. If the C_5H_5 ligand was static, one would expect a wide range of ^1H and ^{13}C chemical shifts rather than the single, sharp C_5H_5 signal that is observed. In the solution ^1H and ^{13}C NMR spectra of **6** and **7** the (η^5-C_5H_5) signal is a sharp singlet, and remains so down to low temperatures (-100 ^oC), indicating fast reorientation of the ring compared with the NMR timescale (10^{-1} to 10^{-9} seconds). The equivalence of the two C_5H_4 rings also indicates the presence of intramolecular motion such that a time-average "mirror plane" exists, containing the M, Cl and bridging carbon atoms.

The room temperature solution ^1H NMR spectra of [$(C_5H_5)_4M$] and [$(C_5H_5)_3MCl$] (M = Zr, Hf) all show just one sharp singlet for the C_5H_5 resonance. Variable temperature NMR studies have been briefly mentioned and the signals remain sharp down to temperatures as low as -150 ^oC.[50,53,56] It is believed that the disorder of the C_5H_5 rings in the [$(C_5H_5)_3ZrCl$] crystal structure, and possibly the poor quality of the [$(C_5H_5)_3HfCl$] structure, is related to the low energy barrier for ligand rearrangement in these compounds.[53] The variable temperature solution ^1H NMR spectra of the compounds [$(C_5H_5)_2Mo(NO)X$], where X = I, CH_3 or (η^1-C_5H_5), showed no evidence of any freezing out of the rotation of the unsymmetrically coordinated (η^5-C_5H_5) rings.[63, 64]

The solution ^1H NMR spectrum of [$(C_5H_5)_3TiCl$] shows a single sharp line down to -100 ^oC. It has been proposed on the basis of calculations that the ground state of [$(C_5H_5)_3TiCl$] is [$(\eta^5$-$C_5H_5)_2Ti(\eta^1$-$C_5H_5)Cl$] and that the low barrier to ligand rearrangement may result from a transition state in which two of the (C_5H_5) ligands adopt "pseudo η^3" coordination modes.[69]

In contrast, the variable temperature ^1H NMR spectrum of $[(C_5H_5)_4Ti]$ shows the $(\eta^5\text{-}C_5H_5)$-$(\eta^1\text{-}C_5H_5)$ interchange on the NMR timescale, and also the sigmatropic reorientation of the $(\eta^1\text{-}C_5H_5)$ ring.[70] The activation energies were estimated to be 67.3 ± 1.3 kJ mol^{-1} for the $(\eta^5\text{-}C_5H_5)$-$(\eta^1\text{-}C_5H_5)$ interchange and around 35 to 40 kJ mol^{-1} for the sigmatropic reorientation. An accurate determination of the activation energy of the sigmatropic reorientation of the $(\eta^1\text{-}C_5H_5)$ ring was not possble because the low temperature limit was not reached in the solution NMR studies.

In 1991, Heyes and Dobson reported the variable temperature ^{13}C CP/MAS spectra of $[(C_5H_5)_4Ti]$ in which the low temperature limit of the sigmatropic reorientation of the $(\eta^1\text{-}C_5H_5)$ ring was reached. An activation energy of 33.2 ± 1.0 kJ mol^{-1} was calculated on the basis of lineshape analysis.[71]

Since the low temperature solution NMR spectra of **6** and **7** showed no sign of freezing out of any fluxionality or lowering of symmetry, it was decided to study the solid state ^{13}C NMR properties of these compounds.

2.6.1 Experimental details

Solid state ^{13}C CP/MAS NMR spectra were recorded by Dr. Steven Heyes and Jacqueline Horne on a Bruker MSL200 spectrometer with a wide bore superconducting magnet, with a field strength of 4.7 T and resonant frequencies of 50.32 MHz for ^{13}C and 200.13 MHz for ^1H. All chemical shifts were referenced externally to TMS using adamantane as a secondary standard (upfield methine resonance δ 29.5 ppm).[72]

In CP/MAS solid state NMR experiments, the Brownian motion of molecules in solution, which causes the chemical shift anisotropy to be averaged to its isotropic value, is simulated by the fast rotation of the sample at the "magic angle" to the field. This drastically improves the resolution of the experiment. High power proton decoupling (HPPD) removes another major source of ^{13}C line broadening (^1H-^{13}C dipolar coupling), and "cross polarisation" (CP) makes use of magnetisation transfer

from protons to carbon atoms to give a greatly increased ^{13}C signal-to-noise ratio.[71-73]

2.6.2. Room temperature ^{13}C CP/MAS NMR experiments

The room temperature ^{13}C CP/MAS solid state NMR spectra of [{$Me_2C(\eta^5$-$C_5H_4)_2$}$M(\eta^5$-$C_5H_5)Cl$] [M = Zr (**6**) and Hf (**7**)] were recorded at a spinning speed of 2.9 kHz for **6** and 3.3 kHz for **7**. The spectra of **6** and **7** are very similar; the spectrum of **7** is shown in Figure 2.6.1 together with the NQS (non-quaternary suppression) spectrum. The room temperature solid state spectra of **6** and **7** closely resemble the solution ^{13}C NMR spectra except for one important feature; a sharp signal corresponding to the C_5H_5 ligand is not observed in the solid state spectra. The other signals closely match the solution spectra, with a quaternary C_5H_4 ipso carbon signal at about 145 ppm, four C_5H_4 signals at about 121, 117, 108 and 97 ppm, a quarternary bridging carbon signal at about 36 ppm and two methyl signals at around 20-25 ppm (methyl signals are typically observed in NQS spectrum due to fast motional averaging of dipolar coupling).

2.6.3. Variable temperature ^{13}C CP/MAS NMR experiments

Variable temperature ^{13}C CP/MAS solid state NMR spectra were recorded between 215 K and 371 K for **7** and between 221 K and 375 K for **6**. The cyclopentadienyl regions of the spectra are shown in Figure 2.6.2 for compound **7** and Figure 2.6.3 for compound **6**.

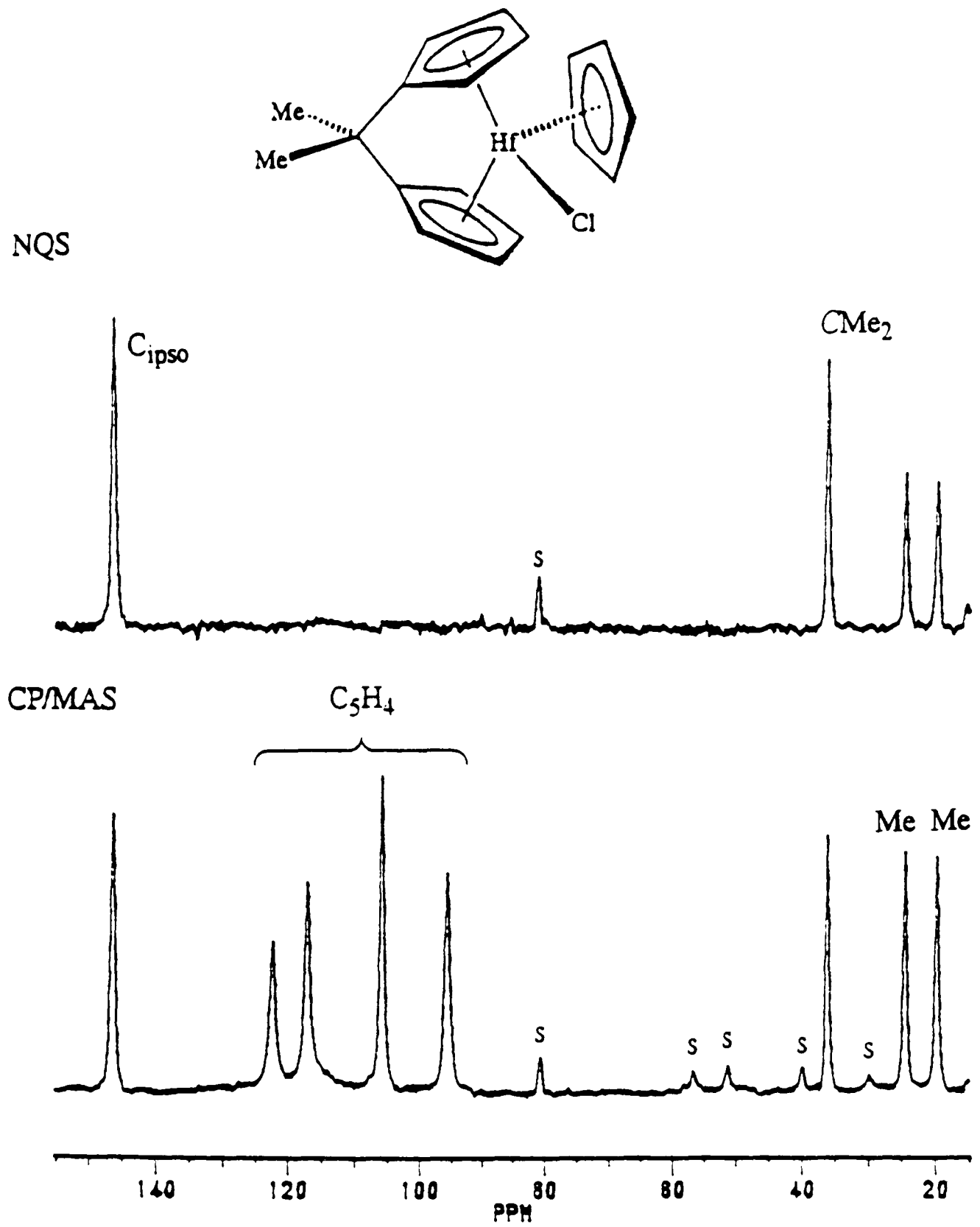

(s - denotes spinning side band)

Figure 2.6.1. Room temperature ^{13}C CP/MAS solid state NMR spectrum of $[\{Me_2C(\eta^5\text{-}C_5H_4)_2\}Hf(\eta^5\text{-}C_5H_5)Cl]$ (**7**), with NQS spectrum above.

The variable temperature ^{13}C CP/MAS solid state NMR spectra of both **7** and **6** are consistent with reorientation of the C_5H_5 ring on the NMR time scale.[74] In the highest temperature spectra the C_5H_5 signal is a relatively sharp singlet, indicating fast reorientation of the ring, with fast exchange of the carbon atoms over all the sites. As the temperature is lowered, exchange broadening is observed, with eventual splitting of the C_5H_5 signal into three signals which sharpen at low temperature with relative intensities 1 : 2 : 2. This process is reversible, and the weighted average chemical shifts at low temperature closely match the high temperature chemical shift, as expected for restricted rotation of a C_5H_5 ligand. For the ^{13}C CP/MAS spectrum of **7** at 215 K the weighted average C_5H_5 chemical shift is 0.2[135.2 + 2(111.8) + 2(109.0)] = 115.7 ppm, compared with a shift of 116.3 ppm for the C_5H_5 signal at 371 K. For **6**, the weighted average C_5H_5 chemical shift at 221 K is 0.2[135.6 + 2(113.2) + 2(110.7)] = 116.7 ppm, compared with a shift of 117.5 ppm for the C_5H_5 signal at 371 K.

The spectra of **7** and **6** are very similar, except that the exchange broadening is frozen out at a slightly lower temperature for **6**, indicating a lower activation barrier.[73, 74] This might be expected because Zr-C bonds are typically slightly longer and slightly weaker than Hf-C bonds.[32, 74, 75] Over the whole temperature range, the ^{13}C signals of the $\{Me_2C(C_5H_4)_2\}$ ligand show little change and the two C_5H_4 rings are still equivalent in the lowest temperature spectra. The observed 1 : 2 : 2. pattern of the C_5H_5 signals also suggests the presence of a mirror plane containing the M, Cl and CMe_2 groups, the C_5H_5 centroid and one of the C_5H_5 carbon atoms. Alternatively there might still be fluxional processes going on even at the lowest temperatures that result in the two C_5H_4 rings and the two halves of the C_5H_5 ring appearing equivalent on the NMR time scale.

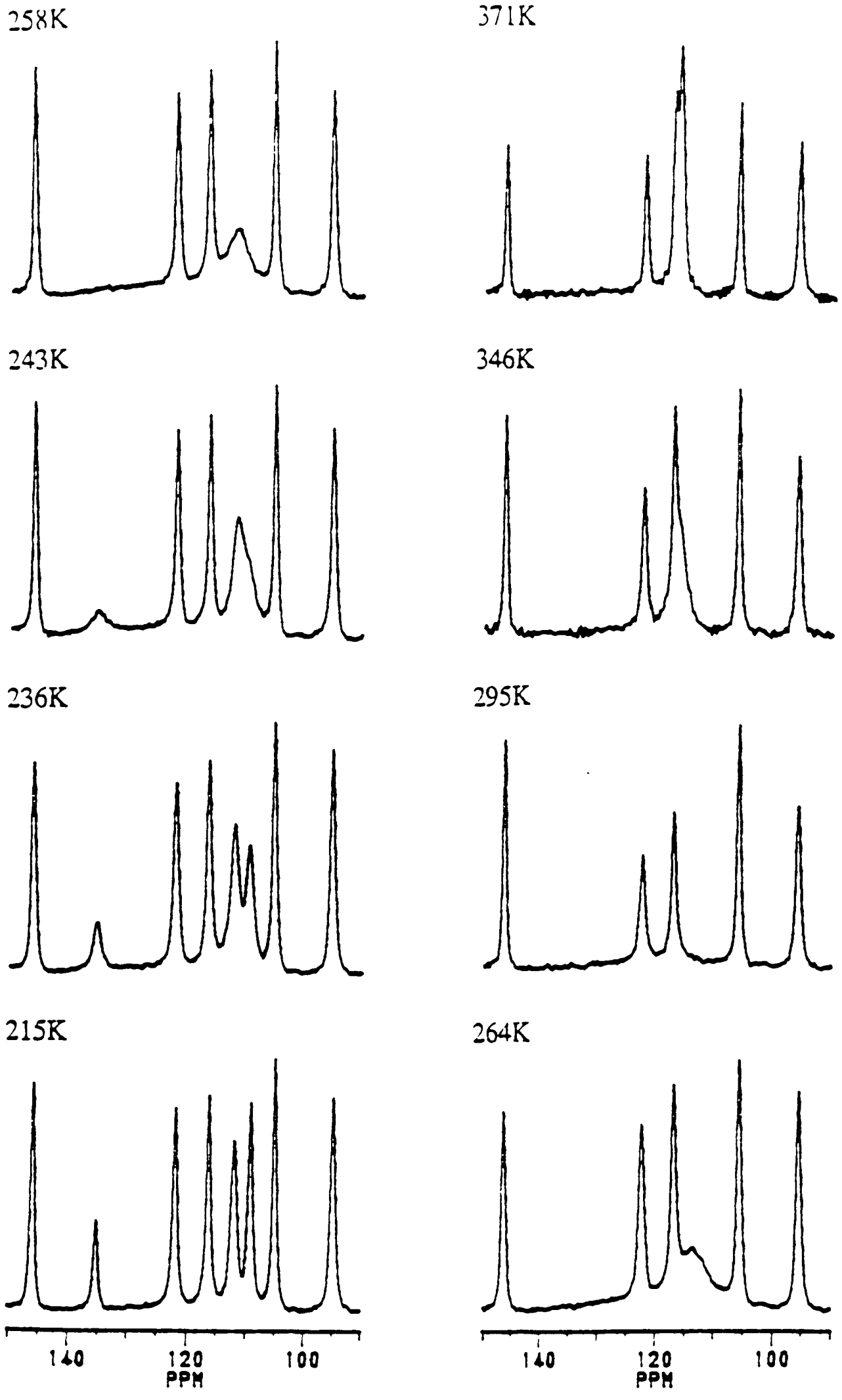

Figure 2.6.2. Variable temperature ^{13}C CP/MAS solid state NMR spectra of $[\{Me_2C(\eta^5\text{-}C_5H_4)_2\}Hf(\eta^5\text{-}C_5H_5)Cl]$ (7) (cyclopentadienyl region)

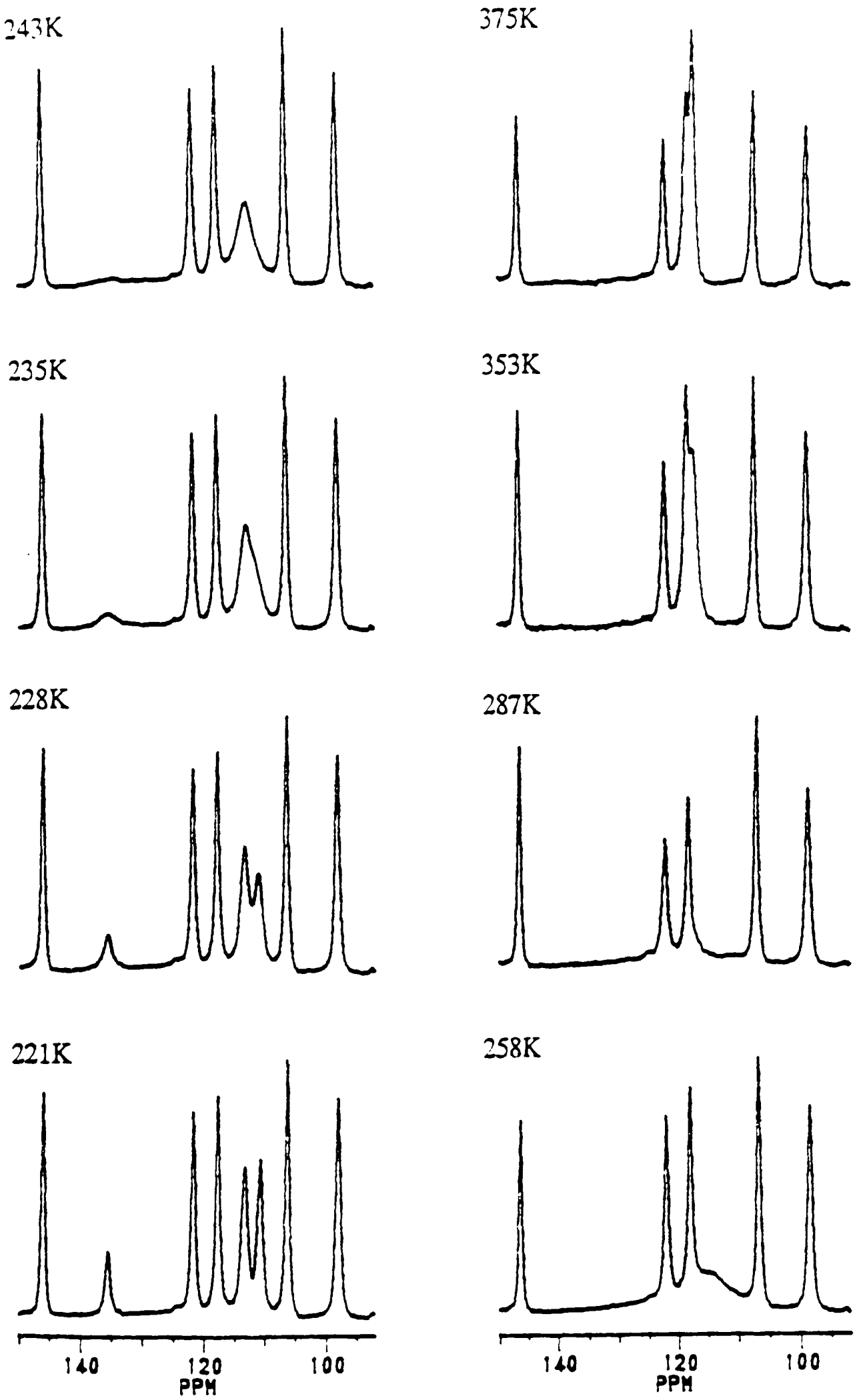

Figure 2.6.3. Variable temperature ^{13}C CP/MAS solid state NMR spectra of $[\{Me_2C(\eta^5\text{-}C_5H_4)_2\}Zr(\eta^5\text{-}C_5H_5)Cl]$ (**6**) (cyclopentadienyl region)

Lineshape simulations of the variable temperature spectra were carried out by Jacqueline Horne and Dr. Steven Heyes.[72] The data from the lineshape simulation experiments were fitted to an Arrhenius expression, [$k = A \exp(E_a/RT)$], giving estimated activation barriers (E_a) for the C_5H_5 ring reorientation of 74.0 ± 3.0 kJ mol^{-1} for **7** and 69 ± 3.0 kJ mol^{-1} for **6**.[72]

The energy barrier for rotation of (η^5-C_5H_5) rings in organometallic compounds is generally very low.[73, 74] Despite many earlier attempts to observe restricted rotation of (η^5-C_5H_5) rings in the NMR spectra of organometallic compounds in solution at low temperature, the first example was not reported until 1990 by Mynott *et al.*[77] In this first report, the solution ^1H and ^{13}C NMR spectra of the sterically crowded complexes $[(\eta^5\text{-}C_5H_5)M(CH_2{=}CHPh)(PPh_3)_2]^+[BF_4]^-$ (M = Ru or Os, Figure 2.6.4) showed splitting of the (η^5-C_5H_5) signal at low temperatures (-100 °C). At the slow exchange limit, the five (η^5-C_5H_5) ^{13}C signals ranged from about 75 to 100 ppm, the proton signals from about 3.2 to 5.7 ppm.

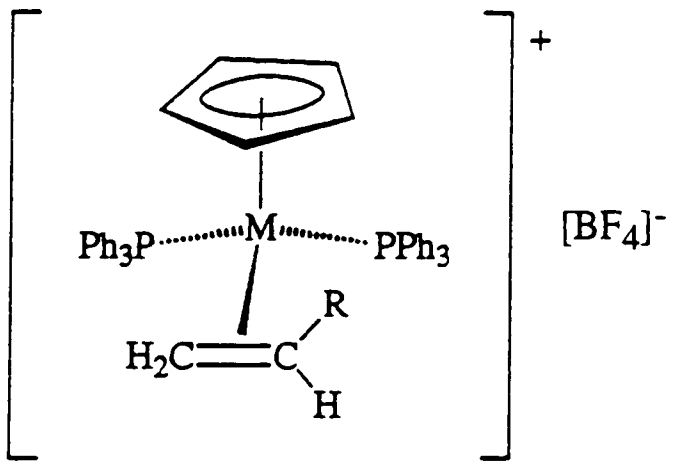

Figure 2.6.4. $[(\eta^5\text{-}C_5H_5)M(CH_2{=}CHR)(PPh_3)_2]^+[BF_4]^-$ (M = Ru, Os). Restricted rotation of (η^5-C_5H_5) is observed in solution ^1H and ^{13}C NMR spectra for R = Ph.

Lineshape analysis of the solution ^{13}C NMR spectra of the ruthenium complex suggested a barrier to rotation of 34.2 ± 1.5 kJ mol^{-1}. It was proposed that this unusually large barrier to rotation resulted mainly from steric crowding; when the styrene group was replaced by ethylene, no significant broadening of the (η^5-C_5H_5)

^{13}C resonance was observed down to -95 ^{o}C.[77] It was suggested that the large range of ^{13}C and ^{1}H chemical shifts for the (η^5-C_5H_5) ligand at low temperature suggested that the bonding between the carbon atoms and the metal centre varied considerably, for example by ring tilting similar to that observed in the tris(η^5-cyclopentadienyl) compounds.

The energy barriers for fluxional processes are generally higher in the solid state than in solution.[73,76] Whereas molecular rearrangements in solution are controlled by the nature of the chemical bonds and by intramolecular (steric) constraints, in the solid state **crystal packing** imposes additional **intermolecular** constraints which can forbid or limit significantly the motional freedom of molecules and molecular fragments. However; the rotation of flat, disclike fragments such as (η^5-C_5H_5) groups is not easily blocked, and even in crystalline organometallic solids the barriers to reorientation of (η^5-C_5H_5) ligands are generally quite low, seldom exceeding 20-30 kJ mol^{-1}. Some values are given in Table 2.6.

The first high resolution solid state ^{13}C CP/MAS spectra showing an (η^5-C_5H_5) in the slow exchange limit were reported by Erker in 1990.[82] Erker showed that for the zirconocene butadiene derivative [(η^5-C_5H_5)$_2$Zr(η^4-C_4H_5Me)] (Figure 2.6.5), the ^{13}C NMR signal of one of the (η^5-C_5H_5) rings broadens as the temperature is lowered and finally splits into five lines at 110 K. As for **6** and **7**, the process is reversible, and the average chemical shift of the ^{13}C signals at low temperature closely matches the high temperature chemical shift.

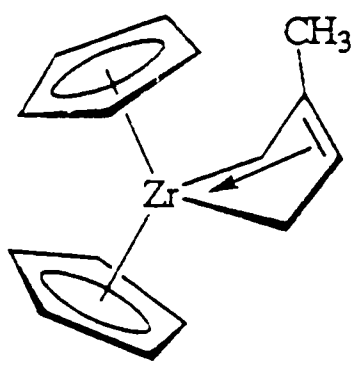

Figure 2.6.5. [(η^5-C_5H_5)$_2$Zr(η^4-C_4H_5Me)]

Table 2.6. Some activation energies for (η^5-C_5H_5) ring reorientation in organometallic solids, and some values for substituted rings

Organometallic species	Activation energies for ring reorientation kJ mol^{-1}	ref.
$(\eta^5\text{-}C_5H_5)_2Fe$, monoclinic	2.7 - 9.6	73[a]
$(\eta^5\text{-}C_5H_5)_2Fe$, orthorhombic	23, 33	78[b]
$(\eta^5\text{-}C_5H_5)_2Ru$, orthorhombic	25, 50	78[b]
$(\eta^5\text{-}C_5H_5)Fe(\eta^5\text{-}C_5H_4Bu^t)$	unsubstituted ring 35.1 substituted ring 39.7	79[c]
$(\eta^5\text{-}C_5H_5)_2MoCl_2$	1.5 - 12.8	80[a]
$(\eta^5\text{-}C_5H_5)_2ZrCl_2$	6.3 - 10.8	81,[d] 82
$(\eta^5\text{-}C_5H_5)_2Zr(\eta^4\text{-}C_4H_5Me)$	16.0, 23.0	82[e]
$(\eta^5\text{-}C_5H_4Me)_2ZrCl_2$	70.7	82[e]
$(\eta^5\text{-}C_5H_4Et)_2ZrCl_2$	ring rotation forbiddden	82[e]
$(\eta^5\text{-}C_5H_4Bu^t)_2ZrCl_2$	ring rotation forbiddden >200	82[e] 81[f]

[a] from ^1H spin-lattice relaxation times

[b] calculated from anisotropic displacement parameters

[c] from wide-line ^1H NMR spectroscopy

[d] calculated atom-atom potential energy barrier, reorientation not frozen out in CP/MAS experiment

[e] from ^{13}C CP/MAS experiment

[f] calculated atom-atom potential energy barrier

Erker also commented on the fact that at low temperature the chemical shifts covered a range of nearly 20 ppm (between 90 and 110 ppm), which suggested that the chemical environment at each carbon atom was quite different. The signal of the

second (η^5-C_5H_5) group of [(η^5-C_5H_5)$_2$Zr(η^4-C_4H_5Me)] broadened but did not split into sharp signals at low temperature. It was suggested that the first ring, for which slow exchange was observed, was that closest to the methyl substituent of the (η^4-C_4H_5Me) ligand, and that steric interaction with the methyl group gave rise to the higher barrier to rotation.[82] Erker also reported that upon introduction of alkyl substituents at the cyclopentadienyl rings, the barrier to ring rotation increases dramatically, as shown in Table 2.6.

The activation barriers for C_5H_5 ring reorientation calculated for **6** and **7** are high compared with typical values for (η^5-C_5H_5) ring reorientation in organometallic compounds. For most crystalline organometallic solids the barrier to (η^5-C_5H_5) ring reorientation has been measured or calculated as less than 30 kJ mol^{-1}. The high rotational barriers calculated for orthorhombic ferrocene and ruthenocene have been attributed to intermolecular crystal packing effects.[73, 78] It was initially thought that the high energy barrier for C_5H_5 ring reorientation calculated for **7** and **6** might indicate some tendency towards η^3 coordination of the C_5H_5 ring. As Table 2.7 shows, the calculated activation energies of around 70 kJ mol^{-1} for **7** and **6** are closer to the energy barriers for reported for the reorientation of η^3-allyl ligands.

Table 2.7. Some activation energies for reorientation of η^3-allyl groups

Organometallic species	Activation energies kJ mol^{-1}	ref.
(η^3-C_3H_5)$_3$Rh	40 ± 8	83
(η^3-C_3H_5)Mo(CO)$_2$Cp	51.5 ± 5.0	84
(η^3-2-Me-C_3H_4)Mo(CO)$_2$Cp	70.3 ± 1.7	84

However, whilst the chemical shifts observed for the C_5H_5 ligand at low temperature might be similar to those expected for an (η^3-C_5H_5) coordinated to

zirconium and hafnium (which is debatable), the C_5H_4 rings remain equivalent at low temperature and a 1 : 2 : 2 pattern is observed for the C_5H_5 ring signals. This suggests that either: (i) the (η^3-C_5H_5) group would have to coordinate in a symmetric manner **across** the equatorial plane of the metallocene fragment (structure **I** below), for which good π-orbital overlap would not be expected,[29-31] or (ii) there would have to be a fast rearrangement process interconverting the two more favourable orientations of the (η^3-C_5H_5) ring (**II** and **III** in Figure 2.6.6) that would be expected to give better π-orbital overlap, but for which the C_5H_4 rings are not equivalent and each C_5H_5 carbon atom is in a different chemical environment.

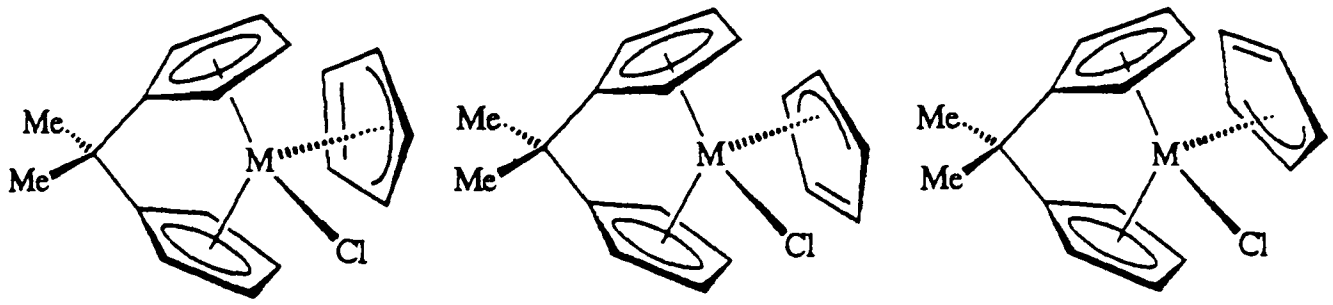

I	**II**	**III**
symmetric but poor π-orbital overlap	good π-orbital overlap but asymmetric	

Figure 2.6.6. Possible orientations of (η^3-C_5H_5) ring in **6** and **7**.

However, if the large barrier to reorientation of the C_5H_5 rings in **6** and **7** was mainly **intramolecular** in origin, one would expect to observe broadening and splitting of the C_5H_5 ring ^1H and ^{13}C NMR signals **in solution**. For example, the sigmatropic reorientation of the (η^1-C_5H_5) rings of [$(C_5H_5)_4Ti$], with an activation energy of around 35 kJ mol^{-1}, was observed in both solid and solution NMR experiments.[70, 71] Also, as discussed above, Mynott reported broadening and splitting of 300 MHz ^1H and 75.5 MHz ^{13}C NMR signals due to restricted rotation of C_5H_5 rings in solution at low tempertaure (173 K) with a barrier to rotation of around 34 kJ mol^{-1},

approximately half the barrier to rotation calcluated for **6** and **7** in the solid.[77] Similar solution NMR experiments for **6** and **7** revealed no such restricted rotation. If the broadening and splitting of the C_5H_5 ring solid state ^{13}C NMR signals of **6** and **7** is due to the mode of bonding of the C_5H_5 ligand to the metal, then this bonding would have to be significantly different in solution compared with in the solid state.

The absence of broadening or splitting of the solution ^{1}H and ^{13}C NMR signals of **6** and **7** suggests that that large barrier to C_5H_5 ring reorientation observed in the solid state ^{13} C NMR spectra is largely due to **crystal packing effects** (intermolecular interactions). The large barriers to ring rotation in orthorhombic ferrocene (up to 40 kJ mol^{-1}) and ruthenocene (up to 50 kJ mol^{-1}) have been attributed to intermolecular interactions resulting from the packing in these metallocene crystals.[73,78]

The room temperature X-ray crystal structures of **6** and **7** are both approximately symmetrical about a plane containing the metal, chlorine and bridging carbon atoms. The C_5H_5 ring centroid and one of the C_5H_5 ring atoms, C(3), also lie close to this plane. This is shown more clearly in the line diagram of the X-ray crystal structure of **7**, shown below.

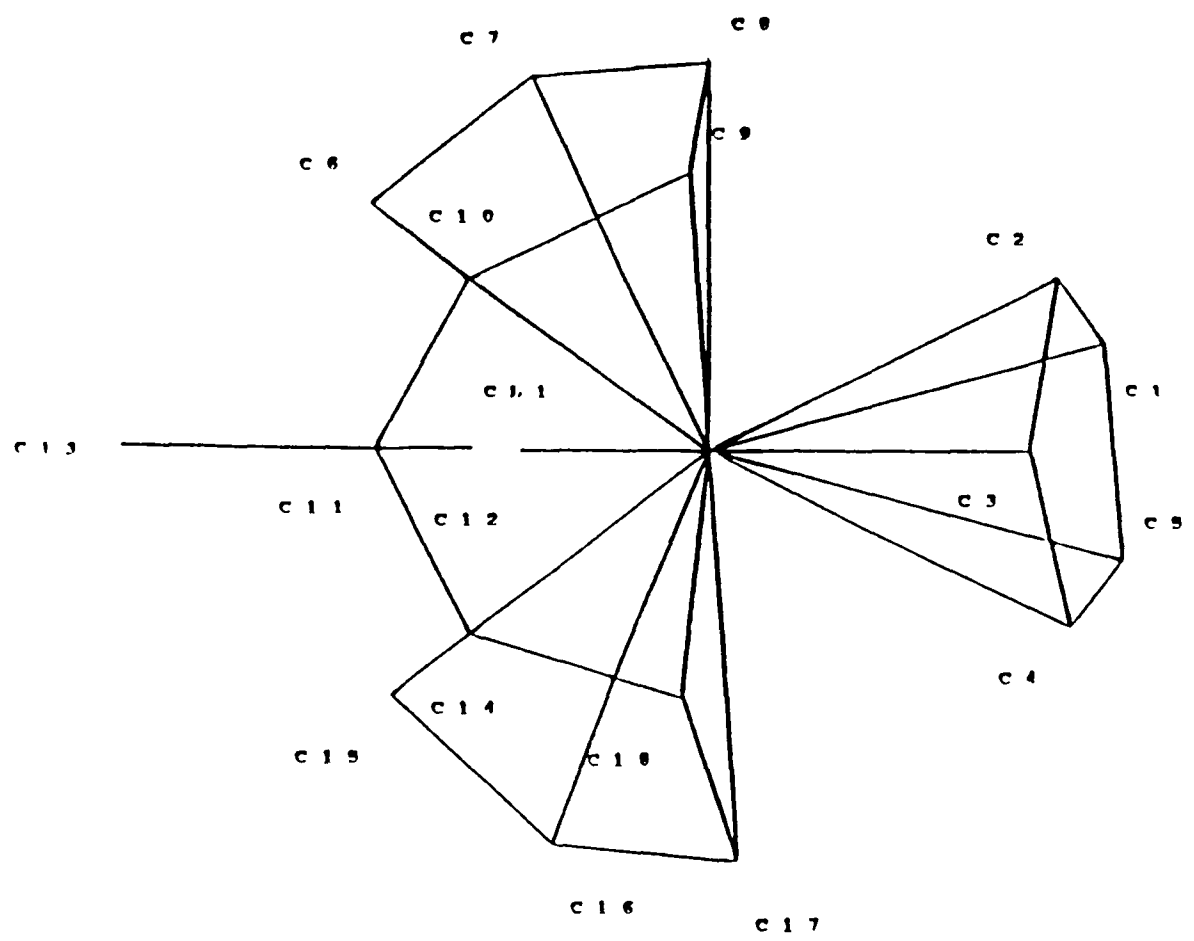

Figure 2.6.7. Molecular structure of **7** from room temperature X-ray crystal structure.

The variable temperature solid state NMR spectra of **6** and **7** are consistent with this molecular structure being maintained over the whole temperature range, with exchange of the C_5H_5 carbon atoms over the five sites corresponding to C(1) to C(5) in the crystal structure. The sites represented by C(2) and C(4) have approximately the same chemical environment and would be expected to result in very similar chemical shifts. The sites occupied by C(1) and C(5) are similarly related, whilst C(3) occupies a unique site. Hence slow exchange between these sites would give rise to a 1 : 2 : 2 pattern of chemical shifts.

Whilst at low temperature the range of C_5H_5 ^{13}C chemical shifts for **6** and **7** is large (spanning 25 ppm), it is not much larger than the range reported for $[(\eta^5\text{-}C_5H_5)_2Zr(\eta^4\text{-}C_4H_5Me)]$ in the solid state (20 ppm), and is similar to the range reported for $[(\eta^5\text{-}C_5H_5)Os(CH_2{=}CHPh)(PPh_3)_2]^+[BF_4]^-$ in solution (24 ppm). The different neighbouring group effects experienced by the C_5H_5 carbon atoms, together with the unsymmetrical (tilted) coordination of the C_5H_5 ring to the metal, probably account for the observed chemical shifts in **6** and **7**. Hence there seems to be no need to invoke η^3 coordination of the C_5H_5 ring to explain either the chemical shifts or the barrier to rotation observed for **6** and **7**.

Even compared with orthorhombic ferrocene and ruthenocene, the barriers to C_5H_5 ring rotation in **6** and **7** are high. This may reflect the steric crowding in **6** and **7**, which may also contribute to the unsymmetrical coordination (tilting) of the C_5H_5 ring. It can be seen from Table 2.6 that steric crowding dramatically increases the barrier to ring rotation. It is possible that crystal packing effects may reinforce the steric crowding in **6** and **7**. The solution NMR spectra of **6** and **7** suggest that the barrier to ring rotation is much lower in solution that in the solid. It may be that in solution the *ansa* ligand is able to adopt conformations which relieve steric crowding of the C_5H_5 ring and allow less-hindered rotation. The *ansa* ligand may have considerably less conformational freedom in the solid due to crystal packing effects. Hence the high barriers to rotation in **6** and **7** may reflect **indirect** crystal packing effects, reinforcing

intramolecular steric effects, as well as direct intermolecular hindrance of ring rotation (although the latter was not obvious from the X-ray crystal structure).

The solid state ^{13}C CP/MAS NMR spectra of compound **2**, [{$Me_2C(\eta^5$-$C_5H_4)(\eta^2$-$C_9H_6)$}$Hf(\eta^5$-$C_5H_5)Cl$], and compound **5**, [{$Me_2C(\eta^5$-$C_5H_4)(\eta^3$-$C_{13}H_8)$}$Zr(\eta^5$-$C_5H_5)Cl$], were also measured.[72] The solid state spectra of both compounds resembled the solution ^{13}C NMR spectra, and the C_5H_5 signals remained sharp at low temperatures, suggesting a much lower barrier to rotation compared with **6** and **7**.

The solid state ^{13}C CP/MAS NMR spectra of [$(\eta^5$-$C_5H_5)_3ZrCl$] has also been recently measured in this laboratory,[85] and there is no evidence for freezing out the (η^5-C_5H_5) ring rotation even at 197 K. This might reflect different crystal packing effects, but might also reflect the more flexible molecular structure of the non-bridged compound which might allow less hindered ring rotation in [$(\eta^5$-$C_5H_5)_3ZrCl$] compared with **6** and **7**.

In conclusion, the solid state ^{13}C CP/MAS NMR spectra of **6** and **7** are consistent with rotation of the (η^5-C_5H_5) ring about the ring-metal axis, with a molecular structure at the slow exchange limit similar to that observed in the room temperature X-ray crystal structure. The large energy barrier to ring rotation for **6** and **7** probably reflects mainly intermolecular crystal packing effects, probably reinforcing intramolecular steric effects resulting from the unusual tris(η^5-cyclopentadienyl) coordination and the rigidity of the *ansa* bridge.

2.7 Summary

The ligands $[Me_2C(C_5H_4)(C_9H_6)Li_2]$ and $[(CH_2)_5C(C_5H_4)(C_9H_6)Li_2]$ react with one equivalent of $[(\eta^5\text{-}C_5H_5)MCl_3\cdot 2L]$ (M = Zr, Hf, 2L = DME, 2THF) to give the novel, *ansa*-bridged mononuclear compounds $[\{Me_2C(\eta^5\text{-}C_5H_4)(\eta^2\text{-}C_9H_6)\}M(\eta^5\text{-}C_5H_5)Cl]$ [M = Zr (**1**), Hf (**2**)] and $[\{(CH_2)_5C(\eta^5\text{-}C_5H_4)(\eta^2\text{-}C_9H_6)\}M(\eta^5\text{-}C_5H_5)Cl]$ [M = Zr (**3**), Hf (**4**)] in which the indenyl ligand is coordinated to the metal in a highly unusual η^2 fashion. The ligand $[Me_2C(C_5H_4)(C_{13}H_8)Li_2]$ reacts with one equivalent of $[(\eta^5\text{-}C_5H_5)ZrCl_3\cdot DME]$ to give the novel, *ansa*-bridged mononuclear complex $[\{Me_2(\eta^5\text{-}C_5H_4)(\eta^3\text{-}C_{13}H_8)\}Zr(\eta^5\text{-}C_5H_5)Cl]$ (**5**), in which the fluorenyl-metal bonding resembles η^3 benzyl-like coordination. The unprecedented η^2-indenyl and η^3-fluorenyl coordination modes in these compounds probably reflect not only competition between the indenyl (or fluorenyl) and cyclopentadienyl ligands for coordination of the metal centre, but also constraints imposed on the molecular structures by the short *ansa*-bridges.[86]

The *ansa*-bis(cyclopentadienyl) ligand $[\{Me_2C(C_5H_4)_2\}Li_2]$ reacts with $[(\eta^5\text{-}C_5H_5)MCl_3\cdot 2L]$ (M = Zr, Hf; 2L = DME, 2THF) to give the novel, mononuclear *ansa*-bridged compounds $[\{Me_2C(\eta^5\text{-}C_5H_4)_2\}M(\eta^5\text{-}C_5H_5)Cl]$ [M = Zr (**6**), Hf (**7**)]. Compound **7** is the first example of a tris(η^5-cyclopentadienyl) derivative of hafnium, or of any transition metal (groups 4 to 10) other than zirconium. The molecular structure of **7** compared with the non-bridged compound $[(\eta^5\text{-}C_5H_5)_2Hf(\eta^1\text{-}C_5H_5)Cl]$ demonstrates the effect that an *ansa* bridge can have on the gross structure of a complex.[49] The variable temperature solid state ^{13}C CP/MAS NMR spectra of **6** and **7** show slow rotation of the C_5H_5 ring on the NMR timescale. The large barrier to ring rotation calculated for both **6** and **7** is probably due to crystal packing effects reinforcing intramolecular steric effects. A summary of the reactions described in Chapter 2 is given in Figure 2.7.

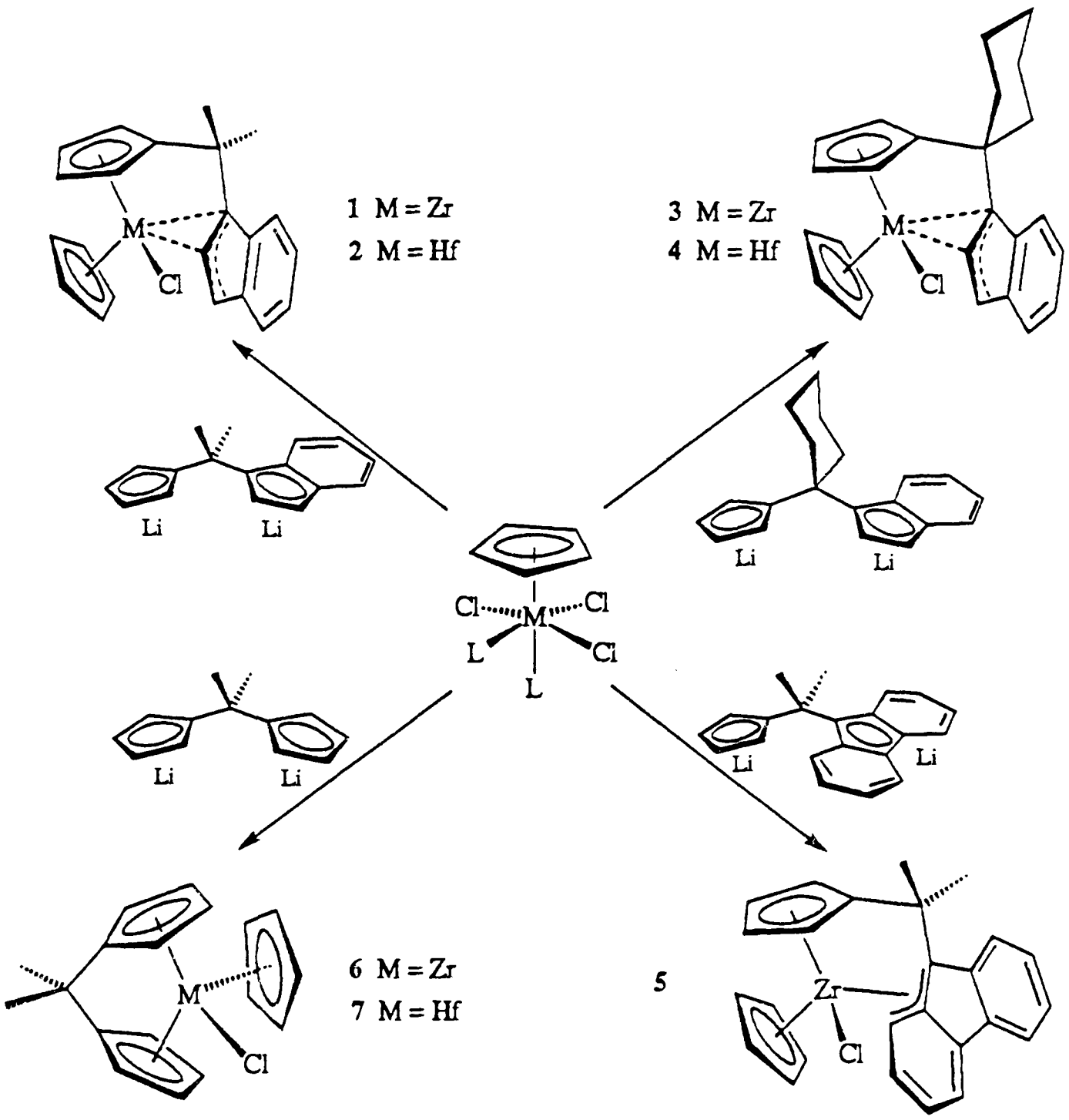

Figure 2.7. Summary of the reactions described in Chapter 2

References for Chapter 2

1. K. P. Reddy and J. L. Petersen, *Organometallics*, 1989, **8**, 2107.
2. J. A. Ewen, R. L. Jones, A. Razavi and J. D. Ferrara, *J. Am. Chem. Soc.*, 1988, **110**, 6255.
3. W. Spalek, M. Antberg, V. Dolle, R. Klein, J. Rohrmann and A. Winter, *New. J. Chem.*, 1990, **14**, 499.
4. D. T. Mallin, M. D. Rausch, Y. G. Lin, S. Dong and J. C. W. Chien, *J. Am. Chem. Soc.*, 1990, **112**, 2030.
5. G. S. Herrmann, H. G. Alt and M. D. Rausch, *J. Organomet. Chem.*, 1991, **401**, C5.
6. J. A. Ewen, M. J. Elder, R. L. Jones, L. Haspeslagh, J. L. Atwood, S. G. Bott and K. Robinson, *Makromol. Chem., Makromol. Symp.*, 1991, **48/49**, 253.
7. R. L. Halterman, *Chem. Rev.*, 1992, **92**, 965.
8. W. Kaminsky, R. Engehausen, K. Zoumis, W. Spalek and J. Rohrmann, *Makromol. Chem.*, 1992, **193**, 1643.
9. I. E. Nifant'ev, P. V. Ivchenko and M. V. Borzov, *J. Chem. Res. (S)*, 1992, 162.
10. G. H. Llinas, R. O. Day, M. D. Rausch and J. C. W. Chien, *Organometallics*, 1993, **12**, 1283.
11. K. J. Stone and R. D. Little, *J. Org. Chem.*, 1984, **49**, 1849.
12. M. Neuenschwander, in *The Chemistry of Double-bonded Functional Groups*, Ed. S. Patai, Wiley, Chichester, 1989, ch. 16, pp. 1131-1268.
13. D. M. Bensley and E. A. Mintz, *J. Organomet. Chem.*, 1988, **353**, 93.
14. Nobuhide Ishihara, D. Phil. Thesis, University of Oxford, 1990.
15. A. E. Derome, *Modern NMR Techniques for Chemistry Research*, Pergamon Press, Oxford, 1987.
16. D. H. Williams and I. Fleming, *Spectroscopic Methods in Organic Chemistry*, McGraw-Hill, London, 1989.

17. Aspect 3000 NMR Software Manual, Bruker Spectrospin Ltd., 1987.

18. J. M. O'Connor and C. P. Casey, *Chem. Rev.*, 1987, **87**, 307.

19. F. H. Kohler, *Chem. Ber.*, 1974, **107**, 570.

20. A. D. Horton, *Organometallics*, 1992, **11**, 3271.

21. S. Bellomo, A. Ceccon, A. Gambaro, S. Santi and A. Venzo, *J. Organomet. Chem.*, 1993, **453**, C4.

22. C. P. Casey and J. M. O'Connor, *Organometallics*, 1985, **4**, 384.

23. C. R. Lucas, M. L. H. Green, R. A. Forder and K. Prout, *J. Chem. Soc., Chem. Commun.*, 1973, 97.

24. G. Erker, R. Noe, C. Kruger and S. Werner, *Organometallics*, 1992, **11**, 4174.

25. R. F. Jordan, R. E. LaPointe, C. S. Bajgur, S. F. Echolls and R. Willet, *J. Am. Chem. Soc.*, 1987, **109**, 4111.

26. J. Scholz, F. Rehbaum, K. H. Thiele, R. Goddard, P. Betz and C. Kruger, *J. Organomet. Chem.*, 1993, **443**, 93.

27. K. Prout, T. S. Cameron and R. A. Forder, *Acta. Crystallogr., Sect. B*, 1974, **30**, 2290.

28. G. L. Soloviechik, T. M. Arkhireeva, V. K. Bel'skii and B. M. Bulychev, *Organomet. Chem. USSR*, 1988, **1**, 125.

29. J. C. Green, M. L. H. Green and C. K. Prout, *J. Chem. Soc., Chem. Commun.*, 1972, 421.

30. J. W. Lauher and R. Hoffmann, *J. Am. Chem. Soc.*, 1976, **98**, 1729.

31. L. Zhu and N. M. Kostic, *J. Organomet. Chem.*, 1987, **335**, 395.

32. A. G. Orpen, L. Brammer, F. H. Allen, O. Kennard, D. G. Watson and R. Taylor, *J. Chem. Soc., Dalton Trans.*, 1989, S1.

33. C. J. Cardin, D. J. Cardin, D. A. Morton-Blake, H. E. Parge and A. Roy, *J. Chem. Soc., Dalton Trans.*, 1987, 1641.

34. N. E. Schore, S. J. Young, M. M. Olmstead and P. Hofmann, *Organometallics*, 1983, **2**, 1769.

35. I. H. Kryspin, R. Gleiter, C. Kruger, R. Zwettler and G. Erker, *Organometallics*, 1990, **9**, 517.

36. M. F. Lappert, P. I. Riley, P. I. W. Yarrow, J. L. Atwood, W. E. Hunter and M. J. Zawarotko, *J. Chem. Soc., Dalton Trans.*, 1981, 814.

37. H. H. Karsch, G. Grauvogl, B. Deubelly and G. Muller, *Organometallics*, 1992, **11**, 4238.

38. H. H. Karsch, B. Deubelly, G. Grauvogl, J. Lachmann and G. Muller, *Organometallics*, 1992, **11**, 4245.

39. Y. Wielstra, R. Duchateau, S. Gambarotta, C. Bensimon and E. Gabe, *J. Organomet. Chem.*, 1991, **418**, 183.

40. J. A. Ewen, L. Haspeslagh, J. L. Atwood and H. Zhang, *J. Am. Chem. Soc.*, 1987, **109**, 6544.

41. J. A. Ewen, L. Haspeslagh, M. J. Elder, J. L. Atwood, H. Zhang and H. N. Cheng, in *Transition Metals and Organometallics as Catalysts for Olefin Polymerization*, W. Kaminsky and H. Sinn, Eds., Springer, New York, 1988.

42. J. A. Ewen, M. J. Elder, R. L. Jones, L. Haspeslagh, J. L. Atwood, S. G. Bott and K. Robinson, *Makromol. Chem., Makromol. Symp.*, 1991, **48/49**, 253.

43. A. Razavi and J. Ferrara, *J. Organomet. Chem.*, 1992, **435**, 299.

44. C. Kowala, P. C. Wailes, H. Weigold and J. A. Wunderlich, *J. Chem. Soc., Chem. Commun.*, 1974, 993.

45. C. Kowala, J. A. Wunderlich, *Acta. Crystallogr., Sect. B*, 1976, **32**, 820.

46. R. B. King and A. Fronzaglia, *J. Am. Chem. Soc.*, 1966, **88**, 709.

47. F. A. Cotton and M. D. LaPrade, *J. Am. Chem. Soc.*, 1968, **90**, 5418.

48. M. Booij, A. Meetsma and J. H. Teuben, *Organometallics*, 1991, **10**, 3246.

49. G. M. Diamond, M. L. H. Green, N. A. Popham and A. N. Chernega, *J. Chem. Soc., Dalton Trans.*, 1993, 2535.

50. R. D. Rogers, R. V. Bynum and J. L. Atwood, *J. Am. Chem. Soc.*, 1978, **100**, 5238.

51. V. I. Kulishov, E. M. Brainiana, N. G. Bokiy and Y. T. Struchkov, *J. Chem. Soc., Chem. Commun.*, 1970, 475.

52. J. Kopf, H. J. Vollmer and W. Kaminsky, *Cryst. Struct. Commun.*, 1980, **9**, 985.

53. R. J. Strittmatter, Ph.D. Thesis, Ohio State University, 1990; R. J. Strittmatter and B. E. Bursten, *J. Am. Chem. Soc.*, 1991, **113**, 552.

54. R. D. Rogers, R. V. Bynum and J. L. Atwood, *J. Am. Chem. Soc.*, 1981, **103**, 692.

55. V. I. Kulishov, E. M. Brainiana, N. G. Bokiy and Y. T. Struchkov, *J. Organomet. Chem.*, 1972, **36**, 333.

56. J. L. Calderon, F. A. Cotton, B. G. DeBoer and J. Takats, *J. Am. Chem. Soc.*, 1971, **93**, 3592.

57. L. M. Hansen, and D. S. Marynick, *Organometallics*, 1989, **8**, 2173.

58. I. E. Nifant'ev, A. V. Churakov, I. F. Urazowski, S. G. Mkoyan and L. O. Atovmyan, *J. Organomet. Chem.*, 1992, **435**, 37.

59. J. A. Smith, J. V. Seyerl, G. Huttner and H. H. Brintzinger, *J. Organomet. Chem.*, 1979, **173**, 175.

60. R. B. King, *Inorg. Chem.*, 1968, **7**, 90.

61. F. A. Cotton and P. Legzdins, *J. Am. Chem. Soc.*, 1968, **90**, 6232.

62. J. L. Calderon, F. A. Cotton and P. Legzdins, *J. Am. Chem. Soc.*, 1969, **91**, 2528.

63. F. A. Cotton, *Discuss. Faraday Soc.*, 1969, **47**, 79.

64. F. A. Cotton and G. A. Rushholme, *J. Am. Chem. Soc.*, 1972, **94**, 402.

65. F. A. Cotton, *J. Am. Chem. Soc.*, 1968, **90**, 6230.

66. J. W. Lauher and R. Hoffmann, *J. Am. Chem. Soc.*, 1976, **98**, 1729.

67. T. J. Marks and R. D. Ernst, in *Comprehensive Organometallic Chemistry*, G. Wilkinson, F. G. A. Stone and E. W. Abel, Eds., Pergamon Press, Oxford, 1982, vol. 3, ch. 21, pp 173-270.

68. B. E. Bursten, L. F. Rhodes and R. J. Strittmatter, *J. Am. Chem. Soc.*, 1989, **111**, 2756.

69. L. M. Hansen, and D. S. Marynick, *J. Am. Chem. Soc.*, 1988, **110**, 2538.

70. J. L. Calderon, F. A. Cotton and J. Takats, *J. Am. Chem. Soc.*, 1971, **93**, 3587.

71. S. J. Heyes and C. M. Dobson, *J. Am. Chem. Soc.*, 1991, **113**, 463.

72. J. A. Horne, Part II thesis, University of Oxford, 1993.

73. D. Braga, *Chem. Rev.*, 1992, **92**, 633.

74. L. E. Schock and T. J. Marks, *J. Am. Chem. Soc.*, 1988, **110**, 7701.

75. J. A. Martinho Simoes and J. L. Beauchamp, *Chem. Rev.*, 1990, **90**, 629.

76. B. E. Mann, in *Comprehensive Organometallic Chemistry*, G. Wilkinson, F. G. A. Stone and E. W. Abel, Eds., Pergamon Press, Oxford, 1982, vol. 3, ch. 20, pp 89-171.

77. R. Mynott, H. Lehmkuhl, E. M. Kruzer and E. Joussen, *Angew. Chem., Int. Ed. Engl.*, 1990, **29**, 289.

78. E. Maverick and J. D. Dunitz, *Mol. Phys.*, 1987, **62**, 451.

79. M. K. Makova, E. V. Lenova, Y. S. Karimov and N. S. Kochetkova, *J. Organomet. Chem.*, 1973, **55**, 185.

80. I. S. Butler, P. J. Fitzpatrick, D. F. R. Gilson, G. Gomez and A. Shaver, *Mol. Cryst. Liq. Cryst.*, 1981, **71**, 213.

81. D. Braga, F. Grepioni and E. Parsini, *Organometallics*, 1991, **10**, 3735.

82. R. Benn, H. Grondey, G. Erker, R. Aul and R. Nolte, *Organometallics*, 1990, **9**, 2493; R. Benn, H. Grondey,R. Nolte and G. Erker, *Organometallics*, 1988, **7**, 777.

83. J. K. Becconsall and S. O'Brien, *J. Chem. Soc., Chem. Commun.*, 1966, 720.

84. J. W. Faller and M. J. Incorvia, *Inorg. Chem.*, 1968, **7**, 840.

85. S. J. Heyes and S. Knight, personal communication.

86. G. M. Diamond, M. L. H. Green, P. Mountford, N. A. Popham and A. N. Chernega, *J. Chem. Soc., Chem. Commun.*, 1994, 103.

CHAPTER THREE

ansa-Bridged Binuclear Compounds of Zirconium and Hafnium

3.1 Introduction

Chapter 1 described how mononuclear group 4 metallocene derivatives have become recognised as an important class of homogeneous catalysts, especially for the stereospecific polymerization of olefins. The aim of this project was to synthesize novel binuclear complexes in which group 4 metallocenes are joined by an *ansa*-bridge.

Few *ansa*-bridged binuclear group 4 metallocene compounds have been previously prepared. In 1989, Petersen reported the reaction between the lithium salts of *ansa*-bridged bis(cyclopentadienyl) ligands $[\{X(C_5H_4)_2\}Li_2]$ ($X = CH_2$, $SiMe_2$) with $[(\eta^5\text{-}C_5H_5)ZrCl_3{\cdot}2THF]$ or $[(\eta^5\text{-}C_5Me_5)ZrCl_3]$ to give the symmetrical, homobinuclear zirconocene derivatives $[\{X(\eta^5\text{-}C_5H_4)_2\}\{(\eta^5\text{-}C_5R_5)ZrCl_2\}_2]$ ($R = H$, CH_3).[1] Heterobinuclear complexes containing bridging bis(cyclopentadienyl)-type ligands are very rare, in part because it is inherently difficult to add one metal selectively to one ring and a different metal to the second.[2] The only report of a heterobinuclear *ansa*-bridged group 4 metallocene compound was by Nifant'ev in 1992, who prepared the compound $[(\eta^5\text{-}C_5H_5)ZrCl_2\{(\eta^5\text{-}C_5H_4)SiMe_2(\eta^5\text{-}C_5H_4)\}TiCl_2(\eta^5\text{-}C_5H_5)]$ from the reaction of Zr-Sn complex $[(\eta^5\text{-}C_5H_5)ZrCl_2\{(\eta^5\text{-}C_5H_4)SiMe_2(\eta^1\text{-}C_5H_4)SnClMe_2\}]$ with $[(\eta^5\text{-}C_5H_5)TiCl_3]$.[3]

Binuclear group 4 metallocene complexes bridged by unsymmetrical *ansa* ligands have not yet been reported. Such complexes would be of interest since the two metals would experience a different ligand environment, and, if the bridging ligand was suitably substituted, chiral binuclear complexes might be prepared. The chemistry of binuclear group 4 metallocene complexes remains under-developed, and the catalytic properties of such complexes have not yet been reported.

As discussed in Chapter 2, a synthetic route to both homo- and hetero-bimetallic complexes was sought. It was thought that this might be achieved if a mononuclear compound could be isolated from the reaction of a dilithium salt of an *ansa* ligand with one equivalent of $[(\eta^5\text{-}C_5H_5)MCl_3]$ (M = group 4), followed by the treatment of this complex with a second, different transition metal halide compound.

The first ligand chosen for study was [{$Me_2C(C_5H_4)(C_9H_6)$}Li_2], because binuclear complexes bridged by this ligand would be chiral, and the two metals would experience different ligand environments.

Chapter 2 described the reaction of [$Me_2C(C_5H_4)(C_9H_6)Li_2$] with one equivalent of [(η^5-C_5H_5)MCl_3·DME] (M = Zr, Hf) to give the novel, *ansa*-bridged mononuclear compounds [{$Me_2C(\eta^5$-$C_5H_4)(\eta^2$-$C_9H_6)$}M(η^5-C_5H_5)Cl] [M = Zr (**1**), Hf (**2**)] in which the indenyl ligand is coordinated to the metal in an unusual η^2 fashion. In this chapter the reactions of these complexes with some transition metal halide compounds are discussed, and the syntheses of many novel homo- and hetero-binuclear complexes are described.

3.2. Synthesis of *ansa*-bridged homobimetallic compounds

3.2.1. Synthesis of [(η^5-C_5H_5)$ZrCl_2${(η^5-C_5H_4)CMe_2(η^5-C_9H_6)}$ZrCl_2$(η^5-C_5H_5)]

It was decided to begin by studying the reaction of [$Me_2C(C_5H_4)(C_9H_6)Li_2$] with two equivalents of [(η^5-C_5H_5)$ZrCl_3$·DME], under conditions similar to those employed by Petersen for the synthesis of the homobinuclear compounds [(η^5-C_5H_5)$ZrCl_2${X(η^5-C_5H_4)$_2$}$ZrCl_2$(η^5-C_5H_5)] (X = CH_2, $SiMe_2$).[1] The pale yellow powder [{$Me_2C(C_5H_4)(C_9H_6)$}Li_2{0.75(Et_2O)}] and two equivalents of the white powder [(η^5-C_5H_5)$ZrCl_3$·DME] were weighed into a thick-walled Rotaflo ampoule. When toluene was added at room temperature, an immediate colour change was observed, resulting in a deep red coloured reaction mixture. The ampoule was then partially evacuated and placed in an oil bath at 105 °C for 20 hours, during which time the colour of the reaction mixture changed from red to yellow. After cooling to room temperature, a clear yellow solution was filtered from a pale solid residue, presumably lithium chloride. The removal of volatiles from the yellow filtrate under reduced pressure gave the crude product as a bright yellow coloured solid. The crude product

was washed with petroleum ether (bp. 40-60 °C) / toluene and extracted into hot toluene. The yellow toluene extract was then cooled to -20 °C and after several days a yellow crystalline solid was isolated from the solution. This was characterised as the novel *ansa*-bridged binuclear compound $[(\eta^5\text{-}C_5H_5)ZrCl_2\{(\eta^5\text{-}C_5H_4)CMe_2(\eta^5\text{-}C_9H_6)\}ZrCl_2(\eta^5\text{-}C_5H_5)]$ (**8**). Concentration of the toluene solution under reduced pressure and cooling again to -20 °C gave two further crops of the yellow crystalline product. The overall yield was 54 %.

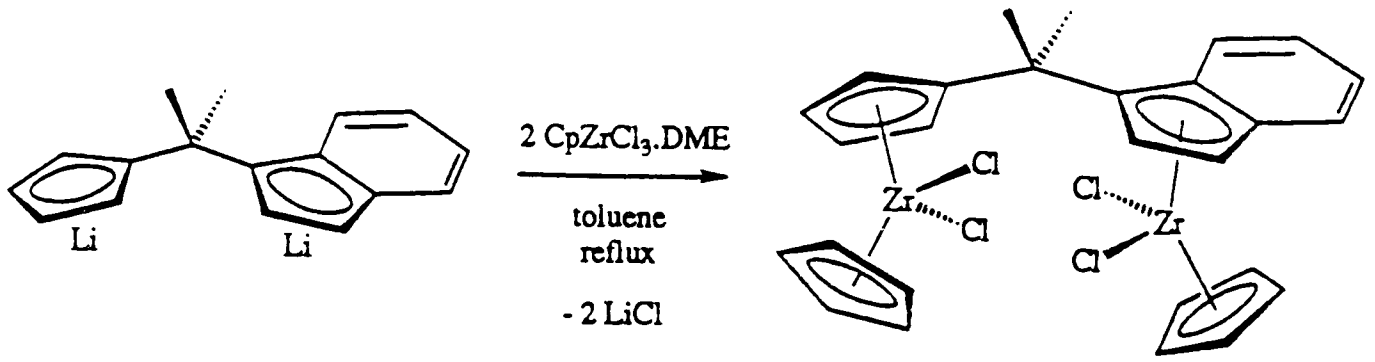

Figure 3.2.1. Synthesis of compound **8**, $[(\eta^5\text{-}C_5H_5)ZrCl_2\{(\eta^5\text{-}C_5H_4)CMe_2(\eta^5\text{-}C_9H_6)\}ZrCl_2(\eta^5\text{-}C_5H_5)]$

In an improved preparation of compound **8**, toluene at -78 °C was added to a stirred mixture of $[\{Me_2C(C_5H_4)(C_9H_6)\}Li_2\{0.6(Et_2O)\}]$ and two equivalents of $[(\eta^5\text{-}C_5H_5)ZrCl_3\cdot DME]$, also at -78 °C. An orange coloured reaction mixture was obtained, becoming deep red in colour when allowed to warm to room temperature. After stirring at room temperature for 2 hours, the ampoule was partially evacuated and placed in an oil bath at 105 °C for 20 hours during which time the colour changed from deep red to yellow/orange. The resulting mixture was filtered, and the clear, yellow/orange coloured filtrate was reduced in volume and cooled to -20 °C, giving large yellow/orange coloured crystals of $[(\eta^5\text{-}C_5H_5)ZrCl_2\{(\eta^5\text{-}C_5H_4)CMe_2(\eta^5\text{-}C_9H_6)\}ZrCl_2(\eta^5\text{-}C_5H_5)]$ (**8**) in 80 % yield. When these crystals were crushed, they gave a bright yellow solid with the same colour as the crystalline solid from the initial preparation.

The yellow crystalline solid $[(\eta^5\text{-}C_5H_5)ZrCl_2\{(\eta^5\text{-}C_5H_4)CMe_2(\eta^5\text{-}C_9H_6)\}ZrCl_2(\eta^5\text{-}C_5H_5)]$ (**8**) was characterised by elemental analysis and ^1H and ^{13}C NMR studies, including selective ^1H decoupling and ^{13}C-^1H shift correlation experiments. Compound **8** is moderately air and moisture sensitive and is soluble in benzene and toluene and very soluble in dichloromethane and THF. The elemental analysis was consistent with the proposed molecular formula $C_{27}H_{26}Cl_4Zr_2$, whilst the ^1H and ^{13}C NMR spectra of compound **8** were consistent with η^5 coordination of the C_5H_5, C_5H_4 and C_9H_6 ligands to the metal centres.

The ^1H NMR spectrum of compound **8** in CD_2Cl_2 is shown in Figure 3.2.2. Integration of the intensities of the signals indicates the presence of one $\{(C_5H_4)CMe_2(C_9H_6)\}$ ligand and two different C_5H_5 ligands. The proposed molecular structure of compound **8** is **chiral**, the different enantiomers corresponding to the coordination of either face of the indenyl ligand to zirconium. The methyl groups on the bridging carbon atom are diastereotopic and have different chemical shifts.

Selective ^1H decoupling revealed two overlapping doublets for the indenyl protons **f** and **c**, two overlapping multiplets for the indenyl protons **e** and **d**, and two doublets for the indenyl C_5-ring protons **a** and **b**. Selective ^1H decoupling also revealed two multiplets each of integrated intesity 1 H and one multiplet of intesity 2 H for the C_5H_4 protons, the 2 H multiplet overlapping the C_5H_5 signal at 6.13 ppm. Comparison with the NMR spectra of other compounds described later in this Chapter indicates that the C_5H_5 signal at 6.43 ppm corresponds to the C_5H_5 ring coordinated to the metal bonded to the C_5H_4 ring of the *ansa* ligand, whilst the C_5H_5 signal at 6.13 ppm corresponds to the C_5H_5 ring coordinated to the metal which is bonded to the indenyl group. The lower chemical shift of the latter might be due to a shielding effect of the induced aromatic ring current in the indenyl group.

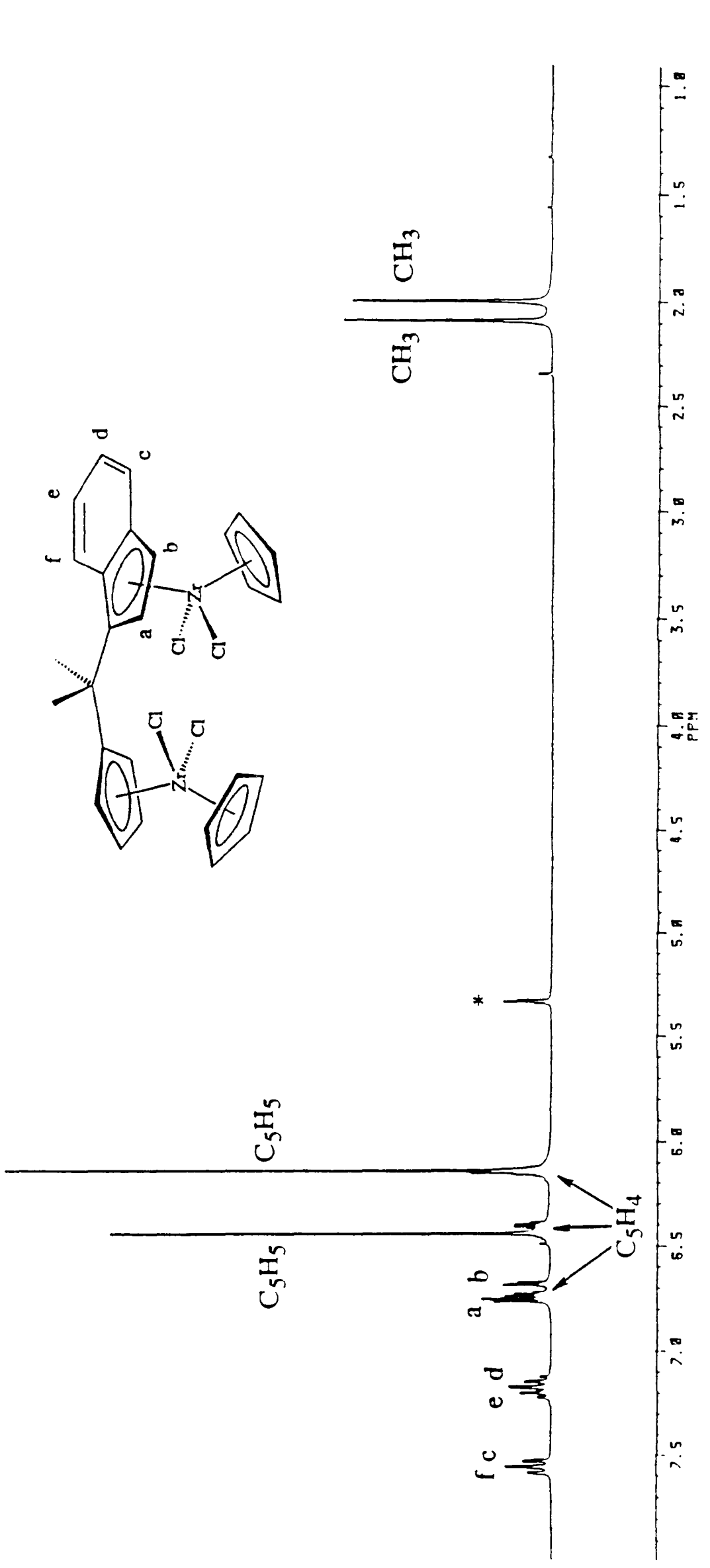

Figure 3.2.2. 300 MHz ^{1}H NMR spectrum of

$[(\eta^5\text{-}C_5H_5)ZrCl_2\{(\eta^5\text{-}C_5H_4)CMe_2(\eta^5\text{-}C_9H_6)\}ZrCl_2(\eta^5\text{-}C_5H_5)]$ (**8**)

in CD_2Cl_2 at r.t. (* = residual protio solvent)

A ^{13}C-^{1}H shift correlation experiment for compound **8** in CD_2Cl_2 was performed, to assist assignment of the ^{13}C NMR spectrum. The region of the ^{13}C-^{1}H correlation spectrum covering the indenyl and cyclopentadienyl signals is shown in Figure 3.2.3. The order of chemical shifts for the C_5H_5 ^{13}C NMR signals is opposite to that found for the ^{1}H signals. Since the carbon atoms are directly bonded to the metals, one might expect the through-bond inductive effects of other ligands coordinated to the metal to have relatively more effect on the ^{13}C chemical shifts, whereas induced field effects of other ligands (such as the shielding effect of the induced aromatic ring current of the indenyl group) are expected to have relatively more effect on the ^{1}H chemical shifts. The ^{1}H nucleus is more sensitive than other nuclei to such non-local shielding effects.

In the synthesis of compound **8**, the colour changes observed when toluene was added to the reactants were very similar to those observed in the synthesis of compound **1**, $[\{Me_2C(\eta^5\text{-}C_5H_4)(\eta^2\text{-}C_9H_6)\}Zr(\eta^5\text{-}C_5H_5)Cl]$. In both cases, when toluene was added to the reactants at room temperature, an immediate colour change was observed giving a deep red coloured reaction mixture. When toluene was added at -78 ^{o}C an orange coloured reaction mixture was obtained, becoming deep red in colour when allowed to warm to room temperature.

In the synthesis of compound **1** only one equivalent of $[(\eta^5\text{-}C_5H_5)ZrCl_3\cdot DME]$ was used and the deep red coloured product $[\{Me_2C(\eta^5\text{-}C_5H_4)(\eta^2\text{-}C_9H_6)\}Zr(\eta^5\text{-}C_5H_5)Cl]$ was obtained in good yield. In the synthesis of compound **8**, two equivalents of $[(\eta^5\text{-}C_5H_5)ZrCl_3\cdot DME]$ were used, and when the deep red coloured reaction mixture was refluxed overnight, the yellow coloured binuclear compound $[(\eta^5\text{-}C_5H_5)ZrCl_2\{(\eta^5\text{-}C_5H_4)CMe_2(\eta^5\text{-}C_9H_6)\}ZrCl_2(\eta^5\text{-}C_5H_5)]$ was obtained. These observations are consistent with the proposal that in the synthesis of **8**, $[Me_2C(C_5H_4)(C_9H_6)Li_2]$ initially reacts with one equivalent $[(\eta^5\text{-}C_5H_5)ZrCl_3\cdot DME]$ in toluene at room temperature to form compound **1**, which then reacts with the second equivalent of $[(\eta^5\text{-}C_5H_5)ZrCl_3\cdot DME]$ on heating to give the binuclear compound **8**.

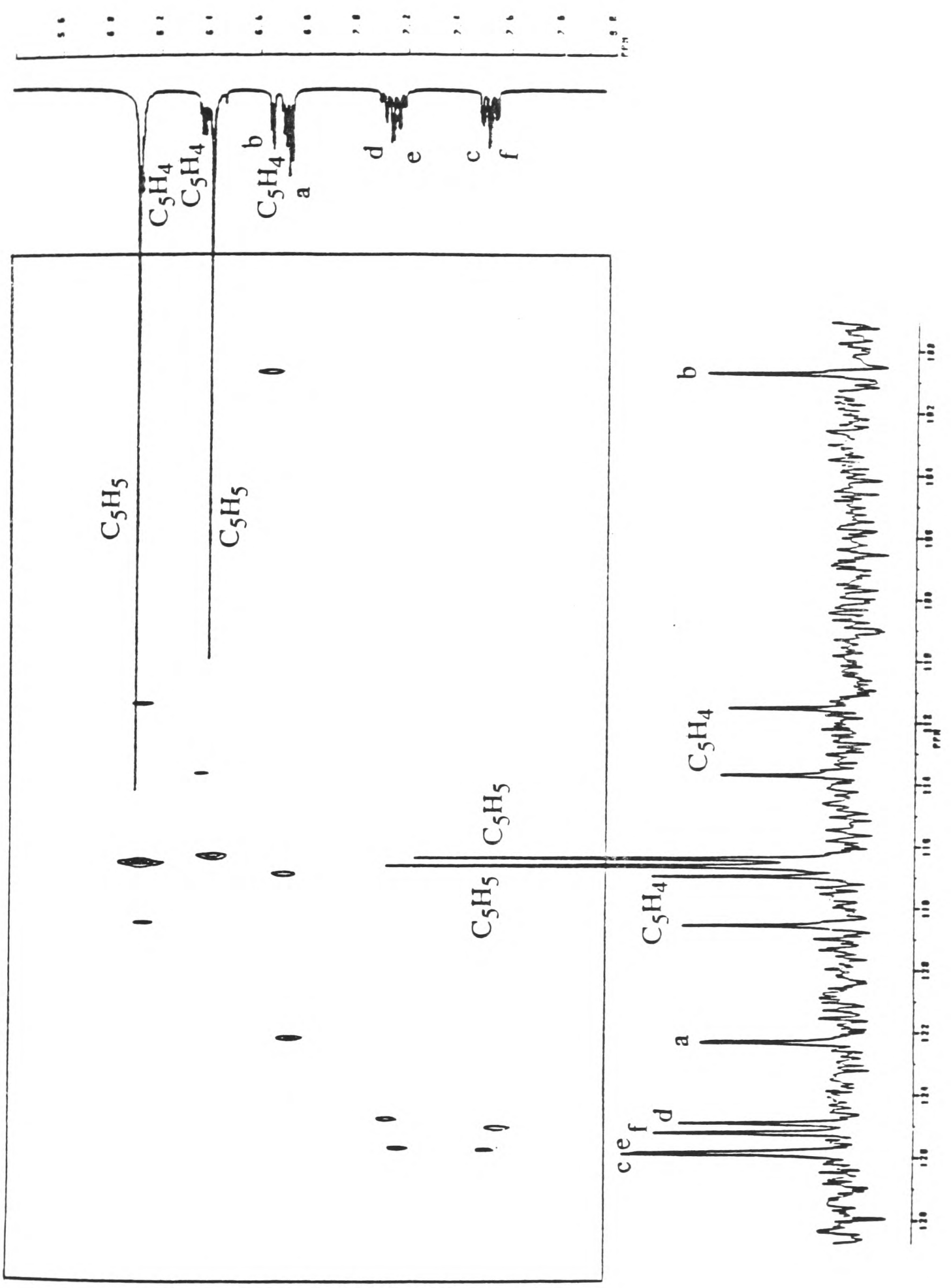

Figure 3.2.3. Part of the 75.5 MHz ^{13}C-^{1}H NMR shift correlation spectrum of $[(\eta^5\text{-}C_5H_5)ZrCl_2\{(\eta^5\text{-}C_5H_4)CMe_2(\eta^5\text{-}C_9H_6)\}ZrCl_2(\eta^5\text{-}C_5H_5)]$ (**8**) in CD_2Cl_2 at r.t.

In a separate experiment, when [{$Me_2C(\eta^5\text{-}C_5H_4)(\eta^2\text{-}C_9H_6)$}$Zr(\eta^5\text{-}C_5H_5)Cl$] (**1**) and one equivalent of [$(\eta^5\text{-}C_5H_5)ZrCl_3$·DME] were refluxed in toluene overnight, compound **8** was obtained in 70 % yield, suggesting that compound **1** is indeed an intermediate in the synthesis of compound **8**.

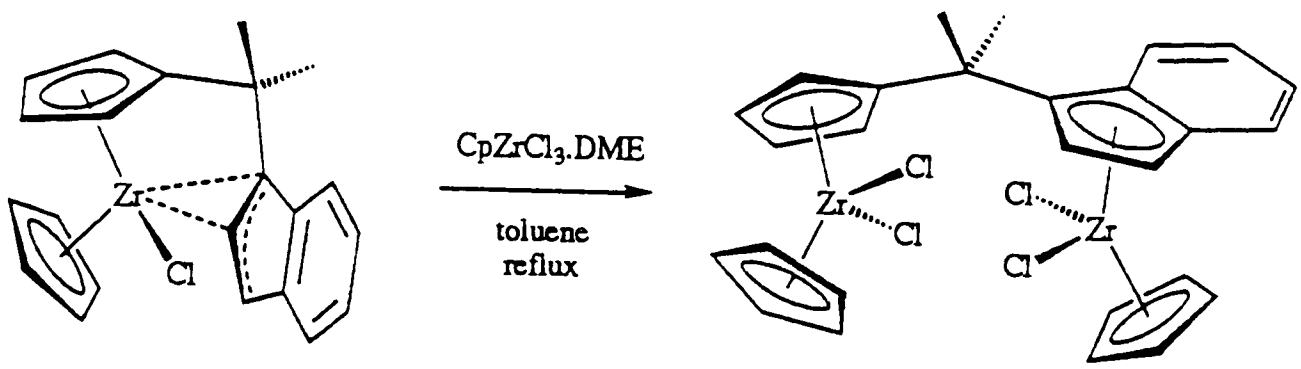

Figure 3.2.4. The reaction of compound **1** with [$(\eta^5\text{-}C_5H_5)ZrCl_3$·DME]

3.2.2. Synthesis of [$(\eta^5\text{-}C_5H_5)HfCl_2\{(\eta^5\text{-}C_5H_4)CMe_2(\eta^5\text{-}C_9H_6)\}HfCl_2(\eta^5\text{-}C_5H_5)$]

It was decided to attempt to prepare the homobinuclear hafnium analogue of compound **8**. Toluene at -78 °C was added to a stirred mixture of [{$Me_2C(C_5H_4)(C_9H_6)$}Li_2{$0.6(Et_2O)$}] and two equivalents of [$(\eta^5\text{-}C_5H_5)HfCl_3$·DME] in a thick-walled Rotaflo ampoule also at -78 °C. The resulting yellow mixture was allowed to warm to room temperature, becoming orange in colour. After stirring at room temperature for one hour, the ampoule was partially evacuated and placed in an oil bath at 105 °C for 18 hours. The resulting suspension was allowed to settle, and the clear yellow solution was decanted into a Schlenk tube, concentrated under reduced pressure and cooled to -20 °C. After several days, yellow crystals were separated from the solution and were characterised as the novel *ansa*-bridged binuclear compound [$(\eta^5\text{-}C_5H_5)HfCl_2\{(\eta^5\text{-}C_5H_4)CMe_2(\eta^5\text{-}C_9H_6)\}HfCl_2(\eta^5\text{-}C_5H_5)$] (**9**). Compound **9** was obtained in 68 % yield.

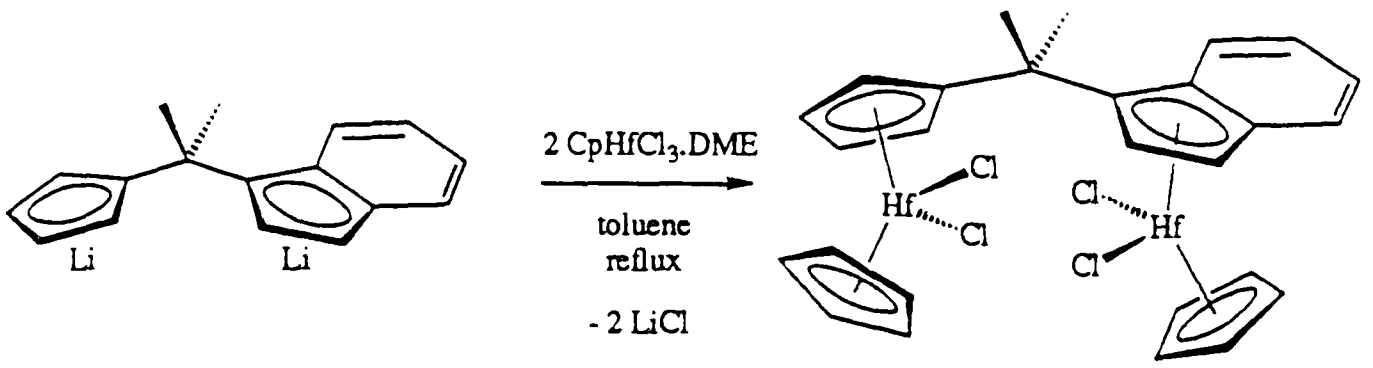

Figure 3.2.5. Synthesis of compound **9**,

$[(\eta^5\text{-}C_5H_5)HfCl_2\{(\eta^5\text{-}C_5H_4)CMe_2(\eta^5\text{-}C_9H_6)\}HfCl_2(\eta^5\text{-}C_5H_5)]$

The yellow crystalline solid $[(\eta^5\text{-}C_5H_5)HfCl_2\{(\eta^5\text{-}C_5H_4)CMe_2(\eta^5\text{-}C_9H_6)\}HfCl_2(\eta^5\text{-}C_5H_5)]$ (**9**) was characterised by elemental analysis and ^1H and ^{13}C NMR spectroscopy. Compound **9** is moderately air and moisture sensitive and is soluble in benzene and toluene, and very soluble in dichloromethane. The elemental analysis was consistent with the proposed formula $C_{27}H_{26}Cl_4Hf_2$.

The ^1H and ^{13}C NMR spectra of compound **9** in CD_2Cl_2 were very similar to those of compound **8**, suggesting an analogous molecular structure. The ^1H chemical shifts of the C_5H_5 signals lie at 6.33 ppm and 6.00 ppm, approximately 0.1 ppm lower than for the zirconium analogue, which is typical of cyclopentadienyl hafnium compounds compared with zirconium analogues.[4-6] To assist the assignment of the NMR spectra of compound **9** and other related compounds, a NOESY experiment was performed. The experimental parameters used were similar to those employed for NOESY Experiment 1 for compound **1**, with a two second mixing time.

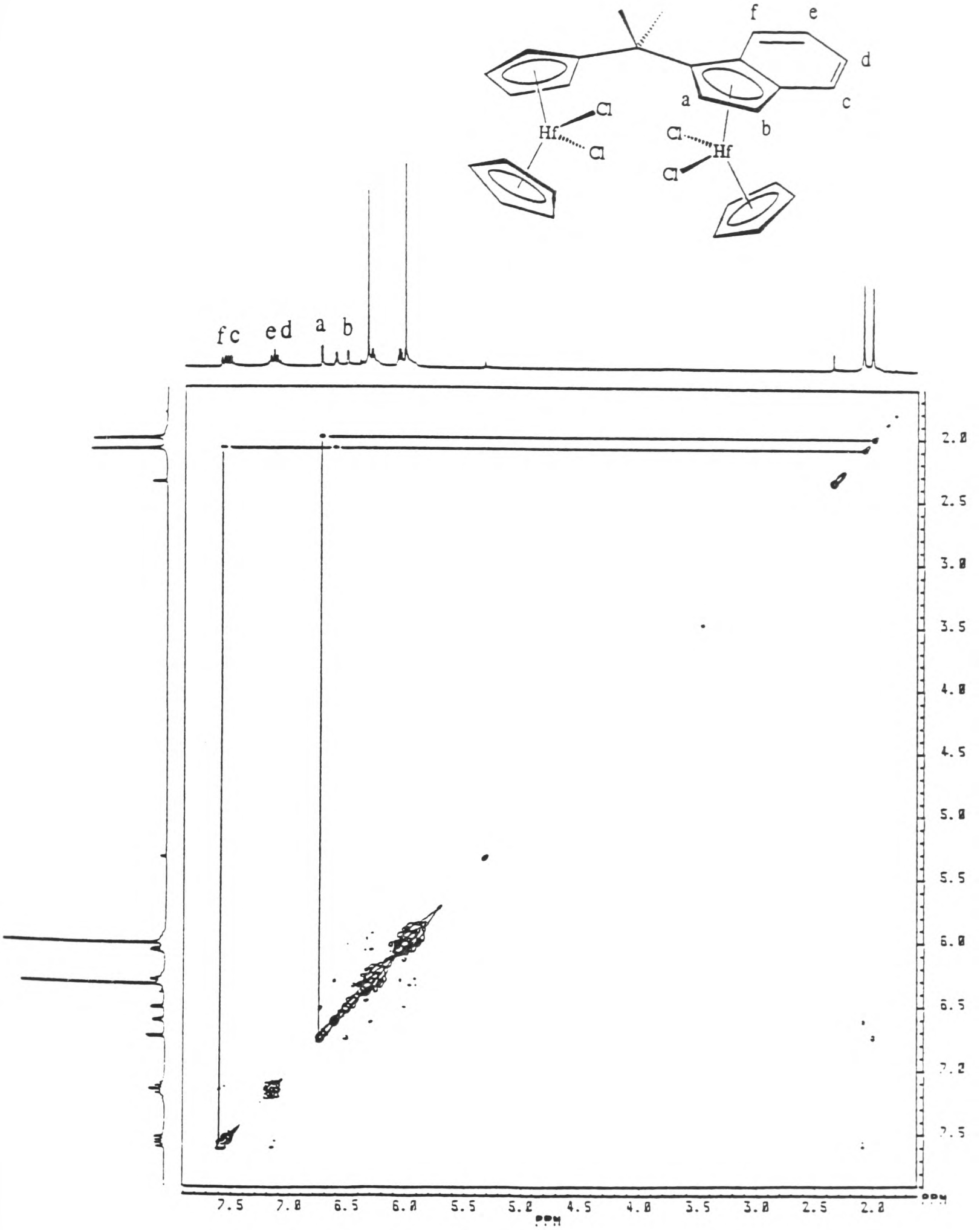

Figure 3.2.6. 300 MHz ^{1}H NOESY spectrum of $[(\eta^5\text{-}C_5H_5)HfCl_2\{(\eta^5\text{-}C_5H_4)CMe_2(\eta^5\text{-}C_9H_6)\}HfCl_2(\eta^5\text{-}C_5H_5)]$ (**9**) in CD_2Cl_2 at r.t.

The NOESY spectrum of compound **9** in CD_2Cl_2 at room temperature (Figure 3.2.6) shows that one of the methyl groups of the bridge is correlated to one of the indenyl C_5-ring protons (**a**), whilst the other methyl group is correlated to one of the indenyl C_6-ring protons (**f**) and one of the C_5H_4 protons. These correlations are consistent with the proposed assignments of the indenyl signals, and also suggest that there may be a preferred molecular conformation of **9** in solution in which proton **a** is close to one of the methyl groups and proton **f** is close to the other methyl group.

3.3. Synthesis of *ansa*-bridged heterobimetallic compounds

If the compounds [{$Me_2C(\eta^5$-$C_5H_4)(\eta^2$-$C_9H_6)$}$M(\eta^5$-$C_5H_5)Cl$] [M = Zr (**1**), Hf (**2**)] are intermediates in the synthesis of the homobinuclear compounds **8** and **9**, then the reaction of **1** with [$(\eta^5$-$C_5H_5)HfCl_3$·DME], and the reaction of **2** with [$(\eta^5$-$C_5H_5)ZrCl_3$·DME], might allow the **selective** synthesis of the heterobinuclear analogues of **8** and **9**.

3.3.1. Synthesis of [$(\eta^5$-$C_5H_5)ZrCl_2${$(\eta^5$-$C_5H_4)CMe_2(\eta^5$-$C_9H_6)$}$HfCl_2(\eta^5$-$C_5H_5)$]

The red solid [{$Me_2C(\eta^5$-$C_5H_4)(\eta^2$-$C_9H_6)$}$Zr(\eta^5$-$C_5H_5)Cl$] (**1**) and the white solid [$(\eta^5$-$C_5H_5)HfCl_3$·DME] were weighed into a thick-walled Rotaflo ampoule. Toluene was added and the red coloured reaction mixture was stirred at room temperature for one hour. The ampoule was then partially evacuated and placed in an oil bath at 105 °C for 16 hours. The resulting clear, orange solution was transferred to a Schlenk tube, concentrated under reduced pressure and cooled to -20 °C. After several days the toluene solution was removed from the yellow crystals that had formed. The solution was again concentrated and cooled to -20 °C, affording a second crop of yellow crystals. The yellow crystalline solid was characterised as the novel,

ansa-bridged heterobinuclear compound $[(\eta^5\text{-}C_5H_5)ZrCl_2\{(\eta^5\text{-}C_5H_4)CMe_2(\eta^5\text{-}C_9H_6)\}HfCl_2(\eta^5\text{-}C_5H_5)]$ (**10**), and was obtained in an overall yield of 74 %.

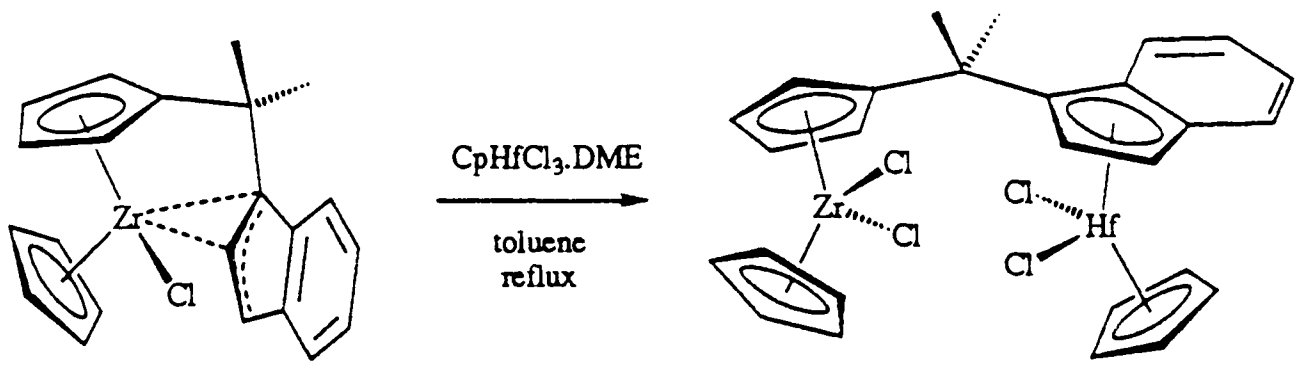

Figure 3.3.1. Synthesis of compound **10**,
$[(\eta^5\text{-}C_5H_5)ZrCl_2\{(\eta^5\text{-}C_5H_4)CMe_2(\eta^5\text{-}C_9H_6)\}HfCl_2(\eta^5\text{-}C_5H_5)]$

The yellow crystalline solid $[(\eta^5\text{-}C_5H_5)ZrCl_2\{(\eta^5\text{-}C_5H_4)CMe_2(\eta^5\text{-}C_9H_6)\}HfCl_2(\eta^5\text{-}C_5H_5)]$ (**10**) was characterised by elemental analysis and ^1H and ^{13}C NMR spectroscopy. The elemental analysis was consistent with the proposed molecular formula $C_{27}H_{26}Cl_4ZrHf$. The ^1H and ^{13}C NMR spectra of compound **10** in CD_2Cl_2 closely resembled those of compounds **8** and **9**. The $^{13}C\{^1H\}$ NMR spectrum of **10**, shown in Figure 3.3.2, was assigned on the basis of a ^{13}C-^1H shift correlation experiment and by comparison with the spectra of compounds **8** and **9**.

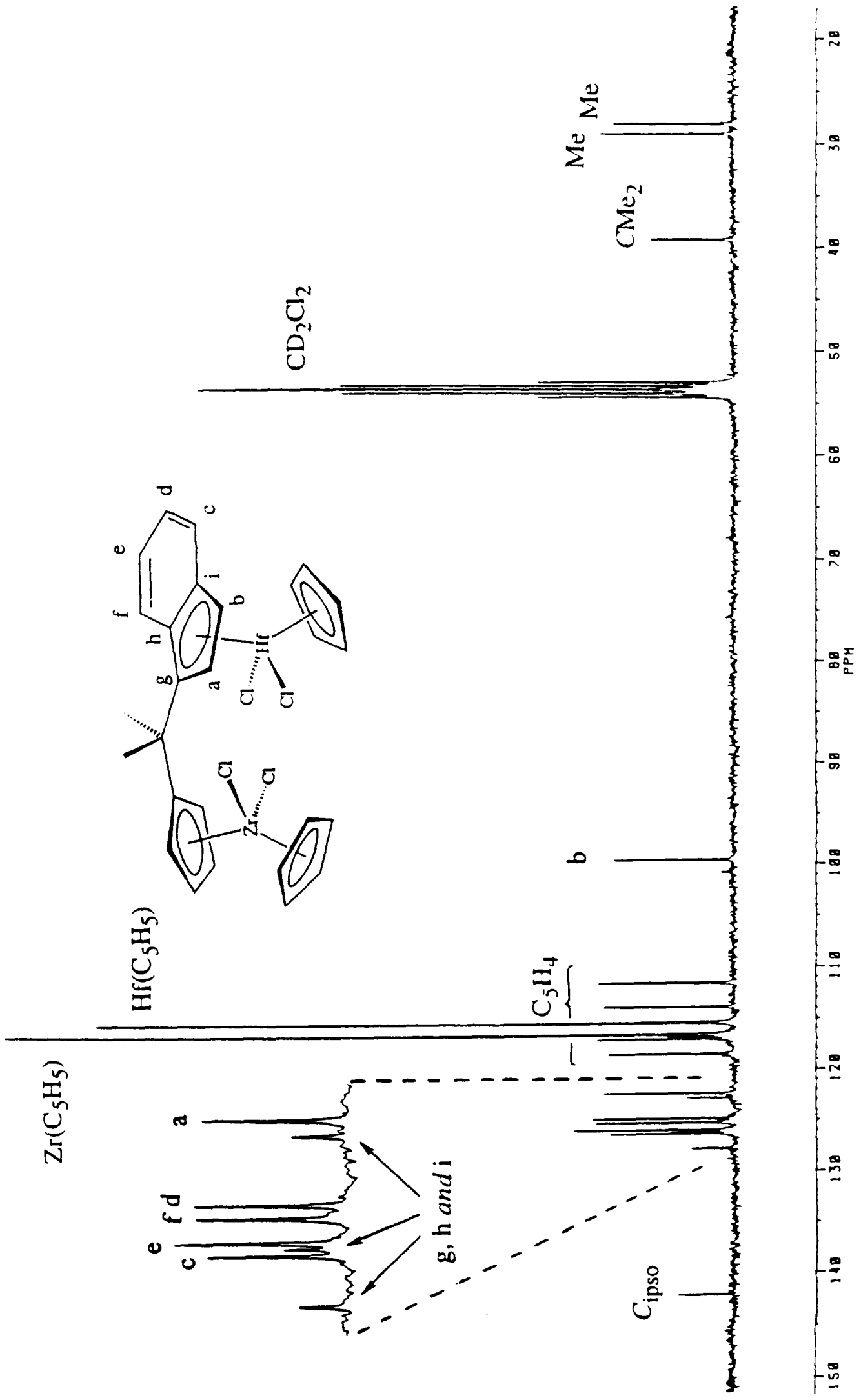

Figure 3.3.2. 75.5 MHz $^{13}C\{^1H\}$ NMR spectrum of compound **10**, $[(\eta^5\text{-}C_5H_5)ZrCl_2\{(\eta^5\text{-}C_5H_4)CMe_2(\eta^5\text{-}C_9H_6)\}HfCl_2(\eta^5\text{-}C_5H_5)]$, in CD_2Cl_2 at r.t.

The ^{1}H NMR spectrum of **10** (Figure 3.3.3) shows that the chemical shifts of the C_5H_4 signals are almost identical to those of compound **8**, while the shifts of the indenyl proton signals are almost identical to those of compound **9** (the chemical shifts of the protons **f**, **c**, **e** **d** and the methyl groups are almost identical in all three cases). These observations are consistent with the proposed identity of compound **10**, as the heterobimetallic analogue of **8** and **9** in which the zirconium is coordinated to the C_5H_4 ring and the hafnium is coordinated to the indenyl group. The ^{13}C chemical shifts of **8**, **9** and **10** are also consistent with this proposal.

In the ^{1}H NMR spectrum of **10**, one of the C_5H_5 signals lies at the same shift as the higher shift (downfield) C_5H_5 signal in the zirconium compound **8** (6.43 ppm), whilst the lower shift (upfield) C_5H_5 signal of **10** lies at almost exactly the same chemical shift as the corresponding signal of the hafnium compound **9** (6.01 ppm). These observations are consistent with the proposal that for compounds **8**, **9** and **10**, the C_5H_5 signal at **higher** chemical shift corresponds to the C_5H_5 ring coordinated to the metal which is bonded to the **C_5H_4 ring** of the *ansa* ligand, whilst the C_5H_5 signal at the **lower** chemical shift corresponds to the C_5H_5 ring coordinated to the metal which is bonded to the **indenyl** group.

Heterobinuclear complexes containing bridging bis(cyclopentadienyl)-type ligands are very rare, in part because it is inherently difficult to add one metal selectively to one ring and a different metal to the second. The NMR spectra of **10** suggest that the reaction of **1** with $[(\eta^5\text{-}C_5H_5)HfCl_3\cdot DME]$ provides a **selective synthesis** of the heterobinuclear compound $[(\eta^5\text{-}C_5H_5)ZrCl_2\{(\eta^5\text{-}C_5H_4)CMe_2(\eta^5\text{-}C_9H_6)\}HfCl_2(\eta^5\text{-}C_5H_5)]$, in which the zirconium is found exclusively at the C_5H_4 site and the hafnium is found exclusively at the indenyl site. The NMR spectra of **10** show no evidence for exchange of the metals between the C_5H_4 and indenyl sites.

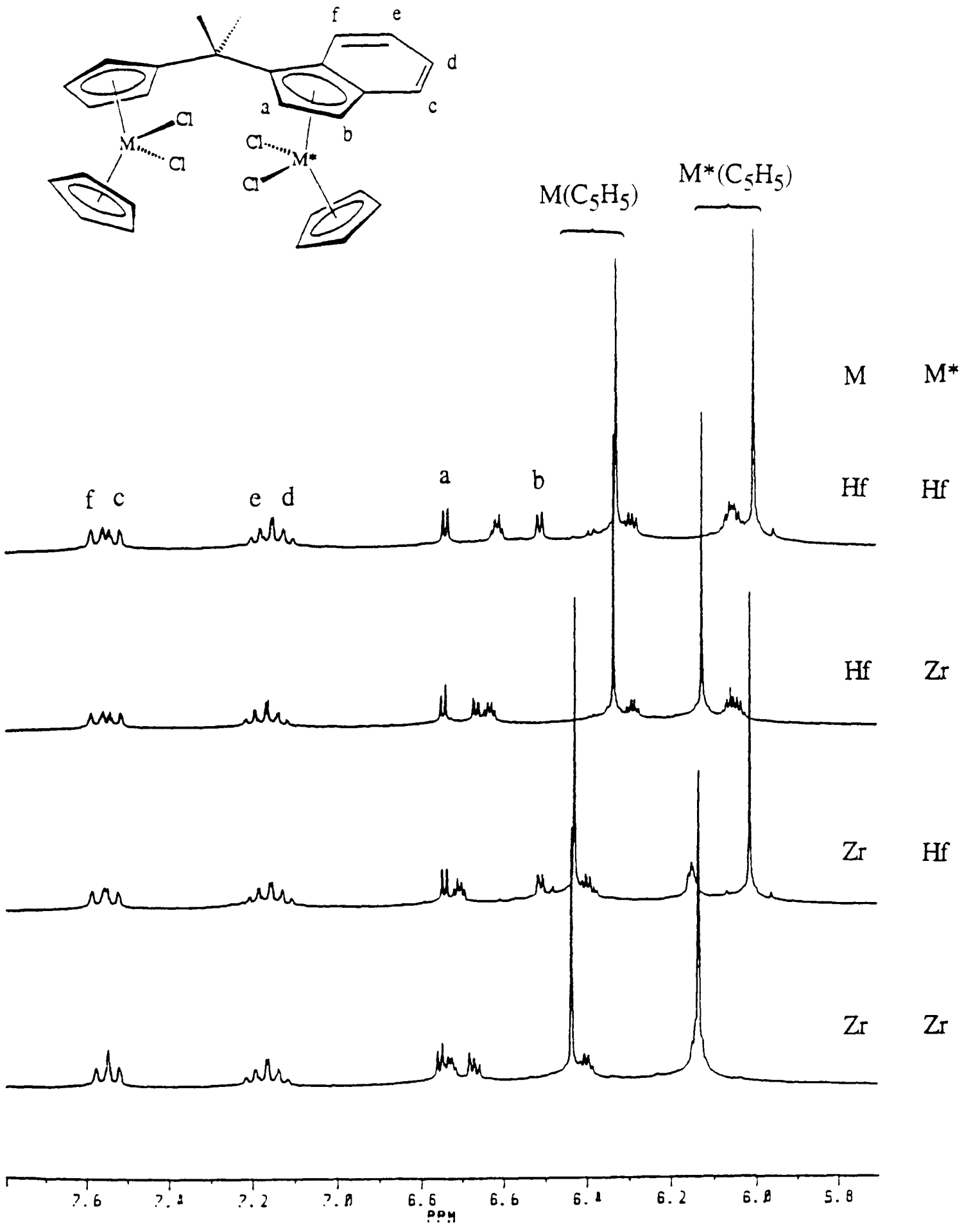

Figure 3.3.3. Cyclopentadienyl and indenyl regions of the 300 MHz ^{1}H NMR spectra of $[(\eta^5\text{-}C_5H_5)MCl_2\{(\eta^5\text{-}C_5H_4)CMe_2(\eta^5\text{-}C_9H_6)\}M^*Cl_2(\eta^5\text{-}C_5H_5)]$ in CD_2Cl_2 at r.t. [M = M* = Hf (**9**); M = Hf, M* = Zr (**11**); M = Zr, M* = Hf (**10**); M = M* = Zr (**8**)]

3.3.2. Synthesis of $[(\eta^5\text{-}C_5H_5)HfCl_2\{(\eta^5\text{-}C_5H_4)CMe_2(\eta^5\text{-}C_9H_6)\}ZrCl_2(\eta^5\text{-}C_5H_5)]$

It was decided to attempt to synthesise the alternative hafnium-zirconium heterobinuclear analogue of **8**, **9** and **10**, namely $[(\eta^5\text{-}C_5H_5)HfCl_2\{(\eta^5\text{-}C_5H_4)CMe_2(\eta^5\text{-}C_9H_6)\}ZrCl_2(\eta^5\text{-}C_5H_5)]$. The reaction of $[\{Me_2C(\eta^5\text{-}C_5H_4)(\eta^2\text{-}C_9H_6)\}Hf(\eta^5\text{-}C_5H_5)Cl]$ (**2**) and one equivalent of $[(\eta^5\text{-}C_5H_5)ZrCl_3\cdot DME]$, following the same procedure as for compound **10** (refluxed in toluene overnight) gave the desired product $[(\eta^5\text{-}C_5H_5)HfCl_2\{(\eta^5\text{-}C_5H_4)CMe_2(\eta^5\text{-}C_9H_6)\}ZrCl_2(\eta^5\text{-}C_5H_5)]$ (**11**) but in low yield (typically less than 20 % isolated yield). It was found, however, that when the reactants were refluxed overnight in THF rather than toluene, the desired product could be isolated in greater than 70 % yield.

In a typical reaction, the dark orange solid $[\{Me_2C(\eta^5\text{-}C_5H_4)(\eta^2\text{-}C_9H_6)\}Hf(\eta^5\text{-}C_5H_5)Cl]$ (**2**) and the white solid $[(\eta^5\text{-}C_5H_5)ZrCl_3\cdot DME]$ were weighed into a thick-walled Rotaflo ampoule. THF was added and the orange/red coloured solution was stirred at room temperature for one hour. The ampoule was then partially evacuated and placed in an oil bath at 80 °C for 15 hours. The resulting clear, yellow solution was transferred to a Schlenk tube and all volatiles were removed under reduced pressure, leaving the crude product as a slightly oily yellow solid (*ca.* 90 % desired product by ^1H NMR). Washing with diethyl ether left the pure product as a fine yellow powder, in 78 % yield. The yellow powder was characterised as the novel *ansa*-bridged heterobinuclear compound $[(\eta^5\text{-}C_5H_5)HfCl_2\{(\eta^5\text{-}C_5H_4)CMe_2(\eta^5\text{-}C_9H_6)\}ZrCl_2(\eta^5\text{-}C_5H_5)]$ (**11**), by elemental analysis and ^1H and ^{13}C NMR spectroscopy.

The elemental analysis of compound **11** was consistent with proposed molecular formula $C_{27}H_{26}Cl_4HfZr$. The ^1H and ^{13}C NMR spectra of compound **11** in CD_2Cl_2 were similar to those of compounds **8**, **9** and **10**. The cyclopentadienyl and indenyl region of the ^1H NMR spectrum of $[(\eta^5\text{-}C_5H_5)HfCl_2\{(\eta^5\text{-}C_5H_4)CMe_2(\eta^5\text{-}C_9H_6)\}ZrCl_2(\eta^5\text{-}C_5H_5)]$ (**11**) is shown in Figure 3.3.3, together with those of compounds **8**, **9** and **10**.

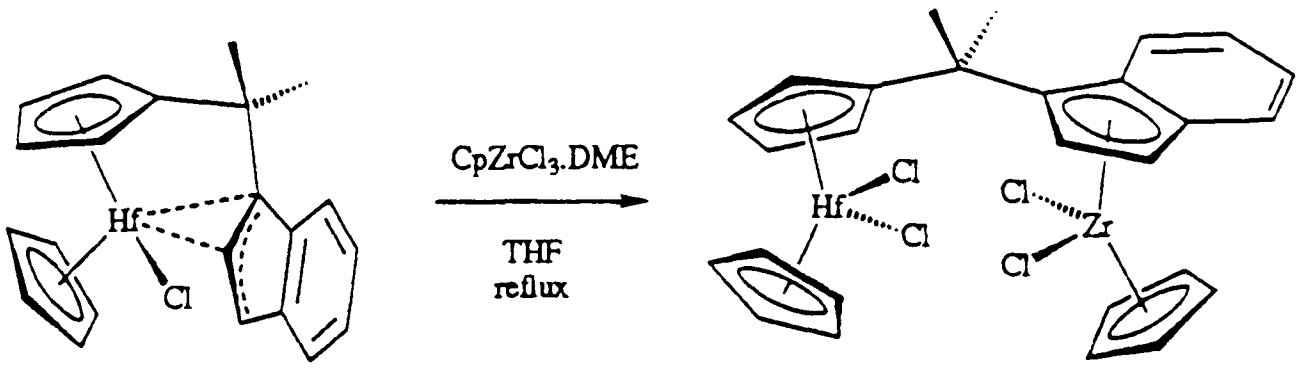

Figure 3.3.4. Synthesis of compound **11**,

$[(\eta^5\text{-}C_5H_5)HfCl_2\{(\eta^5\text{-}C_5H_4)CMe_2(\eta^5\text{-}C_9H_6)\}ZrCl_2(\eta^5\text{-}C_5H_5)]$

It can be seen that the chemical shifts of the C_5H_4 signals of **11** are almost identical to those of the dihafnium compound **9**, while the shifts of the indenyl proton signals are almost identical to those of the dizirconium compound **8**. The chemical shifts of the C_5H_5 signals of **11** are also consistent with the proposed molecular structure, closely matching the higher shift signal of **9** (6.33 ppm) and the lower shift signal of **8** (6.12 ppm).

The ^1H and ^{13}C NMR chemical shifts of C_5H_5 ligands of compounds **8**, **9**, **10** and **11** are shown in Table 3.1. It can be seen that the ^1H and ^{13}C NMR chemical shifts of the C_5H_5 ligands are dependent on which metal the C_5H_5 ligand is coordinated to, and also on the "site" occupied by the metal, i.e. whether the metal is coordinated to the C_5H_4 ring or the indenyl group of the *ansa*-ligand. However, whilst the ^1H chemical shift appears to be primarily determined by the "site", with the nature of the metal having a lesser effect on the shift, the opposite is true for the ^{13}C chemical shift. It also appears that the "site effect" on the chemical shifts is opposite for ^{13}C and ^1H nuclei. As discussed earlier, the through-bond inductive effects of other ligands coordinated to the metal would be expected to have more influence on the ^{13}C chemical shift, whilst non-local shielding effects such as the aromatic ring current effect of the indenyl ligand, would be expected to have more effect on the ^1H chemical shifts.

Table 3.1. ^{1}H and ^{13}C chemical shifts of C_5H_5 ligands of compounds **8**, **10**, **11** and **9**.

^{1}H NMR chemical shifts (CD_2Cl_2) for the C_5H_5 ligands in the series $[(\eta^5\text{-}C_5H_5)MCl_2\{(\eta^5\text{-}C_5H_4)CMe_2(\eta^5\text{-}C_9H_6)\}M^*Cl_2(\eta^5\text{-}C_5H_5)]$				
Compound	M	δ M(C_5H_5) / ppm	M*	δ M*(C_5H_5) / ppm
8	Zr	6.43	Zr	6.13
10	Zr	6.43	Hf	6.01
11	Hf	6.33	Zr	6.12
9	Hf	6.33	Hf	6.00

^{13}C NMR chemical shifts (CD_2Cl_2) for the C_5H_5 ligands in the series $[(\eta^5\text{-}C_5H_5)MCl_2\{(\eta^5\text{-}C_5H_4)CMe_2(\eta^5\text{-}C_9H_6)\}M^*Cl_2(\eta^5\text{-}C_5H_5)]$				
Compound	M	δ M(C_5H_5) / ppm	M*	δ M*(C_5H_5) / ppm
8	Zr	116.4	Zr	116.6
10	Zr	116.4	Hf	115.3
11	Hf	115.0	Zr	116.6
9	Hf	115.0	Hf	115.3

The spectra in Figure 3.3.3 and the data in Table 3.1 provide strong evidence the compounds **8**, **9**, **10** and **11** are indeed a series of homo- and hetero-bimetallic compounds with analogous molecular structures.

The reactions discussed so far in this chapter are summarised in Figure 3.3.5. The novel, *ansa*-bridged homobinuclear complexes **8** and **9** may be prepared by the reaction of $[Me_2C(C_5H_4)(C_9H_6)Li_2]$ two equivalents of $[(\eta^5\text{-}C_5H_5)MCl_3\cdot DME]$ (M = Zr, Hf), whilst the reaction of the *ansa*-bridged mononuclear complexes $[\{Me_2C(\eta^5\text{-}C_5H_4)(\eta^2\text{-}C_9H_6)\}M(\eta^5\text{-}C_5H_5)Cl]$ (M = Zr, Hf) with $[(\eta^5\text{-}C_5H_5)M^*Cl_3\cdot DME]$ (M* = Hf, Zr) allows the selective synthesis of the heterobinuclear analogues **10** and **11**

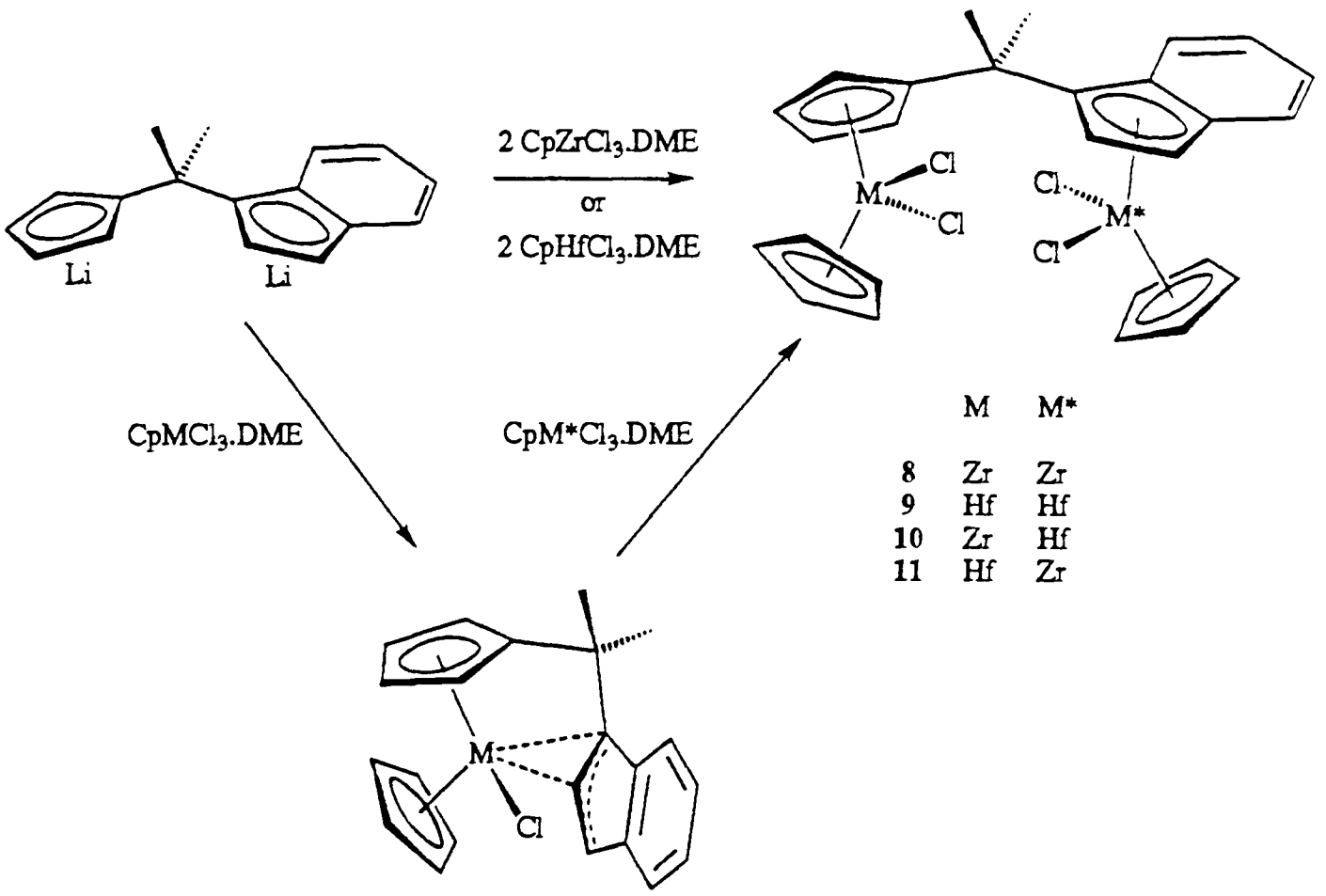

Figure 3.3.5. Synthesis of compounds **8**, **9**, **10** and **11**.

The reactions of [{$Me_2C(\eta^5\text{-}C_5H_4)(\eta^2\text{-}C_9H_6)$}$MCl(\eta^5\text{-}C_5H_5)$] with [($\eta^5$-$C_5H_5$)M*$Cl_3$·DME] might be considered to be "metathesis" reactions, in which M-C and M*-Cl bonds are broken and M-Cl and M*-C bonds are formed:

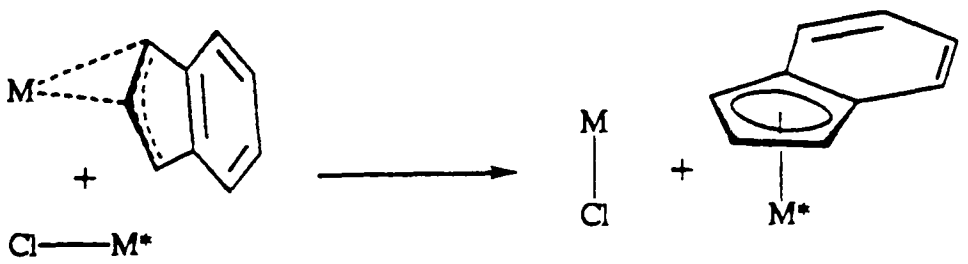

It seems likely that one factor favouring these reactions is a more favourable M*(η^5-indenyl) bonding mode in the product compared with the M(η^2-indenyl) bonding of the chelating *ansa* ligand in the starting material. The relief of the strained *ansa* ligand coordination in the starting material may also drive the reaction. Since Zr-Cl and Hf-Cl bond enthalpies are very similar, and are little effected by ancillary ligands, the

breaking and forming of the M-Cl bonds probably has little effect on the enthalpy of reaction.[7] The bridging *ansa* ligand in the product would be expected to have more degrees of freedom than the chelating *ansa* ligand, which would be expected to make the reaction more entropically favourable.

3.4. Synthesis of $[(\eta^5\text{-}C_5H_5)ZrCl_2\{(\eta^5\text{-}C_5H_4)CMe_2(\eta^5\text{-}C_9H_6)\}ZrCl_2(\eta^5\text{-}C_5Me_5)]$

The previous section described how the reactions between the *ansa*-bridged mononuclear complexes $[\{Me_2C(\eta^5\text{-}C_5H_4)(\eta^2\text{-}C_9H_6)\}M(\eta^5\text{-}C_5H_5)Cl]$ [M = Zr (**1**), Hf (**2**)] and one equivalent of $[(\eta^5\text{-}C_5H_5)MCl_3\cdot DME]$ (M = Hf, Zr) provided **selective** syntheses of the novel heterobinuclear compounds **10** and **11**. It was decided to test whether similar reactions with other monocyclopentadienyl group 4 metal halide derivatives might allow the selective synthesis of other unsymmetrical *ansa*-bridged binuclear metallocene compounds.

When toluene was added to a mixture of $[\{Me_2C(\eta^5\text{-}C_5H_4)(\eta^2\text{-}C_9H_6)\}Zr(\eta^5\text{-}C_5H_5)Cl]$ (**1**) and $[(\eta^5\text{-}C_5Me_5)ZrCl_3\cdot 2THF]$, a red coloured reaction mixture was obtained. When stirred at room temperature for two days, no colour change was observed. However, on heating to 95 °C and stirring for 18 hours, the colour slowly changed from deep red to yellow/orange. The reaction mixture was then filtered, and the yellow filtrate was concentrated under reduced pressure and cooled to -20 °C. After several days a yellow crystalline solid was isolated from the solution and was characterised as the novel binuclear compound $[(\eta^5\text{-}C_5H_5)ZrCl_2\{(\eta^5\text{-}C_5H_4)CMe_2(\eta^5\text{-}C_9H_6)\}ZrCl_2(\eta^5\text{-}C_5Me_5)]$ (**12**). Concentration of the toluene solution under reduced pressure and cooling again to -20 °C gave two further crops of the yellow crystalline product; the overall yield was 52 %.

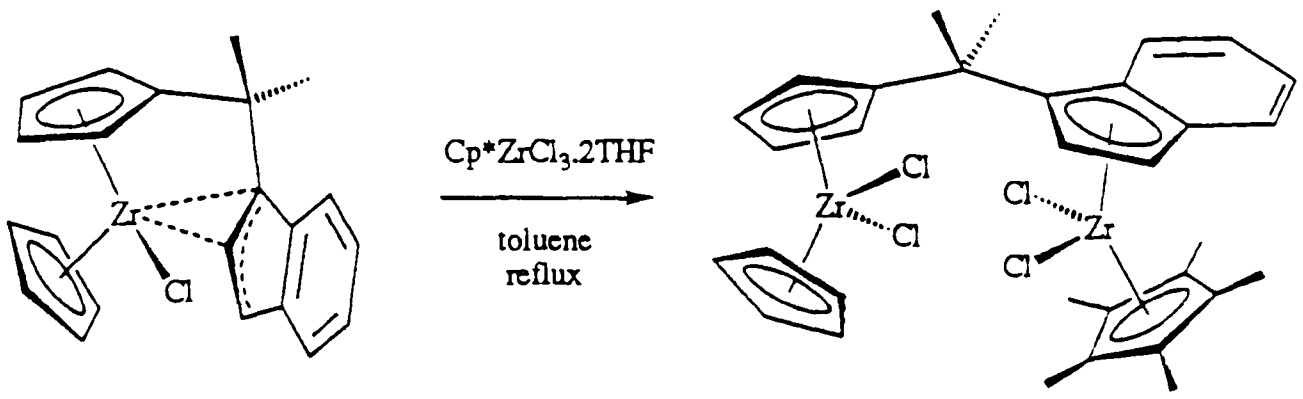

Figure 3.4.1. Synthesis of compound **12**,

$[(\eta^5\text{-}C_5H_5)ZrCl_2\{(\eta^5\text{-}C_5H_4)CMe_2(\eta^5\text{-}C_9H_6)\}ZrCl_2(\eta^5\text{-}C_5Me_5)]$

The elemental analysis of compound **12** was consistent with the proposed molecular formula $C_{32}H_{36}Cl_4Zr_2$. The ^1H and ^{13}C DEPT NMR spectra of compound **12** in CD_2Cl_2 are shown in Figures 3.4.2 and 3.4.3 respectively. The spectra are quite similar to those of the dizirconium compound **8**, except that the signals typical of a $(\eta^5\text{-}C_5Me_5)$ ligand[8, 9] are observed, instead of one of the $(\eta^5\text{-}C_5H_5)$ ligands. In particular, the ^1H chemical shifts for the C_5H_4 and C_5H_5 groups of **12** are very similar to those of the C_5H_4 signals and the higher shift C_5H_5 signal of compound **8**. For compound **12** the chemical shifts of the indenyl C_5-ring ^1H signals **a** and **b** are approximately 0.5 ppm lower than in compound **8**, and the corresponding ^{13}C signals are approximately 3 to 5 ppm lower, which may reflect the electron donating character of the methyl substituents on the C_5Me_5 ring.

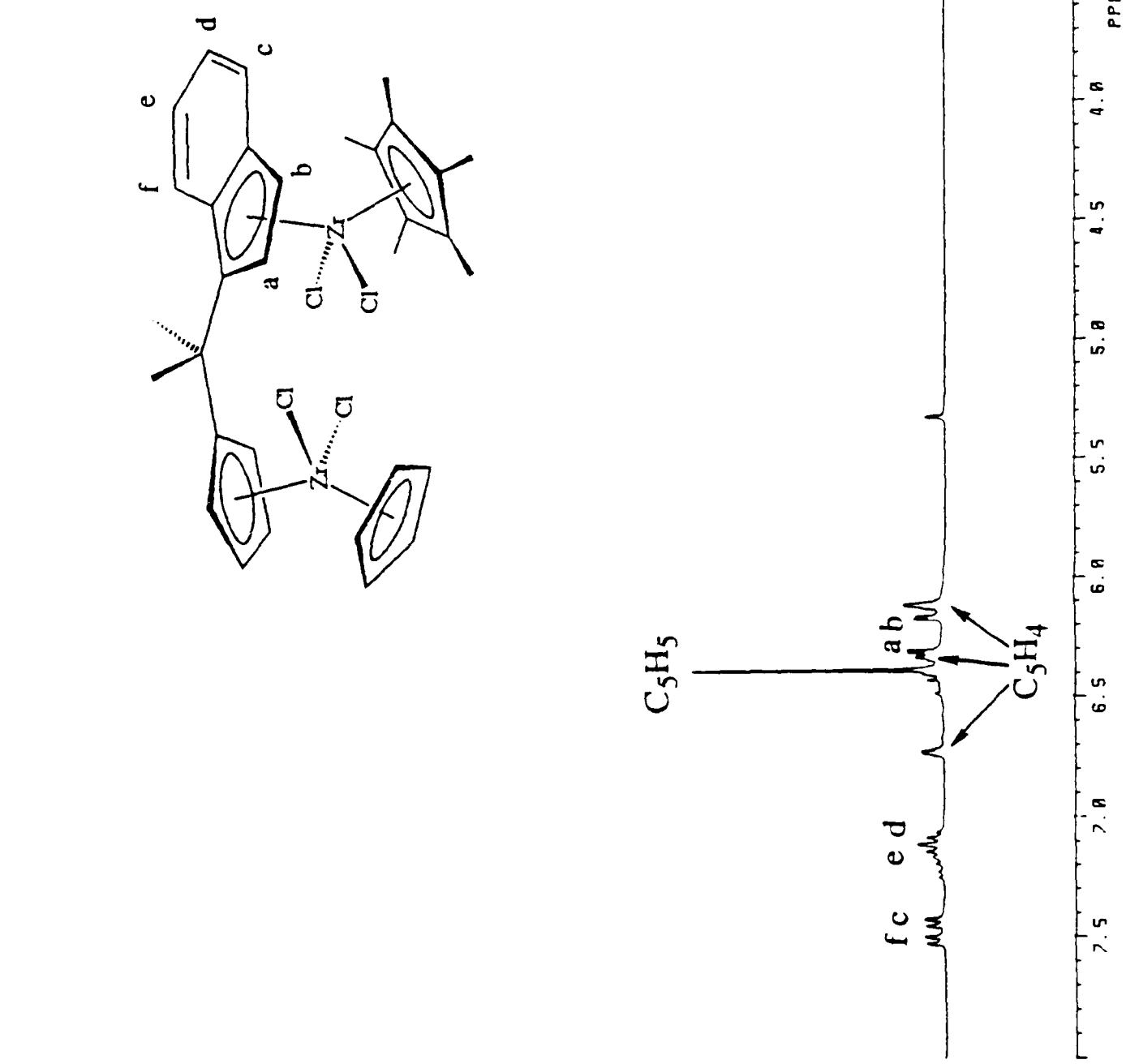

Figure 3.4.2. 300 MHz ^{1}H NMR spectrum of compound **12**, $[(\eta^5\text{-}C_5H_5)ZrCl_2\{(\eta^5\text{-}C_5H_4)CMe_2(\eta^5\text{-}C_9H_6)\}ZrCl_2(\eta^5\text{-}C_5Me_5)]$, in CD_2Cl_2 at r.t.

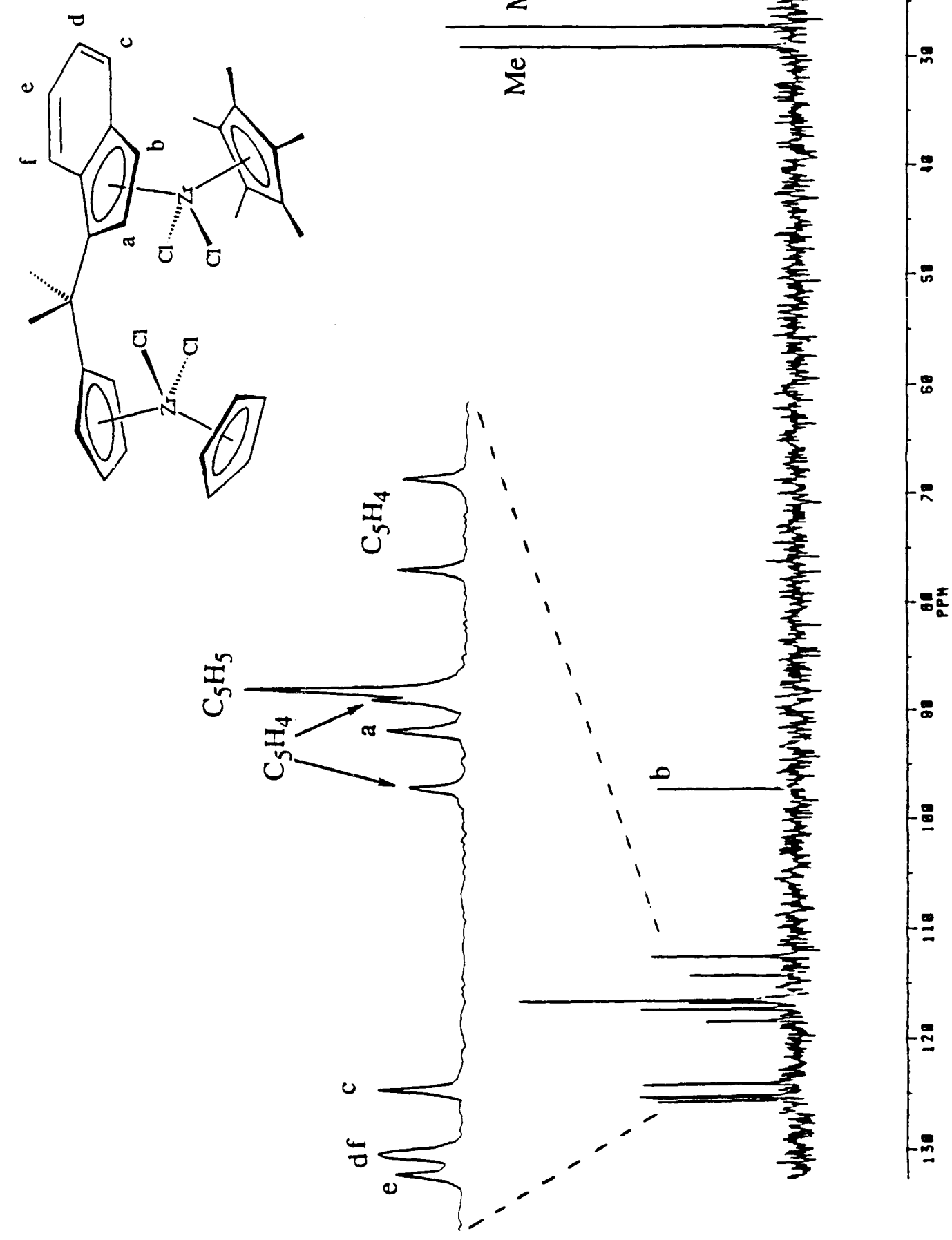

Figure 3.4.3. 75.5 MHz ^{13}C DEPT NMR spectrum of compound **12**, $[(\eta^5\text{-}C_5H_5)ZrCl_2\{(\eta^5\text{-}C_5H_4)CMe_2(\eta^5\text{-}C_9H_6)\}ZrCl_2(\eta^5\text{-}C_5Me_5)]$, in CD_2Cl_2 at r.t.

3.5. Synthesis of binuclear metallocene-dimethyl derivatives

Chapter 1 described how zirconocene and hafnocene dichloride derivatives together with methylaluminoxane co-catalyst have been recognised as an important class of olefin polymerization catalysts.[10-12] It has been proposed that the active catalyst is a cationic or "cation-like" metallocene alkyl species $[Cp'_2M(R)]^{\delta+}$.[13, 14] In 1991, Marks and co-workers demonstrated that $B(C_6F_5)_3$ is capable of abstracting a methide (CH_3^-) group from a variety of $Cp'_2Zr(CH_3)_2$ complexes (Cp' = η^5-C_5H_5, η^5-1,2-$Me_2C_5H_3$, η^5-C_5Me_5) to form the highly active "cation-like" zirconocene polymerization catalysts, $[Cp'_2Zr(CH_3)]^+[CH_3B(C_6F_5)_3]^-$.[15, 16] Soon after the use of $B(C_6F_5)_3$ as an alkide abstraction co-catalyst was reported, Chien and co-workers demonstrated that the triphenylcarbenium complex $[Ph_3C]^+[B(C_6F_5)_4]^-$ could play a similar role. The $[Ph_3C]^+$ was shown to abstract a CH_3^- group from the *ansa*-metallocene dimethyl derivative $[\{Et(Ind)_2\}Zr(CH_3)_2]$ to form Ph_3CCH_3 and the cationic zirconocene complex $[Et(Ind)_2Zr(CH_3)]^+[B(C_6F_5)_4]^-$, which was shown to be a highly active propylene polymerization catalyst.[17]

It was decided to attempt to prepare methyl derivatives of the binuclear group 4 metallocene compounds. The catalytic properties of the methyl derivatives together with $B(C_6F_5)_3$ or $[Ph_3C]^+[B(C_6F_5)_4]^-$ co-catalysts might then be compared with the catalytic properties of the chloride derivatives with methylaluminoxane co-catalyst.

3.5.1. Synthesis of

$[(\eta^5\text{-}C_5H_5)Zr(CH_3)_2\{(\eta^5\text{-}C_5H_4)CMe_2(\eta^5\text{-}C_9H_6)\}Zr(CH_3)_2(\eta^5\text{-}C_5H_5)]$

Dimethyl derivatives of zirconocenes and hafnocenes are typically prepared by the reaction of the zirconocene and hafnocene dichloride derivatives with methyl lithium or methyl Grignard reagents, in diethyl ether or toluene solvent.[5, 18-20] Four equivalents of methyl lithium (in diethyl ether solution) was added to a stirred suspension of $[(\eta^5\text{-}C_5H_5)ZrCl_2\{(\eta^5\text{-}C_5H_4)CMe_2(\eta^5\text{-}C_9H_6)\}ZrCl_2(\eta^5\text{-}C_5H_5)]$ (**8**) in

toluene at -78 °C, then the reaction mixture was allowed to warm to room temperature and was stirred for two hours. Filtration, and removal of volatiles from the orange coloured filtrate under reduced pressure, gave an orange oil. Extraction into petroleum ether (bp. 40-60 °C) gave a pale yellow solution, from which very pale orange crystals were obtained after concentration under reduced pressure and cooling to -80 °C.

The pale orange crystalline product was characterised as the tetramethyl binuclear metallocene derivative $[(\eta^5\text{-}C_5H_5)Zr(CH_3)_2\{(\eta^5\text{-}C_5H_4)CMe_2(\eta^5\text{-}C_9H_6)\}Zr(CH_3)_2(\eta^5\text{-}C_5H_5)]$ (**13**), and was obtained in 75 % yield. It was found that when more than four equivalents of methyl lithium was used, significant amounts of dark, petroleum-insoluble residue was obtained, and the yield of the desired product was much lower.

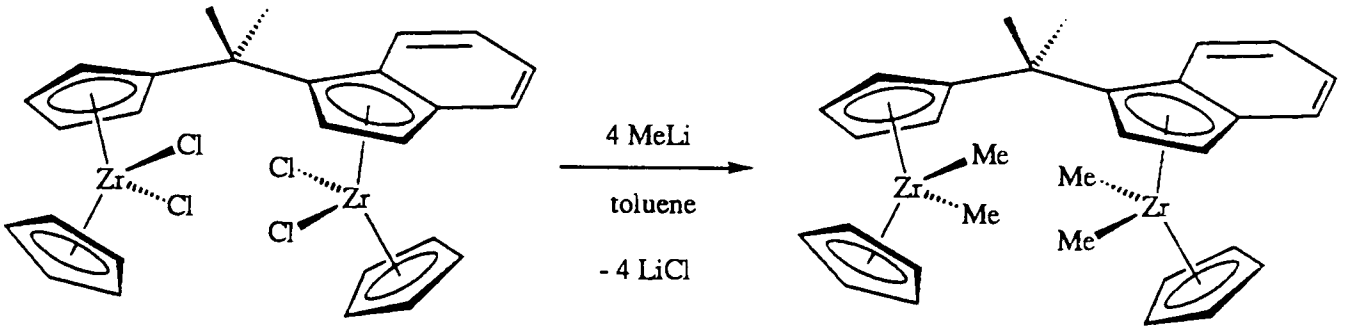

Figure 3.5.1. Synthesis of compound **13**,
$[(\eta^5\text{-}C_5H_5)Zr(CH_3)_2\{(\eta^5\text{-}C_5H_4)CMe_2(\eta^5\text{-}C_9H_6)\}Zr(CH_3)_2(\eta^5\text{-}C_5H_5)]$

The air and moisture sensitive, very pale orange crystalline solid $[(\eta^5\text{-}C_5H_5)Zr(CH_3)_2\{(\eta^5\text{-}C_5H_4)CMe_2(\eta^5\text{-}C_9H_6)\}Zr(CH_3)_2(\eta^5\text{-}C_5H_5)]$ (**13**) was characterised by elemental analysis, which was consistent with proposed molecular formula $C_{31}H_{38}Zr_2$, and by ^1H and ^{13}C NMR spectroscopy. As expected, compound **13** is significantly more soluble than compound **8** in hydrocarbon solvents. The ^1H NMR spectrum of **13** in C_6D_6 is shown in Figure 3.5.2.

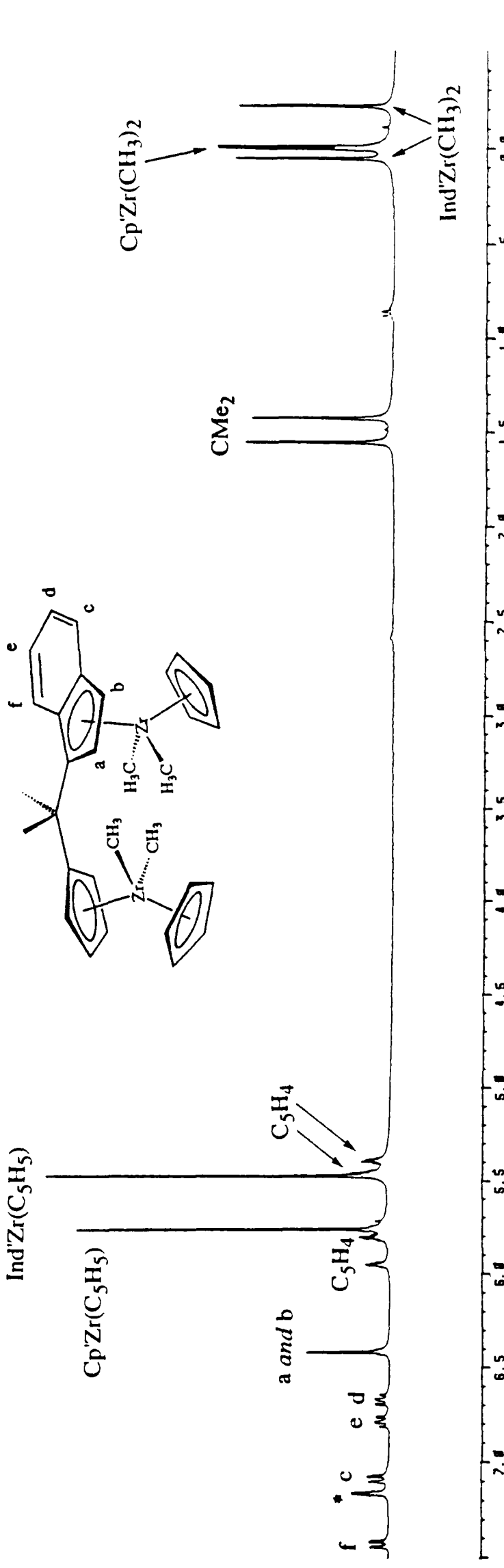

Figure 3.5.2. 300 MHz ^{1}H NMR spectrum of

$[(\eta^5\text{-}C_5H_5)Zr(CH_3)_2\{(\eta^5\text{-}C_5H_4)CMe_2(\eta^5\text{-}C_9H_6)\}Zr(CH_3)_2(\eta^5\text{-}C_5H_5)]$ (**13**)

in C_6D_6 at r.t. (* = residual protio solvent)

The cyclopentadienyl and indenyl region of the ^1H NMR spectrum of **13** resembles that of compound **8** in C_6D_6, except (i) the C_5H_4 and C_5H_5 chemical shifts for **13** are around 0.3 ppm lower than those of compound **8**, and (ii) for compound **13** the signals of protons **a** and **b** coincide, and appear as a pseudo singlet (an extreme example of the "roofing effect" observed when a pair af doublets have similar chemical shifts).

The methyl group ^1H NMR chemical shifts of dimethyl zirconocene and hafnocene derivatives typically lie between 0.5 and -1.5 ppm.[5, 9] For compound **13**, four sharp singlets each of integrated intensity 3 H are observed in this region. The proposed molecular structure of compound **13** is chiral, and the two methyl groups on each of the metal atoms are diastereotopic and would be expected to have different chemical shifts.

Comparison with the NMR spectra of compounds described later in this Chapter indicates that the close pair of singlets at 0.00 and -0.01 ppm correspond to the methyl groups bonded to the metal at the C_5H_4 site, whilst the singlets at 0.05 and -0.22 ppm correspond to the methyl groups bonded to the metal at the indenyl site. The different enantiomers of compound **13** correspond to the coordination of either face of the indenyl ligand to zirconium. It can be seen that the pair signals assigned to the $Zr(CH_3)_2$ group coordinated to the indenyl ligand have a much larger chemical shift difference than the other $Zr(CH_3)_2$ group which is more distant from the chiral centre of the molecule.

The $^{13}C\{^1H\}$ NMR spectrum of compound **13** in C_6D_6 is shown in Figure 3.5.3. The assignments are proposed on the basis of a ^{13}C-^1H shift correlation experiment. The ^1H-coupled ^{13}C NMR spectrum of **13** reveals one of the quaternary carbon signals (**g**, **h** or **i**) at 125.3 ppm, which in the decoupled spectrum shown in Figure 3.5.3 is coincident with signals **f** and **c**.

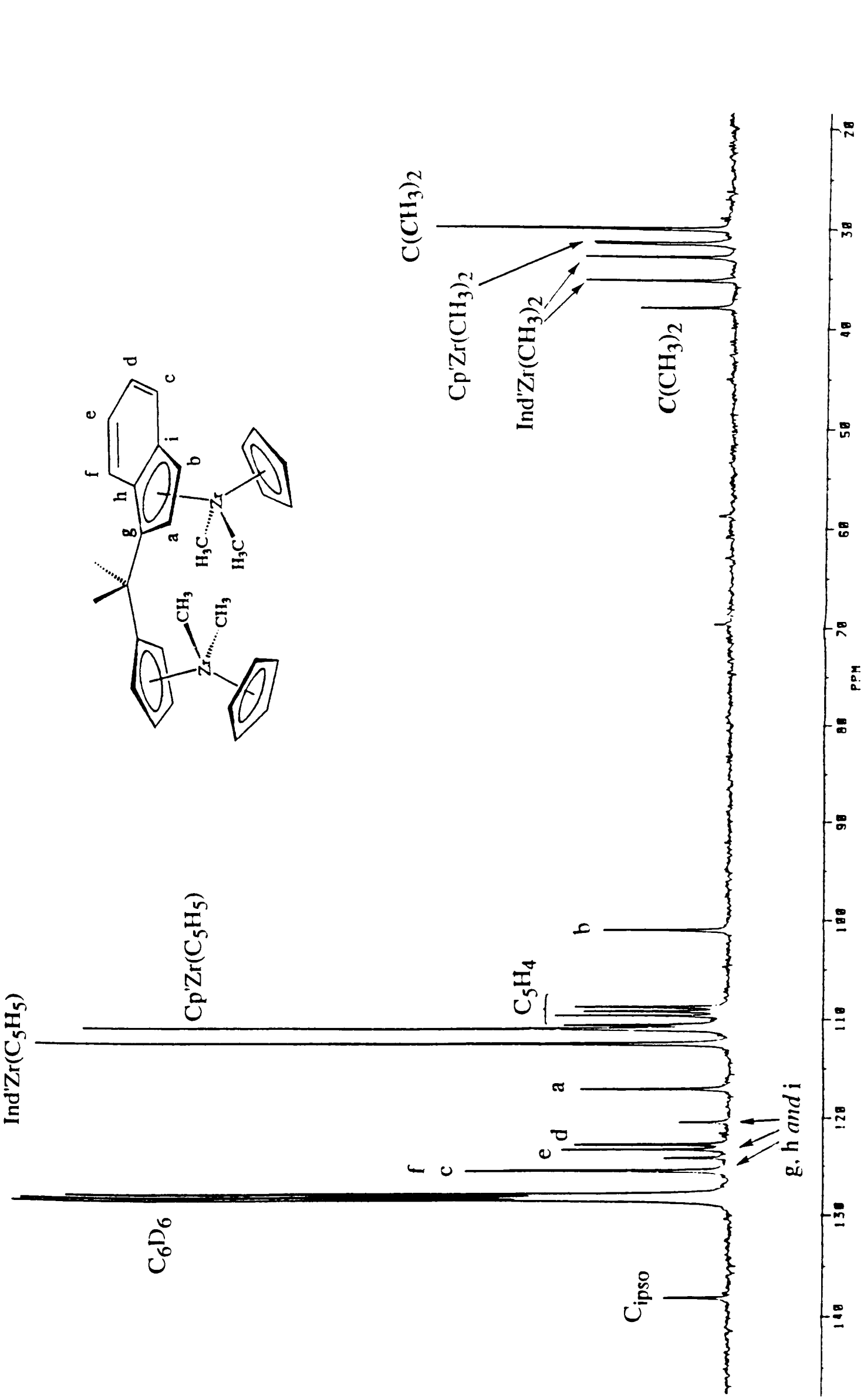

Figure 3.5.3. 75.5 MHz $^{13}C\{^1H\}$ NMR spectrum in C_6D_6 at r.t. of $[(\eta^5\text{-}C_5H_5)Zr(CH_3)_2\{(\eta^5\text{-}C_5H_4)CMe_2(\eta^5\text{-}C_9H_6)\}Zr(CH_3)_2(\eta^5\text{-}C_5H_5)]$ (**13**) .

The two close ^{13}C signals at 31.4 and 31.6 ppm were assigned to the $Zr(CH_3)_2$ group at the C_5H_4 site (based on the ^{13}C-^1H shift correlation experiment), whilst the signals at 35.3 and 32.9 ppm were assigned to the $Zr(CH_3)_2$ group at the indenyl site. The pair of ^{13}C signals assigned to the $Zr(CH_3)_2$ group coordinated to the indenyl ligand have a much larger chemical shift difference than the pair of signals assigned to the other $Zr(CH_3)_2$ group which is more distant from the chiral centre of the molecule, the same was found for the ^1H NMR signals. It also appears that the "site effect" on the $Zr(CH_3)_2$ ^{13}C chemical shift is similar to that observed for the C_5H_5 signals, i.e. the signals assigned to the $Zr(CH_3)_2$ group coordinated to the indenyl ligand are at higher chemical shift than the signals of the $Zr(CH_3)_2$ group coordinated to the C_5H_4 ligand. In the ^1H-coupled ^{13}C NMR spectrum the $Zr(CH_3)_2$ signals are quartets with C-H coupling constants of around 117 Hz, typical of dimethyl zirconocene derivatives.[21]

3.5.2. Synthesis of

$[(\eta^5\text{-}C_5H_5)Zr(CH_3)_2\{(\eta^5\text{-}C_5H_4)CMe_2(\eta^5\text{-}C_9H_6)\}Hf(CH_3)_2(\eta^5\text{-}C_5H_5)]$

A suspension of compound **10**, $[(\eta^5\text{-}C_5H_5)ZrCl_2\{(\eta^5\text{-}C_5H_4)CMe_2(\eta^5\text{-}C_9H_6)\}HfCl_2(\eta^5\text{-}C_5H_5)]$, in toluene was treated with four equivalents of methyl lithium (in diethyl ether solution) under conditions similar to those employed for the preparation of compound **13** above. The same work-up procedure was followed and pale yellow crystals of the novel heterobinuclear compound $[(\eta^5\text{-}C_5H_5)Zr(CH_3)_2\{(\eta^5\text{-}C_5H_4)CMe_2(\eta^5\text{-}C_9H_6)\}Hf(CH_3)_2(\eta^5\text{-}C_5H_5)]$ (**14**) were obtained from petroleum ether (bp. 40-60 °C) at -80 °C, in 64 % yield. Compound **14** was characterised by elemental analysis and ^1H and ^{13}C NMR studies.

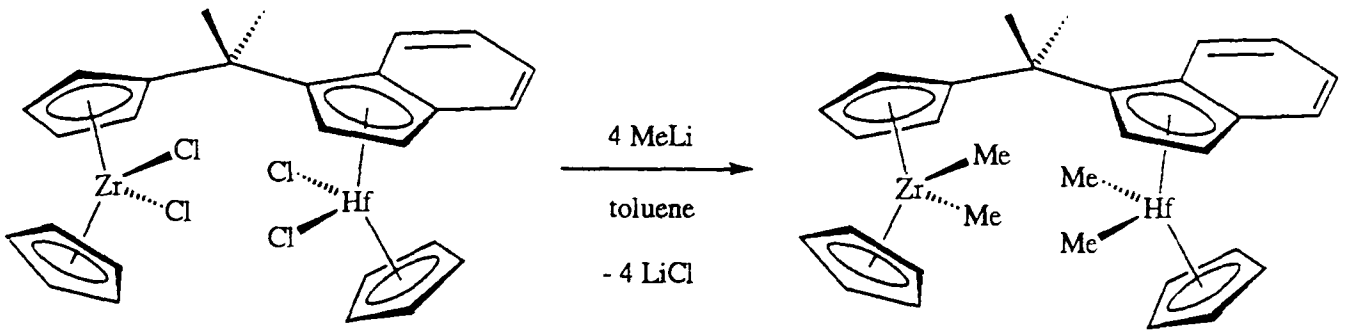

Figure 3.5.4. Synthesis of compound **14**,

$[(\eta^5\text{-}C_5H_5)Zr(CH_3)_2\{(\eta^5\text{-}C_5H_4)CMe_2(\eta^5\text{-}C_9H_6)\}Hf(CH_3)_2(\eta^5\text{-}C_5H_5)]$

The cyclopentadienyl and indenyl region of the ^1H NMR spectrum of **14** in C_6D_6 (shown in Figure 3.5.7) is very similar to that of compound **13**, except (i) the lower shift C_5H_5 signal lies at 5.39 ppm for **14** compared with 5.48 ppm for **13**, indicating that these signals correspond to the C_5H_5 ligand coordinated to the metal at the indenyl site, and (ii) the indenyl proton signals **a** and **b** are found at 6.36 and 6.32 ppm for compound **14** compared with 6.41 ppm for compound **13**. These observations are consistent with the presence of hafnium at the indenyl site in **14**.

The $M(CH_3)_2$ region of the ^1H NMR spectrum of compound **14**, $[(\eta^5\text{-}C_5H_5)Zr(CH_3)_2\{(\eta^5\text{-}C_5H_4)CMe_2(\eta^5\text{-}C_9H_6)\}Hf(CH_3)_2(\eta^5\text{-}C_5H_5)]$, shown in Figure 3.5.8, includes two close singlets at 0.00 and 0.01 ppm, assigned to the $Zr(CH_3)_2$ group at the C_5H_4 site (closely matching the corresponding signals of compound **13**), and two singlets at -0.11 and -0.39 ppm assigned to the $Hf(CH_3)_2$ group at the indenyl site (about 0.17 ppm more negative shift compared with the corresponding $Zr(CH_3)_2$ signals of **13**). This metal-dependence of chemical shift is similar to those reported for the methyl protons of $[(\eta^5\text{-}C_5H_5)_2Zr(CH_3)_2]$ and $[(\eta^5\text{-}C_5H_5)_2Hf(CH_3)_2]$ (-0.39 and -0.50 ppm respectively), and $[(\eta^5\text{-}C_9H_6)_2Zr(CH_3)_2]$ and $[(\eta^5\text{-}C_9H_6)_2Hf(CH_3)_2]$ (-1.13 and -1.30 ppm respectively).[5]

The methyl regions of the $^{13}C\{^1H\}$ spectra are shown in Figure 3.5.9. It can be seen that the ^{13}C signals assigned to the $Zr(CH_3)_2$ group at the C_5H_4 site of **14** lie at 31.5 and 31.4 ppm, closely matching those of compound **13**, where as the signals assigned to the $Hf(CH_3)_2$ group at the indenyl site of **14** are found at 41.1 and 38.5 ppm, approximately 6 ppm **higher** shift than the corresponding $Zr(CH_3)_2$ signals of compound **13**. A similar metal-dependence of ^{13}C chemical shifts has been found for the methyl carbons of the compounds $[(\eta^5\text{-}C_5H_5)_2Hf(CH_3)_2]$ (36 ppm) and $[(\eta^5\text{-}C_5H_5)_2Zr(CH_3)_2]$ (30 ppm).[22]

3.5.3. Synthesis of

$[(\eta^5\text{-}C_5H_5)Hf(CH_3)_2\{(\eta^5\text{-}C_5H_4)CMe_2(\eta^5\text{-}C_9H_6)\}Zr(CH_3)_2(\eta^5\text{-}C_5H_5)]$

A suspension of compound **11**, $[(\eta^5\text{-}C_5H_5)HfCl_2\{(\eta^5\text{-}C_5H_4)CMe_2(\eta^5\text{-}C_9H_6)\}ZrCl_2(\eta^5\text{-}C_5H_5)]$, in toluene was treated with four equivalents of methyl lithium (in diethyl ether solution) under the conditions similar to those employed for the preparation of compounds **13** and **14**. The same work-up procedure was followed and pale yellow crystals of the novel heterobinuclear compound $[(\eta^5\text{-}C_5H_5)Hf(CH_3)_2\{(\eta^5\text{-}C_5H_4)CMe_2(\eta^5\text{-}C_9H_6)\}Zr(CH_3)_2(\eta^5\text{-}C_5H_5)]$ (**15**) were obtained from petroleum ether (bp. 40-60 °C) at -80 °C, in 67 % yield. Compound **15** was characterised by elemental analysis and by ^1H and ^{13}C NMR studies, including selective ^1H decoupling and ^{13}C-^1H shift correlation experiments.

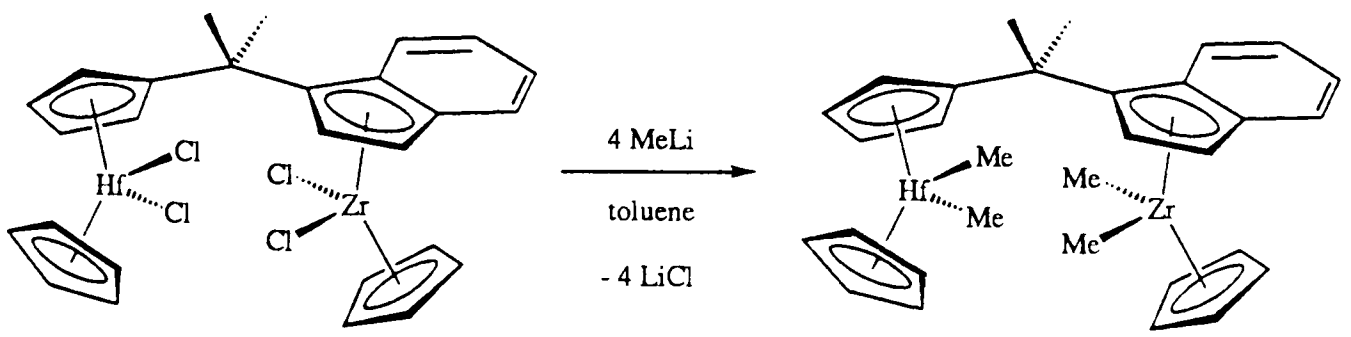

Figure 3.5.5. Synthesis of compound **15**, $[(\eta^5\text{-}C_5H_5)Hf(CH_3)_2\{(\eta^5\text{-}C_5H_4)CMe_2(\eta^5\text{-}C_9H_6)\}Zr(CH_3)_2(\eta^5\text{-}C_5H_5)]$

The cyclopentadienyl and indenyl region of the ^1H NMR spectrum of **15** in C_6D_6 (shown in Figure 3.5.7) is very similar to that of the dizirconium compound **13**, except that the higher shift C_5H_5 signal and the C_5H_4 signals of **15** lie at approximately 0.1 ppm lower chemical shift than the corresponding signals of **13**. These same observations were made for the ^1H NMR spectra of $[(\eta^5\text{-}C_5H_5)HfCl_2\{(\eta^5\text{-}C_5H_4)CMe_2(\eta^5\text{-}C_9H_6)\}ZrCl_2(\eta^5\text{-}C_5H_5)]$ (**11**) compared with $[(\eta^5\text{-}C_5H_5)ZrCl_2\{(\eta^5\text{-}C_5H_4)CMe_2(\eta^5\text{-}C_9H_6)\}ZrCl_2(\eta^5\text{-}C_5H_5)]$ (**8**).

The methyl regions of the ^1H and ^{13}C NMR spectra of compound **15** (Figures 3.5.8 and 3.5.9) are also consistent with the proposed molecular structure, with hafnium at the C_5H_4 site and zirconium at the indenyl site of the binuclear molecule. The ^1H NMR signals assigned to the $Hf(CH_3)_2$ group at the C_5H_4 site lie at approximately 0.18 ppm more negative shift, and the ^{13}C signals at approximately 6 ppm more positive shift, compared with the $Zr(CH_3)_2$ group at the C_5H_4 site of the dizirconium compound **13**. The ^1H and ^{13}C NMR signals assigned to the $Zr(CH_3)_2$ group at the indenyl site in compound **15** closely match those of compound **13**.

3.5.4. Synthesis of

$[(\eta^5\text{-}C_5H_5)Hf(CH_3)_2\{(\eta^5\text{-}C_5H_4)CMe_2(\eta^5\text{-}C_9H_6)\}Hf(CH_3)_2(\eta^5\text{-}C_5H_5)]$

A suspension $[(\eta^5\text{-}C_5H_5)HfCl_2\{(\eta^5\text{-}C_5H_4)CMe_2(\eta^5\text{-}C_9H_6)\}HfCl_2(\eta^5\text{-}C_5H_5)]$ (**9**) in toluene was treated with four equivalents of methyl lithium, folowing the same procedure employed for the preparation of compound **13**. Very pale yellow crystals of the novel homobinuclear compound $[(\eta^5\text{-}C_5H_5)Hf(CH_3)_2\{(\eta^5\text{-}C_5H_4)CMe_2(\eta^5\text{-}C_9H_6)\}Hf(CH_3)_2(\eta^5\text{-}C_5H_5)]$ (**16**) were obtained from petroleum ether (bp. 40-60 ^oC) at -80 ^oC, in 44 % yield. Compound **16** was characterised by elemental analysis and by ^1H and ^{13}C NMR studies, including selective ^1H decoupling, ^1H NOESY and ^{13}C-^1H shift correlation experiments.

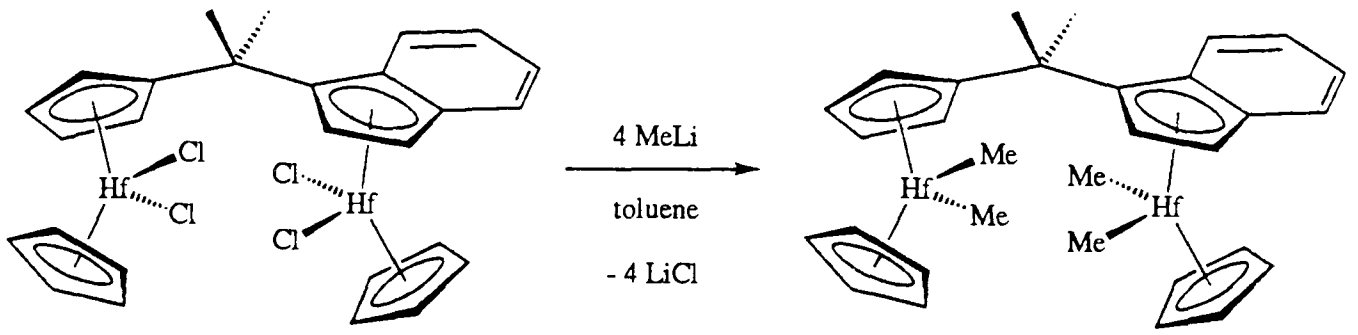

Figure 3.5.6. Synthesis of compound **16**,

$[(\eta^5\text{-}C_5H_5)Hf(CH_3)_2\{(\eta^5\text{-}C_5H_4)CMe_2(\eta^5\text{-}C_9H_6)\}Hf(CH_3)_2(\eta^5\text{-}C_5H_5)]$

The cyclopentadienyl and indenyl region of the ^1H NMR spectrum of **16** in C_6D_6 is shown in Figure 3.5.7, together with the spectra of **13**, **14** and **15**. A ^1H NOESY experiment (recycle delay = 1 second, mixing time = 0.5 seconds) showed correlations between one of the indenyl C_5-ring protons (**a**) and one of the methyl groups of the CMe_2 bridge, and between one of the indenyl C_6-ring protons (**f**) and the other methyl group of the CMe_2 bridge. Similar correlations were observed in the NOESY spectrum of compound **9**, and they are consistent with the proposed assignments of the indenyl signals. The NOESY spectrum also showed a correlation between the indenyl C_5-ring proton **b** and the singlet at -0.11 ppm asssigned to one of the methyl groups coordinated to hafnium at the indenyl site.

The the C_5H_4 signals, and the higher shift C_5H_5 signal (5.67 ppm), of compound **16** closely match those of compound **15**, with hafnium at the C_5H_4 site. The indenyl signals and the lower shift C_5H_5 signal (5.39 ppm) of compound **16** closely match those of compound **14**, with hafnium at the indenyl site. The ^1H and ^{13}C NMR chemical shifts for the C_5H_5 ligands of compounds **13**, **14**, **15** and **16** are given in Table 3.2.

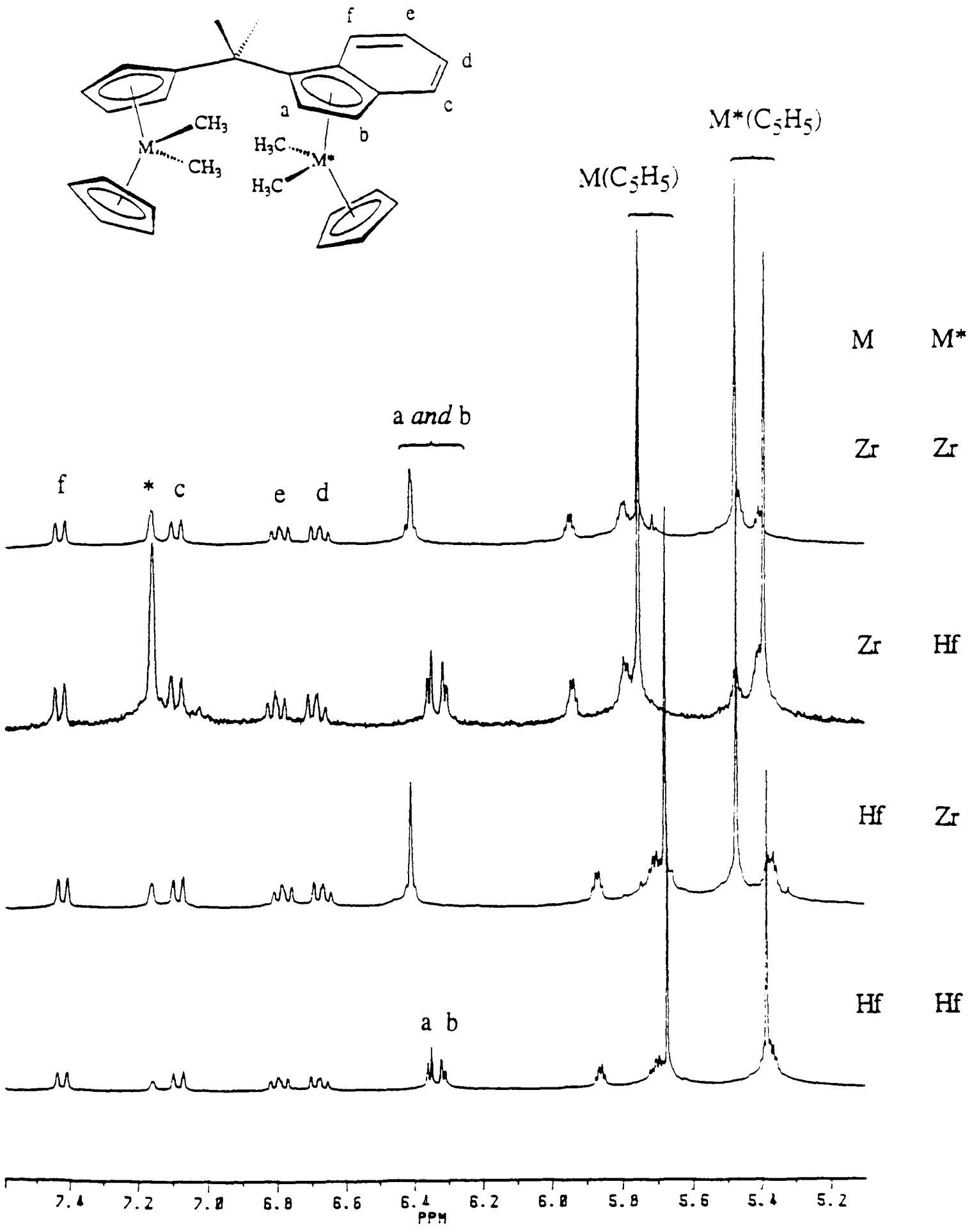

Figure 3.5.7. Cyclopentadienyl and indenyl regions of the 300 MHz ^{1}H NMR spectra of $[(\eta^5\text{-}C_5H_5)M(CH_3)_2\{(\eta^5\text{-}C_5H_4)CMe_2(\eta^5\text{-}C_9H_6)\}M^*(CH_3)_2(\eta^5\text{-}C_5H_5)]$ in C_6D_6 at r.t. (* = residual protio solvent)

[M = M* = Zr (**13**); M = Zr, M* = Hf (**14**); M = Hf, M* = Zr (**15**); M = M* = Hf (**16**)]

Table 3.2. ^{1}H and ^{13}C NMR data for C_5H_5 ligands of compounds **13**, **14**, **15** and **16**.

^{1}H NMR chemical shifts (C_6D_6) for the C_5H_5 ligands in the series $[(\eta^5\text{-}C_5H_5)M(CH_3)_2\{(\eta^5\text{-}C_5H_4)CMe_2(\eta^5\text{-}C_9H_6)\}M^*(CH_3)_2(\eta^5\text{-}C_5H_5)]$				
Compound	M	δ M(C_5H_5) / ppm	M*	δ M*(C_5H_5) / ppm
13	Zr	5.75	Zr	5.48
14	Zr	5.75	Hf	5.39
15	Hf	5.68	Zr	5.47
16	Hf	5.67	Hf	5.39

^{13}C NMR chemical shifts (C_6D_6) for the C_5H_5 ligands in the series $[(\eta^5\text{-}C_5H_5)M(CH_3)_2\{(\eta^5\text{-}C_5H_4)CMe_2(\eta^5\text{-}C_9H_6)\}M^*(CH_3)_2(\eta^5\text{-}C_5H_5)]$				
Compound	M	δ M(C_5H_5) / ppm	M*	δ M*(C_5H_5) / ppm
13	Zr	110.8	Zr	112.4
14	Zr	110.8	Hf	111.6
15	Hf	110.3	Zr	112.4
16	Hf	110.3	Hf	111.6

The $M(CH_3)_2$ region of the ^{1}H NMR spectrum of **16** in C_6D_6 is shown in Figure 3.5.8, together with the spectra of **13**, **14** and **15**, and the data are given in Table 3.3. It appears that, as for the C_5H_5 signals, the chemical shifts of the signals are dependent on (i) whether the methyl is bound to zirconium or hafnium, and (ii) whether the metal is coordinated to the C_5H_4 site or the indenyl site of the *ansa* bridging ligand. However, for the methyl signals the identity of the metal has a larger effect on the mean chemical shift of the $M(CH_3)_2$ ^{1}H NMR signals, whilst for the C_5H_5 signals the "site effect" is larger.

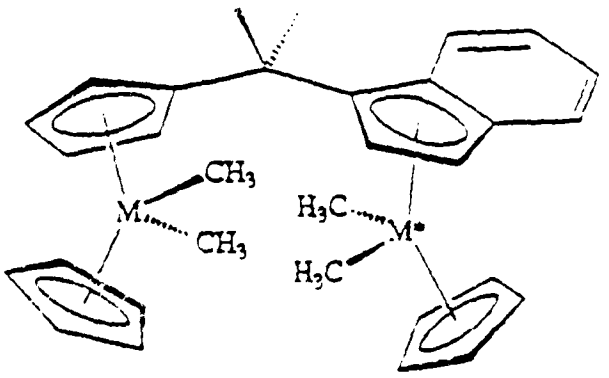

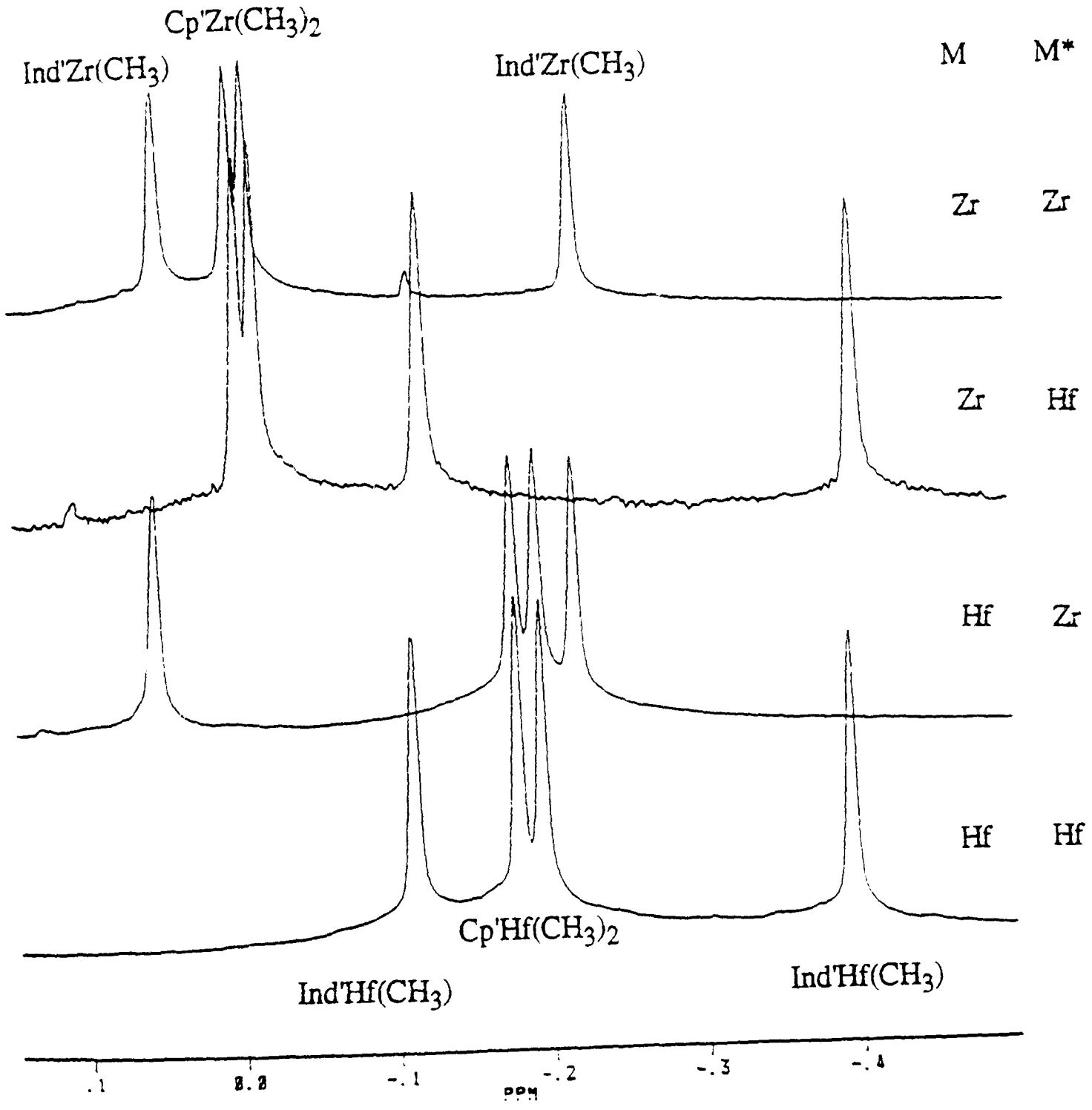

Figure 3.5.8. $M(CH_3)_2$ and $M^*(CH_3)_2$ region of the 300 MHz ^1H NMR spectra of $[(\eta^5\text{-}C_5H_5)M(CH_3)_2\{(\eta^5\text{-}C_5H_4)CMe_2(\eta^5\text{-}C_9H_6)\}M^*(CH_3)_2(\eta^5\text{-}C_5H_5)]$ in C_6D_6 at r.t.

[M = M* = Zr (**13**); M = Zr, M* = Hf (**14**); M = Hf, M* = Zr (**15**); M = M* = Hf (**16**)]

Table 3.3. ^{1}H NMR data for $M(CH_3)$ groups of compounds **13**, **14**, **15** and **16**.

^{1}H NMR chemical shifts (C_6D_6) for the $M(CH_3)_2$ and $M^*(CH_3)_2$ groups in the series $[(\eta^5\text{-}C_5H_5)M(CH_3)_2\{(\eta^5\text{-}C_5H_4)CMe_2(\eta^5\text{-}C_9H_6)\}M^*(CH_3)_2(\eta^5\text{-}C_5H_5)]$				
Compound	M	δ $M(CH_3)_2$ / ppm	M*	δ $M^*(CH_3)_2$ / ppm
13	Zr	0.00, -0.01	Zr	0.05, -0.22
14	Zr	0.00, -0.01	Hf	-0.11, -0.39
15	Hf	-0.18, -0.19	Zr	0.05, -0.22
16	Hf	-0.18, -0.19	Hf	-0.11, -0.39

The methyl regions of the ^{13}C NMR spectra of compounds **13**, **14**, **15** and **16** are shown in Figure 3.5.9. In all four spectra the quaternary bridging carbon signal lies at about 37.9 ppm, whilst the bridge methyl carbon signals lie at around 30 ppm.

The signals corresponding to the $M(CH_3)_2$ groups coordinated to the C_5H_4 ring of the *ansa* ligand are labelled $Cp'M(CH_3)_2$, and those at the indenyl site are labelled $Ind'M(CH_3)_2$. For both zirconium and hafnium, the ^{13}C NMR signals of the diastereotopic $Cp'M(CH_3)_2$ methyl groups are separated by only 0.2 ppm, whilst the signals of the $Ind'M(CH_3)_2$ methyl carbons (closer to the chiral centre of the molecule) are separated by about 2.3 ppm. For both metals the mean chemical shift of the $Ind'M(CH_3)_2$ signals is about 2.5 ppm higher than the mean shift of the $Cp'M(CH_3)_2$ signals, and for both sites the $Hf(CH_3)_2$ signals are at about 6 ppm higher shift than the corresponding zirconium signals. The ^{13}C NMR data for $M(CH_3)_2$ groups of compounds **13**, **14**, **15** and **16** are given in Table 3.4.

The spectra in Figures 3.5.7, 3.5.8 and 3.5.9, and the data in Tables 3.2, 3.3 and 3.4 provide strong evidence the compounds **15**, **16**, **17** and **18** are indeed a series of homo- and hetero-bimetallic compounds with analogous molecular structures.

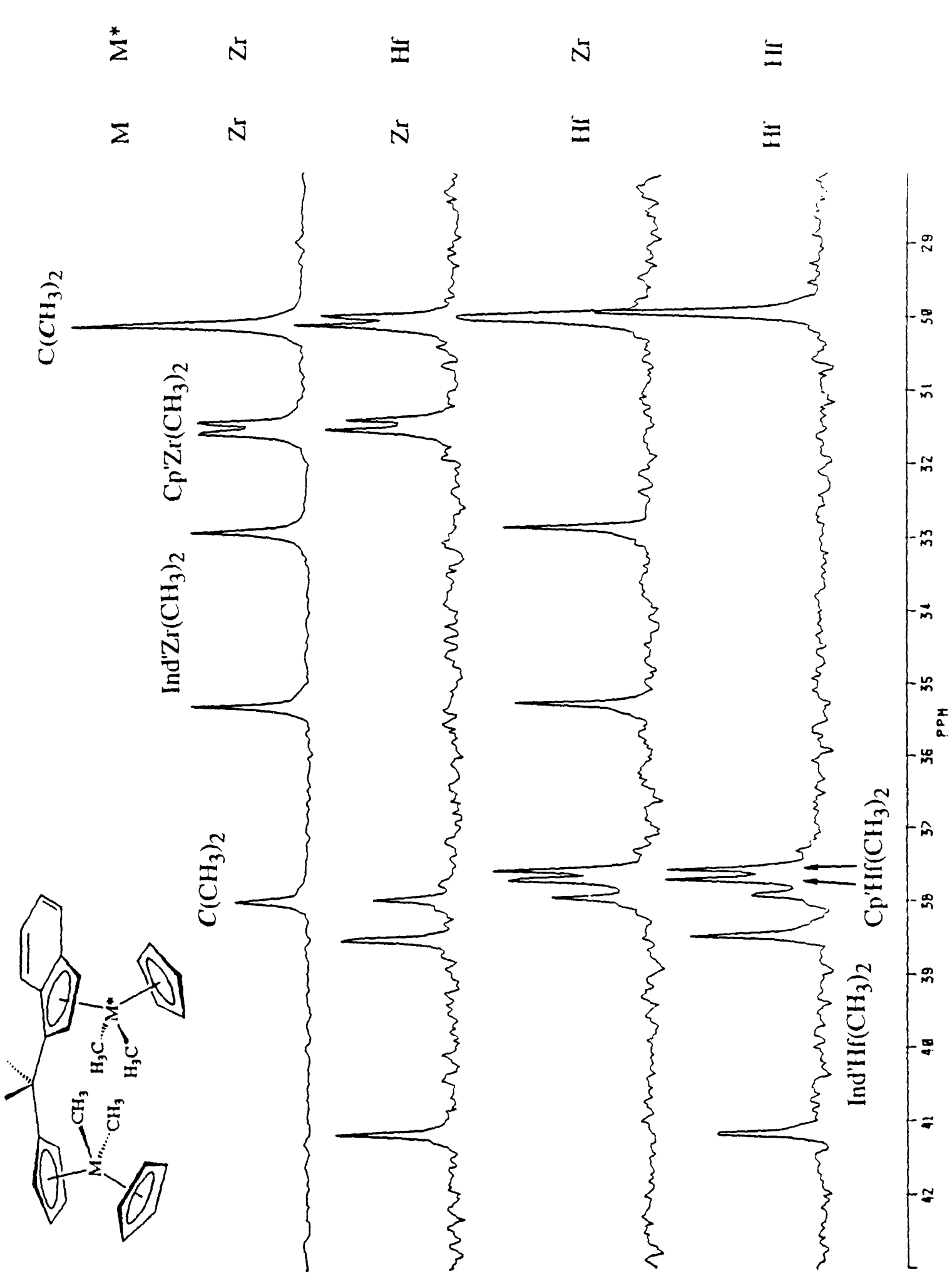

Figure 3.5.9. $M(CH_3)_2$ and $M^*(CH_3)_2$ region of the 75.5 MHz ^{13}C NMR spectra of

$[(\eta^5\text{-}C_5H_5)M(CH_3)_2\{(\eta^5\text{-}C_5H_4)CMe_2(\eta^5\text{-}C_9H_6)\}M^*(CH_3)_2(\eta^5\text{-}C_5H_5)]$

in C_6D_6 at r.t.

[M = M* = Zr (**13**); M = Zr, M* = Hf (**14**); M = Hf, M* = Zr (**15**); M = M* =Hf (**16**)]

Table 3.4. ^{13}C NMR data for $M(CH_3)_2$ groups of compounds **13**, **14**, **15** and **16**.

^{13}C NMR chemical shifts (C_6D_6)for the CH_3 groups in the series $[(\eta^5\text{-}C_5H_5)M(CH_3)_2\{(\eta^5\text{-}C_5H_4)CMe_2(\eta^5\text{-}C_9H_6)\}M^*(CH_3)_2(\eta^5\text{-}C_5H_5)]$				
Compound	M	δ $M(CH_3)_2$ / ppm	M*	δ $M^*(CH_3)_2$ / ppm
13	Zr	31.6, 31.4	Zr	35.3, 32.9
14	Zr	31.5, 31.4	Hf	41.1, 38.5
15	Hf	37.7, 37.5	Zr	35.2, 32.8
16	Hf	37.7, 37.5	Hf	41.1, 38.4

It is not clear why the ^{13}C NMR chemical shifts of the methyl groups coordinated to hafnium should be higher than those coordinated to zirconium, when the ^{13}C and ^{1}H NMR signals for the C_5H_5 ligands, and the ^{1}H NMR signals for the methyl groups, are found at lower chemical shift when coordinated to hafnium compared with zirconium.

One of the factors that influences the chemical shift of a nucleus is the electron density surrounding it. In a uniform magnetic field, the electrons surrounding a nucleus circulate, setting up a secondary magnetic field opposed to the applied field at the nucleus. As a result, a higher field (or lower frequency) is required to bring the nucleus into resonance, and the electrons are said to shield the nucleus from the applied field.[22] A higher electron density shields the nucleus more effectively, and a reduced electron density deshields the nucleus. Neighbouring atoms in a molecule can have a strong inductive effect on the chemical shift of a nucleus. For example, ^{1}H and ^{13}C chemical shifts are strongly influenced by the electronegativity of the elements to which the carbon atom is bonded.[22] Electronegativity was defined by Pauling as "the power of an atom in a molecule to attract electrons towards itself".[23] The more electronegative the element is, the more it tends to attract electrons towards itself, and the more the ^{13}C and ^{1}H nuclei are deshielded, resulting in higher chemical shifts. The

Pauling electronegativities (based on bond energies) of the group 4 metals decrease as the group is descended. The exact values quoted vary according to the source, but lie at around 1.5 for titanium, 1.4 to 1.33 for zirconium and 1.3 for hafnium.[23, 24, 25]

For the group 4 metallocene dichlorides Cp_2TiCl_2, Cp_2ZrCl_2 and Cp_2HfCl_2, the ^{13}C NMR chemical shifts for the C_5H_5 ligands have been reported as 119.7, 115.7 and 114.4 ppm respectively, and the ^1H shifts as 6.57, 6.47 and 6.37 ppm respectively.[5, 26] These chemical shifts follow the pattern that might be expected from the Pauling electronegativities of the metals. The ^1H chemical shifts of the methyl protons of the group 4 metallocene dimethyl derivatives Cp_2TiMe_2, Cp_2ZrMe_2 and Cp_2HfMe_2, follow a similar pattern (-0.17, -0.39 and -0.50 ppm respectively), becoming more negative as the group is descended.[5]

However, the ^{13}C chemical shifts of the methyl groups are 46 ppm for Cp_2TiMe_2, 30 ppm for Cp_2ZrMe_2 and 36 ppm for Cp_2HfMe_2.[22] Similarly, for the binuclear compounds **13**, **14**, **15** and **16**, the ^{13}C chemical shifts of the $Hf(CH_3)_2$ signals are about 6 ppm higher for than the corresponding $Zr(CH_3)_2$ signals. Many other properties of hafnium do not follow the trends that might be expected if one were to extrapolate from those of titanium and zirconium. Often this may be a consequence of the so-called "lanthanide contraction".

The filling of the 4f orbitals through the lanthanide series is accompanied by a steady contraction in the atomic and ionic radii of the lanthanides. The major cause of the lanthanide contraction is the electrostatic effect of the increasing nuclear charge being imperfectly screened by the 4f electrons, due to the spatial characteristics of the 4f orbitals.[26, 29] Relativistic effects are also thought to contribute to the lanthanide contraction.[30]

One result of the lanthanide contraction is that the expected increase in atomic size, on progressing from the second to the third row of the d-block, is almost exactly offset. The post-lanthanide elements in the third row thus have sizes and properties very similar to the second row elements. This effect is most apparent in group 4, and hafnium, which immediately follows the lanthanides, has atomic, ionic and covalent

radii slightly **smaller** than zirconium.[25] For the group 4 elements, these effects are seen in an alternative scale of electronegativity, devised by Allred and Rochow.[29, 30] In the Allred-Rochow scale of electronegativity, the electrostatic force of attraction between a nucleus and an electron from a bonded atom is calculated, taking into account the effective nuclear charge and the covalent radius of an atom. The Allred-Rochow electronegativity for hafnium (1.23) is fractionally higher than that of zirconium (1.22), whilst both are lower than that of titanium (1.32).

Because of the spatial characteristics of the 4f orbitals, some electrons are less well screened from the nuclear charge than others, depending on which orbitals the electrons occupy. If the electrons in the Hf-CH_3 bonding orbitals were less well screened from the nuclear charge than those in the Hf-Cp bonding orbitals, then this could possibly account for the observed ^{13}C chemical shifts.

3.6. Related mononuclear complexes

One of the reasons for preparing a range of novel homo- and hetero-binuclear compounds was so that the chemical behaviour, and especially the catalytic properties, might be compared with related mononuclear compounds. This section describes the synthesis of novel mononuclear zirconocene and hafnocene derivatives, structurally related to the binuclear compounds in described in this chapter.

3.6.1 Preparation of $[Li(C_5H_4)CMe_2(C_9H_7)]$

A diethyl ether solution of 6,6-dimethylfulvene was added dropwise to a diethyl ether solution of lithium indenide at 0 °C, then stirred at room temperature overnight. The lithium cyclopentadienide derivative $[Li(C_5H_4)CMe_2(C_9H_7)]$ was isolated as pale orange crystals by the addition of petrol (bp. 40-60 °C) followed by cooling to -80 °C. The pale orange crystalline solid $[Li(C_5H_4)CMe_2(C_9H_7)]$ was very air- and moisture-

sensitive, which limited the accuracy of the elemental analysis. However, the ^{1}H and ^{13}C NMR spectra were consistent with the proposed molecular structure and indicated a high level of purity.

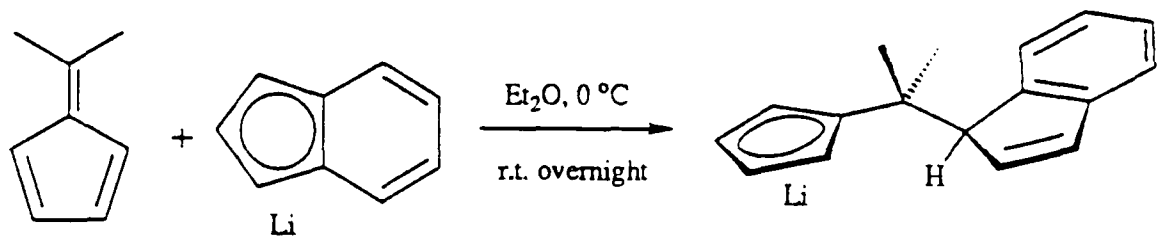

Figure 3.6.1. Synthesis of $[Li(C_5H_4)CMe_2(C_9H_7)]$

3.6.2 Synthesis of $[(\eta^5\text{-}C_5H_5)MCl_2\{(\eta^5\text{-}C_5H_4)CMe_2(C_9H_7)\}]$ (M = Zr, Hf)

A solution of $[Li(C_5H_4)CMe_2(C_9H_7)]$ in THF was added dropwise to a stirred solution of one equivalent of $[(\eta^5\text{-}C_5H_5)MCl_3\cdot DME]$ (M = Zr or Hf) in THF at room temperature. The resulting yellow solution was stirred overnight at room temperature. Removal of volatiles under reduced pressure, followed by extraction into toluene, concentration of the solution under reduced pressure and cooling to -20 °C, afforded the products as white microcrystalline solids. The zirconocene derivative $[(\eta^5\text{-}C_5H_5)ZrCl_2\{(\eta^5\text{-}C_5H_4)CMe_2(C_9H_7)\}]$ (**17**) was obtained in 58 % yield, whilst the hafnocene derivative $[(\eta^5\text{-}C_5H_5)HfCl_2\{(\eta^5\text{-}C_5H_4)CMe_2(C_9H_7)\}]$ (**18**) was obtained in 56 % yield.

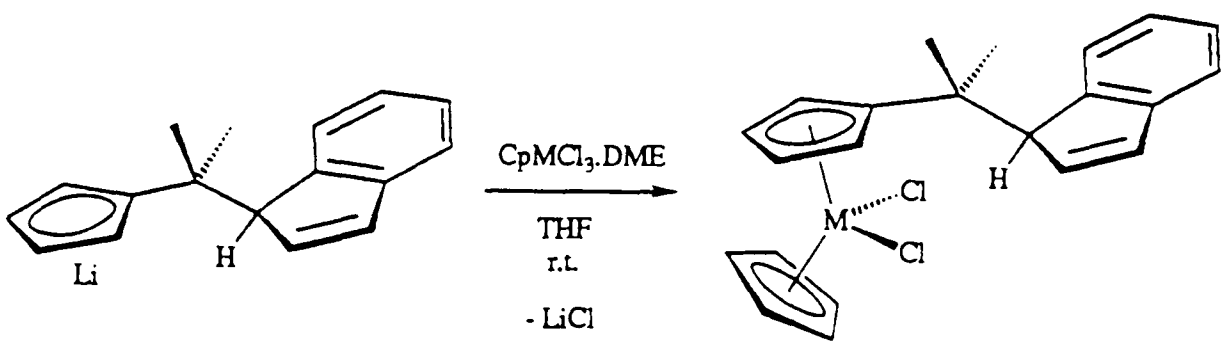

Figure 3.6.2. Synthesis of $[(\eta^5\text{-}C_5H_5)MCl_2\{(\eta^5\text{-}C_5H_4)CMe_2(C_9H_7)\}]$

[M = Zr (**17**), Hf (**18**)]

Compounds **17** and **18** were characterised by elemental analysis and by ^{1}H and ^{13}C NMR studies. The ^{1}H NMR spectra of **17** and **18** in CD_2Cl_2 are shown together in Figure 3.6.3. Both were assigned on the basis of selective ^{1}H decoupling, but for clarity only the ^{1}H spectrum of **17** is labelled.

The ^{1}H NMR spectra of both **17** and **18** show two doublets for the indenyl protons **f** and **c**, two pseudo-triplets for the indenyl protons **d** and **e** and two doublets of doublets for the indenyl protons **a** and **b**. Signals **a** and **b** show a 6 Hz coupling to eachother and a 2 Hz coupling to proton **g** at the indenyl bridge-head. The proposed molecular structures are chiral, the indenyl bridge-head carbon atom is the chiral centre, and the diastereotopic methyl groups of the CMe_2 bridge have different chemical shifts, at about 1.55 and 1.3 ppm for both **17** and **18**.

The largest difference between the two spectra are the chemical shifts of the C_5H_5 and C_5H_4 signals, which are on average about 0.1 ppm lower for the hafnocene compound **18** than for the zirconocene compound **17**. This is typical of cyclopentadienyl hafnium compounds compared with zirconium analogues,[4-6] and was also observed for the binuclear compounds described above.

^{13}C-^{1}H shift correlation experiments were performed for both **17** and **18**, and the ^{13}C NMR spectra of the two compounds are very similar. The DEPT and $^{13}C\{^{1}H\}$ spectra for the hafnium compound **18** are shown in Figure 3.6.4. The chemical shifts of the indenyl signals **a**, **b**, **c**, **d**, **e**, **f**, **h** and **i** are similar to those of indene (C_9H_8), whilst the shift of the indenyl bridge-head carbon signals (**g**) at around 64 ppm is (not unsurprisingly) about 25 ppm higher than the CH_2 signal of indene.[31] The chemical shifts of the C_5H_5 and C_5H_4 signals are on average about 1.3 ppm lower for the hafnocene compound **18** than for the zirconocene compound **17**. Similar observations were made for the binuclear compounds **8** to **11**.

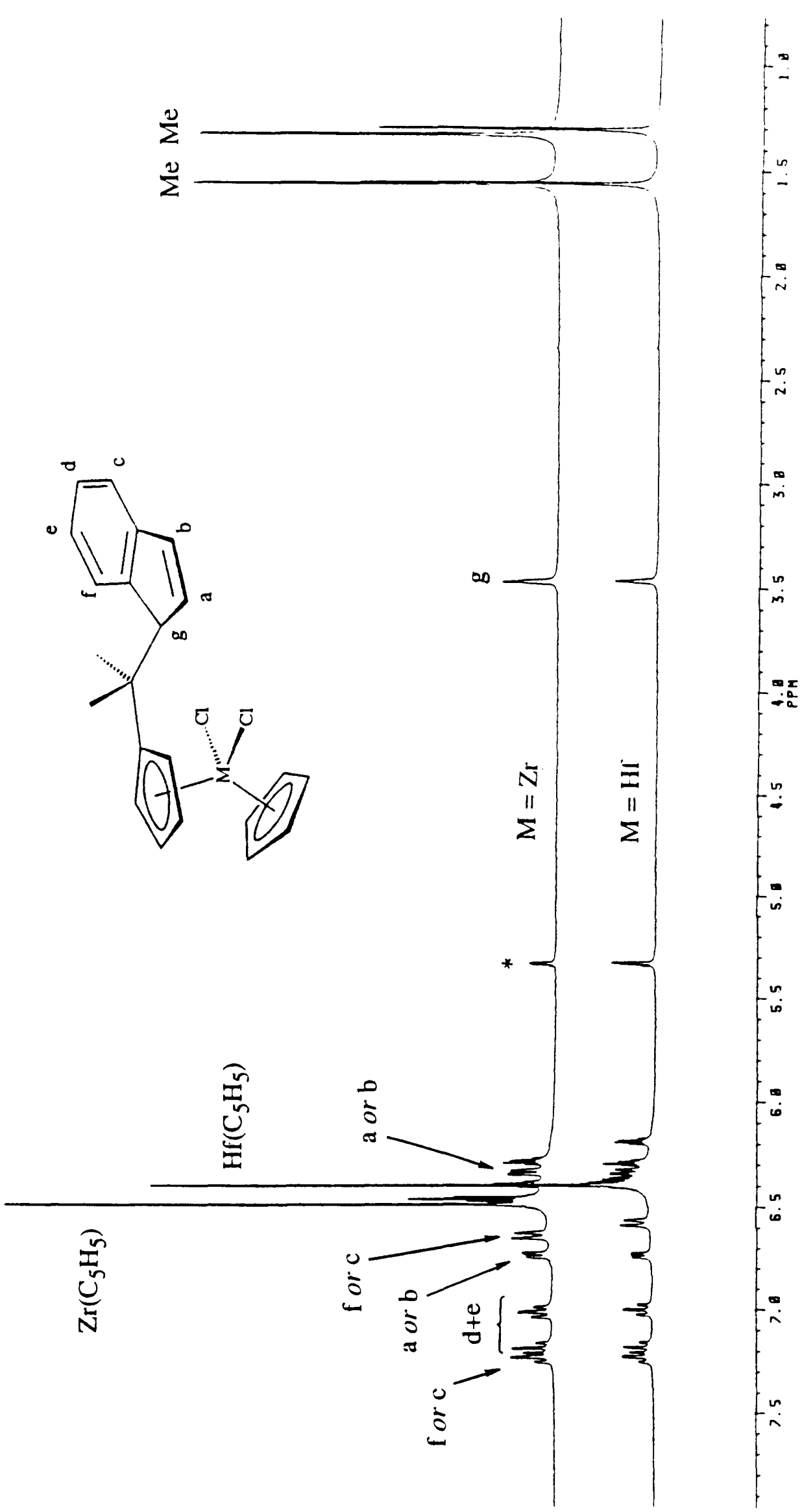

Figure 3.6.3. 300 MHz ^{1}H NMR spectra of $[(\eta^5\text{-}C_5H_5)MCl_2\{(\eta^5\text{-}C_5H_4)CMe_2(C_9H_7)\}]$ [M = Zr (**17**), Hf (**18**)] in CD_2Cl_2 at r.t. (* = residual protio solvent)

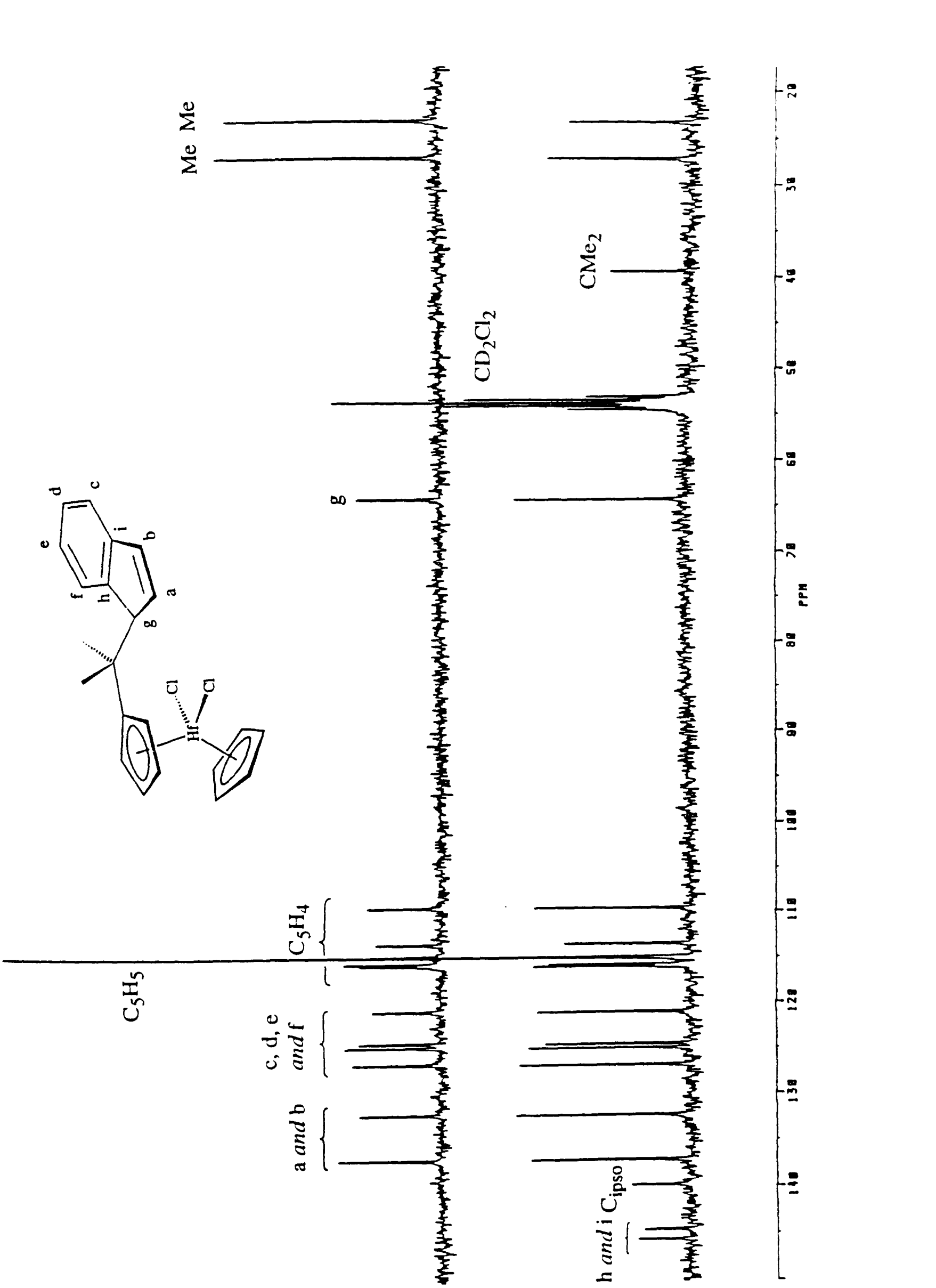

Figure 3.6.4. 75.5 MHz ^{13}C DEPT and $^{13}C\{^{1}H\}$ NMR spectra of $[(\eta^5\text{-}C_5H_5)HfCl_2\{(\eta^5\text{-}C_5H_4)CMe_2(C_9H_7)\}]$ (**18**) in CD_2Cl_2 at r.t.

3.6.3 Synthesis of $[(\eta^5\text{-}C_5H_5)Zr(CH_3)_2\{(\eta^5\text{-}C_5H_4)CMe_2(C_9H_7)\}]$

Two equivalents of methyl lithium (in diethyl ether solution) was added to a stirred suspension of $[(\eta^5\text{-}C_5H_5)ZrCl_2\{(\eta^5\text{-}C_5H_4)CMe_2(C_9H_7)\}]$ (**17**) in diethyl ether at -78 °C, then the reaction mixture was allowed to warm to room temperature and was stirred for five hours. Filtration, and removal of volatiles from the colourless filtrate under reduced pressure, gave a white solid. Extraction into petroleum ether (bp. 40-60 °C) gave a colourless solution, from which white crystals were obtained after concentration under reduced pressure and cooling to -80 °C. The white crystalline solid was characterised as the novel dimethyl zirconocene derivative $[(\eta^5\text{-}C_5H_5)Zr(CH_3)_2\{(\eta^5\text{-}C_5H_4)CMe_2(C_9H_7)\}]$ (**19**), and was obtained in 61 % yield.

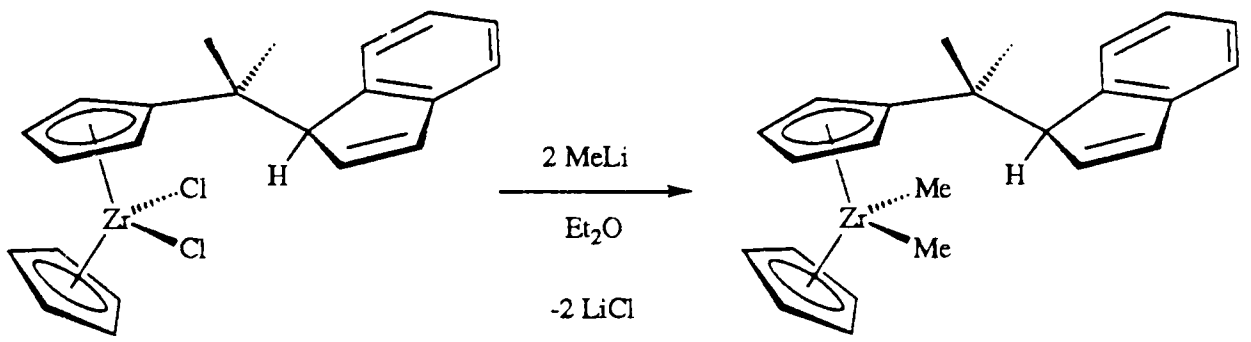

Figure 3.6.5. Synthesis of $[(\eta^5\text{-}C_5H_5)Zr(CH_3)_2\{(\eta^5\text{-}C_5H_4)CMe_2(C_9H_7)\}]$ (**19**)

Compound **19** was by characterised by elemental analysis and by ^1H and ^{13}C NMR studies. The ^1H NMR spectrum of **19** in C_6D_6 is shown in Figure 3.6.6; the assignments were based on selective ^1H decoupling experiments. The two close singlets at -0.03 and -0.05 ppm were assigned to the $Zr(CH_3)_2$ protons.

The ^{13}C DEPT NMR spectrum of compound **19** is shown in Figure 3.6.7. A ^{13}C-^1H shift correlation experiment assisted the assignment and showed that one of the C_5H_4 signals coincides with the C_5H_5 signal at 110.8 ppm. The $Zr(CH_3)_2$ ^{13}C NMR signals lie at 31.6 and 31.4 ppm, identical to those of the $Zr(CH_3)_2$ groups at the C_5H_4 sites of the binuclear compounds **13** and **14**.

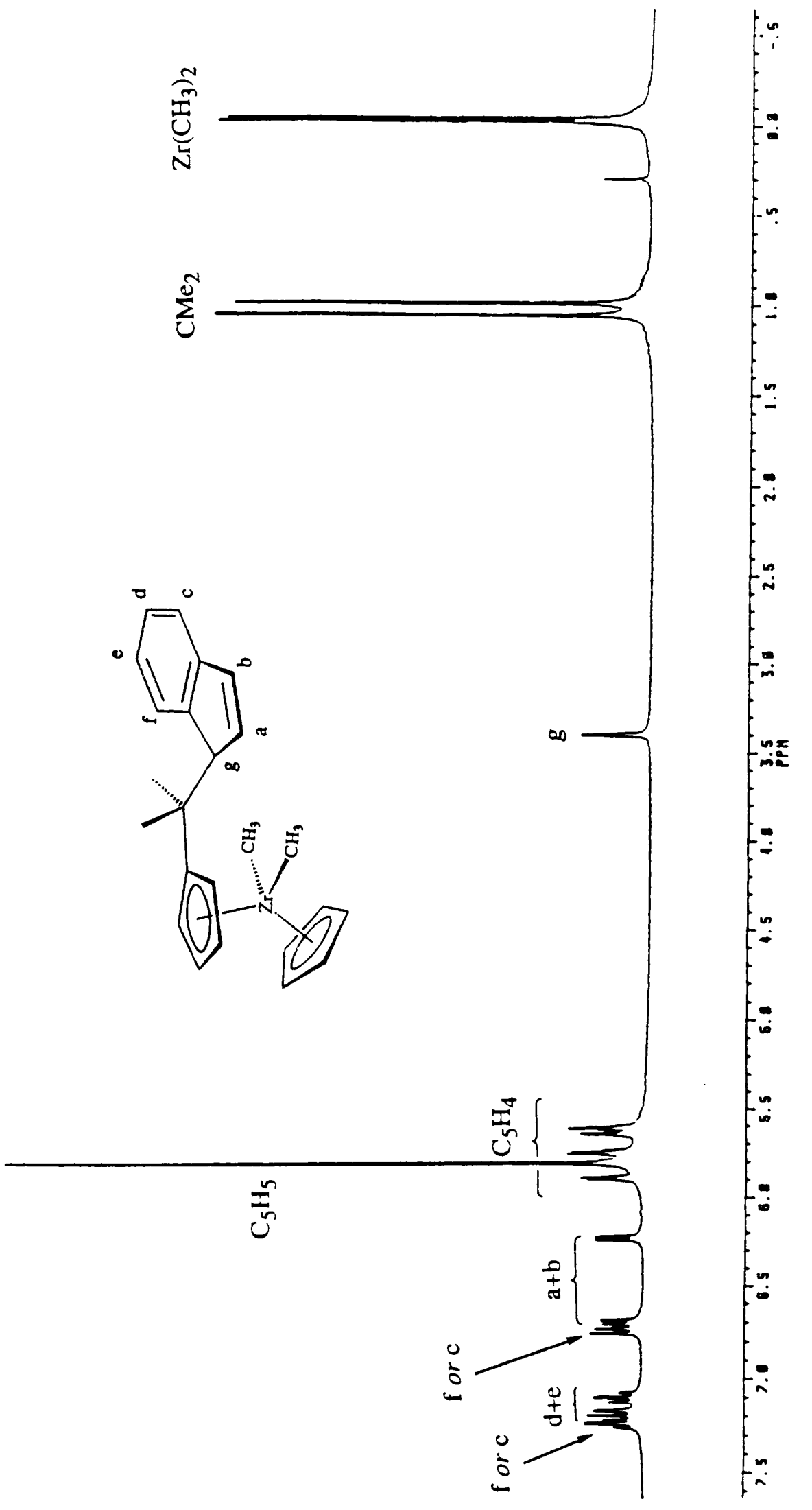

Figure 3.6.6. 300 MHz ^{1}H NMR spectrum in C_6D_6 at r.t. of $[(\eta^5\text{-}C_5H_5)Zr(CH_3)_2\{(\eta^5\text{-}C_5H_4)CMe_2(C_9H_7)\}]$ (**19**)

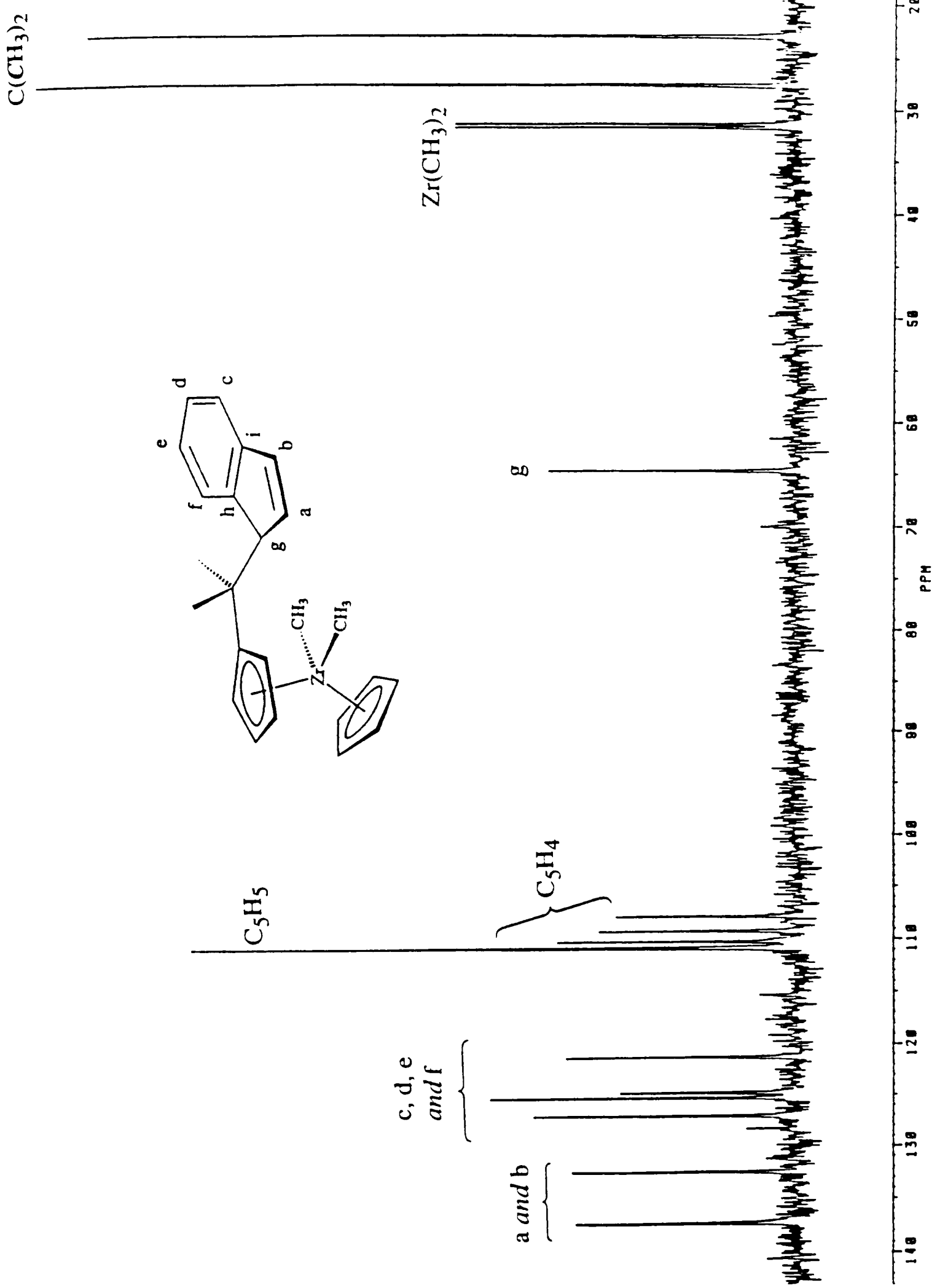

Figure 3.6.7. 75.5 MHz ^{13}C DEPT NMR spectrum in C_6D_6 at r.t. of $[(\eta^5\text{-}C_5H_5)Zr(CH_3)_2\{(\eta^5\text{-}C_5H_4)CMe_2(C_9H_7)\}]$ (**19**)

3.7 Summary

The reaction of $[Me_2C(C_5H_4)(C_9H_6)Li_2]$ with two equivalents of $[(\eta^5\text{-}C_5H_5)MCl_3\cdot DME]$ (M = Zr, Hf) affords the novel, chiral, homobinuclear compounds $[(\eta^5\text{-}C_5H_5)MCl_2\{(\eta^5\text{-}C_5H_4)CMe_2(\eta^5\text{-}C_9H_6)\}MCl_2(\eta^5\text{-}C_5H_5)]$ [M = Zr (**8**), Hf (**9**)], in which the metals are bridged by an unsymmetrical *ansa* ligand and experience different ligand environments. The reaction of the *ansa*-bridged mononuclear complexes $[\{Me_2C(\eta^5\text{-}C_5H_4)(\eta^2\text{-}C_9H_6)\}M(\eta^5\text{-}C_5H_5)Cl]$ [M = Zr (**1**), Hf (**2**)] with one equivalent of $[(\eta^5\text{-}C_5H_5)MCl_3\cdot DME]$ (M = Hf, Zr) provides a **selective** synthesis of the novel, chiral, heterobinuclear compounds $[(\eta^5\text{-}C_5H_5)MCl_2\{(\eta^5\text{-}C_5H_4)CMe_2(\eta^5\text{-}C_9H_6)\}M^*Cl_2(\eta^5\text{-}C_5H_5)]$ [M = Zr, M* = Hf (**10**); M = Hf, M* = Zr (**11**)]. The reaction of compound **1** with $[(\eta^5\text{-}C_5Me_5)ZrCl_3\cdot 2THF]$ gives the homobinuclear compound $[(\eta^5\text{-}C_5H_5)ZrCl_2\{(\eta^5\text{-}C_5H_4)CMe_2(\eta^5\text{-}C_9H_6)\}ZrCl_2(\eta^5\text{-}C_5Me_5)]$ (**12**), in which the steric crowding is considerably greater at one metal site than the other.

Treatment of the group 4 binuclear metallocene derivative $[(\eta^5\text{-}C_5H_5)ZrCl_2\{(\eta^5\text{-}C_5H_4)CMe_2(\eta^5\text{-}C_9H_6)\}ZrCl_2(\eta^5\text{-}C_5H_5)]$ (**8**) with four equivalents of methyl lithium gives the novel, chiral binuclear compound $[(\eta^5\text{-}C_5H_5)Zr(CH_3)_2\{(\eta^5\text{-}C_5H_4)CMe_2(\eta^5\text{-}C_9H_6)\}Zr(CH_3)_2(\eta^5\text{-}C_5H_5)]$ (**13**). The homo- and hetero-bimetallic analogues $[(\eta^5\text{-}C_5H_5)M(CH_3)_2\{(\eta^5\text{-}C_5H_4)CMe_2(\eta^5\text{-}C_9H_6)\}M^*(CH_3)_2(\eta^5\text{-}C_5H_5)]$ [M = Zr, M* = Hf (**14**); M = Hf, M* = Zr (**15**); M = M* = Hf (**16**)] were prepared in a similar fashion.

Some structurally related mononuclear compounds were also prepared. The reaction of $[Li(C_5H_4)CMe_2(C_9H_7)]$ with one equivalent of $[(\eta^5\text{-}C_5H_5)MCl_3\cdot DME]$ (M = Zr, Hf) gives the mononuclear zirconocene and hafnocene derivatives $[(\eta^5\text{-}C_5H_5)MCl_2\{(\eta^5\text{-}C_5H_4)CMe_2(C_9H_7)\}]$ [M = Zr (**17**), Hf (**18**)], and the treatment of **17** with two equivalents of methyl lithium gives the the zirconocene dimethyl derivative $[(\eta^5\text{-}C_5H_5)Zr(CH_3)_2\{(\eta^5\text{-}C_5H_4)CMe_2(C_9H_7)\}]$ (**19**).

This Chapter has demonstrated the use of compounds **1** and **2** as reagents for the **selective** synthesis of hetero- and homo-bimetallic group 4 compounds with unsymmetrical ligand environments. Following on from this work, a colleague Neil Popham has shown that compound **1** reacts with $[Rh(CO)_2Cl]_2$ to give the novel zirconium-rhodium bimetallic compound $[(\eta^5\text{-}C_5H_5)ZrCl_2\{(\eta^5\text{-}C_5H_4)CMe_2(\eta^5\text{-}C_9H_6)\}Rh(CO)_2]$ (**20**), and with $[Mn(CO)_5Cl]$ to give the novel zirconium-manganese bimetallic compound $[(\eta^5\text{-}C_5H_5)ZrCl_2\{(\eta^5\text{-}C_5H_4)CMe_2(\eta^5\text{-}C_9H_6)\}Mn(CO)_3]$ (**21**).[32] These reactions, shown in Figure 3.7 along with the others described in this Chapter, demonstrate the potential versatility of this approach to the synthesis of binuclear compounds.

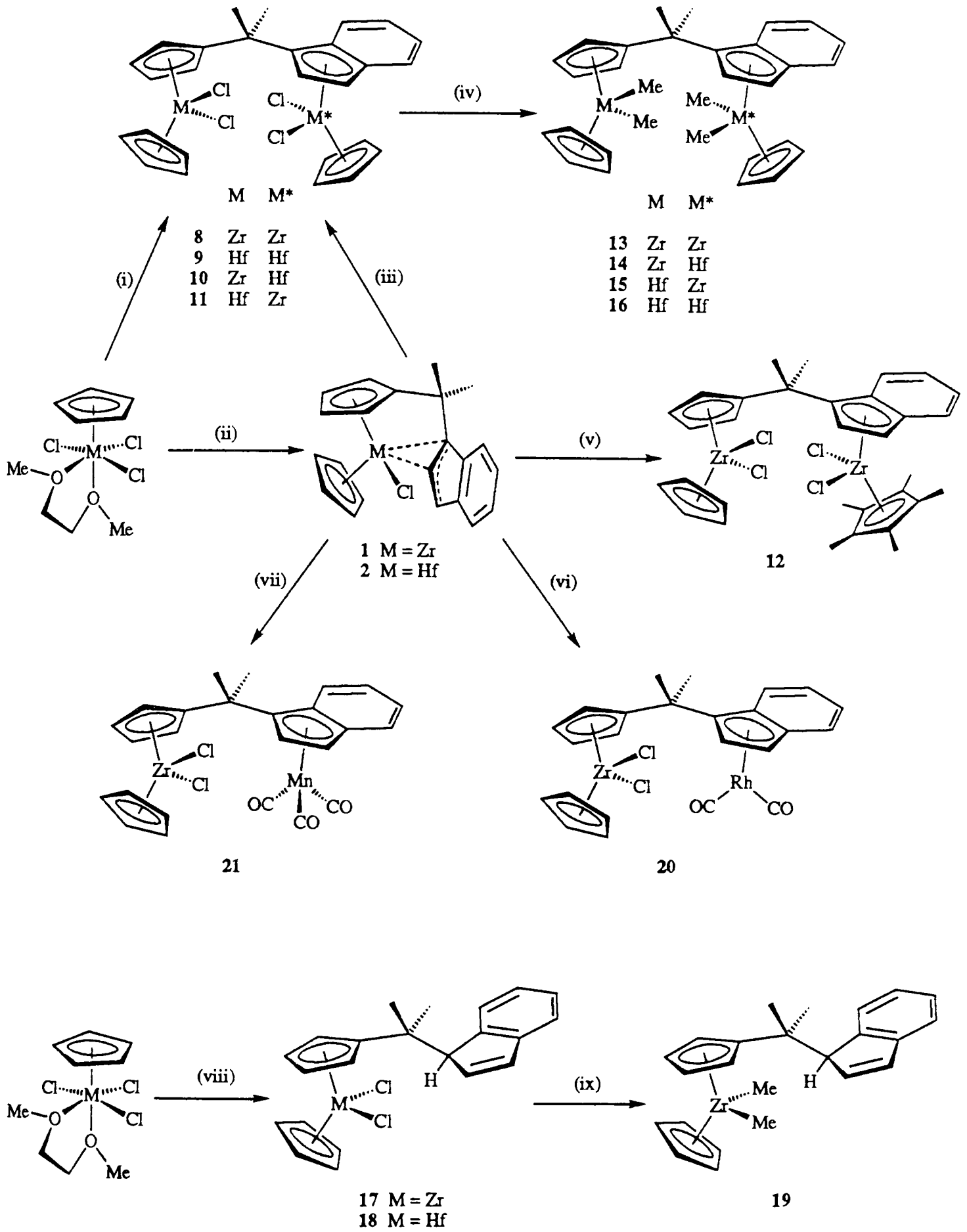

Figure 3.7. Summary of the reactions described in Chapter 3.

Reagents: (i) 0.5 $[Me_2C(C_5H_4)(C_9H_6)Li_2]$, (ii) $[Me_2C(C_5H_4)(C_9H_6)Li_2]$, (iii) $[(\eta^5\text{-}C_5H_5)M^*Cl_3\cdot DME]$, (iv) 4 MeLi, (v) $[(\eta^5\text{-}C_5Me_5)ZrCl_3\cdot 2THF]$, (vi) 0.5 $[Rh(CO)_2Cl]_2$, (vii) $[Mn(CO)_5Cl]$, (viii) $[Li(C_5H_4)CMe_2(C_9H_7)]$, (ix) 2 MeLi.

References for Chapter 3

1. K. P. Reddy and J. L. Petersen, *Organometallics*, 1989, **8**, 2107.
2. J. F. Buzinkai and R. R. Schrock, *Organometallics*, 1987, **6**, 1447.
3. I. E. Nifant'ev, M. V. Borsov, A. V. Churakov, S. G. Mkoyan and L. O. Atovmyan, *Organometallics*, 1992, **11**, 3942.
4. E. C. Lund and T. Livinghouse, *Organometallics*, 1990, **9**, 2426.
5. E. Samuel and M. D. Rausch, *J. Am. Chem. Soc.*, 1973, **95**, 6263.
6. P. Renaut, G. Tainturier and B. Gautheron, *J. Organomet. Chem.*, 1978, **148**, 35.
7. L. E. Schock and T. J. Marks, *J. Am. Chem. Soc.*, 1988, **110**, 7701.
8. A. D. Horton, *Organometallics*, 1992, **11**, 3271.
9. P. T. Wolczanski and J. E. Bercaw, *Organometallics*, 1982, **1**, 793.
10. W. Spalek , M. Antberg, V. Dolle, R. Klein, J. Rohrmann and A. Winter, *New J. Chem.*, 1990, **14**, 499.
11. J. A. Ewen, M. J. Elder, R. L. Jones, L. Haspeslagh, J. L. Atwood, S. G. Bott and K. Robinson, *Makromol. Chem., Makromol. Symp.*, 1991, **48/49**, 253.
12. W. Kaminsky, R. Engehausen, K. Zoumis, W. Spalek and J. Rohrmann, *Makromol. Chem.*, 1992, **193**, 1643.
13. T. J. Marks, *Acc. Chem. Res.*, 1992, **25**, 57.
14. M. Bochmann and S. J. Lancaster, *Organometallics*, 1993, **12**, 633.
15. X. Yang, C. L. Stern and Tobin J. Marks, *J. Am. Chem. Soc.*, 1991, **113**, 3623.
16. M. R. Kesti, G. W. Coates and R. M. Waymouth, *J. Am. Chem. Soc.*, 1992, **114**, 9679.
17. J. C. W. Chien, W. M. Tsai and M. D. Rausch, *J. Am. Chem. Soc.*, 1991, **113**, 8570.
18. W. Wielstra, S. Gambarotta, A. L. Spek and W. J. J. Smeets, *Organometallics*, 1990, **9**, 2142.

19. W. Wielstra, R. Duchateau, S. Gambarotta, C. Benismon and E. Gabe, *J. Organomet. Chem.*, 1991, **418**, 183.

20. J. Cacciola, K. P. Reddy and J. L. Petersen, *Organometallics*, 1992, **11**, 665.

21. Neil Popham, Part II Thesis, University of Oxford, 1991.

22. D. H. Williams and I. Fleming, *Spectroscopic Methods in Organic Chemistry*, McGraw-Hill, London, 1989.

23. L. Pauling, *The Chemical Bond*, Cornell University Press, Ithaca, New York, 1967.

24. N. N. Greenwood and A. Earnshaw, *Chemistry of the Elements*, Pergamon Press, Oxford, 1984.

25. J. Emsley, *The Elements*, Clarendon Press, Oxford, 1991.

26. F. P. Pruchnik, *Organometallic Chemistry of the Transition Elements*, Plenum Press, New York, 1990.

27. F. A. Cotton and G. Wilkinson, *Advanced Inorganic Chemistry*, Wiley, New York, 1988.

28. K. S. Pitzer, *Acc. Chem. Res.*, 1979, **12**, 271.

29. A. L. Allred and E. G. Rochow, *J. Inorg. Nucl. Chem.*, 1958, **5**, 264.

30. A. L. Allred, *J. Inorg. Nucl. Chem.*, 1961, **17**, 215.

31. F. H. Kohler, *Chem. Ber.*, 1974, **107**, 570.

32. G. M. Diamond, M. L. H. Green, N. A. Popham and A. N. Chernega, *J. Chem. Soc., Chem. Commun.*, 1994, in press.

CHAPTER FOUR

Polymerization Studies

4.1 Introduction

In Chapter 1 it was described how mononuclear group 4 metallocene derivatives have become recognised as an important class of homogeneous catalysts, especially for the polymerization of olefins. The proposed mechanism of polymerization, the role of co-catalysts, and the effect of molecular structure on reactivity, were discussed. Chapter 3 described the synthesis of a series of novel, chiral, homo- and hetero-binuclear group 4 metallocene compounds, and some related mononuclear compounds. This chapter describes a study of the binuclear compounds as catalysts for the polymerization of ethylene and propylene, and comparisons are made with the catalytic properties of mononuclear compounds.

4.2. Preparation of the co-catalysts

The methylaluminoxane (MAO) used in this work was prepared by the partial hydrolysis of trimethylaluminium using $CuSO_4.5H_2O$, following the procedures of Kaminsky[1] and Giannetti,[2] as modified by Ishihara.[3] The other co-catalysts $B(C_6F_5)_3$ and $[Ph_3C]^+[B(C_6F_5)_4]^-$ were prepared by literature methods without modification; $B(C_6F_5)_3$ as described by Massey and Park[4] and $[Ph_3C]^+[B(C_6F_5)_4]^-$ as described by Chien *et. al.*.[5]

4.3 General description of procedure

The apparatus used for the polymerization reactions consisted of a Fischer-Porter reactor connected to a computer-controlled gas supply system, shown schematically in Figure 4.3.1. Details of the polymerization procedure are given in section 5.4.

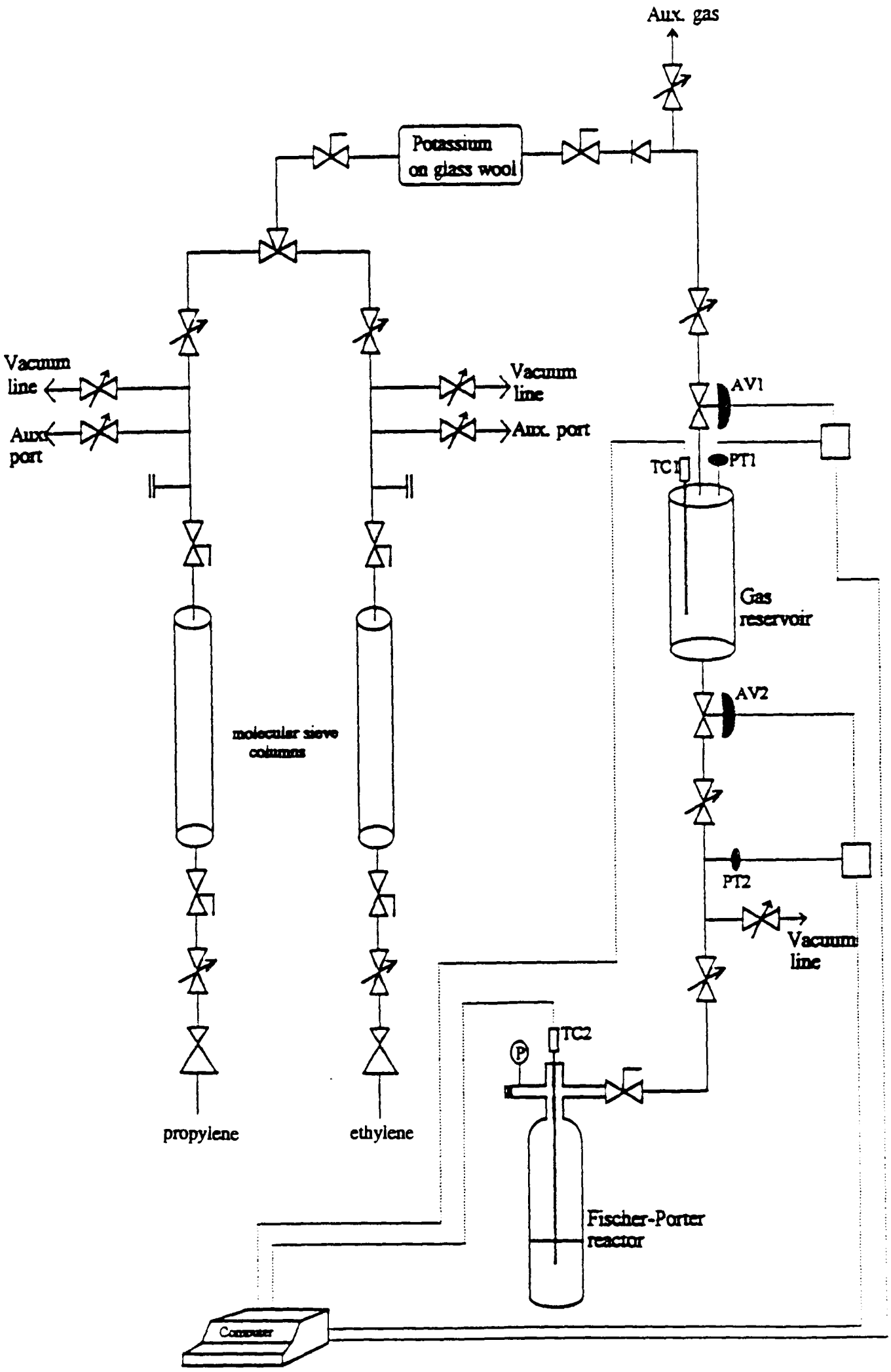

Figure 4.3.1. Apparatus used for the polymerization of ethylene and propylene

As shown in Figure 4.3.1, the ethylene or propylene (pure grade) was further purified by passage through columns of 4 Å molecular sieves and then over finely divided potassium metal supported on glass wool. The gas then passed into a known-volume reservoir, fitted with a pressure transducer (PT1) and thermocouple (TC1), both connected to the computer. The pressure and temperature in the reactor were also monitored (*via* PT2 and TC2). Upper and lower pressure limits were set for both the reactor and reservoir, and when the pressure fell below the lower limit, the appropriate computer-controlled valve (AV1 or AV2) was opened until the upper pressure limit was reached. The pressure limits for the Fischer-Porter reactor were set at 1.95 and 2.05 bar for all experiments.

A wide variety of different conditions (solvents, temperatures, monomer pressures, *etc.*) have been used by different workers for the study of olefin polymerization catalysed by group 4 metallocenes. This variety of conditions has made comparison of the results of different workers very difficult. In 1992, Kaminsky reported the polymerization of ethylene and propylene by eleven different zirconocene and hafnocene catalysts with MAO co-catalyst, under one standard set of polymerization conditions (2 bar monomer pressure, 30 °C, toluene solvent). It was decided to follow Kaminsky's procedure as closely as possible so that comparisons might be made with a range of other metallocene catalysts.

The ethylene polymerization experiments using the metallocene/MAO catalyst systems were performed at least twice and were found to be reproducible. Sufficient time was not available to allow repeat experiments to be performed for the other polymerization reactions.

4.4. Polymerization of ethylene using metallocene / MAO catalyst systems

4.4.1. Polymerization experiments

The polymerization reactions were carried out under conditions as close as possible to those employed by Kaminsky in 1992.[6] Experimental details are given in section 5.4.3.

4.4.2. Results of ethylene polymerization reactions

The ethylene polymerization results for the binuclear compounds [(η^5-C_5H_5)MCl_2{(η^5-C_5H_4)CMe_2(η^5-C_9H_6)}M*Cl_2(η^5-C_5H_5)] [M = M* = Zr (**8**); M = M* = Hf (**9**); M = Zr, M* = Hf (**10**); M = Hf, M* = Zr (**11**)] are given in the top part of Table 4.1. The results for the mononuclear compounds [(η^5-C_5H_5)MCl_2{(η^5-C_5H_4)CMe_2(C_9H_7)}] [M = Zr (**17**), Hf (**18**)] and the binuclear zirconium-rhodium compound [(η^5-C_5H_5)$ZrCl_2${(η^5-C_5H_4)CMe_2(η^5-C_9H_6)}$Rh(CO)_2$] (**20**) are given in the lower part of Table 4.1.

When comparing the activities of the binuclear compounds with the mononuclear compounds, one should bear in mind that the activities are quoted per mole of compound. The same number of moles of compound and the same amount of methylaluminoxane were used in each experiment (and the same were used by Kaminsky).[6] Thus the aluminium/compound molar ratio is the same for each experiment (830/1), but the experiments with the binuclear compounds have twice the number of transition metal sites and thus half the aluminium/transition-metal ratio (415/1), compared with the mononuclear compounds. For mononuclear group 4 metallocene/MAO catalyst systems, doubling the aluminium/transition-metal ratio is typically associated with an increase in activity of between 5 and 30 %.[7, 8]

Table 4.1. Polymerization of ethylene using metallocene / MAO catalyst systems

$[(\eta^5\text{-}C_5H_5)MCl_2\{(\eta^5\text{-}C_5H_4)CMe_2(\eta^5\text{-}C_9H_6)\}M^*Cl_2(\eta^5\text{-}C_5H_5)]$ compounds

Compound	M	M*	Yield (g)	Activity ($kgPE.mol^{-1}.hr^{-1}$)	Relative Activity ($kgPE.mol^{-1}.hr^{-1}.C_{mon}^{-1}$)
8	Zr	Zr	2.14	342	1460
9	Hf	Hf	0.59	94	400
10	Zr	Hf	1.69	270	1150
11	Hf	Zr	0.45	72	310

$[(\eta^5\text{-}C_5H_5)MCl_2(\eta^5\text{-}C_5H_4CMe_2C_9H_6X)]$ compounds

Compound	M	X	Yield (g)	Activity ($kgPE.mol^{-1}.hr^{-1}$)	Relative Activity ($kgPE.mol^{-1}.hr^{-1}.C_{mon}^{-1}$)
17	Zr	H	4.94	790	3360
18	Hf	H	1.71	274	1170
20	Zr	$Rh(CO)_2$	0.85	136	580

2 bar absolute monomer pressure, 30 °C, 210 cm^3 toluene solvent, one hour, 6.25×10^{-6} moles of compound, 0.300 g MAO, $C_{mon} = 0.235$ mol dm^{-3}

In Table 4.1, the activity of each compound is given as kg of polyethylene produced per mole of compound per hour. A "relative activity" is also quoted, which is the activity divided by the monomer concentration, calculated from the monomer solubility in toluene (0.235 $mol.dm^{-3}$ for ethylene in toluene at 30 °C and 2 bar ethylene pressure).[6, 9] The monomer concentration is dependent on temperature and pressure and is different for ethylene and propylene. The relative activity thus allows more meaningful comparison of catalyst activities over a range of temperatures and pressures, and allows the comparison of catalyst activities for ethylene and propylene polymerization.

The relative activities of even the most active compounds in Table 4.1. (**8**, **10**, **17** and **18**) are much lower than that reported by Kaminsky for Cp_2ZrCl_2 / MAO under similar conditions (60900 $kgPE.mol^{-1}.hr^{-1}.C_{mon}^{-1}$) but are similar to that of the *ansa* metallocene $[\{Me_2C(\eta^5\text{-}C_5H_4)(\eta^5\text{-}C_9H_6)\}ZrCl_2]$ (1550 $kgPE.mol^{-1}.hr^{-1}.C_{mon}^{-1}$).[6] The rate of gas uptake by the polymerization reactions was monitored and all of the catalyst systems in Table 4.1 remained active for the whole hour of the experiment.

The binuclear zirconium compound **8** and the mononuclear zirconium compound **17** are both considerably more active than their hafnium analogues **9** and **18**. For the polymerization of both ethylene and propylene, zirconocene/MAO systems are typically much more active than analogous hafnocene catalysts (often by an order of magnitude), but the hafnocene catalysts produce much higher molecular weight polymers.[2, 3, 6, 10-14] These results might be accounted for by the greater strength of hafnium-carbon σ bonds, which would be expected to make both simple bond breaking (chain termination) and insertion into the bond (chain propagation) more difficult. For the compounds $Cp^*_2MMe_2$, the metal-methyl bond enthalpy is around 306 kJ mol^{-1} for hafnium compared with 284 kJ mol^{-1} for zirconium.[15, 16]

The activity of the heterobinuclear compound $[(\eta^5\text{-}C_5H_5)ZrCl_2\{(\eta^5\text{-}C_5H_4)CMe_2(\eta^5\text{-}C_9H_6)\}HfCl_2(\eta^5\text{-}C_5H_5)]$ (**10**) is closer to the activity of the dizirconium analogue **8** and is significantly higher than that of the dihafnium analogue **9**. The activity of $[(\eta^5\text{-}C_5H_5)HfCl_2\{(\eta^5\text{-}C_5H_4)CMe_2(\eta^5\text{-}C_9H_6)\}ZrCl_2(\eta^5\text{-}C_5H_5)]$

(**11**) is much closer to that of **9** and is much lower than the activity of **8**. These observations suggest that the ethylene polymerization activity of the binuclear compounds has a greater dependence on the metal at the C_5H_4 site of the bridging ligand than on the metal at the indenyl site.

Comparing the activities of **8**, **9**, **10** and **11**, it seems reasonable to propose that for both of the homobimetallic compounds **8** and **9** the metal centre at the C_5H_4 site of the bridging ligand has a higher activity than the metal centre at the indenyl site. The metal centre at the C_5H_4 site is the less sterically crowded of the two centres, which would be expected to favour ethylene polymerization at this site. Kaminsky reported that, under similar ethylene polymerization conditions, Cp_2ZrCl_2 was about five times more active than the more sterically crowded neomenthyl-substituted zirconocene compound $(NmCp)_2ZrCl_2$ (Nm = neomenthyl).[6]

It has been proposed that electronic factors have a large effect on ethylene polymerization. Consiglio and co-workers have shown that the ethylene polymerization activity of the compounds $[(\eta^5\text{-}4,7\text{-}X_2C_9H_5)\}ZrCl_2]$ (with MAO) showed a large dependence on the nature of the substituents at the 4- and 7-positions of the indenyl rings. Electron-withdrawing substituents resulted in a decrease of both activity and polymer molecular weight, supporting the hypothesis that the active species is a cationic or "cation-like" metallocene alkyl species, $[Cp'_2M(R)]^{(\delta)+}$.[17]

^{13}C NMR chemical shifts are strongly influenced by the inductive effects of electron withdrawing/donating groups. In the ^{13}C NMR spectra of the methylated homobimetallic compounds $[(\eta^5\text{-}C_5H_5)M(CH_3)_2\{(\eta^5\text{-}C_5H_4)CMe_2(\eta^5\text{-}C_9H_6)\}M(CH_3)_2(\eta^5\text{-}C_5H_5)]$ [M = Zr (**13**) or Hf (**16**)], the signals of the $M^*(CH_3)_2$ methyl carbons (at the indenyl site) are found at higher chemical shift (more deshielded) compared with the signals of the the $M(CH_3)_2$ methyl carbons (at the C_5H_4 site), suggesting that the indenyl ligand is more electron withdrawing (or less electron donating) than the C_5H_4 ligand. The same electronic effects might favour ethylene polymerization at the C_5H_4 site rather than the indenyl site of the binuclear metallocene/MAO systems.

The ethylene polymerization activity of the zirconium-rhodium compound [(η^5-C_5H_5)$ZrCl_2${(η^5-C_5H_4)CMe_2(η^5-C_9H_6)}$Rh(CO)_2$] (**20**) is about half that of the dizirconium compound **8** and the zirconium-hafnium binuclear compound **10**. The activities of all of these binuclear compounds with zirconium at the C_5H_4 site are significantly lower that that of the related mononuclear compound [(η^5-C_5H_5)$ZrCl_2${(η^5-C_5H_4)CMe_2(C_9H_7)}] (**17**). So far as polyethylene productivity is concerned, there would appear to be no advantage in incorporating a second metal centre in these molecules. In fact the second metal centre, whether MCl_2Cp (M = Zr or Hf) or $Rh(CO)_2$, has a negative effect on polyethylene productivity.

The lower activity of the binuclear compounds might reflect steric and/or electronic effects of the second metal centre. It is also possible that there might be more direct interaction between the metal sites. For example, atoms or groups might be exchanged from one metal to another, or might bridge between them. Several binuclear zirconocene compounds with bridging methyls or hydrides have been reported.[18-23] For the zirconium-rhodium bimetallic compound (**20**), one might imagine species in which the metals are bridged by a carbonyl group, or by an RCO or HCO group derived from the insertion of a rhodium-bound carbonyl ligand into a Zr-C or Zr-H bond (species with Zr-H bonds would be expected to be formed by β-elimination of the polymer chain). Erker has described a reaction between $CpRh(CO)_2$ and (butadiene)zirconocene, in which one of the rhodium-bound carbonyl ligands inserts into a Zr-C bond to give a bridged binuclear compound.[24, 25]

4.5. Polymerization of propylene using metallocene / MAO catalyst systems

4.5.1. Polymerization experiments

The binuclear compounds **8**, **9**, **10**, **11** and **20**, and the mononuclear zirconocene compound **17**, were tested as catalysts for the polymerization of propylene under conditions similar to those used for ethylene (210 cm^3 toluene solvent, 30 °C, 2 bar monomer pressure). When the same amount of catalyst (6.25 x 10^{-6} mol) and MAO (0.300 g) were used, the activities were found to be very low, yielding less than 0.02 g of viscous liquid after work up. It was decided that if the activities of the compounds were to be compared with any confidence, and if the ^{13}C NMR spectroscopy of the polypropylene was to be studied, then more polymer product would be required.

It was decided to keep the temperature, pressure and solvent volume the same but to use eight times the amount of compound and co-catalyst compared with the ethylene experiments (and Kaminsky's comparative study).[6] The experimental details are given in section 5.4.4. Because of the higher catalyst concentration, the results cannot be compared quite so directly with the ethylene results in Table 4.1 and Kaminsky's results from a range of metallocene catalysts. However since the temperature and pressure were unchanged, cautious comparisons might still be made. The yields and activities for these reactions are given in Table 4.2.

4.5.2. Results of propylene polymerization reactions

Table 4.2. Polymerization of propylene using metallocene / MAO catalyst systems

$[(\eta^5\text{-}C_5H_5)MCl_2\{(\eta^5\text{-}C_5H_4)CMe_2(\eta^5\text{-}C_9H_6)\}M^*Cl_2(\eta^5\text{-}C_5H_5)]$ compounds

Compound	M	M*	Yield (g)	Activity ($kgPP.mol^{-1}.hr^{-1}$)	Relative Activity ($kgPP.mol^{-1}.hr^{-1}.C_{mon}^{-1}$)
8	Zr	Zr	2.22	11.1	8.8
9	Hf	Hf	1.33	6.7	5.3
10	Zr	Hf	0.42	2.1	1.7
11	Hf	Zr	0.32	1.6	1.3

$[(\eta^5\text{-}C_5H_5)MCl_2(\eta^5\text{-}C_5H_4CMe_2C_9H_6X)]$ compounds

Compound	M	X	Yield (g)	Activity ($kgPP.mol^{-1}.hr^{-1}$)	Relative Activity ($kgPP.mol^{-1}.hr^{-1}.C_{mon}^{-1}$)
17	Zr	H	0.36*	7.2	5.7
20	Zr	$Rh(CO)_2$	0.22	1.1	0.9

2 bar monomer pressure, 30 °C, 210 cm^3 toluene solvent, four hours

(* one hour for compound **17**), 5.0 x 10^{-5} moles of compound, 2.40 g MAO,

C_{mon} = 1.26 mol dm^{-3} for propylene in toluene at 2 bar monomer pressure at 30 °C

The propylene polymerization results for the binuclear compounds [(η^5-C_5H_5)MCl_2{(η^5-C_5H_4)CMe_2(η^5-C_9H_6)}M*Cl_2(η^5-C_5H_5)] [M = M* = Zr (**8**); M = M* = Hf (**9**); M = Zr, M* = Hf (**10**); M = Hf, M* = Zr (**11**)] are given in the top part of Table 4.2. The results for the mononuclear compound [(η^5-C_5H_5)$ZrCl_2${(η^5-C_5H_4)CMe_2(C_9H_7)}] (**17**) and the binuclear zirconium-rhodium compound [(η^5-C_5H_5)$ZrCl_2${(η^5-C_5H_4)CMe_2(η^5-C_9H_6)}$Rh(CO)_2$] (**20**) are given in the lower part of Table 4.2.

All of the metallocene/MAO systems in Table 4.2. have very low propylene polymerization activities. Kaminsky has reported relative activities for propylene polymerization of 140 kgPP.mol^{-1}.hr^{-1}.C_{mon}^{-1} for Cp_2ZrCl_2 and 400 kgPP.mol^{-1}.hr^{-1}.C_{mon}^{-1} for *rac*-[{Me_2C(η^5-C_5H_4)(η^5-C_9H_6)}$ZrCl_2$] under similar conditions, and activities of over 1000 kgPP.mol^{-1}.hr^{-1}.C_{mon}^{-1} for some highly stereospecific *ansa*-zirconocene/MAO ststems.[6]

All of the new compounds tested showed much lower relative activities for propylene polymerization than for ethylene polymerization. In Kaminsky's comparative study of the ethylene and propylene polymerization activities of metallocene/MAO catalysts, the relative activity was higher for ethylene than for propylene in every case.[6] However, the ratio [ethylene activity / propylene activity] showed very large variations: 435 for Cp_2ZrCl_2, 70 for $(NmCp)_2ZrCl_2$ (Nm = neomenthyl), 24 for *rac*-[{$(CH_2)_2$(η^5-$C_9H_6)_2$}$ZrCl_2$], 5 for *rac*-[{$(CH_2)_2$(η^5-$C_9H_6)_2$}$HfCl_2$] and only 1.3 for [{Me_2C(η^5-C_5H_4)(η^5-$C_{13}H_8$)}$ZrCl_2$]. Kaminsky noted that, for propylene polymerization, all of the systems lacking a high degree of stereospecificity also showed low activities. The system Cp_2ZrCl_2/MAO showed the highest activity in ethylene polymerization but the lowest in propylene polymerization of all the systems compared, and gave atactic polypropylene. Kaminsky concluded that for the prochiral propene monomer, stereospecific polymerization is strongly favoured over aspecific polymerization, and that this factor seemed to dominate electronic and steric influences arising from the metallocene structure.[6]

For the binuclear compounds $[(\eta^5\text{-}C_5H_5)MCl_2\{(\eta^5\text{-}C_5H_4)CMe_2(\eta^5\text{-}C_9H_6)\}M^*Cl_2(\eta^5\text{-}C_5H_5)]$ (**8** to **11**), the propylene polymerization activities are not only much lower the for ethylene, but also show a different order. For ethylene polymerization it was found that the metal at the C_5H_4 site had a larger effect than the metal at the indenyl site on the activity of the binuclear compound. For propylene polymerization this does not appear to be the case. The dizirconium compound **8** is more active than the dihafnium compound **9**, but compound **9** is considerably more active than both of the heterobimetallic zirconium-hafnium analogues **10** and **11**. This would not be predicted from the typical behaviour of mononuclear metallocene/MAO systems. Mononuclear zirconocene/MAO catalysts typically have higher propylene polymerization activities than hafnium analogues.[3, 6, 11-14]

Whilst the metal-dependence of the ethylene polymerization activity of the binuclear compounds **8** to **11** is close to that of mononuclear systems, this seem not to be the case for propylene polymerization. For compounds **8** to **11** the average turnover rate for ethylene polymerization is about 2 insertions per second, compared with 0.04 insertions per second for propylene. This corresponds to one insertion every 0.5 seconds for ethylene and only one insertion every 25 seconds for propylene. Possible binuclear processes, requiring close approach of the two metal centres, might thus be expected to compete more effectively with propylene polymerization compared with the much faster ethylene polymerization.

Kaminsky and others have noted some interesting relationships between propylene polymerization activity and the stereoregularity and molecular weights of the polymers formed.[3, 6, 12-14] It was decided to investigate the nature of the polypropylene formed in the polymerization reactions discussed above.

4.6 Characterisation of polypropylene

4.6.1. Stereochemistry of polypropylene

The stereoselective polymerization of propylene was discussed in Chapter 1 and the terms isotactic, syndiotactic and atactic were explained. The stereochemical notation used here is that described by Frisch *et al.*[25] Technically, each methine carbon in a polypropylene chain is asymmetric and can have one of two possible configurations. In ideally isotactic polypropylene each methine carbon has the same configuration, either all *R* or all *S*, while in syndiotactic polypropylene the configurations are alternately *R* and *S*, and in atactic polypropylene there is a random distribution of *R* and *S* configurations. A neighbouring pair of monomer units is called a **dyad**. If the neighbouring units have the same stereochemical configuration then the dyad is ***meso*** (m), if the configurations differ then the dyad is ***racemic*** (r). Two neighbouring dyads (three monomer units) are known as a **triad** and may have mm, mr, rm or rr configurations, and so on.

..RRRRRRRRRRRR.. or *..SSSSSSSSSSSSS..* = **isotactic** = mmmmmmmmmm

...RSRSRSRSRSRSRSRS.... = **syndiotactic** = rrrrrrrrrrrrrrrrrr

...RRSRSSRSSRRRSRSSRR... = **atactic** = mrrrmrrmrmmrrrmrm

4.6.2 NMR spectroscopy of polypropylene

NMR spectroscopy provides the most direct evidence for determining the structure of polymer chains. For hydrocarbon polymers the stereoregularity is determined by ^{13}C NMR spectroscopy. The ^{13}C NMR chemical shifts are very

sensitive to the stereochemical configuration of nearby monomer units, because of the effect on chain conformation. Figure 4.6.1 shows the 25 MHz ^{13}C NMR spectra of isotactic, atactic and syndiotactic polypropylene. Spectra are normally recorded at around 130 °C in a polychlorinated benzene such as 1,2,4-trichlorobenzene. The high temperature is necessary to gain maximum resolution.

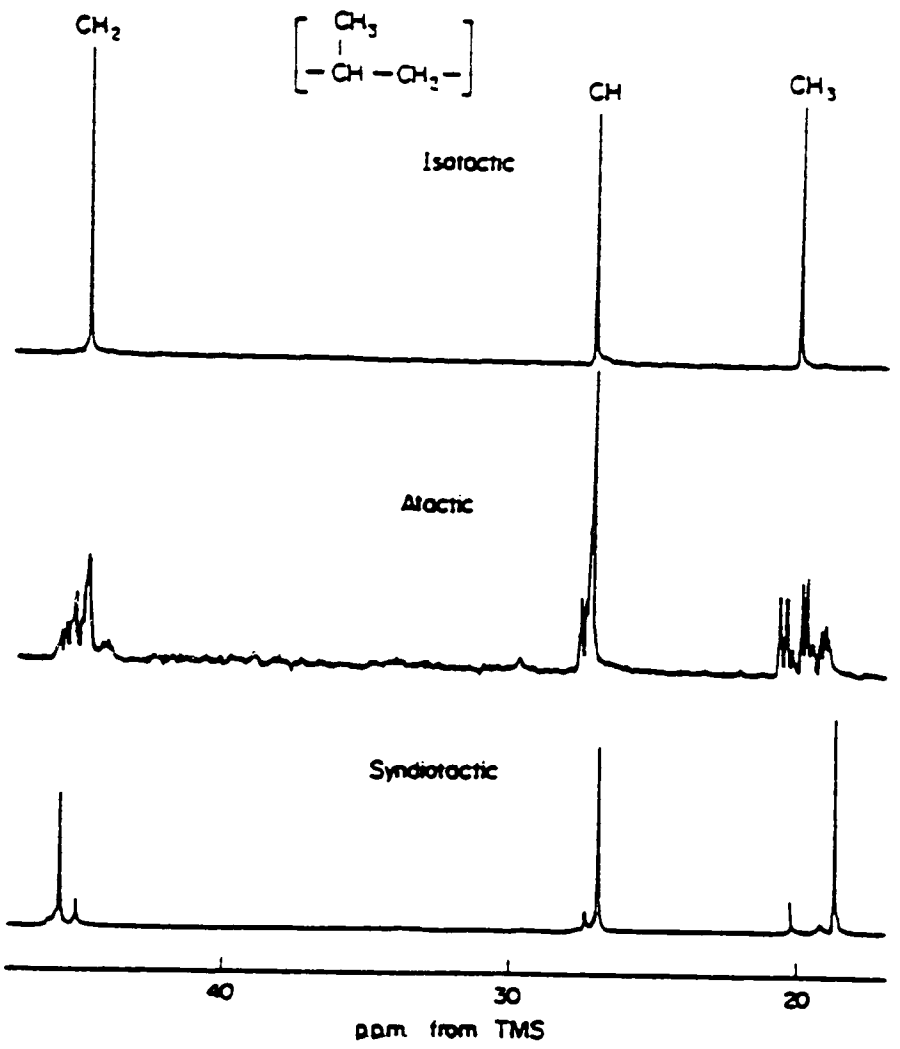

Figure 4.6.1. The 25 MHz ^{13}C NMR spectra of polypropylene: isotactic (top), atactic (middle) and syndiotactic (bottom), observed in 1,2,4-trichlorobenzene at 140 °C.[26]

The polypropylene ^{13}C NMR spectra shown in Figure 4.6.1 all have three distinct regions, corresponding to the methylene (48-45 ppm), methine (30-26 ppm) and methyl (23-19 ppm) carbon atoms. Although configurational sensitivity is shown by all three spectral regions, the methyl region exhibits by far the greatest sensitivity and is of the most value. The chemical shift of each methyl carbon atom in polypropylene is most influenced by the configurations of the neighbouring monomer units, and is influenced to a lesser extent by the configurations of the next-nearest

neighbours. The configurations of more distant monomer units have little effect. As a result of this, the methyl region of stereoirreigular polypropylene shows nine distinguishable bands which have been assigned to the ten unique steric arrangements of five adjacent monomer units, or **pentads**.[27]

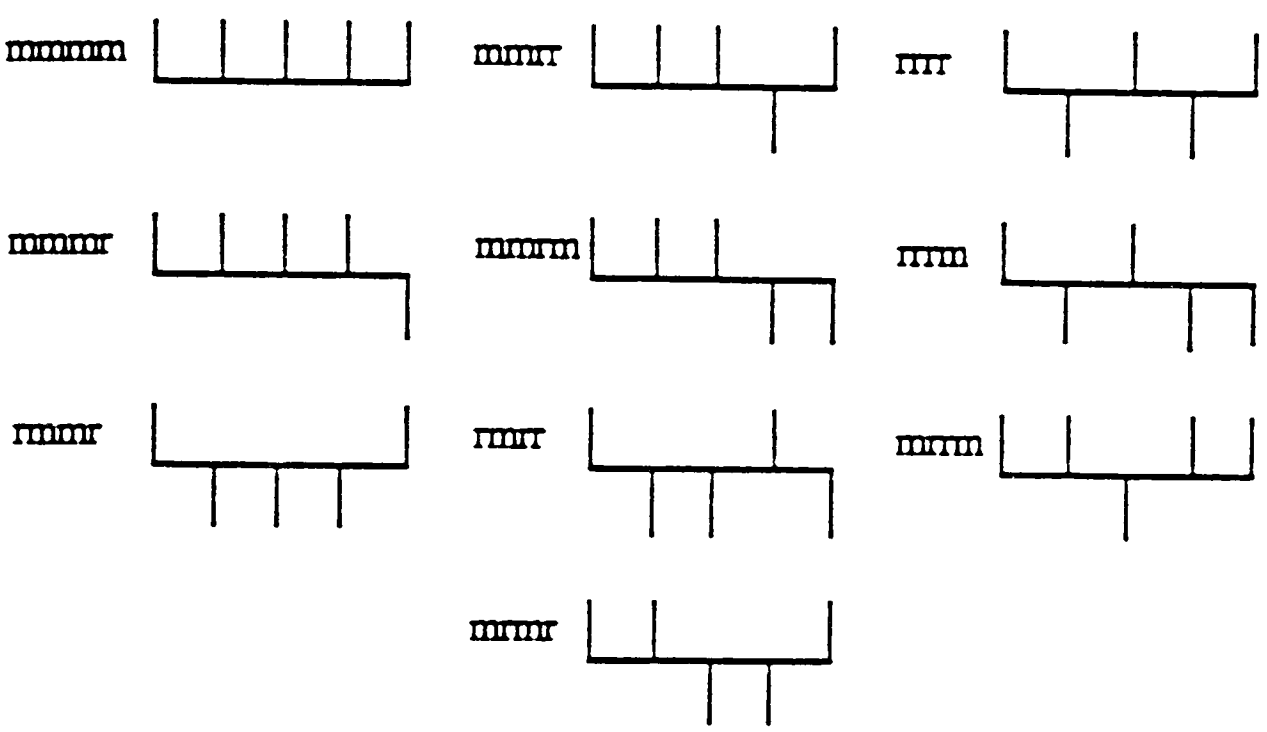

Figure 4.6.2. The ten unique steric pentads

Only nine bands are observed because the mmrm and rmrr pentads have the same chemical shift. The nine bands are divided into three distinct regions corresponding to mm- mr- and rr-centred pentads. The ^{13}C NMR assignments were made by Zambelli, based on model compounds.[27] The methyl region of atactic polypropylene, together with the pentad assignments, is shown if Figure 4.6.3.

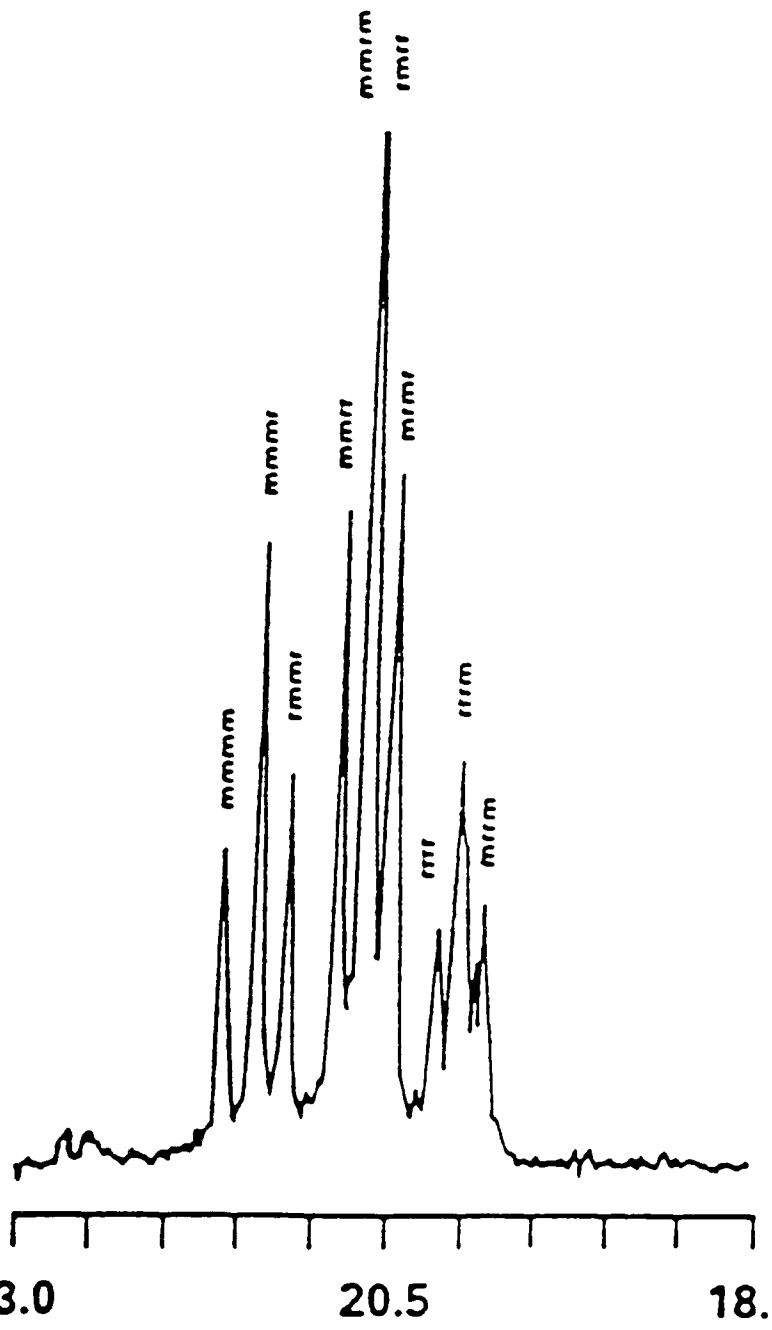

Figure 4.6.3. Methyl region of ^{13}C NMR spectrum of atactic polypropylene[28] showing pentad assignments

The polypropylene samples produced by the new binuclear and mononuclear compounds (with MAO co-catalyst) were all toluene-soluble, highly viscous liquids. The polypropylene ^{1}H and ^{13}C NMR spectra were recorded at 120 ^{o}C in a solvent mixture of 1,2,4-trichlorobenzene and d^{6}-benzene (v/v = 80/20). The ^{1}H and ^{13}C NMR spectra of the polypropylene obtained using $[(\eta^5\text{-}C_5H_5)ZrCl_2\{(\eta^5\text{-}C_5H_4)CMe_2(\eta^5\text{-}C_9H_6)\}ZrCl_2(\eta^5\text{-}C_5H_5)]$ (**8**) / MAO are shown in Figures 4.6.4 and 4.6.5.

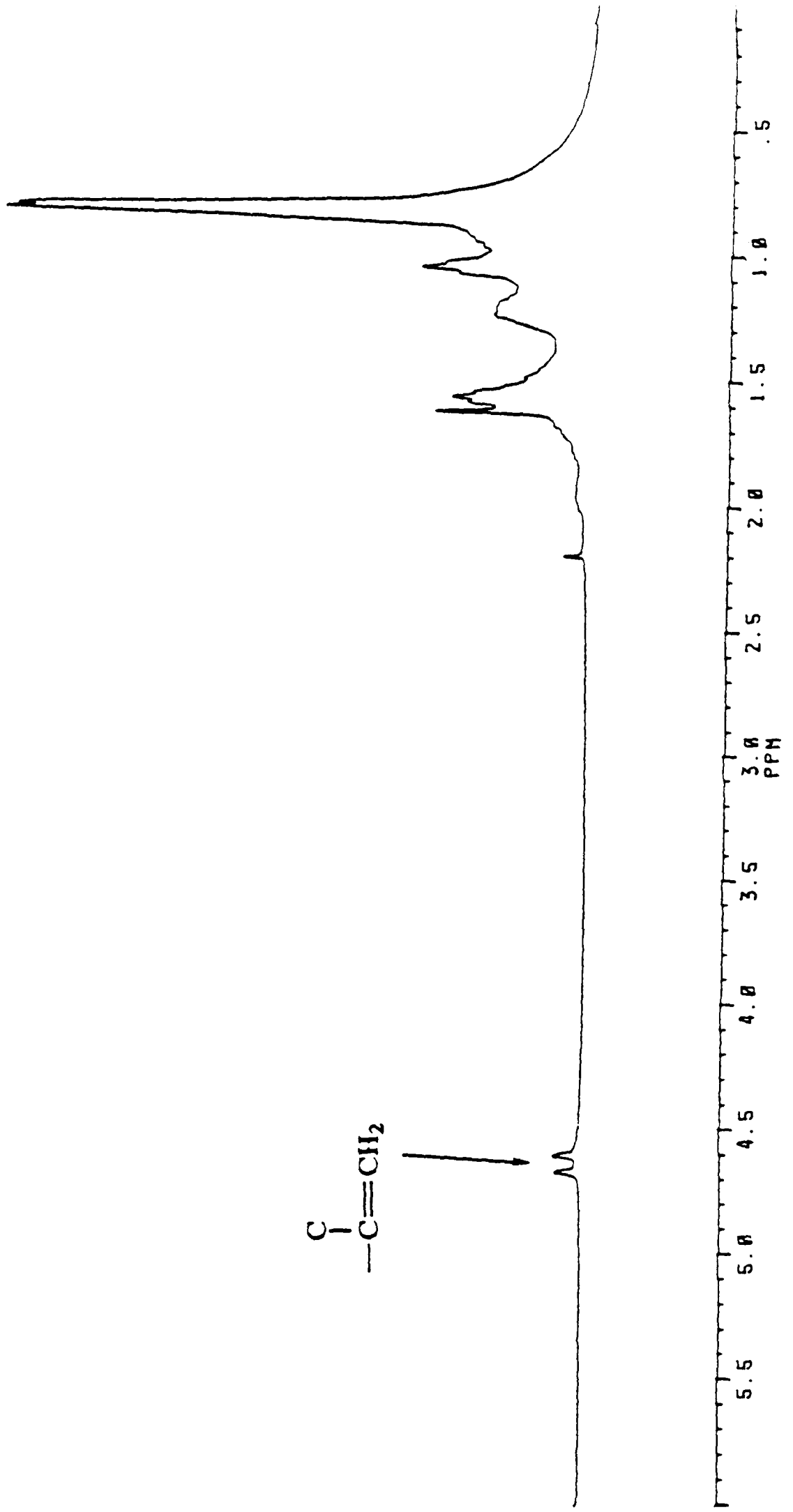

Figure 4.6.4. 300 MHz ^{1}H NMR spectrum

(1,2,4-trichlorobenzene/C_6D_6, 120 °C) of the polypropylene obtained using

$[(\eta^5\text{-}C_5H_5)ZrCl_2\{(\eta^5\text{-}C_5H_4)CMe_2(\eta^5\text{-}C_9H_6)\}ZrCl_2(\eta^5\text{-}C_5H_5)]$ (**8**) / MAO

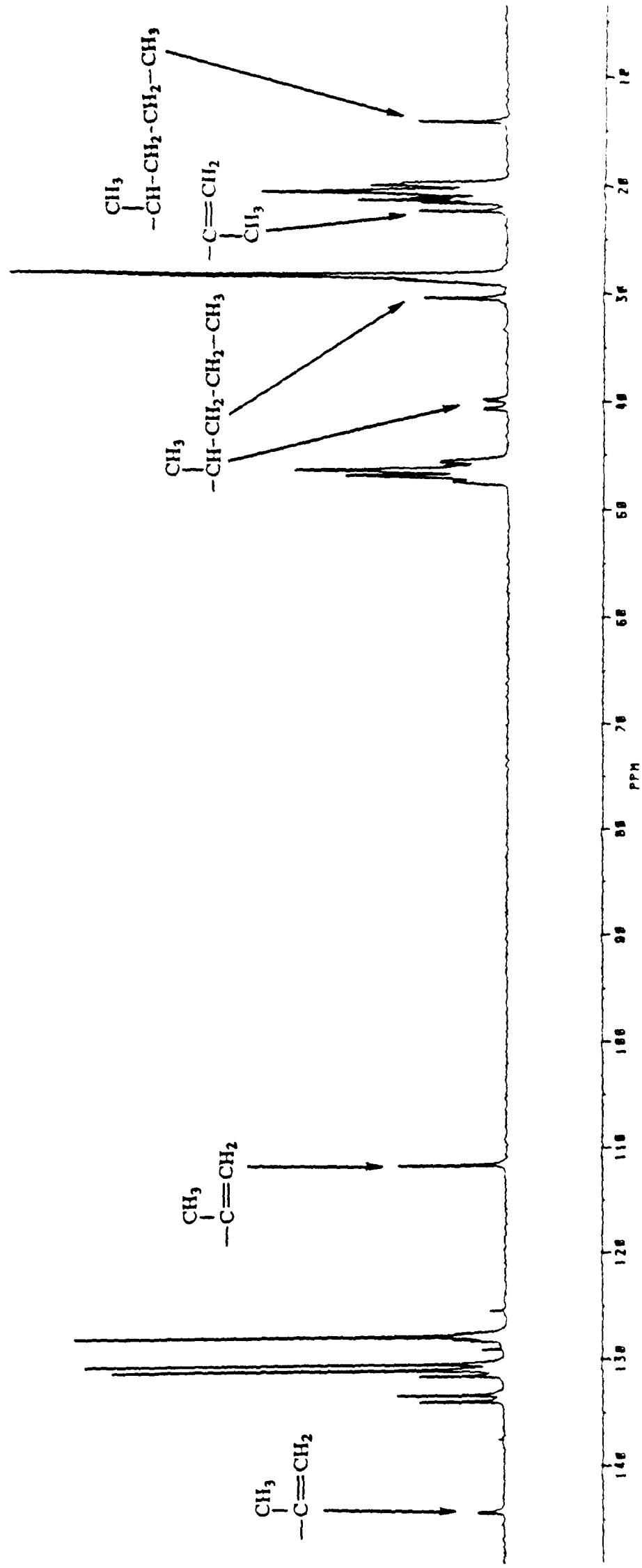

Figure 4.6.5. 75.5 MHz $^{13}C\{^1H\}$ NMR spectrum (1,2,4-trichlorobenzene/C_6D_6, 120 °C) of the polypropylene obtained using $[(\eta^5\text{-}C_5H_5)ZrCl_2\{(\eta^5\text{-}C_5H_4)CMe_2(\eta^5\text{-}C_9H_6)\}ZrCl_2(\eta^5\text{-}C_5H_5)]$ (**8**) / MAO

The ^{13}C NMR spectrum of the polymer obtained using [(η^5-C_5H_5)$ZrCl_2${(η^5-C_5H_4)CMe_2(η^5-C_9H_6)}$ZrCl_2$(η^5-C_5H_5)] (**8**) / MAO is that expected for atactic, low molecular weight polypropylene.[27-31] The methyl region of the spectrum shows the pattern of signals typical of atactic polypropylene.[27-29] The signals labelled in Figure 4.6.5 are those corresponding to the chain-end structures and the significant intensity of these signals indicates low average molecular weight.[29-31] The spectrum shows no detectable signals corresponding to regioirregular (head-to-head or tail-to-tail) structures, suggesting that the polymerization proceeds in a regioregular fashion, probably by primary (1-2) insertion.[31, 32]

The signals at 40.5, 30.8 and 14.3 ppm can be attributed to the presence of n-propyl at the chain end, and the signals at 144.2, 111.5 and 22.4 ppm can be attributed to the presence of vinylidene at the chain-end, by comparison with previous assignments.[29-31] The signals at 22.4 and 14.3 ppm, corresponding to the methyl groups of the vinylidene and n-propyl chain-ends respectively, have approximately equal intensity, suggesting that the n-propyl and vinylidene chain-ends occur in approximately equal amounts. This observation, together with the absence of signals corresponding to other types of chain-end structure, suggests that the main chain transfer process involves β-hydrogen elimination from a regioregular (1-2) monomer unit, followed by initiation of a new polymer chain at a metal-hydrogen bond *via* primary (1-2) insertion, as shown below. The vinylidene chain-end proton signals are seen in the ^1H NMR spectrum of the polypropylene (Figure 4.6.4).

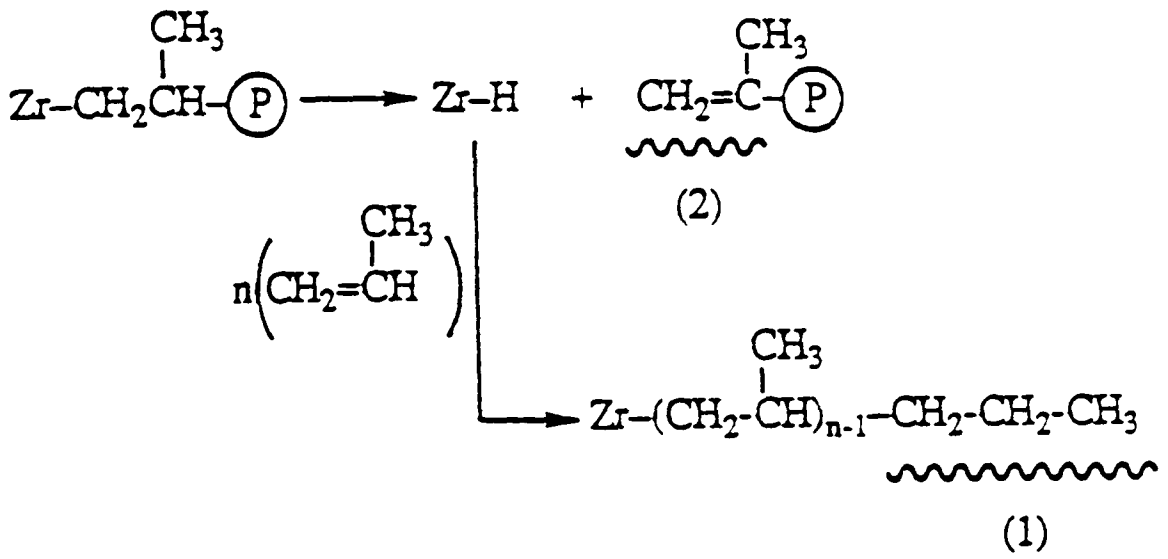

Figure 4.6.6. Primary β-hydrogen elimination / insertion mechanism, giving n-propyl (1) and vinylidene (2) chain end structures.

The ^{1}H and ^{13}C NMR spectra of the polypropylene obtained using compounds **10**, **17** and **20** are very similar to those of the polypropylene produced by compound **8**. The NMR spectra of the polypropylene produced by the compounds $[(\eta^5\text{-}C_5H_5)ZrCl_2\{(\eta^5\text{-}C_5H_4)CMe_2(\eta^5\text{-}C_9H_6)\}M^*Cl_2(\eta^5\text{-}C_5H_5)]$, where M* = Hf (**9**) and M* = Zr (**11**), are also quite similar, except that the chain-end signals are considerably weaker, suggesting higher molecular weights, and the methyl regions of the ^{13}C NMR spectra suggest that the polymers are slightly more isotactic than the polymer obtained using compound **8**.

4.6.3 Stereoregularity

Table 4.3 shows the triad fractions, dyad fractions and triad mechanistic tests for each set of polypropylene ^{13}C NMR data. The methyl pentad signals are divided into three distinct regions corresponding to mm-, mr- and rr-centred pentads. The

integrated intensity of each of these regions corresponds to the [mm], [mr] and [rr] triad fractions. The fractions of meso and racemic dyads are given by:

$$[m] = [mm] + \tfrac{1}{2}[mr] \qquad\qquad [r] = [rr] + \tfrac{1}{2}[mr]$$

The fraction of meso dyads, [m], is sometimes called the statistical isotacticity, and the fraction of racemic dyads, [r], the statistical syndiotacticity.[6]

The data in Table 4.3 show that although the compounds are all chiral, the metallocene/MAO catalyst systems have very low stereospecificities; all of the polymers would normally be considered atactic. In this respect, the low propylene polymerization activity of these systems might be predicted from the properties of mononuclear metallocene/MAO systems, for which high propylene polymerization activity is often associated with high stereospecificity.[6] Compounds **9** and **11** produce slightly more isotactic polymer than the other compounds, and both have hafnium at the C_5H_4 site.

Table 4.3 also shows the results of the triad mechanistic tests. These tests are often applied to ^{13}C NMR data to try to distinguish between enantiomorphic-site control of stereospecificity and chain-end control. These were discussed in Chapter 1. For **enantiomorphic-site control** of olefin polymerization, the stereochemistry of olefin insertion is controlled by the chirality of the catalyst. The test usually applied to determine if enantiomorphic site control is responsible for the stereoselectivity is:

$$2[rr] / [mr] = 1$$

For **chain-end control**, the configuration of the last inserted monomer unit determines the stereochemistry of monomer insertion, resulting in a stereoblock microstructure.[28] The triad test for chain end control is:

$$4[mm][rr] / [mr]^2 = 1$$

Table 4.3. Triad and dyad fractions and triad mechanistic model tests for methyl pentad region of ^{13}C NMR spectra

	triad fractions			dyad fractions		triad tests	
Compound (metals)	[mm]	[mr]	[rr]	[m]	[r]	$4[mm][rr]/[mr]^2$ chain-end	2[rr]/[mr] site
8 (Zr,Zr)	0.26	0.47	0.27	0.49	0.51	1.26	1.16
9 (Hf,Hf)	0.42	0.47	0.11	0.65	0.35	0.82	0.46
10 (Zr,Hf)	0.32	0.48	0.21	0.55	0.45	1.16	0.87
11 (Hf,Zr)	0.39	0.44	0.17	0.61	0.39	1.40	0.78
17 (Zr)	0.28	0.48	0.24	0.52	0.48	1.14	0.98
20 (Zr,Rh)	0.22	0.48	0.29	0.47	0.53	1.15	1.23

The data in Table 4.3 show that the polymer obtained using the mononuclear compound **17** is the only sample to give good agreement one of the mechanistic tests, and it would appear that enantiomorphic-site control is favoured. However, for ideally atactic polypropylene, [m] = [r] = 0.5, and $2[rr] / [mr] = 4[mm][rr] / [mr]^2 = 1$. In other words, these tests can only distinguish between mechanisms of stereoselectivity

when there is significant selectivity, and since all the polymer samples were close to atactic, this is not the case.

It should also be noted that the triad tests described above are simple one-parameter tests and would not be expected to apply if two or more different active catalytic centres were present.[33] The failure of the data to fit these "single active site" models might be due to the presence of two or more different active sites. This might explain why the binuclear compounds give poorer agreement with the tests than the mononuclear compound **17**. Erker has shown that the failure of chiral, non-*ansa*-bridged mononuclear metallocene catatysts to conform to either one model or the other may be due to "double stereodifferentiation", the combined influence of both types of stereochemical control.[34] Similar "double stereodifferentiation" might contribute to the poor agreement of the data in Table 4.3 to the simple mechanistic tests.

4.6.4 Molecular weight

As mentioned before, the intensities of the chain-end signals in the ^{13}C and ^{1}H NMR spectra were significantly lower for the polymers obtained using compounds **9** and **11** than for the other polymer samples, suggesting that the polymers produced by compounds **9** and **11** (with hafnium at the C_5H_4 site) had higher molecular weights. For all of the polymer samples the only chain-end signals observed in the ^{13}C NMR spectra were vinylidene and n-propyl signals, suggesting that the main chain transfer process involves β-hydrogen elimination from a regioregular (1-2) monomer unit, followed by initiation of a new polymer chain at a metal-hydrogen bond via primary (1-2) insertion. This results in an n-propyl group at one end of the chain and a vinylidene group at the other end (see Figure 4.6.6). If this is the case, then the sum of the methyl pentad signal intensities, divided by the intensity of the methyl group at the vinylidene chain end, should give the approximate number of monomer units per polymer chain. Multiplying this number by the molecular mass of the monomer gives an approximate

value for the number-average polymer molecular weight, M_n. The relevant methyl signal integrated intensities were measured, and the results are shown in Table 4.4, together with the [m] and [r] dyad fractions for comparison of polymer molecular weight and tacticity.

Table 4.4. Average polymer chain length and molecular weight (M_n) from ^{13}C NMR

	dyad fractions		average chain length and molecular weight from ^{13}C NMR	
Compound (metals)	[m]	[r]	**chain length** (monomer units)	**M_n** (g mol^{-1})
8 (Zr,Zr)	0.49	0.51	21	870
9 (Hf,Hf)	0.65	0.35	115	4860
10 (Zr,Hf)	0.55	0.45	26	1090
11 (Hf,Zr)	0.61	0.39	76	3180
17 (Zr)	0.52	0.48	34	1430
20 (Zr,Rh)	0.47	0.53	22	920

The data in Table 4.4 suggest that the polypropylene produced by all of the systems is of low molecular weight, which was expected since the polymer samples were all highly viscous liquids. The binuclear catalysts with zirconium at the C_5H_4 site, and the mononuclear compound **17**, produced low molecular weight propylene

oligomers. The highest molecular weight polymer is produced by the dihafnium compound **9**, whilst compound **11** (with hafnium at the C_5H_4 site) produces polymer with an intermediate molecular weight. Mononuclear hafnocene/MAO catalysts typically produce higher molecular weight polymer than analogous zirconocene systems.[3, 6, 12-14] Compound **9** produced the highest molecular weight polymer and the most isotactic. Kaminsky noted that for mononuclear metallocene/MAO systems, the more stereospecific systems produced the higher molecular weight polymer.[6]

4.7 Polymerization of ethylene and propylene using binuclear metallocene-dimethyl derivatives with $[Ph_3C]^+[B(C_6F_5)_4]^-$ and $B(C_6F_5)_3$ co-catalysts

Methylaluminoxane (MAO) is a product of the partial hydrolysis of trimethylaluminium, and is believed to be a mixture of linear and/or cyclic oligomers $[-Al(CH_3)-O-]_n$, together with some coordinated $AlMe_3$.[35, 36] The use of a large excess (typically 500 to 5000 equivalents) of an ill-defined co-catalyst makes study of the detailed polymerization mechanism very difficult. Variations in the exact composition of the methylaluminoxane might mask other, more subtle, factors in comparative studies.[35]

Marks has recently shown that the strong Lewis acid $B(C_6F_5)_3$ is capable of abstracting a methide (CH_3^-) group from a variety of $Cp'_2Zr(CH_3)_2$ complexes (Cp' = η^5-C_5H_5, η^5-1,2-$Me_2C_5H_3$, η^5-C_5Me_5) to form the first stoichiometrically precise, isolable, crystallographically characterised, highly active "cation-like" zirconocene polymerization catalysts, $[Cp'_2Zr(CH_3)]^{\delta+}[CH_3B(C_6F_5)_3]^{\delta-}$.[39, 40] Chien and co-workers have demonstrated that the Lewis acid triphenylcarbenium cation $[Ph_3C]^+$ can perform a similar role. The chiral *ansa*-metallocene dimethyl derivative *rac*-$[\{Et(Ind)_2\}Zr(CH_3)_2]$ and one equivalent of $[Ph_3C]^+[B(C_6F_5)_4]^-$ co-catalyst were shown to catalyse the isospecific polymerization of propylene. It was proposed that

$[Ph_3C]^+$ abstracted a CH_3^- group from the metallocene to form Ph_3CCH_3 and the cationic zirconocene complex $[Et(Ind)_2Zr(CH_3)]^+[B(C_6F_5)_4]^-$.[41]

This section presents the results of a preliminary investigation of the use of these new, well defined co-catalysts, together with two of the novel binuclear metallocene dimethyl compounds, $[(\eta^5\text{-}C_5H_5)M(CH_3)_2\{(\eta^5\text{-}C_5H_4)CMe_2(\eta^5\text{-}C_9H_6)\}M^*(CH_3)_2(\eta^5\text{-}C_5H_5)]$ [M = M* = Zr (**13**) and M = Hf, M* = Zr (**15**)], as olefin polymerization catalysts.

4.7.1. Ethylene polymerization experiments

The polymerizations were carried out under similar conditions (2 bar monomer pressure, 30 °C, 6.25×10^{-6} mol of metallocene compound) and using procedures similar to those employed for the metallocene/MAO experiments. The reaction mixture was stirred for one hour when using $B(C_6F_5)_3$ co-catalyst, or 2 minutes when using $[Ph_3C]^+[B(C_6F_5)_4]^-$ co-catalyst. A two minute reaction time was chosen for the $[Ph_3C]^+[B(C_6F_5)_4]^-$ co-catalysed reactions because the very high activity caused stirring problems if the reaction time was increased. The results of these experiments are shown in Table 4.5.

The polymerization experiments were performed in a total solvent (toluene) volume of 40 cm^3, compared with 210 cm^3 for the metallocene/MAO experiments. When the polymerization experiment using one equivalent (6.25×10^{-6} mol) of $[(\eta^5\text{-}C_5H_5)Zr(CH_3)_2\{(\eta^5\text{-}C_5H_4)CMe_2(\eta^5\text{-}C_9H_6)\}Zr(CH_3)_2(\eta^5\text{-}C_5H_5)]$ (**13**) and two equivalents (1.25×10^{-5} mol) of $[Ph_3C]^+[B(C_6F_5)_4]^-$ was repeated in 200 cm^3 of toluene, no polymerization was observed. However, when a second equivalent of catalyst solution and two more equivalents of co-catalyst solution were added, rapid polymerization was observed and 3.92 g of polyethylene was produced in 10 minutes. This corresponds to an activity of 3800 $kgPE.mol^{-1}.hr^{-1}$ and a relative activity of 16000 $kgPE.mol^{-1}.hr^{-1}C_{mon}^{-1}$ for the second equivalent of catalyst, which is very

similar to the activity obtained when 40 cm^3 of toluene and one equivalent of catalyst was used.

One of the advantages of using a large excess of methylaluminoxane co-catalyst is that this highly reactive alkylaluminium reagent is very effective at "conditioning" the solvent (and reactor surfaces), reacting with trace impurities which might otherwise react with and deactivate the catalyst. This is why most of the methylaluminoxane was added to the reactor, and stirred with the solvent, before the metallocene was added. Like the proposed cationic active species, $[Cp_2M(R)]^+$, methylaluminoxane is highly Lewis acidic and oxophilic, and would be expected to react with many of the same species that would deactivate the catalyst (e.g. traces of water, sulphur compounds, *etc.*). Since a very large excess of MAO is used, this would not be expected to have a significant effect on activity. In contrast, the recently developed $B(C_6F_5)_3$ and $[Ph_3C]^+[B(C_6F_5)_4]^-$ co-catalysts are used in stoichiometric amounts and the resulting catalyst systems are highly sensitive to any trace impurities.

For compound **13** and $[Ph_3C]^+[B(C_6F_5)_4]^-$ co-catalyst, it was found that two equivalents of catalyst in 200 cm^3 of toluene produced almost the same amount of polymer as one equivalent of catalyst in 40 cm^3 of toluene. This suggests that if the cause of the different activites is an impurity in the toluene (and if all other factors are equal), then about 160 cm^3 of toluene would deactivate one equivalent of catalyst, and that for both experiments about 0.75 equivalents of catalyst are active, or at least are not deactivated. If the impurity reacts stoichiometrically with the catalyst, then this would indicate an impurity level of about 40 μM (about 5 ppm). The experiments in Table 4.3 were all preformed using toluene that was pre-dried by standing over 4 Å molecular sieves and then refluxed over molten sodium for at least eight hours before being distilled under a nitrogen atmosphere, then thoroughly deoxygenated before use by bubbling nitrogen through the solvent for approximately one hour.

Table 4.5. Polymerization of ethylene using ~~using~~ binuclear metallocene-dimethyl derivatives with $[Ph_3C]^+[B(C_6F_5)_4]^-$ and $B(C_6F_5)_3$ co-catalysts

Compound (metals)	**co-catalyst**	**equiv. of co-cat.**	**time** (mins)	**Yield** (g)	**Activity** (kgPE. $mol^{-1}.hr^{-1}$).	**Relative Activity** (kgPE.mol^{-1} $.hr^{-1}.C_{mon}^{-1}$)
13 (Zr, Zr)	$[Ph_3C]^+$ $[B(C_6F_5)_4]^-$	2	2	0.85	4100	17000
15 (Hf, Zr)	$[Ph_3C]^+$ $[B(C_6F_5)_4]^-$	2	2	0.46	2200	9400
15 (Hf, Zr)	$B(C_6F_5)_3$	1	60	0.10	16	68
15 (Hf, Zr)	$B(C_6F_5)_3$	2	60	0.33	53	220
15 (Hf, Zr)	$B(C_6F_5)_3$	16	60	0.25	40	170

2 bar absolute monomer pressure, 30 °C, 40 cm^3 toluene solvent

6.25 x 10^{-6} moles of compound, C_{mon} = 0.235 mol dm^{-3}

The dizirconium compound $[(\eta^5\text{-}C_5H_5)Zr(CH_3)_2\{(\eta^5\text{-}C_5H_4)CMe_2(\eta^5\text{-}C_9H_6)\}Zr(CH_3)_2(\eta^5\text{-}C_5H_5)]$ (**13**) with two equivalents of $[Ph_3C]^+[B(C_6F_5)_4]^-$ co-catalyst was the most active system, with a relative activity more than ten times that of the analogous compound **8** / MAO system. The turnover rate (41 insertions per second) is similar to that reported by Marks for the polymerization of ethylene by $[(\eta^5\text{-}C_5H_5)_2Zr(CH_3)]^+[CH_3B(C_6F_5)_3]^-$ at 25 °C (45 insertions per second).[39]

The hafnium-zirconium heterobimetallic compound $[(\eta^5\text{-}C_5H_5)Hf(CH_3)_2\{(\eta^5\text{-}C_5H_4)CMe_2(\eta^5\text{-}C_9H_6)\}Zr(CH_3)_2(\eta^5\text{-}C_5H_5)]$ (**15**) was tested with two equivalents of $[Ph_3C]^+[B(C_6F_5)_4]^-$ co-catalyst, and also with 1, 2 and 16 equivalents of $B(C_6F_5)_3$. The activity of **15** with two equivalents of $[Ph_3C]^+[B(C_6F_5)_4]^-$ was very high, producing 0.42 g of polyethylene in only 2 minutes, corresponding to a relative activity of 9400 kgPE.mol^{-1}.hr$^{-1}C_{mon}^{-1}$. However, the relative activity with two equivalents of $B(C_6F_5)_3$ co-catalyst was much lower (220 kgPE.mol^{-1}.hr$^{-1}C_{mon}^{-1}$), and was similar to the activity of the analogous compound **11** / MAO stysem.

When compound **15** was used with two equivalents of $B(C_6F_5)_3$ co-catalyst, the system remained active for the whole hour of the experiment and 0.33 g of polyethylene was obtained. When one equivalent (6.25×10^{-6} mol) of $B(C_6F_5)_3$ co-catalyst was used, the system was again active for the whole hour of the experiment but only 0.10 g of polyethylene was obtained. When 16 equivalents (1.0×10^{-4} mol) of $B(C_6F_5)_3$ was used, the system appeared to be more active initially but after ten minutes the activity was very low, and only 0.25 g of polyethylene was obtained after one hour. These observations are consistent with a stoichiometric reaction between the binuclear compound **15** and the $B(C_6F_5)_3$ co-catalyst. It would appear that the catalyst becomes deactivated in the presence of excess of $B(C_6F_5)_3$.

The reaction of $[Ph_3C]^+[B(C_6F_5)_4]^-$ with zirconocene dialkyl compounds, $[Cp'_2ZrR_2]$, is thought to form a cationic zirconocene alkyl species, $[Cp'_2ZrR]^+[B(C_6F_5)_4]^-$, whilst $B(C_6F_5)_3$ has been shown to only partially abstract the alkide (R^-) group to give a "cation-like" species, with a very close association between the cation and the anion.[39-42] Methylaluminoxane is also believed to partially abstract a halide or alkide group, to give a tight ion pair or a strongly polarized species. The higher ethylene polymerization activity of compound **15** with $[Ph_3C]^+[B(C_6F_5)_4]^-$ might reflect the presence of a more "naked" cationic centre, rather than a "tight ion pair" with $B(C_6F_5)_3$ co-catalyst, or compound **11** with MAO. It was shown that neither the $[Ph_3C]^+[B(C_6F_5)_4]^-$ nor $B(C_6F_5)_3$ co-catalysts polymerized ethylene in the absence of the metallocene compounds.

4.7.2. Propylene polymerization experiments

The binuclear zirconium compound $[(\eta^5\text{-}C_5H_5)Zr(CH_3)_2\{(\eta^5\text{-}C_5H_4)CMe_2(\eta^5\text{-}C_9H_6)\}Zr(CH_3)_2(\eta^5\text{-}C_5H_5)]$ (**13**) was tested as a propylene polymerization catalyst with $[Ph_3C]^+[B(C_6F_5)_4]^-$ and $B(C_6F_5)_3$ co-catalysts. The polymerization experiments were performed under conditions similar to those employed for the ethylene polymerizations, except: (i) a solution of 5.0×10^{-5} mol of compound **13** in 10 cm^3 of toluene was pre-saturated with propene at 2 bar pressure and 30 °C, (ii) 1.0×10^{-4} mol of the co-catalyst in 10 cm^3 of toluene was then added, and (iii) the reaction mixture was stirred at 30 °C under 2 bar propylene pressure for four hours. Compared with the ethylene polymerization experiments, eight times the amount of catalyst and half the total solvent volume was used. The polypropylene was soluble in toluene and was isolated as described previously. The results are shown in Table 4.6.

Table 4.6. Polymerization of propylene using a binuclear metallocene-dimethyl derivative with $[Ph_3C]^+[B(C_6F_5)_4]^-$ and $B(C_6F_5)_3$ co-catalysts

Compound (metals)	**co-catalyst**	**equiv. of co-cat.**	**Yield** (g)	**Activity** (kgPP. $mol^{-1}.hr^{-1}$)	**Relative Activity** (kgPP.mol^{-1} $.hr^{-1}.C_{mon}^{-1}$)
13 (Zr, Zr)	$[Ph_3C]^+$ $[B(C_6F_5)_4]^-$	2	0.15	0.75	0.60
13 (Zr, Zr)	$B(C_6F_5)_3$	2	trace	---	---

2 bar absolute monomer pressure, 30 °C, 20 cm^3 toluene solvent

5.0×10^{-5} moles of compound, C_{mon} = 1.26 mol dm^{-3}

Compound **13** with two equivalents of $[Ph_3C]^+[B(C_6F_5)_4]^-$ co-catalyst showed very low activity for propylene polymerization. The relative activity was less than one tenth that of the analogous compound **8** / MAO system. This is in sharp contrast to the ethylene polymerization activity of **13** with $[Ph_3C]^+[B(C_6F_5)_4]^-$ co-catalyst, which was more than ten times higher that of the compound **8** / MAO system. The ^{13}C NMR spectrum of the polypropylene produced by compound **13** showed it to be an atactic, low molecular weight polymer. Compound **13** with two equivalents of $B(C_6F_5)_3$ co-catalysts showed almost no activity, only a trace of oily product was obtained from the reaction.

4.8 Summary

This Chapter describes the results of some preliminary olefin polymerization reactions using novel homo- and hetero-binuclear compounds and related monounclear compounds as catalysts. The novel binuclear metallocene compounds $[(\eta^5\text{-}C_5H_5)MCl_2\{(\eta^5\text{-}C_5H_4)CMe_2(\eta^5\text{-}C_9H_6)\}M^*Cl_2(\eta^5\text{-}C_5H_5)]$ [M = M* = Zr (**8**); M = M* = Hf (**9**); M = Zr, M* = Hf (**10**); M = Hf, M* = Zr (**11**)] together with methylaluminoxane co-catalyst, were tested as catalysts for the polymerization of ethylene and propylene. For ethylene polymerization, the activities of the catalysts appeared to be primarily determined by the metal at the C_5H_4 site, and the metal-dependence of activity was similar to that observed for the related mononuclear compounds $[(\eta^5\text{-}C_5H_5)MCl_2\{(\eta^5\text{-}C_5H_4)CMe_2(C_9H_7)\}]$ [M = Zr (**17**), Hf (**18**)]. For propylene polymerization catalysed by the binuclear compounds with MAO co-catalyst, the the activity showed a strong dependence on the metals at both sites, and was much less well predicted from the activity of mononuclear compounds. ^{13}C NMR studies showed that the polypropylene produced by all of the binuclear compounds was of low molecular weight and atactic. The polymer produced by the dihafnium

compound **9** had the highest molecular weight and was the most isotactic, but the molecular weight and stereoregularity were still very low.

The novel binuclear compounds $[(\eta^5\text{-}C_5H_5)M(CH_3)_2\{(\eta^5\text{-}C_5H_4)CMe_2(\eta^5\text{-}C_9H_6)\}M^*(CH_3)_2(\eta^5\text{-}C_5H_5)]$ [M = M* = Zr (**13**) and M = Hf, M* = Zr (**15**)] were tested as olefin polymerization catalysts together with the Lewis acid co-catalysts $[Ph_3C]^+[B(C_6F_5)_4]^-$ and $B(C_6F_5)_3$. Compounds **13** and **15** both showed very high ethylene polymerization activities when used with two equivalents of $[Ph_3C]^+[B(C_6F_5)_4]^-$ co-catalyst. Compound **15** showed much lower ethylene polymerization activity when used with $B(C_6F_5)_3$ co-catalyst, and the activity was sensitive to the amount of co-catalyst used. The dizirconium compound **13** catalysed the polymerization of propylene with low activity when used with $[Ph_3C]^+[B(C_6F_5)_4]^-$ co-catalyst, and was inactive when used with $B(C_6F_5)_3$ co-catalyst.

The binuclear compounds show some interesting differences in their activities for ethylene and propylene polymerization, but it is difficult to say much more. If the catalytic behaviour of the novel binuclear systems is to be understood, then many more experiments would be necessary, using different polymerization conditions (temperature, monomer pressure, catalyst and co-catalyst concentrations, *etc.*). The properties of the binuclear compounds would need to be compared with those of model compounds for **both** sites, and the model compounds should be tested both individually and in combination. Only then might the consequences of linking the metal centres with an inter-annular bridge become clear.

References for Chapter 4

1. W. Kaminsky, M. Miri, H. Sinn and R. Woldt, *Makromol. Chem., Rapid Commun.*, 1983, **4**, 417.
2. E. Giannetti, G. M. Nicoletti and R. Mazzocchi, *J. Polym. Sci., Polym. Chem. Ed.*, 1985, **23**, 2117.
3. Nobuhide Ishihara, D. Phil. Thesis, University of Oxford, 1990; M. L. H. Green and N. Ishihara, *J. Chem., Soc., Dalton Trans*, 1994, in press.
4. A. G. Massey and A. J. Park, *J. Organomet. Chem.*, 1964, **2**, 245.
5. J. C. W. Chien, W.M. Tsai and M. D. Rausch, *J. Am. Chem. Soc.*, 1991, **113**, 8570.
6. W. Kaminsky, R. Engerhausen, K. Zoumis, W. Spalek and J. Rohrmann, *Makromol. Chem.*, 1992, **193**, 1643.
7. B. Rieger, X. Mu, D. T. Mallin, M. D. Rausch and J. C. W. Chien, *Macromolecules*, 1990, **23**, 3559.
8. S. Jungling, R. Mulhaupt and H. Plenio, *J. Organomet. Chem.*, 1993, **460**, 191.
9. Landolt-Bornstein, Springer-Verlag, Berlin, 6th edition, 1976, vol. IV, part 4-c1.
10. A. Ahlers and W. Kaminsky, *Makromol. Chem., Rapid Commun.*, 1988, **9**, 457.
11. J. A. Bandy, M. L. H. Green, I. M. Gardiner and K. C. Prout, *J. Chem., Soc., Dalton Trans*, 1991, 2207.
12. W. Spalek , M. Antberg, V. Dolle, R. Klein, J. Rohrmann and A. Winter, *New J. Chem.*, 1990, **14**, 499.
13. J. A. Ewen, L. Haspeslagh, J. L. Atwood and H. Zhang, *J. Am. Chem. Soc.*, 1987, **109**, 6544.
14. J. A. Ewen, L. Haspeslagh, M. J. Elder, J. L. Atwood, H. Zhang and H. N. Cheng, in *Transition Metals and Organometallics as Catalysts for Olefin Polymerization*, W. Kaminsky and H. Sinn, Eds., Springer, New York, 1988.

15. L. E. Schock and T. J. Marks, *J. Am. Chem. Soc.*, 1988, **110**, 7701.

16. J. A. Martinho Simoes and J. L. Beauchamp, *Chem. Rev.*, 1990, **90**, 629.

17. N. Piccolrovazzi, P. Pino, G. Consiglio, A. Sironi and M. Moret, *Organometallics*, 1990, **9**, 3098.

18. R. M. Waymouth, B. D. Santarsiero and R. H. Grubbs, *J. Am. Chem. Soc.*, 1984, **106**, 4050.

19. K. P. Reddy and J. L. Petersen, *Organometallics*, 1989, **8**, 547.

21. K. P. Reddy and J. L. Petersen, *Organometallics*, 1989, **8**, 2107.

22. J. Cacciola, K. P. Reddy and J. L. Petersen, *Organometallics*, 1992, **11**, 665.

23. C. J. Curtis and R. C. Haltiwanger, *Organometallics*, 1991, **10**, 3220.

24. G. Erker, R. Noe, C. Kruger and S. Werner, *Organometallics*, 1992, **11**, 4174.

25. H. L. Frisch, C. L. Mallows and F. A. Bovey, *J. Chem. Phys.*, 1966, **45**, 1565.

26. *Comprehensive Polymer Science*, G. Allen and J. C. Bevington, Eds., Pergamon Press, Oxford, 1989, vol. 1, ch. 17, pp 354.

27. A. Zambelli, P. Locatelli, G. Bajo and F. A. Bovey, *Macromolecules*, 1975, **8**, 687.

28. J. A. Ewen, *J. Am. Chem. Soc.*, 1984, **106**, 6355.

29. T. Tsutsui, A. Mizuno and N. Kashiwa, *Polymer*, 1989, **30**, 428.

30. H. N. Cheng and D. A. Smith, *Macromolecules*, 1986, **19**, 2065.

31. H. N. Cheng and J. A. Ewen, *Makromol. Chem.*, 1989, **190**, 1931.

32. H. N. Cheng and G. H. Lee, *Macromolecules*, 1987, **20**, 436.

33. Y. Inoue, Y. Itabashi, R. Chujo and Y. Doi, *Polymer*, 1989, **30**, 428.

34. G. Erker, R. Nolte, R. Aul, S. Wilker, C. Kruger and R. Noe, *J. Am. Chem. Soc.*, 1991, **113**, 7594.

35. E. Giannetti, G. M. Nicoletti and R. Mazzocchi, *J. Polym. Sci., Polym. Chem. Ed.*, 1985, **23**, 2117.

36. W. Kaminsky and R. Steiger, *Polyhedron*, 1988, **7**, 2375.

37. C. Sishta, R. M. Hathorn and T. Marks, *J. Am. Chem. Soc.*, 1992, **114**, 1112.

38. D. Cam and U. Giannini, *Makromol. Chem.*, 1992, **193**, 1049.

39. X. Yang, C. L. Stern and Tobin J. Marks, *J. Am. Chem. Soc.*, 1991, **113**, 3623.

40. T. J. Marks, *Acc. Chem. Res.*, 1992, **25**, 57.

41. J. C. W. Chien, W. M. Tsai and M. D. Rausch, *J. Am. Chem. Soc.*, 1991, **113**, 8570.

42. M. Bochmann and S. J. Lancaster, *Organometallics*, 1993, **12**, 633.

CHAPTER FIVE

Experimental Details

5.1 General experimental details

5.1.1 Techniques

All manipulations of air- and/or moisture-sensitive materials were carried out in an inert atmosphere using either a dual vacuum/nitrogen line and standard Schlenk techniques, or in an inert atmosphere dry box containing nitrogen. In each case the nitrogen was purified by passage over 4 Å molecular sieves, and either BASF catalyst for the dry box, or MnO for the Schlenk line. Solvents and solutions were transferred, using a positive pressure of nitrogen, through stainless steel cannulae. Filtrations were generally performed using modified stainless steel cannulae which could be fitted with glass fibre filter discs. All glassware and cannulae were dried overnight at 200 °C before use.

5.1.2 Solvents and general materials

Solvents were pre-dried by standing over 4 Å molecular sieves and then refluxed and distilled under a nitrogen atmosphere from sodium/potassium alloy (1:3 w/w) [pentane, petroleum ether (bp. 40-60 °C), diethyl ether]; sodium [1,2-bis(methoxy)ethane, toluene]; potassium (tetrahydrofuran) or phosphorus pentoxide (dichloromethane). All solvents were thoroughly deoxygenated before use by bubbling dinitrogen through the solvent for at least 30 minutes.

Deuterated solvents for NMR studies were stored in Young's ampoules over 4 Å molecular sieves under a nitrogen atmosphere (C_6D_6, CD_2Cl_2), or refluxed with potassium metal and stored over a potassium film in a Young's ampoule under a nitrogen atmosphere (d^8-THF). NMR solvents were transferred using a teat pipette in an inert atmosphere dry box.

5.2 Experimental details for Chapter 2

5.2.1 Preparation of 6,6-dimethylfulvene

A modification of a literature preparation[1] of 6,6-dimethylfulvene was used, in which pyrrolidine catalyses the condensation reaction between cyclopentadiene and acetone. Cyclopentadiene monomer (33 g, 0.50 mol) and acetone (29 g, 0.50 mol) were added to degassed reagent grade methanol (200 cm^3). The solution was stirred and cooled to 0 °C, then pyrrolidine (53.3 g, 0.75 mol) was added. The resulting bright yellow solution was stirred for a further hour at room temperature, cooled to 0 °C and neutralised with acetic acid (45 g, 0.75 mol). The mixture was diluted with diethyl ether (200 cm^3) and deionised water (150 cm^3) and transferred to a separating funnel. The aqueous layer was separated and washed with diethyl ether (2 x 50 cm^3). The combined organic fractions were washed with water (4 x 50 cm^3) and saturated NaCl solution (3 x 50 cm^3) then dried over $MgSO_4$. The mixture was then filtered, and the bright yellow filtrate was concentrated under reduced pressure at 0 °C until all the diethyl ether was removed, leaving the pure product as an orange oil. Yield 43 g (81 %).

5.2.2 Preparation of $[\{Me_2C(C_5H_4)(C_9H_6)\}Li_2\{0.6(Et_2O)\}]$

A solution of 6,6-dimethylfulvene (12.4 g, 0.117 mol) in diethyl ether (50 cm^3) was added dropwise, over one hour, to a stirred solution of lithium indenide (LiC_9H_7, 15 g, 0.123 mol) in diethyl ether (300 cm^3) at 0 °C. The ice bath was then removed and the solution stirred for a further 22 hours at room temperature. The reaction mixture was then cooled to 0 °C and n-BuLi (0.117 mol, 68 cm^3 of 1.7 M hexane solution) was added dropwise over one hour. After stirring for a further 20 hours at room temperature, the pale yellow solid product was isolated by filtration, washed with four 50 cm^3 portions of diethyl ether and dried *in vacuo*. Yield 29 g (89 %). (The

amount of solvating diethyl ether, as determined by ^1H NMR, varied between 0.6 and 0.8 equivalents in subsequent preparations).

5.2.3 Preparation of $[(\eta^5\text{-}C_5H_5)MCl_3\cdot DME]$ (M = Zr, Hf) and $[(\eta^5\text{-}C_5H_5)HfCl_3\cdot 2THF]$

$[(\eta^5\text{-}C_5H_5)ZrCl_3\cdot DME]$ and $[(\eta^5\text{-}C_5H_5)HfCl_3\cdot DME]$ were prepared by the literature method.[2] It was found that the hafnium compound prepared in this fashion was contaminated with $[(n\text{-}Bu)_3SnCl]$ (a by-product), but could be purified by washing with petroleum ether (bp. 40-60 °C), or by re-crystallisation from THF giving $[(\eta^5\text{-}C_5H_5)HfCl_3\cdot 2THF]$.

5.2.4 Preparation of $[\{Me_2C(\eta^5\text{-}C_5H_4)(\eta^2\text{-}C_9H_6)\}Zr(\eta^5\text{-}C_5H_5)Cl]$ (1)

The pale yellow powder $[\{Me_2C(C_5H_4)(C_9H_6)\}Li_2\{0.6(Et_2O)\}]$ (3.95 g, 14.2 mmol) and the white powder $[(\eta^5\text{-}C_5H_5)ZrCl_3\cdot DME]$ (5.0 g, 14.2 mmol) were weighed into a Schlenk tube. Toluene (300 cm^3) was added at room temperature resulting in an immediate colour change, giving a deep red reaction mixture which was stirred for a further 16 hours at room temperature. Filtration, followed by concentration of the solution under reduced pressure and cooling to -20 °C afforded red crystals of **1**. Yield 3.75 g (64 %).

In a modified procedure, toluene (300 cm^3) at -78 °C was added to a stirred mixture of $[\{Me_2C(C_5H_4)(C_9H_6)\}Li_2\{0.75(Et_2O)\}]$ (4.11 g, 14.2 mmol) and $[(\eta^5\text{-}C_5H_5)ZrCl_3\cdot DME]$ (4.95 g, 14.0 mmol) also at -78 °C. The resulting orange mixture was allowed to warm to room temperature over one hour, during which time it slowly darkened to a deep red colour, and was stirred at room temperature for a further 16 hours. Filtration, followed by concentration of the solution under reduced pressure and cooling to -20 °C afforded red crystals of **1**. Yield 4.35 g (75 %).

5.2.5 Preparation of [{$Me_2C(\eta^5\text{-}C_5H_4)(\eta^2\text{-}C_9H_6)$}$Hf(\eta^5\text{-}C_5H_5)Cl$] (**2**)

Toluene (250 cm^3) was added to a stirred mixture of [{$Me_2C(C_5H_4)(C_9H_6)$}Li_2{$0.6(Et_2O)$}] (3.2 g, 11.3 mmol) and [(η^5-C_5H_5)$HfCl_3$·2THF] (5.6 g, 11.3 mmol) at room temperature. The resulting orange/red coloured mixture was stirred for a further 16 hours. Filtration, followed by concentration of the solution under reduced pressure and cooling to -20 °C afforded dark orange crystals of **2**. Yield 4.0 g (71 %).

In a modified procedure, toluene (300 cm^3) at -78 °C was added to a stirred mixture of [{$Me_2C(C_5H_4)(C_9H_6)$}Li_2{$0.75(Et_2O)$}] (4.11 g, 14.2 mmol) and [(η^5-C_5H_5)$HfCl_3$·DME] (6.13 g, 13.9 mmol) at -78 °C. The resulting yellow mixture was allowed to warm to room temperature over one hour, during which time it slowly darkened to an orange colour, and was stirred for a further 18 hours at room temperature. Filtration, followed by concentration of the solution under reduced pressure and cooling to -20 °C afforded orange crystals of **2**. Yield 5.65 g (81 %).

5.2.6 Preparation of 6,6-pentamethylenefulvene

A modification of a literature preparation[1] of 6,6-pentamethylenefulvene was used. Cyclopentadiene monomer (19.8 g, 0.30 mol) and cyclohexanone (29.4 g, 0.30 mol) were added to degassed reagent grade methanol (100 cm^3). The solution was stirred and cooled to 0 °C, then pyrrolidine (32 g, 0.45 mol) was added. The resulting bright yellow solution was stirred for a further hour at room temperature then cooled to 0 °C and neutralised with acetic acid (27 g, 0.45 mol). The mixture was diluted with diethyl ether (100 cm^3) and deionised water (100 cm^3) and transferred to a separating funnel. The aqueous layer was separated and washed with diethyl ether (2 x 50 cm^3). The combined organic fractions were washed with water (4 x 50 cm^3) and saturated NaCl solution (3 x 50 cm^3) then dried over $MgSO_4$. The mixture was then filtered and the bright yellow filtrate was concentrated under reduced pressure at 0 °C

until all the diethyl ether was removed, leaving the pure product as an orange oil. Yield 41.2 g (94 %).

5.2.7 Preparation of $[\{(CH_2)_5C(C_5H_4)(C_9H_6)\}Li_2\{0.8(Et_2O)\}]$

A solution of 6,6-pentamethylenefulvene (2.68 g, 18.3 mmol) in diethyl ether (20 cm^3) was added dropwise, over one hour, to a stirred solution of lithium indenide (LiC_9H_7, 2.24 g, 18.3 mmol) in diethyl ether (180 cm^3) at 0 °C. The ice bath was then removed and the solution was stirred for a further 22 hours at room temperature. The reaction mixture was then cooled to 0 °C and n-BuLi (22 mmol, 13 cm^3 of 1.7 M hexane solution) was added dropwise over 20 minutes. After stirring for a further 20 hours at room temperature, the pale yellow solid product was isolated by filtration, washed with two 30 cm^3 portions of diethyl ether and dried *in vacuo*. Yield 5.6 g (92 %).

5.2.8 Preparation of

$$[\{(CH_2)_5C(\eta^5\text{-}C_5H_4)(\eta^2\text{-}C_9H_6)\}Zr(\eta^5\text{-}C_5H_5)Cl]\cdot[0.5(C_6H_5CH_3)] \quad (3)$$

Toluene (90 cm^3) was added to a stirred mixture of $[\{(CH_2)_5C(C_5H_4)(C_9H_6)\}Li_2\{0.8(Et_2O)\}]$ (0.50 g, 1.5 mmol) and $[(\eta^5\text{-}C_5H_5)ZrCl_3\cdot DME]$ (0.53 g, 1.5 mmol) at room temperature. The resulting red coloured mixture was stirred for a further 16 hours. Filtration, followed by concentration of the solution under reduced pressure, and cooling to -20 °C, afforded red crystals of **3**. Yield 0.59 g (79 %).

5.2.9 Preparation of

$[\{(CH_2)_5C(\eta^5\text{-}C_5H_4)(\eta^2\text{-}C_9H_6)\}Hf(\eta^5\text{-}C_5H_5)Cl]\cdot[0.5(C_6H_5CH_3)]$ (4)

Toluene (90 cm^3) was added to a stirred mixture of $[\{(CH_2)_5C(C_5H_4)(C_9H_6)\}Li_2\{0.8(Et_2O)\}]$ (0.50 g, 1.5 mmol) and $[(\eta^5\text{-}C_5H_5)HfCl_3\cdot 2THF]$ (0.74 g, 1.5 mmol) at room temperature. The resulting orange/red mixture was stirred for a further 16 hours. Filtration followed by concentration of the solution under reduced pressure and cooling to -20 °C, afforded dark orange crystals of **4**. Yield 0.51 g (58 %).

5.2.10 Preparation of $[\{Me_2C(C_5H_4)(C_{13}H_8)\}Li_2\{0.75(Et_2O)\}]$

A solution of 6,6-dimethylfulvene (2.16 g, 2.45 cm^3, 20.3 mmol) in diethyl ether (60 cm^3) was added dropwise, over 40 minutes, to a stirred solution of lithium fluorenide $[LiC_{13}H_9\cdot Et_2O$, 5.0 g, 20.3 mmol] in diethyl ether (200 cm^3) at 0 °C. The ice bath was then removed and the solution was stirred for a further 22 hours at room temperature. The reaction mixture was then cooled to 0 °C and n-BuLi (21.6 mmol, 12 cm^3 of 1.8 M hexane solution) was added dropwise over 40 minutes. After stirring for a further 4 hours at room temperature, the bright yellow solid product was isolated by filtration, washed with 50 cm^3 of diethyl ether and dried *in vacuo*. Yield 6.2 g (90 %).

5.2.11 Preparation of $[\{Me_2C(\eta^5\text{-}C_5H_4)(\eta^3\text{-}C_{13}H_8)\}Zr(\eta^5\text{-}C_5H_5)Cl]$ (5)

Toluene (90 cm^3) was added to a stirred mixture of $[\{Me_2C(C_5H_4)(C_{13}H_8)\}Li_2\{0.75(Et_2O)\}]$ (0.96 g, 2.8 mmol) and $[(\eta^5\text{-}C_5H_5)ZrCl_3\cdot DME]$ (1.0 g, 2.8 mmol) at room temperature. The resulting red mixture was stirred for a further 16 hours. Filtration followed by removal of volatiles under reduced pressure gave crude product (*ca.* 80 % compound **5** by NMR). This red solid

was washed with petroleum ether (bp. 40-60 °C) then extracted into toluene (110 cm^3). The toluene solution, when concentrated under reduced pressure and cooled to -20 °C, afforded red crystals of **5**. Yield 0.75 g (57 %).

5.2.12 Preparation of [{$Me_2C(\eta^5\text{-}C_5H_4)_2$}Zr($\eta^5$-$C_5H_5$)Cl] (6)

Toluene (400 cm^3) was added to a stirred mixture of [{$Me_2C(C_5H_4)_2$}Li_2] (1.0 g, 5.4 mmol)[3] and [(η^5-C_5H_5)$ZrCl_3$·DME] (1.9 g, 5.4 mmol) at room temperature. The resulting pale yellow mixture was stirred for a further 60 hours at room temperature. Filtration, followed by concentration of the filtrate under reduced pressure and cooling to -20 °C, afforded pale yellow crystals of **6** (0.43 g). The reaction residue was extracted with a further 300 cm^3 of toluene, which yielded a further 0.38 g of **6**. Total yield 0.81 g (41 %).

5.2.13 Preparation of [{$Me_2C(\eta^5\text{-}C_5H_4)_2$}Hf($\eta^5$-$C_5H_5$)Cl] (7)

Toluene (200 cm^3) was added to a stirred mixture of [{$Me_2C(C_5H_4)_2$}Li_2] (0.5 g, 2.7 mmol)[3] and [(η^5-C_5H_5)$HfCl_3$·2THF] (1.34 g, 2.7 mmol) at room temperature. The resulting yellow mixture was stirred for a further 60 hours at room temperature. The solution was filtered from the solid residue, which was extracted with a further 80 cm^3 of toluene. The combined toluene solutions, when concentrated under reduced pressure and cooled to -20 °C, afforded pale yellow crystals of the product. Yield 0.52 g (43 %).

5.3 Experimental details for Chapter 3

5.3.1 Preparation of

$[(\eta^5\text{-}C_5H_5)ZrCl_2\{(\eta^5\text{-}C_5H_4)CMe_2(\eta^5\text{-}C_9H_6)\}ZrCl_2(\eta^5\text{-}C_5H_5)]$ (8)

Toluene (200 cm^3) at -78 °C was added to a stirred mixture of $[\{Me_2C(C_5H_4)(C_9H_6)\}Li_2\{0.6(Et_2O)\}]$ (2.0 g, 7.18 mmol) and $[(\eta^5\text{-}C_5H_5)ZrCl_3\cdot DME]$ (5.05 g, 14.3 mmol) at -78 °C in a thick-walled Rotaflo ampoule. The resulting orange mixture was allowed to warm to room temperature, becoming deep red in colour. After stirring at room temperature for 2 hours the ampoule was partially evacuated and placed in an oil bath at 105 °C for 20 hours. The resulting mixture was filtered to give a clear, yellow/orange coloured solution which was concentrated under reduced pressure and cooled to -20 °C, giving large yellow/orange crystals **8**. Yield 3.87 g (80 %).

5.3.2 Preparation of

$[(\eta^5\text{-}C_5H_5)HfCl_2\{(\eta^5\text{-}C_5H_4)CMe_2(\eta^5\text{-}C_9H_6)\}HfCl_2(\eta^5\text{-}C_5H_5)]$ (9)

Toluene (200 cm^3) at -78 °C was added to a stirred mixture of $[\{Me_2C(C_5H_4)(C_9H_6)\}Li_2\{0.6(Et_2O)\}]$ (2.0 g, 7.18 mmol) and $[(\eta^5\text{-}C_5H_5)HfCl_3\cdot DME]$ (6.32 g, 14.3 mmol) also at -78 °C, in a thick-walled Rotaflo ampoule. The resulting yellow mixture was allowed to warm to room temperature, becoming orange in colour. After stirring at room temperature for one hour the ampoule was partially evacuated and placed in an oil bath at 105 °C for 18 hours. The resulting suspension was allowed to settle and the clear yellow solution was decanted into a Schlenk tube, concentrated under reduced pressure and cooled to -20 °C, giving yellow crystals of **9**. Yield 4.09 g (68 %).

5.3.3 Preparation of

$[(\eta^5\text{-}C_5H_5)ZrCl_2\{(\eta^5\text{-}C_5H_4)CMe_2(\eta^5\text{-}C_9H_6)\}HfCl_2(\eta^5\text{-}C_5H_5)]$ (10)

$[\{Me_2C(\eta^5\text{-}C_5H_4)(\eta^2\text{-}C_9H_6)\}Zr(\eta^5\text{-}C_5H_5)Cl]$ (0.50 g, 1.21 mmol) and $[(\eta^5\text{-}C_5H_5)HfCl_3\cdot DME]$ (0.53 g, 1.20 mmol) were weighed into a thick-walled Rotaflo ampoule. Toluene (90 cm^3) was added and the red coloured reaction mixture was stirred at room temperature for one hour. The ampoule was then partially evacuated and placed in an oil bath at 105 °C for 16 hours. The resulting clear, orange solution was transferred to a Schlenk tube, concentrated under reduced pressure and cooled to -20 °C, affording yellow crystals of **10**. Yield 0.68 g (74 %).

5.3.4 Preparation of

$[(\eta^5\text{-}C_5H_5)HfCl_2\{(\eta^5\text{-}C_5H_4)CMe_2(\eta^5\text{-}C_9H_6)\}ZrCl_2(\eta^5\text{-}C_5H_5)]$ (11)

$[\{Me_2C(\eta^5\text{-}C_5H_4)(\eta^2\text{-}C_9H_6)\}Hf(\eta^5\text{-}C_5H_5)Cl]$ (1.50 g, 3.00 mmol) and $[(\eta^5\text{-}C_5H_5)ZrCl_3\cdot DME]$ (1.00 g, 2.83 mmol) were weighed into a thick-walled Rotaflo ampoule. THF (130 cm^3) was added and the orange/red coloured solution was stirred at room temperature for one hour. The ampoule was then partially evacuated and placed in an oil bath at 80 °C for 15 hours. The resulting clear, yellow solution was transferred to a Schlenk tube and volatiles were removed, leaving the crude product as a slightly oily yellow solid (*ca.* 90 % compound **11** by ^1H NMR). Washing with diethyl ether (140 cm^3) left the pure product (**11**) as a fine yellow powder. Yield 1.69 g (78 %).

5.3.5 Preparation of

$[(\eta^5\text{-}C_5H_5)ZrCl_2\{(\eta^5\text{-}C_5H_4)CMe_2(\eta^5\text{-}C_9H_6)\}ZrCl_2(\eta^5\text{-}C_5Me_5)]$ (12)

$[\{Me_2C(\eta^5\text{-}C_5H_4)(\eta^2\text{-}C_9H_6)\}Zr(\eta^5\text{-}C_5H_5)Cl]$ (0.70 g, 1.70 mmol) and $[(\eta^5\text{-}C_5Me_5)ZrCl_3\cdot 2THF]$ (0.81 g, 1.70 mmol)[4] were weighed into a thick-walled Rotaflo

ampoule. Toluene (100 cm^3) was added and the red coloured reaction mixture was stirred at room temperature for 2 days. The ampoule was then partially evacuated and placed in an oil bath at 95 °C for 18 hours. The resulting orange suspension was filtered to give a clear orange solution, which was concentrated under reduced pressure and cooled to -20 °C, affording compound **12** as a yellow crystalline solid. Yield 0.66 g (52 %).

5.3.6 Preparation of

$[(\eta^5\text{-}C_5H_5)Zr(CH_3)_2\{(\eta^5\text{-}C_5H_4)CMe_2(\eta^5\text{-}C_9H_6)\}Zr(CH_3)_2(\eta^5\text{-}C_5H_5)]$ (13)

Toluene (50 cm^3) was added to $[(\eta^5\text{-}C_5H_5)ZrCl_2\{(\eta^5\text{-}C_5H_4)CMe_2(\eta^5\text{-}C_9H_6)\}ZrCl_2(\eta^5\text{-}C_5H_5)]$ (0.50 g, 0.74 mmol) and the yellow suspension was stirred and cooled to -78 °C. Four equivalents of methyl lithium (1.8 cm^3 of a 1.7 M diethyl ether solution) were added, then the reaction mixture was allowed to warm to room temperature over *ca.* 30 minutes, giving a pale orange cloudy solution. This was stirred at room temperature for a further 90 minutes. Filtration and removal of volatiles under reduced pressure, at room temperature, gave an orange oil. Petroleum ether (bp. 40-60 °C, 160 cm^3) was added and the mixture was stirred vigorously at room temperature for 4 hours. The resulting pale yellow solution was filtered from the residues, concentrated under reduced pressure and cooled to -80 °C, affording very pale orange crystals of **13**. Yield 0.33 g (75 %).

5.3.7 Preparation of

$[(\eta^5\text{-}C_5H_5)Zr(CH_3)_2\{(\eta^5\text{-}C_5H_4)CMe_2(\eta^5\text{-}C_9H_6)\}Hf(CH_3)_2(\eta^5\text{-}C_5H_5)]$ (14)

Toluene (30 cm^3) was added to $[(\eta^5\text{-}C_5H_5)ZrCl_2\{(\eta^5\text{-}C_5H_4)CMe_2(\eta^5\text{-}C_9H_6)\}HfCl_2(\eta^5\text{-}C_5H_5)]$ (0.25 g, 0.33 mmol) and the pale yellow suspension was stirred and cooled to -78 °C. Four equivalents of methyl lithium (0.8 cm^3 of a 1.7 M diethyl ether solution) were added, then the reaction mixture was allowed to warm to

room temperature and was stirred for 2 hours. Filtration, and removal of volatiles from the filtrate under reduced pressure gave a pale yellow oil. Petroleum ether (bp. 40-60 °C, 100 cm^3) was added and the mixture was stirred vigorously at room temperature for one hour The resulting colourless solution was filtered from the residues, concentrated under reduced pressure and cooled to -80 °C, affording the product (**14**) as a very pale yellow crystalline solid. Yield 0.15 g (64 %).

5.3.8 Preparation of

$[(\eta^5\text{-}C_5H_5)Hf(CH_3)_2\{(\eta^5\text{-}C_5H_4)CMe_2(\eta^5\text{-}C_9H_6)\}Zr(CH_3)_2(\eta^5\text{-}C_5H_5)]$ (15)

Toluene (70 cm^3) was added to $[(\eta^5\text{-}C_5H_5)HfCl_2\{(\eta^5\text{-}C_5H_4)CMe_2(\eta^5\text{-}C_9H_6)\}ZrCl_2(\eta^5\text{-}C_5H_5)]$ (1.00 g, 1.31 mmol) and the bright yellow suspension was stirred and cooled to -78 °C. Four equivalents of methyl lithium (3.2 cm^3 of a 1.7 M diethyl ether solution) were added, then the reaction mixture was allowed to warm to room temperature and was stirred for 4 hours. Filtration, and removal of volatiles from the filtrate under reduced pressure gave a yellow oil. Petroleum ether (bp. 40-60 °C, 170 cm^3) was added and the mixture was stirred vigorously at room temperature for 2 hours. The resulting yellow solution was filtered from the residues, concentrated under reduced pressure and cooled to -80 °C, giving the product (**15**) as a pale yellow crystalline solid. Yield 0.595 g (67 %).

5.3.9 Preparation of

$[(\eta^5\text{-}C_5H_5)Hf(CH_3)_2\{(\eta^5\text{-}C_5H_4)CMe_2(\eta^5\text{-}C_9H_6)\}Hf(CH_3)_2(\eta^5\text{-}C_5H_5)]$ (16)

Toluene (35 cm^3) was added to $[(\eta^5\text{-}C_5H_5)HfCl_2\{(\eta^5\text{-}C_5H_4)CMe_2(\eta^5\text{-}C_9H_6)\}HfCl_2(\eta^5\text{-}C_5H_5)]$ (0.50 g, 0.59 mmol) and the pale yellow suspension was stirred and cooled to -78 °C. Four equivalents of methyl lithium (1.5 cm^3 of a 1.7 M diethyl ether solution) were added, then the reaction mixture was allowed to warm to room temperature and was stirred for 3 hours. Filtration and removal of volatiles from

the filtrate under reduced pressure gave a yellow oil. Petroleum ether (bp. 40-60 °C, 140 cm^3) was added and the mixture was stirred vigorously at room temperature for one hour. The solution was then filtered from the residues, concentrated under reduced pressure and cooled to -80 °C, giving the product (**16**) as a very pale yellow crystalline solid. Yield 0.20 g (44 %).

5.3.10 Preparation of $[Li(C_5H_4)CMe_2(C_9H_7)]$

A solution of 6,6-dimethylfulvene (4.43 g, 41.7 mmol) in diethyl ether (30 cm^3) was added dropwise over 40 minutes to a stirred solution of lithium indenide (LiC_9H_7, 4.9 g, 40.1 mmol) in diethyl ether (300 cm^3) at 0 °C. The ice bath was then removed and the solution stirred for a further 15 hours at room temperature. Petroleum ether (bp. 40-60 °C, 60 cm^3) was then added and the reaction mixture was allowed to stand for 30 minutes, during which time a small amount of dark oil settled to the bottom of the Schlenk tube. The desired clear orange solution was then carefully decanted from the oil and cooled to -80 °C, giving the product as pale orange crystals. Yield 5.65 g (63 %).

5.3.11 Preparation of $[(\eta^5\text{-}C_5H_5)ZrCl_2\{(\eta^5\text{-}C_5H_4)CMe_2(C_9H_7)\}]$ (17)

A solution of $[Li(C_5H_4)CMe_2(C_9H_7)]$ (0.73 g, 3.20 mmol) in THF (30 cm^3) was added dropwise to a stirred solution of $[(\eta^5\text{-}C_5H_5)ZrCl_3\cdot DME]$ (1.07 g, 3.04 mmol) in THF (70 cm^3) at room temperature. The resulting yellow solution was stirred for a further 13 hours at room temperature. Removal of volatiles under reduced pressure, followed by extraction into toluene (150 cm^3), concentration of the filtrate under reduced pressure and cooling to -20 °C, afforded the product (**17**) as a white microcrystalline solid. Yield 0.79 g (58 %).

5.3.12 Preparation of $[(\eta^5\text{-}C_5H_5)HfCl_2\{(\eta^5\text{-}C_5H_4)CMe_2(C_9H_7)\}]$ (18)

A solution of $[Li(C_5H_4)CMe_2(C_9H_7)]$ (0.30 g, 1.31 mmol) in THF (15 cm^3) was added dropwise to a stirred solution of $[(\eta^5\text{-}C_5H_5)HfCl_3\cdot DME]$ (0.578 g, 1.31 mmol) in THF (35 cm^3) at room temperature. The resulting yellow solution was stirred for a further 13 hours at room temperature. Removal of volatiles under reduced pressure, followed by extraction into toluene (70 cm^3), concentration of the filtrate under reduced pressure and cooling to -20 °C, afforded the product (**18**) as a white microcrystalline solid. Yield 0.39 g (56 %).

5.3.13 Preparation of $[(\eta^5\text{-}C_5H_5)Zr(CH_3)_2\{(\eta^5\text{-}C_5H_4)CMe_2(C_9H_7)\}]$ (19)

Diethyl ether (60 cm^3) was added to $[(\eta^5\text{-}C_5H_5)ZrCl_2\{(\eta^5\text{-}C_5H_4)CMe_2(C_9H_7)\}]$ (0.68 g, 1.52 mmol) and the suspension was stirred and cooled to -78 °C. Two equivalents of methyl lithium (1.8 cm^3 of a 1.7 M diethyl ether solution) was added, then the reaction mixture was allowed to warm to room temperature and was stirred for a further 5 hours. Filtration and removal of volatiles under reduced pressure gave a white solid. Petroleum ether (bp. 40-60 °C, 120 cm^3) was added and the mixture was stirred vigorously at room temperature for one hour. The colourless solution was then filtered from the residues, concentrated under reduced pressure and cooled to -80 °C, affording the product (**19**) as white crystals. Yield 0.38 g (61 %).

5.4 Experimental details for Chapter 4

5.4.1 Preparation of methylaluminoxane (MAO)

Methylaluminoxane (MAO) was prepared by the partial hydrolysis of trimethylaluminium using $CuSO_4.5H_2O$, following the procedures of Kaminsky[5] and Giannetti,[6] as modified by Ishihara.[7] Finely pulverized $CuSO_4.5H_2O$ (76.9 g, 0.31 mol = 1.54 mol H_2O) and toluene (550 cm^3) were added to a nitrogen-filled 1-litre, 3-necked round bottomed flask fitted with a thermometer. The flask was then placed in a cold water bath and the contents were stirred. Trimethylaluminium (74.0 g, 1.03 mol) was then added very slowly, dropwise, whilst the temperature of the reaction mixture was maintained at approximately 20 °C by adjusting the rate of addition, and adding ice to the water bath when necessary. The reaction mixture was stirred for 24 hours at room temperature, then the solution was filtered from the solid residues. The filtrate was concentrated under reduced pressure and then dried *in vacuo* at 50 °C to give the product as a white glassy solid Yield 22 g (37 %).

5.4.2 General details of polymerizations

All manipulations of catalysts and co-catalysts were carried out in an inert atmosphere using either a dual vacuum/nitrogen line and standard Schlenk techniques or in an inert atmosohere dry box containing nitrogen. Ethylene and propylene (pure grade) were further purified by passage through columns of 4 Å molecular sieves and then over finely divided potassium metal supported on glass wool. Polymerizations were carried out in a Fischer-Porter reactor placed in a thermostatically heated bath and equipped with a magnetic stirrer. The apparatus used for the polymerizations is shown in Figure 4.3.1.

5.4.3 Polymerization of ethylene using metallocene/MAO catalysts

The polymerizations were carried out under conditions as close as possible to those employed by Kaminsky in 1992.[8] 250 mg of methylaluminoxane (MAO) was weighed into the Fischer-Porter bottle, which was then connected to the ethylene supply *via* the computer-controlled gas supply system (Figure 4.3.1). The flexible steel hose joining the Fischer-Porter bottle to the supply system was evacuated and filled with ethylene three times, then the Fischer-Porter bottle was evacuated and filled with ethylene. Toluene (200 cm^3) was then added, the ethylene pressure increased to 2 bar (absolute pressure) and the mixture was stirred at 30 °C until saturated with ethylene. Meanwhile, 6.25 x 10^{-6} mol of the metallocene in 10 cm^3 of toluene [taken from a standard solution of 6.25 x 10^{-5} mol of metallocene (*ca.* 42 to 53 mg) in 100 cm^3 toluene] was added to 50 mg of MAO and stirred for 15 minutes pre-activation. The stirring of the contents of the Fischer-Porter reactor was then stopped, to minimise the loss of ethylene from solution when the presure was released to enable the metallocene/MAO mixture to be added quickly, *via* a cannula, to the reactor. The ethylene pressure was then increased to 2 bar again and the experiment was started. The reaction mixture was stirred vigorously at 30 °C under a 2 bar pressure of ethylene for one hour.

After one hour the polymerization was quenched by venting the ethylene and adding a small amount of ethanol. The contents of the reactor were transferred to a conical flask and 300 cm^3 of a 20 % (by volume) solution of conc. HCl in ethanol was added and the mixture stirred overnight. The polymer was then separated from the solution using a sintered glass funnel (on a Buchner flask, connected to a water aspirator for suction) and was washed with water, ethanol and finally diethyl ether, then dried *in vacuo* at 50 °C to constant weight.

5.4.4 Polymerization of propylene using metallocene/MAO catalysts

These polymerization reactions were performed under the same conditions (2 bar monomer pressure, 30 °C) and using essentially the same procedure as for ethylene, except: (i) 2.00g of MAO and 130 cm^3 of toluene were pre-saturated with propylene at 2 bar and 30 °C, (ii) 5.0 x 10^{-5} mol of metallocene in 80 cm^3 of toluene was added to 400 mg of MAO for 15 minutes pre-activation, (iii) the reaction mixture was stirred under 2 bar propylene pressure at 30 °C for 4 hours.

After four hours the polymerization was quenched by venting the propylene then adding a small amount of ethanol. The contents of the reactor were transferred to a conical flask and 300 cm^3 of a 20 % (by volume) solution of conc. HCl in ethanol was added and the mixture stirred overnight. The polypropylene was soluble in toluene, so the toluene layer was separated, washed well with water (5 x 100 cm^3) then stirred with $MgSO_4$ drying agent. After filtration, the toluene was removed under reduced pressure leaving the polypropylene, typically a highly viscous liquid, which was dried to constant weight *in vacuo* at 50 °C.

5.4.5 Preparation of $B(C_6F_5)_3$ and $[Ph_3C]^+[B(C_6F_5)_4]^-$ co-catalysts

Both co-catalysts were prepared by literature methods without modification, $B(C_6F_5)_3$ as described by Massey and Park,[9] $[Ph_3C]^+[B(C_6F_5)_4]^-$ as described by Chien *et. al.*.[10]

5.4.6 Polymerization of ethylene using methylated metallocenes and $B(C_6F_5)_3$ or $[Ph_3C]^+[B(C_6F_5)_4]^-$ co-catalysts

The Fischer-Porter reactor was connected to the gas supply system, evacuated while the glass was still hot from the 200 °C oven, then filled with nitrogen. The evacuation/filling procedure was repeated three times with nitrogen then twice with

ethylene. Toluene (36 cm^3) was then added, the ethylene pressure increased to 2 bar and the solution stirred at 30 °C until saturated with ethylene. The stirring of the Fischer-Porter reactor was then stopped, so that a minimum of ethylene was released from solution when the pressure was released to enable the catalyst solution (6.25 x 10^{-6} mol of the metallocene in 2 cm^3 toluene) and the co-catalyst solution (2 cm^3) to be added quickly, *via* cannulae, to the reactor. The ethylene pressure was then increased to 2 bar, and the experiment started. The reaction mixture was stirred vigorously at 30 °C under an ethylene pressure of 2 bar, for one hour with $B(C_6F_5)_3$ co-catalyst, or for two minutes with $[Ph_3C]^+[B(C_6F_5)_4]^-$ co-catalyst. The polymerization was quenched by venting the ethylene then adding ethanol. The contents of the reactor were transferred to a conical flask and 3 cm^3 of conc. HCl was added, followed by water, and the mixture stirred overnight. The polymer was separated from the solution using a sinterer glass funnel (and suction) and was washed with water, ethanol and finally diethyl ether, then dried *in vacuo* at 50 °C to constant weight.

5.4.7 Polymerization of propylene using methylated metallocenes and $B(C_6F_5)_3$ or $[Ph_3C]^+[B(C_6F_5)_4]^-$ co-catalysts

The Fischer-Porter bottle evacuated and filled with propylene following the same procedure described above for ethylene. A solution of 5.0 x 10^{-5} mol of the binuclear metallocene in 10 cm^3 of toluene was then added, the propylene pressure increased to 2 bar, and the solution stirred at 30 °C until saturated with the monomer. The stirring of the Fischer-Porter reactor was then stopped, and the pressure was released to enable the co-catalyst solution (1.0 x 10^{-4} mol in 10 cm^3 toluene) to be added quickly, *via* a cannula, to the reactor. The propylene pressure was then increased to 2 bar and the experiment started. The reaction mixture was stirred vigorously at 30 °C under 2 bar of propylene for four hours, then the polymerization was quenched by venting the propylene and adding ethanol. The contents of the

reactor were transferred to a conical flask and 3 cm^3 of conc. HCl was added followed by water and more toluene, and the mixture stirred overnight. The toluene layer was then separated, washed with water and stirred with $MgSO_4$ drying agent. After filtration the toluene was removed under reduced pressure leaving the product which was dried to constant weight *in vacuo* at 50 °C.

References for Chapter 5

1. K. J. Stone and R. D. Little, *J. Org. Chem.*, 1984, **49**, 1849.
2. E. C. Lund and T. Livinghouse, *Organometallics*, 1990, **9**, 2426.
3. I. E. Nifant'ev, P. V. Ivchenko and M. V. Borzov, *J. Chem. Research (S)*, 1992, 162.
4. G. H. Llinas, M. Mena, F. Palacios, P. Royo and R. Serrano, *J. Organomet. Chem.*, 1988, **340**, 37.
5. W. Kaminsky, M. Miri, H. Sinn and R. Woldt, *Makromol. Chem., Rapid Commun.*, 1983, **4**, 417.
6. E. Giannetti, G. M. Nicoletti and R. Mazzocchi, *J. Polym. Sci., Polym. Chem. Ed.*, 1985, **23**, 2117.
7. Nobuhide Ishihara, D. Phil. Thesis, University of Oxford, 1990; M. L. H. Green and N. Ishihara, *J. Chem., Soc., Dalton Trans*, 1994, in press.
8. W. Kaminsky, R. Engerhausen, K. Zoumis, W. Spalek and J. Rohrmann, *Makromol. Chem.*, 1992, **193**, 1643.
9. A. G. Massey and A. J. Park, *J. Organomet. Chem.*, 1964, **2**, 245.
10. J. C. W. Chien, W.M. Tsai and M. D. Rausch, *J. Am. Chem. Soc.*, 1991, **113**, 8570.

CHAPTER SIX

Characterising Data

6.1 General comments

6.1.1 Nuclear magnetic resonance spectra

Solution NMR spectra were recorded on a Bruker AM 300 spectrometer (^{1}H 300 MHz, ^{13}C 75.5 MHz). Spectra were referenced internally using the residual protio solvent (^{1}H) and solvent (^{13}C) resonances relative to tetramethylsilane ($\delta = 0$ ppm). All chemical shifts are quoted in δ (ppm) and coupling constants (J) are in Hertz. The ^{13}C NMR spectra of polypropylene were recorded at 120 ^{o}C in a solvent mixture of 1,2,4-trichlorobenzene and d^{6}-benzene (v/v = 80/20).

6.1.2 Elemental analysis

Elemental analyses were performed by the Microanalytical Department of the Inorganic Chemistry Laboratory, University of Oxford.

6.1.3 X-ray crystal structure determinations

See Appendices A to D.

6.1.4 Mass spectrum

The mass spectrum (electron impact) of compound **1** was recorded by Neil Popham on an AEI MS902 mass spectrometer updated by a data handling system supplied by Mass Spectroscopy Services Ltd.

6.2 Characterising data for new compounds described in Chapter 2

6.2.1 Data characterising [{$Me_2C(\eta^5\text{-}C_5H_4)(\eta^2\text{-}C_9H_6)$}Zr ($\eta^5\text{-}C_5H_5$)Cl] (1)

Description: Red crystals

Elemental analysis for $C_{22}H_{21}ClZr$ (M.W. = 412.06):

found (required) / % C, 64.1 (64.1); H, 5.2 (5.1); Cl, 8.8 (8.6)

Single crystal X-ray structure: $R = 0.044$; $R_w = 0.050$

See Appendix A for further details

Mass spectrum (electron impact): $m/z = 410$, M^+

^{1}H NMR data: (300 MHz, d^8-THF, room temperature)

7.59 [1 H, d, $J(H_fH_e)$ 8, H_f]

7.47 [1 H, d, $J(H_cH_d)$ 8, H_c]

7.29 [1 H, d, $J(H_bH_a)$ 4, H_b]

7.03 [1 H, pseudo t, $J(H_eH_{d,f})$ 8, H_e]

6.81 [1 H, pseudo t, $J(H_dH_{c,e})$ 8, H_d]

6.43 [1 H, d, $J(H_aH_b)$ 4, H_a]

6.28 [1 H, pseudo q, $J(H_kH_{i,j,l})$ 3 H_k]

6.24 [1 H, pseudo q, $J(H_iH_{j,k,l})$ 3, H_i]

5.97 [1 H, pseudo q, $J(H_jH_{i,k,l})$ 3, H_j]

5.74 [1 H, pseudo q, $J(H_lH_{i,j,k})$ 3, H_l]

5.41 [5 H, s, H_m]

2.08 [3 H, s, H_g]

1.70 [3 H, s, H_h]

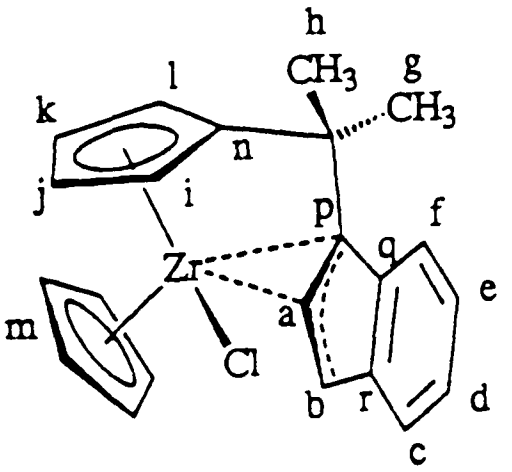

^{13}C NMR data: (75.5 MHz, d^{8}-THF, room temperature)

142.4 [s, C_n]

137.6 [s, $C_{q\ or\ r}$]

129.8 [d, J(CH) 170, C_b]

127.9 [s, $C_{q\ or\ r}$]

123.9 [d, J(CH) 157, C_e]

123.3 [d, J(CH) 156, C_c]

121.4 [d, J(CH) 175, C_j]

120.4 [d, J(CH) 159, C_d]

119.7 [d, J(CH) 157, C_f]

114.6 [d, J(CH) 174, C_m]

112.0 [d, J(CH) 174, C_k]

111.7 [d, J(CH) 156, C_a]

107.8 [d, J(CH) 173, C_i]

99.4 [d, J(CH) 173, C_l]

84.4 [s, C_p]

39.2 [s, C_o]

31.2 [s, C_h]

26.7 [s, C_g]

^{1}H assignments from selective decoupling, COSY and NOESY experiments

^{13}C assignments from ^{13}C-^{1}H shift correlation experiment

6.2.2 Data characterising $[\{Me_2C(\eta^5\text{-}C_5H_4)(\eta^2\text{-}C_9H_6)\}Hf(\eta^5\text{-}C_5H_5)Cl]$ (2)

Description: Orange crystals

Elemental analysis for $C_{22}H_{21}ClHf$ (M.W. = 499.33):

found (required) / % C, 53.2 (52.9); H, 4.2 (4.2); Cl, 7.15 (7.1)

^{1}H NMR data: (300 MHz, d^8-THF, room temperature)

7.60 [1 H, d, J(H_fH_e) 8, H_f]

7.53 [1 H, d, J(H_cH_d) 8, H_c]

7.29 [1 H, d, J(H_bH_a) 4, H_b]

7.07 [1 H, pseudo t, J($H_eH_{d,f}$) 8, H_e]

6.78 [1 H, pseudo t, J($H_dH_{c,e}$) 8, H_d]

6.27 [1 H, d, J(H_aH_b) 4, H_a]

6.25 [1 H, m, H_k]

6.22 [1 H, m, H_i]

6.00 [1 H, pseudo q, J($H_jH_{i,k,l}$) 3, H_j]

5.67 [1 H, pseudo q, J($H_lH_{i,j,k}$) 3, H_l]

5.32 [5 H, s, H_m]

2.06 [3 H, s, H_g]

1.66 [3 H, s, H_h]

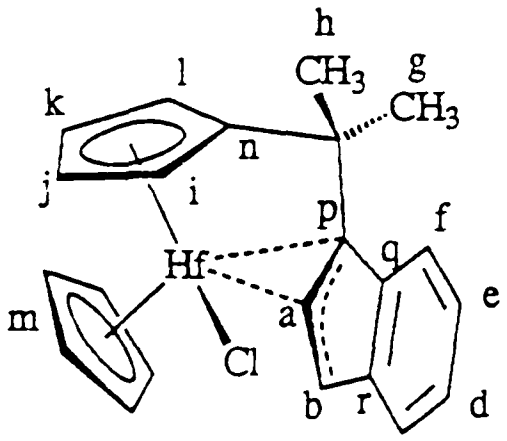

^{13}C NMR data: $^{13}C\{^1H\}$ (75.5 MHz, d^8-THF, room temperature)

141.6 [s, C_n]

138.2 [s, $C_{q\text{ or }r}$]

129.4 [s, C_b]

127.9 [s, $C_{q\text{ or }r}$]

123.2 [s, C_e]

122.6 [s, C_c]

120.7 [s, C_j]

120.6 [s, C_d]

120.5 [s, C_f]

113.0 [s, C_m]

110.5 [s, C_k]

108.6 [s, C_a]

106.1 [s, C_i]

98.0 [s, C_l]

85.1 [s, C_p]

39.0 [s, C_o]

32.3 [s, C_h]

27.0 [s, C_g]

^1H and ^{13}C assignments from selective ^1H decoupling experiments, ^{13}C-^1H shift correlation experiment and comparison with compound **1**

6.2.3 Data characterising

$[\{(CH_2)_5C(\eta^5\text{-}C_5H_4)(\eta^2\text{-}C_9H_6)\}Zr(\eta^5\text{-}C_5H_5)Cl][0.5\ (C_6H_5CH_3)]$ **(3)**

Description: Red crystals

Elemental analysis for $C_{25}H_{25}ClZr[0.5(C_7H_8)] = C_{28.5}H_{29}ClZr$ (M.W. = 498.2):

found (required) / % C, 68.7 (68.7); H, 5.9 (5.9); Cl, 7.4 (7.1)

Single crystal X-ray structure: $R = 0.033$; $R_w = 0.035$

See Appendix B for further details

^{1}H NMR data: (300 MHz, C_6D_6, room temperature)

7.43 [1 H, d, $J(H_cH_d)$ 8, H_c or $J(H_fH_e)$ 8, H_f]

7.42 [1 H, d, $J(H_bH_a)$ 4, H_b]

7.40 [1 H, d, $J(H_cH_d)$ 8, H_c or $J(H_fH_e)$ 8, H_f]

7.10 [1 H, pseudo t, $J(H_dH_{c,e})$ 8, H_d or $J(H_eH_{d,f})$ 8, H_e]

6.91 [1 H, pseudo t, $J(H_dH_{c,e})$ 8, H_d or $J(H_eH_{d,f})$ 8, H_e]

6.35 [1 H, d, $J(H_aH_b)$ 4, H_a]

5.82 [1 H, pseudo q, J(HH) 3, C_5H_4]

5.72 [1 H, pseudo q, J(HH) 3, C_5H_4]

5.37 [1 H, pseudo q, J(HH) 3, C_5H_4]

5.15 [5 H, s, C_5H_5]

4.77 [1 H, pseudo q, J(HH) 3, C_5H_4]

2.28 [2 H, m, CH_2]

2.02 [1 H, m, CH_2]

1.7 to 1.2 [7 H, br. m, CH_2]

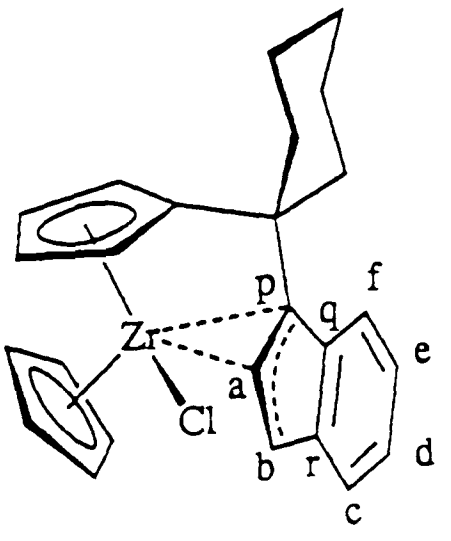

^{13}C NMR data: (75.5 MHz, C_6D_6, room temperature)

140.6 [s, C_{ipso} (C_5H_4)]

137.0 [s, $C_{q\ or\ r}$]

128.9 [coupling obscured by solvent, C_b]

126.8 [s, $C_{q\ or\ r}$]

123.8 [d, J(CH) 155, $C_{d\ or\ e}$]

123.3 [d, J(CH) 165, $C_{c\ or\ f}$]

120.5 [d, J(CH) 159, $C_{d\ or\ e}$]

119.9 [d, J(CH) 157, $C_{c\ or\ f}$]

119.7 [d, J(CH) 172, C_5H_4]

114.1 [d, J(CH) 174, C_5H_5]

112.0 [d, J(CH) 171, C_5H_4]

111.0 [d, J(CH) 152, C_a]

107.5 [d, J(CH) 179, C_5H_4]

97.8 [d, J(CH) 172, C_5H_4]

85.7 [s, C_p]

43.8 [s, $C(CH_2)_5$]

39.2 [t, J(CH) 127, CH_2]

34.8 [t, J(CH) 125, CH_2]

26.3 [t, J(CH) 130, CH_2]

23.2 [t, J(CH) 121, CH_2]

22.0 [t, J(CH) 130, CH_2]

^{1}H assignments from selective decoupling experiments

^{13}C assignments from comparison with compound **4**

6.2.4 Data characterising

$[\{(CH_2)_5C(\eta^5\text{-}C_5H_4)(\eta^2\text{-}C_9H_6)\}Hf(\eta^5\text{-}C_5H_5)Cl][0.5\ (C_6H_5CH_3)]$ **(4)**

Description: Orange crystals

Elemental analysis for $C_{25}H_{25}ClHf[0.5(C_7H_8)] = C_{28.5}H_{29}ClHf$ (M.W. = 585.5):

found (required) / % C, 59.0 (58.5); H, 5.0 (5.0); Cl, 6.4 (6.1)

^{1}H NMR data: (300 MHz, C_6D_6, room temperature)

7.55 [1 H, d, $J(H_cH_d)$ 8, H_c or $J(H_fH_e)$ 8, H_f]

7.48 [1 H, d, $J(H_bH_a)$ 4, H_b]

7.44 [1 H, d, $J(H_cH_d)$ 8, H_c or $J(H_fH_e)$ 8, H_f]

7.20 [1 H, pseudo t, $J(H_dH_{c,e})$ 8, H_d or $J(H_eH_{d,f})$ 8, H_e]

6.94 [1 H, pseudo t, $J(H_dH_{c,e})$ 8, H_d or $J(H_eH_{d,f})$ 8, H_e]

6.19 [1 H, d, $J(H_aH_b)$ 4, H_a]

5.84 [1 H, pseudo q, J(HH) 3, C_5H_4]

5.67 [1 H, pseudo q, J(HH) 3, C_5H_4]

5.30 [1 H, pseudo q, J(HH) 3, C_5H_4]

5.03 [5 H, s, C_5H_5]

4.64 [1 H, pseudo q, J(HH) 3, C_5H_4]

2.28 [2 H, m, CH_2]

2.02 [1 H, m, CH_2]

1.66 [1 H, m, CH_2]

1.5 [4 H, br.m, CH_2]

1.30 [1 H, m, CH_2]

1.18 [1 H, m, CH_2]

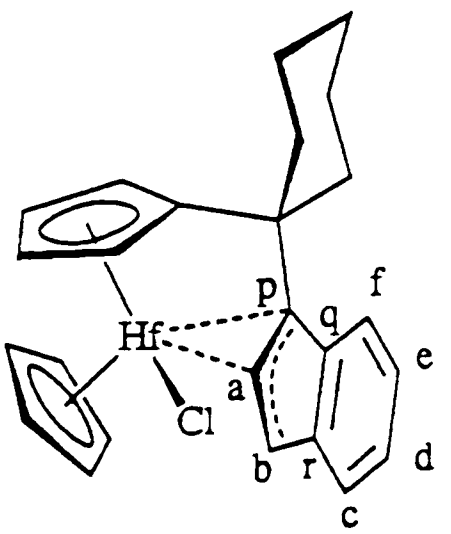

^{13}C NMR data: (75.5 MHz, C_6D_6, room temperature)

141.3 [s, C_{ipso} (C_5H_4)]

137.8 [s, $C_{q\ or\ r}$]

129.5 [coupling obscured by solvent, C_b]

125.6 [s, $C_{q\ or\ r}$]

123.2 [d, J(CH) 161, $C_{d\ or\ e}$]

122.9 [d, J(CH) 156, $C_{c\ or\ f}$]

120.6 [d, J(CH) 162, $C_{d\ or\ e}$]

120.5 [d, J(CH) 162, $C_{c\ or\ f}$]

119.4 [d, J(CH) 179, C_5H_4]

112.3 [d, J(CH) 178, C_5H_5]

110.0 [d, J(CH) 174, C_5H_4]

108.0 [d, J(CH) 156, C_a]

105.7 [d, J(CH) 174, C_5H_4]

96.5 [d, J(CH) 180, C_5H_4]

84.9 [s, C_p]

43.7 [s, $C(CH_2)_5$]

40.4 [t, J(CH) 128, CH_2]

35.1 [t, J(CH) 128, CH_2]

26.4 [t, J(CH) 123, CH_2]

23.3 [t, J(CH) 126, CH_2]

22.3 [t, J(CH) 126, CH_2]

^1H assignments from selective decoupling experiments

^{13}C assignments from ^{13}C-^1H shift correlation experiment

6.2.5 Data characterising $[\{Me_2C(\eta^5\text{-}C_5H_4)(\eta^3\text{-}C_{13}H_8)\}Zr(\eta^5\text{-}C_5H_5)Cl]$ (5)

Description: Red crystals

Elemental analysis for $C_{26}H_{23}ClZr$ (M.W. = 462.12):

found (required) / % C, 67.5 (67.6); H, 5.0 (5.0); Cl, 7.8 (7.7)

Single crystal X-ray structure: $R = 0.0376$; $R_w = 0.0369$

See Appendix C for further details

^{1}H NMR data: (300 MHz, CD_2Cl_2, room temperature)

8.26 [1 H, m, H_d]

8.11 [1 H, d, $J(H_eH_f)$ 8, H_e]

7.91 [1 H, d, $J(H_hH_g)$ 8, H_h]

7.42 [2 H, m, H_b and H_c]

7.41 [1 H, m, H_g]

7.31 [1 H, m, H_a]

7.20 [1 H, pseudo t, $J(H_fH_{e,g})$ 8, H_f]

6.31 [1 H, pseudo q, $J(H_lH_{k,m,n})$ 3, H_l]

6.28 [1 H, pseudo q, $J(H_mH_{k,l,n})$ 3, H_m]

6.06 [1 H, pseudo q, $J(H_kH_{l,m,n})$ 3, H_k]

5.59 [1 H, pseudo q, $J(H_nH_{k,l,m})$ 3, H_n]

4.84 [5 H, s, H_o]

2.20 [3 H, s, H_i]

1.35 [3 H, s, H_j]

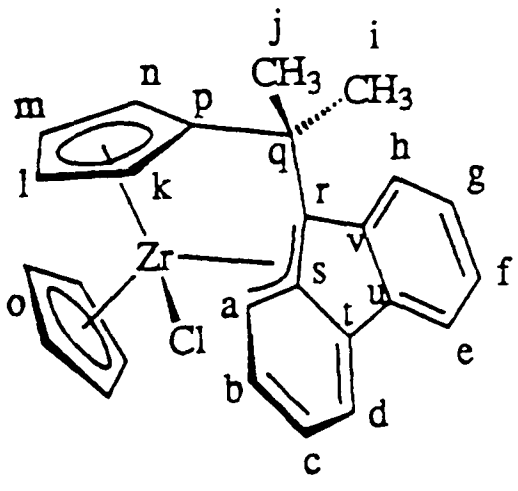

^{13}C NMR data: (75.5 MHz, CD_2Cl_2, room temperature)

145.3 [s, C_p]

137.6 [s, $C_{s,t,u\ or\ v}$]

133.4 [s, $C_{s,t,u \text{ or } v}$]

133.0 [d, J(CH) 162, $C_{b \text{ or } c}$]

126.3 [d, J(CH) 158, C_g]

125.4 [s, $C_{s,t,u \text{ or } v}$]

123.1 [d, J(CH) 178, C_l]

121.8 [d, J(CH) 161, $C_{b \text{ or } c}$]

121.6 [d, J(CH) 155, C_d]

121.4 [d, J(CH) 158, C_h]

121.1 [d, J(CH) 161, C_f]

120.1 [d, J(CH) 157, C_e]

120.1 [s, $C_{s,t,u \text{ or } v}$]

113.6 [d, J(CH) 175, C_o]

109.7 [d, J(CH) 174, C_m]

107.3 [d, J(CH) 180, C_k]

105.0 [d, J(CH) 158, C_a]

97.1 [d, J(CH) 178, C_n]

70.4 [s, C_r]

36.6 [s, C_q]

30.9 [q, J(CH) 127, C_i]

24.2 [q, J(CH) 127, C_j]

^1H assignments from selective decoupling, COSY45 and NOESY experiments

^{13}C assignments from ^{13}C-^1H shift correlation experiment

6.2.6 Data characterising $[\{Me_2C(\eta^5\text{-}C_5H_4)_2\}Zr(\eta^5\text{-}C_5H_5)Cl]$ (6)

Description: Pale yellow crystals

Elemental analysis for $C_{18}H_{19}ClZr$ (M.W. = 362.0):

found (required) / % C, 60.2 (59.7); H, 5.3 (5.3); Cl, 9.85 (9.8)

^{1}H NMR data: (300 MHz, C_6D_6, room temperature)

6.00 [2 H, pseudo q, J(HH) 3, C_5H_4]

5.83 [2 H, pseudo q, J(HH) 3, C_5H_4]

5.70 [5 H, s, C_5H_5]

5.35 [2 H, pseudo q, J(HH) 3, C_5H_4]

5.22 [2 H, pseudo q, J(HH) 3, C_5H_4]

1.30 [3 H, s, CH_3]

1.24 [3 H, s, CH_3]

^{13}C NMR data: $^{13}C\{^1H\}$ (75.5 MHz, CD_2Cl_2, room temperature)

146.7 [s, $C_{ipso}(C_5H_4)$]

122.9 [s, C_5H_4]

115.5 [s, C_5H_5]

112.5 [s, C_5H_4]

110.0 [s, C_5H_4]

93.1 [s, C_5H_4]

35.4 [s, CMe_2]

24.0 [s, CH_3]

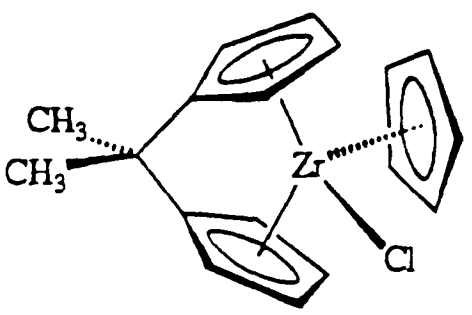

6.2.7 Data characterising [{$Me_2C(\eta^5\text{-}C_5H_4)_2$}Hf($\eta^5$-$C_5H_5$)Cl] (7)

Description: Pale yellow crystals

Elemental analysis for $C_{18}H_{19}ClHf$ (M.W. = 449.27):

found (required) / % C, 48.3 (48.1); H, 4.3 (4.3); Cl, 7.9 (7.9)

Single crystal X-ray structure: R = 0.0244; R_w = 0.0263

See Appendix D for further details

^{1}H NMR data: (300 MHz, d^8-THF, room temperature)

6.09 [2 H, m, C_5H_4]

5.94 [2 H, m, C_5H_4]

5.93 (5 H, s, C_5H_5]

5.82 [2 H, pseudo q, J(CH) 2.5, C_5H_4]

5.66 [2 H, pseudo q, J(CH) 2.5, C_5H_4]

1.64 [3 H, s, CH_3]

1.55 [3 H, s, CH_3]

^{1}H NMR data: (300 MHz, C_6D_6, room temperature)

5.99 [2 H, m, C_5H_4]

5.75 [2 H, m, C_5H_4]

5.58 [5 H, s, C_5H_5]

5.52 [2 H, m, C_5H_4]

5.18 [2 H, m, C_5H_4]

1.34 [3 H, s, CH_3]

1.30 [3 H, s, CH_3]

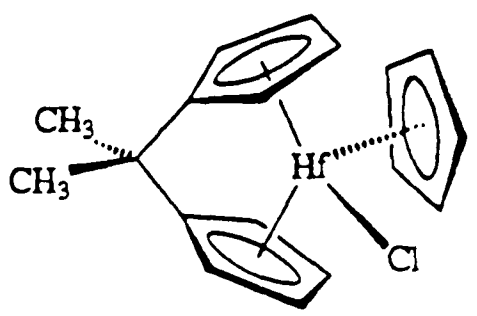

^{13}C NMR data: (75.5 MHz, d^8-THF, room temperature)

142.1 [s, $C_{ipso}(C_5H_4)$]

120.4 [d, J(CH) 172, C_5H_4]

117.0 [d, J(CH) 178, C_5H_4]

114.6 [d, J(CH) 174, C_5H_5]

105.5 [d, J(CH) 173, C_5H_4]

96.9 [d, J(CH) 173, C_5H_4]

35.9 [s, CMe_2]

27.3 [q, J(CH) 130, CH_3]

25.0 [coupling obscured by solvent, CH_3]

Other NMR Techniques:

Low temperature ^1H solution NMR experiments (500 MHz, d^8-THF, 304 to 173 K)

^{13}C CP/MAS solid state NMR experiments (50 MHz, 215 to 371 K)

6.3 Characterising data for new compounds described in Chapter 3

6.3.1 Data characterising

$[(\eta^5\text{-}C_5H_5)ZrCl_2\{(\eta^5\text{-}C_5H_4)CMe_2(\eta^5\text{-}C_9H_6)\}ZrCl_2(\eta^5\text{-}C_5H_5)]$ **(8)**

Description: Yellow crystalline solid

Elemental analysis for $C_{27}H_{26}Cl_4Zr_2$ (M.W. = 674.75):

found (required) / % C, 48.0 (48.1); H, 4.1 (3.9); Cl, 21.3 (21.0)

^{1}H NMR data: (300 MHz, CD_2Cl_2, room temperature)

7.56 [1 H, d, J(H_fH_e) 9, H_f]

7.53 [1 H, d, J(H_cH_d) 8, H_c]

7.19 [1 H, m, H_e]

7.14 [1 H, m, H_d]

6.75 [1 H, d, J(H_aH_b) 4, H_a]

6.73 [1 H, pseudo q, J(HH) 3, C_5H_4]

6.67 [1 H, d, J(H_bH_a) 4, H_b]

6.43 [5 H, s, Cp'Zr(C_5H_5)]

6.40 [1 H, pseudo q, J(HH) 3, C_5H_4]

6.14 [2 H, m, C_5H_4]

6.13 [5 H, s, Ind'Zr(C_5H_5)]

2.09 [3 H, s, CH_3]

2.00 [3 H, s, CH_3]

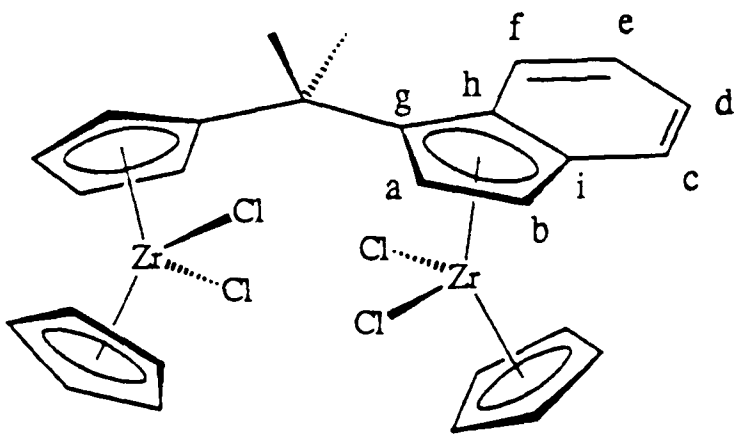

^{13}C NMR data: $^{13}C\{^1H\}$ (75.5 MHz, CD_2Cl_2, room temperature)

141.9 [s, $C_{ipso}(C_5H_4)$]

129.8 [s, $C_{g,\ h\ or\ i}$]

125.9 [s, C_c]

125.8 [s, C_e]

125.4 [s, $C_{g,\ h\ or\ i}$]

125.2 [s, C_f]

124.9 [s, C_d]

123.4 [s, $C_{g,\ h\ or\ i}$]

122.3 [s, C_a]

118.5 [s, C_5H_4]

116.9 [s, C_5H_4]

116.6 [s, Ind'Zr(C_5H_5)]

116.4 [s, Cp'Zr(C_5H_5)]

113.6 [s, C_5H_4]

111.5 [s, C_5H_4]

100.7 [s, C_b]

39.3 [s, CMe_2]

29.1 [s, CH_3]

28.2 [s, CH_3]

^1H and ^{13}C assignments from selective ^1H decoupling experiments, ^{13}C-^1H shift correlation experiment and comparison with compound **9**, **10** and **11**

6.3.2 Data characterising

$[(\eta^5\text{-}C_5H_5)HfCl_2\{(\eta^5\text{-}C_5H_4)CMe_2(\eta^5\text{-}C_9H_6)\}HfCl_2(\eta^5\text{-}C_5H_5)]$ (9)

Description: Yellow crystalline solid

Elemental analysis for $C_{27}H_{26}Cl_4Hf_2$ (M.W. = 849.29):

found (required) / % C, 38.6 (38.2); H, 3.1 (3.1); Cl, 16.6 (16.7)

^{1}H NMR data: (300 MHz, CD_2Cl_2, room temperature)

7.58 [1 H, d, J(H_fH_e) 9, H_f]

7.53 [1 H, d, J(H_cH_d) 9, H_c]

7.18 [1 H, m, H_e]

7.13 [1 H, m, H_d]

6.74 [1 H, d, J(H_aH_b) 4, H_a]

6.61 [1 H, pseudo q, J(HH) 3, C_5H_4]

6.50 [1 H, d, J(H_bH_a) 4, H_b]

6.33 [5 H, s, Cp'Hf(C_5H_5)]

6.29 [1 H, pseudo q, J(HH) 3, C_5H_4]

6.06 [2 H, m, C_5H_4]

6.00 [5 H, s, Ind'Hf(C_5H_5)]

2.08 [3 H, s, CH_3]

2.00 [3 H, s, CH_3]

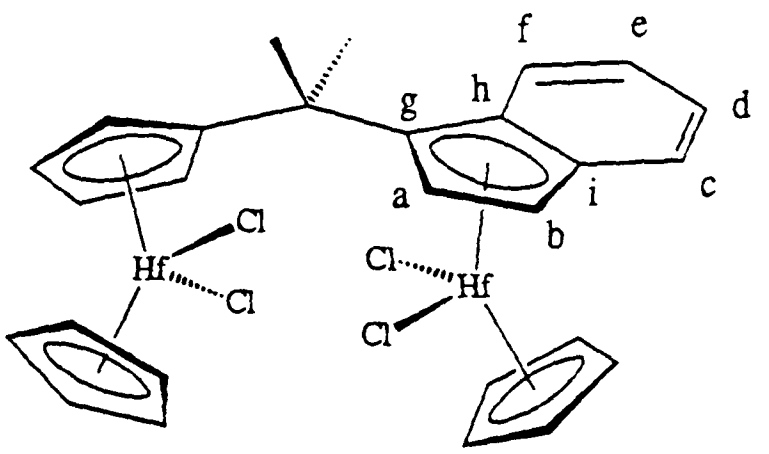

^{13}C NMR data: $^{13}C\{^1H\}$ (75.5 MHz, CD_2Cl_2, room temperature)

139.9 [s, $C_{ipso}(C_5H_4)$]

127.6 [s, $C_{g,\ h\ or\ i}$]

126.1 [s, C_c]

125.8 [s, C_e]

125.4 [s, $C_{g,\ h\ or\ i}$]

125.2 [s, C_f]

124.9 [s, C_d]

122.7 [s, $C_{g,\ h\ or\ i}$]

122.2 [s, C_a]

116.9 [s, C_5H_4]

115.5 [s, C_5H_4]

115.3 [s, Ind'Hf(C_5H_5)]

115.0 [s, Cp'Hf(C_5H_5)]

112.8 [s, C_5H_4]

110.2 [s, C_5H_4]

99.6 [s, C_b]

39.1 [s, *C*Me_2]

29.1 [s, CH_3]

28.2 [s, CH_3]

^1H and ^{13}C assignments from selective ^1H decoupling, ^1H NOESY and ^{13}C-^1H shift correlation experiments, and comparison with compound **8**, **10** and **11**

6.3.3 Data characterising

$[(\eta^5\text{-}C_5H_5)ZrCl_2\{(\eta^5\text{-}C_5H_4)CMe_2(\eta^5\text{-}C_9H_6)\}HfCl_2(\eta^5\text{-}C_5H_5)]$ **(10)**

Description: Yellow crystalline solid

Elemental analysis for $C_{27}H_{26}Cl_4ZrHf$ (M.W. = 762.02):

found (required) / % C, 42.4 (42.6); H, 3.5 (3.4); Cl, 18.7 (18.6)

^{1}H NMR data: (300 MHz, CD_2Cl_2, room temperature)

7.57 [1 H, d, J(H_fH_e) 9, H_f]

7.53 [1 H, d, J(H_cH_d) 8, H_c]

7.18 [1 H, m, H_e]

7.13 [1 H, m, H_d]

6.74 [1 H, d, J(H_aH_b) 4, H_a]

6.71 [1 H, pseudo q, J(HH) 3, C_5H_4]

6.51 [1 H, d, J(H_bH_a) 4, H_b]

6.43 [5 H, s, Zr(C_5H_5)]

6.40 [1 H, pseudo q, J(HH) 3, C_5H_4]

6.15 [2 H, m, C_5H_4]

6.01 [5 H, s, Hf(C_5H_5)]

2.10 [3 H, s, CH_3]

2.01 [3 H, s, CH_3]

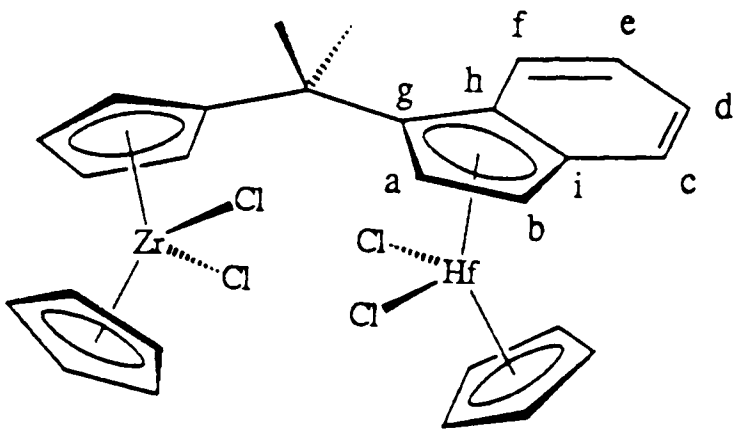

^{13}C NMR data: (75.5 MHz, CD_2Cl_2, room temperature)

142.1 [s, $C_{ipso}(C_5H_4)$]

127.7 [s, $C_{g,\ h\ or\ i}$]

126.2 [d, J(CH) 166, C_c]

126.0 [s, $C_{g,\ h\ or\ i}$]

125.8 [d, J(CH) 163, C_e]

125.1 [d, J(CH) 164, C_f]

124.7 [d, J(CH) 166, C_d]

122.6 [s, $C_{g,\ h\ or\ i}$]

122.2 [d, J(CH) 173, C_a]

118.4 [d, J(CH) 179, C_5H_4]

116.7 [d, J(CH) 176, C_5H_4]

116.4 [d, J(CH) 173, $Zr(C_5H_5)$]

115.3 [d, J(CH) 174, $Hf(C_5H_5)$]

113.7 [d, J(CH) 175, C_5H_4]

111.5 [d, J(CH) 173, C_5H_4]

99.6 [d, J(CH) 177, C_b]

39.2 [s, CMe_2]

29.1 [s, CH_3]

28.1 [s, CH_3]

^1H and ^{13}C assignments from selective ^1H decoupling experiments, ^{13}C-^1H shift correlation experiment and comparison with compounds **8**, **9** and **11**

6.3.4 Data characterising

$[(\eta^5\text{-}C_5H_5)HfCl_2\{(\eta^5\text{-}C_5H_4)CMe_2(\eta^5\text{-}C_9H_6)\}ZrCl_2(\eta^5\text{-}C_5H_5)]$ **(11)**

Description: Yellow powder

Elemental analysis for $C_{27}H_{26}Cl_4HfZr$ (M.W. = 762.02):

found (required) / % C, 42.4 (42.6); H, 3.5 (3.4); Cl, 18.6 (18.6)

^{1}H NMR data: (300 MHz, CD_2Cl_2, room temperature)

7.57 [1 H, d, J(H_fH_e) 9, H_f]

7.52 [1 H, d, J(H_cH_d) 8, H_c]

7.19 [1 H, m, H_e]

7.14 [1 H, m, H_d]

6.74 [1 H, d, J(H_aH_b) 3, H_a]

6.66 [1 H, d, J(H_bH_a) 3, H_b]

6.63 [1 H, pseudo q, J(HH) 3, C_5H_4]

6.33 [5 H, s, Hf(C_5H_5)]

6.29 [1 H, pseudo q, J(HH) 3, C_5H_4]

6.12 [5 H, s, Zr(C_5H_5)]

6.04 [2 H, m, C_5H_4]

2.09 [3 H, s, CH_3]

2.00 [3 H, s, CH_3]

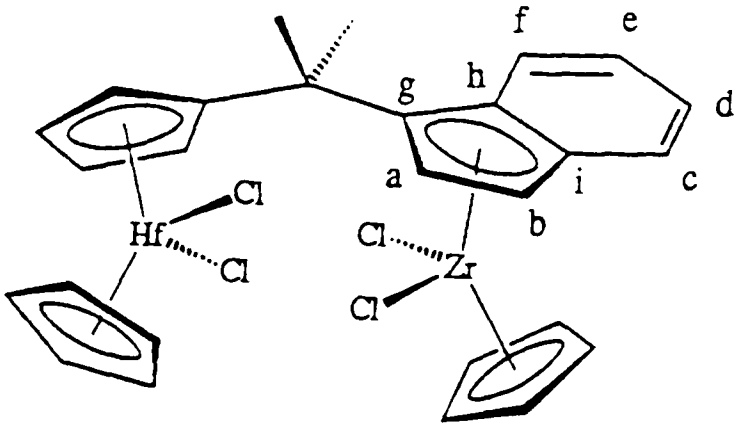

^{13}C NMR data: $^{13}C\{^1H\}$ (75.5 MHz, CD_2Cl_2, room temperature)

139.6 [s, $C_{ipso}(C_5H_4)$]

130.1 [s, $C_{g,\ h\ or\ i}$]

128.6 [s, $C_{g,\ h\ or\ i}$]

125.9 [s, C_c]

125.8 [s, C_e]

125.3 [s, C_f]

124.8 [s, C_d]

123.4 [s, $C_{g,\ h\ or\ i}$]

122.3 [s, C_a]

117.1 [s, C_5H_4]

116.6 [s, $Zr(C_5H_5)$]

115.8 [s, C_5H_4]

115.0 [s, $Hf(C_5H_5)$]

112.5 [s, C_5H_4]

110.2 [s, C_5H_4]

100.7 [s, C_b]

39.3 [s, CMe_2]

29.1 [s, CH_3]

28.2 [s, CH_3]

^1H and ^{13}C assignments from selective ^1H decoupling experiments, ^{13}C-^1H shift correlation experiment and comparison with compounds **8**, **9** and **10**

6.3.5 Data characterising

$[(\eta^5\text{-}C_5H_5)ZrCl_2\{(\eta^5\text{-}C_5H_4)CMe_2(\eta^5\text{-}C_9H_6)\}ZrCl_2(\eta^5\text{-}C_5Me_5)]$ **(12)**

Description: Yellow crystalline solid

Elemental analysis for $C_{32}H_{36}Cl_4Zr_2$ (M.W. = 744.86):

found (required) / % C, 51.5 (51.6); H, 4.8 (4.9); Cl, 18.6 (19.0)

^{1}H NMR data: (300 MHz, CD_2Cl_2, room temperature)

7.51 [1 H, d, J(H_fH_e) 8, H_f]

7.43 [1 H, d, J(H_cH_d) 8, H_c]

7.14 [1 H, m, H_e]

7.08 [1 H, m, H_d]

6.73 [1 H, pseudo q, J(HH) 3, C_5H_4]

6.38 [5 H, s, C_5H_5]

6.33 [1 H, pseudo q, J(HH) 3, C_5H_4]

6.30 [1 H, d, J(H_aH_b) 3, H_a]

6.16 [1 H, d, J(H_bH_a) 3, H_b]

6.11 [2 H, m, C_5H_4]

2.14 [3 H, s, CH_3]

1.97 [15 H, s, $C_5(CH_3)_5$]

1.95 [3 H, s, CH_3]

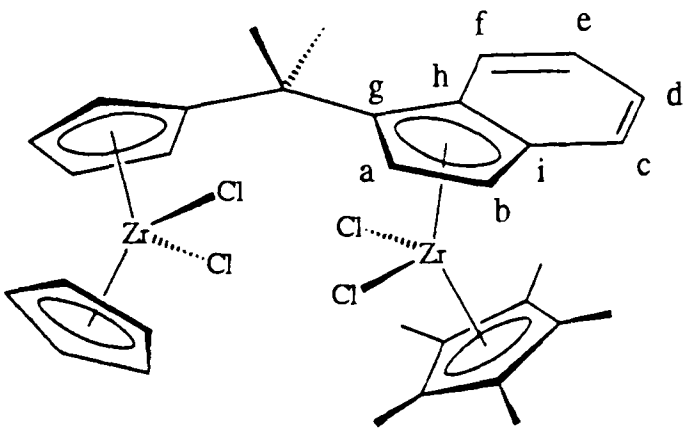

^{13}C NMR data: $^{13}C\{^1H\}$ (75.5 MHz, CD_2Cl_2, room temperature)

142.6 [s, $C_{ipso}(C_5H_4)$]

130.5 [s, $C_{g,\ h\ or\ i}$]

129.1 [s, $C_{g,\ h\ or\ i}$]

128.3 [s, $C_{g,\ h\ or\ i}$]

125.5 [s, C_e]

125.2 [s, C_d]

125.1 [s, C_f]

125.0 [s, $C_5(CH_3)_5$]

123.7 [s, C_c]

118.2 [s, C_5H_4]

117.1 [s, C_a]

116.5 [s, C_5H_4]

116.3 [s, C_5H_5]

113.9 [s, C_5H_4]

112.4 [s, C_5H_4]

97.0 [s, C_b]

39.7 [s, CMe_2]

28.9 [s, CH_3]

27.2 [s, CH_3]

12.6 [s, $C_5(CH_3)_5$]

^1H assignments from selective decoupling experiments and comparison with compounds **8** and **10**, ^{13}C assignments from ^{13}C-^1H shift correlation experiment

6.3.6 Data characterising

$[(\eta^5\text{-}C_5H_5)Zr(CH_3)_2\{(\eta^5\text{-}C_5H_4)CMe_2(\eta^5\text{-}C_9H_6)\}Zr(CH_3)_2(\eta^5\text{-}C_5H_5)]$ **(13)**

Description: Very pale orange crystalline solid

Elemental analysis for $C_{31}H_{38}Zr_2$ (M.W. = 593.05):

found (required) / % C, 62.6 (62.8); H, 6.4 (6.5)

^{1}H NMR data: (300 MHz, C_6D_6, room temperature)

7.43 [1 H, d, J(H_fH_e) 9, H_f]

7.09 [1 H, d, J(H_cH_d) 8, H_c]

6.79 [1 H, m, H_e]

6.67 [1 H, m, H_d]

6.41 [2 H, m, H_a and H_b]

5.95 [1 H, m, C_5H_4]

5.79 [1 H, m, C_5H_4]

5.75 [5 H, s, Cp'Zr(C_5H_5)]

5.48 [5 H, s, Ind'Zr(C_5H_5)]

5.46 [1 H, m, C_5H_4]

5.40 [1 H, m, C_5H_4]

1.56 [3 H, s, C(CH_3)]

1.43 [3 H, s, C(CH_3)]

0.05 [3 H, s, Ind'Zr(CH_3)]

0.00 [3 H, s, Cp'Zr(CH_3)]

-0.01 [3 H, s, Cp'Zr(CH_3)]

-0.22 [3 H, s, Ind'Zr(CH_3)]

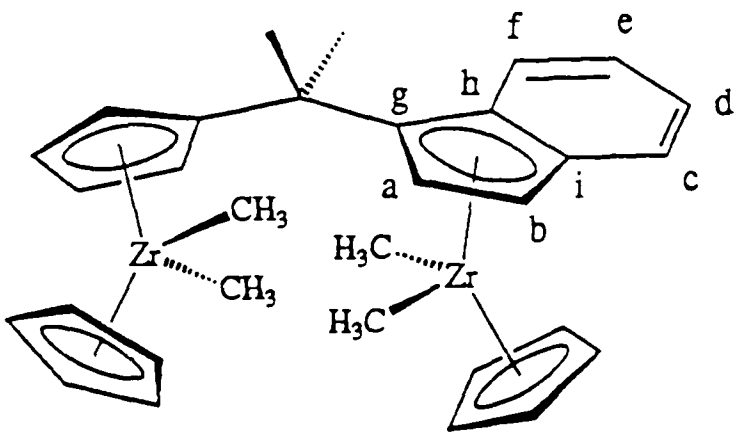

^{13}C NMR data: (75.5 MHz, C_6D_6, room temperature)

138.1 [s, $C_{ipso}(C_5H_4)$]

125.3 [d, J(CH) 161, C_c and C_f]

125.3 [s, $C_{g, h \text{ or } i}$]

124.0 [s, $C_{g, h \text{ or } i}$]

123.1 [d, J(CH) 159, C_e]

122.6 [d, J(CH) 160, C_d]

120.3 [s, $C_{g, h \text{ or } i}$]

116.9 [d, J(CH) , C_a]

112.4 [d, J(CH) 172, Ind'Zr(C_5H_5)]

110.8 [d, J(CH) 172, Cp'Zr(C_5H_5)]

110.5 [d, J(CH) 164, C_5H_4]

109.5 [d, J(CH) 170, C_5H_4]

109.1 [d, J(CH) 163, C_5H_4]

108.6 [d, J(CH) 164, C_5H_4]

100.9 [d, J(CH) 175, C_b]

37.9 [s, CMe_2]

35.3 [q, J(CH) 117, Ind'Zr(CH_3)]

32.9 [q, J(CH) 117, Ind'Zr(CH_3)]

31.6 [q, J(CH) 117, Cp'Zr(CH_3)]

31.4 [q, J(CH) 116, Cp'Zr(CH_3)]

30.1 [q, J(CH) 125, $C(CH_3)_2$]

^{1}H and ^{13}C assignments from selective ^{1}H decoupling experiments, ^{13}C-^{1}H shift correlation experiment and comparison with compounds **14**, **15** and **16**

6.3.7 Data characterising

$[(\eta^5\text{-}C_5H_5)Zr(CH_3)_2\{(\eta^5\text{-}C_5H_4)CMe_2(\eta^5\text{-}C_9H_6)\}Hf(CH_3)_2(\eta^5\text{-}C_5H_5)]$ **(14)**

Description: Pale yellow crystalline solid

Elemental analysis for $C_{31}H_{38}ZrHf$ (M.W. = 680.33):

found (required) / % C, 54.4 (54.7); H, 5.5 (5.6)

^{1}H NMR data: (300 MHz, C_6D_6, room temperature)

7.42 [1 H, d, J(H_fH_e) 9, H_f]

7.09 [1 H, d, J(H_cH_d) 8, H_c]

6.80 [1 H, m, H_e]

6.69 [1 H, m, H_d]

6.36 [1 H, d, J(H_aH_b) 4, H_a]

6.32 [1 H, d, J(H_bH_a) 4, H_b]

5.93 [1 H, pseudo q, J(HH) 3, C_5H_4]

5.78 [1 H, m, C_5H_4]

5.75 [5 H, s, $Zr(C_5H_5)$]

5.46 [1 H, pseudo q, J(HH) 3, C_5H_4]

5.41 [1 H, m, C_5H_4]

5.39 [5 H, s, $Hf(C_5H_5)$]

1.57 [3 H, s, $C(CH_3)$]

1.43 [3 H, s, $C(CH_3)$]

0.00 [3 H, s, $Zr(CH_3)$]

-0.01 [3 H, s, $Zr(CH_3)$]

-0.11 [3 H, s, $Hf(CH_3)$]

-0.39 [3 H, s, $Hf(CH_3)$]

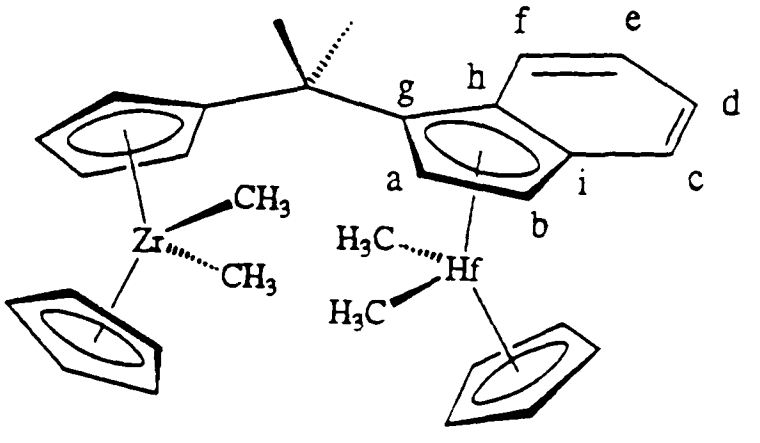

^{13}C NMR data: $^{13}C\{^1H\}$ (75.5 MHz, C_6D_6, room temperature)

138.1 [s, $C_{ipso}(C_5H_4)$]

125.5 [s, C_c]

125.2 [s, C_f]

123.4 [s, C_e]

123.0 [s, $C_{g,\ h\ or\ i}$]

122.7 [s, C_d]

120.6 [s, $C_{g,\ h\ or\ i}$]

117.2 [s, C_a]

111.6 [s, $Hf(C_5H_5)$]

110.8 [s, $Zr(C_5H_5)$]

110.5 [s, C_5H_4]

109.9 [s, C_5H_4]

109.0 [s, C_5H_4]

108.6 [s, C_5H_4]

100.2 [s, C_b]

41.1 [s, $Hf(CH_3)$]

38.5 [s, $Hf(CH_3)$]

37.9 [s, CMe_2]

31.5 [s, $Zr(CH_3)$]

31.4 [s, $Zr(CH_3)$]

30.1 [s, $C(CH_3)$]

30.0 [s, $C(CH_3)$]

^1H and ^{13}C assignments from selective ^1H decoupling experiments, ^{13}C-^1H shift correlation experiment and comparison with compounds **13**, **15** and **16**. One of the quaternary signals (g, h or i) is not observed, presumably obscured by another signal.

6.3.8 Data characterising

$[(\eta^5\text{-}C_5H_5)Hf(CH_3)_2\{(\eta^5\text{-}C_5H_4)CMe_2(\eta^5\text{-}C_9H_6)\}Zr(CH_3)_2(\eta^5\text{-}C_5H_5)]$ **(15)**

Description: Pale yellow crystalline solid

Elemental analysis for $C_{31}H_{38}HfZr$ (M.W. = 680.33):

found (required) / % C, 53.2 (54.7); H, 5.4 (5.6)

^{1}H NMR data: (300 MHz, C_6D_6, room temperature)

7.42 [1 H, d, J(H_fH_e) 9, H_f]

7.09 [1 H, d, J(H_cH_d) 8, H_c]

6.78 [1 H, m, H_e]

6.66 [1 H, m, H_d]

6.41 [2 H, m, H_a and H_b]

5.87 [1 H, pseudo q, J(HH) 3, C_5H_4]

5.72 [1 H, m, C_5H_4]

5.68 [5 H, s, $Hf(C_5H_5)$]

5.47 [5 H, s, $Zr(C_5H_5)$]

5.37 [2 H, m, C_5H_4]

1.56 [3 H, s, $C(CH_3)$]

1.45 [3 H, s, $C(CH_3)$]

0.05 [3 H, s, $Zr(CH_3)$]

-0.18 [3 H, s, $Hf(CH_3)$]

-0.19 [3 H, s, $Hf(CH_3)$]

-0.22 [3 H, s, $Zr(CH_3)$]

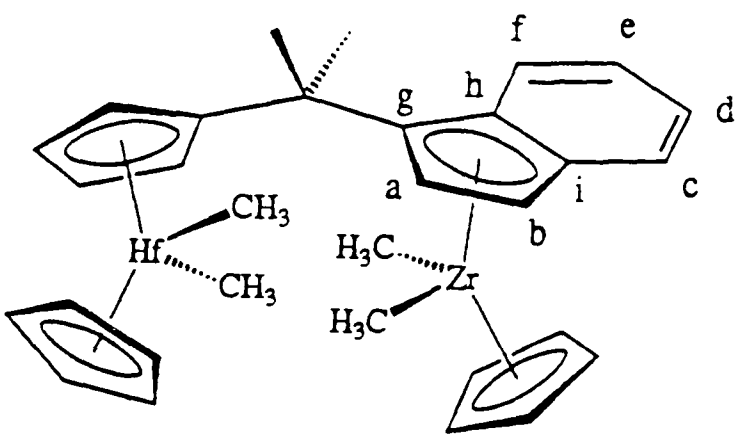

^{13}C NMR data: $^{13}C\{^{1}H\}$ (75.5 MHz, C_6D_6, room temperature)

136.7 [s, $C_{ipso}(C_5H_4)$]

125.3 [s, C_c and C_f]

124.0 [s, $C_{g, h \text{ or } i}$]

123.1 [s, C_e]

122.6 [s, C_d]

120.3 [s, $C_{g, h \text{ or } i}$]

117.0 [s, C_a]

112.4 [s, $Zr(C_5H_5)$]

110.3 [s, $Hf(C_5H_5)$]

109.9 [s, C_5H_4]

108.8 [s, C_5H_4]

108.7 [s, C_5H_4]

108.5 [s, C_5H_4]

101.0 [s, C_b]

37.9 [s, CMe_2]

37.7 [s, $Hf(CH_3)$]

37.5 [s, $Hf(CH_3)$]

35.2 [s, $Zr(CH_3)$]

32.8 [s, $Zr(CH_3)$]

30.0 [s, $C(CH_3)_2$]

^{1}H and ^{13}C assignments from selective ^{1}H decoupling experiments, ^{13}C-^{1}H shift correlation experiment and comparison with compounds **13**, **14** and **16**. One of the quaternary signals (g, h or i) is not observed, presumably obscured by another signal.

6.3.9 Data characterising

$[(\eta^5\text{-}C_5H_5)Hf(CH_3)_2\{(\eta^5\text{-}C_5H_4)CMe_2(\eta^5\text{-}C_9H_6)\}Hf(CH_3)_2(\eta^5\text{-}C_5H_5)]$ (16)

Description: Very pale yellow crystalline solid

Elemental analysis for $C_{31}H_{38}Hf_2$ (M.W. = 767.59):

found (required) / % C, 48.9 (48.5); H, 4.9 (5.0)

^{1}H NMR data: (300 MHz, C_6D_6, room temperature)

7.43 [1 H, d, J(H_fH_e) 9, H_f]

7.08 [1 H, d, J(H_cH_d) 8, H_c]

6.80 [1 H, m, H_e]

6.68 [1 H, m, H_d]

6.36 [1 H, d, J(H_aH_b) 4, H_a]

6.31 [1 H, d, J(H_bH_a) 4, H_b]

5.86 [1 H, pseudo q, J(HH) 3, C_5H_4]

5.70 [1 H, m, C_5H_4]

5.67 [5 H, s, Cp'Hf(C_5H_5)]

5.39 [5 H, s, Ind'Hf(C_5H_5)]

5.36 [2 H, m, C_5H_4]

1.58 [3 H, s, C(CH_3)]

1.46 [3 H, s, C(CH_3)]

-0.11 [3 H, s, Ind'Hf(CH_3)]

-0.18 [3 H, s, Cp'Hf(CH_3)]

-0.19 [3 H, s, Cp'Hf(CH_3)]

-0.39 [3 H, s, Ind'Hf(CH_3)]

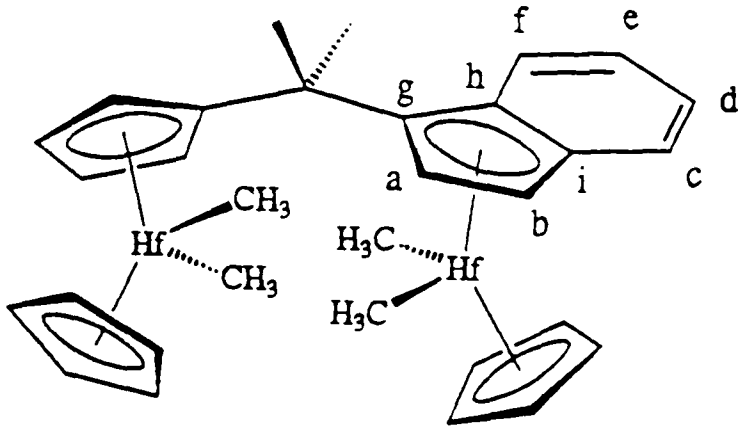

^{13}C NMR data: $^{13}C\{^{1}H\}$ (75.5 MHz, C_6D_6, room temperature)

136.7 [s, $C_{ipso}(C_5H_4)$]

125.5 [s, C_c]

125.3 [s, C_f]

123.4 [s, C_e]

123.0 [s, $C_{g,\ h\ or\ i}$]

122.7 [s, C_d]

120.5 [s, $C_{g,\ h\ or\ i}$]

117.2 [s, C_a]

111.6 [s, Ind'Hf(C_5H_5)]

110.3 [s, Cp'Hf(C_5H_5)]

109.8 [s, C_5H_4]

108.7 [s, $2(C_5H_4)$]

108.4 [s, C_5H_4]

100.2 [s, C_b]

41.1 [s, Ind'Hf(CH_3)]

38.4 [s, Ind'Hf(CH_3)]

37.9 [s, CMe_2]

37.7 [s, Cp'Hf(CH_3)]

37.5 [s, Cp'Hf(CH_3)]

29.9 [s, $C(CH_3)_2$]

^{1}H and ^{13}C assignments from selective ^{1}H decoupling, ^{1}H NOESY and ^{13}C-^{1}H shift correlation experiments, and comparison with compounds **13**, **14** and **15**. One of the quaternary signals (g, h or i) is not observed, presumably obscured by another signal.

6.3.10 Data characterising $[Li(C_5H_4)CMe_2(C_9H_7)]$

Description: Pale orange crystals

Elemental analysis for $C_{17}H_{17}Li$ (M.W. = 228.25):

found (required) / % C, 85.6 (89.5); H, 7.8 (7.5); Li, 3.0 (2.9)

(too air/moisture sensitive to get more satisfactory analysis from ICL analytical department)

^{1}H NMR data: (300 MHz, d^8-THF, room temperature)

7.15 [1 H, d, J(H_fH_e) 7, H_f or J(H_cH_d) 7, H_c]

7.02 [1 H, pseudo t, J($H_dH_{c,e}$) 7, H_d, or J($H_eH_{d,f}$) 7, H_e]

6.78 [1 H, pseudo t, J($H_dH_{c,e}$) 7, H_d, or J($H_eH_{d,f}$) 7, H_e]

6.71 [1 H, d, J(H_aH_b) 6, H_a or H_b]

6.54 [1 H, d, J(H_aH_b) 6, H_a or H_b]

6.17 [1 H, d, J(H_fH_e) 7, H_f or J(H_cH_d) 7, H_c]

5.64 [2 H, m, C_5H_4]

5.60 [2 H, m, C_5H_4]

3.69 [1 H, br.s, H_g]

1.47 [3 H, s, CH_3]

0.98 [3 H, s, CH_3]

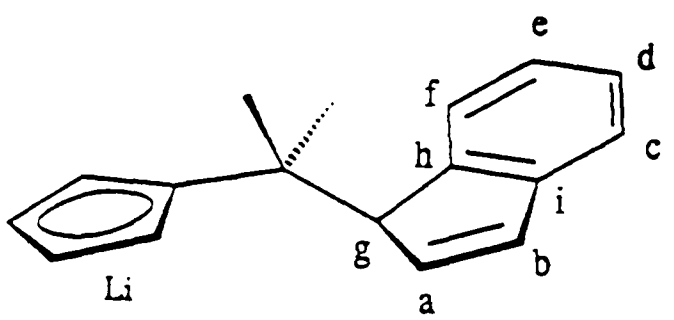

^{13}C NMR data: $^{13}C\{^1H\}$ (75.5 MHz, d^8-THF, room temperature)

147.7 [s, $C_{h\ or\ i}$]

145.9 [s, $C_{h\ or\ i}$]

139.9 [s, $C_{a\ or\ b}$]

131.0 [s, $C_{a\ or\ b}$]

130.0 [s, $C_{ipso}(C_5H_4)$]

126.7 [s, $C_{c\ or\ f}$]

125.9 [s, $C_{d\ or\ e}$]

124.3 [s, $C_{d\ or\ e}$]

120.1 [s, $C_{c\ or\ f}$]

102.5 [s, C_5H_4]

101.8 [s, C_5H_4]

65.5 [s, C_g]

38.4 [s, CMe_2]

31.3 [s, CH_3]

24.5 [s, CH_3]

^1H assignments from selective decoupling experiments, ^{13}C assignments from ^{13}C-^1H shift correlation experiment and by comparison with ^{13}C NMR spectrum of indene (C_9H_8)

^{7}Li NMR Data: (116.6 MHz, d^8-THF, room temperature)

-4.0 ppm (relative to 1.0 M LiCl in D_2O)

6.3.11 Data characterising $[(\eta^5\text{-}C_5H_5)ZrCl_2\{(\eta^5\text{-}C_5H_4)CMe_2(C_9H_7)\}]$ (17)

Description: White microcrystalline solid

Elemental analysis for $C_{22}H_{22}Cl_2Zr$ (M.W. = 448.53):

found (required) / % C, 59.0 (58.9); H, 5.0 (5.0); Cl, 15.9 (15.8)

^{1}H NMR data: (300 MHz, CD_2Cl_2, room temperature)

7.25 [1 H, d, J(H_fH_e) 7, H_f or J(H_cH_d) 7, H_c]

7.19 [1 H, pseudo t, J($H_dH_{c,e}$) 7, H_d, or J($H_eH_{d,f}$) 7, H_e]

7.02 [1 H, pseudo t, J($H_dH_{c,e}$) 7, H_d, or J($H_eH_{d,f}$) 7, H_e]

6.73 [1 H, dd, J(H_aH_b) 6, J($H_{a\text{ or }b}H_g$) 2, H_a or H_b]

6.65 [1 H, d, J(H_fH_e) 7, H_f or J(H_cH_d) 7, H_c]

6.49 [5 H, s, C_5H_5]

6.46 [2 H, m, C_5H_4]

6.39 [1 H, m, C_5H_4]

6.33 [1 H, dd, J(H_aH_b) 6, J($H_{a\text{ or }b}H_g$) 2, H_a or H_b]

6.28 [1 H, m, C_5H_4]

3.46 [1 H, m, H_g]

1.56 [3 H, s, CH_3]

1.34 [3 H, s, CH_3]

^{13}C NMR data: $^{13}C\{^1H\}$ (75.5 MHz, CD_2Cl_2, room temperature)

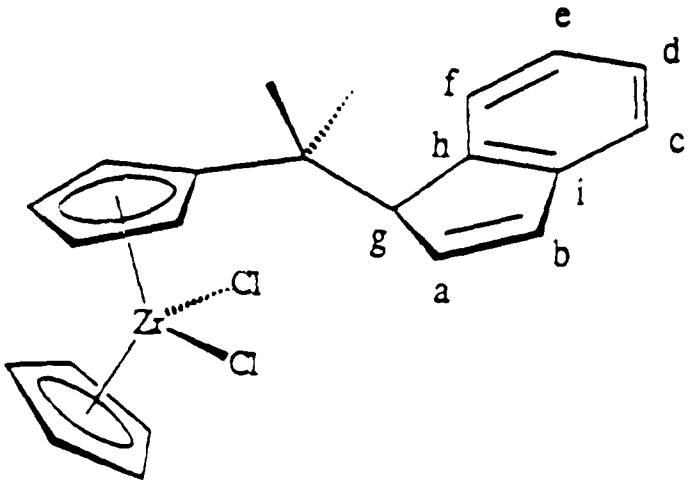

145.6 [s, $C_{h\text{ or }i}$]

144.5 [s, $C_{h\text{ or }i}$]

142.0 [s, $C_{ipso}(C_5H_4)$]

137.0 [s, $C_{a\text{ or }b}$]

132.3 [s, $C_{a\text{ or }b}$]

126.9 [s, $C_{d\text{ or }e}$]

124.8 [s, $C_{c\ or\ f}$]

124.5 [s, $C_{d\ or\ e}$]

121.0 [s, $C_{c\ or\ f}$]

117.3 [s, C_5H_4]

117.3 [s, C_5H_4]

116.3 [s, C_5H_5]

114.3 [s, C_5H_4]

111.0 [s, C_5H_4]

64.0 [s, C_g]

39.4 [s, CMe_2]

27.0 [s, CH_3]

23.4 [s, CH_3]

^1H assignments from selective decoupling experiments

^{13}C assignments from ^{13}C-^1H shift correlation experiment

6.3.12 Data characterising $[(\eta^5\text{-}C_5H_5)HfCl_2[(\eta^5\text{-}C_5H_4)CMe_2(C_9H_7)\}]$ (18)

Description: White microcrystalline solid

Elemental analysis for $C_{22}H_{22}Cl_2Hf$ (M.W. = 535.80):

found (required) / % C, 49.2 (49.3); H, 4.0 (4.1); Cl, 13.4 (13.2)

^{1}H NMR data: (300 MHz, CD_2Cl_2, room temperature)

7.24 [1 H, d, J(H_fH_e) 7, H_f or J(H_cH_d) 7, H_c]

7.18 [1 H, pseudo t, J($H_dH_{c,e}$) 7, H_d, or J($H_eH_{d,f}$) 7, H_e]

7.00 [1 H, pseudo t, J($H_dH_{c,e}$) 7, H_d, or J($H_eH_{d,f}$) 7, H_e]

6.73 [1 H, dd, J(H_aH_b) 6, J($H_{a\text{ or }b}H_g$) 2, H_a or H_b]

6.57 [1 H, d, J(H_fH_e) 7, H_f or J(H_cH_d) 7, H_c]

6.39 [5 H, s, C_5H_5]

6.39 [1 H, m, C_5H_4]

6.36 [1 H, m, C_5H_4]

6.33 [1 H, dd, J(H_aH_b) 6, J($H_{a\text{ or }b}H_g$) 2, H_a or H_b]

6.28 [1 H, m, C_5H_4]

6.19 [1 H, m, C_5H_4]

3.46 [1 H, m, H_g]

1.56 [3 H, s, CH_3]

1.30 [3 H, s, CH_3]

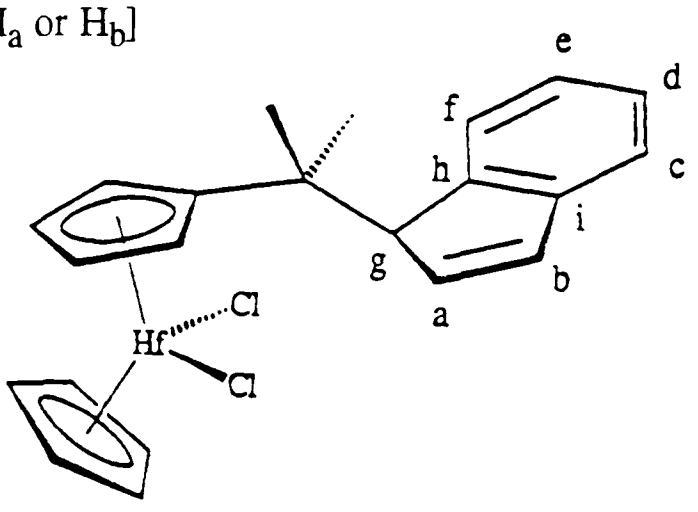

^{13}C NMR data: $^{13}C\{^1H\}$ (75.5 MHz, CD_2Cl_2, room temperature)

145.6 [s, $C_{h\text{ or }i}$]

144.6 [s, $C_{h\text{ or }i}$]

139.8 [s, $C_{ipso}(C_5H_4)$]

137.1 [s, $C_{a\text{ or }b}$]

132.3 [s, $C_{a\text{ or }b}$]

126.9 [s, $C_{d\ or\ e}$]

125.0 [s, $C_{c\ or\ f}$]

124.5 [s, $C_{d\ or\ e}$]

121.0 [s, $C_{c\ or\ f}$]

116.0 [s, C_5H_4]

115.7 [s, C_5H_4]

114.9 [s, C_5H_5]

113.4 [s, C_5H_4]

109.5 [s, C_5H_4]

64.3 [s, C_g]

39.3 [s, CMe_2]

27.0 [s, CH_3]

23.1 [s, CH_3]

^1H assignments from selective decoupling experiments

^{13}C assignments from ^{13}C-^1H shift correlation experiment

6.3.13 Data characterising $[(\eta^5\text{-}C_5H_5)Zr(CH_3)_2[(\eta^5\text{-}C_5H_4)CMe_2(C_9H_7)]]$ (19)

Description: Very pale yellow crystalline solid

Elemental analysis for $C_{24}H_{28}Zr$ (M.W. = 407.68):

found (required) / % C, 70.6 (70.7); H, 7.1 (6.9)

^{1}H NMR data: (300 MHz, C_6D_6, room temperature)

7.24 [1 H, d, J(H_fH_e) 7, H_f or J(H_cH_d) 7, H_c]

7.21 [1 H, m (coupling obscured by solvent), H_d, or H_e]

7.09 [1 H, pseudo t, J($H_dH_{c,e}$) 7, H_d, or J($H_eH_{d,f}$) 7, H_e]

6.74 [1 H, d, J(H_fH_e) 7, H_f or J(H_cH_d) 7, H_c]

6.69 [1 H, d, J(H_aH_b) 6, H_a or H_b]

6.22 [1 H, d, J(H_aH_b) 6, H_a or H_b]

5.88 [1 H, m, C_5H_4]

5.80 [5 H, s, C_5H_5]

5.75 [1 H, m, C_5H_4]

5.64 [1 H, m, C_5H_4]

5.61 [1 H, m, C_5H_4]

3.39 [1 H, br. s, H_g]

1.05 [3 H, s, C(CH_3)]

0.98 [3 H, s, C(CH_3)]

-0.03 [3 H, s, Zr(CH_3)]

-0.05 [3 H, s, Zr(CH_3)]

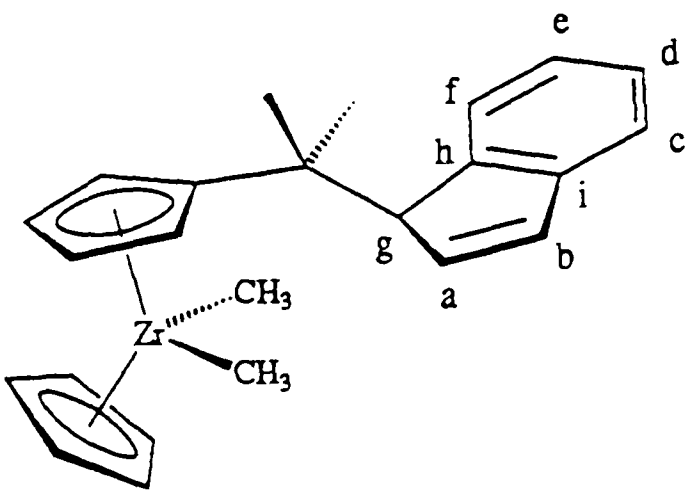

^{13}C NMR data: $^{13}C\{^1H\}$ (75.5 MHz, C_6D_6, room temperature)

145.6 [s, $C_{h\ or\ i}$]

145.1 [s, $C_{h\ or\ i}$]

137.6 [s, $C_{ipso}(C_5H_4)$]

137.3 [s, $C_{a\ or\ b}$]

132.5 [s, $C_{a\ or\ b}$]

127.0 [s, $C_{d\ or\ e}$]

125.3 [s, $C_{c\ or\ f}$]

124.7 [s, $C_{d\ or\ e}$]

121.2 [s, $C_{c\ or\ f}$]

110.8 [s, C_5H_4]

110.8 [s, C_5H_5]

110.1 [s, C_5H_4]

109.2 [s, C_5H_4]

107.9 [s, C_5H_4]

64.6 [s, C_g]

38.4 [s, CMe_2]

31.6 [s, $Zr(CH_3)$]

31.2 [s, $Zr(CH_3)$]

27.4 [s, $C(CH_3)$]

22.9 [s, $C(CH_3)$]

^1H assignments from selective decoupling experiments

^{13}C assignments from ^{13}C-^1H shift correlation experiment

APPENDICES

X-Ray Crystal Structure Data

A. X-ray structure analysis of [{$Me_2C(\eta^5\text{-}C_5H_4)(\eta^2\text{-}C_9H_6)$}$Zr(\eta^5\text{-}C_5H_5)Cl$] (1)

A.1 Crystal data, data collection and refinement

Compound **1**; $C_{22}H_{21}ClZr$, M = 412.06, tetrahedral, space group $P\bar{4}2_1c$, a = b = 22.794(1), c = 7.0667(8) Å, V = 3671.8 Å^3, F(000) = 1680, Z = 8, D_c = 1.49 gcm^{-3}, μ = 7.35 cm^{-1}, crystal size *ca.* 0.22 x 0.28 x 0.45 mm, 4174 total (3696 independent) reflections, R = 0.044 and R_w = 0.050 from 1552 reflections with $I > 3\sigma(I)$ (217 variables, observations / variables 7.15), maximum peak in final Fourier difference synthesis 0.57 eÅ^{-3}.

Data were collected at room temperature on an Enraf-Nonius CAD4 diffractometer using graphite-monochromated MoK_α radiation ($\omega/2\theta$ scan mode, ratio of scan rates ω/θ = 1.2, θ_{max} = 32.5°). The structure was solved by direct methods and refined by full-matrix least-squares technique in the anisotropic approximation (Chebyshev weighting scheme, parameters 9.65, -6.15, 7.84, -0.81).[1] About 75 % of hydrogen atoms were located in the difference Fourier maps, positions of the remainder were calculated geometrically. In the final refinement, all hydrogen atoms were included with the fixed positional and thermal parameters. Corrections for Lorentz and polarisation effects and an empirical correction for absorption were applied.[2] Anomalous dispersion contributions were included in the calculated structure factors. Crystallographic calculations were carried out using the CRYSTALS program package[3] on a Micro VAX 3800 computer. The data were collected and the structure was solved by Dr. Alexander Chernega.

A.2 Interatomic distances (Å) and angles (°) for [{$Me_2C(\eta^5$-$C_5H_4)(\eta^2$-$C_9H_6)$}$Zr(\eta^5$-$C_5H_5)Cl$] (1)

ZR(1)	- CL(1)	2.489(2)
ZR(1)	- C(1)	2.511(9)
ZR(1)	- C(2)	2.49(1)
ZR(1)	- C(3)	2.492(9)
ZR(1)	- C(4)	2.520(9)
ZR(1)	- C(5)	2.540(9)
ZR(1)	- C(6)	2.438(8)
ZR(1)	- C(7)	2.479(8)
ZR(1)	- C(8)	2.514(8)
ZR(1)	- C(9)	2.483(8)
ZR(1)	- C(10)	2.451(8)
ZR(1)	- C(14)	2.587(8)
ZR(1)	- C(15)	2.497(8)
C(1)	- C(2)	1.39(2)
C(1)	- C(5)	1.42(2)
C(2)	- C(3)	1.40(1)
C(3)	- C(4)	1.37(2)
C(4)	- C(5)	1.38(1)
C(6)	- C(7)	1.40(1)
C(6)	- C(10)	1.43(1)
C(7)	- C(8)	1.37(1)
C(8)	- C(9)	1.41(1)
C(9)	- C(10)	1.41(1)
C(10)	- C(11)	1.51(1)
C(11)	- C(12)	1.52(1)
C(11)	- C(13)	1.53(1)
C(11)	- C(14)	1.53(1)
C(14)	- C(15)	1.43(1)
C(14)	- C(18)	1.45(1)
C(15)	- C(16)	1.40(1)
C(16)	- C(17)	1.41(1)
C(17)	- C(18)	1.43(1)
C(17)	- C(22)	1.42(1)
C(18)	- C(19)	1.41(1)
C(19)	- C(20)	1.39(1)
C(20)	- C(21)	1.41(2)
C(21)	- C(22)	1.35(2)

C(1)	- ZR(1) - CL(1)	95.5(3)
C(2)	- ZR(1) - CL(1)	127.2(3)
C(2)	- ZR(1) - C(1)	32.2(4)
C(3)	- ZR(1) - CL(1)	127.0(3)
C(3)	- ZR(1) - C(1)	53.9(3)
C(3)	- ZR(1) - C(2)	32.7(3)
C(4)	- ZR(1) - CL(1)	95.6(3)
C(4)	- ZR(1) - C(1)	53.7(3)
C(4)	- ZR(1) - C(2)	53.3(4)
C(4)	- ZR(1) - C(3)	31.8(4)
C(5)	- ZR(1) - CL(1)	77.8(3)
C(5)	- ZR(1) - C(1)	32.6(4)
C(5)	- ZR(1) - C(2)	53.1(4)
C(5)	- ZR(1) - C(3)	52.8(3)
C(5)	- ZR(1) - C(4)	31.8(3)
C(6)	- ZR(1) - CL(1)	133.2(2)
C(6)	- ZR(1) - C(1)	96.1(4)
C(6)	- ZR(1) - C(2)	77.9(4)
C(6)	- ZR(1) - C(3)	95.8(4)
C(6)	- ZR(1) - C(4)	127.2(4)
C(6)	- ZR(1) - C(5)	127.9(4)
C(7)	- ZR(1) - CL(1)	106.0(2)
C(7)	- ZR(1) - C(1)	80.4(4)
C(7)	- ZR(1) - C(2)	79.1(4)
C(7)	- ZR(1) - C(3)	108.9(4)
C(7)	- ZR(1) - C(4)	131.0(3)
C(7)	- ZR(1) - C(5)	111.4(4)
C(8)	- ZR(1) - CL(1)	79.2(2)
C(8)	- ZR(1) - C(1)	99.9(3)
C(8)	- ZR(1) - C(2)	109.0(4)
C(8)	- ZR(1) - C(3)	140.5(4)
C(8)	- ZR(1) - C(4)	152.8(3)
C(8)	- ZR(1) - C(5)	122.2(4)
C(9)	- ZR(1) - CL(1)	84.6(3)
C(9)	- ZR(1) - C(1)	132.0(3)
C(9)	- ZR(1) - C(2)	130.6(4)
C(9)	- ZR(1) - C(3)	148.5(4)
C(9)	- ZR(1) - C(4)	174.3(3)
C(9)	- ZR(1) - C(5)	152.9(3)
C(10)	- ZR(1) - CL(1)	116.6(2)
C(10)	- ZR(1) - C(1)	130.1(4)
C(10)	- ZR(1) - C(2)	109.2(3)
C(10)	- ZR(1) - C(3)	115.9(3)
C(10)	- ZR(1) - C(4)	144.8(4)
C(10)	- ZR(1) - C(5)	161.8(4)
C(14)	- ZR(1) - CL(1)	117.1(2)
C(14)	- ZR(1) - C(1)	140.1(3)
C(14)	- ZR(1) - C(2)	109.6(3)
C(14)	- ZR(1) - C(3)	87.0(3)
C(14)	- ZR(1) - C(4)	98.3(3)
C(14)	- ZR(1) - C(5)	129.8(3)
C(15)	- ZR(1) - CL(1)	85.2(2)
C(15)	- ZR(1) - C(1)	149.6(3)
C(15)	- ZR(1) - C(2)	133.1(3)
C(15)	- ZR(1) - C(3)	102.0(3)
C(15)	- ZR(1) - C(4)	96.0(3)
C(15)	- ZR(1) - C(5)	119.9(4)
C(7)	- ZR(1) - C(6)	33.1(3)
C(8)	- ZR(1) - C(6)	54.1(3)
C(8)	- ZR(1) - C(7)	31.9(3)
C(9)	- ZR(1) - C(6)	54.8(4)
C(9)	- ZR(1) - C(7)	54.1(4)
C(9)	- ZR(1) - C(8)	32.8(3)

C(10)	- ZR(1)	- C(6)	34.1(3)
C(10)	- ZR(1)	- C(7)	55.5(3)
C(10)	- ZR(1)	- C(8)	55.0(3)
C(10)	- ZR(1)	- C(9)	33.1(3)
C(14)	- ZR(1)	- C(6)	78.5(3)
C(14)	- ZR(1)	- C(7)	109.2(3)
C(14)	- ZR(1)	- C(8)	107.9(3)
C(14)	- ZR(1)	- C(9)	76.7(3)
C(14)	- ZR(1)	- C(10)	55.7(3)
C(15)	- ZR(1)	- C(6)	105.5(3)
C(15)	- ZR(1)	- C(7)	128.7(3)
C(15)	- ZR(1)	- C(8)	110.0(3)
C(15)	- ZR(1)	- C(9)	78.4(3)
C(15)	- ZR(1)	- C(10)	74.4(3)
C(15)	- ZR(1)	- C(14)	32.6(3)
C(2)	- C(1)	- ZR(1)	72.9(5)
C(5)	- C(1)	- ZR(1)	74.8(6)
C(5)	- C(1)	- C(2)	106.4(9)
C(1)	- C(2)	- ZR(1)	74.8(6)
C(3)	- C(2)	- ZR(1)	73.9(6)
C(3)	- C(2)	- C(1)	108.7(11)
C(2)	- C(3)	- ZR(1)	73.4(5)
C(4)	- C(3)	- ZR(1)	75.2(6)
C(4)	- C(3)	- C(2)	108.1(9)
C(3)	- C(4)	- ZR(1)	73.0(5)
C(5)	- C(4)	- ZR(1)	74.9(6)
C(5)	- C(4)	- C(3)	108.5(10)
C(1)	- C(5)	- ZR(1)	72.6(5)
C(4)	- C(5)	- ZR(1)	73.3(5)
C(4)	- C(5)	- C(1)	108.3(10)
C(7)	- C(6)	- ZR(1)	75.0(5)
C(10)	- C(6)	- ZR(1)	73.4(5)
C(10)	- C(6)	- C(7)	108.3(8)
C(6)	- C(7)	- ZR(1)	71.9(5)
C(8)	- C(7)	- ZR(1)	75.5(5)
C(8)	- C(7)	- C(6)	108.8(9)
C(7)	- C(8)	- ZR(1)	72.6(4)
C(9)	- C(8)	- ZR(1)	72.4(4)
C(9)	- C(8)	- C(7)	108.3(9)
C(8)	- C(9)	- ZR(1)	74.8(5)
C(10)	- C(9)	- ZR(1)	72.2(4)
C(10)	- C(9)	- C(8)	108.9(10)
C(6)	- C(10)	- ZR(1)	72.5(5)
C(9)	- C(10)	- ZR(1)	74.7(5)
C(9)	- C(10)	- C(6)	105.8(8)
C(11)	- C(10)	- ZR(1)	104.6(5)
C(11)	- C(10)	- C(6)	125.5(8)
C(11)	- C(10)	- C(9)	126.4(9)
C(12)	- C(11)	- C(10)	108.9(9)
C(13)	- C(11)	- C(10)	111.4(8)
C(13)	- C(11)	- C(12)	108.3(9)
C(14)	- C(11)	- C(10)	101.5(6)
C(14)	- C(11)	- C(12)	114.2(8)
C(14)	- C(11)	- C(13)	112.3(9)
C(11)	- C(14)	- ZR(1)	98.1(5)
C(15)	- C(14)	- ZR(1)	70.2(4)
C(15)	- C(14)	- C(11)	120.6(7)
C(18)	- C(14)	- ZR(1)	107.8(5)
C(18)	- C(14)	- C(11)	131.8(8)
C(18)	- C(14)	- C(15)	106.4(8)
C(14)	- C(15)	- ZR(1)	77.2(5)
C(16)	- C(15)	- ZR(1)	103.9(6)
C(16)	- C(15)	- C(14)	109.4(8)
C(17)	- C(16)	- C(15)	108.4(8)
C(18)	- C(17)	- C(16)	108.3(7)
C(22)	- C(17)	- C(16)	130.8(10)
C(22)	- C(17)	- C(18)	120.9(10)
C(17)	- C(18)	- C(14)	107.4(8)
C(19)	- C(18)	- C(14)	133.6(10)
C(19)	- C(18)	- C(17)	119.0(8)
C(20)	- C(19)	- C(18)	119.1(12)
C(21)	- C(20)	- C(19)	120.2(11)
C(22)	- C(21)	- C(20)	122.8(9)
C(21)	- C(22)	- C(17)	118.0(11)

A.3 Fractional atomic coordinates and isotropic thermal parameters for all non-hydrogen atoms of [{$Me_2C(\eta^5\text{-}C_5H_4)(\eta^2\text{-}C_9H_6)$}$Zr(\eta^5\text{-}C_5H_5)Cl$] (1)

Atom	x/a	y/b	z/c	U(iso)
ZR(1)	0.29312(3)	0.01834(3)	0.6727(1)	0.0362
CL(1)	0.3370(1)	0.0620(1)	0.3825(3)	0.0624
C(1)	0.3891(4)	-0.0005(4)	0.836(2)	0.0567
C(2)	0.3460(5)	-0.0288(5)	0.940(2)	0.0635
C(3)	0.3229(4)	-0.0746(4)	0.831(2)	0.0516
C(4)	0.3517(4)	-0.0753(4)	0.661(2)	0.0580
C(5)	0.3930(4)	-0.0308(5)	0.661(2)	0.0658
C(6)	0.2435(4)	0.0603(4)	0.947(1)	0.0459
C(7)	0.2907(4)	0.0980(4)	0.911(1)	0.0503
C(8)	0.2812(4)	0.1259(3)	0.742(2)	0.0480
C(9)	0.2278(4)	0.1055(3)	0.666(2)	0.0502
C(10)	0.2032(4)	0.0644(3)	0.792(1)	0.0432
C(11)	0.1552(4)	0.0208(4)	0.747(1)	0.0525
C(12)	0.1276(5)	0.0003(5)	0.932(2)	0.0647
C(13)	0.1073(5)	0.0485(5)	0.625(2)	0.0737
C(14)	0.1895(3)	-0.0269(3)	0.641(1)	0.0399
C(15)	0.2131(4)	-0.0157(4)	0.458(1)	0.0490
C(16)	0.2348(4)	-0.0679(4)	0.381(1)	0.0533
C(17)	0.2236(4)	-0.1138(4)	0.511(2)	0.0477
C(18)	0.1946(3)	-0.0895(3)	0.672(2)	0.0408
C(19)	0.1783(4)	-0.1270(4)	0.822(2)	0.0591
C(20)	0.1917(4)	-0.1863(4)	0.810(2)	0.0612
C(21)	0.2220(4)	-0.2084(4)	0.651(2)	0.0617
C(22)	0.2382(4)	-0.1742(4)	0.504(2)	0.0607

A.4 Anisotropic thermal parameters for [{$Me_2C(\eta^5\text{-}C_5H_4)(\eta^2\text{-}C_9H_6)$}$Zr(\eta^5\text{-}C_5H_5)Cl$] (1)

Atom	U(11)	U(22)	U(33)	U(23)	U(13)	U(12)
ZR(1)	0.0416(4)	0.0329(4)	0.0355(3)	-0.0018(4)	0.0042(4)	0.0033(3)
CL(1)	0.088(2)	0.071(2)	0.047(1)	0.000(1)	0.017(1)	-0.024(1)
C(1)	0.046(5)	0.048(5)	0.105(9)	-0.005(7)	-0.032(7)	0.001(4)
C(2)	0.065(6)	0.059(6)	0.080(7)	0.010(6)	-0.023(6)	0.011(5)
C(3)	0.046(5)	0.043(4)	0.091(7)	0.010(6)	-0.027(6)	0.008(4)
C(4)	0.061(6)	0.056(5)	0.075(7)	-0.023(7)	-0.018(7)	0.020(4)
C(5)	0.046(5)	0.082(7)	0.094(8)	0.027(8)	0.015(7)	0.018(5)
C(6)	0.066(6)	0.039(4)	0.042(4)	-0.007(4)	0.013(4)	0.003(4)
C(7)	0.052(5)	0.046(5)	0.060(5)	-0.016(4)	0.006(5)	-0.001(5)
C(8)	0.060(6)	0.027(4)	0.073(6)	-0.010(4)	0.009(5)	-0.002(4)
C(9)	0.068(5)	0.029(3)	0.069(5)	0.004(5)	0.011(6)	0.007(4)
C(10)	0.046(5)	0.036(4)	0.056(6)	0.001(4)	0.005(4)	0.015(4)
C(11)	0.035(5)	0.051(5)	0.083(6)	0.012(5)	0.005(4)	-0.001(4)
C(12)	0.060(6)	0.063(6)	0.13(1)	0.006(7)	0.058(7)	0.006(5)
C(13)	0.047(5)	0.069(7)	0.16(1)	-0.003(8)	-0.035(7)	0.012(5)
C(14)	0.044(4)	0.030(4)	0.048(5)	-0.002(3)	-0.002(4)	-0.001(3)
C(15)	0.062(5)	0.043(4)	0.051(4)	0.002(4)	-0.011(4)	-0.017(5)
C(16)	0.056(5)	0.056(5)	0.053(5)	-0.005(4)	-0.001(4)	-0.016(4)
C(17)	0.047(5)	0.039(4)	0.074(6)	-0.009(4)	-0.015(5)	-0.012(4)
C(18)	0.039(4)	0.036(4)	0.054(4)	0.001(4)	-0.009(4)	-0.009(3)
C(19)	0.060(5)	0.053(5)	0.079(6)	0.026(6)	0.005(6)	-0.002(4)
C(20)	0.054(6)	0.057(6)	0.12(1)	0.043(7)	-0.015(7)	-0.020(5)
C(21)	0.048(5)	0.040(4)	0.14(1)	0.012(8)	-0.025(7)	-0.004(4)
C(22)	0.063(6)	0.040(5)	0.099(8)	-0.011(6)	-0.016(6)	-0.008(4)

B. X-ray structure analysis of $[\{(CH_2)_5C(\eta^5\text{-}C_5H_4)(\eta^2\text{-}C_9H_6)\}Zr(\eta^5\text{-}C_5H_5)Cl]$ $[0.5(C_6H_5CH_3)]$ (3)

B.1 Crystal data, data collection and refinement

Compound **3**; $[C_{25}H_{25}ClZr][(0.5)C_7H_8]$, M = 498.22, monoclinic, space group $P2_1/n$, a = 12.123(2), b = 7.069(3), c = 27.504(7) Å, β = 101.76(2), V = 2307.5 Å^3, F(000) = 1028, Z = 4, D_c = 1.43 gcm^{-3}, μ = 5.98 cm^{-1}, crystal size *ca.* 0.16 x 0.31 x 0.71 mm, 4539 total (3843 independent) reflections, R = 0.033 and R_w = 0.035 from 2086 reflections with $I > 4\sigma(I)$ (280 variables, observations / variables 7.5), maximum peak in final Fourier difference synthesis 0.28 eÅ^{-3}.

Data were collected at room temperature on an Enraf-Nonius CAD4 diffractometer using graphite-monochromated MoK_α radiation ($\omega/2\theta$ scan mode, θ_{max} = 24.5°). Corrections were made for Lorentz and polarization effects for both structures as well as an empirical correction for absorption.[2] The structure was solved by direct methods and refined by full-matrix least-squares technique in the anisotropic approximation (Chebyshev weighting scheme, parameters 3.66, -2.49, 2.39).[1] All hydrogen atoms were located in the difference Fourier maps, except the H atoms of the toluene solvate molecules whose positions were calculated geometrically. In the final refinement all H atoms were included with the fixed positional and thermal parameters. Crystallographic calculations were carried out using the CRYSTALS program package[3] on a MicroVAX 3800 computer. The data were collected and the structure was solved by Dr. Alexander Chernega.

B.2 Interatomic distances (Å) and angles (°) for [{$(CH_2)_5C(\eta^5\text{-}C_5H_4)(\eta^2\text{-}C_9H_6)$}$Zr(\eta^5\text{-}C_5H_5)Cl$] [0.5($C_6H_5CH_3$)] (3)

ZR(1)	-	CL(1)	2.500(1)	C(1)	- ZR(1) -	CL(1)	127.8(2)
ZR(1)	-	C(1)	2.481(6)	C(2)	- ZR(1) -	CL(1)	125.1(2)
ZR(1)	-	C(2)	2.497(5)	C(2)	- ZR(1) -	C(1)	32.2(2)
ZR(1)	-	C(3)	2.532(5)	C(3)	- ZR(1) -	CL(1)	93.5(2)
ZR(1)	-	C(4)	2.526(5)	C(3)	- ZR(1) -	C(1)	53.0(2)
ZR(1)	-	C(5)	2.481(5)	C(3)	- ZR(1) -	C(2)	31.8(2)
ZR(1)	-	C(6)	2.483(5)	C(4)	- ZR(1) -	CL(1)	77.3(2)
ZR(1)	-	C(7)	2.527(5)	C(4)	- ZR(1) -	C(1)	53.2(2)
ZR(1)	-	C(8)	2.500(5)	C(4)	- ZR(1) -	C(2)	52.3(2)
ZR(1)	-	C(9)	2.446(5)	C(4)	- ZR(1) -	C(3)	30.9(2)
ZR(1)	-	C(10)	2.461(4)	C(5)	- ZR(1) -	CL(1)	95.9(2)
ZR(1)	-	C(17)	2.564(4)	C(5)	- ZR(1) -	C(1)	32.6(2)
ZR(1)	-	C(18)	2.508(5)	C(5)	- ZR(1) -	C(2)	53.0(2)
C(1)	-	C(2)	1.383(9)	C(5)	- ZR(1) -	C(3)	52.2(2)
C(1)	-	C(5)	1.394(9)	C(5)	- ZR(1) -	C(4)	31.7(2)
C(2)	-	C(3)	1.378(9)	C(6)	- ZR(1) -	CL(1)	83.9(1)
C(3)	-	C(4)	1.349(8)	C(6)	- ZR(1) -	C(1)	132.5(2)
C(4)	-	C(5)	1.369(9)	C(6)	- ZR(1) -	C(2)	151.0(2)
C(6)	-	C(7)	1.426(7)	C(6)	- ZR(1) -	C(3)	174.1(2)
C(6)	-	C(10)	1.411(7)	C(6)	- ZR(1) -	C(4)	151.7(2)
C(7)	-	C(8)	1.394(7)	C(6)	- ZR(1) -	C(5)	133.2(2)
C(8)	-	C(9)	1.406(6)	C(7)	- ZR(1) -	CL(1)	78.4(1)
C(9)	-	C(10)	1.421(6)	C(7)	- ZR(1) -	C(1)	111.1(2)
C(10)	-	C(11)	1.527(6)	C(7)	- ZR(1) -	C(2)	142.8(2)
C(11)	-	C(12)	1.539(6)	C(7)	- ZR(1) -	C(3)	151.4(2)
C(11)	-	C(16)	1.538(7)	C(7)	- ZR(1) -	C(4)	120.9(2)
C(11)	-	C(17)	1.543(6)	C(7)	- ZR(1) -	C(5)	100.9(2)
C(12)	-	C(13)	1.531(7)	C(8)	- ZR(1) -	CL(1)	105.6(1)
C(13)	-	C(14)	1.506(8)	C(8)	- ZR(1) -	C(1)	80.9(2)
C(14)	-	C(15)	1.507(8)	C(8)	- ZR(1) -	C(2)	111.1(2)
C(15)	-	C(16)	1.522(7)	C(8)	- ZR(1) -	C(3)	131.4(2)
C(17)	-	C(18)	1.439(7)	C(8)	- ZR(1) -	C(4)	110.7(2)
C(17)	-	C(21)	1.456(6)	C(8)	- ZR(1) -	C(5)	81.2(2)
C(18)	-	C(19)	1.376(7)	C(9)	- ZR(1) -	CL(1)	132.5(1)
C(19)	-	C(20)	1.409(7)	C(9)	- ZR(1) -	C(1)	79.1(2)
C(20)	-	C(21)	1.440(6)	C(9)	- ZR(1) -	C(2)	98.6(2)
C(20)	-	C(25)	1.415(7)	C(9)	- ZR(1) -	C(3)	129.6(2)
C(21)	-	C(22)	1.396(7)	C(9)	- ZR(1) -	C(4)	128.1(2)
C(22)	-	C(23)	1.372(7)	C(9)	- ZR(1) -	C(5)	96.7(2)
C(23)	-	C(24)	1.399(8)	C(10)	- ZR(1) -	CL(1)	116.1(1)
C(24)	-	C(25)	1.369(8)	C(10)	- ZR(1) -	C(1)	109.8(2)
C(26)	-	C(27)	1.19(6)	C(10)	- ZR(1) -	C(2)	118.2(2)
C(26)	-	C(28)	1.28(3)	C(10)	- ZR(1) -	C(3)	147.7(2)
C(27)	-	C(28)	1.50(4)	C(10)	- ZR(1) -	C(4)	161.7(2)
C(28)	-	C(29)	1.13(3)	C(10)	- ZR(1) -	C(5)	130.3(2)
				C(17)	- ZR(1) -	CL(1)	117.5(1)
				C(17)	- ZR(1) -	C(1)	107.9(2)
				C(17)	- ZR(1) -	C(2)	86.9(2)
				C(17)	- ZR(1) -	C(3)	99.7(2)
				C(17)	- ZR(1) -	C(4)	130.6(2)
				C(17)	- ZR(1) -	C(5)	138.8(2)
				C(18)	- ZR(1) -	CL(1)	85.3(1)
				C(18)	- ZR(1) -	C(1)	130.7(2)
				C(18)	- ZR(1) -	C(2)	100.5(2)
				C(18)	- ZR(1) -	C(3)	95.7(2)
				C(18)	- ZR(1) -	C(4)	119.8(2)
				C(18)	- ZR(1) -	C(5)	147.9(2)
				C(7)	- ZR(1) -	C(6)	33.1(2)
				C(8)	- ZR(1) -	C(6)	54.5(2)
				C(8)	- ZR(1) -	C(7)	32.2(2)
				C(9)	- ZR(1) -	C(6)	55.0(2)
				C(9)	- ZR(1) -	C(7)	54.3(2)
				C(9)	- ZR(1) -	C(8)	33.0(2)

C(10) - ZR(1) - C(6)	33.1(2)
C(10) - ZR(1) - C(7)	54.8(1)
C(10) - ZR(1) - C(8)	55.1(1)
C(10) - ZR(1) - C(9)	33.7(1)
C(17) - ZR(1) - C(6)	77.0(1)
C(17) - ZR(1) - C(7)	108.5(1)
C(17) - ZR(1) - C(8)	109.5(2)
C(17) - ZR(1) - C(9)	78.6(2)
C(17) - ZR(1) - C(10)	56.4(1)
C(18) - ZR(1) - C(6)	78.9(2)
C(18) - ZR(1) - C(7)	110.8(2)
C(18) - ZR(1) - C(8)	129.5(2)
C(18) - ZR(1) - C(9)	106.0(2)
C(18) - ZR(1) - C(10)	75.5(2)
C(18) - ZR(1) - C(17)	32.9(2)
C(2) - C(1) - ZR(1)	74.5(3)
C(5) - C(1) - ZR(1)	73.7(3)
C(5) - C(1) - C(2)	106.2(6)
C(1) - C(2) - ZR(1)	73.2(3)
C(3) - C(2) - ZR(1)	75.5(3)
C(3) - C(2) - C(1)	108.4(5)
C(2) - C(3) - ZR(1)	72.7(3)
C(4) - C(3) - ZR(1)	74.3(3)
C(4) - C(3) - C(2)	108.5(6)
C(3) - C(4) - ZR(1)	74.8(3)
C(5) - C(4) - ZR(1)	72.3(3)
C(5) - C(4) - C(3)	108.5(6)
C(1) - C(5) - ZR(1)	73.7(3)
C(4) - C(5) - ZR(1)	75.9(3)
C(4) - C(5) - C(1)	108.4(5)
C(7) - C(6) - ZR(1)	75.1(3)
C(10) - C(6) - ZR(1)	72.6(3)
C(10) - C(6) - C(7)	108.2(5)
C(6) - C(7) - ZR(1)	71.8(3)
C(8) - C(7) - ZR(1)	72.8(3)
C(8) - C(7) - C(6)	107.9(4)
C(7) - C(8) - ZR(1)	75.0(3)
C(9) - C(8) - ZR(1)	71.4(3)
C(9) - C(8) - C(7)	108.3(4)
C(8) - C(9) - ZR(1)	75.6(3)
C(10) - C(9) - ZR(1)	73.8(3)
C(10) - C(9) - C(8)	108.6(4)
C(6) - C(10) - ZR(1)	74.3(3)
C(9) - C(10) - ZR(1)	72.6(2)
C(9) - C(10) - C(6)	106.9(4)
C(11) - C(10) - ZR(1)	103.4(3)
C(11) - C(10) - C(6)	125.5(4)
C(11) - C(10) - C(9)	124.6(4)
C(12) - C(11) - C(10)	111.8(4)
C(16) - C(11) - C(10)	110.1(4)
C(16) - C(11) - C(12)	108.4(4)
C(17) - C(11) - C(10)	101.5(3)
C(17) - C(11) - C(12)	111.3(4)
C(17) - C(11) - C(16)	113.5(4)
C(13) - C(12) - C(11)	112.5(4)
C(14) - C(13) - C(12)	111.8(4)
C(15) - C(14) - C(13)	110.9(4)
C(16) - C(15) - C(14)	111.2(5)
C(15) - C(16) - C(11)	111.7(4)
C(11) - C(17) - ZR(1)	98.6(2)
C(18) - C(17) - ZR(1)	71.4(2)
C(18) - C(17) - C(11)	121.2(4)
C(21) - C(17) - ZR(1)	109.0(3)
C(21) - C(17) - C(11)	130.7(5)
C(21) - C(17) - C(18)	106.3(4)
C(17) - C(18) - ZR(1)	75.6(3)
C(19) - C(18) - ZR(1)	105.6(3)
C(19) - C(18) - C(17)	109.3(4)
C(20) - C(19) - C(18)	109.4(4)
C(21) - C(20) - C(19)	108.2(4)
C(25) - C(20) - C(19)	132.3(5)
C(25) - C(20) - C(21)	119.4(5)
C(20) - C(21) - C(17)	106.6(4)
C(22) - C(21) - C(17)	134.0(5)
C(22) - C(21) - C(20)	119.4(4)
C(23) - C(22) - C(21)	119.5(5)
C(24) - C(23) - C(22)	121.6(5)
C(25) - C(24) - C(23)	120.9(5)
C(24) - C(25) - C(20)	119.2(5)
C(28) - C(26) - C(27)	132.9(41)
C(28) - C(27) - C(26)	101.1(26)
C(27) - C(28) - C(26)	126.0(30)
C(29) - C(28) - C(26)	128.2(39)
C(29) - C(28) - C(27)	105.8(38)

B.3 Fractional atomic coordinates and isotropic thermal parameters for all non-hydrogen atoms of $[\{(CH_2)_5C(\eta^5\text{-}C_5H_4)(\eta^2\text{-}C_9H_6)\}Zr(\eta^5\text{-}C_5H_5)Cl]$ $[0.5(C_6H_5CH_3)]$ (3)

Atom	x/a	y/b	z/c	U(iso)
ZR(1)	0.08483(4)	0.04867(7)	0.81733(2)	0.0331
CL(1)	0.1577(1)	-0.2559(2)	0.79011(5)	0.0503
C(1)	-0.0095(6)	0.3094(9)	0.7642(2)	0.0572
C(2)	-0.0956(5)	0.204(1)	0.7767(2)	0.0523
C(3)	-0.0980(5)	0.030(1)	0.7537(2)	0.0543
C(4)	-0.0152(6)	0.025(1)	0.7275(2)	0.0602
C(5)	0.0406(5)	0.195(1)	0.7336(2)	0.0531
C(6)	0.2579(4)	0.0370(8)	0.8835(2)	0.0413
C(7)	0.2952(4)	0.1005(8)	0.8403(2)	0.0447
C(8)	0.2458(4)	0.2759(8)	0.8269(2)	0.0412
C(9)	0.1787(4)	0.3240(7)	0.8612(2)	0.0343
C(10)	0.1870(3)	0.1771(7)	0.8970(2)	0.0307
C(11)	0.1047(3)	0.1479(7)	0.9317(2)	0.0317
C(12)	0.1561(4)	0.0256(8)	0.9769(2)	0.0416
C(13)	0.2531(4)	0.1252(9)	1.0119(2)	0.0503
C(14)	0.2182(5)	0.3155(9)	1.0282(2)	0.0549
C(15)	0.1698(4)	0.4372(9)	0.9840(2)	0.0450
C(16)	0.0707(4)	0.3400(7)	0.9504(2)	0.0396
C(17)	0.0068(3)	0.0444(8)	0.8972(2)	0.0345
C(18)	0.0188(4)	-0.1477(8)	0.8818(2)	0.0352
C(19)	-0.0851(4)	-0.2168(7)	0.8591(2)	0.0420
C(20)	-0.1682(4)	-0.0794(7)	0.8612(2)	0.0366
C(21)	-0.1132(4)	0.0867(7)	0.8850(2)	0.0358
C(22)	-0.1775(4)	0.2460(8)	0.8906(2)	0.0428
C(23)	-0.2919(5)	0.2416(9)	0.8735(2)	0.0545
C(24)	-0.3460(4)	0.082(1)	0.8499(2)	0.0538
C(25)	-0.2863(4)	-0.078(1)	0.8436(2)	0.0539
C(26)	0.472(2)	0.669(4)	-0.005(1)	0.1314
C(27)	0.493(2)	0.644(5)	0.039(1)	0.1587
C(28)	0.524(1)	0.438(4)	0.0417(9)	0.1438
C(29)	0.545(2)	0.401(4)	0.083(1)	0.0876

B.4 Anisotropic thermal parameters for [{$(CH_2)_5C(\eta^5\text{-}C_5H_4)(\eta^2\text{-}C_9H_6)$}Zr($\eta^5$-$C_5H_5$)Cl] [0.5($C_6H_5CH_3$)] (3)

Atom	U(11)	U(22)	U(33)	U(23)	U(13)	U(12)
ZR(1)	0.0336(2)	0.0330(2)	0.0323(2)	0.0007(3)	0.0058(2)	-0.0014(3)
CL(1)	0.0689(9)	0.0383(7)	0.0603(8)	-0.0043(7)	0.0301(7)	0.0031(7)
C(1)	0.083(5)	0.042(4)	0.060(4)	0.009(3)	-0.024(4)	-0.007(3)
C(2)	0.044(3)	0.095(5)	0.041(3)	0.017(3)	0.003(3)	0.024(3)
C(3)	0.050(3)	0.070(5)	0.053(3)	0.011(3)	-0.008(3)	-0.023(3)
C(4)	0.079(4)	0.076(5)	0.037(3)	-0.010(3)	-0.007(3)	0.005(4)
C(5)	0.044(4)	0.110(6)	0.038(3)	0.030(4)	0.000(3)	-0.006(4)
C(6)	0.030(2)	0.049(3)	0.047(3)	0.000(3)	0.005(2)	-0.002(3)
C(7)	0.033(3)	0.063(4)	0.053(3)	-0.006(3)	0.019(2)	-0.005(2)
C(8)	0.044(3)	0.052(3)	0.037(3)	-0.003(2)	0.013(2)	-0.018(3)
C(9)	0.034(3)	0.035(3)	0.034(2)	-0.000(2)	0.005(2)	-0.003(2)
C(10)	0.022(2)	0.038(3)	0.035(2)	-0.006(2)	0.000(2)	-0.006(2)
C(11)	0.026(2)	0.038(3)	0.033(2)	0.005(2)	0.006(2)	-0.003(2)
C(12)	0.039(3)	0.050(3)	0.041(3)	0.010(2)	0.012(2)	0.001(2)
C(13)	0.050(3)	0.067(4)	0.038(3)	0.009(3)	0.001(2)	-0.003(3)
C(14)	0.052(3)	0.077(4)	0.043(3)	-0.011(3)	0.004(3)	-0.011(3)
C(15)	0.044(3)	0.054(3)	0.049(3)	-0.017(3)	0.017(2)	-0.008(3)
C(16)	0.039(3)	0.040(3)	0.043(3)	-0.004(2)	0.014(2)	0.001(2)
C(17)	0.031(2)	0.034(2)	0.041(2)	0.005(3)	0.010(2)	0.001(3)
C(18)	0.032(3)	0.040(3)	0.039(3)	0.000(2)	0.014(2)	-0.003(2)
C(19)	0.052(3)	0.039(3)	0.040(3)	-0.002(2)	0.013(2)	-0.010(3)
C(20)	0.030(3)	0.052(4)	0.034(2)	0.001(2)	0.007(2)	-0.010(2)
C(21)	0.031(2)	0.044(3)	0.035(2)	0.001(2)	0.009(2)	0.001(2)
C(22)	0.031(3)	0.059(3)	0.045(3)	-0.001(3)	0.007(2)	0.007(3)
C(23)	0.039(3)	0.076(4)	0.055(3)	-0.001(3)	0.004(3)	0.013(3)
C(24)	0.028(3)	0.094(6)	0.058(3)	-0.001(4)	-0.005(2)	0.002(3)
C(25)	0.046(3)	0.080(5)	0.046(3)	-0.008(3)	-0.000(2)	-0.017(3)
C(26)	0.12(1)	0.19(2)	0.52(5)	-0.22(3)	0.19(3)	-0.05(1)
C(27)	0.12(1)	0.25(3)	0.48(5)	-0.21(3)	0.18(3)	-0.11(1)
C(28)	0.067(9)	0.19(2)	0.31(2)	-0.01(2)	0.07(1)	-0.02(1)
C(29)	0.034(8)	0.11(2)	0.22(3)	0.02(2)	-0.02(1)	0.021(9)

C. X-ray structure analysis of [{$Me_2(\eta^5\text{-}C_5H_4)(\eta^3\text{-}C_{13}H_8)$}$Zr(\eta^5\text{-}C_5H_5)Cl$] (5)

C.1 Crystal data, data collection and refinement

Compound **5**; $C_{26}H_{23}ClZr$, M = 462.12, monoclinic, space group $P2_1/c$, a = 15.249(3), b = 8.588(2), c = 16.185(6) Å, β = 108.65(2), V = 2008.4 $Å^3$, F(000) 944, Z = 4, D_c = 1.53 gcm^{-3}, μ = 6.81 cm^{-1}, crystal size *ca.* 0.2 x 0.3 x 0.3 mm, 4335 total (3138 independent) reflections, R = 0.038 and R_w = 0.037 from 2037 reflections with $I > 3\sigma(I)$ (253 variables, observations / variables 8.1), maximum peak in final Fourier difference synthesis 0.41 $eÅ^{-3}$.

Data were collected at room temperature on an Enraf-Nonius CAD4 diffractometer using graphite-monochromated MoK_α radiation ($\omega/2\theta$ scan mode, θ_{max} = 24°). Corrections were made for Lorentz and polarization effects as well as an empirical correction for absorption.[2] The structure was solved by direct methods and refined by full-matrix least-squares technique in the anisotropic approximation (Chebyshev weighting scheme, parameters 13.0, -19.3, 13.0, -5.50, 1.51).[1] The hydrogen atoms were located in the difference Fourier maps except the $\eta^5\text{-}C_5H_5$ hydrogen atoms which were placed geometrically. In the final refinement of both structures all H atoms were included with the fixed positional and thermal parameters. Crystallographic calculations were carried out using the CRYSTALS program package[3] on a MicroVAX 3800 computer. The data collection was preformed by Dr. Vince Murphy and the structure was solved by Dr. Philip Mountford.

C.2. Interatomic distances (Å) and angles (°) for [{$Me_2(\eta^5\text{-}C_5H_4)(\eta^3\text{-}C_{13}H_8)$}Zr($\eta^5$-$C_5H_5$)Cl] (5)

ZR(1) - CL(1)	2.560(1)
ZR(1) - C(5)	2.692(5)
ZR(1) - C(6)	2.633(5)
ZR(1) - C(7)	2.649(5)
ZR(1) - C(17)	2.453(5)
ZR(1) - C(18)	2.505(5)
ZR(1) - C(19)	2.531(6)
ZR(1) - C(20)	2.529(6)
ZR(1) - C(21)	2.442(5)
ZR(1) - C(22)	2.510(6)
ZR(1) - C(23)	2.502(6)
ZR(1) - C(24)	2.467(6)
ZR(1) - C(25)	2.479(6)
ZR(1) - C(26)	2.483(6)
C(1) - C(2)	1.370(7)
C(1) - C(6)	1.460(6)
C(1) - C(13)	1.440(7)
C(2) - C(3)	1.384(7)
C(3) - C(4)	1.397(7)
C(4) - C(5)	1.389(7)
C(5) - C(6)	1.406(7)
C(6) - C(7)	1.445(7)
C(7) - C(8)	1.489(7)
C(7) - C(14)	1.539(6)
C(8) - C(9)	1.402(7)
C(8) - C(13)	1.412(6)
C(9) - C(10)	1.396(7)
C(10) - C(11)	1.393(8)
C(11) - C(12)	1.370(8)
C(12) - C(13)	1.394(6)
C(14) - C(15)	1.548(7)
C(14) - C(16)	1.538(7)
C(14) - C(17)	1.516(7)
C(17) - C(18)	1.426(7)
C(17) - C(21)	1.413(8)
C(18) - C(19)	1.434(8)
C(19) - C(20)	1.395(9)
C(20) - C(21)	1.412(8)
C(22) - C(23)	1.35(1)
C(22) - C(26)	1.35(1)
C(23) - C(24)	1.34(1)
C(24) - C(25)	1.40(1)
C(25) - C(26)	1.39(1)

C(5) - ZR(1) - CL(1)	74.9(1)
C(6) - ZR(1) - CL(1)	105.0(1)
C(6) - ZR(1) - C(5)	30.6(1)
C(7) - ZR(1) - CL(1)	132.1(1)
C(7) - ZR(1) - C(5)	58.6(1)
C(7) - ZR(1) - C(6)	31.8(1)
C(17) - ZR(1) - CL(1)	115.8(1)
C(17) - ZR(1) - C(5)	87.5(2)
C(17) - ZR(1) - C(6)	79.3(2)
C(17) - ZR(1) - C(7)	55.8(1)
C(18) - ZR(1) - CL(1)	82.6(1)
C(18) - ZR(1) - C(5)	82.1(2)
C(18) - ZR(1) - C(6)	91.3(2)
C(18) - ZR(1) - C(7)	80.7(2)
C(18) - ZR(1) - C(17)	33.4(2)
C(19) - ZR(1) - CL(1)	74.5(2)
C(19) - ZR(1) - C(5)	110.3(2)
C(19) - ZR(1) - C(6)	124.4(2)
C(19) - ZR(1) - C(7)	109.9(2)
C(19) - ZR(1) - C(17)	54.7(2)
C(19) - ZR(1) - C(18)	33.1(2)
C(20) - ZR(1) - CL(1)	100.5(2)
C(20) - ZR(1) - C(5)	136.4(2)
C(20) - ZR(1) - C(6)	133.8(2)
C(20) - ZR(1) - C(7)	105.3(2)
C(20) - ZR(1) - C(17)	54.8(2)
C(20) - ZR(1) - C(18)	54.5(2)
C(21) - ZR(1) - CL(1)	128.8(1)
C(21) - ZR(1) - C(5)	120.0(2)
C(21) - ZR(1) - C(6)	103.8(2)
C(21) - ZR(1) - C(7)	73.1(2)
C(21) - ZR(1) - C(17)	33.6(2)
C(21) - ZR(1) - C(18)	55.3(2)
C(22) - ZR(1) - CL(1)	108.1(3)
C(22) - ZR(1) - C(5)	94.1(2)
C(22) - ZR(1) - C(6)	79.7(2)
C(22) - ZR(1) - C(7)	87.1(2)
C(22) - ZR(1) - C(17)	134.8(3)
C(22) - ZR(1) - C(18)	167.4(2)
C(23) - ZR(1) - CL(1)	79.5(2)
C(23) - ZR(1) - C(5)	98.7(2)
C(23) - ZR(1) - C(6)	98.8(2)
C(23) - ZR(1) - C(7)	115.9(3)
C(23) - ZR(1) - C(17)	164.6(2)
C(23) - ZR(1) - C(18)	161.2(2)
C(24) - ZR(1) - CL(1)	80.1(2)
C(24) - ZR(1) - C(5)	127.9(3)
C(24) - ZR(1) - C(6)	129.3(2)
C(24) - ZR(1) - C(7)	136.9(2)
C(24) - ZR(1) - C(17)	144.6(3)
C(24) - ZR(1) - C(18)	138.8(2)
C(25) - ZR(1) - CL(1)	111.1(3)
C(25) - ZR(1) - C(5)	146.5(2)
C(25) - ZR(1) - C(6)	126.5(3)
C(25) - ZR(1) - C(7)	113.8(3)
C(25) - ZR(1) - C(17)	116.0(3)
C(25) - ZR(1) - C(18)	130.7(2)
C(26) - ZR(1) - CL(1)	130.7(2)
C(26) - ZR(1) - C(5)	118.3(3)
C(26) - ZR(1) - C(6)	94.0(3)
C(26) - ZR(1) - C(7)	84.8(2)
C(26) - ZR(1) - C(17)	112.2(2)
C(26) - ZR(1) - C(18)	142.9(3)

C(20) - ZR(1) - C(19)	32.0(2)
C(21) - ZR(1) - C(19)	54.3(2)
C(21) - ZR(1) - C(20)	32.9(2)
C(22) - ZR(1) - C(19)	155.0(2)
C(22) - ZR(1) - C(20)	127.2(3)
C(22) - ZR(1) - C(21)	118.1(3)
C(23) - ZR(1) - C(19)	133.8(3)
C(23) - ZR(1) - C(20)	123.5(3)
C(23) - ZR(1) - C(21)	135.4(2)
C(23) - ZR(1) - C(22)	31.2(2)
C(24) - ZR(1) - C(19)	105.9(2)
C(24) - ZR(1) - C(20)	92.5(3)
C(24) - ZR(1) - C(21)	111.4(3)
C(24) - ZR(1) - C(22)	52.0(2)
C(24) - ZR(1) - C(23)	31.3(3)
C(25) - ZR(1) - C(19)	102.9(3)
C(25) - ZR(1) - C(20)	76.3(2)
C(25) - ZR(1) - C(21)	83.0(3)

C(25)	- ZR(1) - C(22)	52.4(2)	
C(25)	- ZR(1) - C(23)	52.9(3)	
C(25)	- ZR(1) - C(24)	32.9(3)	
C(26)	- ZR(1) - C(19)	129.2(3)	
C(26)	- ZR(1) - C(20)	97.8(3)	
C(26)	- ZR(1) - C(21)	87.8(3)	
C(26)	- ZR(1) - C(22)	31.3(3)	
C(26)	- ZR(1) - C(23)	52.5(3)	
C(26)	- ZR(1) - C(24)	53.6(2)	
C(26)	- ZR(1) - C(25)	32.6(3)	
C(6)	- C(1) - C(2)	120.4(4)	
C(13)	- C(1) - C(2)	132.2(4)	
C(13)	- C(1) - C(6)	107.1(4)	
C(3)	- C(2) - C(1)	121.2(5)	
C(4)	- C(3) - C(2)	119.2(5)	
C(5)	- C(4) - C(3)	121.6(5)	
C(4)	- C(5) - ZR(1)	120.1(4)	
C(6)	- C(5) - ZR(1)	72.4(3)	
C(6)	- C(5) - C(4)	120.2(5)	
C(1)	- C(6) - ZR(1)	118.9(3)	
C(5)	- C(6) - ZR(1)	77.0(3)	
C(5)	- C(6) - C(1)	117.3(4)	
C(7)	- C(6) - ZR(1)	74.7(3)	
C(7)	- C(6) - C(1)	109.3(4)	
C(7)	- C(6) - C(5)	132.8(4)	
C(6)	- C(7) - ZR(1)	73.5(3)	
C(8)	- C(7) - ZR(1)	118.2(3)	
C(8)	- C(7) - C(6)	105.4(4)	
C(14)	- C(7) - ZR(1)	95.3(3)	
C(14)	- C(7) - C(6)	124.6(4)	
C(14)	- C(7) - C(8)	126.3(4)	
C(9)	- C(8) - C(7)	132.5(4)	
C(13)	- C(8) - C(7)	108.9(4)	
C(13)	- C(8) - C(9)	118.4(4)	
C(10)	- C(9) - C(8)	118.7(5)	
C(11)	- C(10) - C(9)	122.1(5)	
C(12)	- C(11) - C(10)	119.7(5)	
C(13)	- C(12) - C(11)	119.5(5)	
C(8)	- C(13) - C(1)	109.2(4)	
C(12)	- C(13) - C(1)	128.8(4)	
C(12)	- C(13) - C(8)	121.7(5)	
C(15)	- C(14) - C(7)	114.1(4)	
C(16)	- C(14) - C(7)	111.5(4)	
C(16)	- C(14) - C(15)	108.4(4)	
C(17)	- C(14) - C(7)	103.1(4)	

C(17)	- C(14) - C(15)	108.5(4)	
C(17)	- C(14) - C(16)	111.1(4)	
C(14)	- C(17) - ZR(1)	104.2(3)	
C(18)	- C(17) - ZR(1)	75.3(3)	
C(18)	- C(17) - C(14)	126.2(5)	
C(21)	- C(17) - ZR(1)	72.8(3)	
C(21)	- C(17) - C(14)	123.5(5)	
C(21)	- C(17) - C(18)	108.0(5)	
C(17)	- C(18) - ZR(1)	71.3(3)	
C(19)	- C(18) - ZR(1)	74.5(3)	
C(19)	- C(18) - C(17)	106.4(5)	
C(18)	- C(19) - ZR(1)	72.4(3)	
C(20)	- C(19) - ZR(1)	73.9(3)	
C(20)	- C(19) - C(18)	109.1(5)	
C(19)	- C(20) - ZR(1)	74.1(3)	
C(21)	- C(20) - ZR(1)	70.1(3)	
C(21)	- C(20) - C(19)	107.9(6)	
C(17)	- C(21) - ZR(1)	73.7(3)	
C(20)	- C(21) - ZR(1)	76.9(3)	

C(20)	- C(21) - C(17)	108.6(5)	
C(23)	- C(22) - ZR(1)	74.1(4)	
C(26)	- C(22) - ZR(1)	73.3(4)	
C(26)	- C(22) - C(23)	110.0(7)	
C(22)	- C(23) - ZR(1)	74.7(4)	
C(24)	- C(23) - ZR(1)	72.9(4)	
C(24)	- C(23) - C(22)	108.6(8)	
C(23)	- C(24) - ZR(1)	75.8(4)	
C(25)	- C(24) - ZR(1)	74.0(4)	
C(25)	- C(24) - C(23)	108.1(7)	
C(24)	- C(25) - ZR(1)	73.0(4)	
C(26)	- C(25) - ZR(1)	73.8(4)	
C(26)	- C(25) - C(24)	106.1(7)	
C(22)	- C(26) - ZR(1)	75.5(4)	
C(25)	- C(26) - ZR(1)	73.6(4)	
C(25)	- C(26) - C(22)	107.3(7)	

C.3 Fractional atomic coordinates and isotropic thermal parameters for [{$Me_2(\eta^5\text{-}C_5H_4)(\eta^3\text{-}C_{13}H_8)$}$Zr(\eta^5\text{-}C_5H_5)Cl$] (5)

Atom	x/a	y/b	z/c	U(iso)
ZR(1)	0.16907(3)	0.26263(6)	0.12474(3)	0.0325
CL(1)	-0.00487(9)	0.2120(2)	0.08547(9)	0.0533
C(1)	0.2914(3)	-0.0361(5)	0.2700(3)	0.0313
C(2)	0.2420(4)	-0.1002(6)	0.3188(3)	0.0402
C(3)	0.1489(4)	-0.1350(7)	0.2823(4)	0.0485
C(4)	0.1053(4)	-0.1063(7)	0.1936(4)	0.0466
C(5)	0.1535(3)	-0.0472(6)	0.1408(3)	0.0381
C(6)	0.2477(3)	-0.0087(5)	0.1768(3)	0.0296
C(7)	0.3114(3)	0.0738(6)	0.1429(3)	0.0342
C(8)	0.3963(3)	0.0978(6)	0.2191(3)	0.0358
C(9)	0.4783(3)	0.1809(7)	0.2295(3)	0.0465
C(10)	0.5438(4)	0.1902(7)	0.3124(4)	0.0500
C(11)	0.5302(4)	0.1190(7)	0.3848(3)	0.0486
C(12)	0.4502(4)	0.0381(6)	0.3753(3)	0.0403
C(13)	0.3835(3)	0.0275(6)	0.2932(3)	0.0341
C(14)	0.3053(3)	0.0778(6)	0.0462(3)	0.0341
C(15)	0.3977(4)	0.1183(9)	0.0306(4)	0.0556
C(16)	0.2699(4)	-0.0777(7)	0.0006(3)	0.0504
C(17)	0.2369(3)	0.2081(6)	0.0093(3)	0.0340
C(18)	0.1397(4)	0.1912(7)	-0.0318(3)	0.0366
C(19)	0.1003(5)	0.3432(8)	-0.0333(4)	0.0514
C(20)	0.1709(5)	0.4493(8)	0.0045(4)	0.0577
C(21)	0.2551(4)	0.3661(6)	0.0330(4)	0.0452
C(22)	0.2328(7)	0.3086(9)	0.2861(4)	0.0580
C(23)	0.1423(6)	0.346(1)	0.2629(5)	0.0677
C(24)	0.1273(6)	0.470(1)	0.2106(5)	0.0616
C(25)	0.2120(9)	0.5152(8)	0.2012(5)	0.0712
C(26)	0.2770(5)	0.408(1)	0.2485(6)	0.0668
H(21)	0.2748(4)	-0.1154(6)	0.3898(3)	0.1000
H(31)	0.1147(4)	-0.1713(7)	0.3187(4)	0.1000
H(41)	0.0356(4)	-0.1166(7)	0.1743(4)	0.1000
H(51)	0.1203(3)	-0.0631(6)	0.0796(3)	0.1000
H(91)	0.4817(3)	0.2415(7)	0.1770(3)	0.1000
H(101)	0.6092(4)	0.2718(7)	0.3257(4)	0.1000
H(111)	0.5897(4)	0.1269(7)	0.4401(3)	0.1000
H(121)	0.4317(4)	-0.0259(6)	0.4220(3)	0.1000
H(151)	0.3862(4)	0.1023(9)	-0.0240(4)	0.1000
H(152)	0.4182(4)	0.2359(9)	0.0599(4)	0.1000
H(153)	0.4387(4)	0.0452(9)	0.0606(4)	0.1000
H(161)	0.2179(4)	-0.1381(7)	0.0116(3)	0.1000
H(162)	0.3181(4)	-0.1653(7)	0.0262(3)	0.1000
H(163)	0.2688(4)	-0.0656(7)	-0.0497(3)	0.1000
H(181)	0.1048(4)	0.0775(7)	-0.0511(3)	0.1000
H(191)	0.0279(5)	0.3815(8)	-0.0750(4)	0.1000
H(201)	0.1601(5)	0.5683(8)	0.0046(4)	0.1000
H(211)	0.3198(4)	0.4009(6)	0.0716(4)	0.1000
H(221)	0.2623(7)	0.2243(9)	0.3237(4)	0.0864
H(231)	0.0967(6)	0.291(1)	0.2813(5)	0.1024
H(241)	0.0686(6)	0.520(1)	0.1836(5)	0.0937
H(251)	0.2230(9)	0.6027(8)	0.1689(5)	0.1032
H(261)	0.3414(5)	0.405(1)	0.2534(6)	0.1124

C.4 Anisotropic thermal parameters for [{$Me_2(\eta^5\text{-}C_5H_4)(\eta^3\text{-}C_{13}H_8)$}$Zr(\eta^5\text{-}C_5H_5)Cl$] (5)

Atom	U(11)	U(22)	U(33)	U(23)	U(13)	U(12)
Zr(1)	0.03668(22)	0.03798(23)	0.02845(22)	-0.00006(22)	0.00770(22)	0.00764(23)
Cl(1)	0.03885(77)	0.0468(11)	0.04016(88)	-0.00746(77)	0.01233(65)	0.00897(77)
C(11)	0.0402(33)	0.0383(33)	0.0322(32)	-0.0011(32)	0.0108(32)	0.0013(32)
C(12)	0.0553(39)	0.0485(38)	0.0301(33)	0.0106(32)	0.0145(32)	-0.0064(33)
C(13)	0.0521(38)	0.0585(46)	0.0495(38)	0.0104(33)	0.0221(33)	-0.0099(34)
C(14)	0.0410(33)	0.0544(38)	0.0351(33)	0.0011(33)	0.0146(33)	-0.0059(34)
C(15)	0.0333(33)	0.0463(38)	0.0327(33)	-0.0001(32)	0.0106(32)	0.0065(32)
C(16)	0.0229(33)	0.0396(36)	0.0325(32)	-0.0013(32)	0.0107(32)	0.0064(32)
C(17)	0.0388(38)	0.0482(38)	0.0324(32)	0.0032(32)	0.0105(32)	0.0107(32)
C(18)	0.0339(33)	0.0453(38)	0.0327(33)	0.0032(32)	0.0109(32)	0.0103(32)
C(19)	0.0413(33)	0.0461(38)	0.0339(33)	0.0109(32)	0.0110(33)	-0.0092(33)
C(110)	0.0422(33)	0.0451(46)	0.0447(33)	-0.0032(33)	0.0103(33)	-0.0124(33)
C(111)	0.0448(33)	0.0538(38)	0.0398(33)	0.0032(33)	-0.0104(33)	-0.0103(33)
C(122)	0.0521(33)	0.0446(38)	0.0325(32)	0.0032(32)	0.0103(32)	-0.0101(33)
C(133)	0.0388(33)	0.0398(38)	0.0326(32)	0.0104(32)	0.0106(32)	0.0104(32)
C(144)	0.0333(33)	0.0544(38)	0.0325(32)	0.0032(32)	0.0122(32)	0.0107(32)
C(155)	0.0501(33)	0.0613(46)	0.0394(33)	0.0011(33)	0.0127(33)	0.0123(34)
C(166)	0.0772(44)	0.0538(46)	0.0335(33)	-0.0105(33)	0.0113(33)	0.0222(33)
C(177)	0.0339(33)	0.0621(46)	0.0329(32)	0.0110(32)	0.0110(32)	0.0109(32)
C(188)	0.0532(33)	0.0666(46)	0.0346(32)	0.0107(32)	0.0110(32)	0.0123(33)
C(199)	0.0684(44)	0.0779(46)	0.0332(33)	0.0115(33)	0.0122(33)	0.0226(34)
C(201)	0.0885(55)	0.0539(46)	0.0495(46)	0.0148(33)	0.0222(33)	0.0122(34)
C(211)	0.0652(44)	0.0447(33)	0.0327(33)	0.0113(33)	0.0116(33)	-0.0104(33)
C(221)	0.1330(88)	0.0657(55)	0.0333(46)	-0.0129(33)	-0.0116(46)	0.0466(55)
C(231)	0.1005(77)	0.0597(55)	0.0495(46)	-0.0330(46)	0.0333(46)	-0.0123(55)
C(241)	0.0755(55)	0.0553(55)	0.0558(55)	-0.0338(46)	-0.0110(46)	0.0463(55)
C(251)	0.08(11)	0.0495(46)	0.0556(55)	-0.0127(46)	0.0463(55)	-0.0228(55)
C(261)	0.0555(44)	0.1226(88)	0.0564(55)	-0.0173(55)	0.0220(46)	-0.0135(55)

D. X-ray structure analysis of [{$Me_2C(\eta^5\text{-}C_5H_4)_2$}Hf($\eta^5$-$C_5H_5$)Cl] (7)

D.1 Crystal data, data collection and refinement

Compound **7**; $C_{18}H_{19}ClHf$, M = 449.27, monoclinic, space group $P2_1$, a = 7.115(6), b = 9.572(6), c = 10.883(6) Å, β = 92.39(7)°, V = 740.5 Å^3, F(000) = 432, Z = 2, D_c = 2.02 gcm^{-3}, μ = 71.5 cm^{-1}, crystal size *ca.* 0.19 x 0.22 x 0.50 mm, 3575 total (2881 independent) reflections, R = 0.0244 and R_w = 0.0263 from 2453 reflections with $I > 3\sigma(I)$ (181 variables, observations / variables 13.5), maximum peak in final Fourier difference synthesis 0.86 eÅ^{-3}.

Data were collected at room temperature on an Enraf-Nonius CAD4 diffractometer using graphite-monochromated MoK_α radiation (ω-2θ scan mode, ratio of scan rates ω/θ = 1.2, θ_{max} = 33°). The structure was solved by direct methods and refined by full-matrix least-squares technique in the anisotropic approximation (Chebyshev weighting scheme, parameters 8.24, -6.88, 5.75).[1] All hydrogen atoms were located in the difference Fourier maps and included in the final refinement with the fixed positional and thermal parameters. Corrections for Lorentz and polarisation effects and an empirical correction for absorption were applied.[2] Polar axis direction was determined using enantiopole parameter.[4] Crystallographic calculations were carried out using the CRYSTALS program package[3] on a Micro VAX 3800 computer. The data were collected and the structure was solved by Dr. Alexander Chernega.

D.2 Interatomic distances (Å) and angles (°) for [{$Me_2C(\eta^5\text{-}C_5H_4)_2$}Hf($\eta^5$-$C_5H_5$)Cl] (7)

HF(1) - CL(1)	2.510(1)
HF(1) - C(1)	2.49(2)
HF(1) - C(2)	2.57(1)
HF(1) - C(3)	2.632(6)
HF(1) - C(4)	2.67(2)
HF(1) - C(5)	2.60(2)
HF(1) - C(6)	2.62(2)
HF(1) - C(7)	2.64(2)
HF(1) - C(8)	2.58(1)
HF(1) - C(9)	2.52(2)
HF(1) - C(10)	2.51(2)
HF(1) - C(14)	2.559(6)
HF(1) - C(15)	2.53(1)
HF(1) - C(16)	2.63(1)
HF(1) - C(17)	2.69(2)
HF(1) - C(18)	2.48(2)
C(1) - C(2)	1.41(2)
C(1) - C(5)	1.42(1)
C(2) - C(3)	1.41(3)
C(3) - C(4)	1.39(4)
C(4) - C(5)	1.46(3)
C(6) - C(7)	1.40(3)
C(6) - C(10)	1.51(2)
C(7) - C(8)	1.41(3)
C(8) - C(9)	1.31(3)
C(9) - C(10)	1.50(3)
C(10) - C(11)	1.52(2)
C(11) - C(12)	1.533(8)
C(11) - C(13)	1.533(8)
C(11) - C(14)	1.56(2)
C(14) - C(15)	1.33(2)
C(14) - C(18)	1.35(2)
C(15) - C(16)	1.44(2)
C(16) - C(17)	1.37(2)
C(17) - C(18)	1.52(2)

C(1) - HF(1) - CL(1)	123.0(3)
C(2) - HF(1) - CL(1)	91.3(4)
C(2) - HF(1) - C(1)	32.2(5)
C(3) - HF(1) - CL(1)	73.6(2)
C(3) - HF(1) - C(1)	53.0(5)
C(3) - HF(1) - C(2)	31.5(8)
C(4) - HF(1) - CL(1)	90.7(4)
C(4) - HF(1) - C(1)	53.6(6)
C(4) - HF(1) - C(2)	51.7(3)
C(4) - HF(1) - C(3)	30.3(9)
C(5) - HF(1) - CL(1)	122.2(5)
C(5) - HF(1) - C(1)	32.3(2)
C(5) - HF(1) - C(2)	52.2(6)
C(5) - HF(1) - C(3)	51.7(6)
C(5) - HF(1) - C(4)	32.2(6)
C(6) - HF(1) - CL(1)	77.4(5)
C(6) - HF(1) - C(1)	122.9(6)
C(6) - HF(1) - C(2)	114.6(5)
C(6) - HF(1) - C(3)	132.0(9)
C(6) - HF(1) - C(4)	162.2(6)
C(6) - HF(1) - C(5)	153.1(6)
C(7) - HF(1) - CL(1)	74.5(5)
C(7) - HF(1) - C(1)	97.9(6)
C(7) - HF(1) - C(2)	83.8(5)
C(7) - HF(1) - C(3)	103.5(10)
C(7) - HF(1) - C(4)	133.2(6)
C(7) - HF(1) - C(5)	130.2(7)
C(8) - HF(1) - CL(1)	103.3(5)
C(8) - HF(1) - C(1)	72.0(6)
C(8) - HF(1) - C(2)	71.0(5)
C(8) - HF(1) - C(3)	100.4(10)
C(8) - HF(1) - C(4)	121.3(6)
C(8) - HF(1) - C(5)	103.5(6)
C(9) - HF(1) - CL(1)	127.3(5)
C(9) - HF(1) - C(1)	75.3(6)
C(9) - HF(1) - C(2)	89.5(6)
C(9) - HF(1) - C(3)	121.0(9)
C(9) - HF(1) - C(4)	128.4(7)
C(9) - HF(1) - C(5)	98.9(7)
C(10) - HF(1) - CL(1)	110.1(4)
C(10) - HF(1) - C(1)	109.4(6)
C(10) - HF(1) - C(2)	122.2(5)
C(10) - HF(1) - C(3)	152.7(9)
C(10) - HF(1) - C(4)	159.0(5)
C(10) - HF(1) - C(5)	126.8(6)
C(14) - HF(1) - CL(1)	111.2(2)
C(14) - HF(1) - C(1)	124.9(4)
C(14) - HF(1) - C(2)	157.2(4)
C(14) - HF(1) - C(3)	151.4(9)
C(14) - HF(1) - C(4)	121.8(5)
C(14) - HF(1) - C(5)	109.4(5)
C(15) - HF(1) - CL(1)	82.2(4)
C(15) - HF(1) - C(1)	149.3(4)
C(15) - HF(1) - C(2)	165.9(4)
C(15) - HF(1) - C(3)	134.6(8)
C(15) - HF(1) - C(4)	115.5(5)
C(15) - HF(1) - C(5)	121.6(5)
C(16) - HF(1) - CL(1)	80.6(4)
C(16) - HF(1) - C(1)	127.1(5)
C(16) - HF(1) - C(2)	134.3(5)
C(16) - HF(1) - C(3)	104.6(10)
C(16) - HF(1) - C(4)	83.2(6)
C(16) - HF(1) - C(5)	94.9(6)

C(17)	- HF(1)	- CL(1)	106.9(4)	C(2)	- C(3)	- HF(1)	71.8(6)
C(17)	- HF(1)	- C(1)	99.9(4)	C(4)	- C(3)	- HF(1)	76.4(9)
C(17)	- HF(1)	- C(2)	118.7(5)	C(4)	- C(3)	- C(2)	109.6(6)
C(17)	- HF(1)	- C(3)	98.6(9)	C(3)	- C(4)	- HF(1)	73.3(8)
C(17)	- HF(1)	- C(4)	69.6(6)	C(5)	- C(4)	- HF(1)	71.1(10)
C(17)	- HF(1)	- C(5)	69.2(5)	C(5)	- C(4)	- C(3)	106.3(18)
C(18)	- HF(1)	- CL(1)	131.0(5)	C(1)	- C(5)	- HF(1)	69.6(13)
C(18)	- HF(1)	- C(1)	98.1(6)	C(4)	- C(5)	- HF(1)	76.7(11)
C(18)	- HF(1)	- C(2)	128.8(6)	C(4)	- C(5)	- C(1)	108.0(21)
C(18)	- HF(1)	- C(3)	124.6(8)	C(7)	- C(6)	- HF(1)	75.6(11)
C(18)	- HF(1)	- C(4)	94.4(6)	C(10)	- C(6)	- HF(1)	68.9(9)
C(18)	- HF(1)	- C(5)	78.4(6)	C(10)	- C(6)	- C(7)	108.0(17)
C(7)	- HF(1)	- C(6)	30.9(6)	C(6)	- C(7)	- HF(1)	73.5(11)
C(8)	- HF(1)	- C(6)	50.9(6)	C(8)	- C(7)	- HF(1)	71.9(10)
C(8)	- HF(1)	- C(7)	31.3(6)	C(8)	- C(7)	- C(6)	105.3(17)
C(9)	- HF(1)	- C(6)	55.0(7)	C(7)	- C(8)	- HF(1)	76.8(10)
C(9)	- HF(1)	- C(7)	53.2(7)	C(9)	- C(8)	- HF(1)	72.7(11)
C(9)	- HF(1)	- C(8)	29.7(6)	C(9)	- C(8)	- C(7)	116.6(17)
C(10)	- HF(1)	- C(6)	34.3(6)	C(8)	- C(9)	- HF(1)	77.6(12)
C(10)	- HF(1)	- C(7)	54.4(5)	C(10)	- C(9)	- HF(1)	72.2(10)
C(10)	- HF(1)	- C(8)	52.3(5)	C(10)	- C(9)	- C(8)	105.9(18)
C(10)	- HF(1)	- C(9)	34.7(6)	C(6)	- C(10)	- HF(1)	76.8(10)
C(14)	- HF(1)	- C(6)	75.3(5)	C(9)	- C(10)	- HF(1)	73.2(10)
C(14)	- HF(1)	- C(7)	104.9(4)	C(9)	- C(10)	- C(6)	104.0(14)
C(14)	- HF(1)	- C(8)	105.5(5)	C(11)	- C(10)	- HF(1)	105.6(8)
C(14)	- HF(1)	- C(9)	79.7(5)	C(11)	- C(10)	- C(6)	126.2(14)
C(14)	- HF(1)	- C(10)	54.3(2)	C(11)	- C(10)	- C(9)	128.6(14)
C(15)	- HF(1)	- C(6)	76.3(3)	C(12)	- C(11)	- C(10)	112.9(14)
C(15)	- HF(1)	- C(7)	106.3(5)	C(13)	- C(11)	- C(10)	111.5(12)
C(15)	- HF(1)	- C(8)	122.6(5)	C(13)	- C(11)	- C(12)	111.0(5)
C(15)	- HF(1)	- C(9)	104.4(6)	C(14)	- C(11)	- C(10)	97.7(5)
C(15)	- HF(1)	- C(10)	71.9(5)	C(14)	- C(11)	- C(12)	110.3(13)
C(15)	- HF(1)	- C(14)	30.3(4)	C(14)	- C(11)	- C(13)	112.9(12)
C(16)	- HF(1)	- C(6)	107.4(6)	C(11)	- C(14)	- HF(1)	102.0(5)
C(16)	- HF(1)	- C(7)	134.9(3)	C(15)	- C(14)	- HF(1)	73.5(7)
C(16)	- HF(1)	- C(8)	154.7(6)	C(15)	- C(14)	- C(11)	124.0(7)
C(16)	- HF(1)	- C(9)	130.8(6)	C(18)	- C(14)	- HF(1)	71.2(9)
C(16)	- HF(1)	- C(10)	102.7(5)	C(18)	- C(14)	- C(11)	121.7(10)
C(16)	- HF(1)	- C(14)	51.2(4)	C(18)	- C(14)	- C(15)	109.6(11)
C(17)	- HF(1)	- C(6)	126.3(6)	C(14)	- C(15)	- HF(1)	76.1(7)
C(17)	- HF(1)	- C(7)	157.1(5)	C(16)	- C(15)	- HF(1)	77.7(8)
C(17)	- HF(1)	- C(8)	147.8(2)	C(16)	- C(15)	- C(14)	107.9(12)
C(17)	- HF(1)	- C(9)	118.4(6)	C(15)	- C(16)	- HF(1)	69.9(8)
C(17)	- HF(1)	- C(10)	105.6(5)	C(17)	- C(16)	- HF(1)	77.5(9)
C(17)	- HF(1)	- C(14)	52.8(4)	C(17)	- C(16)	- C(15)	110.6(15)
C(18)	- HF(1)	- C(6)	103.3(6)	C(16)	- C(17)	- HF(1)	72.7(8)
C(18)	- HF(1)	- C(7)	128.9(6)	C(18)	- C(17)	- HF(1)	65.4(9)
C(18)	- HF(1)	- C(8)	114.8(6)	C(18)	- C(17)	- C(16)	101.7(14)
C(18)	- HF(1)	- C(9)	85.1(3)	C(14)	- C(18)	- HF(1)	77.8(9)
C(18)	- HF(1)	- C(10)	74.5(5)	C(17)	- C(18)	- HF(1)	80.7(10)
C(18)	- HF(1)	- C(14)	31.0(5)	C(17)	- C(18)	- C(14)	109.0(15)
C(16)	- HF(1)	- C(15)	32.4(5)				
C(17)	- HF(1)	- C(15)	52.5(4)				
C(17)	- HF(1)	- C(16)	29.8(5)				
C(18)	- HF(1)	- C(15)	51.9(6)				
C(18)	- HF(1)	- C(16)	51.9(6)				
C(18)	- HF(1)	- C(17)	33.8(5)				
C(2)	- C(1)	- HF(1)	77.0(8)				
C(5)	- C(1)	- HF(1)	78.0(13)				
C(5)	- C(1)	- C(2)	107.1(19)				
C(1)	- C(2)	- HF(1)	70.7(7)				
C(3)	- C(2)	- HF(1)	76.7(6)				
C(3)	- C(2)	- C(1)	108.7(15)				

D.3 Fractional atomic coordinates and isotropic thermal parameters for all non-hydrogen atoms of [{$Me_2C(\eta^5\text{-}C_5H_4)_2$}Hf($\eta^5$-$C_5H_5$)Cl] (7)

Atom	x/a	y/b	z/c	U(iso)
HF(1)	-0.80009(2)	0.1900(3)	-0.80128(1)	0.0206
CL(1)	-1.1527(2)	0.182(1)	-0.8215(2)	0.0368
C(1)	-0.594(2)	0.119(2)	-0.970(2)	0.0236
C(2)	-0.772(2)	0.071(1)	-1.011(1)	0.0192
C(3)	-0.888(1)	0.188(4)	-1.0385(5)	0.0340
C(4)	-0.785(3)	0.310(2)	-1.022(2)	0.0436
C(5)	-0.595(3)	0.267(2)	-0.981(2)	0.0325
C(6)	-0.887(3)	0.022(2)	-0.623(2)	0.0337
C(7)	-0.895(3)	-0.063(2)	-0.728(2)	0.0390
C(8)	-0.709(3)	-0.068(1)	-0.768(2)	0.0317
C(9)	-0.584(3)	0.008(2)	-0.706(2)	0.0254
C(10)	-0.688(2)	0.075(2)	-0.605(1)	0.0413
C(11)	-0.6233(8)	0.193(1)	-0.5201(4)	0.0237
C(12)	-0.4093(9)	0.197(4)	-0.4971(5)	0.0353
C(13)	-0.725(1)	0.189(3)	-0.3986(5)	0.0382
C(14)	-0.688(1)	0.3167(9)	-0.6045(5)	0.0103
C(15)	-0.867(2)	0.353(1)	-0.626(1)	0.0204
C(16)	-0.876(2)	0.446(1)	-0.730(2)	0.0261
C(17)	-0.702(2)	0.460(1)	-0.778(1)	0.0265
C(18)	-0.585(3)	0.361(2)	-0.698(2)	0.0220

D.4 Anisotropic thermal parameters for [{$Me_2C(\eta^5\text{-}C_5H_4)_2$}Hf($\eta^5$-$C_5H_5$)Cl] (7)

Atom	U(11)	U(22)	U(33)	U(23)	U(13)	U(12)
HF(1)	0.02066(7)	0.02064(7)	0.02041(7)	0.0008(4)	0.00101(4)	-0.0003(4)
CL(1)	0.0222(4)	0.045(2)	0.0505(7)	-0.003(1)	0.0015(4)	0.000(1)
C(1)	0.024(4)	0.030(5)	0.023(4)	-0.005(3)	0.007(3)	-0.008(3)
C(2)	0.047(6)	0.017(3)	0.012(3)	-0.006(2)	-0.008(3)	0.001(3)
C(3)	0.038(2)	0.048(6)	0.024(2)	-0.007(7)	-0.007(2)	-0.002(8)
C(4)	0.037(6)	0.060(8)	0.038(6)	-0.005(6)	-0.004(4)	0.002(6)
C(5)	0.052(7)	0.036(7)	0.022(4)	-0.001(4)	0.003(4)	-0.019(5)
C(6)	0.034(5)	0.046(8)	0.035(5)	0.013(5)	0.003(4)	-0.017(4)
C(7)	0.055(8)	0.045(7)	0.034(6)	-0.004(5)	-0.001(4)	-0.027(5)
C(8)	0.08(1)	0.016(4)	0.030(5)	-0.002(3)	-0.007(5)	0.013(4)
C(9)	0.038(5)	0.019(5)	0.029(5)	0.000(4)	0.002(4)	0.012(4)
C(10)	0.055(8)	0.022(5)	0.073(9)	0.009(5)	-0.005(7)	-0.014(5)
C(11)	0.043(3)	0.030(2)	0.023(2)	-0.015(5)	0.003(2)	-0.019(5)
C(12)	0.041(2)	0.037(6)	0.040(2)	-0.016(7)	-0.014(2)	0.003(6)
C(13)	0.058(3)	0.050(4)	0.022(2)	-0.008(8)	0.004(2)	0.01(1)
C(14)	0.020(3)	0.018(4)	0.003(2)	-0.002(2)	-0.001(2)	-0.003(3)
C(15)	0.026(4)	0.017(3)	0.022(3)	-0.001(3)	0.004(3)	0.007(3)
C(16)	0.031(4)	0.019(4)	0.038(5)	-0.011(4)	-0.004(3)	0.005(3)
C(17)	0.035(5)	0.026(5)	0.023(4)	0.001(3)	0.009(3)	0.007(3)
C(18)	0.030(5)	0.015(4)	0.026(3)	0.006(3)	-0.001(3)	0.003(3)

References for Appendices

1. J. S. Rollet, *Computing Methods in Crystallography*, Pergamon Press, Oxford, 1965.
2. N. Walker and D. Stuart, *Acta Crystallogr., Sect. A*, 1983, **39**, 158.
3. D. J. Watkin, J. R. Carruthers and P. W. Betteridge, CRYSTALS user guide, Chemical Crystallography Laboratory, University of Oxford, 1985.
4. H. D. Fluck, *Acta Crystallogr., Sect. A*, 1983, **39**, 876.